Impact of Sea Level Rise on
Groundwater Flow Regimes

A Sensitivity Analysis for the Netherlands

Impact of Sea Level Rise on

Groundwater Flow Regimes
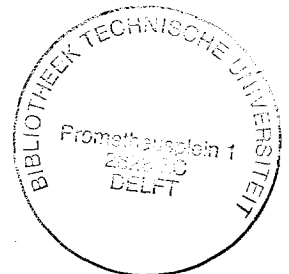
A Sensitivity Analysis for the Netherlands

by

G. H. P. Oude Essink

Volume 7

Delft Studies in Integrated Water Management

Delft University of Technology

Delft, April 1996

Cover designed by Anne-Marie Oude Essink

"De kwel van vooral zoet en zout water zal in laag-Nederland toenemen. Ook is het niet uitgesloten dat de omvang van de zoetwaterbellen onder de duinen zal worden beïnvloed. Voorts zal tot ver landinwaarts de waterinfrastructuur aanpassing behoeven: óf de waterniveaus stijgen in laag-Nederland mee met de zeespiegelstijging, óf de pompcapaciteit zal moeten worden opgevoerd. De precieze gevolgen voor de waterhuishouding en de bedrijfssectoren, en de benodigde oplossingen, zijn nog onderwerp van studie."

Derde Nota Waterhuishouding: Water voor nu en later.
Tweede Kamer, vergaderjaar 1988-1989, **21 250**, *nrs. 1-2.*

aan Gerard en Berendina, mijn ouders.

Acknowledgements

In front of you lies the result of five years of research at the Hydrology Group of the Faculty of Civil Engineering. The number of pages of this thesis may suggest it's a life's work: well, it's not, though the comprehensive analysis of numerous variables and aspects in this Ph.D. study was time-consuming.

Four persons I want to acknowledge especially. First of all, Prof. J.C. van Dam is thanked for the warm-hearted way he advised me on more than only (geo)hydrological topics. Moreover, he patiently taught me the ropes of writing technical English. Secondly, I thank my daily companion Reinder Boekelman with whom I published a few articles and who truly supported and guided me in my choices during the whole research. Thirdly, Tom Rientjes is thanked for his commitment to my Ph.D. adventures. Fourthly, I thank my former roommate Theo Brandsma, whose well-balanced personality supported me during the first four years.

I thank my other colleagues of the Hydrology Group who have created an environment in which working on this thesis was a real pleasure: in particular Margreet Evertman, Betty Rothfusz, Som Gan, Marc van Dijk, Marcel Boomgaard, Herbert Berger, Pieter Huisman, Antal Koçan and Hans Vermeulen. Ruud Bosters is acknowledged for his efforts to bring up material for chapter 2. Thanks to Humphrey Paap who relieved my efforts in data-processing for the profile in section 8.3.

Rob Klomp, Dick Lyklema, Matt Mann, Herman van der Most, Jos Streng, Frans van de Ven and Wouter Zijl are acknowledged for being (temporary) members of the guidance committee, which was active during the first three years.

Luc Lebbe, Jan Kooiman and Hans van der Eem are thanked for their release of documentation which made it possible for me to adapt the MOC version of 1989 for density differences. Based on their articles, I was inspired to choose the numerical modelling approach applied in this thesis. Hans van Duijn and Ruud Schotting are acknowledged for their release of documentation applied in section 6.4. I thank Theo Olsthoorn for his release of data of the studied area in chapter 7 and section 8.2.

I am indebted to Geke and Loek van der A who corrected my technical English in nearly half of the chapters of this thesis.

Delft Hydraulics is sincerely thanked for supporting me financially during this study.

Last but not least, I want to render my deepest thanks to my three housemates, my parents and my brother Erik, as well as to my girlfriend Sheila Pels for accompanying me during these past years, for relieving my household-commitments, and for preventing sea level rise to permeate my private life.

"(...) the only base of credibility (...) of long term forecasting and prediction (...) is a hydrologically sound theory, since an opportunity to correct a wrong extrapolation will always come either too late or never."

[Klemeš, 1986]

Contents

Chapter 1

Introduction

1.1 Problem definition

In the Netherlands, mankind has been attracted for ages to coastal areas because of an abundance of food (fisheries and agriculture) and the presence of economic activities (e.g. trade, ports and infrastructure). As a consequence, these coastal areas are densely populated. Many coastal areas, especially the low-lying deltaic areas with a ground level situated within a few metres above or even below mean sea level, have directly been affected by variations in the level of the sea. Coastal defence systems had to be set up to protect mankind against flooding. Management of water resources (or water management[1]) in these coastal areas is rather complex and hence, sophisticated (technical and organizational) systems have been required.

In the near future, climate change will probably jeopardize the water management systems in the vulnerable Dutch coastal areas even more. Relevant mechanisms related to climate change are the (enhanced) greenhouse effect, global warming and an accelerated rise in global mean sea level. All these mechanisms are probably caused by natural as well as man-induced processes. Though the effects of several feedbacks of the climate system (e.g. clouds and oceans) are difficult to assess, a global mean sea level rise of 60 centimetres for the next century is still considered the best estimate (in 1996).

As the Netherlands is a low-lying country[2], sea level rise will directly affect the Dutch society from an environmental, social and economic point of view. As a consequence, great (economic) interests may be at stake. The impact of sea level rise on water management in the Dutch coastal areas is subdivided into three main sectors:

---

[1]Water management is defined here as [CHO-TNO, 1986]:

> *"The total of research, planning, technical activities and administrative measures that should lead to the most efficient integrated management of the available groundwater and surface water. The way water resources in a specific area are assimilated, displaced, utilized, consumed and transported. In most cases, this process is affected by human interventions."*

[2]About 25 % of the land is situated below mean sea level (*M.S.L.*), whereas about 65 % would be flooded regularly by the sea or the rivers in the absence of dunes and dikes. Accordingly, some 8 million people would be endangered.

Enhanced greenhouse effect	Changes in solar output Milankovitch cycli	Changes in hydrological regime

origin trace gases:
-natural
-anthropogenic

changes in natural recharge:
-precipitation
-evapotranspiration
changes in land use and crops

Climate Change

Global warming

Coastal zone and hinterland	Sea Level Rise (relative)	Estuaries and rivers

increased risk of flooding
increase of wave attack
increase of tidal range
increase of storm surges
population at risk
changes in morphology:
-coastal erosion
-dune erosion
-shoreline retreat
land losses, land degradation

global mean rise
land-subsidence
uplift

increased risk of flooding
population at risk
changes in sediment load:
-river bed elevation
backwater effect
salt water intrusion
increased seepage
crop losses, land degradation
changes in ecosystems:
-decrease in diversity of species

Coastal groundwater flow regimes

salt water intrusion in aquifers
rise of piezometric levels
extra upconing saline groundwater
decrease of freshwater resources
increase of seepage:
-quantitative
-qualitative

Human activities on groundwater flow regimes

exploiting groundwater
mining of gas, oil, water and sand
land reclamation
man-induced land-subsidence
drainage
irrigation
countermeasures:
-extraction saline groundwater
-infiltration surface water
-inundation low-lying polders
-physical barriers
-increase natural recharge

Impacts on water management:

safety
domestic & industrial water supply
agriculture & horticulture: salt damage to crops
flushing of water courses
(beach) recreation: narrowing of sand-dune areas
discharge: blocking of (natural) discharge
ecosystems: degradation
navigation
irrigation
infrastructure

Figure 1.1: Relevant aspects affecting the coastal areas in case of climate change and a relative sea level rise.

(I) the coastal zone and the hinterland; (II) the estuaries and the rivers; and (III) the coastal groundwater flow regimes. Figure 1.1 shows a diagram of relevant aspects that affect the coastal areas in case of climate change and a relative sea level rise.

ad I. Coastal zone and hinterland

The coastal zone and deltaic areas will directly bear the impact of sea level rise (figure 1.2). A possible increase in storm surges due to climate change and an increase in wave attack could lead to collapse of coastal defence systems (dykes and dunes). Subsequently, this could induce flooding of populated areas in the hinterland and loss of lives should be feared. In the medium term, sea level rise could cause an increase in coastal erosion. If no countermeasures such as sand-suppletion are carried out, coastal erosion could result in a severe shoreline
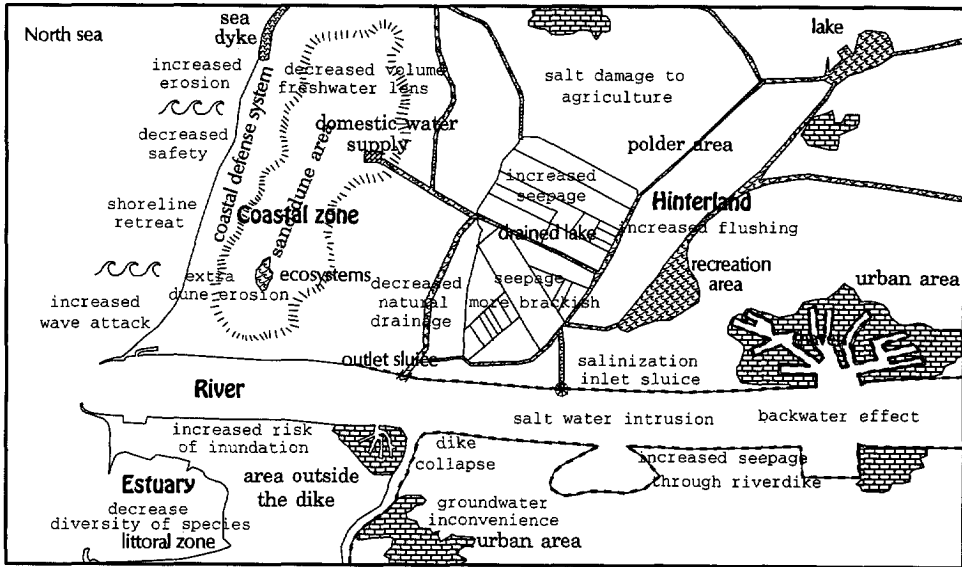
Figure 1.2: Possible impacts of sea level rise on a coastal lowland.

retreat and in a decrease of the natural recharge area. Furthermore, a rise in water level (due to the backwater effect) could block the natural discharge of low-lying areas and the excess water must be discharged by pumpage at the expense of higher energy costs.

ad II. Estuaries and rivers

Estuaries and rivers could experience an increased salt water intrusion if the river bed elevation cannot match sea level rise (figure 1.2). This can be expected in numerous river mouths where the sediment load has been reduced significantly during the last decades because of, among others, sand-mining and the construction of dams and barrages. Moreover, the backwater effect of sea level rise will decrease the safety against flooding over large distances upstream of the river mouth.

ad III. Coastal groundwater flow regimes

At this moment, a large number of coastal groundwater flow regimes, especially shallow ones, experience a severe *salt water intrusion* (a permanent inflow of saline groundwater) caused by both natural as well as man-induced processes. Figure 1.3 displays several possible impacts of sea level rise on the groundwater flow regime in the low-lying western part of the Netherlands.

Coastal groundwater flow regimes within the zone of influence of mean sea level, situated nearby the coast, are threatened by the rise in global mean sea level even more than they are endangered already. The rise in sea level will accelerate

Coastal zone   Hinterland
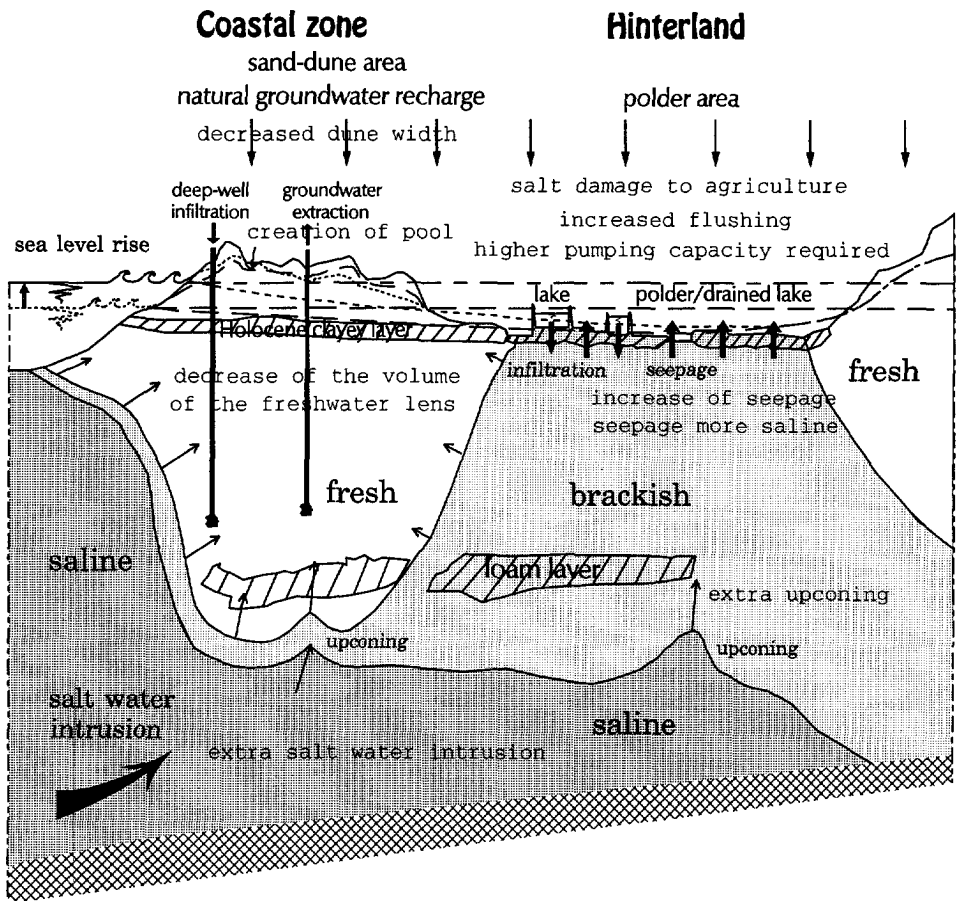
Figure 1.3: Possible impacts of sea level rise on the groundwater flow regime in the low-lying western part of the Netherlands.

the salinisation process in these coastal regimes. This process could result in a reduction of fresh water resources. Furthermore, the seepage quantity will increase in those coastal areas which are below $M.S.L.$. The present capacity of the discharge systems in several polders may be insufficient to cope with the excess of seepage water. This seepage will probably have a higher salinity than at present. In consequence, crops may suffer from salt damage and fertile arable land might eventually become barren land.

The mixing zone between fresh and saline groundwater will be shifted further inland. Groundwater extraction wells, which were originally located in fresh groundwater, will then be located in or nearby brackish or saline groundwater,

so that upconing can easily occur.

Shoreline retreat will also affect the Dutch coastal groundwater flow regimes by narrowing the width of the sand-dune areas, thus diminishing the area over which natural groundwater recharge occurs. This may lead to a decrease in fresh water resources which could affect domestic, agricultural and industrial water supply. If shoreline retreat is counteracted, the phreatic groundwater level in the sand-dune areas along the coast will rise due to sea level rise. As a result, the soil is moistened and dune pools may develop. On the other hand, if the shoreline retreat is severe, the phreatic groundwater level further inland in the sand-dune area may drop, and consequently drier conditions might occur. It depends on local conditions and human interference whether flora and fauna of vulnerable ecosystems will be able to adapt to such hydrological changes.

In addition, higher salinities due to an increased salt water intrusion in rivers and estuaries may jeopardize adjacent aquifers through recharge from surface water with a higher solute content. Consequently, the extraction rates of existing pumped wells will have to be reduced or the wells might even have to be abandoned.

Note that, besides sea level rise, human activities also could highly affect the coastal groundwater flow regimes, for instance by means of:

- exploiting or eventually mining of fresh groundwater, which is extracted for domestic, agricultural and industrial water supply,

- reducing natural groundwater recharge areas, e.g. the sand-dunes along the coast, for the development of housing and recreational areas,

- reclaiming land, thus causing the lowering of phreatic groundwater levels and eventually land subsidence.

1.2 Objective definition

The last sector Coastal groundwater flow regimes in section 1.1 appears to be rather underexposed in most of the descriptions of the impact of sea level rise (see also chapter 2). Nevertheless, the impact of sea level rise on groundwater flow regimes and consequently on water management can be far-reaching. Virtually all relevant literature treats coastal groundwater flow regimes only very superficially and concludes that the volume of fresh water resources is likely to decrease and saline seepage in groundwater flow regimes is likely to increase. Therefore, in order to partly fill the gap of knowledge, the scope of this thesis is the study of the coastal groundwater flow regimes in the Netherlands.

The main objective of this thesis is to investigate the possible impact of several scenarios of sea level rise and human activities on vulnerable coastal groundwater flow regimes in the Netherlands during the next millennium. The most important tool

which leads to the objective is numerical modelling. A two-dimensional groundwater flow model is chosen which simulates density-dependent groundwater flow and solute transport in a number of specific groundwater flow regimes.

It should be noted that the methodology followed in this thesis to fulfil the main objective can also be extended to similar vulnerable coastal groundwater flow regimes around the world. Moreover, the conclusions drawn from the Dutch groundwater flow regimes by means of numerical modelling can serve in understanding the mechanisms involving sea level rise and its impact on coastal groundwater flow regimes.

This study has four sub-objectives. They are formulated as follows:

a. **assess the propagation of sea level rise in the piezometric level distribution**
    If the length (the so-called *zone of influence*) over which the impact of sea level rise can be noticed in the groundwater flow regime is long, changes in the salinity distribution of the groundwater flow regime due to sea level rise may be considerable.

b. **assess the changes in salt water intrusion in the groundwater flow regime**
    If the salinisation rate of the groundwater flow regimes increases, saline groundwater may reach the top layer more rapidly. Note that, for centuries, human activities have already caused salinisation of the Dutch subsoil since (low-lying) polder areas have been created (the so-called drained lakes) and great quantities of (fresh) groundwater have been extracted.

c. **assess the changes in volumes of freshwater lenses in sand-dune areas**
    If saline groundwater intrudes from the sea in the aquifers more rapidly because of sea level rise than under present conditions, the volumes of fresh groundwater resources along the coast may decrease and/or freshwater lenses may displace further inland. Subsequently, drinking water companies, which extract groundwater from the sand-dune areas, should anticipate on future deficiencies. As a result, future domestic, agricultural and industrial water supply may be threatened.

d. **assess the changes in seepage (both quantity and quality) in low-lying polder areas**
    If the gradient of the piezometric level in coastal groundwater flow regimes increases because of sea level rise, seepage quantity will increase. Areas in which surface water had previously infiltrated, may in the future be subject to seepage. Furthermore, seepage in polder areas will eventually contain a higher salinity than at this moment, as sea level rise accelerates the inflow of saline groundwater and the redistribution of salinity in the subsoil. The saline seepage, mixed with fresh surface water, will eventually end up in water courses. Agriculture may suffer from salt damage, causing economic implications. In order to control the solute concentrations in surface water, the water courses in the low-lying areas in the vicinity of the coast (e.g. in the water control system of Rijnland) will probably have to be flushed more frequently and/or more intensively.

After the impact of sea level rise on the groundwater flow regime is investigated, the relation of the sub-objectives with three water management sectors[3] relevant to this study will be assessed. They are: (1) domestic and industrial water supply from coastal sand-dune areas, (2) flushing of water courses of low-lying areas and (3) agriculture in terms of salt damage.

An accurate assessment of the impact of sea level rise on coastal groundwater flow regimes is difficult to achieve, as so many processes are involved. A single assessment of the impact of sea level rise is impossible, since the exact impact of sea level rise on coastal groundwater flow regimes is very site-specific and depends on features such as geometry of the geohydrologic system, (geo)hydrological parameters and human activities.

It is important to realize that impact of sea level rise must be considered in relation to that of human activities. The present state of the groundwater flow regime is not yet in a dynamic equilibrium. A reason for this is the time lag between cause and effect, which can amount to several decades or centuries. Human activities in the past, such as reclaiming lakes or extracting groundwater at high rates causing upconing, are still not completely effective concerning the salinity distribution of most of the groundwater flow regimes. In addition, in the future, the influence of a gradual rise in sea level and human activities (e.g. countermeasures) will also affect the groundwater flow regime. It is quite possible that, in the future, not sea level rise, but past, present and future human activities will dominate the salinisation process of numerous coastal groundwater flow regimes.

As groundwater flow is a very slow process, the impact of sea level rise will only be noticed after at least several decades. In order to assure that mankind can anticipate to it in due time by taking adequate measures, the impact of sea level rise on groundwater flow regimes should be recognized, estimated, investigated and analysed in time: i.e. at this very moment.

1.3   Organization of the thesis

The chapters 2 and 3 introduce the reader into the topic of sea level rise and its impact. In chapter 2, an overview is given of possible impacts of sea level rise on the coastal zone and the hinterland, on estuaries and rivers, on coastal groundwater flow regimes and on water management. In chapter 3, the causes of climate change, temperature rise and sea level rise respectively are discussed, and the variations of sea level in the past and the predictions of future sea level rise are summarized.

The chapters 4, 5, 6 and 7 present the features of the numerical modelling process. In chapter 4, a concise summary of available suitable groundwater flow models is given and the selection of one groundwater flow model is argued. In chapter 5, the

---

[3]In the study Policy Analysis for the Watermanagement of the Netherlands (PAWN) [Pulles, 1985] the water management sectors are: agriculture; horticulture; domestic water supply; industry; power generation; navigation; recreation; and environment, ecology and nature preservation.

different theoretical aspects are described of the selected groundwater flow model MOC which has been adapted by the author for density differences. In chapter 6, additional testing is done for the adapted MOC model for three hypothetical cases. In chapter 7, a sensitivity analysis of both subsoil and model parameters is executed for a profile through the sand-dune area of Gemeentewaterleidingen Amsterdam and polders lying more inland.

The chapters 8 and 9 discuss and analyse the results of simulations with the adapted MOC model on Dutch groundwater flow regimes. In chapter 8, the simulations of two specific profiles perpendicular to the Dutch coastline are discussed for several rates of sea level rise. In chapter 9, the sensitivity analysis of the groundwater flow regime in the Netherlands for sea level rise is described, based on eight representative profiles. Moreover, scenarios with countermeasures and with varying subsoil parameters are considered.

In chapter 10, the impact of sea level rise on the groundwater flow regime is reproduced for the following three water management sectors: domestic and industrial water supply, flushing and agriculture.

Finally, conclusions are drawn and recommendations are given in chapter 11.

Chapter 2

Overview of the physical impacts of sea level rise

2.1 Introduction

From ancient times on, man has always preferred deltaic and coastal areas for settlement, mainly because of the abundance of food from fishery and from agriculture due to the presence of fertile soils. Also nowadays a great deal of the earth's population is still concentrated in these areas. Living in these areas, however, has also some drawbacks. One of them being the danger of flooding. Storm surges and river floods may cause flooding of low-lying areas and may eventually lead to many casualties and great economic damage. Many measures have been taken to minimize this risk: maintenance of natural levees, construction of dams, dikes and embankments, prevention of scouring to avoid a sudden collapse of dykes, etc.

In addition, climate change will affect the level of the sea by global warming (namely the global mean air temperature rises due to the enhanced greenhouse effect). As a result, (geo)hydrologic and subsequently socio-economic consequences can be expected.

It is evident that a rise in sea level will increase the risk of flooding. Moreover, a sea level rise will also affect other aspects of the environment. Although a relative sea level rise may show very different local effects, e.g. because of different (geo)hydrological and topographical circumstances, the phenomenon of sea level rise will be felt throughout the world. Especially in case of a rapid rise in sea level, the consequences will therefore be diverse. In figure 2.1, an overview is given of the areas vulnerable to sea level rise. All these areas over the world will in some way be affected by sea level rise. Most directly noticeable are changes along the shoreline and changes in estuaries and rivers. In the long-term, changes in the salinity distribution of coastal groundwater flow regimes may also occur. Eventually, these changes will induce changes in water management as well (see figure 1.1).

Especially during the last decade, numerous initiatives have been taken to assess the vulnerability for sea level rise on coastal zone management. Two initiatives are briefly mentioned here.

Firstly, the impact of a rise in mean sea level on society was considered during
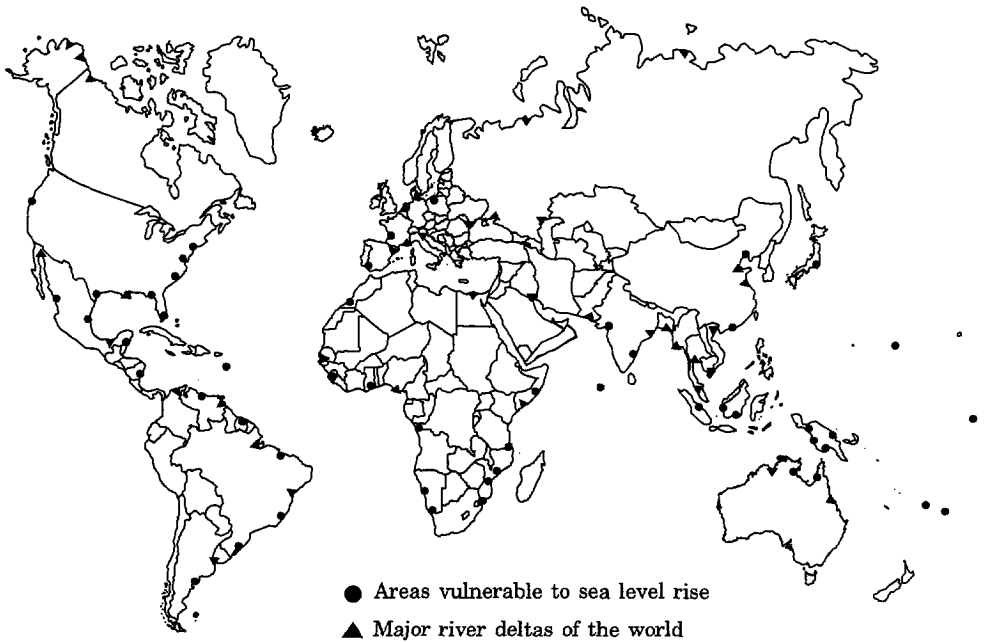
Figure 2.1: Areas in the world vulnerable to sea level rise, based on information about major river deltas and low-lying polder areas of the world, coastal wetlands (marshes, mangrove forests), and various other qualitative descriptions of vulnerable areas due to sea level rise [e.g. Snead, 1972; Miami Conference, 1990; Gilbert *et al.*, 1990; Tsyban *et al.*, 1990; Perdomo *et al.*, 1992].

a Workshop in Delft, the Netherlands, in 1986: Impact of Sea Level Rise on Society (ISOS) [Wind, 1987]. The session was intended to provide information on possible impacts of sea level rise on coastal lowlands and to indicate the consequences of possible strategies open to decision makers. The impact on three case studies was evaluated: the Netherlands, Bangladesh and the Maldives Islands. The results of the case study the Netherlands are extensively presented in Peerbolte *et al.* [1991].

Secondly, exploratory investigations under the terms of the activities of the Intergovernmental Panel of Climate Change (IPCC) have resulted, in 1990 and 1992, in interesting findings and recommendations. The IPCC was set up jointly by the World Meteorological Organization and the United Nations Environment Programme in 1988. Several hundreds of scientists have participated in the preparation and review of this assessment. The IPCC has established three working groups:

I. Science Group
  to assess the scientific and technical information related to climate change issues. The Working Group I has inquired how human activities can change the

Earth's climate through the greenhouse effect. The First Assessment Report was released in 1990 [Houghton *et al.*]. The IPCC Supplement [Perdomo *et al.*, 1992] did not update the estimates of sea level rise of the 1990 Assessment Report. This IPCC-update report was prepared for the UN Conference on Environment and Development in Rio de Janeiro, June 1992. A comprehensive Second Assessment Report is in preparation, which will probably be released by the begin of 1996.

II. Impacts Group
to describe for the next decades the environmental and socio-economic implications of possible climate changes, caused by increasing concentrations of greenhouse gases [Izrael *et al.*, 1990]. Conclusions were drawn concerning agriculture and forestry, natural terrestrial ecosystems, hydrology and water resources, human settlements, oceans and coastal zones, seasonal snow cover, ice and permafrost.

III. Response Strategies Group
to formulate appropriate strategies: (a) *"limiting climate change by reducing emissions and increasing sinks and reservoirs"*, and (b) *"adapting to climate change"*. The Coastal Zone Management Subgroup (CZMS) is one of the subgroups dealing with adaptive responses, viz. retreat, accommodation and protection [Gilbert *et al.*, 1990; Perdomo *et al.*, 1992]. The 1992 Report of the CZMS has presented the results of the workshop **The Rising Challenge of the Sea**, organized on Margarita Island in Venezuela, March 1992. This report describes several case studies on the vulnerability to an accelerated sea level rise. In addition, a extensive vulnerability analysis for the Netherlands is presented in August 1992 [Bijlsma *et al.*, 1992].

The physical impacts of sea level rise are described in this chapter. The descriptions are mainly of a qualitative character, as the knowledge of the many processes involved and their interrelation is still limited. For that reason, it is rather difficult to assess the impact of sea level rise in a quantitative way.

In section 2.2, the impact of sea level rise on the coastal zone and the hinterland is described, whereas in section 2.3, the impact on estuaries and rivers is discussed. The boundary conditions for the coastal groundwater flow regimes are set in these two sections. In section 2.4, the impact of sea level rise on coastal groundwater flow regimes is discussed. In section 2.5, the impact on water management problems is briefly dealt with.

Substantial portions of the sections 2.2 to 2.5 have been derived from chapter V of the report prepared for the UNESCO Workshop SEACHANGE'93 in Noordwijkerhout, the Netherlands, in April 1993 on behalf of the IHP-IV Project H-2-2 [Oude Essink, Boekelman and Bosters, 1993].

2.2   Impact on the coastal zone and the hinterland

The coastal zone and the hinterland include deltaic regions throughout the world that have been involved in the active processes induced by sea level rise. Thus wetlands, regularly inundated because of tides, but also dunes, affected only by severe storms, are included. Sea level rise is first sensed in the coastal zone by higher water levels, followed by morphological changes.

Coastal lowlands are very young phenomena in geological terms. The present situation of coastal lowlands is considerably affected by the rise of sea level of about 100 m, associated mainly with the melting of land ice caps from the last glacial period. The rise in sea level started about 18,000 years ago and has flooded large parts of the continental shelf. The shorelines moving in inland direction were interacting with a landscape resulting from continental processes. Thus, the configuration and other characteristics of the coastal zone and the shoreline are partly the result of stream erosion and sedimentation, marine erosion and sedimentation, and tectonic movement.

The impacts of sea level rise on the shoreline of sandy coasts, hard (fixed) coasts and coastal wetlands are discussed respectively in the following subsections: 2.2.1, 2.2.2 and 2.2.3. Four cases are discussed in subsection 2.2.4.

2.2.1   Sandy coasts

Introduction

Sandy shorelines occur all over the world. They often form, by means of sand-dunes, the primary protection against the sea for densely populated coastal areas. Many holiday resorts are found along these coasts. Obviously, there is quite some interest as to how these shorelines will respond to an accelerated sea level rise, because the consequences may be substantial with respect to safety but also from an economic point of view. Despite this interest, relatively little is known about this subject. Though various empirical formulae have been derived for the response of a sandy coast to a rise in sea level, most of the literature gives only qualitative descriptions [e.g. van der Does, 1990]. One of the reasons is that the precise influence of many processes involved is scarcely known, such as that of sediment transport, waves and tides. Generally speaking, any sea level variation will affect the position of the shoreline.

In this study, sandy coasts are subdivided into four categories: beaches, barriers, tidal inlets and sand-dunes.

Beaches

The impact of sea level variation on beaches depends for a great deal on processes which take place along the beach. For beaches a so-called *equilibrium profile* is defined. This is the beach profile which is created if the climatic and hydraulic conditions would remain constant for a long time. A well-known relationship for this equilibrium

profile is an expression, developed by Bruun in 1954 for beach profiles at the southeast coast of Florida and confirmed by Dean in 1977 for beach profiles at the Atlantic and Gulf coasts of the Unites States [Dean *et al.*, 1987]:

$$h = \xi \, x^{2/3} \tag{2.1}$$

where

- h = water depth (L),

- ξ = shape factor for a certain profile depending on stability characteristics of the bed material, $\approx 0.117 \, m^{1/3}$ for steep profiles at the southeast coast of Florida [Bruun, 1973],

- x = horizontal distance from the shoreline (at $M.S.L.$) in seaward direction (L).

In reality, however, climatic and hydraulic conditions are time-dependent. Thus the beach profile is always adapting to the present conditions, which cause sediment to move up and down the profile. The two most important processes for the sand transport perpendicular to the shoreline are:

1. Storms

    The natural beach profile is generally concave upward. The wave energy is dissipated in an area where the water depth is less than a certain depth. When during severe storms the water level rises, the concave shape of the profile causes the wave energy to be dissipated in a relatively smaller body of water. This will lead to greater turbulence, resulting in erosion of the higher part of the beach, thus creating a gentler overall profile.

2. Wind

    Between the storm periods, the wind will blow the sand back from the foreshore, where it was deposited during heavy storms, higher up the beach.

Other causes of sand transport, that influence the development of the shoreline, are the occurrence of:

- Tidal currents, causing longshore sand transport[1] at greater depths, further away from the coastline. Longshore sand transport is capable to move great quantities of sand. Changes in longshore sand transport indirectly affect the shoreline: a deficit of sand may cause a beach to erode, a surplus of sand may cause a beach to accrete,

- Waves, which approach a beach obliquely, causing longshore transport closer to the shoreline,

---

[1]It must be admitted that the processes of longshore sand transport are complex and difficult to describe, which is the reason why their impacts are difficult to assess.

- Large influx of sediment, originating from a great river debouching into the sea.

The way a sea level variation will affect the position of the shoreline depends to a large extent on local circumstances:

- In certain places, like sheltered bays with a very subdued wave climate, the most important direct impact of sea level rise is inundation, as the profile requires a long time to adapt. The shoreline retreat will depend on the slope of the coastal profile: the gentler the slope, the greater the shoreline retreat (see figure 2.2). The beach profile will respond to sea level rise by adjusting itself to the new conditions. Obviously, there is a time lag: at first the sea level will rise and the profile will turn into a non-equilibrium state. Subsequently, heavy storms will step by step lead to a new state of dynamic equilibrium by moving sediment. In general, it can be assumed that the configuration of the beach profile will not basically change, only its position will do so.
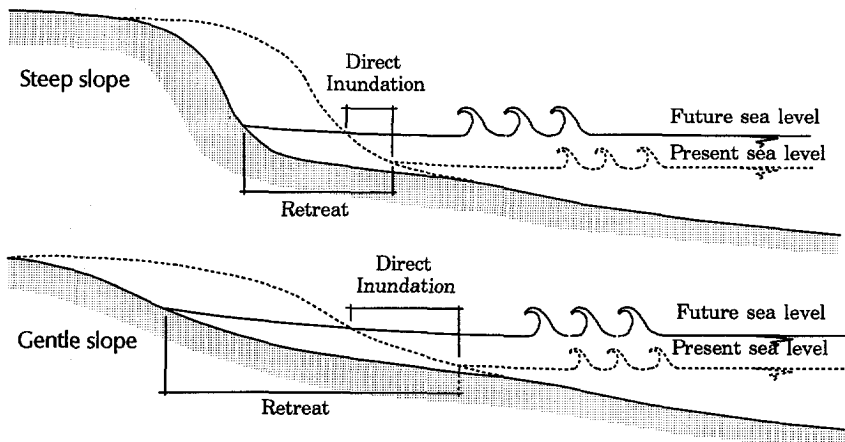
Figure 2.2: Shifting of the equilibrium profile.

- In some cases, where great influxes of sediment occur, e.g. in the vicinity of a large river mouth, the shoreline may be able to maintain its position by simply building-up the profile. In general, however, there is no such influx and the shoreline will thus be eroded considerably. Then the land loss due to the retreat of the profile will be several times greater than the land loss due to direct inundation (see figure 2.2).

There are various methods to determine the shoreline retreat due to sea level rise [Dean et al., 1987]. Four methods are mentioned here:

1. extrapolation of historical trends [e.g. Leatherman, 1984]. A method often applied is to estimate future shoreline changes by means of the analysis of historical

records. For example, from those records it is concluded that currently about 60 % of the world's sandy shorelines is retreating, 30 % seems to be stable and only about 10 % is advancing [Dean *et al.*, 1987]. Advancing sandy shorelines are mainly due to tectonic uplift or a great sediment influx from a nearby river mouth.

2. a sediment budget method by Everts [1985].

3. the dynamic equilibrium model by Kriebel and Dean [1985], which describes dynamic cross-shore transport including the time-varying water level and wave height.

4. the use of the so-called **Bruun's Rule**, formulated by P. Bruun [1962], though the Russian scientist V. Zenkovich [1959] drew up an equivalent formula. Bruun's Rule formulates the relationship between sea level rise and the rate of shoreline erosion. It is a much cited and applied method to predict shoreline response. Several laboratory and field studies have been carried out to evaluate Bruun's Rule, usually with confirmation. Especially for several case studies in the United States, the predictions of Bruun's Rule agree with actual figures in horizontal shoreline retreat of approximately 50-100 times the sea level rise [U.S. Department of Energy, 1989].
   In many publications, Bruun's Rule is often presented without reservation. However, it is in fact only valid for a narrow range of parameters: e.g. steep bottom surface, sufficient sediment supply, wave direction dominantly transverse to the coast and absence of emerged and submerged coastal barrier features [Selivanov, 1993]. There are various remarks to be made on the original Bruun's Rule:

   - it is a (steady state) two-dimensional approach which only considers cross-shore conditions, whereas it does not consider, among others, longshore sand transport and deposition of suspended transport,
   - the time lag between sea level rise and the adjustment of the equilibrium profile is neglected,
   - the relationship is upset when sediments move beyond the water depth (the so-called *closure depth*) where waves have no influence,
   - biogenic production of sediment is neglected.

   Therefore, according to the principle that the equilibrium beach profile will only move upwards and backwards, the shoreline retreat as expressed in Bruun's Rule has been modified by various authors. Equation 2.2 gives such a modification of Bruun's Rule by Hands in 1981 (see also figure 2.3):

$$R = G_a \frac{\text{SLR } W}{H} \qquad (2.2)$$

   where

- R = shoreline retreat (L),

- G_a = overfill ratio, to account for loss of suspended load from the eroded material $(-)$. In Bruun's Rule, G_a equals 1,

- SLR = sea level rise (L),

- W = width of profile taking part in the process, i.e. from the point in the profile that remains unchanged till the point where the water depth is such (5-10 m) that waves have no influence (L),

- H = height of responding profile or vertical relief of active beach, total depth of profile (L).
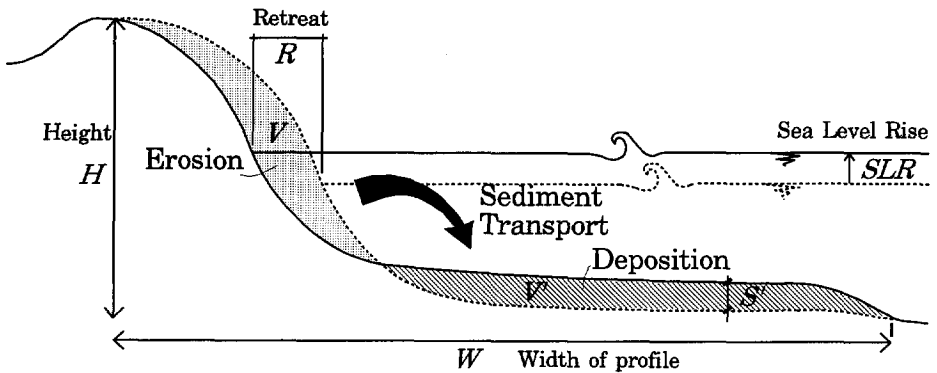
$V \stackrel{.}{=} V'$ = resp. eroded and deposited quantity of material (L^3)
S' = average rise in bottom level (L)

Figure 2.3: Bruun's Rule

Studies on the coast of the Caspian Sea [Kaplin, 1990] and on other former U.S.S.R. coasts [Selivanov, 1993] show that the original Bruun scheme for submerging coasts is not universal. For instance, the Caspian Sea provides very interesting data for studies of coastal deformations related to sea level variations. From 1929 on, the Caspian Sea coast was exposed to a relatively quick fall of the lake level, to a minimum of -29.2 m $M.S.L.$. By contrast, from 1978 to present the level rose with 12 cm per $year$. The development of the coastal zone during sea level rise appeared to depend mainly on the inclination of the submarine coastal profile [Kaplin, 1990], as depicted in figure 2.4. At the most gentle coast (gradient ≈ 0.0005), land flooding has occurred without coastal zone reformation, as waves lose their energy on the gentle slopes. Where the gradient ≈ 0.001, sea level rise has resulted in the formation of a coastal ridge in the breaking zone at some distance from the coast, forming a lagoon (that is a shallow body of saline or brackish water partially connected with the sea).
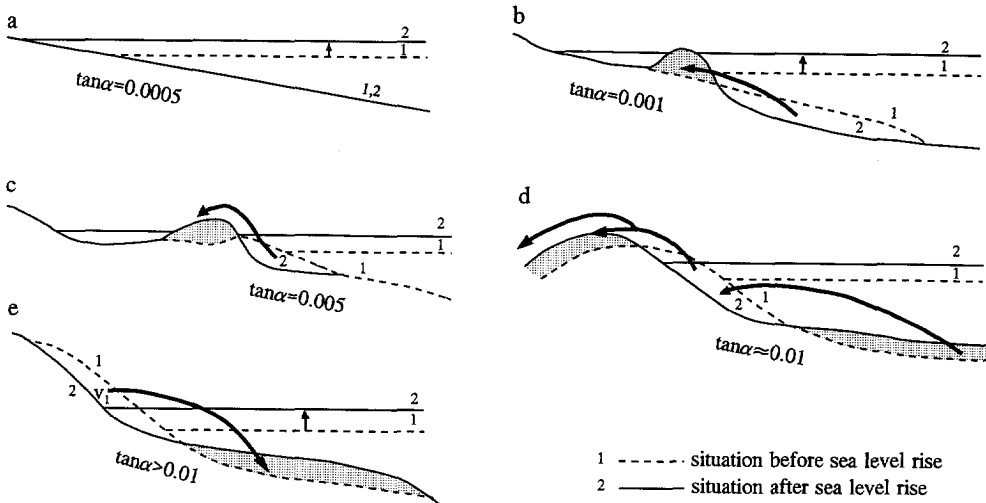
Figure 2.4: Development of the coastal zone at the Caspian Sea due to sea level rise, for different submarine slopes [after Kaplin, 1990]. Source: *Greenhouse Effect, Sea Level and Drought. Paepe, R., Fairbridge, R.W. & Jelgersma, S. (eds), p. 388.* Copyright © 1990 Kluwer Academic Publishers, reprinted by permission of Kluwer Academic Publishers.

Steeper slopes (≈ 0.005) have caused waves to break near the shoreline and a beach ridge could become a barrier with behind it a shallow lagoon. For slopes ≈ 0.01, no lagoon has been created, in case the area behind the barrier is more elevated and the beach ridge is rising and migrating. Development of the coastal zone according to Bruun's Rule has only occurred for gradients > 0.01. According to Selivanov [1993], landward migration and destruction of accumulative barriers may become the most disastrous consequences of the anticipated sea level rise on the other coasts of the former U.S.S.R.

In contrast with Bruun's Rule, it is also suggested that slow rates of sea level rise can form accumulative coastal barriers. Assuming the wave climate remains the same, Dean *et al.* [1987] suggested, after analysing responses from the past, that a sea level rise would cause a landward rather than a seaward sediment transport, as required by Bruun's Rule (compare figure 2.3 with figure 2.5). During the rapid rise of the sea level (rate $\approx 0.8 \ m/c$) up to 6000 year BP, the shoreward sediment transport was not sufficient to maintain a stable shoreline. By contrast, during the slow rise of the sea level (rate $\approx 0.08 \ m/c$) from 6000 year BP, the same rates of shoreward sediment transport have generally led to reduced erosion rates and in some cases to stable or even accreting shorelines [U.S. Department of Energy, 1989].
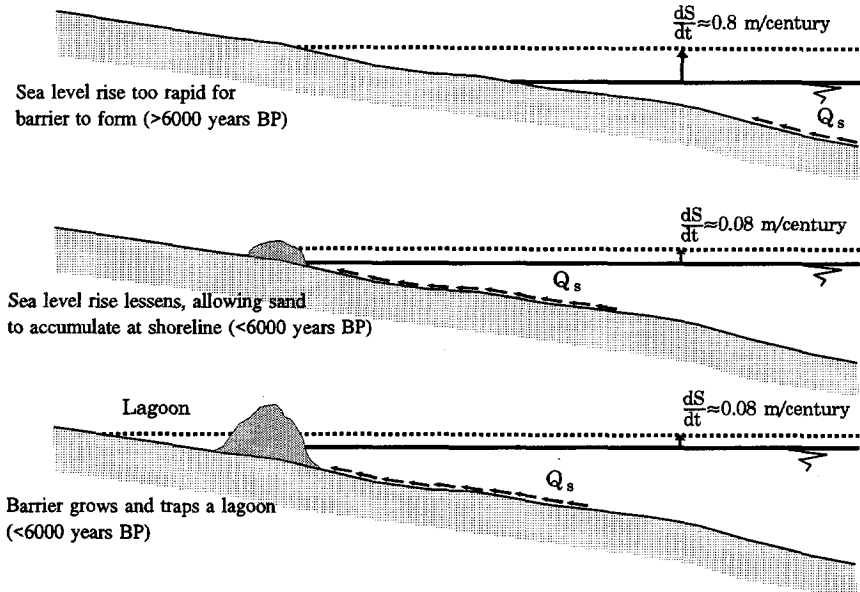
Figure 2.5: Shoreward sediment transport Q_s and rate of sea level rise dS/dt related to barrier island formation [after Dean, 1987].

Barriers

Along many shorelines barriers or barrier islands are found. A barrier is an oblong piece of land close and parallel to the shore, at one end also in connection with the mainland. When the sea breaks through the barrier at one or more places and creates one or more inlets, the connection with the mainland is gone and so-called barrier islands are created. Barriers are developed under various circumstances:

- longshore currents are transporting sediments, supplied by a large river, along the coast where sedimentation is taking place. Wind and wave activities are building up the barrier,

- longshore sand transport, caused by tidal currents, is developing a spit where a straight coast is abruptly cut off. If the spit becomes very long, it is also called a barrier,

- sea level rise is displacing sediments towards the shore to form barriers, in case of very gently sloping coastal profiles (see figure 2.5).

Barriers and barrier islands show up in wave dominated coastal areas with low-gradient underwater profiles and, of course, sufficient sediment supply. Behind barriers lagoons are found. Lagoons may become completely isolated from the sea, in

which case they transform into coastal ponds or lakes or eventually swamps. Sometimes they contain fresh water if there is a sufficient supply of e.g. river water.

When sea level rises, the response of the barrier will depend on the sediment supply:

a. if there is enough sediment supply, the barrier will not be affected by sea level rise and will simply continue to grow in seaward direction due to sedimentation, while building itself upward,

b. if sediment supply is rather limited, the barrier will be built upward and also landward. During storm surges, when higher water levels occur, a certain number of waves will be able to overtop the barrier. These waves will wash away sand from the seaside of the barrier, which will settle at the land side. So the barrier is able to maintain itself by moving landward: *barrier rollover* (figure 2.6). When sea level rises, surge levels will become higher and thus more sand will be transported from the seaside to the land side of the barrier. However, if sea level rise is even greater, the barrier eventually will become part of the new shore,

c. if sand supply is that small that the barrier will not be able to react on sea level rise at all, the barrier will simply be drowned at the place: *barrier drowning* or *barrier overstepping* (figure 2.6).

Thus, the determining factor for these alternatives is again the amount of sediment supply. The more the sea level rises, the more sand will be needed to maintain a certain stable profile. From the moment sand demand exceeds sand supply, the barrier will not be able to maintain its position, and, depending on the sediment deficit, it will be submerged.

Tidal inlets

In general, a tidal inlet is considered as the connection between the sea and certain sheltered waters. For instance, tidal inlets are channels through which water flows in and out of estuaries because of tides, but they are also channels through a barrier transporting water to and from the bay behind it.

During every high tide, tidal inlets allow a certain volume of water to enter the bay, which accordingly is flowing out into the sea again during low tide. This volume of water is the *tidal prism* of the bay. These flood and ebb flows are transporting sediment through the inlet. As soon as this sediment-loaded flow gets beyond the inlet, flow velocities are decreasing which results in sedimentation on both sides of the inlet. This process often induces the development of a delta on both sides of the inlet: an ebb delta on the seaward side coming about due to the ebb flows and a flood delta on the landward side resulting from the flood flows. Their size can normally be expressed by a more or less linear relationship with the tidal prism [Dean *et al.*, 1987]. The required amount of sediment is generally provided by longshore sand

Barrier rollover

Land   Sea

Barrier

Salt marsh peat

high tide

low tide

Lagoon mud

Nearshore marine sediments

Land   Salt marsh peat   Barrier   Sea Level Rise   Sea

High tide

Low tide

Lagoon mud   high tide

low tide

Barrier drowning

Land   Sea

sea level 2

sea level 1

Transgressive backbarrier   Barrier
          sediments

Land   Sea

sea level 3

sea level 2

New barrier   sea level 1

Transgressive backbarrier   Drowned barrier
          sediments

Figure 2.6: Barrier movement [modified from Rampino and Sanders, 1980]. Source: *Rampino, M.R. & Sanders, J.E. Holocene transgression in south-central Long Island, New York. J. of Sedimentary Petrology, 50: 1063-1080, p. 1075.* Copyright ©1980 The Society of Economic Paleontologists and Mineralogists, reprinted by permission of The Society of Economic Paleontologists and Mineralogists, Tusla, Oklahoma.

transport. Especially when the inlet is fixed, for example for navigational purposes, this may lead to serious erosion of the downdrift beaches, because the longshore sand transport carries away the sand downdrift of the inlet to account for the sand loss because of the aforementioned delta formation.

When sea level rises and the shores of the bay behind the tidal inlet are quite steep, the increase of the tidal prism of the bay will be relatively small, roughly equal to the surface of the bay multiplied by the sea level rise. As a result, the flood and ebb deltas are probably growing accordingly. However, the increase of the tidal prism of the bay is often negligible compared to the increase of the cross-sectional area of the tidal inlet. Consequently, flow velocities through the tidal inlet will go down and the sediment transport capacity will decrease. Thus, sedimentation will occur

in the estuary as well as in the tidal inlet until a new state of dynamic equilibrium
has been established. The level of the ebb and flood deltas are being heightened,
apart from being extended. These sedimentation processes will cause a decrease in
the sediment load of the longshore sand transport, resulting in erosion of downdrift
beaches. Again, this erosion will be even more serious if the tidal inlet is fixed by
human structures.

When sea level rises and the slopes along the shores of the bay are gentle, some-
thing else is likely to happen, especially when large wetlands are present. Then, the
increase of the tidal prism due to sea level rise will be relatively greater than the
increase of the cross-sectional area of the tidal inlet. As a result, erosion will occur
throughout the whole estuary or bay which may lead to the destruction of wetlands.

Sand-dunes

Sand-dunes are well-known features along sandy coastlines. Protection of the hin-
terland often depends on these sand-dunes. The most important factor concerning
safety of the hinterland is the width of the dune zone. Research done in the field
of dynamics of sand-dunes is rather limited. There seems to be no general rule for
dune development associated with sea level variations. Many processes, not or hardly
known, influence sand transport and dune formation, thus the overall impact is very
hard to assess. It appears that sand-dunes, which have experienced sea level rise,
keep the same profile though a certain retreat has to be encountered: they shift in
landward direction.

2.2.2   Hard coasts

Hard coasts of natural origin

The two main types of hard coasts of natural origin are: (1) rocky coasts and (2)
coral islands.

ad 1. Rocky coasts
   Rocky coasts and cliffs occur all over the world [Snead, 1972]. They are normally
   very stable. They do erode but only at a very slow rate. The time scale of these
   erosional processes goes far beyond the time scale of a significant sea level rise.
   Therefore, sea level rise is supposed to have no noticeable impact on rocky
   shorelines for the next century. Only in case of gently sloping rocky shorelines
   direct inundation, and thus shoreline retreat, may take place.

ad 2. Coral islands
   In general, coral islands are hardly elevated above $M.S.L.$, at most about three
   metres. Thus, when the sea level rises, say one metre, a relatively large part
   of these islands may be inundated. Obviously, a sea level rise would have great
   impact on the people living on these islands. Their society might even be
   endangered [Gilbert et al., 1990; Perdomo et al., 1992].

Apart from coral islands there are coral reefs[2]. They often serve as natural breakwaters and protect islands and coasts against tropical storms. Sea level rise may reduce this function considerably. Under natural circumstances, however, the growth of coral reefs can keep pace with sea level rise, as growth rates of several centimetres per year have been observed. Naturally, the growth process of corals is a sensitive one. Any human activity causing pollution upsets the growth process and may bring it to a halt entirely. Thus, the impact on these islands does not only depend on the rate of sea level rise and the local rate of coral growth, but also on human behaviour.

Manmade protectional structures

The overtopping frequency of protectional structures such as dams, dikes and sea-walls, can be calculated, given certain parameters such as mean sea level, storm level occurrence and wave run-up.

When sea level rises, water depths increase and higher waves are developed. Accordingly, the wave run-up increases, see figure 2.7. The reference level, on top of which storm surges build up their extra high levels, is elevated, and thus an increase in overtopping frequency can be expected. For example, in the Netherlands a sea level rise of one metre is estimated to increase the risk of flooding rather dramatically, from 1:10,000 to about 1:500 [den Elzen and Rotmans, 1988]. Furthermore, the wave attack on foot and front of the dike is intensified, which may lead to erosion and hence may endanger the structure's stability. In addition, climate change, which is expected to cause an accelerated sea level rise, is also likely to cause an increased storm activity in certain parts of the world. These factors all point in the same direction: an increase of overtopping frequency and eventually a collapse of protectional structures.
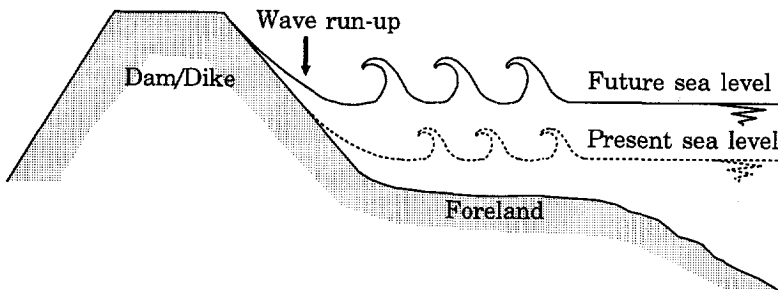
Figure 2.7: Increased wave run-up.

---

[2]The optimum growth of coral reefs is between 25 $^\circ C$ and 29 $^\circ C$, and hence, they flourish under tropical conditions.

2.2.3   Coastal wetlands

Introduction

Coastal wetlands are areas which occupy area between land and sea. They are in-
undated regularly, not because of extreme situations, but simply because of the tide.
In table 2.1, the areas of coastal wetlands of international importance are given in
km^2 and as a percentage of the area of the region [Gilbert *et al.*, 1990]. Coastal
wetlands are of great importance from an ecological point of view [e.g. Brouns, 1988;
Wolff *et al.*, 1993[3]]: they serve as nursery grounds for fish, provide food for birds and
are a habitat for many other animals. Apart from that, they also provide protection
against storms and flooding.

Table 2.1: Wetlands areas. From: A global survey of coastal wetlands, their function and
threats in relation to adaptive responses to sea level rise. IPCC-CZM Workshop, Australia
1990.

Region	wetlands (km^2)	% of the region
North America	32,330	1.64
Central America	25,319	0.88
Caribbean Islands	24,452	9.43
South America (Atlantic coast)	158,260	1.13
South America (Pacific coast)	12,413	0.53
Small islands (Atlantic)	400	3.29
North and West Europe	31,515	0.71
Baltic Sea Coast	2,123	0.18
Northern Mediterranean	6,497	0.61
Southern Mediterranean	3,941	0.10
Africa Atlantic Ocean Coast	44,369	0.56
Africa Indian Ocean Coast	11,755	0.16
Gulf States	1,657	0.08
Asia Indian Ocean Coast	59,530	1.20
Southeast Asia	122,595	3.42
East Asia	102,074	1.00
Pacific Ocean Large Islands	89,500	19.39
former USSR	4,191	0.02
Total	732,921	0.85

Coastal wetlands have the ability to adapt to sea level rise by building themselves
upwards. It is because of this so-called accretion that in the past few thousand years
the coastal wetlands have generally managed to keep pace with sea level rise and

---

[3] Wolff *et al.* have investigated the expected ecological effects of sea level rise from different points
of view.

have even extended. The accretion is partly from mineral origin (sediments), partly from biological origin (organic production or peat). Peat production in the coastal wetlands is very important, since generally more than half the wetland accretion is due to peat production. Sediments serve not only as building material but also deliver the necessary nutrients for the wetland vegetation. The sediment supply for coastal wetlands has two main sources:

a. **sediment from a river:** during floods, the river delta is inundated and flow velocities in the inundated areas are small. Accordingly, sedimentation is taking place,

b. **resuspended sediment:** sediments, which were deposited near the coast in fairly shallow waters, can be resuspended during severe storms. The seawater, enriched with resuspended sediments, inundates the coastal wetlands where the sediments have the opportunity to settle down.

Coastal wetlands can roughly be subdivided in three categories, depending on their salinity levels [Dean *et al.*, 1987]:

1. **Salt marshes and mangrove forests**
   Salt marshes and mangrove forests occur in a saline environment, the former at higher latitudes, the latter in tropical regions. Mangrove forests are important as they act as an effective protection against floods,

2. **Brackish marshes**
   In brackish marshes salinity levels are less than 30 *p.p.t.*[4]. They can be found in estuaries at places with calm water and abundant sediment supply,

3. **Tidal freshwater marshes**
   Tidal freshwater marshes occur in the more elevated parts of estuaries. Consequently, they are less frequently inundated and have low salinity levels, namely less than 5 *p.p.t.* Access canals for navigation may accelerate the salinisation of freshwater marshes [Day, 1987].

Impact of sea level rise on coastal wetlands

When sea level rises, the impact may be as follows:

- the coastal wetland accretion is that much that it can keep pace with sea level rise. Under these circumstances, the marsh area will extend, because accretion becomes possible in areas which were originally situated above the high tide level, see figure 2.8a. Salt marshes are found at the landward side of barriers. In that position they are mainly indirectly threatened by sea level rise, in the sense that they may be buried under a barrier which is moving in landward direction. Brackish marshes are supposed to keep pace with a rising sea level due to the abundant sediment supply and their own organic production.

---

[4]*p.p.t.* stands for *parts per thousand*. The salinity level or total dissolved solids (*TDS*) is expressed in *p.p.t.* which approximates *g/l*.
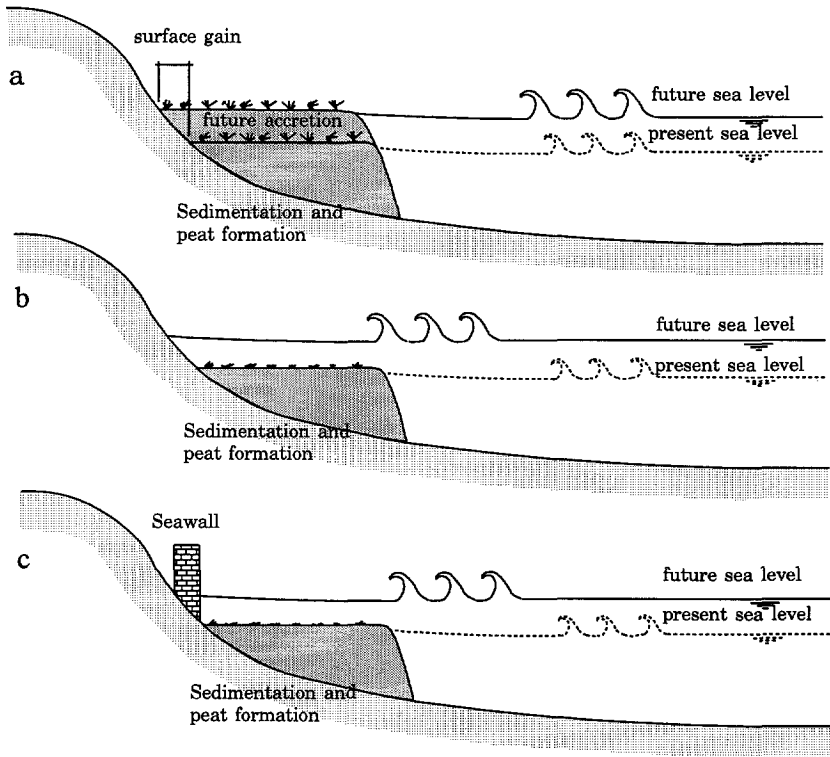
Figure 2.8: Effects of sea level rise on coastal wetlands: (a) accretion can keep pace with sea level rise; (b) accretion cannot keep pace with (rapid) sea level rise; and (c) human interference impedes wetland movements.

- coastal wetland accretion cannot keep pace with sea level rise, but the difference between the rate of accretion and sea level rise is small. The coastal wetlands will have to face losses, though they are able to adapt to the new condition to at least some extent.

  Normally, freshwater marshes can be found at the highest elevations of a wetland area and salt marshes at the lowest elevations. Brackish marshes may appear in between, which depends on local morphological history. When sea level rises, a redistribution will take place. In general, freshwater marshes will then develop in the new area which is under tidal influence. Meanwhile, original freshwater marshes will slowly change into brackish or salt marshes due to salt water intrusion, which results in original plant species being replaced by more salt resistant ones. The brackish marshes will become salt marshes, whereas the original salt marshes will eventually be submerged.

- sea level rise is so rapid that a coastal wetland area cannot respond accordingly. Consequently, the whole coastal wetland area will be submerged and get lost (see figure 2.8b). Some new marshes may develop as new area comes under tidal influence. Even if this gain is included, the overall losses are extensive.

Human interference

Human interference can influence the coastal wetlands significantly. As mentioned before and shown in figure 2.8a, new coastal wetlands may develop in areas which only come under tidal influence after a sea level rise, e.g. higher on the shore and/or further inland. However, this does not happen if marshes are impeded from moving upward by e.g. structures such as dams and seawalls (see figure 2.8c). On a worldwide scale the losses due to impediment of upward migration will not be that great, though locally they may be significant. For instance, in the Netherlands, most of the areas just above the intertidal zones are occupied by human activities (e.g. grazing cattle), which might probably lead to a decrease in the species diversity of flora and fauna.

Many rivers throughout the world, and especially their deltas, have been subject to human interference to avoid flooding, such as the construction of dams and embankments. Accordingly, flooding of those deltaic areas is less frequent or does not occur any more. Furthermore, the original inflow of sediments, freshwater and nutrients is reduced significantly or is stopped completely. The coastal wetlands then mainly depend on their organic production, which, as research has proven [Dean et al., 1987], is normally too little for their survival because of a deficit of nutrients.

In addition, canals have been built through deltas to facilitate navigation by improving the access to the main river. In general, these canals have spoil banks, constructed of the material which is dredged from the canal. Normally, even during storm surges, these spoil banks are not overtopped, which means that the areas next to such a canal are not flooded any more by the sea. Thus, also the sediment supply from the sea (that is the resuspended sediment) is blocked, which implies another reduction of the accretion rate. At the same time these canals, because of their much greater capacity, do allow saline water to penetrate much further inland, which may lead to losses or conversion of freshwater marshes into brackish or salt marshes.

Moreover, it is also possible that estuaries will be cut off from their connection with the sea by man-made dams, subsequently forming brackish to fresh estuarine reservoirs or basins. Actual examples during the past centuries can, among others, be found in France, India, Japan, and the Netherlands. Sluices discharge the excess of river water and precipitation, and shiplocks enable navigation. The former coastal wetlands in the enclosed reservoir will be affected in the accretion of peat and subsequently in their ecology.

2.2.4   Cases

Introduction

Assessing the impact of sea level rise on a particular location is rather complex, as numerous factors should be considered, such as the future rate of coastal wetland accretion, the elevation of the water level, the increase of wave-activity due to deeper tidal canals, a possible increase in frequency of storm surges and floods, and the landward displacement or disappearance of barriers. In addition, the effect of future human interference should also be considered, such as the construction of coastal defence works and sand management practices.

Obviously, areas with high tidal ranges will be the least vulnerable to sea level rise: then a sea level rise will make relatively little difference. On the other hand, areas with small tidal ranges are rather vulnerable to sea level rise. For instance, the Mediterranean Basin is vulnerable to sea level rise, since the amplitude of the spring tide is very small in the Mediterranean Basin: usually less than 0.2 to 0.3 m, increasing little near the Strait of Gibraltar (0.9 m) and at the Gulf of Gabes, southeast coast of Tunisia (1.7 m) [Pirazzoli, 1987].

Not only many qualitative studies about the impact of sea level rise have been performed, e.g. for the Mediterranean Basin [Sestini, 1990; Oueslati, 1990; Jeftic *et al.*, 1992], also a number of site-specific quantitative studies have been carried out, such as in Barth and Titus [1984] and Schröder [1988]. Furthermore, coastal defense strategies of several case studies have already been discussed in the Coastal Zone Management Strategies of the Intergovernmental Panel of Climate Change [Gilbert *et al.*, 1990; Perdomo *et al.*, 1992].

In this subsection, four cases are discussed: (I) the Mississippi delta, (II) the Galveston bay, Texas and the Charleston area, South Carolina, (III) the Dutch shoreline and (IV) the Nile delta.

I. Mississippi delta, USA

The Mississippi delta can serve as an excellent example of the impact to be expected from an accelerated sea level rise [Day, 1987; Day *et al.*, 1993]. The compaction of riverine sediments along with mining activities (oil and gas) and groundwater recovery induce a rapid land subsidence. This causes a relative sea level rise of about 10 mm/yr, which fits well with the rate of sea level rise of one metre per century, often assumed by scientists during the 1980's.

In spite of the fact that the Mississippi delta is rapidly subsiding for at least thousands of years, a large deltaic plain (50,000 km^2) of lakes, bays, near sea level coastal wetlands and low-lying uplands has been formed. The greater part of the 20,000 km^2 coastal wetlands is situated within one metre above $M.S.L.$ The historical growth rate over the past 5000 years was somewhat greater than 4 km^2/yr. However, during the past decades the process has reversed into an accelerated land loss of about

100 km^2/yr. As a result, the Louisiana coast is retreating at an average rate of 4.2 m/yr [U.S. Department of Energy, 1989].

The causes of the land deterioration of especially coastal wetlands appear to be mainly man-induced:

- embanking the Mississippi river by dikes (which extend almost to its mouth) in order to protect the delta against flooding from both river and sea. As a consequence, the influx of riverine sediments on the coastal wetlands is reduced significantly.

- dredging canals for navigation, discharge and mostly as an access for oil and gas exploration and production. As the spoil banks from deposition of excavated material are not overtopped frequently, the influx of resuspended sediments on the coastal wetlands is reduced.

Studies have shown that embankments and canals have the following effects:

- change in the (geo)hydrologic and hydraulic systems,

- increase of salt water intrusion into originally freshwater areas. Salt water intrusion increases the salinity level of freshwater and brackish marshes and probably also converts cypress swamps, which are very sensitive to saline water, into (open water) lakes. Sea level rise might speed up this process [Titus, 1987]. A number of studies has shown a correlation between the salinity of the surface water in canals and the loss of wetlands,

- reduction of the coastal wetland vegetation, thus decreasing the vertical accretion significantly,

- deterioration of the natural channels.

The results from the Mississippi delta plain indicate that a complex system determines the present land loss. One interesting observation in the Mississippi delta plain is that there seems to be a considerable time lag (of several decades) between relative sea level rise and its impacts such as the rate of land loss.

II. Galveston bay, Texas and Charleston, South Carolina, USA

The impact of higher average water levels on flooding has been investigated for the area around Galveston bay, Texas, by Leatherman [1984] and for the area of Charleston, South Carolina, by Kana *et al.* [1984]. For both cases, the shoreline response is determined by extrapolating the historical trend of local sea level variations.

For Galveston bay, Texas, a relative sea level rise is occurring due to eustatic and isostatic effects such as land subsidence. Local sea level variations has been analysed from 1850 to 1960, derived from tidal gauge records on 40 shoreline positions. The plain is intersected by estuaries and lagoons along the Galveston bay. The impact of

sea level rise on the gently sloping floodplains of the Galveston bay, which are mostly situated less than 5 m above $M.S.L.$, would be significant. For instance, in 1980 the area covered by the 100-year floodplain was 58.4 % of an area of 275 km^2. For a sea level rise of 92.4 cm by the year 2075 (a so-called low scenario of sea level rise), the 100-year floodplain area would be increased to 94.1 % of that area. Furthermore, Leatherman estimated that by 2075, the 5 metre Galveston seawall, which protects Galveston city, would be overtopped by a 100-year storm for the medium (164.5 cm) and high (236.9 cm) scenarios of sea level rise.

For Charleston, South Carolina, Kana *et al.* conclude that up to one-half of the area could be flooded permanently due to sea level rise if no countermeasures are taken. The impact of sea level rise on shoreline retreat is substantial: for instance, by the year 2075 around 15 %, 31 % and 46 % of the area would get lost due to a sea level rise of 88 cm, 159 cm and 231.6 cm respectively. In case of the medium scenario (159 cm), a 10-year storm would cause by the year 2075 as much flooding as a 100-year storm would inflict today.

III. The Dutch shoreline

Already in 1960, the Delta Commission advised to account for a relative sea level rise of 0.2 m/c over the life span of newly designed coastal water defences [Tweede Kamer, explanatory memory Wet op de waterkering, 1989]. Sea level rise has played an important part in the discussion on long-term coastal defence policies in the Netherlands [Rijkswaterstaat, 1990]. Four policy alternatives have been evaluated: (1) retreat except when erosion threatens the safety of the polders; (2) selective preservation of polders and major interests in the dunes and on the beach; (3) preservation of the entire coastline; and (4) seaward expansion at points of marked erosion through artificial defences, while elsewhere the present coastline would be preserved. In 1990, the Government of the Netherlands chose the option of *Dynamic Preservation*: that is preservation, though some conditional allowance should be made for the natural movement of the coastline.

In the late 1980's, the Tidal Waters Division of Rijkswaterstaat has commissioned several consultants to determine the development of the entire Dutch shoreline, among others, for the period 1990-2090. For this purpose, a dynamic model has been applied to assess the sediment balance of the entire Dutch coast [Delft Hydraulics, 1989]. Three scenarios of sea level rise were considered. The shoreline movement has been estimated for 17 coast segments. For a sea level rise of 0.2 m/c, which is supposed to be the reference case, the shoreline movements could vary from +3.9 m/yr (advance) to -2.2 m/yr (retreat), see table 2.2. Obviously, there are some coast segments which show advancing shorelines due to sediment deposition. However, if the rate of sea level rise increases, the additional shoreline movements will be as follows: from -0.2 to -1.1 m/yr for a sea level rise of 0.6 m/c and from -0.4 to -2.6 m/yr for a sea level rise of 0.85 m/c.

The probability of exceedance of a critical water level, called the safety frequency

Table 2.2: Prediction of the Dutch shoreline displacement in case of three sea level rise scenarios [after Delft Hydraulics, 1989].

Segment	Sea level rise		
	0.2 m/c	0.6 m/c	0.85 m/c^*
	Shoreline movement (m/yr)	Additional movement (m/yr)	Additional movement (m/yr)
Zeeuws Vlaanderen	-1.1	-0.4	-1.1
Walcheren	-1.1	-0.4	-1.1
Schouwen	1.5	-0.3	-0.8
Goeree	-0.7	-0.3	-0.9
Voorne	-0.7	-0.3	-0.9
Hoek van Holland-Scheveningen	-0.1	-0.2	-0.4
Scheveningen-Noordwijk	0.3	-0.2	-0.5
Noordwijk-IJmuiden	0.4	-0.2	-0.5
IJmuiden-Egmond	0.2	-0.2	-0.4
Egmond-Groet	-0.5	-0.2	-0.7
Petten-Gr. Keeten	-0.9	-0.2	-0.9
Gr. Keeten-Den Helder	-1.1	-0.3	-1.0
Texel	-1.6	-0.5	-1.6
Vlieland	-1.9	-0.6	-1.9
Terschelling	-1.9	-0.6	-1.9
Ameland	-2.2	-0.6	-2.0
Schiermonnikoog	3.9	-1.1	-2.6

*: this scenario includes changes in wind, tide and wave climate.

or overtopping frequency, is likely to increase significantly in case of a sea level rise [de Ronde, 1991; den Elzen and Rotmans, 1992]. Computations have indicated that in order to maintain the present safety standard for the central part of the Netherlands, that is 1:10,000 years which equals the *Delta standard*, several billion *guilders* are necessary to adapt dikes. For instance, according to the first computations of the IPCC [Perdomo *et al.*, 1992], the total protection and adaptation costs (without annual maintenance costs) to maintain the present standard in case of a sea level rise of one metre will amount to some 24 billion *guilders* during the next century. This value corresponds with about 0.05 % of the Dutch Gross National Product (1990). According to de Ronde [1991], some 7 billion *guilders* are needed to raise dikes in case of a sea level rise of 60 *cm*. Note that Rijkswaterstaat manages some 2500 *km* primary water defences (700 *km* of dunes and dikes along the coast and tidal rivers and 1800 *km* of water defences along the large rivers).

IV. Nile delta, Egypt

The Nile delta comprises the most important coastal lowland along the Mediterranean Sea, covering an area of approximately 22,000 km^2. The coastal zone of the Nile delta consists of a number of brackish lagoons separated from the sea by barrier islands and coastal dunes with elevations up to +30 m $M.S.L.$ (see figure 2.9). Agricultural land, recently reclaimed, is situated in the deltaic area with an elevation below +2 m $M.S.L.$ Furthermore, three regions seem to be in particular vulnerable to sea
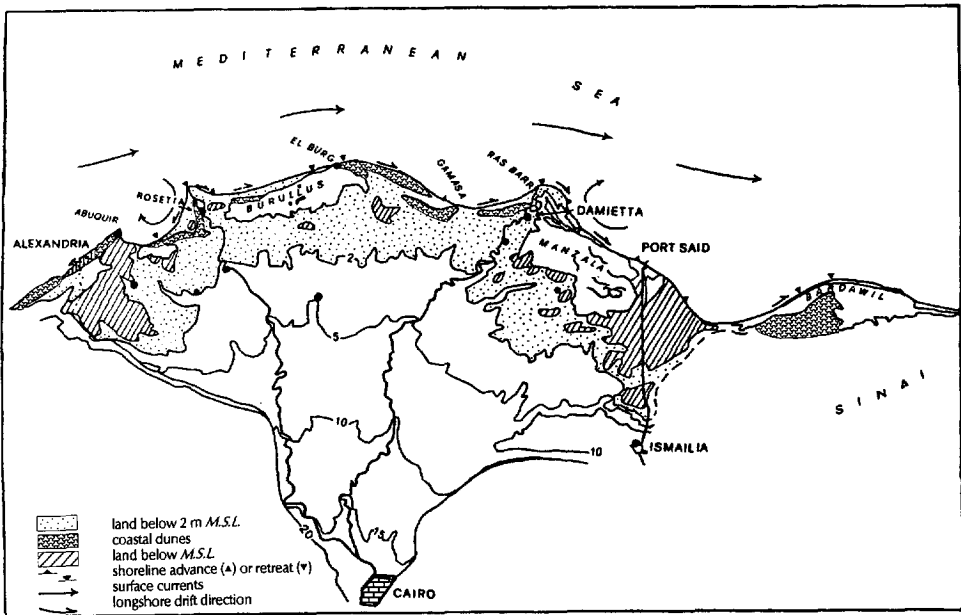
Figure 2.9: The Nile delta [modified from Sestini, 1992]. Source: *Impacts of Sea-level Rise on European Coastal Lowlands. Tooley, M.J. & Jelgersma, S. (eds), p. 183.* Copyright © 1992 The Institute of British Geographers, reprinted by kind permission of Sestini and Blackwell Publishers.

level rise: the Alexandria region with extensive seaport facilities, urban seafronts and beaches; Lake Burullus which is under consideration for a freshwater storage project; and the Lake Manzala region which includes the cities Damietta and Port Said [El-Raey, 1990].

The Nile delta is subject to the following two processes, both induced by natural causes as well as by human activities:

a. High rate of land subsidence

In this area, subsidence has mainly natural causes. For the last 5 million years, not only the Nile delta, but also other great deltas in the Mediterranean Area (e.g. Po, Rhône, Ebro) show a rapid sedimentation rate from a geological point

of view. As a result, the crust is buried under several kilometres of sediment. The basins have subsided some hundreds of metres due to this weight of sediment. For instance, according to Stanley [1988], the northeastern part of the Nile delta has rapidly subsided since about 7500 years ago with rates of up to 5 mm/yr. From historic times, ancient monuments give evidence of subsidence rates of millimetres per year. At present, the Nile delta is still subsiding at high rates, according to several studies ranging between 0.5 and 5.0 mm/yr [El-Fishawi, 1989].

b. Severe shoreline retreat

From drill-cores it has been derived that the shoreline has advanced in northern direction by as much as 50 km during the past 5000 years (an average rate of 10 m/yr). Already for centuries, the Nile delta coast has been unstable. Before 1900, the delta front was propagated seaward, e.g. the advance of the Rosetta promontory was about 30 m/yr [Sestini, 1992]. However, from 1900 on (or after about 1910 according to Sestini, 1992), a severe coastal erosion has occurred. For instance, west of Rosetta the average maximum erosion rate has been 58 m/yr [El-Fishawi, 1989]. Figure 2.10 shows the shoreline changes at Rosetta, Burullus and Damietta during the period 1909-1988. The causes of the shoreline retreat are assumed to be twofold: subsidence and reduced sediment load from the river Nile.

To improve water management in Egypt, series of dams and barrages on the Nile have been constructed since the nineteenth century [Kashef, 1981]. The turn of the century can roughly be considered as the turning point. From then on, both annual sediment load and river discharge of the Nile have been reduced significantly and, subsequently, the coast has eroded. It is, however, somewhat uncertain to attribute the sudden change in annual sediment load and river discharge in the Nile to the effect of the construction of the Low Aswan Dam, which was completed in 1902.

However, at least a substantial contribution of the present coastal erosion has been induced by the High Aswan Dam. The High Aswan Dam, which was completed in the year 1964, is the last and most important one of the dams and barriers on the Nile. This dam has reduced the sediment load downstream to insignificant quantities, which has resulted in erosion of the Nile riverbed, drainage ditches and irrigation canals, and in a decrease of the fertility of agricultural land.

The rapid land subsidence in combination with a predicted acceleration in sea level rise during the next decades will result in a relative sea level rise which could threaten human activities in the area, such as present and planned land-reclamation, irrigation, agricultural and housing projects. Stanley [1988] has predicted that relative sea level rise in the Nile delta could lead to increased flooding and salt water intrusion in the eastern delta.
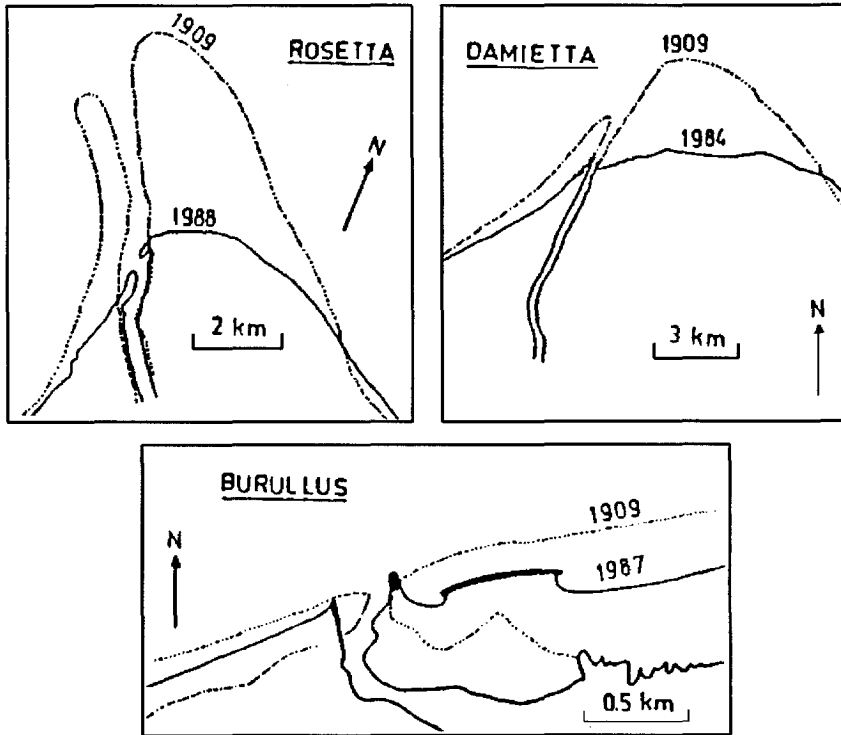
Figure 2.10: Shoreline changes at Rosetta, Burullus and Damietta during the period 1909-1988 [El-Fishawi, 1989].

The accelerated sea level rise in combination with a greater wave attack may reduce the width of beaches (e.g. of Alexandria), decrease the extent of coastal dunes and damage harbour structures. Furthermore, lagoons with a specific water circulation and salinity could alter and especially bird habitats, fisheries and aquaculture could be jeopardized, causing great socio-economic impacts [Sestini, 1992].

2.3   Impact on estuaries and rivers

Nowadays, many estuaries, deltas and rivers already experience salt water intrusion, such as the Mississippi delta, the Nile delta, the Indus river estuary [Naeem *et al.*, 1993], the Mekong delta [Jelgersma *et al.*, 1993] and the Gambia river [Manneh, 1993]. When estuaries are widened and deepened to be able to cope with greater ship capacities at harbours or when river discharges are low during extended droughts, severe problems can be expected, e.g. for drinking water intakes and for ecosystems. Based on analyses of estuary evolutions in the past and the present prognosis of sea

level rise, it can be assumed that sea level rise will augment the present salt water
intrusion problems in estuaries and rivers.

Up to some years ago, most research was focused on the impact of sea level rise
on the coastal zone, such as shoreline retreat and increased flooding. However, also
estuaries and rivers demand the scientific attention. As the phenomenon of salt water
intrusion is rather complex, mainly qualitative descriptions of the impact of sea level
rise on estuaries and rivers have been given. Local parameters and properties, such
as river discharge, sediment transport, shape of the estuary and changes in river
discharges due to changes in the hydrological regime, highly determine the overall
impact of sea level rise in a specific area. Research activities should be stimulated in
the field of mixing under wave action, combined wave and tide action, development of
fronts due to salinity, temperature and sediment gradients. So far, case studies have
mainly been focused on the effects of canal deepening and of changes in upstream
river hydrology (such as changes in runoff) on salt water intrusion, as paradigms for
what would occur in case sea level rises.

In subsection 2.3.1, the mechanisms, that determine salt water intrusion into
estuaries and rivers, are described, followed by possible impacts of sea level rise on
estuaries and rivers. In subsection 2.3.2, four cases are briefly discussed.

2.3.1   Salt water intrusion in estuaries and rivers

The following phenomena determine salt water intrusion in estuaries and in the lower
reaches of rivers:

- Density differences
  The tidal average velocity near the bottom is directed inland due to differences
  in density. This induces saline water near the bottom to intrude upstream the
  river,

- Tidal range
  A higher tidal range leads to a more severe salt water intrusion. The differ-
  ence in salt water intrusion between high water slack and low water slack can
  illustrate what would occur in case of sea level rise. It is evident that only
  a small rise is required to cause a significant horizontal movement of the salt
  water front [U.S. Department of Energy, 1989],

- River discharge
  Salt water enters a river or an estuary during the rising tide unless the river
  regime is such that the discharge is great enough to completely fill the en-
  tire tidal prism during the rising tide phase. Only a few rivers have sufficient
  discharge over the entire year to prevent salt water intrusion. Mostly, the dis-
  charge is insufficient to prevent the intrusion of saline water. Especially during
  extended droughts river discharges are low and salt water intrusion causes se-
  vere problems. An extreme case is the Gambia river in Western Africa where

at minimum discharge the saline effect is felt up to 235 km upstream from the
sea [Volker, 1987; Savenije, 1992],

- **Cross-sectional area**
  When the cross-sectional area increases due to sea level rise or due to widening
  and deepening of the estuary (e.g. dredging of waterways) in order to make
  harbours accessible for ships of greater capacities, saline water can intrude
  further upstream,

- **Mixing**
  One of the factors that limit the distance over which saline water can intrude
  inland is vertical mixing and vertical advective salt transport. In case of mixing,
  salt from the bottom layers, where predominantly landward advective transport
  occurs, is carried in the upper layers, where predominantly seaward transport
  occurs.

  The degree of mixing in an estuary can be related to the ratio between the
  river discharge times the period of tidal oscillation and the volume of the tidal
  prism. An example of a mixing parameter is:

$$M = \frac{Q_r\, T'}{P} \tag{2.3}$$

where

- M = mixing parameter or flood number (Canter Cremers Number) $(-)$,
- Q_r = fresh water river discharge $(L^3\,T^{-1})$,
- T' = tidal period (T),
- P = volume of the tidal prism (L^3).

Some sketches of the isohalines (lines of constant salinity) of three river types
are shown in figure 2.11.

Fundamental approaches to the salt water intrusion problem have been applied by
Ippen and Harleman [1961] and by Abraham [1976]. Langeweg and van Weerden
[1976] summarized various empirical methods for salinity movement in estuaries, such
as stationary models [e.g. Ippen and Harleman, 1961] and non-stationary models [e.g.
Thatcher and Harleman, 1972].

Savenije [1992] developed a rapid assessment technique to determine the salt water
intrusion in alluvial estuaries of the well-mixed type, based on 18 different estuaries
world wide. The cross-sectional area and the width of these alluvial estuaries are
described with negative exponential functions. The technique can be applied to
assess the impact of sea level rise on salt water intrusion. The salt water intrusion
length in steady state can be calculated for estimated greater depth and tidal velocity
amplitude due to sea level rise [van Dam, 1993].

M<0.1
Mixed estuary

river

sea

0.1≤M<1
Partially mixed estuary

river

sea

M≥1
Stratified estuary

river

sea
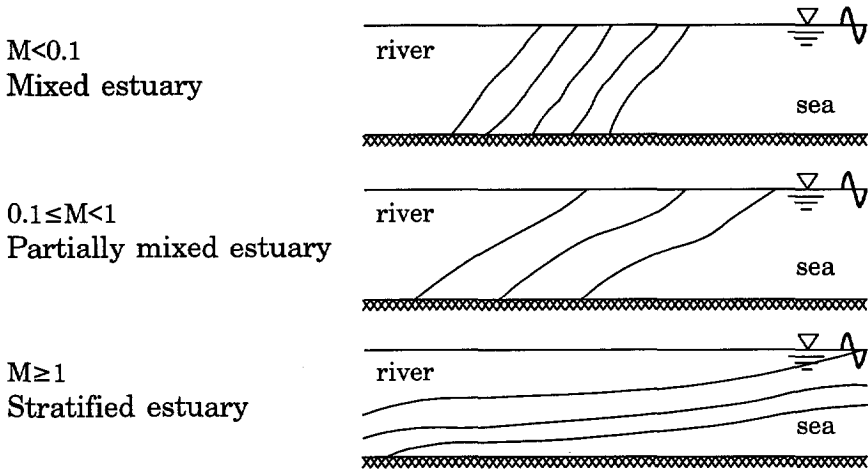
Figure 2.11: River mixing criteria.

Salt water wedge

When mixing is such that a salt water wedge occurs (the so-called *stratified estuary*), methods are available to estimate the salt water wedge length for stationary situations. The salt water wedge length is the distance over which saline water manages to intrude.

A salt water wedge occurs when a river discharges into a saline body of water, such as a sea or an ocean (see figure 2.12). Sea water intrudes along the river bottom under the fresh river water due to the difference in density. The length of the intruding wedge is determined by an equilibrium between the friction forces along the interface (no mixing is assumed) and the horizontal pressure gradient resulting from the inclination of the interface. A state of dynamic equilibrium occurs, if the salt water wedge is in stationary position with fresh water flowing seaward near the water surface and spreading out into a thin surface layer at sea.

For example, the length of such a salt water wedge in a prismatic, horizontal, rectangular canal, discharging into an infinite sea, with no tidal oscillations, is given by equation 2.4 [Kranenburg, 1986]:

$$L_w = \frac{h}{k_I} \left[\frac{1}{20 \, Fr^2} - 0.5 + 0.75 \, Fr^{2/3} - 0.3 \, Fr^{4/3} \right]$$

and

$$Fr = \frac{V_r}{\sqrt{\alpha \, g \, h}} \tag{2.4}$$

where

- L_w = length of the salt water wedge (L),
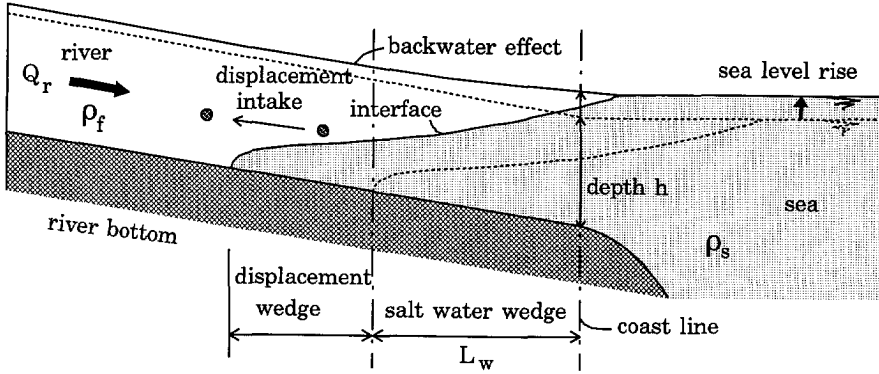
Figure 2.12: Salt water wedge in estuaries and rivers.

- h = water depth of the river (L),

- k_I = friction factor representing the stress along the interface $(-)$, (reasonable value in the order of $4 \cdot 10^{-4}$),

- Fr = Froude number $(-)$,

- V_r = velocity in the river, upstream of the wedge, Q_r/A (LT^{-1}),

- Q_r = fresh water river discharge $(L^3\,T^{-1})$,

- A = cross-sectional area (L^2),

- α = relative density difference, $(\rho_s - \rho_f)/\rho_f$, $(-)$,

- ρ_s = density of saline water $(M\,L^{-3})$,

- ρ_f = density of fresh water $(M\,L^{-3})$,

- g = acceleration of gravity $(L\,T^{-2})$.

Note that it was assumed that no mixing occurs across the interface and that the salt water wedge is at rest. The expression illustrates the significant parameters of the salt water intrusion, such as the water depth, the river discharge velocity and density differences.

Sea level rise versus river bed elevation

The change in length of the salt water wedge, initiated by a sea level rise SLR, can be approximated by the aforementioned equation 2.4. If the position of the river bed is fixed, the total water depth at the river mouth becomes h + SLR, and the corresponding salt water intrusion length can be calculated.

However, once the sea level is rising, this will lead to a reaction in the river: water depths in the lower reach of the river increase, flow velocities go down and sedimentation occurs. As a result, the river bed rises also. In theory, the river bed elevation will finally take place over the whole length of the river, since river flow is subcritical. Whether and how fast the river adapts to changes in boundary conditions depends on local conditions. The time lag between the rise and the response of the river by creating a higher bed appears to be considerable [van den Berg and de Vries, 1979]. The rate of rise of the river bed depends, among others, on the discharge and the sediment load of the river, the bottom gradient, the geometry of the river mouth and the rate of sea level rise. Also human activities determine the rate of rise of the river bed, for instance by damming and embanking the river (e.g. the Nile), by withdrawing sand and water, and by dredging of harbour entries and waterways for navigation.

As a matter of fact, the actual salt water intrusion length L_w should be calculated for a depth equal to $h + \zeta$ SLR, $0 \le \zeta \le 1$, where ζ depends on the river bed elevation. If the river bed elevation follows the sea level rise closely, then there will be hardly any impact ($\zeta \approx 0$). This can be expected for the Chinese rivers Hwang Ho and Yangthze Kiang, which have huge sediment loads. However, if there is a constant increase in water depth because the river bed elevation cannot match sea level rise due to a deficit of sediment, then an increase of salt water intrusion in estuaries and rivers can be expected (e.g. $\zeta > 0.5$). This could happen in rivers such as the Nile, the Indus, etc.

Effect of sea level rise

When estuaries and rivers experience an increased salt water intrusion, then the following problems may arise:

- along major rivers, intakes for domestic, agricultural and industrial water supply are threatened. Normally, these upstream intakes are located far enough beyond the saline zone, even during dry periods. However, sea level rise may cause the salt water wedge to shift beyond such intakes, with the result that they can be used only temporarily or, at worst, not any more (see figure 2.12).

- the seepage quantity from estuaries and rivers towards adjacent areas increases, e.g. in the Delaware estuary [Lennon et al., 1986]. Vulnerable areas are those in which the phreatic groundwater level is kept low with respect to the water level in estuary or river for reasons of land-use. The seepage may become more saline in the long-term, thus increasing the salt load in the adjacent areas and, depending on the climatic conditions, decreasing the crop yields.

Backwater effect

Not only areas along the coast should be protected against the impact of sea level rise. Also large areas along estuaries and, in upstream direction, rivers should be

defended against flooding due to the backwater effect. Especially areas adjacent
to rivers with average valley slopes only slightly steeper than average river slopes
have to be protected by (higher) embankments. Both average slopes are based on
the distance between the coastline and the 100 m contourline, however, the average
valley slope is measured in a straight line whereas the average river slope is measured
along the river axis [Gilbert *et al.*, 1990].

For instance, the Nile river has an average valley slope of approximately 8.3
cm/km, whereas the average river slope is about 8.0 cm/km. This implies that
the backwater effect of sea level rise may threaten areas along the river over at least
tens of kilometres. A characteristic length of the backwater effect has been applied
as a guideline to determine the distance upstream from the river mouth, where the
backwater effect of the expected sea level rise of one metre is reduced to 30 % (this is
an arbitrary chosen figure) [Gilbert *et al.*, 1990]. The length is based on the average
annual river discharge, the number of main branches and the average river slope. For
instance, the characteristic length for the Nile river is 58 km.

2.3.2 Cases

I. Delaware estuary, USA

The implications of sea level rise on increased salinity have been examined in detail
for the Delaware estuary which has a well-mixed character [Hull and Titus, 1986].
During the worst period of the severe drought in the 1960's, the salt water front
(250 mg Cl^-/l) advanced 53 km up the river. Since 1979, the Delaware River Basin
Commission has considered not only implications of droughts, but has also focused
its investigations on the implications of greenhouse warming. In a joint report by the
Delaware River Basin Commission and the Environmental Protection Agency, the
implications of sea level rise on the salinity distribution in the estuary are examined.
A mathematical salinity model of the estuary was applied, which relates chloride
distribution in the estuary to freshwater inflows, tides, and ocean salinities. It was
assumed that the position of the river bed is fixed. The computations showed that
a rise in sea level would substantially exacerbate today's salinity problems in the
Delaware estuary. For instance, the salt water front (the 250 mg Cl^-/l isochlor[5])
would move about 11 and 39 km upstream in case of a repeat of the drought of the
1960's, combined with a sea level rise of 73 and 250 cm respectively.

The upper part of the estuary (above Philadelphia) would become too salty for
most of the users, such as municipal and industrial water supply. Furthermore, an
accelerated sea level rise could even threaten the New Jersey aquifers (the Potomac-
Raritan-Magothy aquifer system), which are recharged by the Delaware river (see
also subsection 2.4.4).

---

[5] An isochlor is a line of equal Cl^--concentration.

II. Nile delta, Egypt

Near the river mouths of the Rosetta and Damietta branches and the lake outlets (see figure 2.9), the salinity ranges from 100 to 380 $mg\ Cl^-/l$. Salinity levels respond to tidal movements and to (seasonal) changes in river discharge. A relative sea level rise at the Nile delta coast of about 94 cm by 2050 is likely to increase the salinity of the river mouths to 500-800 $mg\ Cl^-/l$ [El-Fishawi, 1993]. The salt water intrusion would affect the area of the Nile delta which is lying below +2 $m\ M.S.L.$ This area comprises a densely populated area up to 20 to 30 km from the coast, which is characterized by a high level of agriculture, industry and commerce. Furthermore, the ecosystems in the estuaries and coastal lakes could be upset and fish catches could alter in composition or even vanish.

III. Gambia river, Gambia

As a result of the flat topography of the estuary, the Gambia river in western Africa, which has a well-mixed character, experiences tidal effects up to some 500 km inland. Accordingly, more than half the total length of the river in the Republic of the Gambia is affected by salt water intrusion. During the wet season, a great river discharge is moving the salt water front down to a distance of about 100 km from the mouth, while afterwards at the minimum river discharge the salt water front is intruding up to some 250 to 300 km upstream from the mouth [Volker, 1987, Savenije, 1992].

When sea level rises, not only fresh water resources could be affected, also a severe soil degradation in the form of soil salinisation could be expected [Manneh, 1993]. Large potential agricultural areas along the river may become unexploitable and more barren lands in the floodplain may be expected due to higher salinities in the river.

IV. Rijn delta near Rotterdam, the Netherlands

A simulation model is applied to assess the socio-economic impacts of greenhouse effect for the Netherlands [den Elzen and Rotmans, 1988]. A variety of aspects is evaluated, such as the coastal defence, water management and energy use. Salt water intrusion in the Rijn delta, which has a stratified character, is treated for the aspect water management. The length of the salt water wedge is approximated by the following simple formula [de Hoog, 1988] (see figure 2.13):

$$L_w \approx \frac{\rho_s - \rho_f}{\rho_s} \frac{h}{I_b} \tag{2.5}$$

where $I_b = \tan\beta =$ bottom gradient of the river $(-)$. When sea level rises, the salt water wedge itself will not basically change. However, the salt water wedge will shift in upstream direction over a distance ΔL_w, on condition that the river bed stays the same:

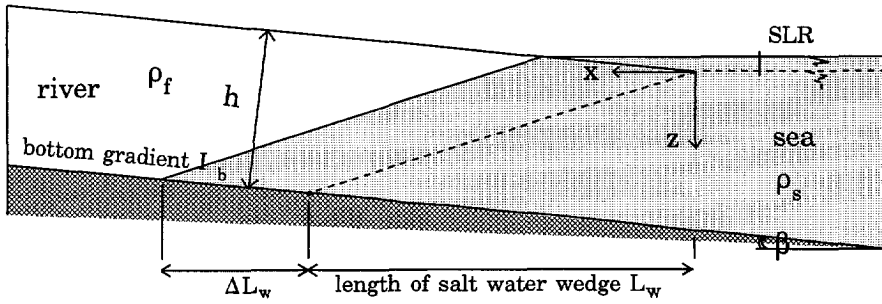$$\Delta L_w = \frac{\text{SLR}}{I_b} \tag{2.6}$$

Figure 2.13: Shift of the salt water wedge due to sea level rise.

where ΔL_w = shift of the salt water wedge (L) and SLR = sea level rise (L). From expression 2.6, it is clear that the smaller the bottom gradient, the greater the shift of the salt water wedge and the further the influence of sea level rise will be sensed. Climate change, which is expected to cause an accelerated sea level rise, may also result in an increase in precipitation and may result in a greater discharge of the river. Consequently, the salt water wedge is pushed further seaward, since a greater discharge means greater water depths. The overall effect on the shift of the salt water wedge becomes:

$$\Delta L_w = \frac{\text{SLR} - \frac{\rho_f}{\rho_s} \Delta h}{I_b} \qquad (2.7)$$

where Δh = increase in water depth of the river because of climate change (L). Obviously, a decrease in precipitation would induce the opposite effect: the salt water wedge will be pushed further inland.

These straightforward expressions are applied for the waterways in the Rijn delta near Rotterdam, the Netherlands. For instance, the present length, determined from the coastline, of the salt water wedge in the Rotterdam seaway, the Netherlands is 29.2 km. The horizontal shift of the salt water wedge has been computed at 4.6 km in case sea level rises one metre (precipitation and river discharge remain the same).

2.4 Impact on coastal groundwater flow regimes

Any variation in sea level will affect the coastal groundwater flow regime, as the sea can be considered as a boundary condition. Aspects that affect coastal groundwater flow regimes have been summarized in figure 1.1. Obviously, from a geohydrological point of view, the most interesting areas are the coastal geohydrologic systems with sedimentary deposits, rather than coastal geohydrologic systems consisting of hard rocks. Coastal geohydrologic systems of the first-mentioned type occur in the Netherlands. The following features should be considered in the classification of the subsoil:

- long-term evolution, e.g. sea water transgressions or regressions, natural subsidence,

- sea behaviour, e.g. storm surges, wave action, tidal regime, sea bottom sediments,

- climate related aspects, e.g. hydrologic regime, wind climate,

- human activities since several centuries, e.g. land reclamation; mining of oil, gas, gravel, sand and clay; extraction of groundwater.

The impact of sea level rise can be substantial on coastal groundwater flow regimes where fresh groundwater occurs and which are subject to human activities now and/or in the future. Nevertheless, this impact is probably the least well known until now, compared to the impact of sea level rise on the coastal zone, hinterland, estuaries and rivers. Virtually all literature has treated the coastal groundwater flow regimes only very roughly and has concluded that volumes of fresh water resources will probably decrease and that saline seepage will probably increase in vulnerable coastal groundwater flow regimes.

    First, in subsection 2.4.1, two important characteristics of the impact of sea level rise are discussed: the zone of influence and the time lag of sea level rise perceptible in the coastal groundwater flow regimes. In subsection 2.4.2, the impact of sea level rise on coastal groundwater flow regimes is clarified by making use of expressions in combination with the Badon Ghyben-Herzberg principle. In subsection 2.4.3, countermeasures to compensate the impact of sea level rise are described. Finally, in subsection 2.4.4, six cases are discussed that are dealing with the impact of sea level rise.

2.4.1   Zone of influence and time lag of sea level rise

Zone of influence

Whether or not the impact of sea level rise is significant depends on the attenuation of the rise in water level in coastal groundwater flow regimes. For the Dutch situation, this implies in other words: to what extent is the rise in sea level perceptible in the polder areas of the western and northern parts of the Netherlands ?

    It is common knowledge that, as a first approximation, the simple straightforward formula 2.8 of Mazure [1936] can be applied to assess the zone of influence of sea level rise for a semi-confined aquifer, the so-called *Holland-profile*[6]:

$$\lambda = \sqrt{kDc} \tag{2.8}$$

where

---

[6]The geohydrological schematisation, which consists of a Pleistocene sandy aquifer overlain by a Holocene (clayey) aquitard, is named the Holland profile. It is representative for large (low-lying) parts of Holland, which is located in the western part of the Netherlands.

- k = hydraulic conductivity of the aquifer (LT^{-1}),

- D = saturated thickness of the semi-confined aquifer (L),

- c = hydraulic resistance of the aquitard (T),

- $\lambda = \sqrt{kDc}$ = the so-called characteristic length or leakage factor of the formation (L).

So, in case the subsoil parameters k, D and c are known, a first approximation of the zone of influence in the aquifer of the rise in open water level (or a sea level rise) can roughly be estimated with the characteristic length λ of the formation. For instance, at distances of $x = 2\ \lambda$ and $x = 3\ \lambda$ from the open water boundary, only e^{-2} (= about 13.5 %) and e^{-3} (= about 5 %) respectively is still perceptible of the rise in the open water level.

In this approach, only fresh groundwater is considered, so no density differences are taken into account. Thus, changes in the salinity distribution of seepage due to sea level rise cannot be assessed. The formula only gives the zone of influence of a water level rise at a boundary like the seaside boundary. In reality, however, density flow and spatially varying subsoil parameters highly affect groundwater flow in coastal aquifers. In addition, human activities, such as groundwater recovery and reclaimed low-lying polders, also disturb the groundwater flow. Hence, the straightforward formula 2.8 should only be applied with the greatest reservation.

Time lag

Groundwater flow in a geohydrologic system responds to changes in boundary conditions, which is in this study the rise in mean sea water level. The time lag, before a new state of dynamic equilibrium is reached, is normally for (semi)-confined aquifers and unconfined aquifers in the order of several hours and a few months respectively. These time lags can be neglected completely compared to the time lag of sea level rise perceptible in a geohydrologic system, which is in the order of decades to centuries, namely a sea level rise of approximately 60 cm is foreseen for the next century.

Unlike the relatively rapid approach to a new state of dynamic equilibrium for piezometric levels, the displacement of solutes in groundwater flow regimes is a very slow process. The real velocity of groundwater, $V = q/n_e$ where q is the filter velocity and n_e is the effective porosity, in the aquifer system plays an important role in the salinisation process. Even in case of sudden sea level rise, salinisation of coastal groundwater flow regimes will take at least several decades to even centuries before a new state of dynamic equilibrium for the salinity distribution is reached, as enormous volumes of fresh groundwater must be replaced by brackish or saline groundwater. Fortunately, this gives mankind the time to counteract the salinisation process, though also human countermeasures probably need a long time to become effective. Therefore, it is important to anticipate on the impact of sea level rise on coastal groundwater flow regimes in due time.

2.4.2 Changes of a sharp interface due to sea level rise

Badon Ghyben-Herzberg principle

Several researchers [e.g. Kana *et al.*, 1984; Leatherman, 1984; de Ronde and de Ruij-ter, 1986; Lennon, 1986] have estimated the extent of salt water intrusion into coastal groundwater flow regimes due to sea level rise with the Badon Ghyben-Herzberg principle. This approximation describes the position of a sharp interface between fresh and saline groundwater. It should be noted that these calculations are only approximations of the real situation in the subsoil, and therefore, they only roughly estimate the impact of sea level rise on the distribution of fresh and saline groundwater.

Unconfined aquifer

Freshwater lenses have been evolving in unconfined (phreatic, water table) aquifers due to natural groundwater recharge. Sea level rise will lead to an upward movement of the freshwater lens and a decrease in width (see figure 2.14). Note that human activities to counteract the shoreline retreat, e.g. by sand suppletion, are left out of consideration.
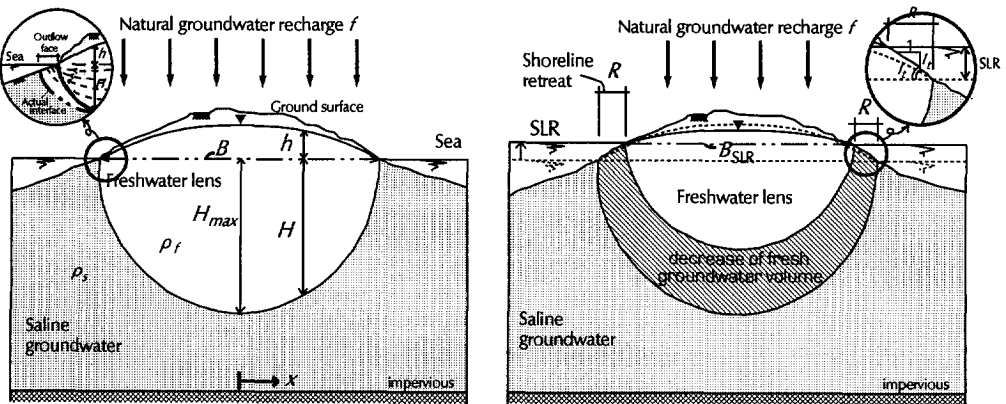
Figure 2.14: Effect of sea level rise on the fresh-salt interface in an unconfined coastal aquifer.

One-dimensional phreatic groundwater flow is considered through a strip of sand-dunes or an elongated island where a freshwater lens has evolved. The depth of the fresh-salt interface and the phreatic groundwater level are given in equation 2.9 [van Dam, 1992a]:

$$H = \sqrt{\frac{f\left(0.25\,B^2 - x^2\right)}{k\left(1 + \alpha\right)\alpha}}$$

$$h = \alpha H, \quad \text{with } \alpha = \frac{\rho_s - \rho_f}{\rho_f} \tag{2.9}$$

where

- H = depth of the fresh-salt interface below mean sea level (L),

- f = natural groundwater recharge $(L\,T^{-1})$,

- B = width of sand-dunes before sea level rise (L),

- x = horizontal position (distance from the axis of symmetry) (L),

- α = relative density difference, $(\rho_s - \rho_f)/\rho_f$, $(-)$,

- h = piezometric level of fresh water with respect to mean sea level (L).

As can be seen, the depth of the fresh-salt interface H is proportional to the width B of the sand-dune area. The volume of fresh groundwater per unit coast length below mean sea level is given by equation 2.10:

$$C' = \frac{1}{4}\pi\, n_e\, B\, H_{max} \tag{2.10}$$

where

- C' = content of fresh groundwater per unit coast length below $M.S.L.$ $(L^3\,L^{-1})$,

- n_e = effective porosity $(-)$,

- H_{max} = deepest position of the fresh-salt interface (in the middle) (L).

Although more sophisticated computations of the shoreline retreat can be applied (see, e.g., section 2.2), a straightforward approximation of the shoreline retreat can be determined as follows:

$$R = \frac{\text{SLR}}{I_t}$$
$$B_{\text{SLR}} = B - 2\,R \tag{2.11}$$

where

- R = landward shift of the shoreline or shoreline retreat (L),

- I_t = slope of the topography $(-)$,

- B_{SLR} = width of sand-dunes after sea level rise (L).

Circular sandy islands could also suffer from shoreline retreat by sea level rise. Consequently, a decrease in the volume of the freshwater lens can be expected. Equation 2.12 gives the formulas for the axial-symmetric situation, that is a circular sandy island with recharge [van Dam, 1992a]:

solution:

$$H = \sqrt{\frac{f\left(R_c^2 - r^2\right)}{2\,k\,(1+\alpha)\,\alpha}}$$

$$h = \alpha\,H$$

$$C = \frac{2}{3}\pi\,n_e\,R_c^2\,H_{max}$$

sea level rise:

$$R = \frac{\text{SLR}}{I_t}, \quad R_{c,\text{SLR}} = R_c - R \tag{2.12}$$

where

- R_c = radius of the sandy island before sea level rise (L),

- r = distance from the center of the circular island (L),

- C = content of the freshwater body (L^3),

- R = landward shift of the shoreline or shoreline retreat (L),

- $R_{c,\text{SLR}}$ = radius of the sandy island after sea level rise (L).

In many shallow phreatic aquifer, the freshwater body originally touches the impervious base, thus creating a salt water wedge of length L_w, see figure 2.15. Stagnant saline groundwater occurs. The length of the salt water wedge is defined by equation 2.13:

$$H = \sqrt{\frac{-f\,x^2 - 2\,q_0\,x}{k\,(1+\alpha)\,\alpha}}$$

$$h = \alpha\,H$$

$$q = f\,x + q_0$$

$$L_w = -\frac{q_0}{f} - \sqrt{\left(\frac{q_0}{f}\right)^2 - \frac{k}{f}\,D^2\,(1+\alpha)\alpha} \tag{2.13}$$

where

- q = groundwater flow per unit coast length $(L^2\,T^{-1})$,

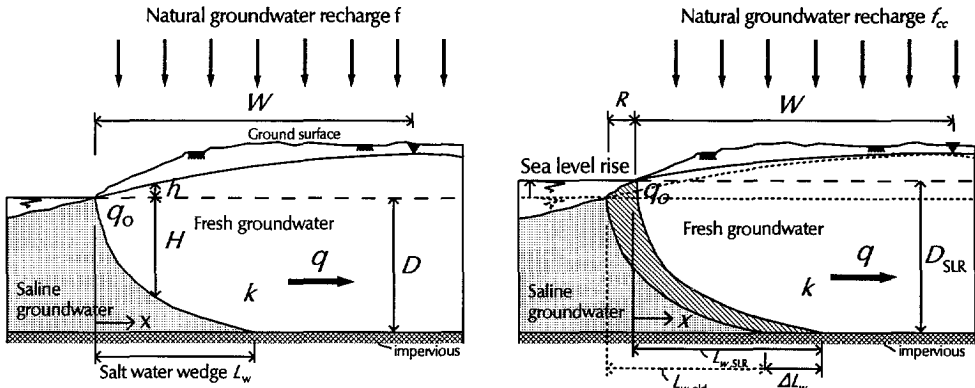- L_w = length of the salt water wedge (L),

Figure 2.15: Shift of the salt water wedge in shallow unconfined aquifers due to sea level rise.

- q_0 = natural groundwater outflow at the coastline x=0 (negative sign) $(L^2 T^{-1})$.

When sea level rises, the position of the wedge toe L_w may shift inland due to several causes, see expression 2.14. First, the wedge may shift landward due to the shoreline retreat R. Second, especially for thin aquifers, the increase in thickness of the aquifer to D_{SLR} may cause an additional landward shift of the salt water wedge. Furthermore, changes in the natural groundwater recharge due to climate change may also be considered.

shoreline retreat:
$$R \;=\; \frac{\text{SLR}}{I_t}$$
aquifer thickness:
$$D_{\text{SLR}} \;=\; D + \text{SLR}$$
climate change:
$$f_{cc} \;=\; \zeta\, f, \;\approx [0.8 \le \zeta \le 1.2]; \quad q_{0,cc} = -f_{cc}\, W$$
shift in the toe of the wedge:
$$\Delta L_w \;=\; R + [L_w(q_{0,cc}, f_{cc}, D_{\text{SLR}}, k, \alpha) - L_w(q_0, f, D, k, \alpha)] \qquad (2.14)$$

where W is the width of the coastal aquifer up to the water divide (L). A different situation occurs for a coastal aquifer with at one boundary the sea and at the other boundary land with a low phreatic groundwater level with respect to $M.S.L.$ Figure 2.16 shows such a situation where the freshwater lens rests upon the impervious base. It is possible that sea level rise may involve the end of the contact between the freshwater lens and the impervious base. Then, saline groundwater will be able to flow underneath the lens in the direction of the low-lying area and flow of saline

groundwater will be introduced in the system. In the new state of dynamic equilibrium, a permanent inflow of saline groundwater will occur. In this situation, fresh or brackish groundwater, if any, at the inland side will be replaced by saline groundwater. Salt water intrusion in this coastal aquifer will permanently increase with sea level rise, according to equation 2.15:
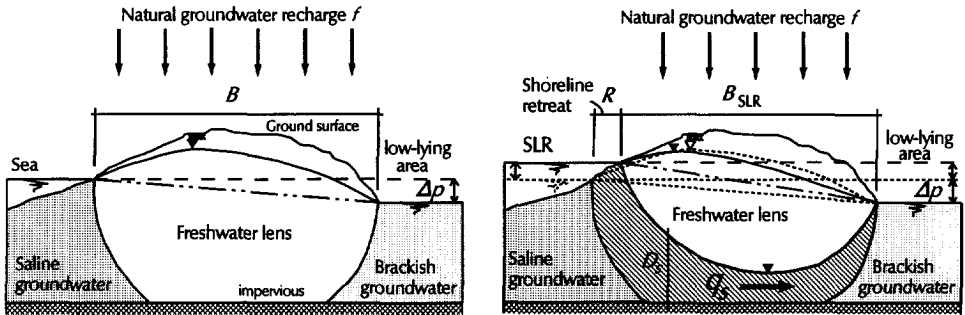
Figure 2.16: Salt water intrusion underneath a freshwater lens into a low-lying area. A permanent inflow of saline groundwater occurs due to sea level rise.

$$q_s = kD_s \frac{\Delta p + \text{SLR}}{B_{\text{SLR}}} \tag{2.15}$$

where

- q_s = flow of saline groundwater underneath the freshwater lens $(L^2\,T^{-1})$,

- kD_s = average transmissivity of the aquifer between the impervious base and the freshwater lens $(L^2\,T^{-1})$,

- Δp = difference between $M.S.L.$ and phreatic groundwater level in low-lying area (L),

- $B_{\text{SLR}} = B - R$ = width of the sand-dunes after sea level rise (L),

- B = width of the sand-dunes before sea level rise (L),

- R = landward shift of the shoreline (retreat) (L).

The permanent salinisation of the subsoil is induced by sea level rise for three reasons. In the first place, the zone with variable thickness D_s between the freshwater lens and the impervious base is increasing with sea level rise, and subsequently, the inflow of saline groundwater is increasing into the low-lying area. Second, due to the increasing difference in head (Δp + SLR) between $M.S.L.$ and the adjacent low-lying area located further inland the seepage quantity is increasing as well. Third, the distance between the sea and the low-lying area is shortening, as the width of the sand-dune

area B_{SLR} is decreasing. Consequently, natural groundwater recharge occurs over a smaller width and the thickness of the freshwater lens is becoming smaller.

Depending on the geometry of the groundwater flow regime, the brackish zone between saline and fresh groundwater will move further inland and seepage will slowly become more saline. In the beginning, the changes in the seepage and the solute concentration in the subsoil will be felt in the polders which are located near the sea with (relatively) low phreatic groundwater levels. Later on, the changes will also be noticeable in polders which are situated further inland but still within the zone of influence of sea level rise.

Semi-confined aquifer

A semi-confined (leaky) aquifer is bounded at the top and/or bottom by aquitards (semi-pervious layers). The aquitard has a hydraulic resistance which suppresses vertical groundwater flow. When sea level rises, the flow of saline groundwater q_s underneath a freshwater lens depends on the characteristic length λ [van Dam, 1993], see figure 2.17 and equation 2.16:

$$q_s = kD_s \frac{\Delta p + \text{SLR}}{\lambda_{sea} + B_{\text{SLR}} + \lambda_{land}} \tag{2.16}$$

where

- kD_s = average transmissivity of the aquifer between impervious base and the freshwater lens ($L^2 T^{-1}$),

- c_{sea}, c_{land} = hydraulic resistance of the aquitard at the seaside and the inland side respectively (T),

- λ_{sea}, $\lambda_{land} = \sqrt{kD_s c_{sea}}$, $\sqrt{kD_s c_{land}}$ = the characteristic lengths of the formation at the seaside and the inland side respectively (L),

- $B_{\text{SLR}} = B$ - R = width of the sand-dunes after a sea level rise (L).

Obviously, as the characteristic lengths are often in the order of kilometres, the aquitards can considerably reduce the flow of saline groundwater q_s, compared with the situation for unconfined aquifers without aquitards.

Confined aquifer

A confined aquifer is enclosed by two aquicludes. The freshwater body touches the impervious base, thus creating a salt water wedge (figure 2.18). The following straightforward formula, based on the Badon Ghyben-Herzberg principle, can be applied to determine the length of the salt water wedge L_w:

$$H = \sqrt{\frac{-2 q_f x}{k \alpha}}$$
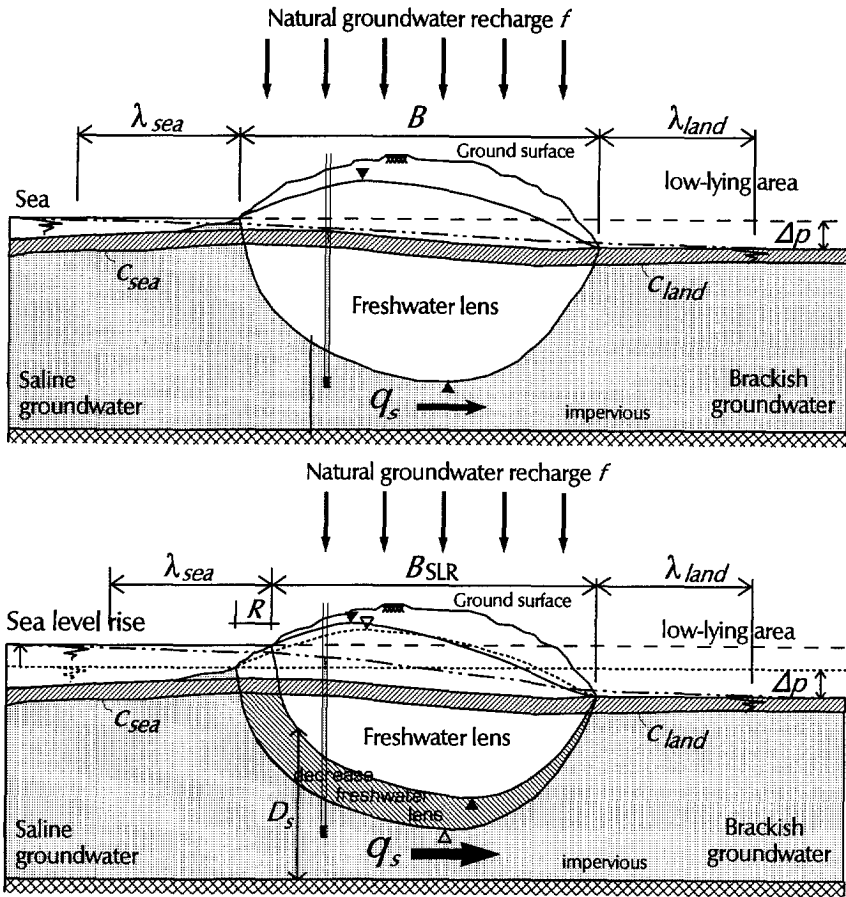
Figure 2.17: Salt water intrusion due to sea level rise in a semi-confined aquifer.

$$h = \alpha (H + A)$$
$$q = q_f$$
$$L_w = -\frac{k D^2 \alpha}{2 q_f} \qquad (2.17)$$

where

- D = saturated thickness of the confined aquifer (L),

- q_f = fresh groundwater flow from recharge in the uplands, possibly diminished by groundwater extractions, per unit coast length $(L^2 T^{-1})$,

- A = height of the sea level with respect to the top of the aquifer (L).

Figure 2.18: No impact of sea level rise on the salt water wedge in confined coastal aquifers.

Equation 2.17 demonstrates that the length of the salt water wedge in confined aquifers is independent of sea level rise. The length of the salt water wedge is only determined (inversely proportional) by the fresh groundwater flow q_f, since all other parameters remain constant. The fresh groundwater flow could differ due to changes in recharge in the uplands. Possible causes are changes in the hydrological regime (e.g. climate change) or human activities such as groundwater extraction or artificial recharge.

2.4.3 Countermeasures against the impact of sea level rise

When sea level rises, the salinisation rate of the subsoil of groundwater flow regimes will probably increase. Nevertheless, it will probably take a considerable time 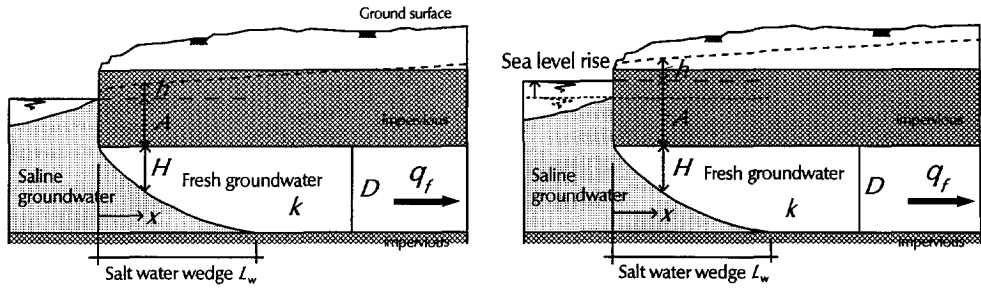before the impact of sea level rise on the groundwater flow regimes is actually observed, since in the salinisation process enormous volumes of fresh groundwater have to be replaced by saline groundwater. As countermeasures to control the salt water intrusion probably also need a long time to become effective, they should be taken in due time. In general, the impact of sea level rise may be substantial in coastal groundwater flow regimes where the existing piezometric levels are lower than a few metres above $M.S.L.$ In those cases, countermeasures should be applied to reduce salt water intrusion. The following countermeasures against the impact of sea level rise can be considered (see also figure 2.19):

1. application of freshwater injection barriers, e.g. through injection or (deep-well) infiltration of fresh sewage water near the shoreline. This is already applied in Israel, at Long Island and in Los Angeles [U.S. Department of Energy, 1989].

2. extraction of saline and brackish groundwater. However, this could regrettable result in undesirably low piezometric levels, especially in shallow coastal groundwater flow regimes. Furthermore, the disposal of the extracted saline or brackish groundwater could meet with problems.

3. land reclamation, thus creating a foreland where a freshwater body may develop.

4. increase of (artificial) recharge in upland areas to enlarge the outflow of fresh groundwater through the coastal groundwater flow regime, and thus, to reduce the length of the salt water wedge.

5. modifying pumping practice through reduction of withdrawal rates and/or adequate location of extraction wells. In most of the situations, groundwater withdrawal for domestic, agricultural and industrial water supply have not been reduced during periods of droughts, so that salt water intrusion tends to occur.

6. creation of physical barriers, such as sheet piles, clay trenches and injection of chemicals. This solution is applicable only in shallow thin aquifers and at the expense of high costs. A small physical barrier through pumping of cement grout has been implemented at Okinawa-Jima Island in Japan [U.S. Department of Energy, 1989].

The possible countermeasures to prevent and/or retard salt water intrusion due to relative sea level rise resemble the present solutions to counteract the negative effects of human activities [Todd, 1980; Sorensen *et al.*, 1984; van Dam, 1992b]. In fact, sea level rise is basically the same as equally lowering the land surface and thus the phreatic groundwater level [van Dam, 1992b]. Nowadays, dramatic lowering of the piezometric levels due to excessive overpumping already occurs in many groundwater flow regimes around the world, such as in the Bangkok region. It is obvious that for those regimes, the impact of a (relatively small) sea level rise (e.g. 0.6 m/c) on the groundwater flow regime will be of marginal importance compared to the effect of an increase in withdrawal rate.

2.4.4   Cases

I. Nile delta, Egypt

The coastal aquifer system of the Nile delta is underlain by an impervious layer which has an inclination of about 4 m/km. The thickness of the aquifer varies from about 100 m near Cairo to 900 m at the Mediterranean coast [Kashef, 1983b; Shahin, 1991; Volker *et al.*, 1993]. A relatively large brackish zone (mixing zone or transition zone) occurs between fresh and saline groundwater in the aquifer system. It is certain that a huge freshwater body occurs, which has probably a maximum thickness of about 300 m. It contains at least $400 \cdot 10^9$ m^3 of fresh water. Nowadays, the recent excess of irrigation water can be considered as a significant source of recharge. In the past, the position of the salt water wedge was probably shifted further inland than today because of less recharge into the aquifer system. At the coastal strip, which has a width of about 50 km, saline groundwater oozes through the aquitard. The agricultural potential in this coastal area of the Nile delta is limited due to this saline seepage, which either reaches the drainage system or evaporates [Shahin, 1991]. Though many scientists have investigated the Nile delta aquifer system and described it by means of sharp interface models [e.g. Kashef, 1983b; Farid and Amer,

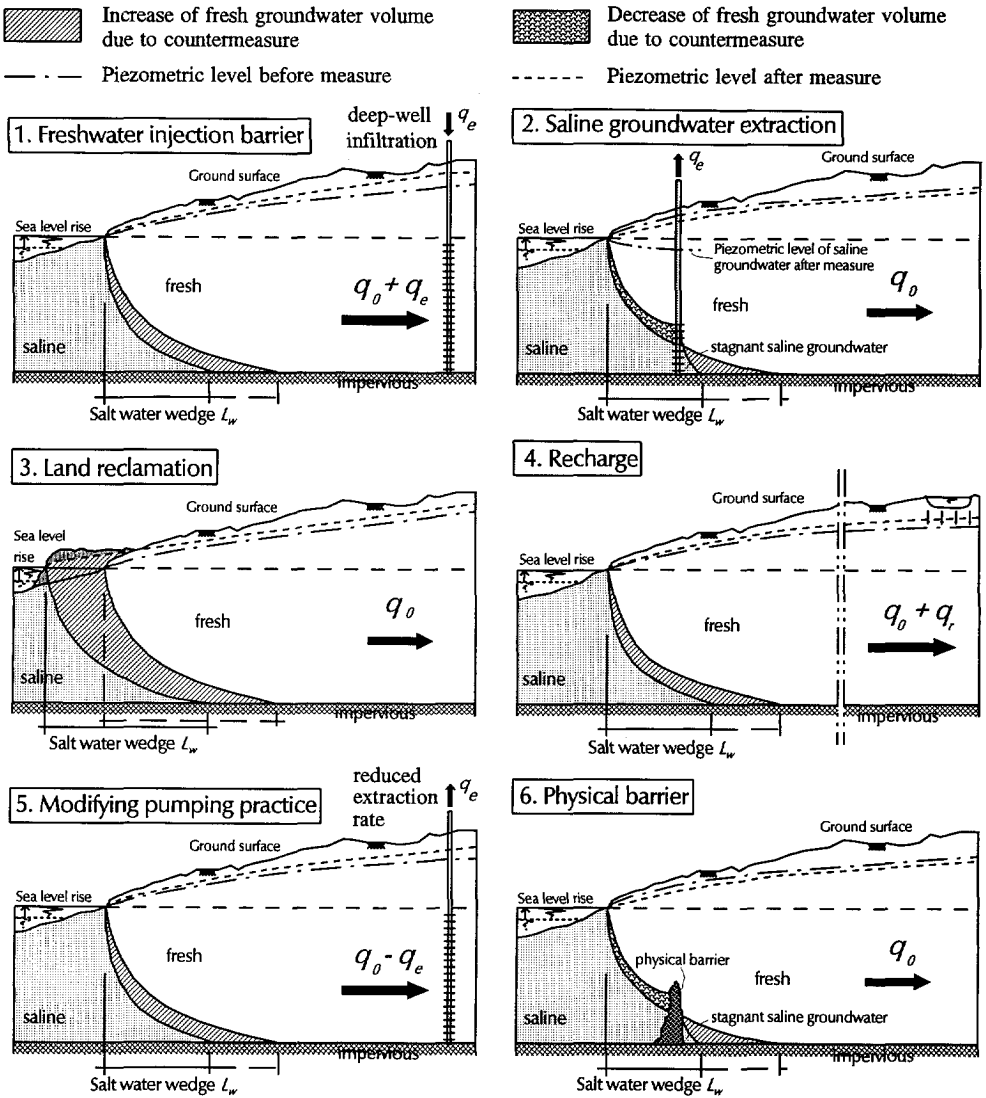**Figure 2.19**: Countermeasures to control salt water intrusion in case of sea level rise.

1986; Farid, 1989], the exact distribution of fresh, brackish and saline groundwater is not yet assessed due to the complexity of the system and a scarcity of accurate field data.

The water policy of the Ministry of Irrigation of Egypt is to extract more groundwater for irrigation and land reclamation purposes. Consequently, an accelerated salt

water intrusion in the Nile delta aquifer system can be expected due to an increase in extraction rates.

In addition, an accelerated (relative) sea level rise could threaten the aquifer system even more than it is jeopardized today. The zone of influence of sea level rise is in the order of tens of kilometres, as the characteristic length λ of the Nile delta aquifer system is long due to high transmissivities and hydraulic resistances[7]. When sea level rises, saline water will intrude further inland. Although the hydraulic resistance of the overlying aquitard near the coast is very high, the northern part of the delta will receive more saline seepage. Special attention should be paid to changes in quality of the groundwater, especially near pumping stations. Higher solute concentrations at water intakes could threaten public health, could increase the costs of water treatment and could damage sanitary facilities and machineries [El-Fishawi, 1993].

II. Galveston bay, Texas, USA

Leatherman *et al.* [1984] have examined the potential impacts of sea level rise on salt water intrusion in the coastal aquifers of Galveston bay, Texas. They concluded that aquifers in the Galveston bay area have already been polluted or salt-contaminated and that any incremental rise in sea level will have little affect on the two important confined aquifers in the region.

III. Charleston, South Carolina, USA

For the case study in Charleston, South Carolina, the Badon Ghyben-Herzberg principle has been applied by Kana *et al.* [1984] for a conservative estimate of the position and change of the sharp interface between fresh and saline groundwater due to a number of accelerated sea level rise scenarios for the years 2025 and 2075. The estimates for the sea level rise vary from 11.2 *cm* to 63.8 *cm* for 2025 and from 23.8 *cm* to 231.6 *cm* for 2075.

Without site-specific modelling of the groundwater flow regime, it is assumed that a new state of dynamic equilibrium could quickly be established after a sea level rise, since the phreatic (unconfined) aquifer has a thickness of about 13 *m* only and there is a high natural groundwater recharge from local precipitation in this shallow sandy aquifer.

The position of the interface toe is estimated at approximately 60 *m* inland of the new shoreline position. This estimate is assumed to be independent of sea level rise scenarios. Thus, the interface will always be estimated to occur at the point where the phreatic groundwater level is about 0.3 *m* above *M.S.L.* (1/40·13 *m*). Note that the increase in thickness of the aquifer due to higher phreatic groundwater levels was

---

[7]The zone of influence of a sea level rise for the Nile delta aquifer can roughly be assessed as a multiple of the characteristic length in equation 2.8.

not taken into consideration. Accordingly, the salt water wedge will eventually shift inland over a length equal to the shift of the shoreline due to sea level rise.

Salt water intrusion will not threaten existing public water supply wells (in Mount Pleasant), except in case of the high sea level rise scenario for 2075. Furthermore, the ultimate impact of sea level rise may be negligible in comparison with the rapid salt water contamination of shallow coastal aquifers due to human activities over the last 50 years (the same has occurred in South Florida, New Jersey and Long Island, New York). The shallow coastal aquifers have already been overpumped, which has resulted in a more severe salt water intrusion than that due to sea level rise as predicted in this case study.

IV. Potomac-Raritan-Magothy aquifer system, New Jersey, USA

Lennon *et al.* [1986] have examined the impacts of increased Delaware river salinity on the adjacent Potomac-Raritan-Magothy aquifer system. This aquifer system is the main resource for domestic and industrial water supply in the coastal plain of southern New Jersey. When the salt water front moved up the Delaware estuary during the severe drought of the 1960's and allowed saline water to recharge the Potomac-Raritan-Magothy aquifer system, salinity levels in groundwater wells were monitored. The zone of influence of sea level rise in the aquifer system is approximated by making use of groundwater velocities that are derived from inflow rates into the aquifer. In this case study, a no solute and dispersion model has been applied to evaluate more adequately the impact of the estuary salinity distribution on the groundwater flow regime.

In the future, saline groundwater will move further into the aquifer, even without sea level rise. However, when sea level rises, the aquifer system would be recharged by river water with higher chloride concentrations[8] than at present. As such, a sea level rise would threaten parts of the New Jersey aquifer system recharged by the Delaware river. The aquifer system, now heavily exploited for domestic water supply, would probably become too saline for drinking water (the drinking water standard for New Jersey equals 78 mg Cl^-/l). As a result, the extractions should be allocated to agricultural and industrial uses. When the sea level rises 250 cm, the groundwater wells in the aquifer would even have to be abandoned.

Also Navoy [1991] has investigated the vulnerability of (potable) groundwater supplies in the Potomac-Raritan-Magothy aquifer system to sea level rise. The interaction between the Delaware river and the aquifer system has been evaluated and the salt water intrusion has been assessed. Navoy has applied the three-dimensional groundwater flow model MODFLOW which is based on the finite-difference method. A constant density is considered under non-equilibrium conditions in a heterogeneous and anisotropic medium. The simulated area of 60 km by 45 km is discretized by 5 layers, 106 columns and 99 rows. The groundwater flow model is combined with a

---

[8] Chloride concentration records constitute the basic data for simulations with several scenarios of sea level rise.

particle tracking procedure and a one-dimensional solute transport model (the longitudinal dispersivity approximates 100 ft), which has been calibrated with historical data of the seawater encroachment event during the severe drought in 1964. The impact of sea level rise is assessed by means of simulations with increased chloride concentrations in the Delaware estuary.

Navoy has assessed that a 30-day encroachment event with a return period of one to five years and chloride concentrations of the river water of 2000 to 4000 $mg\ Cl^-/l$ will have a significant impact on the aquifer system. In the short-term, possible countermeasures are temporary cessation of pumpage during severe encroachment events and/or barrier injection. However, in the long-term, the most feasible action may be to abandon pumpage in the affected area.

V. North Atlantic Coastal Plain, USA

Meisler, Leahy and Knobel [1984] have examined the changes in the distribution of fresh and saline groundwater in a specific profile, the so-called Atlantic City profile, in the North Atlantic Coastal Plain, USA, as a consequence of strong (eustatic) sea level fluctuations in the order of many tens of metres during geologic history.

Saline groundwater is underlying fresh groundwater on the eastern side of North America (New Jersey), see figure 2.20. A transition zone occurs with a thickness varying from 300 to 600 m between the isochlors of 1000 and 18,000 $mg\ Cl^-/l$. The position of the isochlors and thus the thickness of the transition zone during the beginning of the 1980's are shown in figure 2.20. Apart from the broad transition zone between fresh water and saline water at great depth, another (smaller) transition zone occurs between saline and fresh water close to the surface of the sediment wedge (see figure 2.20). The broad transition zone may probably have been developed due to the strong sea level fluctuations in the past million years, whereas the small transition zone at the ocean floor may be the result of short-term cyclic fluctuations of sea level caused by storms and tides.

The profile is about 240 km long. The coastal aquifer consists of a wedge of sediments which thickens from about 50 m at the western boundary to more than 4900 m at the eastern boundary (not displayed in figure 2.20). The hydraulic conductivities of the sediments of the continental shelf are not very well known, though they seem to decrease with both depth and distance from the coast.

The finite-difference computer code INTERA [1979] was applied to simulate variable-density groundwater flow and solute transport. Although the computer code can simulate the transition zone, INTERA only computed in this case study the position of a sharp equilibrium interface between fresh and saline groundwater for several positions of the sea level. Altogether twenty-one simulations were carried out to determine the position of the sharp interface as a function of sea level, hydraulic conductivities and anisotropy factor. In figure 2.20, the effects of four positions of the sea levels are presented, which reflect certain average levels in the geological past: (1) the present sea level; (2) 50 ft ($\sim$ 15 m) and (3) 100 ft ($\sim$ 30 m) below present
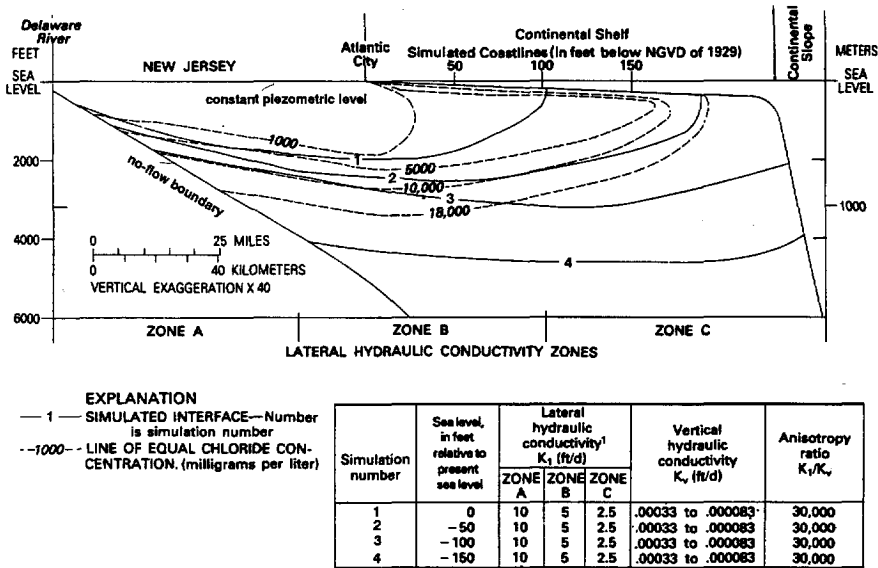
Figure 2.20: Schematisation of the geohydrology of the Atlantic City profile, and positions of the sharp interface for the present sea level and for sea levels -50, -100 and -150 ft with respect to present sea level [after Meisler *et al.*, 1984].

sea level; and (4) 150 ft ($\sim$ 46 m) below present sea level which is the estimated average sea level during the past 900,000 years (see figure 3.9).

The four simulations show that a low sea level forces the freshwater to move to greater depths and, at the same time, to move further away from the new coastline. Note that the coastline itself advances in eastward direction due to the simulated sea level fall. It appears that the observed transition zone is not in equilibrium with the present sea level, but reflects sea levels 50 to 100 ft below the present sea level. This can be deduced from the position of the simulated sharp interface, assuming that the 10,000 mg/l isochlor represents the center of the transition zone. In reality, the observed transition zone is situated considerably further seaward than the simulated sharp interface for the present sea level (that is simulation no. 1). Computations showed that probably the interface is slowly moving landward at an estimated rate of about 300 m per 10,000 $years$.

VI. The Mediterranean Basin and the Near East

Coastal groundwater flow regimes in the Mediterranean Basin and the Near East have suffered from salt water intrusion, mainly due to overexploitation of groundwater. In most of the areas, the impact of sea level rise is probably only significant in the medium term. When sea level rises, the coastal groundwater flow regimes could

become too salty to withdraw from. Under those circumstances, withdrawal of fossil groundwater appears to be an obvious alternative, as fossil groundwater resources are present in all countries of North Africa and the Arabian Peninsula. In these regions, effective infiltration and recharge have probably ceased some 10,000 years ago, thus fossil groundwater is certain to be a nonrenewable resource. Therefore, vital reserves should only be permitted to be mined when all relevant processes are considered and evaluated.

2.5   Impact on water management

Based on the impact of sea level rise described in the previous sections, sea level rise will influence the integrated management of water resources in an entire coastal area. As the management system is too complex to be described completely, only a number of descriptive analyses about the impact of sea level rise on water management have been carried out up till now.

In subsection 2.5.1, the impact of sea level rise on two aspects of water management gets some more attention: seepage and discharge (of excess water). Finally, in subsection 2.5.2, four cases on the impact of sea level rise on water management are discussed.

2.5.1   Effect of seepage and discharge on water management

Sea level rise and seepage

When sea level rises, the head difference between the level of the sea and the phreatic groundwater level of polder areas will become greater, as already indicated [e.g. by Volker, 1987; de Ronde, 1991]. Accordingly, the seepage quantity will increase proportionally. In the low-lying polders in the vicinity of the sea, where the phreatic groundwater level is kept low in an artificial way, an increase in seepage quantity also implies an increase in salt load, as seepage is usually already brackish.

In addition, the seepage quantity will also increase in polders along the lower reaches of estuaries and rivers with an open connection with the sea, because the adjacent surface waters will experience a rise in their water level due to the backwater effect. Seepage may also become more saline because saline water will probably intrude further upstream in these estuaries and rivers in case of sea level rise. However, further upstream in the rivers, the increased seepage will still be fresh. The process mentioned above will probably occur in the Delaware estuary, USA [Lennon et al., 1986].

For the Netherlands, straightforward computations have been executed to assess the increase in seepage quantity due to sea level rise. For instance, straightforward calculations, executed in 1986 by the Tidal Waters Division of the Rijkswaterstaat within the framework of an exploratory investigation on the impact of an extreme sea level rise of 5 m for the next 200 years, predict that the seepage quantity in
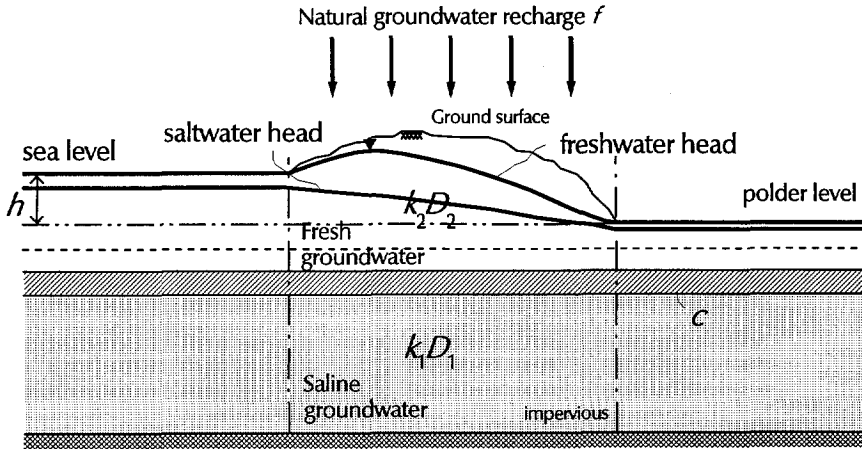
Figure 2.21: Schematisation of the geohydrologic system, applied to assess the increase of (saline) seepage along the Dutch coast due to sea level rise [after Bruggeman, 1987]. By courtesy of Bruggeman.

large low-lying polder areas in the western part of the Netherlands (between 2 to 6 m below $M.S.L.$) will increase twofold to threefold in case of a 5 m sea level rise [de Ronde and de Ruijter, 1986; de Ronde, 1988]. As a result, the amount of fresh water needed for flushing polders will then increase with about 50 %.

Exploratory computations in the IMAGE model (see subsection 2.5.2) also showed an increase in seepage quantity for the coastal areas in the Netherlands [den Elzen and Rotmans, 1988]. In this model analytical expressions have been applied which were formulated by Bruggeman [1987]. Figure 2.21 shows the schematisation of the geohydrologic system: two aquifers separated by an aquitard. In the top aquifer fresh groundwater occurs and in the bottom aquifer saline groundwater. Though the estimates are only indicative, the model has assessed an increase of the total amount of seepage of 40 % and 80 % respectively, for a sea level rise of 0.5 and 1.0 m.

Sea level rise and discharge

Sea level rise will affect discharge of excess water as follows:

- Seepage quantities will increase. This means that more water will have to be disposed of, either by gravity discharge or by pump-lift discharge. In some areas, the natural balance between input and output will be disturbed. In any case, the extra input of seepage will require investments: the capacity of the discharge system has to be increased.

- An increase in seepage quantity will also mean a higher salt load. Too much salt in the upper layers will affect crop yields. To avoid damage by salinisation

of the soils, irrigation may become necessary and the discharge system will have to be flushed more intensively.

- Water that is pumped out of the low-lying areas will be disposed to a river or the sea. Since the mean water levels of those systems will be higher due to sea level rise, an increase of pumping head and consequently an increase in the energy costs can be expected.

- Regions, which are used to drain in a natural way (that is by gravity), will have to cope with higher water levels outside the area. In case they have to maintain their original function, for example for agricultural purposes, pumping stations with greater capacities will have to be built. Moreover, the total area that has to be drained artificially may increase.

2.5.2 Cases

I. ISOS: Impact of sea level rise on society

For the Workshop Impact of Sea level rise On Society (ISOS) in 1986 [Wind, 1987], a model was developed by Delft Hydraulics and Rijkswaterstaat to assess socio-economic impacts of sea level rise for three case studies: the Netherlands, Bangladesh and the Maldives Islands. The interest was also focused on storm frequencies, storm intensities and discharges of large rivers. The illustrative model simulates the situation in a specific country or geographic region. The main components of the model are: scenarios, characteristics of the impact area, measures and effects, see figure 2.22. Various major impacts are foreseen for these three countries:

a. the Netherlands
A substantial rise in sea level would eventually require changes in coastal protection strategies. In 1987, the United Nations Environment Programme (UNEP) and the Government of the Netherlands gave the onset for a further elaboration of the approach developed during the ISOS Workshop in 1986 [Delft Hydraulics, 1988; Peerbolte et al., 1991].

b. Bangladesh
Large parts of Bangladesh would be inundated or threatened by flooding. The exact surface area in jeopardy also depends on the sediment load of the rivers Ganges-Brahmaputra, which probably enable a substantial part of the land to keep pace with sea level rise. Efforts to protect the country would at least require a massive economic effort.

c. the Maldives Islands
The entire nation may be inundated, as the Islands are mostly less than two metres above mean sea level. This depends, however, on the possibility of coral reefs to keep pace with sea level rise. If not, then it might be necessary to abandon entire islands.
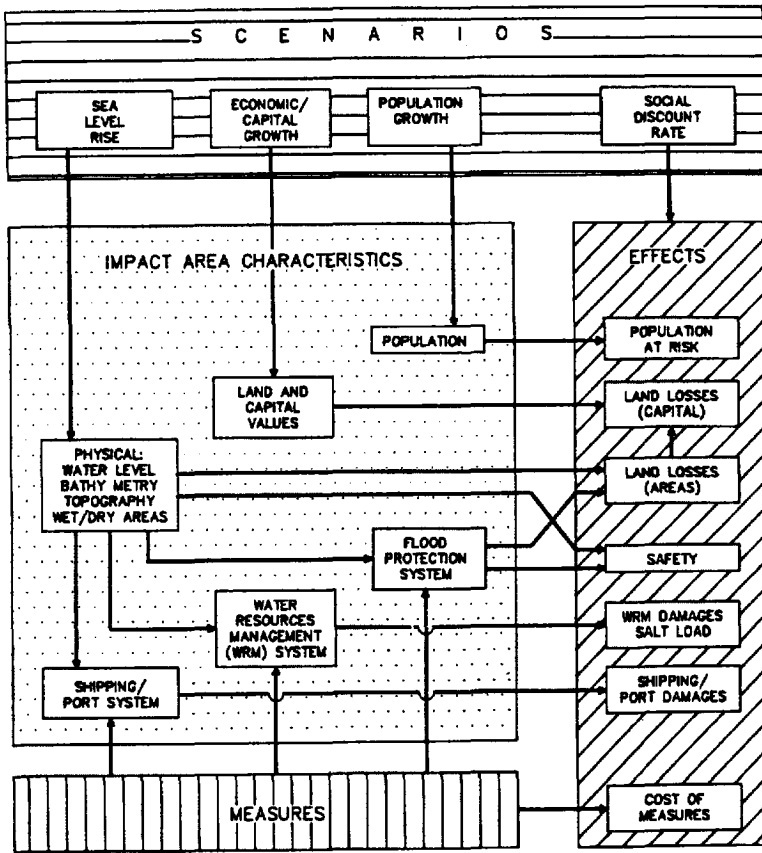
Figure 2.22: Main components and relationships in the ISOS system diagram [from Wind, 1987]. Source: *Impact of Sea level rise On Society. Wind, H.G. (ed), p. 49.* Copyright © 1987 A.A. Balkema, Rotterdam, reprinted by permission of A.A. Balkema.

II. Japan

The Japanese coast is often subjected to typhoons, seasonal strong winds and earthquakes with tsunamis. Moreover, for centuries, reclamation and tidal land reclamation has made many coastal areas in Japan even more vulnerable to sea level rise. The complexity of cause and effect of climate change and sea level rise requires an impact analysis of the whole socio-economic system, starting from climate change to society through physical change and natural effects. A methodology, similar to the ISOS approach, has been applied to assess the vulnerability of Japanese coastal lowlands due to sea level rise[9] [Hosokawa, 1992]. Effects of inundation and flooding

---

[9] The same methodology has been applied by Mimura *et al.* [1992] for two other areas: Tongatapu Island, a small coral island in the Kingdom of Tonga, and the Tianjin area, a large low-lying river delta in China.

related to the magnitude of typhoons, salt water intrusion into rivers and aquifers and wave shoaling along the coast have been evaluated.

III. IMAGE and ESCAPE models

The Netherlands National Institute of Public Health and Environmental Protection (RIVM) uses the simulation model Integrated Model for the Assessment of the Greenhouse Effect (IMAGE) to investigate some socio-economic consequences of the greenhouse effect for the Dutch society. In IMAGE [den Elzen and Rotmans, 1988; Rotmans, 1990], sometimes rather straightforward formulas are defined to assess the socio-economic consequences of sea level rise for the Netherlands. A variety of aspects are evaluated in IMAGE, such as coastal defence (risk analysis, dike raising, dune erosion and intertidal zones), water management (seepage, salt water intrusion, discharge) and energy use (heating and cooling).

The simulation model Evaluation of Strategies to address Climate change by Adapting to and Preventing Emissions (ESCAPE) is based, among others, on the IMAGE model and on models applied by the Intergovernmental Panel on Climate Change [Houghton *et al.*, 1990]. It is an instrument of the European Committee policy based on scientific analysis. ESCAPE assesses the relation between the future emission of greenhouse gases and their impacts on climate and sea level. ESCAPE has been developed by the Dutch National Institute of Public Health and Environmental Protection (RIVM) and the Climate Research Unit of Norwich, United Kingdom.

IV. IJsselmeer, the Netherlands.

As it is of vital importance for the water management of a large part of the Netherlands (about 15,000 km^2), the IJsselmeer is likely to play an important role in the measures against the impact of sea level rise [de Jong, 1986; de Ronde, 1988; den Elzen and Rotmans, 1988, 1992; Volker *et al.*, 1993].

The IJsselmeer, with a surface area of about 1200 km^2, used to have an open connection with the sea. In 1932 an enclosure dam of some 30 km was constructed, the Afsluitdijk. After closure it became a freshwater lake, as there is inflow of fresh water from the river IJssel, a branch of the river Rijn. The IJsselmeer receives about 12 % of the Rijn discharge. It is the main storage basin of fresh water for domestic and agricultural water supply and for flushing of canals. Furthermore, the lake is utilized for navigation and as a source of cooling-water. It has also become an important area for recreation and nature conservation. In winter times, the excess water of this basin is disposed to the sea by gravity via sluice gates. The average discharge from the lake into the Waddenzee (through the sluices) is about 50 million m^3/day. In winter the water level strived after is -0.4 m N.A.P. and in summer -0.2 m N.A.P. There are several sources that contribute to the salt load of the IJsselmeer, such as the river IJssel, water discharged in the IJsselmeer by the great and low-lying polders (in particular the Wieringermeer polder), leakage of saline water through sluices and

shiplocks, and saline seepage through and below the Afsluitdijk (estimated at 35,000 *ton Cl⁻/yr*).

It may be possible that the present (natural) discharge system of the IJsselmeer could not be utilized any more in case of a sea level rise of e.g. 60 *cm*. Two water management strategies and their effects on dike length, seepage, salt load, discharge and water supply are briefly discussed in case of such a sea level rise [den Elzen and Rotmans, 1988, 1992]:

a. maintaining the present level in the IJsselmeer

Sea level rise will deteriorate the possibilities of gravity discharge. Consequently, one or two pumping stations may be required in the future. The Afsluitdijk will have to be heightened to maintain the present degree of safety.

The amount of saline seepage and salt load through the Afsluitdijk on the freshwater lake will increase substantially, as the difference in head between sea and lake increases. Meanwhile, the seepage quantity from the IJsselmeer to the surrounding land will remain the same. In summer, the water supply from the lake will remain unchanged.

b. raising the level in the IJsselmeer in accordance with the sea level rise

The capacity of local pumping stations will have to be increased. Despite the heightening of the lake water level, the capacity of the sluices in the Afsluitdijk will need to be increased also. The reason is that the storage capacity will decrease when water levels will be higher, since water levels will be closer to the maximum acceptable level. Therefore, not only the Afsluitdijk will need to be heightened, but also the dikes along the polders in and around the IJsselmeer and the river IJssel.

The amount of saline seepage through the Afsluitdijk remains the same, whereas the seepage quantity from the IJsselmeer to the surrounding land would considerably increase. As originally the IJsselmeer was part of the sea, groundwater in the region is still mostly saline. Therefore, the seepage will also be saline and the salt load on the polders and subsequently on the IJsselmeer will increase. More water will be available for additional water supply during the summertime, as the difference between summer water level (higher than -0.2 *m N.A.P.*) and winter water level (still strived after -0.4 *m N.A.P.*) is greater[10]. Then, this additional water can be applied for agriculture and for flushing of the adjacent polders to avoid the effects of the increase in saline seepage.

---

[10] As a consequence, harbour structures have to be adapted for a greater difference in water level.

Chapter 3

Sea level rise: causes, mechanisms and estimates

3.1 Introduction

Climate plays a central role in the mechanisms that determine the level of the sea. Climate changes mainly due to a disturbance in the balance of incoming and outgoing energy. The disturbance in the balance is accomplished when, among others, solar radiation varies, the intensity of volcanic eruptions changes, or when the concentration of atmospheric trace gases (called together the greenhouse gases) alters. The most important greenhouse gases are water vapour (H_2O), carbon dioxide (CO_2), nitrous oxide (N_2O), ozone (O_3), methane (CH_4) and chlorofluorocarbons ($CFCs$).

Before the Industrial Revolution (at roughly 1850), natural processes determined the concentration of greenhouse gases, the change of atmospheric temperature, the global changes in climate, and thus the level of the sea. The time scale of the natural processes was in the order of millennia and more. However, there is consensus that since the beginning of the Industrial Revolution the concentration of greenhouse gases has rapidly increased because of human activities. In addition, during the past century, global mean temperature has risen. The global warming is most probably enhanced by the increase in the concentration of greenhouse gases. The mechanism of global warming is called *the greenhouse effect*. Note that even without the man-induced greenhouse effect, a natural greenhouse effect keeps the Earth warmer than it would otherwise be. A doubling of greenhouse gases in the atmosphere is to be expected by the middle or the end of the next century. It is generally to be expected that the increase of greenhouse gases will enhance the greenhouse effect. This mechanism is called *the enhanced greenhouse effect*. As a consequence, the atmospheric temperature is likely to rise some degrees.

When the climate system begins to warm, also other factors, the so-called feedbacks, come into play. Positive feedbacks such as ice and snow, water vapour and permafrost (permanently frozen soils) probably amplify the greenhouse effect, while on the other hand negative feedbacks such as oceans may counteract the greenhouse effect.

At this moment a global warming occurs, although it is not yet clear whether

the present global warming is the result of natural variability on various time-scales in the climatic system or is induced by human activities. Either way, the atmospheric temperature is certain to increase more in the near future than under natural conditions.

When temperature rises, sea level will rise due to the following processes: thermal expansion of ocean water; melting of mountain glaciers and small icecaps; and ablation[1] of the polar ice sheets of Greenland and Antarctica.

As the Netherlands is a low-lying country, sea level rise would affect the society of the Dutch environmentally, socially and economically. The impact of sea level rise has to be estimated in time, so that society can anticipate on them. For this reason, it is essential to know within what range future sea level rise can be expected. More insight can be gained in how the sea level will rise during the next century by analysing data how sea level changed in the past over different periods of time: decades, centuries, millennia and even millions of years.

Quite a number of the above mentioned processes and feedbacks are still based on assumptions only, as they are difficult to analyse. Although much research is being accomplished concerning the cause and the rate of sea level rise, many of the complex aspects that determine the sea level rise are not yet completely understood. First, as climate on Earth is not only changing due to natural causes, but also due to human activities, it is difficult to determine which part of the sea level rise since the beginning of the Industrial Revolution is the consequence of which cause: natural processes or human activities. Second, the effect of various complex feedbacks on global warming such as oceans and clouds is difficult to assess. Third, the rise in sea level is deduced from the rise in temperature, which is already difficult to predict. Fourth, it will still take at least several years before the rise in sea level can truly be detected, since the order of magnitude of sea level rise due to anthropogenic causes and due to natural variability equals each other during the next decades. In conclusion, at this moment, no exact prognosis of the sea level rise for the next century can be given. Hence, scenarios of future sea level rise are presented.

The variation in sea level is determined by a combination of eustatic, tectonic and compaction (of sediment) factors on a local, regional and global scale. In fact, as these factors are hard to separate from each other, the *relative* sea level rise with respect to the land-surface is meant when referring to sea level rise. The eustatic changes in mean sea level are generally ascribed to a large group of phenomena such as folding of the sea bed, sedimentation covering the sea floor and melting or formation of continental ice masses [Lisitzin, 1974]. The term *eustatic* departs from the assumption (of Suess in 1885) that vertical displacements of the ocean surface occur uniformly throughout the oceans and seas on Earth. In reality, the sea level is an equipotential surface of the Earth's gravity field, the so-called geoid. Removal of glacier ice masses changes the Earth's gravity field and deforms the geoid of that moment. Thus, variations in sea level are also influenced by glacio-isostatic

---

[1]Ablation means that accumulated ice evaporates or melts and subsequently runs off.

effects which accompany the present deglaciation phase, with upheaval in areas of ice melting and subsidence in a wide peripheral belt [Pirazzoli, 1991]. In addition, tectonic movements of the crust of the Earth (e.g. isostatic uplift or subsidence) has the same effect as a eustatic sea level fall or rise. These regional circumstances highly determine the relative sea level rise [Robin, 1986]. As can be seen in figure 3.1, the relative sea level rise, as a result of the retreat of Northern Hemisphere ice sheets, is highly determined by regional circumstances. Furthermore, deformation of the geoid on a local scale is also caused by human activities such as mining activities, land reclamation, groundwater recovery and the construction of dams. This should also be added to the relative sea level rise.
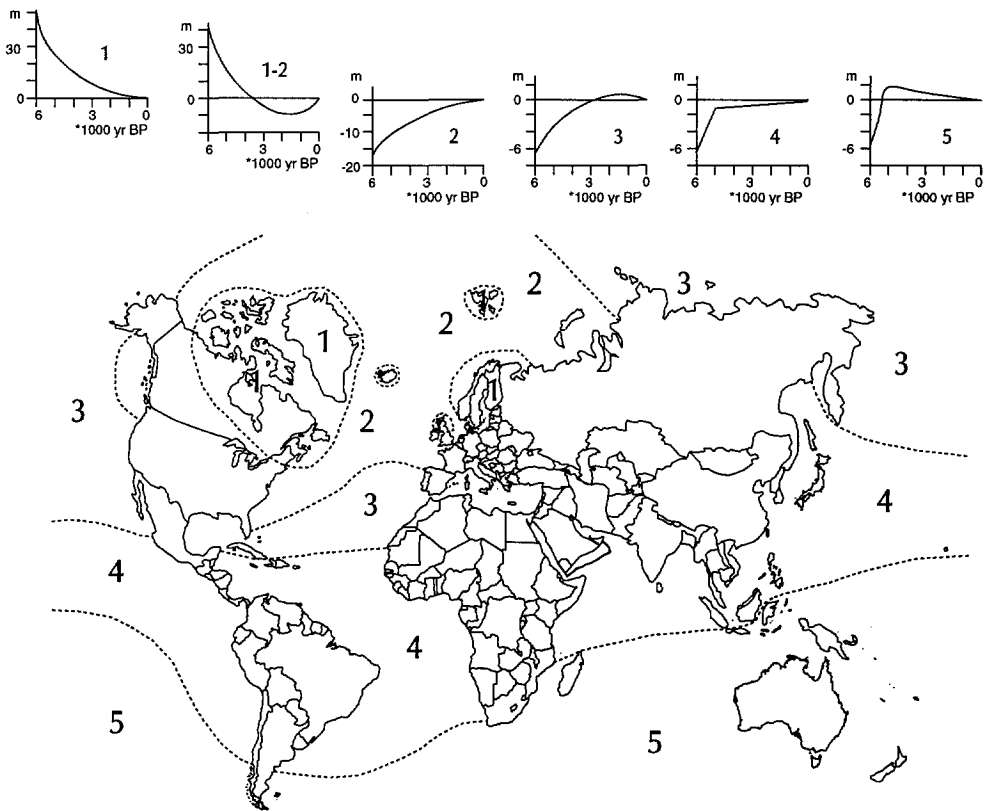
Figure 3.1: Regional distribution of the sea level zones and typical relative sea level curves, under the assumption that no eustatic change has occurred since 5000 years before present [adapted from Clark et al., 1978 by Pirazzoli, 1991]. Source: World Atlas of Holocene Sea-level Changes. Pirazzoli, P.A. & Pluet, J. Elsevier Oceanography Series, Vol. 58, p. 5. Copyright © 1991 Elsevier Science Publishers, reprinted by permission of Elsevier Science Publishers.

The most relevant mechanisms of sea level variations are discussed in this chapter. In section 3.2, a brief summary of the processes involving climate change is given. In section 3.3, the causes of temperature rise and greenhouse effect in relation with feedbacks are discussed. In section 3.4, the physical processes which determine sea level in case of temperature rise are given. In section 3.5, sea level variations in the past during three different periods are described. In section 3.6, several prognoses of future sea level rise are summarized. Finally, in section 3.7, conclusions are drawn.

3.2   Causes of climate change

Since the creation of the Earth, climate has been changing. During the first hundred million years, the upper layers of the Earth's crust were liquid. Slowly, the Earth's crust cooled down to temperatures that made life possible. The general condition of the Earth's crust is determined by a complex self-regulating *geosphere-biosphere system* [Priem, 1989]. This system includes the following components: atmosphere, biosphere, oceans, ice sheets and the Earth's crust itself.

Solar radiation warms up the Earth. External changes in global climate are forced by various processes that change the flows of radiation energy within the geosphere-biosphere system. Consequently, the absorption of solar radiation and the trapping of long-wave radiation by trace gases in the atmosphere may change, which results in a change in global mean temperature or global warming. Five possible causes for change in global climate are [Dickinson, 1986]:

1. a change in solar output. Solar output is known to vary both on very long time scales and on short time scales (days to years),

2. a change in the geometry of the Earth's orbit around the sun (the *Milankovitch cycles*),

3. a change in the fraction of incoming (short-wave) energy at the top of the atmosphere,

4. a change in the amount of net outgoing (long-wave) energy at the top of the troposphere,

5. a change in the amount of heat stored in the deep oceans.

It is rather difficult to detect what change is the effect of what cause, as the global temperature is a combination of the five causes that have different (response-)time scales. The causes 1 and 2 are beyond the scope of this chapter, whereas the causes 3, 4 and 5 are closely related to the geosphere-biosphere system on the Earth, which will probably cause the enhanced greenhouse effect.

3.3 Causes of temperature rise

In subsection 3.3.1, the physical process occurring in the atmosphere of the Earth causing the greenhouse effect is briefly described. In subsection 3.3.2, the origin of present greenhouse gases is subdivided into emission by natural processes and by human activities. In subsection 3.3.3, the most important feedbacks are discussed. In subsection 3.3.4, prognoses of greenhouse gases and atmospheric temperatures during the next century are summarized, using figures of the Villach II Conference, Austria, in 1985 [Oerlemans, 1989] and the IPCC[2] [Houghton et al., 1990].

3.3.1 Relation between greenhouse effect and temperature rise

Solar radiation that is not directly reflected warms up both atmosphere and the Earth's surface. Solar radiation, that reaches the Earth's surface, is partly absorbed by the Earth's surface (short-wave energy) and is partly reflected (determined by the reflection coefficient, called *albedo*). Part of the absorbed fraction is emitted as long-wave (infrared) radiation, which can subsequently be absorbed by the greenhouse gases. The amount of the short-wave energy absorbed by the Earth's surface depends on the state of the geosphere-biosphere system.

Temperature changes when the balance between incoming (short-wave) and outgoing (long-wave and short-wave) radiation energy is disturbed. The concentration of greenhouse gases is the most important factor that keeps the incoming and outgoing energy in balance. In case the concentration of greenhouse gases is higher, more emitted energy will be trapped in the atmosphere. As such, the higher level of greenhouse gases is considered as the main contributor that warms up the atmosphere of the Earth. This process is called the enhanced greenhouse effect.

3.3.2 Origin and concentration of greenhouse gases

Water vapour influences global warming in about the same order of magnitude as all other greenhouse gases together. The greenhouse gases are comprised in the so-called effective CO_2-concentration, since CO_2 is the most important of these gases from the viewpoint of affecting climate change. The other greenhouse gases, with the exception of water vapour, occur in much smaller concentrations than the CO_2-concentration, for instance 1.7 *p.p.m.* (*parts per million*) N_2O related to 350 *p.p.m.* CO_2 [Korevaar, 1989].

Greenhouse gases originate from both natural processes and from human activities. Water vapour (the concentration of which varies widely in space and time) is purely a natural factor, while CFCs, being of strictly anthropogenic origin, are purely artificial. The other greenhouse gases have concentrations that are influenced by human activities, but may also vary naturally as parts of the feedback of the climate system as a whole [Dickinson, 1986].

---

[2] The editors of chapter 9 Sea Level Rise are Warrick and Oerlemans.

Natural processes

The warming up and cooling of the Earth is a natural process, which can be seen in figure 3.2 where global temperatures since the Pleistocene on three time spans are given.
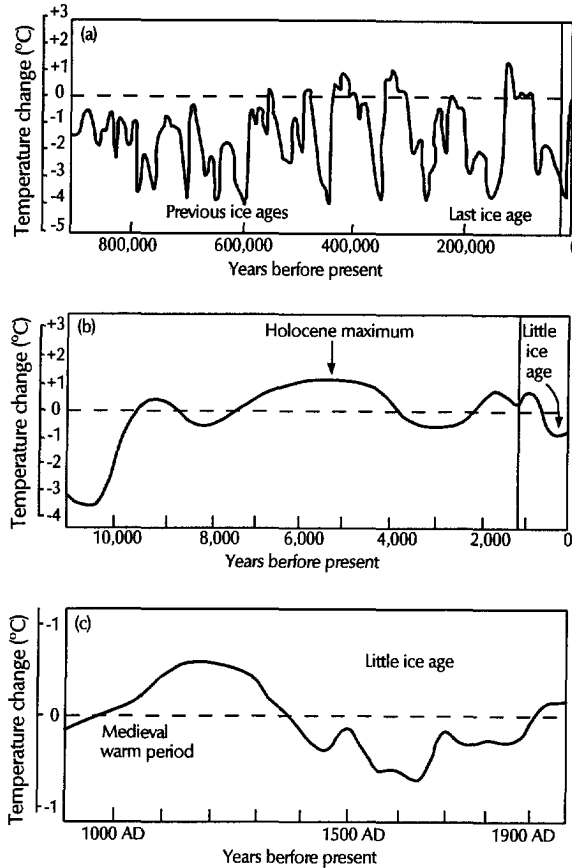
Figure 3.2: Global mean temperature variations since the Pleistocene on three time spans: (a) the last million years; (b) the last ten thousand years; and (c) the last thousand years. The dotted lines nominally represent conditions beginning 20th century. Modified from IPCC [Houghton *et al.*, 1990]. Copyright ©1990 Intergovernmental Panel on Climate Change, reprinted by permission of the Press Syndicate of the University of Cambridge.

The concentrations of natural greenhouse gases in the atmosphere have been built up in several millions of years. Due to, among others, the greenhouse effect of these gases, the climate was mild and made the Earth livable for some 3.5 billion years. Without these greenhouse gases, the Earth would now have a temperature of about -18 °C.

Until the Industrial Revolution, the CO_2-concentration, which is taken as the reference greenhouse gas in this chapter, was the result of the complex self-regulating geosphere-biosphere system. An enormous amount of CO_2 is stored as bicabonate in ocean water and as carbonate and biomass in sedimentary rocks, together some 200,000 times the amount of CO_2 in the atmosphere [Priem, 1989]. In this system, the biosphere plays a crucial role. In case the atmospheric CO_2-concentration would fall substantially below the present level, a worldwide cold period would set in. For instance, during the last Ice Age, the CO_2-concentration was 30 % lower than at the beginning of the Industrial Revolution. This was detected from air bubbles, locked in old ice-layers in Antarctica, e.g. at the station Vostok [Barnola et al., 1987] (figure 3.3).
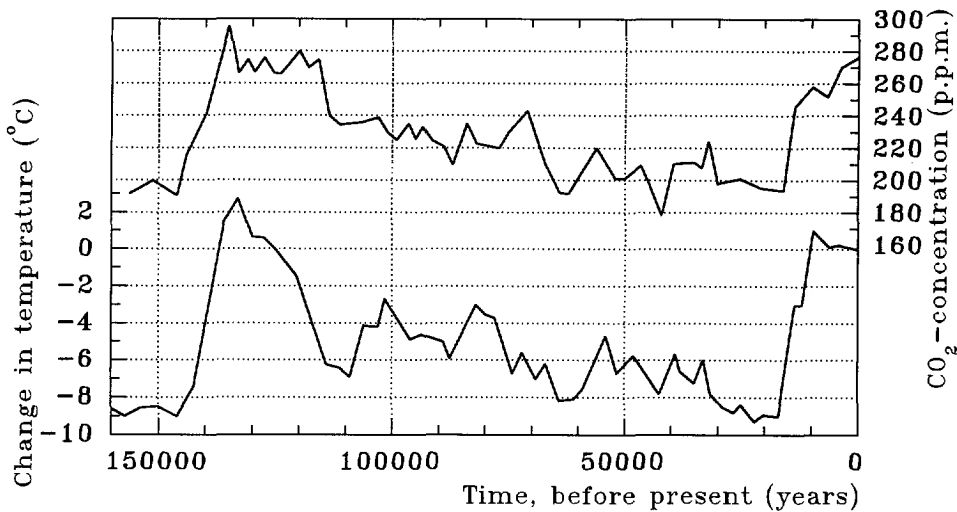

Figure 3.3: The CO_2-concentration and the change in atmospheric surface temperature in the Vostok area during the last 160,000 years. There appears to be a clear relationship. The data are based on ice samples, bored at the station Vostok, Antarctica [Barnola *et al.*, 1987]. Source: *Barnola, J.M., Raynaud, D., Korotkevich, Y.S. & Lorius, C. Vostok ice core provides 160,000-year record of atmospheric CO_2. Nature, 1 Oct., **329**: 408-411, p. 410.* Copyright ©1987 Macmillan Magazines, reprinted by permission of Macmillan Magazines.

The geosphere-biosphere system reacts as follows [Priem, 1989]. During the cold period, the sea is absorbing extra CO_2 and the biological activity as well as the intensity of the chemical erosion at the surface of the Earth is decreasing. As a result, less CO_2 is withdrawn from the atmosphere by formation of carbonate and biomass. Meanwhile, the supply of CO_2 has not been influenced by low temperatures at the surface of the Earth, as volcanic eruptions and geological processes in the Earth's crust kept on taking place. According to this straightforward scenario, the CO_2-concentration in the atmosphere is rising again after a while, and then the climate is warming up. In the course of this process, feedbacks counteract the increase of

the CO_2-concentration in the atmosphere. Currently, the regulating processes in the geosphere-biosphere system are reacting too slow to counteract the present increase of CO_2-concentration substantially.

Human activities

It is common knowledge that since the beginning of the Industrial Revolution at roughly 1850[3] the concentration of greenhouse gases has rapidly increased as a result of intensive human activities. The increasing concentration of greenhouse gases is especially due to deforestation and due to large-scale burning of biomass and fossil fuels (coal, mineral oil and natural gas). Some important contributors are industry, traffic and agriculture.

Anyway, since 1850, the CO_2-concentration increased by about 30 % [Oerlemans, 1993]. At this moment, the CO_2-concentration annually increases by about 0.4 %, the N_2O-concentration by 1 %, the CH_4-concentration by 0.25 % and the $CFCs$-concentration by about 5 % [Korevaar, 1989]. As a consequence of the increasing concentration of greenhouse gases, energy is absorbed and the atmospheric temperature has risen (figure 3.4). It should be noted that the global warming could be the effect of the recovery from the *Little Ice Age*, rather than a direct result of human activities. The Little Ice Age began about 450 years ago and came to an end only in the 19th century (see figure 3.2).
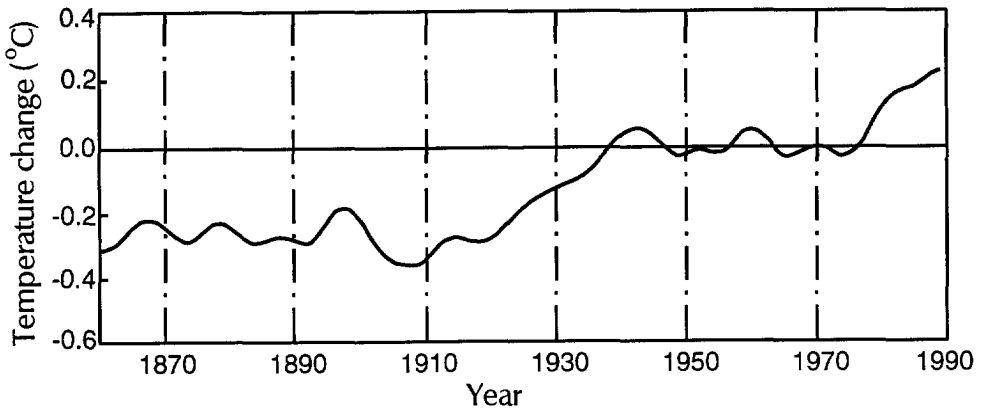
Figure 3.4: Global mean (combined land-air and sea-surface) temperatures 1861-1989, relative to the average for 1951-1980. Modified from IPCC [Houghton *et al.*, 1990]. Copyright ©1990 Intergovernmental Panel on Climate Change, reprinted by permission of the Press Syndicate of the University of Cambridge.

---

[3]Recently drilled ice cores from Greenland indicate that the increase of the concentration of greenhouse gases started earlier, around 1810, which could be the result of changes in land use and deforestation.

3.3.3 Feedbacks

Feedbacks affect the change in the concentration of greenhouse gases and consequently the temperature, as feedbacks are components in the geosphere-biosphere system. They can either counteract or amplify the rise in temperature. It is still quite unclear how most of the feedbacks react exactly to climate changes. Scientific research on the interaction between feedbacks is still in development. The six most important feedbacks are characterized as follows:

1. Influence of water vapour

    A higher concentration of the greenhouse gases will raise the temperature. Thus, more water vapour will enter the atmosphere by evaporation. More outgoing radiation energy is absorbed, and consequently, the temperature is raised even more. As such, this positive feedback amplifies global warming. According to some scientists, e.g. [Rind *et al.*, 1991], the influence of water vapour is underestimated in the so-called *general circulation models* (GCMs); it is of the same order of magnitude as the influence of all other greenhouse gases.

2. Influence of ice and snow

    Much of the solar radiation is absorbed at the Earth's surface. Therefore, the reflection coefficient (albedo) at the surface is the most important factor in determining the actual amount of absorbed solar radiation energy. The albedo may vary from as low as 0.02 (−) to higher than 0.95 (−), depending on the kind of surface [Dickinson, 1986]. In general, ice and snow surfaces have much higher albedos than most of the land surfaces and all water surfaces. Therefore, when temperature rises because of an increasing concentration of greenhouse gases, ice and snow will melt, and thus the extent of ice and snow surfaces on the world will decrease. The incoming solar radiation is reflected less, and as a result, the temperature at the Earth's surface rises even more. This positive feedback also amplifies global warming.

3. Influence of clouds

    Especially this feedback is unclear, because the following parameters of clouds are difficult to assess: cloud-thicknesses, fractional covers, altitudes of the tops of the clouds, liquid water contents, drop sizes and spacial scales. It is possible that future change in cloud properties could alter the net radiation budget of the climate system by either more absorption of outgoing energy or, possibly, by more reflection of incoming energy. Hence, clouds could either amplify or counteract the effect of the increased concentration of greenhouse gases [Dickinson, 1986].

    Ramanathan and Collins [1991] investigated the influence of clouds by measuring, with satellites, the radiation at the top of the atmosphere during the 1987 El Niño event. They found in that particular study that especially highly reflective cirrus clouds counteract the enhanced greenhouse effect.

4. **Influence of oceans**
   Still little is known about the role of oceans if the concentration of greenhouse gases increases. Scientists are familiar with the fact that oceans can absorb large amounts of CO_2, but the precise saturation level is unknown. A first assessment of the saturation level is that about half of what mankind emits in the atmosphere is absorbed by oceans [Zwerver, 1989]. If this is correct, oceans are a reservoir for positive feedback. They counteract the rise of the concentration of greenhouse gases and consequently the rise of temperature.

   Another important aspect of oceans in case of climate change is the possibility that the directions of ocean currents (e.g. the Atlantic conveyor) may alter, which could have great affects on 'regional' climates. For instance, note that the North Atlantic Drift (Gulfstream) is essential for the climate in Western Europe.

5. **Influence of permafrost**
   By warming up permafrost, which are permanently frozen soils occurring at high northern latitudes such as in Canada and Siberia, more methane (CH_4) will enter the atmosphere, which will amplify the greenhouse effect.

6. **Influence of volcanic activities**
   Volcanic eruptions bring, apart from solid material, large amounts of dust particles and gases in the atmosphere. Together with the dust particles emitted by burning biomass and fossil fuels, the volcanic dust will reflect incoming energy. As a result, the greenhouse effect could be counteracted. Furthermore, dust particles form the cores of cloud drops that may probably reflect sunlight (see also item 3.). Anyway, the influence of these *aerosol particles*, which are solid or liquid particles in the size range 0.001-10 μm radius, on cloud processes and thus on the radiation budget of the climate system is very difficult to assess.

3.3.4   Future CO_2-concentration and temperature rise

It is not yet possible for the scientific community to detect statistically significant effects on climate of changing concentrations of greenhouse gases, though the observed global-scale warming experienced over the past century is compatible with model estimates. Hence, in order to avoid this uncertainty, several scenarios have been applied for the future development of the concentration of greenhouse gases.

   Evaluating the results of the GCM's leads to the conclusion that the increase in global mean temperature due to a doubling of the atmospheric CO_2-concentration (referred to as the *climate sensitivity*) is likely to be in the range of 1.5-4.5 °C. This well-known scenario is formulated at the Villach II Conference, Austria, in 1985 [Bolin *et al.*, 1986]. The temperature scenario for the next century of the Villach II Conference is illustrated with a probability range in figure 3.5. Although no value in the range of uncertainty (1.5-4.5 °C) can be excluded, it is plausible that the increase
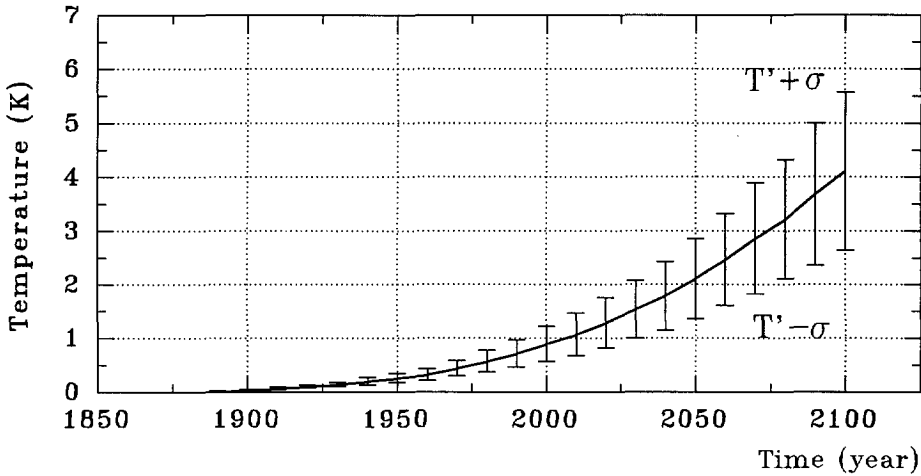
Figure 3.5: The temperature scenario: the outcome of the Villach II Conference discussion. Vertical bars indicate the standard deviation. Modified from Oerlemans [1989]. Source: *Oerlemans, J. A projection of Future Sea Level. Clim. Change*, **15**: 151-174, p. 155. Copyright © 1989 Kluwer Academic Publishers, reprinted by permission of Kluwer Academic Publishers.

in temperature may be found in the lower half of this range. This range is valid in case the present trend of emission of greenhouse gases is continuing.

Another widely known scenario was suggested by the Working Group 1 of the IPCC. The IPCC [Houghton *et al.*] predicted in 1990:

> *"under the IPCC Business-as-Useful (Scenario A) emissions of greenhouse gases, a rate of increase of global mean temperature during the next century of about 0.3 °C per decade (with an uncertainty range of 0.2 °C to 0.5 °C per decade), which is greater than that seen over the past 10,000 years..."*

Furthermore, the IPCC presents three other emission scenarios of the greenhouse gases for the next century. In these scenarios, a broad range of possible controls to limit the emission of greenhouse gases is suggested, and various levels of technological development and environmental controls are described. The rate of increase in global mean temperature is for:

- Scenario B, Low Emission: 0.2 °C *per decade*,

- Scenario C, Control Policy: just above 0.1 °C *per decade*,

- Scenario D, Accelerated Policy: about 0.1 °C *per decade*.

3.4   Causes of sea level rise

An important consequence of the increase of global mean temperature is sea level rise. Four physical processes relate the change in sea level to the change of atmospheric temperature:

1. Thermal expansion of ocean water

Thermal expansion of ocean water is an important factor contributing to sea level rise, depending on the temperature level and the salt concentration of the ocean water. For instance, a layer of ocean water of 100 m thickness at a temperature of 25 $^{\circ}C$ will expand 3 *cm per degree temperature rise*, while a layer of ocean water of 100 m thickness at a temperature of 0 $^{\circ}C$ will only expand 0.5 *cm per degree temperature rise*. Because the warming up of deep ocean layers is a long-term process (it takes at least some centuries), sea level rise during the next centuries is mainly due to thermal expansion of the upper ocean layers of only a few hundred metres thickness.

2. Melting of mountain glaciers and small icecaps

Although mountain glaciers and small icecaps contain only a small part of the total ice mass on Earth (see table 3.1), they are located in warmer climates than the polar ice sheets of Greenland and Antarctica. Therefore, these ice masses are more active and react more quickly to climate change [Oerlemans, 1989]. Since the beginning of the Industrial Revolution, a great number of mountain glaciers has shown a withdrawal of their tongues. In figure 3.6a, a few long records are displayed, showing variations in glacier length. Despite the fact that data of essential mountain glaciers such as in the Andes, Himalaya and Alaska are rare, the impression is that the withdrawal of glacier tongues is worldwide (see figure 3.6b).

The main reason for this withdrawal appears to be that temperature rise melts glacier tongues. Because the albedo of the ice surfaces is great (about 0.3), glacier tongues are quite sensitive to changes in the net radiation budget of the climate system. Moreover, the incoming short-wave radiation is more intensive than before because of two processes. First, as the concentration of $CFCs$[4] increases, the thickness of the ozone layer reduces, and as a result the incoming radiation increases. Second, since the beginning of this century, the number of volcanic activities has been small. As a result, less dust is in the atmosphere, and hence, the incoming radiation is greater than before this century.

3. Accumulation on and ablation of polar ice sheets

The polar ice sheets of Greenland and Antarctica will also react to climate change. These ice sheets differ from the mountain glaciers and small icecaps due to other

---

[4]On a molecule-for-molecule basis, e.g. $CFC-11$ is about 12,000 times more effective than CO_2, whereas methane is about 21 times more effective than CO_2 [IPCC Houghton *et al.*, 1990].

Table 3.1: Some characteristics of the polar ice sheets of Greenland, Antarctica and mountain glaciers and small icecaps. Data from Wilhelm [1975], Flint [1971], Ambach [1980], Radok [1982], Drewry [1983] and Orheim [1985]. From Oerlemans [1989].

Characteristic	Antarctica	Greenland	Glaciers & Icecaps
Area $(10^6\ km^2)$	11.97	1.80	0.60
Volume $(10^6\ km^3)$	29.33	3.00	0.18
Mean thickness (m)	2488	1667	300
Largest thickness (m)	4700	3400	–
Mean elevation (m)	2000	2080	–
Sea level rise at entire melting (m)	65	7.5	0.50
Accumulation (km^3/yr)	2200	500	–
Losses of ice by calving (% of loss)	99	58	–
Losses of ice by melting (% of loss)	1	42	–

physical characteristics (see table 3.1). A higher atmospheric temperature will not immediately imply smaller ice masses on these ice sheets. This depends on the surface temperature above the polar ice sheets.

For most geographical and climatological conditions (when surface temperature is not too low), increasing air temperature indeed implies decreasing ice masses. This is the case for the Greenland Ice Sheet and the edges of the Antarctic continent. By contrast, for the coldest polar regions, particularly over Central Antarctica, the annual surface air temperature is very low and it limits snow (or rime) accumulation. When the annual surface air temperature above Central Antarctica increases, the saturation vapour pressure will increase also. Scientists suggest that the atmosphere above Central Antarctica will then contain more water vapour, and as a consequence, ice masses will accumulate. This leads to the situation that ice masses would increase with air temperature.

Recent computations suggest that the net effect is small: the accumulation of snow on Central Antarctica and the ablation on Greenland and the edges of the Antarctic continent are somewhat in balance. However, this is a temporary situation. In the long run (centuries to millennia, if the warming would last that long), mass loss on Greenland will probably dominate [Oerlemans, 1993]. Meanwhile, there are scientists [e.g. Miller and De Vernal, 1992] who predict that global warming could lead to an accumulation on polar ice-sheets. This would dominate all other contributions during global warming, resulting in a possible sea level fall of -0.7 m/c.

4. Disintegration of West Antarctic Ice Sheets

During the first period of attention for the issue of greenhouse effect and sea level rise, several authors, such as Mercer, Thomas *et al.*, Lingle and van der Veen [from IPCC, Houghton *et al.*, 1990], have argued that the West Antarctic Ice Sheets (WAIS)
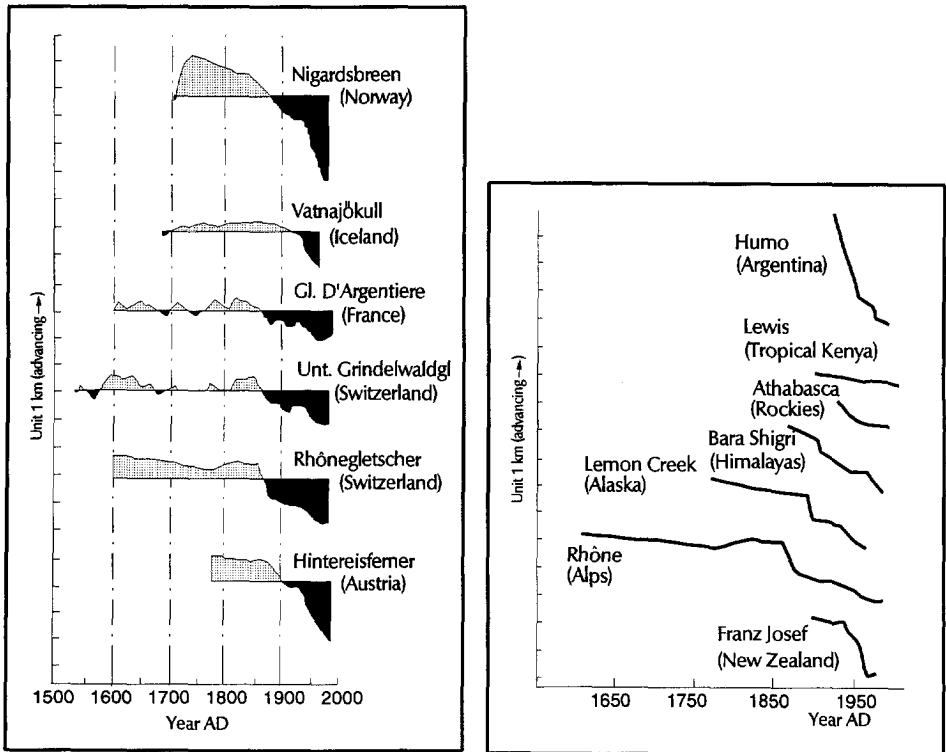
Figure 3.6: Historic variations in the length of some glaciers throughout: (a) Europe, and (b) the world over the last centuries. From IPCC [Houghton *et al.*, 1990]. Ad a.: Data from Bjornsson [1979]; Ostrem *et al.* [1977]; Kasser [1967, 1973]; Kasser and Haeberli [1979]; Muller [1977]; Vivian [1975] and Haeberli [1985]. The position of the glacier tongue is given, relative to the axis that is determined by the average position of the glacier tongue during the whole record. Ad b.: Data from Grove [1988] and other sources. Copyright ⓒ1990 Intergovernmental Panel on Climate Change, reprinted by permission of the Press Syndicate of the University of Cambridge.

(figure 3.7) might be sensitive to small variations in sea level or melting rates of the ice shelves. Then, it might be possible that grounded ice starts to float, which could be the beginning of the disintegration of the WAIS, resulting in a sea level rise of 5 to 6 *m* within a few centuries. Though many aspects still need more research, the present consensus is that the early estimates of the sensitivity of the WAIS were exaggerated.
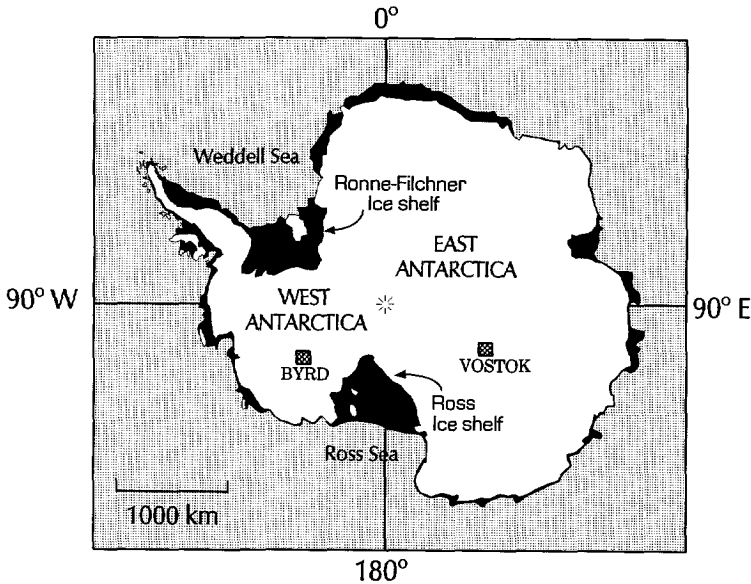
Figure 3.7: Map of Antarctica. The following areas can be distinguished: Central Antarctica ('East Antarctica') with the station Vostok; the two major West Antarctic Ice Sheets: the Ronne-Filchner ice shelve and the Ross ice shelve (the two large black areas); and some smaller polar ice sheets at the edges of the Antarctic continent.

3.5   Sea level variations in the past

Since the creation of the Earth, climate, atmospheric temperature and thus sea level have changed. By analysing sea level variations during different periods of time in the past, the mechanisms involved are better understood. Accordingly, scientists may be able to give more reliable prognoses of sea level rise.

In this section, the variations in sea level during three different periods in the past are presented: (1) the Cenozoic: Tertiary and Quaternary periods; (2) the Holocene; and finally (3) the last few centuries.

ad 1. The Cenozoic: Tertiary and Quaternary periods

Cycles of cold periods on the Earth (Ice Ages) alternated by warm periods (interglacial eras) have already occurred for many millions of years. For instance, the Quaternary is characterized by an alternation of several warmer and colder phases, whereas the uppermost cold phases (Elsterian, Saalian, Weichselian) comprise some interphases of less severe cold [Zagwijn *et al.*, 1986].

Figure 3.8 shows the relative sea level variations during the Tertiary and Quaternary periods. The sea level during the Early Tertiary period was, in general, higher
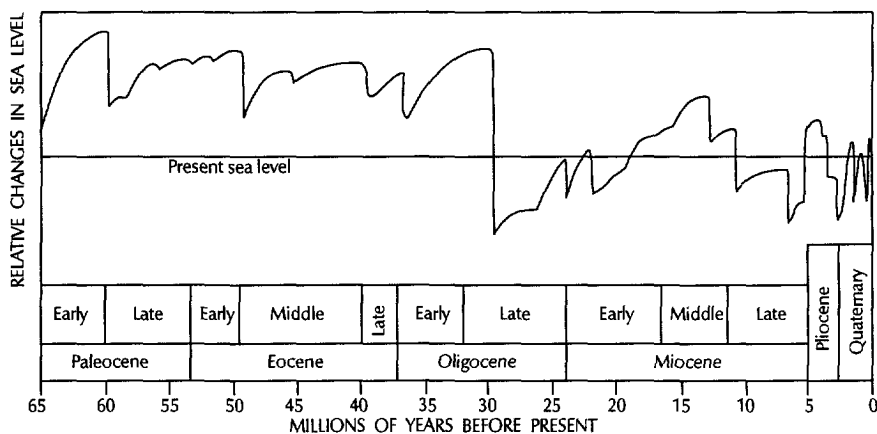
Figure 3.8: Relative sea level curve during the Cenozoic: Tertiary and Quaternary periods. Modified from Vail, Mitchum, and Thompson [1977], figure 3. From Meisler *et al.* [1984].
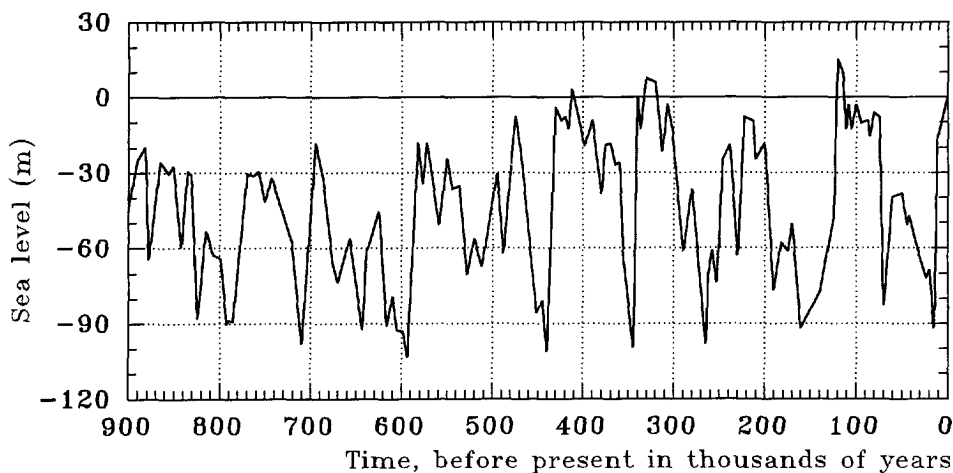
Figure 3.9: Sea level curve. Modified from Zellmer [1979], figure 17. From Meisler *et al.* [1984].

than during the Late Tertiary period. Figure 3.9 displays the sea level during the last 900,000 years, when the mean sea level was approximately 45 m below present $M.S.L.$. It is clear that the present sea level has a high position.

ad 2. The Holocene

At this moment, the Earth finds itself in an interglacial era. The last Ice Age the Weichselian lasted for 60,000 years. Since the beginning of the Holocene era (about 10,000 year ago), the climate has become warmer. As a result, sea level has risen. As can be seen in figure 3.1, the Netherlands are situated in the sea-level zone 2. In figure 3.10 a more detailed time-depth diagram for the Netherlands is shown with the sea level trend curves during the last 8000 years [van de Plassche, 1982a, 1982b]. It shows that during the last millennia, sea level rose less than during the first millennia of the Holocene. Keeping this in mind, it is remotely possible that sea level will rise several tens of metres during the next millennia, because the amounts of ice masses stored in mountain glaciers, small icecaps and in the polar ice sheets of Greenland and Antarctica, which will participate in the melting process, are relatively small.
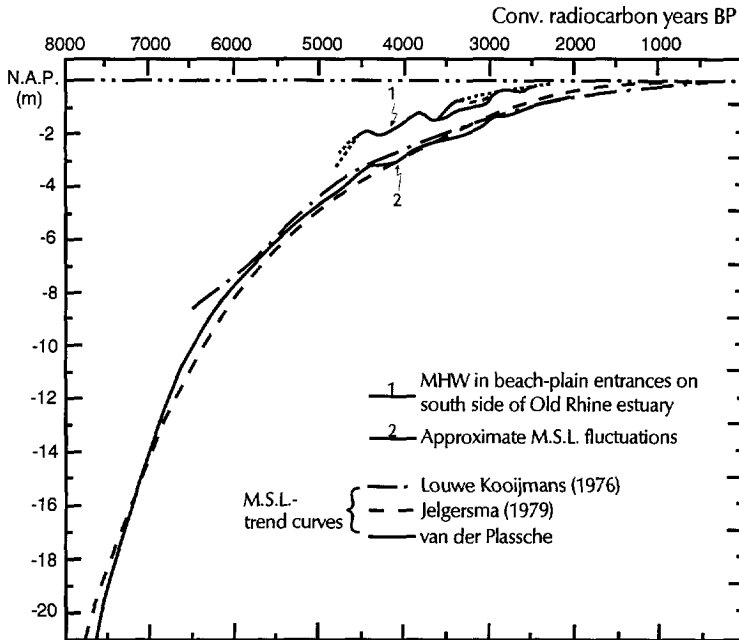
Figure 3.10: Time-depth diagram with sea level trend curves for the Netherlands, developed by Louwe Kooijmans [1976], Jelgersma [1979] and van de Plassche [1982]. From van de Plassche [1982a, 1982b]. Source: *Mededelingen Rijks Geologische Dienst, Vol. 36-1, p. 85*. Reprinted with permission of van de Plassche and the Rijks Geologische Dienst.

A promising pilot area in the world for research on the possible impacts of the global sea level rise is the Caspian Sea, which has a present level of about -28 m with respect to $M.S.L.$. During the Holocene, the Caspian Sea has shown great sea level oscillations, probably due to eustatic and isostatic changes [Pirazzoli, 1991]. The sea

water level in the Caspian Sea was subject to at least four major oscillations of 5 to 10 m for the last 10,000 years. Especially during historic times, strong sea level fluctuations have occurred in the Caspian Sea. For example, during the last decade the sea level has risen one metre.

ad 3. The past few centuries

Since about the beginning of the Industrial Revolution, a deviation in the trend of sea level rise can be detected. This is illustrated for example in figure 3.11, where the mean sea levels of Amsterdam, Brest, Den Helder and 'Global', explicitly show a deviation in the trend of sea level rise.
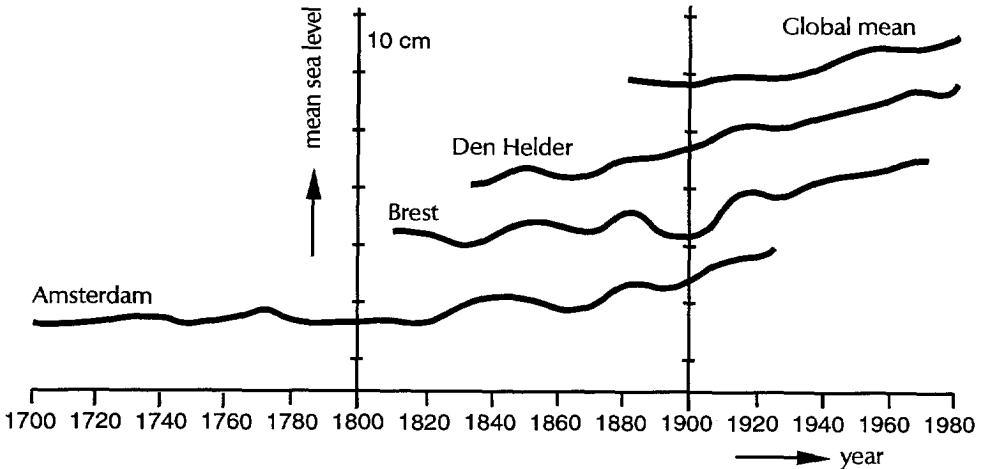
Figure 3.11: Mean (eustatic) sea levels of Amsterdam, Brest, Den Helder and Global mean, put together in one figure. The sea levels of Amsterdam are measured till 1932, when the inlet of the IJsselmeer (former Zuiderzee) was closed by a dam (the so-called Afsluitdijk). The Global mean sea level is derived by Gornitz *et al.* [de Ronde, 1988]. By courtesy of de Ronde.

Table 3.2 shows the results of various scientists who have estimated the change in mean 'global' sea level during the past century. In conclusion, the sea level has risen about 10 à 20 *cm per century* during the period 1880-1980, whereas no author gives a sea level rise of more than a few decimetres over this period. Barnett's estimates show that during the past fifty years sea level has risen faster than during the first fifty years of the period 1880-1980.

The estimates of the IPCC [Houghton et al., 1990] have the same tenor. The panel judges that:

> "*the average rate of rise over the last 100 years has been 1.0-2.0 mm per year.*"

Table **3.2**: Estimates of mean 'global' sea level increase. From Lisitzin [1974]; Barnett [1983]; Robin [1986] and IPCC [Houghton *et al.*, 1990].

Author	Rate (cm/c)	Comments
Thorarinsson [1940]	> 5	Cryologic Estimate
Gutenberg [1941]	$11 \pm 8\ddagger$	1807-1939 (69 stations)
Kuenen [1950]	$12 - 14$	-1942 Different Methods
Lisitzin [1958]	$11.2 \pm 3.6\ddagger$	1807-1943 (six stations)
Wexler [1961]	11.8	Cryologic Estimate
Fairbridge & Krebs [1962]	12	1900-1950 (selected stations)
Emery *et al.* [1980]	30	1935-1975 (many stations)
Gornitz *et al.* [1982]	$12^\star$	1880-1980 (many stations)
Klige [1982]	15	1900-1975 (many stations)
Barnett [1983]	$15.1 \pm 1.5\dagger$	1903-1969 (selected stations)
Barnett [1984]	$14.3 \pm 1.4\dagger$	1881-1980 (many stations)
Barnett [1984]	$22.7 \pm 2.3\dagger$	1930-1980 (many stations)
Gornitz & Lebedeff [1987]	$12 \pm 3\dagger$	1880-1982 (130 stations)
Barnett [1988]	11.5	1880-1986 (155 stations)
Peltier & Tushingham [1989, 1990]	$24 \pm 9\ddagger$	1920-1970 (40 stations)
Trupin & Wahr [1990]	$17 \pm 1.3\ddagger$	1900-1980 (84 stations)

$\star = 12\ cm/c$ is the uncorrected value: $10\ cm/c$ is corrected for crustal motion
     (long range trends, e.g. residual isostatic uplift of continents).
$\dagger =$ value plus 95 % confidence interval.
$\ddagger =$ mean and standard deviation.

and that

> *"there is no firm evidence of accelerations in sea level rise during this century (although there is some evidence that sea level rose faster in this century compared to the previous two centuries)."*

3.6   Predictions of future sea level rise

It is difficult to prove what part of sea level rise is the result of climate changes caused by human activities or by natural processes. For instance, in order to detect the specific part of sea level rise caused by human activities, scientists should detect about one millimetre sea level rise per year in a wave-amplitude of e.g. one metre. Therefore, it will probably take quite a few years before the scientific community can statistically confirm that an accelerated sea level rise occurs due to human activities. As a first step towards a persuasive confirmation, variations in sea level should be observed more intensively through related tide gauge networks around the world.

Even so, many scientists have even so attempted in the meantime to predict the rise in sea level, especially for the next century.

First, in this section, the two processes are described that determine the prognoses of the future sea level rise. Second, the different contributions to the sea level rise (see also section 3.4) are specified for one particular prognosis. Third, some prognoses of future sea level rise for some specific years are given. Finally, future sea level rise scenarios are selected, that are applied in the procedure of numerical groundwater modelling.

Processes of future sea level rise

The two processes that determine the prognoses of sea level rise are:

1. **Natural processes**

   Natural changes in climate with short (order of decades or centuries) and long (order of millennia) *response-time scales* will influence the future sea level rise. Although sea level has not risen much during the past millennia (see figure 3.10), still no steady state situation is reached.

   Short response-time scale processes are associated with upper oceanic layers and adjustment of small glaciers. Response-time scales of the order of a century are associated with deeper oceanic layers and larger glaciers.

   Long response-time scale processes are the melting of continental ice sheets and resultant adjustment of the Earth's crust to changing ice loading, which could lead to relative sea level rise [Robin, 1986]. For instance, since the end of the last Ice Age Scandinavia is rising, whereas, at this moment, some parts near the Dutch coast (Noord-Holland and the area near Rotterdam) are falling more than -0.08 m/c [Noomen, 1989]. This process of land-subsidence is indirectly taken into account in the scenario **g. land-subsidence** in section 9.3. In most cases, however, land-subsidence is small in the Netherlands and it can be neglected with respect to the sea level rise.

2. **Human activities**

   Human activities, such as the extra emission of greenhouse gases, accomplish the changes in climate. They are probably amplifying the greenhouse effect. Therefore, in addition to sea level rise caused by natural processes, sea level is now also rising due to human activities. The response-time scale appears to be short, just in the order of decades.

   According to Sahagian *et al.* [1994], anthropogenic contributions have lead to at least a third of the observed sea level rise in the twentieth century. They have evaluated that human activities, such as storing water in reservoirs (which results in a sea level fall), deforestation, groundwater withdrawal, surface water diversion, destruction of wetlands and land-use changes, have directly affected the level of the sea.

Contributions to future sea level rise

Some scientists, such as Oerlemans [1989, 1993], predict the future sea level rise by subdividing the contributions into the four groups of section 3.4: In figure 3.12, the predicted contributions to changing sea level is demonstrated in case of the 1985 Villach II temperature scenario (figure 3.5). The most important contribution appears to be the thermal expansion of ocean water, directly followed by the melting of mountain glaciers and small icecaps. The contributions of Greenland, Antarctica and the West Antarctic Ice Sheets almost compensate each other. Since for the 1985 Villach II temperature scenario (figure 3.5) a standard deviation is given, also the probability distributions of sea level rise can be determined. This is done in figure 3.13: it indicates how rapid uncertainties of the prognosis of future sea level grow in time [Oerlemans, 1989].
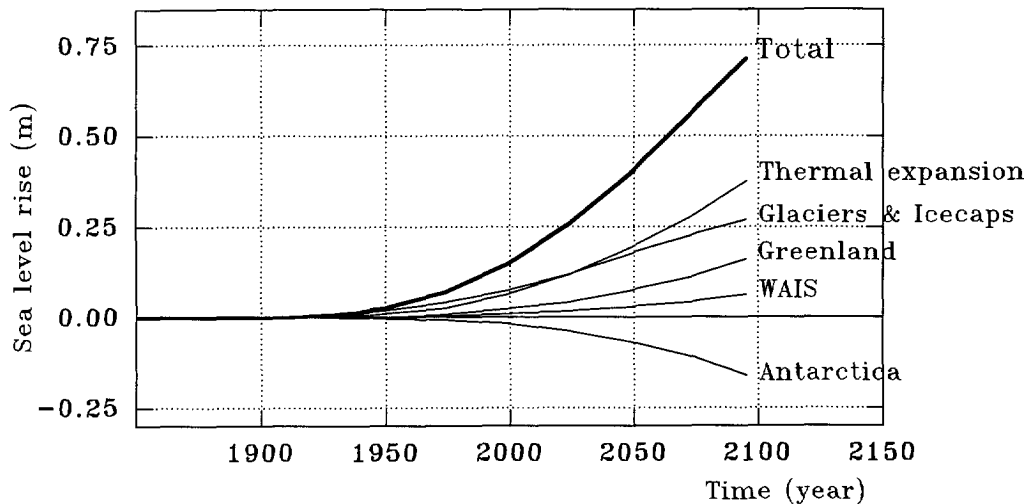

Figure 3.12: Estimated contributions to sea level change for the 1985 Villach II temperature scenario of figure 3.5. Modified from Oerlemans [1989]. Source: *Oerlemans, J. A projection of Future Sea Level. Clim. Change*, **15**: *151-174, p. 167*. Copyright © 1989 Kluwer Academic Publishers, reprinted by permission of Kluwer Academic Publishers.

Still, some scientists suggest that global warming might lead to growing of ice-sheets. For instance, Miller and De Vernal [1992] examined a recent geological record of 130,000 years to present. They found that accumulation on ice-sheets by ice-sheet growth at high northern altitudes (65-80°N) occurred for climate conditions at the begin of the last glacial cycle, under climate conditions rather similar to the present conditions. As a result, they suggest that this accumulation on polar ice-sheets can contribute to sea level rise with a (negative) rate of up to -0.7 m/c.
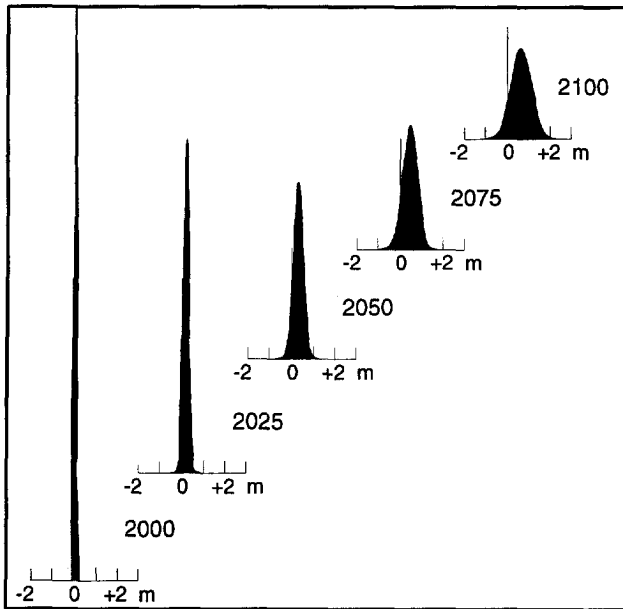
Figure 3.13: Probability distributions of sea level relative to 1985, for some selected times. From Oerlemans [1989]. Source: *Oerlemans, J. A projection of Future Sea Level. Clim. Change,* **15**: *151-174, p. 169.* Copyright © 1989 Kluwer Academic Publishers, reprinted by permission of Kluwer Academic Publishers.

Prognosis of future sea levels for some specific years

It is easy to understand that, after analysing quite a few prognoses of sea level rise, the prognoses by scientists are not very consistent, as so many mechanisms that determine the sea level rise are quite indistinct.

In table 3.3 a few prognoses of the future sea level rise at specific years are summarized. Because many prognoses are calculated with different scenarios and parameters, a straightforward comparison is not entirely possible. Various other prognoses of sea level rise (without projections in specific years) are:

- Revelle predicted in 1983 that the sea level rise is likely to be 70 *cm* in 2085 relative to 1980. He ignored (and not added) the impact of global warming on Antarctica, though he noted that the latter contribution is likely to be 1 to 2 *m/c* after 2050 [Titus, 1987].

- The USA National Academy of Science Polar Research Board [1985] predicted a sea level rise between 50 and 200 *cm* in 2100 relative to 1980 [Titus, 1987].

- Robin [1986] estimated, based on a linear relation between sea level change and global temperature trend), that:

Table 3.3: Comparison of prognoses of future sea level rise in *cm* relative to 1980, except for the prognosis of Oerlemans which is relative to 1985.

Author	2000	2025	2050	2075	2100
Extrapolation of historic data[a]	2-3	4.5-6.8	7-10.5	9.5-14.3	12-18
Hoffman *et al.* [1984]:[b]					
- Conservative Scenario	4.8	13.0	23.8	38.0	56.2
- Mid-range Moderate Scenario	8.8	26.2	52.3	91.2	144.4
- Mid-range High Scenario	13.2	39.3	78.6	136.8	216.6
- High Scenario	17.1	54.9	116.7	212.7	345.0
Robin [1986][c]		25.1	52.6	70.8	89.1
Oerlemans [1989]		20.5	33.0	50.5	65.6

[a] The historical sea level rises have been estimated by Barnett [1983] and Gornitz *et al.* [1982]: 10 à 15 *cm per century* in the period 1880-1980. The data are based on measurements of sea level variations with tidal gauges at particular locations over the past century.

[b] Hoffman *et al.* [1984] made projections of sea level rises for the next century at intermediate years, based on special case scenarios for changes in greenhouse gases. They assumed that the glacial contribution would be one to two times the contribution of thermal expansion.

[c] These prognoses were calculated by Robin from the sea level-time regression (linear relationship) to estimate sea level rise for a 3.5 K warming [Oerlemans, 1989].

"the prediction of global warming of $3.5°C \pm 2.0°C$ due to CO_2 doubling over the next century would lead to a sea level rise of 80^{+85}_{-60} cm."

- In the statement of the Villach II Conference, Austria, in 1985 the following future sea level rise is predicted:

  "on the basis of observed changes since the beginning of this century, global warming of $1.5°C$ to $4.5°C$ would lead to a sea-level rise of 20-140 centimeters" [Bolin, 1986].

The following future sea level rises are presented in two impact studies that predict the effects of climate change on society:

- In the ISOS-study (see subsection 2.5.2) [Wind, 1987; Delft Hydraulics, 1988], the following three scenarios of sea level rise are proposed for the period 1990-2090: (1) the high scenario 85 *cm*, (2) the middle scenario 60 *cm*, and (3) the low scenario 35 *cm*.

- In IMAGE (see subsection 2.5.2), four different scenarios for emissions of the most important greenhouse gases are applied to determine the future sea level

rise (see table 3.4).

Table 3.4: Four scenarios of future sea level rise in the period 1985-2100, as input in the IMAGE model (in *cm* relative to 1985). From den Elzen and Rotmans [1988].

Scenarios of greenhouse gases in IMAGE	2000	2025	2050	2075	2100
Scenario A: unrestricted trends	6.7	21.1	38.9	61.1	86.5
Scenario B: reduced trends	6.3	18.7	33.6	50.5	67.8
Scenario C: changed trends	6.0	17.8	28.8	41.3	53.8
Scenario D: forced trends	5.8	15.8	24.5	33.2	41.8

Finally, the prognoses of the IPCC are given in table 3.5. The IPCC employs simple models to calculate the rise in sea level to the year 2100, relative to 1990. The best estimate of global mean sea level rise under the IPCC Business-as-Usual emission scenario A is about 60 *cm* over the next century with an uncertainty range of 30 to 100 *cm per century*. Note that the rise will not be linear in time, but is supposed to accelerate as a function of time. In table 3.5, also the best estimates of sea level rise of the three other policy emission scenarios of the greenhouse gases are given.

Table 3.5: Four scenarios of future sea level rise in the period 1990-2100, determined by the IPCC (in *cm* relative to 1990). From IPCC [Houghton *et al.*, 1990].

Greenhouse gases scenarios in IPCC		2030	2070	2100
	high	29	71	110
Scenario A: Business-as-Usual	best estimate	18	44	66
	low	8	21	31
Scenario B: Low Emission	best estimate	16	32	47
Scenario C: Control Policy	best estimate	15	29	40
Scenario D: Accelerated Policy	best estimate	14	26	34

Scenarios of future sea level rise

As could be seen, many prognoses of future sea level rise are possible. In order to reckon with all realistic prognoses, six *sea level rise scenarios* are selected:

1. no sea level rise,

2. a sea level fall of -0.6 *m/c*,

3. a *natural* sea level rise of 0.15 *m/c*,

4. a sea level rise of 0.6 m/c, which is the best estimate according to the IPCC [Houghton *et al.*, 1990] during the next century,

5. a sea level rise of 1.0 m/c,

6. an *extreme* sea level rise of 1.5 m/c,

In the procedure of numerical groundwater modelling, all six sea level rise scenarios are applied in chapter 8, whereas only the scenarios (1), (2) and (4) are applied in chapter 9 to arrive at a comprehensive view over the results of the simulations.

3.7 Conclusions

Climate changes especially because of disturbances in the balance of incoming and outgoing radiation energy. The concentration of greenhouse gases in the atmosphere influences the energy balance. The higher the concentration of greenhouse gases in the atmosphere, the more energy is absorbed by the atmosphere. As a result, the atmosphere will warm up: this is the greenhouse effect. Of all greenhouse gases, carbon dioxide (CO_2) is the most important greenhouse gas, though water vapour influences the greenhouse effect in about the same order of magnitude as all other greenhouse gases together.

When the temperature rises, feedbacks such as ice and snow, water vapour and permafrost substantially amplify the greenhouse effect. On the other hand, the scientific community believes that the oceans counteract the greenhouse effect, because large amounts of CO_2 and heat can be stored into the deep oceans. Furthermore, the influence of clouds on the greenhouse effect is still too indistinct, though several scientists assume that clouds counteract the greenhouse effect.

Until the beginning of the Industrial Revolution, a complex self-regulating geosphere-biosphere system had determined the concentration of the greenhouse gases. However, from about 1850 on, human activities have increased the concentration of greenhouse gases in the atmosphere due to deforestation, changes in land use, and burning of biomass and fossil fuels. Scientists predict that as a result of human activities, between 2050 and 2100 the concentration of greenhouse gases in the atmosphere will probably have doubled compared to that at the beginning of the Industrial Revolution. As a result of the established enhanced greenhouse effect, the temperature will probably have risen approximately 3 °C with an uncertainty range of 1.5-4.5 °C.

An important consequence of global mean temperature rise is sea level rise. The following physical processes contribute to sea level rise: thermal expansion of ocean water; melting of mountain glaciers and small icecaps; and ablation of polar ice sheets. Note that accumulation on polar ice sheets contributes to sea level fall, whereas the present consensus is that the West Antarctic Ice Sheets do not disintegrate during the next century. At the beginning of the Holocene, which started about 10,000 year ago, the sea level has risen a few tens of metres within a geologically short period of

some millennia. By contrast, during the last three millennia, the sea level has not risen more than a few decimetres. In the period 1880-1980, the sea level has risen only about 10 à 20 *cm per century*.

As the present era is an interglacial, the level of the sea is already high and relatively small amounts of ice masses are stored. Therefore, a sea level rise of only several decimetres for the next century is to be expected. The present range of predictions of the future sea level rise for the next century is rather consistent: in the range of 30 to 100 *cm*. The main contributors to this sea level rise will be thermal expansion of ocean water as well as melting of mountain glaciers and small icecaps, whereas accumulation on and ablation of polar ice sheets are supposed to be in balance.

Chapter 4

Selection of a suitable model

4.1 Introduction

Groundwater flow models applicable in this study are devices which are able to simulate groundwater flow regimes along the Dutch coast. Mostly non-uniform density distributions occur in these Dutch geohydrologic profiles with Holocene and Pleistocene deposits of marine and fluviatile origin, as the present situation is the result of various processes during geological history [e.g. Meinardi, 1973; Maas, 1989].

Only three groundwater flow models, which are capable of simulating the relevant processes involved, have been selected for further analysis: the adapted MOC model (Method Of Characteristics), SUTRA (Saturated-Unsaturated TRAnsport) and SWICHA. The adapted MOC model and SUTRA are two-dimensional models, whereas SWICHA is a three-dimensional model. In this chapter, it is demonstrated that the adapted MOC model is preferred above SUTRA and SWICHA. Simulations will show that only this adapted MOC model is capable of simulating the actual hydrodynamic dispersion by means of small dispersivities, whereas the other two models cannot accurately match calculated salinity profiles with observed ones. These shortcomings of SUTRA and SWICHA are caused by numerical approximations in the process of spatial discretization, resulting in severe numerical dispersion and oscillation[1].

In section 4.2, various models and solution techniques, that are capable of handling variable density groundwater problems, are summarized. In section 4.3, the program of requirements of suitable models is specified. In section 4.4, truncation and oscillation errors, which occur in groundwater flow models, are briefly discussed. In section 4.5, the influence of longitudinal dispersivities on the solution is pointed out by simulation of the groundwater flow in a profile through Noord-Holland with the three selected models. Finally, the choice of the adapted MOC model, preferred above SUTRA and SWICHA, is argued in section 4.6.

---

[1] Oscillation means that the maximum and minimum solute concentrations, that are originally inserted in the model, are over and undershot.

4.2   Enumeration of groundwater flow models

In the past, the behaviour of density dependent groundwater flow has been investigated by means of *analogue models* (e.g. the Hele Shaw model and electric models [Bear, 1972]) as well as by means of models which apply analytical methods (e.g. the hodograph method).

Since computers appeared on the scene, *mathematical models*[2] gained ground. At present, a large number of mathematical models is available, which are capable of handling fresh and saline groundwater flow in aquifer systems. They are subdivided into *analytical* and *numerical models*. The analytical models are based on (e.g. Laplace) transformations and the hodograph method (conformal mapping), whereas numerical models are based on computer codes. A computer code solves (partial differential) equations by means of numerical methods on a digital computer.

Sharp interface models: Badon Ghyben-Herzberg principle

The Badon Ghyben-Herzberg principle (see also subsection 2.4.2) can be applied to gain a clear insight in the behaviour of fresh and saline groundwater, though some restrictions on the applicability of the principle should be considered. Two restrictions are mentioned here.

First, the Badon Ghyben-Herzberg principle only approximates the actual occurrence of fresh, brackish and saline groundwater in the subsoil. The principle can only be applied in case the brackish zone between fresh and saline groundwater is only a few percents of the thickness of the saturated freshwater body. Subsequently, the situation can be schematised by a fresh-salt interface. In practice, the maximum thickness of the brackish zone that is allowed should be in the order of several metres only. This condition applies only in rare situations where the freshwater lens is evolved by natural recharge, as occurs in sand-dune areas or in (coral) islands.

Second, the Badon Ghyben-Herzberg principle assumes a hydrostatic equilibrium, whereas in reality the groundwater flow regime might considerably deviate from this equilibrium situation. In those cases, e.g. in freshwater bodies near the shoreline, the Badon Ghyben-Herzberg principle should not be applied, as the computed position of the sharp interface significantly deviates from the actual position as the coast is approached.

The sharp interface models are still widely applied. These models are based on the (Badon Ghyben-Herzberg) assumption that a sharp interface between fresh and saline groundwater is able to represent the actual situation. Techniques, that apply sharp fresh-saline interfaces, are given by e.g. van Dam [1976]; Bear and Kapuler [1981]; Wilson and Sa da Costa [1982]; van Dam and Sikkema [1982]; Kashef [1983a, 1983b]; Essaid [1986]; Bear and Verruijt [1987: Beaversoft]; IWACO [SALINA, 1987]; Chan

---

[2] "A mathematical model simulates groundwater flow indirectly by means of a governing equation thought to represent the physical processes that occur in the system." [Anderson and Woessner, 1992].

Hong *et al.* [1989] and Olsthoorn [1993]. Most of the calculation methods are based on the finite-element method or the finite-difference method. Also other techniques are applied to solve groundwater flow in combination with a sharp interface, such as the boundary-integral-equation method [e.g. van der Weiden, 1988]; the analytical element method [e.g. Strack, 1989]; and the method based on the vortex theory which has an analytic character [e.g. de Josselin de Jong, 1977; Haitjema, 1977; Peters, 1983].

Solute transport models

In most of the cases, a relatively thick brackish zone[3] is present, since saline and fresh groundwater have mixed because of, among others, hydrodynamic dispersion. For example, Cooper *et al.* [1964] found that circulation of brackish water occurs in the Biscayne aquifer near Miami due to inflow of saline groundwater in the lower part of the coastal aquifer and hydrodynamic dispersion. The brackish zone of the coastal aquifers is also increasing due to the tidal regime and human activities, such as (artificial) recharge and groundwater extraction at high and variable rates.

Under such conditions, models are required that are more sophisticated than models just with expressions for sharp fresh-salt interfaces, namely models which take into account variable densities. In this chapter, these models are referred to as *solute transport models*. As the solute transport models apply numerical schemes, they can also be utilized to simulate groundwater flow regimes with complex geometries and salt-fresh inversions.

Various calculation methods have been developed to simulate the density dependent flow of groundwater in combination with the (complicated) transport of solute. Four major methods that solve the groundwater and solute equations are [Kinzelbach, 1987a]: (1) the finite-difference method; (2) the finite-element method; (3) the random walk method; and (4) the method of characteristics. Suitable computer codes are already available since at least two decades.

Several two-dimensional models, which take into account the solute (advection-dispersion) transport, apply the finite-difference method, such as a model by Pinder and Cooper [1970], MOC [Konikow and Bredehoeft, 1978] which has been adapted for density differences by Lebbe [1983] and MOCDENSE by Sanford and Konikow [1985]. These models also utilize the method of characteristics by means of particle tracking for solving the solute equation. Other models apply the finite-element method, such as models developed by Lee and Cheng [1974], Segol *et al.* [1975], Frind [1982], SUTRA [Voss, 1984] and Galeati *et al.* [1992].

Three dimensional models, that represent solute transport, are INTERCOMP [1976], INTERA [1979], HST3D by Kipp [1986], SWICHA by Lester [1991] and METROPOL by the Dutch National Institute of Public Health and Environmental Protection RIVM [Sauter *et al.* 1993]. The NAtional GRondwater Model (NAGROM), developed by de Lange [1991], is a model based on Strack's analytical element method

---

[3]Other terms are the mixing zone, zone of dispersion or transition zone.

[Strack, 1989]. The advantage of this model is that refinement of the discretization can easily be accomplished. From April 1995, it is ready for use for density dependent groundwater flow regimes in the Netherlands. The model departs from a quasi-dynamic density distribution. Hydrodynamic dispersion will be implemented in the model after 1996. A recently (1994) new released model is the modular three-dimensional transport model called MT3D that is completely compatible with the well-known MODFLOW model [McDonald and Harbaugh, 1984]. MT3D applies the method of characteristics, the modified method of characteristics or a hybrid of these two methods.

The U.S. Geological Survey is one of the leading institutes in developing two and three dimensional groundwater flow models. Important distributors of affordable models are, among others, the International Ground Water Modeling Center [IG-WMC: Delft, the Netherlands and Golden, U.S.A., 1992] and the Scientific Software Group, Washington D.C. U.S.A. [1995].

Reviews of literature on fresh and saline groundwater and available computer models are given in e.g. Bachmat *et al.* [1980], CHO-TNO [1980], Reilly and Goodman [1985], Custodio *et al.* [1987], Thorborg and Jousma [1989] and Strack [1989].

4.3   Program of requirements

A numerical model, which is applied to simulate groundwater flow in a coastal geohydrologic system, must be validated with available groundwater data in order to prove its predictive capability, accuracy and reliability.

A sea level variation can be simulated by changing the piezometric level at the seaside boundary. Note that a sea level rise can be considered as only one specific scenario among many scenarios such as human interventions (e.g. land reclamation, groundwater extraction and deep-well infiltration). Once the groundwater flow model has proven its credibility, it can also be applied to simulate the groundwater flow in any other scenario.

Sharp interface model versus solute transport model

As broad transition zones are present in Dutch coastal groundwater flow regimes, models have to be applied which can represent the transition zone between fresh, brackish and saline groundwater. As such, sharp fresh-salt interface models are unsuitable[4], whereas solute transport models should be applied which take into account density differences. They are able to simulate, among others, changes in solute concentration, changes in volumes of freshwater in sand-dune areas and changes in the salinity of seepage in low-lying polder areas.

---

[4]Notwithstanding the restrictions of the straightforward sharp interface models, they can be applied as an educational means to get more insight in the behaviour of coastal groundwater flow regimes in case boundary conditions change.

Two-dimensional versus three-dimensional models

Though two-dimensional groundwater flow models require quite some effort before they are completely understood, they can be applied in various situations. Obviously, an important restriction of these codes is that only two-dimensional profiles can be simulated. Therefore, a proper profile should be carefully selected.

It may happen, however, that the groundwater flow perpendicular to the coastline is disturbed in such a way that the schematisation of the actual situation by a two-dimensional profile cannot be allowed any more. Such situations occur for instance in the vicinity of polder areas where the controlled phreatic groundwater levels have led to radial flow patterns, or in the vicinity of singular wells where groundwater is extracted.

Under those circumstances, three-dimensional models should be applied to simulate density dependent groundwater flow. The application of these three-dimensional models on a broad scale is still at a primary stage. Three-dimensional models naturally require even more effort to be understood, implemented and utilized effectively than two-dimensional models.

Availability of data

An important aspect for the calibration of numerical models is the availability of groundwater data. Data, such as subsoil parameters, groundwater extraction rates, and salinity and piezometric level distributions as a function of space and time, are necessary to calibrate the applied groundwater flow model as accurately as possible. Regrettably, in many cases sufficiently reliable data are scarce. For instance, calibration of groundwater flow models with salinities changing over time is still rather laborious. As it takes quite some years before an accelerated salinisation can be detected, long time series of monitored salinities have to be available. Unfortunately, long time series are available only occasionally.

Obviously, the availability of enough reliable data is even more pinching for three-dimensional models than for two-dimensional models.

4.4   Numerical accuracy and stability

The numerical approximations, that define the derivatives of the groundwater flow and solute transport equations, may introduce truncation and oscillation errors. As such, these errors limit the techniques that solve the partial differential equations.

Artificial *numerical dispersion* may occur in the solution of the solute concentration as a result of numerical approximation of the nonlinear solute transport equation (see figure 4.1). It depends on the applied discretization scheme of the advective term in the solute transport equation whether or not a *truncation error* occurs. This truncation error has the appearance of an additional dispersion-like term. It may dominate the numerical accuracy of the solution.

Over and undershooting of the solute concentration values, which is called *oscillation* (see figure 4.1), may lead to *oscillation errors* in the solution of the solute concentration. If the oscillation reaches unacceptable values, the solution may even become unstable.
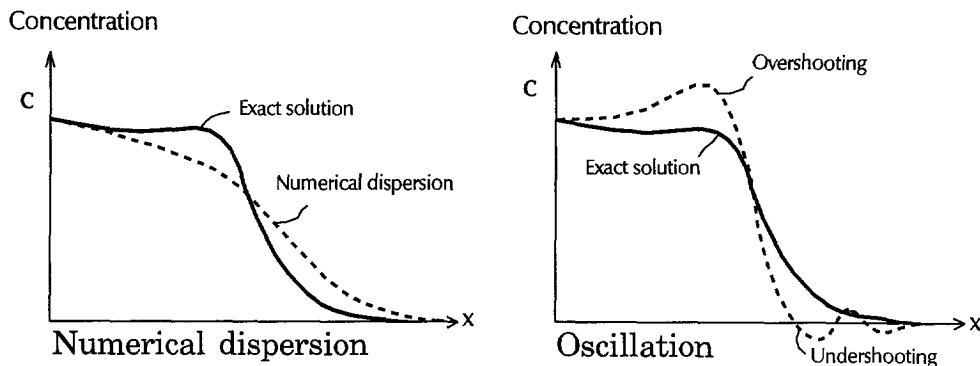

Figure 4.1: Schematisation of numerical dispersion and oscillation.

There exists a close relation between numerical accuracy (numerical dispersion) and stability (oscillation) [Peaceman, 1977; Pinder and Gray, 1977]. In fact, numerical dispersion acts to stabilize the solution of the equation. Numerical dispersion spreads the sharp front by generating a solution which applies a greater dispersion than the hydrodynamic dispersion. In order to suppress the numerical dispersion, the numerical scheme (spatial as well as temporal) can be adapted. Meanwhile, this scheme may lead to over and undershooting, and subsequently, oscillation can be amplified. For these reasons, the discretization scheme should be chosen carefully in order to control both numerical accuracy and stability.

4.4.1   Numerical dispersion

Standard finite-difference methods may generate significant truncation errors. In this subsection, a one-dimensional schematisation is applied to demonstrate in a simple way the principle of assessing truncation errors. The standard (one-dimensional) advection-dispersion equation is defined as follows:

$$\frac{\partial C}{\partial t} = -V\frac{\partial C}{\partial x} + D_h\frac{\partial^2 C}{\partial x^2} \qquad (4.1)$$

where

- V = real velocity of groundwater $(L\,T^{-1})$,

- D_h = hydrodynamic dispersion $(L^2\,T^{-1})$.

Approximations of the first-order derivatives generate errors in the order of magnitude of the second-order derivatives. This can be shown by using Taylor series expansions [e.g. Lantz, 1971; Bear and Verruijt, 1987]. The truncation errors depend on the chosen numerical approximation scheme, presented and discussed below:

- Forward difference in time (explicit)
  A truncation error in the time derivative may cause numerical dispersion for the finite-difference approximation in time:

$$\frac{\partial C}{\partial t} = \frac{C(t + \Delta t) - C(t)}{\Delta t} - \frac{1}{2}\Delta t \frac{\partial^2 C}{\partial t^2} + \dots \tag{4.2}$$

  By applying the original equation 4.1, this expression can be rewritten as [Lantz, 1971]:

$$\frac{\partial C}{\partial t} = \frac{C(t + \Delta t) - C(t)}{\Delta t} - \frac{1}{2}V^2\Delta t \frac{\partial^2 C}{\partial x^2} + \dots \tag{4.3}$$

  Accordingly, the term which contributes to the numerical dispersion is $-\frac{1}{2}V^2\Delta t$. In table 4.1 the truncation error forms for the one-dimensional equation are summarized.

Table 4.1: Summary of numerical dispersion for the one-dimensional equation. Modified from Lantz [1971]; INTERCOMP [1976]; Bear and Verruijt [1987].

Approximation scheme		Numerical dispersion
Time	Spatial	Truncation error
FIT: forward in time	BIS (upstream)	$+\frac{V\Delta x}{2} - \frac{V^2\Delta t}{2}$
(explicit)	CIS (centered)	$-\frac{V^2\Delta t}{2}$
BIT: backward in time	BIS (upstream)	$+\frac{V\Delta x}{2} + \frac{V^2\Delta t}{2}$
(implicit)	CIS (centered)	$\frac{V^2\Delta t}{2}$
CIT: centered in time	BIS (upstream)	$\frac{V\Delta x}{2}$
(Crank-Nicholson)	CIS (centered)	none

- Backward difference in time (implicit)
  Analogous to the forward difference in time, the backward difference in time induces an equivalent error in numerical dispersion, though now the sign is opposite: $+\frac{1}{2}V^2\Delta t$ (see table 4.1).

- Central difference in time (Crank-Nicholson)

  This scheme is the most often applied second order time approximation, as the contribution of the time truncation error to numerical dispersion is removed. Nonetheless, oscillations in time can still occur [INTERCOMP, 1976].

- **Backward difference in space (upstream weighting)**
  The finite-difference approximations in space also introduce truncation errors. The backward difference in space approximation derives the following equation for the term $\frac{\partial C}{\partial x}$:

$$\frac{\partial C}{\partial x} = \frac{C(x) - C(x - \Delta x)}{\Delta x} + \frac{1}{2}\Delta x \frac{\partial^2 C}{\partial x^2} + \dots \tag{4.4}$$

The term $\frac{\partial C}{\partial x}$ should be multiplied with $-V$ to be inserted properly in equation 4.1. In the backward spatial approximation, the numerical dispersion D_{num} due to the truncation error in space is (see also table 4.1):

$$D_{num} = +\frac{1}{2}V\Delta x \tag{4.5}$$

- **Central difference in space**
  As the central finite-difference in space does not generate a space truncation error of the second-order derivative, no numerical dispersion due to this approximation occurs.

$$\frac{\partial C}{\partial x} = \frac{C(x + \Delta x) - C(x - \Delta x)}{2\Delta x} + O\left((\Delta x)^2, \frac{\partial^3 c}{\partial x^3}\right) \tag{4.6}$$

- **Forward difference in space**
  Forward difference in space also results in a truncation error term, as the derivation for the term $\frac{\partial C}{\partial x}$ gives:

$$\frac{\partial C}{\partial x} = \frac{C(x + \Delta x) - C(x)}{\Delta x} - \frac{1}{2}\Delta x \frac{\partial^2 C}{\partial x^2} + \dots \tag{4.7}$$

As this spatial difference approximation is not commonly applied for the advective term, this truncation error is not displayed in table 4.1.

4.4.2   Oscillation

Oscillations may occur in case the total dispersion (that is the sum of hydrodynamic dispersion D_h and numerical dispersion D_{num}) is negative. To counteract oscillations, the following expression should be obeyed:

$$D_h + D_{num} \geq 0 \tag{4.8}$$

A stability analysis indicates whether or not the approximation scheme for the solute transport equation causes an unstable solution [INTERCOMP, 1976; Peaceman, 1977]. Various analyses can be applied to determine the stability criteria for each approximation scheme. Two examples of a central difference in space approximation scheme are briefly discussed:

1. Central difference in time (Crank Nicholson)

No numerical dispersion occurs if a central difference in time scheme is applied in combination with central difference in space (see table 4.1). Hence, this approximation scheme seems to be ideal. There is, however, a tendency of central difference approximations to over and undershoot maximum and minimum solute concentrations, and subsequently, oscillations in time are caused. These oscillation errors can be reduced by limiting the time step. The criterion appears to be related to the criterion of the explicit scheme: in fact, it equals about one-half of the forward in time first order stability criterion [INTERCOMP, 1976]:

$$\frac{V\Delta t}{\Delta x} \leq 2 \qquad (4.9)$$

2. Backward difference in time (implicit)

No stability criteria exist for implicit schemes. However, still, a so-called spatial oscillation may occur in the central in space approximation [Price et al., 1966; INTERCOMP, 1976]. In order to limit this oscillation, the following equation should be fulfilled:

$$\frac{V\Delta x}{2} \leq D_h \quad \text{or} \quad Pe_{grid} = \frac{V\Delta x}{D_h} \leq 2 \qquad (4.10)$$

where Pe_{grid} = grid-Peclet-number $(-)$, which determines the relative size of the advective and dispersive fluxes on the level of a discretization element. This restriction is not really compulsory, because the results can be satisfactory if Pe_{grid} is somewhat greater than 2 though in some places over and undershooting may occur.

4.4.3 Analysis of truncation and oscillation errors

The solution of the solute transport equation may be faced with difficulties, since standard finite-difference and finite-element models may yield unreliable results if the discretization conditions are not met. Although in general, representation of the dispersion by the finite-element method[5] is accurate if numerical dispersion is small with respect to the hydrodynamic dispersion [Bear and Verruijt, 1987], it is recommended to analyse the solute transport equation anyway.

In order to quantify numerical accuracy, an *eigenvalue analysis* of the advection-dispersion equation should be performed. Such an analysis will demonstrate the importance of mesh spacing [e.g. Frind and Pinder, 1983]. In addition, a stability analysis should determine the stability condition [e.g. Peaceman, 1977]. In order to

---

[5]The analysis of (truncation and oscillation) errors due to numerical dispersion and oscillation for the finite-difference method by means of central finite-difference approximations is similar for the finite-element method [Pinder and Gray, 1977, Kinzelbach, 1987a].

obtain real and distinct eigenvalues, the spatial discretization in the finite-element
formulations should meet the condition [Daus *et al.*, 1985]:

$$Pe_{grid} = \frac{V \Delta x}{D_h} \leq 2 \qquad (4.11)$$

In advective-dominant solute transport, the hydrodynamic dispersion D_h can be ex-
pressed as $D_h = \alpha_L V$ (see subsection 5.3.1), and thus, equation 4.11 becomes:

$$Pe_{grid} = \frac{\Delta x}{\alpha_L} \leq 2 \qquad (4.12)$$

Daus *et al.* [1985] derive for the temporal discretization:

$$Co = \frac{V \Delta t}{\Delta x} \leq \frac{Pe_{grid}}{2} \qquad (4.13)$$

where $Co =$ Courant-number $(-)$. The Courant condition Co is physically interpreted
as the ratio of the advective transport distance during one time step to the spatial
discretization. Figure 4.2 illustrates the Courant condition in a numerical scheme. If
the grid-Peclet-number Pe_{grid} is assumed to be maximum (that is $Pe_{grid} = 2$), the
Courant constraint becomes:

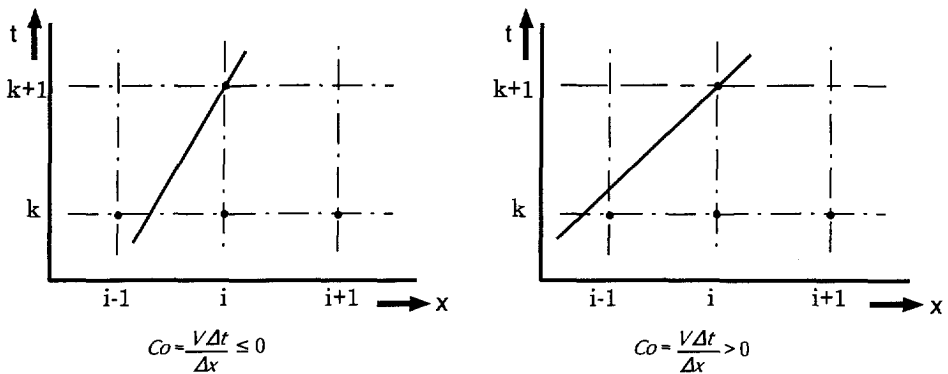$$Co = \frac{V \Delta t}{\Delta x} \leq 1 \qquad (4.14)$$

Figure 4.2: Schematisation of the Courant condition.

Grid-Peclet-numbers and Courant-numbers have been mentioned in various quan-
titative descriptions. Whether or not the numerical dispersion is suppressed, depends
on the applied discretization technique applied [e.g. Jensen and Finlayson, 1978;

Campbell *et al.*, 1981; Voss and Souza, 1987]. In summary, the criteria for the grid-Peclet-number are:

$$Pe_{grid} < 2 \qquad \text{Finite difference algorithm, central in space}$$
$$Pe_{grid} < 2 \qquad \text{Finite element algorithm, linear basic functions}$$
$$Pe_{grid} < 4 \qquad \text{Finite element algorithm, quadratic basic functions} \quad (4.15)$$

or, if mechanical dispersion dominates over molecular diffusion:

$$\Delta x < 2 \, \alpha_L \qquad \text{Finite difference algorithm, central in space}$$
$$\Delta x < 2 \, \alpha_L \qquad \text{Finite element algorithm, linear basic functions}$$
$$\Delta x < 4 \, \alpha_L \qquad \text{Finite element algorithm, quadratic basic functions} \quad (4.16)$$

It appears that hydrodynamic dispersion is small for geohydrologic circumstances in the Netherlands. This manifests itself in sand-dune areas along the Dutch coast, where freshwater lenses with relatively sharp fresh-salt interfaces have been formed. Computations will indicate that if a great hydrodynamic dispersion (that means great dispersivities) is simulated, unrealistic solutions are generated (see, e.g., section 7.5 and subsection 8.2.3).

4.5   Comparison of MOC, SUTRA and SWICHA

In this section, the results of the three selected groundwater flow models MOC (adapted), SUTRA and SWICHA are mutually compared with respect to the magnitude of the longitudinal dispersivity α_L. The interest is focused on numerical dispersion and on numerical stability of the solutions for a case study with a profile through the sand-dune area of Gemeentewaterleidingen Amsterdam along the Dutch coast and the Haarlemmermeer polder lying inland of the sand-dunes.

In subsection 4.5.1, the three models are briefly described and some differences between the models are discussed. Moreover, in this subsection, the maximum number of grid cells for each model is determined that can be applied under the 8 Mb *Extended Memory* RAM of the applied computer. In subsection 4.5.2, the influence of the longitudinal dispersivity α_L on the numerical solution is discussed.

4.5.1   Short description of the three models

The two-dimensional adapted MOC model

The original MOC model is a widely applied and widely accepted groundwater flow model throughout the world. Version 3.0 of MOC [1989] has been adapted by the author for density differences, making use of documentation of Lebbe [1983] and van der Eem [1987]. The adaptation implies that the variations in fluid density now affect the velocity distribution. In order to obtain the adapted MOC model from

the original MOC model, small adjustments due to density differences have been accomplished. As a consequence, the model is capable to simulate density dependent two-dimensional groundwater flow with solute transport. In chapter 5, an extensive description of the theoretical background of the adapted MOC model is given.

As MOC applies the method of characteristics to solve advection through a particle tracking procedure, numerical dispersion is suppressed considerably. This property makes the adapted MOC model a very suitable groundwater flow model for simulating groundwater flow regimes with Holocene and Pleistocene deposits of marine and fluviatile origin such as occur along the Dutch coast.

Note that a computer code similar to the adapted MOC model came on the market in 1985: MOCDENSE [Sanford and Konikow, 1985]. It is a modified version of the original MOC model. Whereas the original and the adapted MOC model are still based on (freshwater) heads, MOCDENSE is based on pressures. Although MOCDENSE was removed from the IGWMC software-list for a few years because of (small) errors in the computer code, it is gaining ground again [e.g. Calvache and Pulido-Bosch, 1991]. It is now beginning to enjoy a good reputation with respect to other solute transport models such as SUTRA.

The two-dimensional model SUTRA

This paragraph only consists of a summary of SUTRA's fundamentals, as the manual of the groundwater flow model SUTRA is well-documented [see Voss, 1984]. The model has been applied successfully for the simulation of salt water intrusion in various types of profiles, which is demonstrated in a large number of publications such as Voss and Souza [1987]; Souza and Voss [1987]; Reilly [1990]; Ghassemi et al. [1990]; Samper and García-Vera [1993]; Shearer and van Wonderen [1993]; Vogel et al. [1993]; and Das Gupta and Loof [1993]. Gradually, SUTRA has become a widely accepted groundwater flow model throughout the world, and accordingly, it has a prosperous future in store in the field of two-dimensional modelling of solute transport in density dependent (coastal) aquifer systems.

SUTRA can simulate two-dimensional density dependent groundwater flow with (thermal) energy transport or chemically reactive (single-species) solute transport. The SUTRA flow simulation can be applied for areal and for cross-sectional modelling of saturated groundwater flow regimes, and for cross-sectional modelling of unsaturated zone flow. It applies a weighted residual numerical method combining Galerkin finite-elements with integrated finite-differences to solve groundwater flow and transport equations (either energy or solute). As SUTRA is a finite-element model, the system is represented by nodes and (quadrilateral) elements. The applied temporal discretization is based on a backward finite-difference approximation for the time derivatives.

A unique aspect of SUTRA is the availability of a flow-direction-dependent longitudinal dispersion form (besides the flow-direction-independent form) which allows the longitudinal dispersivity to vary with direction. However, this feature appears to

be redundant in this study, as the dispersivities are small in geohydrologic systems with Holocene and Pleistocene deposits of marine and fluviatile origin such as occur along the Dutch coast. Longitudinal dispersivities should be in the order of the size of either the largest geohydrologic or flow inhomogeneities along the transport reach or of that of the distance between those inhomogeneities, whichever is the greater value. Narrow transition zones require a careful choice of spatial and temporal discretization. Voss and Souza [1987] stated that oscillations in the numerical method do not occur if the following expression is obeyed:

$$Pe_{grid} = \frac{|V|\,\Delta x_i}{(\alpha_L\,|V| + D_d)} < 4 \qquad (4.17)$$

where

- Δx_i = longest distance between sides of an element (L),

- $|V|$ = magnitude of the real velocity $(L\,T^{-1})$,

- D_d = molecular diffusion $(L^2\,T^{-1})$.

This expression appears to be a severe restriction.

The three-dimensional model SWICHA

SWICHA, developed by Lester [1991], is a three-dimensional finite-element computer code. It simulates variable density fluid flow and solute transport processes in fully-saturated porous media. The groundwater flow and solute equations are solved by the Galerkin finite-element technique. An implicit Picard iterative scheme is applied to treat the nonlinearity of the problems. For a transient solution of the seawater intrusion problem, the Crank-Nicholson time stepping scheme is applied to handle the temporal discretization. Spatial discretization is performed using rectangular and triangular elements. A vertical slicing approach can be applied. Various sets of material properties can describe the subsoil characteristics of aquifers or aquitards in the geohydrologic system.

The version 5.05 of SWICHA is based on an earlier version described in Huyakorn *et al.* [1987]. The mentioned problems range from simple one-dimensional to complex three-dimensional, coupled flow and solute transport.

The solution of the solute transport equation may not converge, if the critical Peclet-number Pe_{crit} is exceeded in an element. In order to solve this problem, SWICHA has introduced a trick at the user's option: a minimum of numerical dispersion (the so-called *artificial dispersion*) is added to the solute transport equation matrix, until the Peclet-number in that element equals the critical Peclet-number Pe_{crit}. Then, spatial oscillations are suppressed by a factor and, subsequently, the solution will converge. Especially when the applied dispersivities are small, a lot of artificial dispersion must be added (see subsection 4.5.2).

HST3D [Kipp, 1986] is another three-dimensional model that has been considered. Ossenkoppele [1993] showed in her M.Sc. thesis that modelling the sand-dune area of Gemeentewaterleidingen Amsterdam along the Dutch coast (dimensions: 12,000 · 20,000 m^2 by 160 m) with HST3D appeared to be rather complicated. She applied a Geographic Information System to determine accurately the hydraulic conductivity matrix of the geohydrologic system. Large dispersivities (e.g. $\alpha_L=200$ m) were applied as otherwise the equations did not converge to a solution. As a consequence of simulations with great dispersivities, excessive hydrodynamic dispersion created unrealistic extensive brackish zones which could not be matched with the observed situation. For this reason, HST3D is certain to be unsuitable in this study.

Differences between the models

Implementation of the boundary conditions differs between the adapted MOC model and both SUTRA and SWICHA. As MOC is a finite-difference model, the (freshwater) heads and concentrations are given in the center of a grid cell. This is in contrast with SUTRA and SWICHA which use the finite-element method. As a consequence, the heads and concentrations are given in the nodes of the elements (or grid cells). Therefore, the freshwater head and the chloride concentration in the vicinity of the boundary conditions will differ somewhat between the models.

In the adapted MOC model, spatial oscillations of concentrations caused by great dispersivities do not occur. As such, the convergence of the solution is not directly influenced by the magnitude of the dispersivities. Hence, the dispersivities that are applied in the adapted MOC model can remain constant during the simulation. In both SUTRA and SWICHA, however, spatial oscillations of concentrations may occur when dispersivities are great and the mesh is coarse. In SUTRA, the dispersivities are not modified automatically, whereas in SWICHA, artificial dispersion can be added, even if the solution does not converge directly.

In the adapted MOC model, an extra procedure enables the user to simulate a sea level variation at a selected boundary on every time step the groundwater flow equation is solved (that is the so-called flow time step, see subsection 5.2.3). In the original SUTRA version, however, a scenario with sea level rise cannot easily be implemented. By contrast, in SWICHA, a sea level variation can easily be simulated, as time-dependent boundary conditions for the head are implemented in the model.

Number of grid cells

The maximum allowable number of grid cells, allocated under the 8 Mb Extended Memory RAM[6] of the applied Highscreen computer, has been determined by trial and error. MOC can reproduce some 20,000 (e.g. 500 · 40) grid cells with 9 particles per grid cell. SUTRA can reproduce only some 5500 grid cells. The main reason for

---

[6]Note that in a 8 Mb Extended Memory RAM computer, only some 7 Mb is available for execution of programs.

this small number of grid cells relative to MOC is that SUTRA has to allocate more arrays. The model applies the finite-element method and it presents more subsoil characteristics for each element (grid cell) than MOC has. For instance, two arrays are required for location of the nodes of the elements, one array is required for the porosity, three arrays for the representation of the permeability and three arrays for the dispersivities. SWICHA can reproduce some 5500 grid cells in combination with 20 slices.

4.5.2   Influence of dispersion on the numerical solution

Introduction

The influence of longitudinal dispersivities on the solution is analysed through simulation of a specific profile in Noord-Holland with the three selected groundwater flow models. The profile through the sand-dune area of Gemeentewaterleidingen Amsterdam up to halfway the Haarlemmermeer polder is taken as the reference case.

The schematisation and calibration of this profile will be discussed extensively in chapter 7. The simulations start with an initial chloride distribution at the beginning of 1854 AD (see figure 4.3), as it is proposed by Kooiman through 'trial and error' [1989]. Each of the models computes the chloride distribution after a simulation time of 134 years, from the reclamation of the Haarlemmermeer polder till the end of 1987. The following longitudinal dispersivities are applied: α_L=0.02 m; α_L=0.2 m; α_L=2.0 m and α_L=20.0 m. In order to compare the three models one with another, the dimension of the grid cells should be equal for each of the models. The dimension is set to Δx=250 m and Δz=10 m. This implies for a profile with the dimensions 12,500 m by 180 m: 50 · 18 = 900 grid cells. Only one slice is modelled in the three-dimensional model SWICHA.

When a three-dimensional situation has to be schematised, the number of elements in SWICHA would be much more than the allowed 5500 elements (and 20 slices) under 8 Mb Extended Memory RAM. For instance, if the geohydrologic system has the following dimensions: 12,500 · 10,000 m^2 by 180 m, and the dimensions of an element would be Δx=250 m, Δy=250 m and Δz=10 m, then the program would require at least 27 Mb Extended Memory RAM. However, in order to obey the numerical restriction (e.g. $\Delta x < 4\,\alpha_L$, see equation 4.16), whereas longitudinal dispersivities should be small, the chosen horizontal dimensions $\Delta x, \Delta y$ of the element of 250 m are very likely to be too large. Moreover, such a number of elements would require a lot of calculation time. In addition, the simulation time for the impact of sea level rise on groundwater flow regimes is very likely to be in the order of centuries. Based on the reflections mentioned above, one can imagine that for the time being three-dimensional modelling for this specific purpose is still unfeasible.
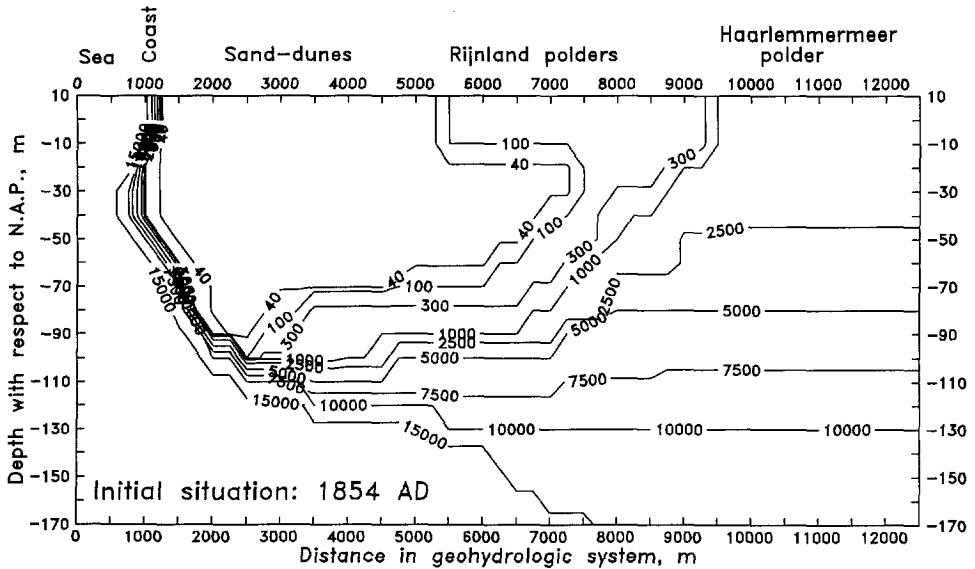
Figure 4.3: Initial chloride distribution (values in $mg\ Cl^-/l$) at the beginning of 1854 AD, computed for 900 grid cells [Kooiman, 1989].

Discussion

Figure 4.4 shows six chloride distributions in the profile at the end of 1987, after a simulation time of 134 years. The three models MOC, SUTRA and SWICHA have simulated the profile in combination with the longitudinal dispersivities $\alpha_L=0.02\ m$ and $\alpha_L=20.0\ m$. In addition, figure 4.5 shows six chloride distributions at the end of 1987 for the three models with $\alpha_L=0.2\ m$ and $\alpha_L=2.0\ m$.

The calculated chloride distribution matches the observed chloride distribution best if the longitudinal dispersivity α_L is small. The cases with small longitudinal dispersivities, that is $\alpha_L=0.02\ m$ and $\alpha_L=0.2\ m$, have freshwater lenses that correspond with observations. In all three models, the case with $\alpha_L=2.0\ m$ shows a freshwater lens that is too small. In all three models, the case with $\alpha_L=20.0\ m$ does not simulate a freshwater lens any more. The geohydrologic system consists of only a large zone with brackish groundwater. Obviously, this situation does not match reality.

Moreover, as can be seen in the figures 4.4 and 4.5, the chloride distributions by the adapted MOC model are smooth. This is in contrast with the distributions by SUTRA and SWICHA. When longitudinal dispersivities are small, these two models compute inaccurate chloride distributions, and over and undershooting of the maximum and minimum chloride concentration frequently occur.

For instance, table 4.2 shows that in SUTRA over and undershooting always occur in several grid cells. The smaller the longitudinal dispersivity, the more grid cells are
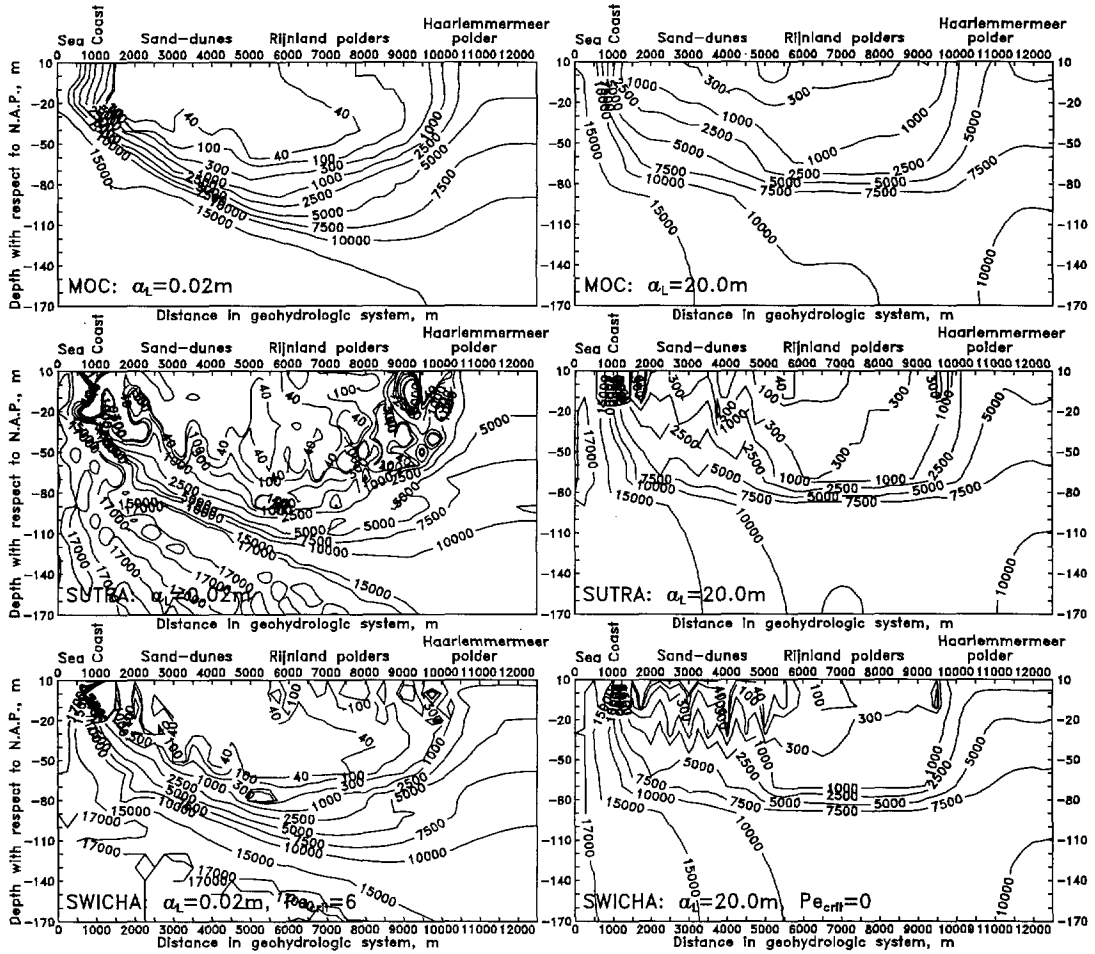
Figure 4.4: Six chloride distributions (in $mg\ Cl^-/l$) at the end of 1987 for the case with 900 grid cells, calculated with MOC, SUTRA and SWICHA for α_L=0.02 m and α_L=20.0 m.

subject to over and undershooting.

When the longitudinal dispersivity is small, the grid-Peclet-number Pe_{grid} appears to be very great. Figure 4.6 displays for the adapted MOC model the grid-Peclet-number in horizontal direction: $Pe_{grid,x} = \left|\frac{V_x \Delta x}{D_{xx}}\right|$ (see also equation 5.48). As the velocities are small near the no-flow boundary at x=12,500 m, the grid-Peclet-number is smaller there than in the center of the geohydrologic system. The figure shows that $Pe_{grid,x}$ is so great that the numerical method of SUTRA obviously produces oscillations in the solution, as the restriction $Pe_{grid} < 4$ predicts (see
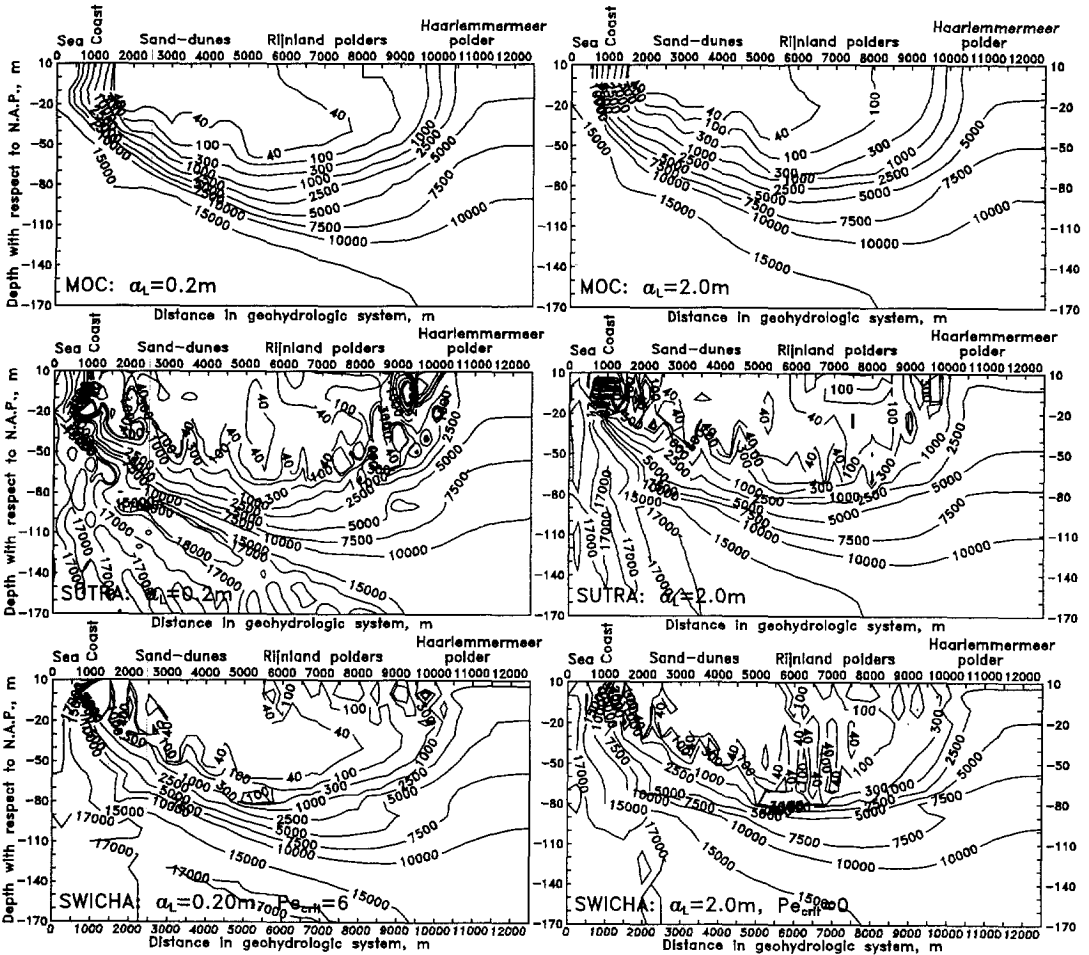
Figure 4.5: Six chloride distributions (in mg Cl^-/l) at the end of 1987 for the case with 900 grid cells, calculated with MOC, SUTRA and SWICHA for α_L=0.2 m and α_L=2.0 m.

equation 4.17).

In SWICHA, when the critical Peclet-number Pe_{crit}=0, the solution does not even converge in case the longitudinal dispersivity α_L equals 0.02 m and 0.2 m. Therefore, artificial dispersion must be added to the solute transport equation matrix. In table 4.3 the influence is demonstrated of the critical Peclet-number Pe_{crit}, applied in SWICHA, on the accuracy of the salinity distribution. By decreasing Pe_{crit} (to a minimum of 0.5[7]) more artificial dispersion is added during the simulation. As a consequence, the over and undershooting decrease in absolute value and in number

---

[7]The smallest critical Peclet-number Pe_{crit} that is allowed in SWICHA equals 0.5.

Table 4.2: Influence of the longitudinal dispersivity on the accuracy of the solution: the minimum and maximum chloride concentrations; and the number of grid cells undershooting a chloride concentration of 0 mg Cl^-/l and overshooting 17,000 mg Cl^-/l.

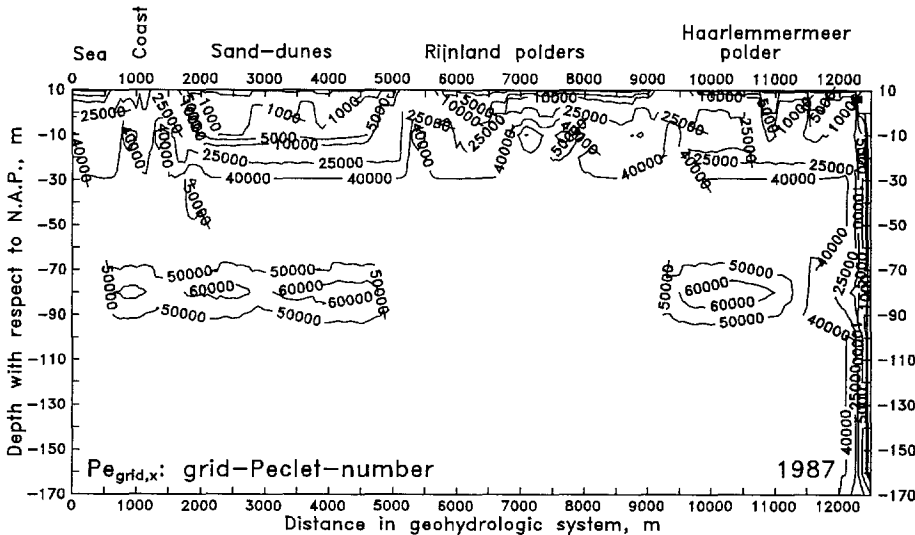| SUTRA				
α_L	Minimum	Maximum	Undershoot	Overshoot
(m)	$(mg$ $Cl^-/l)$	$(mg$ $Cl^-/l)$	(grid cells)	(grid cells)
0.02	-8707	37,580	66	133
0.2	-7506	25,436	50	130
2.0	-7063	27,089	21	70
20.0	-1958	22,970	6	14

Figure 4.6: Distribution of the grid-Peclet-number in x-direction at the end of 1987. The simulation is done with the adapted MOC model: 900 grid cells and α_L=0.02 m.

of grid cells: viz. less grid cells contain chloride concentrations > 17,000 mg Cl^-/l and < 0 mg Cl^-/l. In the cases with small longitudinal dispersivities α_L=0.02 m and α_L=0.2 m, the solution converges for a critical Peclet-number $0.5 < Pe_{crit} \leq$ 6. When the critical Peclet-number Pe_{crit} is greater than 6, apparently not enough artificial dispersion is added and the solution does not converge.

Table 4.3: Influence of the critical Peclet-number of SWICHA on the solution: the longitudinal dispersivity; the critical Peclet-number; the minimum and maximum chloride concentrations; and the number of grid cells undershooting a chloride concentration of 0 mg Cl^-/l and overshooting 17,000 mg Cl^-/l. When Pe_{crit} is set to 0, no artificial dispersion is added.

SWICHA					
α_L	Pe_{crit}	Minimum	Maximum	Undershoot	Overshoot
(m)	$(-)$	$(mg\ Cl^-/l)$	$(mg\ Cl^-/l)$	(grid cells)	(grid cells)
0.02	0.5	-4	18,660	1	10
	1	-2	18,300	1	7
	3	-2291	17,330	10	20
	5	-7875	19,600	16	27
	6	-30,500	28,670	22	36
	$Pe_{crit} = 0$: no convergence				
	$Pe_{crit} \geq 7$: no convergence				
0.2	0.5	-3	18,660	1	3
	6	-30,130	28,330	23	28
	$Pe_{crit} = 0$: no convergence				
	$Pe_{crit} \geq 7$: no convergence				
2.0	0	-2558	20,830	34	73
	6	-4327	21,120	17	11
20.0	0	-2096	18,040	10	23
	1	-	18,290	0	3
	5	-36	18,020	2	3
	6	-217	18,090	4	3

4.6 Choice of the groundwater flow model

In conclusion, small dispersivities should be applied in the simulations of groundwater flow regimes with Holocene and Pleistocene deposits of marine and fluviatile origin such as occur along the Dutch coast in order to match calculated salinity distributions with actual ones. In addition, the spatial discretization (viz. the dimension of a grid cell or grid block) should also be small in order to suppress truncation and oscillation errors.

Whereas the finite-element models SUTRA and SWICHA cannot generate accurate solutions of the salinity distributions in case of small longitudinal dispersivities, the adapted MOC model is very well capable of generating accurate solutions. Mainly for that reason, the adapted MOC model is applied for simulations of the groundwater flow regime along the Dutch coast.

The dimensions of the grid block of (standard) three-dimensional codes with dis-

persive solute transport may not be larger than e.g. two times the magnitude of the (longitudinal) dispersivity that represents the hydrodynamic dispersion. Unfortunately, as the (longitudinal) dispersivities are at maximum in the order of metres for most of the Dutch geohydrologic systems, the dimensions of the grid blocks should be in the order of metres as well.

During the past years of this study, the state of affairs of (personal) computer performances was such that the application of three-dimensional models (solving solute transport by the finite-element method) was limited. As the dispersivities are small, a very large number of grid blocks was necessary to model geometries of a few hundreds of metres. When, however, the scale of the geohydrologic system in question is extensive (e.g. several square kilometres and the thickness of the geohydrologic system equal to a hundred metre), the required number of grid blocks would be enormous. The allowed number of grid blocks was below the required number, as computer memory capacity was limited. In addition, such an enormous number of grid blocks demanded a lot of calculation time, though computer performances increased rapidly. These strict demands severely restricted the practical application of these three-dimensional solute transport models. In conclusion, they made it unfeasible to model the Dutch geohydrologic system with SWICHA.

Now (1996), however, the spectacular boom in computer performances has made it possible to cope indeed with geometries of several kilometres (viz. with grid blocks of only some metres and small dispersivities (order of decimetres)). For instance, in the oil-industry, the maximum possible number of grid cells in three-dimensional models is already in the order of millions. Hence, in the near future, three-dimensional modelling of solute transport by means of the method of characteristics (particle tracking) will certainly be possible.

Chapter 5

Background of the adapted MOC model

5.1 Introduction

In this thesis, an adapted version of the two-dimensional model MOC is applied to simulate the density dependent flow of groundwater in the geohydrologic systems along the Dutch coast. Originally, MOC, which was developed in 1978 by Konikow and Bredehoeft for the United States Geological Survey, was only applied as a horizontal two-dimensional groundwater flow model. The adaptation for density differences was necessary because in most parts along the Dutch coast a non-uniform density distribution occurs, and thus, fluid density variations affect the velocity distribution.

Lebbe was the first to adapt MOC[1] for vertical groundwater flow and density differences. He presented his results on the eighth Salt Water Intrusion Meeting (SWIM) in Bari, Italy, in May 1983. In 1986, van der Eem and Peters of the National Institute of Public Health and Environmental Protection (RIVM, formerly RID), also adapted MOC[2] for density differences.

In March 1990, the author adapted MOC[3] for density differences, using documentation of Lebbe [1981, 1983] and van der Eem [1987]. Since August 2, 1985, MOC is also suited to simulate non-conservative solute transport in saturated groundwater systems, such as transport affected by radioactive decay, sorption and exchange (retardation). Hence, the adapted MOC model applied in this thesis can simulate not only density dependent groundwater flow but also chemical and physical reactions.

In this chapter, different aspects of MOC, adapted by the author and applied in this thesis, are described. In section 5.2, the theoretical background concerning the equations of groundwater flow is summarized. In section 5.3, the theoretical background concerning the equation of solute transport is discussed. In section 5.4, model and subsoil parameters of the adapted MOC model are described. In section 5.5, some limitations of the adapted MOC model are discussed. Finally, in section 5.6, several postprocessors that present the results are summarized.

---

[1] Lebbe, of the Laboratory of Applied Geology and Hydrology of the State University of Ghent, Belgium, adapted the updated version of MOC of August, 1981.

[2] Van der Eem and Peters adapted the updated version of MOC of June-August, 1984.

[3] The author adapted the updated version of MOC of March, 1989. This model (version 3.0, 1989) was purchased from the International Ground Water Modeling Center (IGWMC).

5.2   Groundwater flow

This section comprises the fundamentals of the numerical algorithm, applied in the adapted MOC model, to represent two-dimensional density dependent groundwater flow.

5.2.1   Equation of motion

The equation of motion for two-dimensional laminar groundwater flow in an anisotropic non-homogeneous porous medium in the principle directions is described by Darcy's law [Bear, 1972]:

$$q_x = -\frac{\kappa_x}{\mu_i}\frac{\partial p}{\partial x} \qquad\qquad q_z = -\frac{\kappa_z}{\mu_i}(\frac{\partial p}{\partial z} + \gamma) \qquad\qquad (5.1)$$

where

- q_x, q_z = Darcian specific discharges in the principal directions, respectively horizontal and vertical $(L\,T^{-1})$,

- p = pressure $(M\,L^{-1}\,T^{-2})$,

- κ_x, κ_z = principal intrinsic permeabilities, respectively horizontal and vertical (L^2),

- μ_i = dynamic viscosity of water at point $[x, z]$ $(M\,L^{-1}\,T^{-1})$,

- $\gamma = \rho_i g$ = specific weight $(M\,L^{-2}\,T^{-2})$,

- ρ_i = density of groundwater at point $[x, z]$ $(M\,L^{-3})$,

- g = gravity acceleration $(L\,T^{-2})$.

The dynamic viscosity μ highly depends on the temperature, see table 5.1. Voss [1986] uses in SUTRA the following expression:

$$\mu(T) \simeq (239.4 \cdot 10^{-7})10^{\frac{248.37}{T+133.15}} \qquad\qquad (kg/m\,s) \qquad\qquad (5.2)$$

The dynamic viscosity μ is relatively insensitive to pressure within the limiting values that can occur in the studied areas. Furthermore, the dynamic viscosity also depends on the solute concentration, though only for very high solute concentrations.

   In general, the range in temperature in the deep aquifers of the Dutch groundwater flow regimes is small. For instance, data from Stuyfzand [1986a, 1988] in sand-dune areas along the Dutch coast show that the temperature of groundwater in the aquifers directly under the Holocene aquitard (at roughly -20 m $N.A.P.$) is normally between 10.0 and 11.0 ^oC, while the annual mean air temperature near the coast is roughly

Table 5.1: Variation of the dynamic viscosity μ with temperature T at a pressure of 100 kPa (1 bar) [Verruijt, 1970; Bear, 1972; Voss, 1986; CRC, 1994].

Temperature T	Dynamic viscosity μ $(kg/m\,s)$	
$(^\circ C)$	Verruijt, Bear, CRC	Voss, equation 5.2
0	$1.79 \cdot 10^{-3}$	$1.76 \cdot 10^{-3}$
5	$1.52 \cdot 10^{-3}$	$1.50 \cdot 10^{-3}$
10	$1.31 \cdot 10^{-3}$	$1.30 \cdot 10^{-3}$
15	$1.14 \cdot 10^{-3}$	$1.14 \cdot 10^{-3}$
20	$1.00 \cdot 10^{-3}$	$1.00 \cdot 10^{-3}$
40	$0.65 \cdot 10^{-3}$	$0.65 \cdot 10^{-3}$
70	$0.41 \cdot 10^{-3}$	$0.40 \cdot 10^{-3}$
100	$0.28 \cdot 10^{-3}$	$0.28 \cdot 10^{-3}$

9.5 $^\circ C$. In deeper layers, the mean temperature of the groundwater varies between 11.0 and 12.5 $^\circ C$.

The relation between the pressure and the so-called, *fictive, freshwater head* is as follows [e.g. Lebbe, 1981] (if the atmospheric pressure equals zero):

$$\phi_f = \frac{p}{\rho_f g} + z \tag{5.3}$$

where

- ϕ_f = *fictive* freshwater head (L),

- $\frac{p}{\rho_f g}$ = pressure head, expressed in fresh water (L),

- ρ_f = density of fresh groundwater $(M\,L^{-3})$,

- z = elevation with respect to the reference level $(N.A.P.)$ (L).

The horizontal and vertical hydraulic conductivities of fresh groundwater are defined as follows:

$$k_x = \frac{\kappa_x \rho_f g}{\mu_f} \qquad\qquad k_z = \frac{\kappa_z \rho_f g}{\mu_f} \qquad (L\,T^{-1}) \tag{5.4}$$

Density differences in groundwater flow

The density distribution in the deep groundwater flow regimes along the Dutch coast is non-uniform and varies with depth. As the density ρ_i varies with position, effects of density difference have to be considered. Henceforth, the Darcian specific discharge in vertical direction takes into account density differences [Lebbe, 1983]. Inserting equation 5.3 into equation 5.1 gives:

$$q_x = -\frac{\kappa_x \rho_f g}{\mu_i} \frac{\partial \phi_f}{\partial x} \qquad\qquad q_z = -\frac{\kappa_z \rho_f g}{\mu_i} \left(\frac{\partial \phi_f}{\partial z} - 1 + \frac{\rho_i}{\rho_f} \right) \tag{5.5}$$

If the density varies with position, the intrinsic permeabilities κ_x, κ_z and the dynamic viscosity μ should be applied instead of the hydraulic conductivities k_x or k_z. However, small viscosity differences may be disregarded in case density differences are taken into account in groundwater flow problems in vertical profiles [Verruijt, 1980; Bear and Verruijt, 1987]. As such, the factor μ_f/μ_i, which is close to 1, is ignored in the development of the adapted MOC model from this point on, also because of the lack of accuracy by which the horizontal and vertical hydraulic conductivities are determined. Making use of equation 5.4, equation 5.5 becomes:

$$q_x = -k_x \frac{\partial \phi_f}{\partial x} \qquad\qquad q_z = -k_z \left(\frac{\partial \phi_f}{\partial z} + \Upsilon \right) \tag{5.6}$$

where $\Upsilon = (\rho_i - \rho_f)/\rho_f$ is the relative density difference, the so-called *buoyancy* $(-)$. As can be seen, the vertical Darcian specific discharge has an extra term in comparison with groundwater flow with a uniform density: this term is called the *vertical density gradient velocity*.

5.2.2   Equation of continuity

Equation (5.7) describes the non-steady two-dimensional mass flow in a small element of a saturated anisotropic, porous medium [e.g. Bear 1972, van der Heide and Boswinkel 1982]:

$$-\left[\frac{\partial(\rho_i q_x)}{\partial x} + \frac{\partial(\rho_i q_z)}{\partial z} \right] = \frac{\partial(n_e \rho_i)}{\partial t} + W'(x, z, t) \tag{5.7}$$

or

$$-\left[\rho_i \frac{\partial q_x}{\partial x} + \rho_i \frac{\partial q_z}{\partial z} + n_e V_x \frac{\partial \rho_i}{\partial x} + n_e V_z \frac{\partial \rho_i}{\partial z} \right] = \rho_i \frac{\partial n_e}{\partial t} + n_e \frac{\partial \rho_i}{\partial t} + W'(x, z, t) \tag{5.8}$$

where

- $W'(x, z, t)$ = source function, which describes the mass flux of the fluid into (negative sign) or out of (positive sign) the system $(M\,L^{-3}\,T^{-1})$,

- t = time (T),

- n_e = effective porosity of the medium $(-)$,

- $n_e V_i = q_i$, where V_i = real velocity of the groundwater in the direction of x_i.

When the effective porosity is a function of pressure, $n_e = n_e(p)$, and the density of groundwater is a function of pressure, concentration of dissolved solutes and temperature of the fluid, $\rho_i = \rho_i(p, C, T)$, equation 5.8 gives (Zijl and Nawalany, 1993):

$$-\rho_i \left[\frac{\partial q_x}{\partial x} + \frac{\partial q_z}{\partial z} \right] =$$

$$n_e V_x \left(\frac{\partial \rho_i}{\partial p} \frac{\partial p}{\partial x} + \frac{\partial \rho_i}{\partial C} \frac{\partial C}{\partial x} + \frac{\partial \rho_i}{\partial T} \frac{\partial T}{\partial x} \right) + n_e V_z \left(\frac{\partial \rho_i}{\partial p} \frac{\partial p}{\partial z} + \frac{\partial \rho_i}{\partial C} \frac{\partial C}{\partial z} + \frac{\partial \rho_i}{\partial T} \frac{\partial T}{\partial z} \right)$$

$$+ \rho_i \frac{\partial n_e}{\partial p} \frac{\partial p}{\partial t} + n_e \left(\frac{\partial \rho_i}{\partial p} \frac{\partial p}{\partial t} + \frac{\partial \rho_i}{\partial C} \frac{\partial C}{\partial t} + \frac{\partial \rho_i}{\partial T} \frac{\partial T}{\partial t} \right) + W'(x,z,t) \tag{5.9}$$

or

$$- \left[\frac{\partial q_x}{\partial x} + \frac{\partial q_z}{\partial z} \right] = \frac{1}{\rho_i} \frac{\partial p}{\partial t} \left(\rho_i \frac{\partial n_e}{\partial p} + n_e \frac{\partial \rho_i}{\partial p} \right) + \frac{n_e}{\rho_i} \frac{\partial \rho_i}{\partial C} \left(\frac{\partial C}{\partial t} + V_x \frac{\partial C}{\partial x} + V_z \frac{\partial C}{\partial z} \right)$$

$$+ \frac{n_e}{\rho_i} \frac{\partial \rho_i}{\partial p} \left(V_x \frac{\partial p}{\partial x} + V_z \frac{\partial p}{\partial z} \right) + \frac{n_e}{\rho_i} \frac{\partial \rho_i}{\partial T} \left(\frac{\partial T}{\partial t} + V_x \frac{\partial T}{\partial x} + V_z \frac{\partial T}{\partial z} \right) + \frac{W'(x,z,t)}{\rho_i} \tag{5.10}$$

It is reasonable to assume that the term $\left(\frac{\partial C}{\partial t} + V_x \frac{\partial C}{\partial x} + V_z \frac{\partial C}{\partial z} \right)$, which is in fact a stripped version of the *advection-dispersion equation* for conservative solutes whereas the dispersion is negligible (see equation 5.43), is also negligible small in the equation of continuity (Zijl and Nawalany, 1993). The term $\left(V_x \frac{\partial p}{\partial x} + V_z \frac{\partial p}{\partial z} \right)$ is generally small enough to be neglected in relation to the other terms. Furthermore, if $\frac{\partial \rho_i}{\partial T}$ can be neglected with respect to the pressure gradient term, equation 5.10 is simplified to:

$$- \left[\frac{\partial q_x}{\partial x} + \frac{\partial q_z}{\partial z} \right] = \frac{1}{\rho_i} \frac{\partial p}{\partial t} \left(\rho_i \frac{\partial n_e}{\partial p} + n_e \frac{\partial \rho_i}{\partial p} \right) + \frac{W'(x,z,t)}{\rho_i} \tag{5.11}$$

Due to the fact that a slightly compressible fluid is present, it is necessary to introduce the specific storativity S_s [Bear, 1972]. It is assumed that the specific storativity is independent of variations in fluid density [van der Heide and Boswinkel, 1982]:

$$S_s = g \frac{\partial(n_e \rho_i)}{\partial p} = g(\rho_i \frac{\partial n_e}{\partial p} + n_e \frac{\partial \rho_i}{\partial p}) \tag{5.12}$$

with

$$S_s = \frac{S}{b} \tag{5.13}$$

where

- S_s = specific storativity (L^{-1}),

- S = storage coefficient $(-)$,

- b = saturated thickness of the aquifer (L).

Taking the partial derivative of equation 5.3, that is after rewriting $\frac{\partial p}{\partial t} = \rho_f g \frac{\partial \phi_f}{\partial t}$, and assuming that the factor ρ_f / ρ_i is close to 1, and the pressure gradient can be replaced by a term containing the gradient of the piezometric level ϕ_f:

$$- \left[\frac{\partial q_x}{\partial x} + \frac{\partial q_z}{\partial z} \right] = S_s \frac{\partial \phi_f}{\partial t} + \frac{W'(x,z,t)}{\rho_i} \tag{5.14}$$

5.2.3   Numerical algorithm

The combination of the equations 5.6 and 5.14 gives the *groundwater flow equation*[4]:

$$\frac{\partial(k_x\frac{\partial\phi_f}{\partial x})}{\partial x} + \frac{\partial(k_z(\frac{\partial\phi_f}{\partial z}+\Upsilon))}{\partial z} = S_s\frac{\partial\phi_f}{\partial t} + \frac{W'(x,z,t)}{\rho_i} \tag{5.15}$$

When equation 5.15 is multiplied by the thickness of the aquifer b, and the x and z are the principal directions with respectively principal values T_{xx} and T_{zz}, the following equation is derived:

$$\frac{\partial(T_{xx}\frac{\partial\phi_f}{\partial x})}{\partial x} + \frac{\partial(T_{zz}\frac{\partial\phi_f}{\partial z})}{\partial z} + \frac{\partial(T_{zz}\Upsilon)}{\partial z} = S\frac{\partial\phi_f}{\partial t} + W(x,z,t) \tag{5.16}$$

where

- $W(x,z,t) = (W'(x,z,t)\cdot b)/\rho_i$ = volume flux per unit area (positive sign for outflow, e.g. well pumpage; negative for inflow, e.g. well injection and natural groundwater recharge) $(L\,T^{-1})$,

- T_{xx}, T_{zz} = respectively horizontal and vertical transmissivities $(L^2\,T^{-1})$.

In the original horizontal version of MOC, also evapotranspiration and steady leakage into or from the aquifer through a semi-confining layer can be simulated. However, in the adapted vertical MOC model, this steady leakage is utilized otherwise (see subsection 5.4.2 item 7. **Recharge and discharge**). In the adapted MOC model, the volume flow W comprises fluxes such as injection of surface water by well injection (the so-called *deep-well infiltration*) and extraction of groundwater by well pumpage. The volume flow W also comprises natural groundwater recharge (see subsection 5.4.2 item 7. **Recharge and discharge**).

To solve the equation of groundwater flow numerically, the derivatives are replaced in the finite-difference approximation by values of the difference quotients of the function in separate discrete points, using Taylor-series [Pinder and Bredehoeft, 1968], see figure 5.1:

$$\frac{\partial\phi_f}{\partial x} = \frac{\phi^k_{f(i+1,j)} - \phi^k_{f(i-1,j)}}{2\Delta x} + O(-\frac{1}{6}\Delta x^2\frac{\partial^3\phi_f}{\partial x^3} + ...)$$

$$\frac{\partial^2\phi_f}{\partial x^2} = \frac{\phi^k_{f(i+1,j)} - 2\phi^k_{f(i,j)} + \phi^k_{f(i-1,j)}}{(\Delta x)^2} + O(-\frac{1}{12}\Delta x^2\frac{\partial^4\phi_f}{\partial x^4} + ...) \tag{5.17}$$

and similarly

$$\frac{\partial\phi_f}{\partial z} = \frac{\phi^k_{f(i,j+1)} - \phi^k_{f(i,j-1)}}{2\Delta z} + O(-\frac{1}{6}\Delta z^2\frac{\partial^3\phi_f}{\partial z^3} + ...)$$

$$\frac{\partial^2\phi_f}{\partial z^2} = \frac{\phi^k_{f(i,j+1)} - 2\phi^k_{f(i,j)} + \phi^k_{f(i,j-1)}}{(\Delta z)^2} + O(-\frac{1}{12}\Delta z^2\frac{\partial^4\phi_f}{\partial z^4} + ...) \tag{5.18}$$

---

[4]The fact is ignored that Darcy's law describes flow with respect to the elastically moving solids (Zijl and Nawalany, 1993)
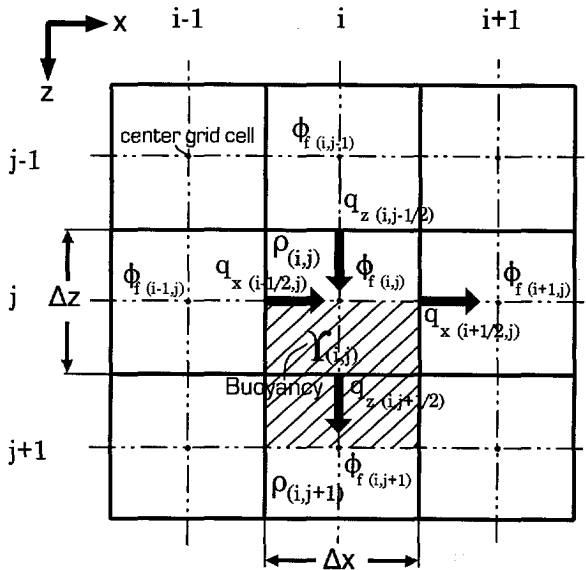
Figure 5.1: Nodal array for development of finite-difference expressions. Note that now the z-axis has been taken as positive downward, so that the gravity acts in positive z-direction. The buoyancy of the vertical velocity $q_{z(i,j+1/2)}$ is determined over the hatched area.

and

$$\Upsilon_{(i,j)} = \frac{\frac{\rho_{(i,j)} + \rho_{(i,j+1)}}{2} - \rho_f}{\rho_f} \tag{5.19}$$

where $\rho_{(i,j)}$, $\rho_{(i,j+1)}$ are the densities of groundwater in respectively the grid cells $[i,j]$ and $[i, j+1]$. The i, j and k are the indices in respectively the x, z and t dimensions, and the Δx, Δz and Δt are increments in respectively the x, z and t dimensions. The approximation for the time derivative is expressed as:

$$\frac{\partial \phi_f}{\partial t} = \frac{\phi_{f(i,j)}^k - \phi_{f(i,j)}^{k-1}}{\Delta t} + O(-\frac{1}{6}\Delta t^2 \frac{\partial^3 \phi_f}{\partial t^3} + ...) \tag{5.20}$$

where Δt is the so-called *flow time step* (T).

The Darcian specific discharges at the boundary of the grid cell $[i,j]$, the so-called *boundary velocities* are given by the explicit finite-difference formulations (see figure 5.1):

$$q_{x(i+1/2,j)}^k = k_{x(i+1/2,j)} \frac{\phi_{f(i,j)}^k - \phi_{f(i+1,j)}^k}{\Delta x} \tag{5.21}$$

and

$$q_{z(i,j+1/2)}^k = k_{z(i,j+1/2)} \left(\frac{\phi_{f(i,j)}^k - \phi_{f(i,j+1)}^k}{\Delta z} + \Upsilon_{(i,j)} \right) \tag{5.22}$$

where

- $q_{x(i+1/2,j)}^k$ = boundary velocity in the x-direction on the boundary between the nodes $[i,j]$ and $[i+1,j]$ $(L\,T^{-1})$,

- $q_{z(i,j+1/2)}^k$ = boundary velocity in the z-direction on the boundary between the nodes $[i,j]$ and $[i,j+1]$ $(L\,T^{-1})$,

- $k_{x(i+1/2,j)}, k_{z(i,j+1/2)}$ = *weighted harmonic mean* of the hydraulic conductivity in respectively the x and z-direction:

$$k_{x(i+1/2,j)} = \frac{2k_{x(i+1,j)}k_{x(i,j)}}{k_{x(i+1,j)} + k_{x(i,j)}}, \qquad k_{z(i,j+1/2)} = \frac{2k_{z(i,j+1)}k_{z(i,j)}}{k_{z(i,j+1)} + k_{z(i,j)}} \quad (5.23)$$

Before November 21, 1988, the original MOC model computed the Darcian specific discharges in the center of the node directly, for example in the x-direction:

$$q_{x(i,j)}^k = k_{x(i,j)}\frac{\phi_{f(i-1,j)}^k - \phi_{f(i+1,j)}^k}{2\Delta x} \quad (5.24)$$

However, in order to avoid discontinuities in velocity in heterogeneous media, the Darcian specific discharges in the center of the node $[i,j]$ have been computed since then by:

$$q_{x(i,j)}^k = \frac{q_{x(i+1/2,j)}^k + q_{x(i-1/2,j)}^k}{2} \qquad q_{z(i,j)}^k = \frac{q_{z(i,j+1/2)}^k + q_{z,(i,j-1/2)}^k}{2} \quad (5.25)$$

The *real velocity* of groundwater flow can be derived by dividing the Darcian specific discharges by the effective porosity n_e of the medium.

Writing out equation 5.16 in terms of finite-difference approximations (and applying equation 5.20) yields:

$$\frac{\partial}{\partial x}\left(T_{xx}\frac{\partial \phi_f}{\partial x}\right)_{(i,j)}^k + \frac{\partial}{\partial z}\left(T_{zz}\frac{\partial \phi_f}{\partial z}\right)_{(i,j)}^k + \frac{\partial}{\partial z}(T_{zz}\Upsilon)_{(i,j)}^k =$$
$$S\left[\frac{\phi_{f(i,j)}^k - \phi_{f(i,j)}^{k-1}}{\Delta t}\right] + W_{(i,j)}(x,z,t) \quad (5.26)$$

The transmissivity midway between $[i,j]$ and $[i-1,j]$ in the x-direction is given by the Taylor-series:

$$T_{xx(i-1/2,j)} = T_{xx(i,j)} - \frac{\Delta x}{2}\frac{\partial T_{xx(i,j)}}{\partial x} + \frac{(\Delta x^2)}{8}\frac{\partial^2 T_{xx(i,j)}}{\partial x^2} \quad (5.27)$$

or after rearranging

$$T_{xx(i,j)} = T_{xx(i-1/2,j)} + \frac{\Delta x}{2}\frac{\partial T_{xx(i,j)}}{\partial x} - \frac{(\Delta x^2)}{8}\frac{\partial^2 T_{xx(i,j)}}{\partial x^2} \quad (5.28)$$

and similarly

$$T_{xx(i,j)} = T_{xx(i+1/2,j)} - \frac{\Delta x}{2}\frac{\partial T_{xx(i,j)}}{\partial x} - \frac{(\Delta x^2)}{8}\frac{\partial^2 T_{xx(i,j)}}{\partial x^2} \qquad (5.29)$$

Now, according to Pinder and Bredehoeft [1968], the transmissivity at the midpoint between two nodes is applied to solve equation 5.26. Rewriting the first term of equation 5.16 yields:

x − direction

$$\frac{\partial}{\partial x}\left(T_{xx}\frac{\partial \phi_f}{\partial x}\right)^k_{(i,j)} = T_{xx(i,j)}\frac{\partial^2 \phi_f}{\partial x^2} + \frac{\partial T_{xx(i,j)}}{\partial x}\frac{\partial \phi_f}{\partial x} \qquad (5.30)$$

or, by applying equation 5.17, after rearranging:

x − direction

$$\frac{\partial}{\partial x}\left(T_{xx}\frac{\partial \phi_f}{\partial x}\right)^k_{(i,j)} = \left[\frac{T_{xx(i,j)}}{(\Delta x)^2} - \frac{1}{2\Delta x}\frac{\partial T_{xx(i,j)}}{\partial x}\right][\phi^k_{f(i-1,j)} - \phi^k_{f(i,j)}]$$

$$+ \left[\frac{T_{xx(i,j)}}{(\Delta x)^2} + \frac{1}{2\Delta x}\frac{\partial T_{xx(i,j)}}{\partial x}\right][\phi^k_{f(i+1,j)} - \phi^k_{f(i,j)}] \qquad (5.31)$$

The expressions of the Taylor-series in the form $(-\frac{1}{6}\Delta x^2\frac{\partial^3 \phi_f}{\partial x^3})$, $(-\frac{1}{12}\Delta x^2\frac{\partial^4 \phi_f}{\partial x^4})$, etc., are neglected. Similarly, the same procedure can be followed for the z-direction:

z − direction

$$\frac{\partial}{\partial z}\left(T_{zz}\frac{\partial \phi_f}{\partial z}\right)^k_{(i,j)} = \left[\frac{T_{zz(i,j)}}{(\Delta z)^2} - \frac{1}{2\Delta z}\frac{\partial T_{zz(i,j)}}{\partial z}\right][\phi^k_{f(i,j-1)} - \phi^k_{f(i,j)}]$$

$$+ \left[\frac{T_{zz(i,j)}}{(\Delta z)^2} + \frac{1}{2\Delta z}\frac{\partial T_{zz(i,j)}}{\partial z}\right][\phi^k_{f(i,j+1)} - \phi^k_{f(i,j)}] \qquad (5.32)$$

Substituting the equations 5.28 and 5.29 into equation 5.31, the finite-difference approximation in the x-direction becomes equation 5.33. Note that the Taylor-series in the equations 5.28 and 5.29 have been truncated after the second term, so that expressions of the form $\frac{(\Delta x)^2}{8}\frac{\partial^2 T_{xx(i,j)}}{\partial x^2}$ have been neglected [Pinder and Bredehoeft, 1968].

x − direction

$$\frac{\partial}{\partial x}\left(T_{xx}\frac{\partial \phi_f}{\partial x}\right)^k_{(i,j)} =$$

$$\left[\frac{1}{(\Delta x)^2}\left(T_{xx(i-1/2,j)} + \frac{\Delta x}{2}\frac{\partial T_{xx(i,j)}}{\partial x}\right) - \frac{1}{2\Delta x}\frac{\partial T_{xx(i,j)}}{\partial x}\right][\phi^k_{f(i-1,j)} - \phi^k_{f(i,j)}]$$

$$+ \left[\frac{1}{(\Delta x)^2}\left(T_{xx(i+1/2,j)} - \frac{\Delta x}{2}\frac{\partial T_{xx(i,j)}}{\partial x}\right) + \frac{1}{2\Delta x}\frac{\partial T_{xx(i,j)}}{\partial x}\right][\phi^k_{f(i+1,j)} - \phi^k_{f(i,j)}] \quad (5.33)$$

or

x − direction

$$\frac{\partial}{\partial x}\left(T_{xx}\frac{\partial \phi_f}{\partial x}\right)^k_{(i,j)} =$$

$$T_{xx(i-1/2,j)}\left(\frac{\phi^k_{f(i-1,j)}-\phi^k_{f(i,j)}}{(\Delta x)^2}\right) + T_{xx(i+1/2,j)}\left(\frac{\phi^k_{f(i+1,j)}-\phi^k_{f(i,j)}}{(\Delta x)^2}\right) \qquad (5.34)$$

and similarly for the z-direction:

z − direction

$$\frac{\partial}{\partial z}\left(T_{zz}\frac{\partial \phi_f}{\partial z}\right)^k_{(i,j)} =$$

$$T_{zz(i,j-1/2)}\left(\frac{\phi^k_{f(i,j-1)}-\phi^k_{f(i,j)}}{(\Delta z)^2}\right) + T_{zz(i,j+1/2)}\left(\frac{\phi^k_{f(i,j+1)}-\phi^k_{f(i,j)}}{(\Delta z)^2}\right) \qquad (5.35)$$

To obtain the final finite-difference approximation for the groundwater flow equation, the equations 5.35 and 5.34 are substituted into equation 5.26:

$$T_{xx(i-1/2,j)}\left(\frac{\phi^k_{f(i-1,j)}-\phi^k_{f(i,j)}}{(\Delta x)^2}\right) + T_{xx(i+1/2,j)}\left(\frac{\phi^k_{f(i+1,j)}-\phi^k_{f(i,j)}}{(\Delta x)^2}\right)$$

$$+T_{zz(i,j-1/2)}\left(\frac{\phi^k_{f(i,j-1)}-\phi^k_{f(i,j)}}{(\Delta z)^2} + \frac{\Upsilon_{(i,j-1)}}{\Delta z}\right) + T_{zz(i,j+1/2)}\left(\frac{\phi^k_{f(i,j+1)}-\phi^k_{f(i,j)}}{(\Delta z)^2} - \frac{\Upsilon_{(i,j)}}{\Delta z}\right) =$$

$$S\left[\frac{\phi^k_{f(i,j)}-\phi^{k-1}_{f(i,j)}}{\Delta t}\right] + W_{(i,j)}(x,z,t) \qquad (5.36)$$

5.2.4 Alternating-direction implicit procedure

In the applied version of MOC, the iterative *alternating-direction implicit* procedure (*ADI*), developed by Peaceman & Rachford and Douglas & Peaceman in 1955[5], is applied to solve the equations. This (backward difference in time) technique is unconditionally stable, and thus, there are no stability restrictions on the length of Δt as in an explicit (forward difference in time) technique. A brief summary of the technique from Pinder and Bredehoeft [1968] is given, though they applied the non-iterative *ADI*, whereas here the iterative version is applied in order to allow greater time steps. The difference between the iterative and the non-iterative version can be concluded from the use of iteration parameters [Trescott, Pinder and Larson, 1976].

The piezometric levels ϕ_f in equation 5.36 are unknown in only one coordinate direction, the known piezometric levels are calculated at the time level k. During one complete cycle of $2N$ calculations, the entire matrix is solved twice, using the two equations 5.37 and 5.38:

column: implicit in z−direction, explicit in x−direction

$$\frac{T_{xx(i-1/2,j)}}{(\Delta x)^2}\left(\phi^k_{f(i-1,j)} - \phi^k_{f(i,j)}\right) + \frac{T_{xx(i+1/2,j)}}{(\Delta x)^2}\left(\phi^k_{f(i+1,j)} - \phi^k_{f(i,j)}\right)$$

---

[5]This procedure has extensively been used by the petroleum industry for predicting oil and gas reservoir behaviour.

$$+\frac{T_{zz(i,j-1/2)}}{(\Delta z)^2}\left(\phi_{f(i,j-1)}^{k+1}-\phi_{f(i,j)}^{k+1}+\Upsilon_{(i,j-1)}\Delta z\right)$$

$$+\frac{T_{zz(i,j+1/2)}}{(\Delta z)^2}\left(\phi_{f(i,j+1)}^{k+1}-\phi_{f(i,j)}^{k+1}-\Upsilon_{(i,j)}\Delta z\right)=$$

$$S\left[\frac{\phi_{f(i,j)}^{k+1}-\phi_{f(i,j)}^{k}}{\Delta t}\right]+W_{(i,j)}(x,z,t) \tag{5.37}$$

and

row: implicit in x–direction, explicit in z–direction

$$\frac{T_{xx(i-1/2,j)}}{(\Delta x)^2}\left(\phi_{f(i-1,j)}^{k+1}-\phi_{f(i,j)}^{k+1}\right)+\frac{T_{xx(i+1/2,j)}}{(\Delta x)^2}\left(\phi_{f(i+1,j)}^{k+1}-\phi_{f(i,j)}^{k+1}\right)$$

$$+\frac{T_{zz(i,j-1/2)}}{(\Delta z)^2}\left(\phi_{f(i,j-1)}^{k+1}-\phi_{f(i,j)}^{k+1}+\Upsilon_{(i,j-1)}\Delta z\right)$$

$$+\frac{T_{zz(i,j+1/2)}}{(\Delta z)^2}\left(\phi_{f(i,j+1)}^{k+1}-\phi_{f(i,j)}^{k+1}-\Upsilon_{(i,j)}\Delta z\right)=$$

$$S\left[\frac{\phi_{f(i,j)}^{k+1}-\phi_{f(i,j)}^{k}}{\Delta t}\right]+W_{(i,j)}(x,z,t) \tag{5.38}$$

The technique first calculates values by sweeping the matrix column by column (using equation 5.37), and then recalculates the matrix by sweeping row by row (using equation 5.38). For instance, rewriting equation 5.37, the finite-difference expression for any column gives:

column

$$\frac{T_{zz(i,j-1/2)}}{(\Delta z)^2}\phi_{f(i,j-1)}^{k+1}-[\frac{T_{zz(i,j+1/2)}}{(\Delta z)^2}+\frac{T_{zz(i,j-1/2)}}{(\Delta z)^2}+\frac{S}{\Delta t}]\phi_{f(i,j)}^{k+1}+\frac{T_{zz(i,j+1/2)}}{(\Delta z)^2}\phi_{f(i,j+1)}^{k+1}=$$

$$-\frac{T_{xx(i-1/2,j)}}{(\Delta x)^2}\phi_{f(i-1,j)}^{k}+[\frac{T_{xx(i-1/2,j)}}{(\Delta x)^2}+\frac{T_{xx(i+1/2,j)}}{(\Delta x)^2}-\frac{S}{\Delta t}]\phi_{f(i,j)}^{k}-\frac{T_{xx(i+1/2,j)}}{(\Delta x)^2}\phi_{f(i+1,j)}^{k}$$

$$-\frac{T_{zz(i,j-1/2)}}{\Delta z}\Upsilon_{(i,j-1)}+\frac{T_{zz(i,j+1/2)}}{\Delta z}\Upsilon_{(i,j)}+W_{(i,j)}(x,z,t) \tag{5.39}$$

Analogous expressions for these equations are of the form:

$$\begin{aligned} B_1\phi_{f,1}+C_1\phi_{f,2} &= D_1 \\ A_j\phi_{f,j-1}+B_j\phi_{f,j}+C_j\phi_{f,j+1} &= D_j, \qquad \text{for } 2\le j\le\eta-1, \\ A_\eta\phi_{f,\eta-1}+B_\eta\phi_{f,\eta} &= D_\eta \end{aligned} \tag{5.40}$$

where

- η is the length of the row or column under consideration,

- A_j, B_j and C_j are the coefficients of the unknown piezometric level values. A_j stands for the term that belongs to $\phi_{f(i,j-1)}^{k+1}$ in equation 5.39, B_j to $\phi_{f(i,j)}^{k+1}$ and C_j to $\phi_{f(i,j+1)}^{k+1}$.

- D_j is the sum of all known parameters, namely all terms on the right hand side of equation 5.39.

The following *dummy variables* w_j (T^{-1}) and g_j (L) are defined:

$$w_j = B_j - \frac{A_j C_{j-1}}{w_{j-1}}$$

$$g_j = \frac{D_j - A_j g_{j-1}}{w_j} \tag{5.41}$$

When the last node in the row or column is reached, the piezometric level is calculated in order of decreasing j as follows:

$$\phi_{f,j} = g_j - \frac{C_j \phi_{f,j+1}}{w_j};$$

$$\text{if} \quad j = \eta \quad \text{then} \quad \phi_{f,j} = g_j \tag{5.42}$$

To take into account the boundary conditions, some small adjustments must be executed. For instance, if the edge is a *barrier boundary*, the reflection technique is employed: $\phi_{f,j-1} = \phi_{f,j+1}$ and $A_1 = C_1$.

In MOC, additional terms are appended in the dummy variables. These terms represent iteration parameters, as the *iterative* version of the *alternating-direction implicit* procedure ADI is applied. Iteration parameters are applied to compute rapidly the acceptable freshwater head ϕ_f. The determination of the iteration parameters is not discussed here. See for more information Trescott, Pinder and Larson [1976].

5.3   Solute transport

The two-dimensional equation for solute transport in homogeneous isotropic porous media can be written as follows [Konikow and Bredehoeft, 1978]:

$$\frac{\partial (Cb)}{\partial t} = \frac{\partial}{\partial x_i}(b\, D_{ij}\, \frac{\partial C}{\partial x_j}) - \frac{\partial}{\partial x_i}(b\, C\, V_i) - \frac{C'\, W}{n_e} \tag{5.43}$$

where

- C = concentration of the dissolved solutes $(M\, L^{-3})$,

- D_{ij} = coefficient of hydrodynamic dispersion (a second-order tensor) $(L^2\, T^{-1})$,

- $V_i = q_i/n_e$ = real velocity of the groundwater in the direction of x_i $(L\, T^{-1})$,

- C' = concentration of the dissolved solutes in a source or sink $(M\, L^{-3})$,

- b = saturated thickness of the aquifer (L).

This equation is called the *advection-dispersion equation* or *transport-dispersion equation*. The first term on the right hand side represents the change in concentration of solutes due to hydrodynamic dispersion. The second term represents the effect of advective transport[6], that is the movement of solutes attributed to transport by flowing

---

[6]Sometimes this *advection* process is erroneously called the *convection* process. In fact, the term *convection* is reserved for thermally driven groundwater flow [Freeze and Cherry, 1979].

groundwater. The third term represents the contribution and removal of solutes due to fluid sources and sinks.

Already since August 2, 1985 (and modified again for more extensive chemical reactions by Goode and Konikow [1989]), MOC is suited to simulate non-conservative solute transport in saturated groundwater flow regimes. Nonetheless, the effects of e.g. radioactive decay, sorption and exchange is not considered in this thesis, as the attention is only focused on a conservative solute, the chloride ion.

The solution technique of the advection-dispersion equation 5.43 in the adapted version of MOC does not differ from the solution technique in the original version. Therefore, the solution technique applied by Konikow and Bredehoeft [1978] is only summarized here.

5.3.1 Dispersion coefficient

Hydrodynamic dispersion D_h is defined as the sum of two processes, $D_h = D_m + D_d$:

1. mechanical (or convective) dispersion D_m
   This process is caused by velocity variations at the microscopic scale. The spreading depends on both fluid flow and the characteristics of the pore system through which the flow takes place,

2. molecular diffusion D_d
   This process is caused by the random movement of molecules in a fluid and depends on concentration gradients, the properties of the fluid and the soil.

Under normal groundwater flow conditions, molecular diffusion is of marginal importance with respect to mechanical dispersion. The subdivision of the hydrodynamic dispersion into mechanical dispersion and molecular diffusion is artificial. From analysis of experimental values in the 1950's, the coefficient of hydrodynamic dispersion D_h is, in general, a function of the *Peclet-number* of molecular diffusion [Bear, 1972]:

$$Pe \equiv \frac{V\,d}{D_d} = \frac{(q/n_e)\,d}{D_d} \tag{5.44}$$

where

- Pe = Peclet-number $(-)$,

- d = mean grain size or any other characteristic medium length (a measure of the pore spacing) (L).

Five zones of mixing were proposed by Pfannkuch (in 1963) which are related to the Peclet-number. For small Peclet-numbers, e.g. $Pe \leq 0.4$, molecular diffusion predominates because the average velocity of the flow is very small. For Peclet-numbers approximately within the range $0.4 \leq Pe \leq 5$, the effects of molecular diffusion and mechanical dispersion are of the same order of magnitude. For $Pe \geq 5$,

three zones can be distinguished, in which the mechanical dispersion dominates. For an extensive description of hydrodynamic dispersion, see, e.g., Bear [1972].

The mechanical dispersion coefficient, which is a second-rank symmetrical tensor, is given by Scheidegger [1961]:

$$D_{ij} = \alpha_{ijmn} \frac{V_m V_n}{|V|} \tag{5.45}$$

where

- D_{ij} = coefficient of mechanical dispersion $(L^2 T^{-1})$,

- α_{ijmn} = *geometrical dispersivity tensor* of the aquifer (L),

- V_m, V_n = components of the real velocity in m and n direction $(L T^{-1})$,

- $|V|$ = magnitude of the real velocity $(L T^{-1})$.

Scheidegger defines the dispersivity tensor for an isotropic aquifer in terms of two constants:

$$\begin{aligned} D_L &= \alpha_L |V| \\ D_T &= \alpha_T |V| \end{aligned} \tag{5.46}$$

where

- α_L = *longitudinal* dispersivity of the aquifer (L),

- α_T = *transversal* dispersivity of the aquifer (L).

In the adapted MOC model, not only mechanical dispersion, but also molecular diffusion D_d is considered. Thus, the components of hydrodynamic dispersion (in the principal directions) for two-dimensional flow in an isotropic aquifer are as follows:

$$\begin{aligned} D_{xx} &= D_L \frac{(V_x)^2}{|V|^2} + D_T \frac{(V_z)^2}{|V|^2} + D_d \\ D_{zz} &= D_T \frac{(V_x)^2}{|V|^2} + D_L \frac{(V_z)^2}{|V|^2} + D_d \\ D_{xz} &= D_{zx} = (D_L - D_T) \frac{V_x V_z}{|V|^2} \end{aligned} \tag{5.47}$$

See subsection 5.4.5 for more information on the applied hydrodynamic dispersion.

5.3.2 Method of characteristics

Which of the terms of the advection-dispersion equation is more prominent depends on the advective and dispersive fluxes at the level of the discretization element [Kinzelbach, 1987a]. The so-called *grid-Peclet-numbers* Pe_{grid} can be applied to assess the most dominant process:

$$Pe_{grid,x} = \left| \frac{V_x \Delta x}{D_{xx}} \right| \qquad \text{and} \qquad Pe_{grid,z} = \left| \frac{V_z \Delta z}{D_{zz}} \right| \tag{5.48}$$

where

- $Pe_{grid,x}, Pe_{grid,z}$ = grid-Peclet-numbers in x and z-direction $(-)$,

- V_x, V_z = real velocity of the groundwater in x and z-direction $(L\,T^{-1})$.

For small grid-Peclet-numbers $(Pe_{grid} < 1)$ the parabolic nature of the advection-dispersion equation prevails, whereas for great grid-Peclet-numbers $(Pe_{grid} > 2)$ the hyperbolic nature dominates. As it appears that advective transport of solute dominates over dispersive transport in most field problems, the hyperbolic nature prevails. Unfortunately, numerical solving of an equation with a hyperbolic nature is more difficult than solving an equation with a parabolic nature.

Equation 5.43 is rewritten by expanding the derivatives:

$$b\frac{\partial C}{\partial t} + C\frac{\partial b}{\partial t} = \frac{\partial}{\partial x_i}\left(b\, D_{ij} \frac{\partial C}{\partial x_j} \right) - bV_i\frac{\partial C}{\partial x_i} - Cb\frac{\partial V_i}{\partial x_i} - CV_i\frac{\partial b}{\partial x_i} - \frac{C'\,W}{n_e} \tag{5.49}$$

Note that in the original MOC model, the thickness b is still considered as a variable. In combination with equation 5.16, which can be rewritten as:

$$-\frac{\partial(bq_i)}{\partial x_i} = S\frac{\partial \phi_f}{\partial t} + W \tag{5.50}$$

or

$$-n_e\left(b\frac{\partial V_i}{\partial x_i} + V_i\frac{\partial b}{\partial x_i} \right) = S\frac{\partial \phi_f}{\partial t} + W \tag{5.51}$$

equation 5.49, divided by b, gives the simplified formulation:

$$\frac{\partial C}{\partial t} = \frac{1}{b}\frac{\partial}{\partial x_i}\left(b\, D_{ij} \frac{\partial C}{\partial x_j} \right) - V_i\frac{\partial C}{\partial x_i} + \frac{C(S\frac{\partial \phi_f}{\partial t} + W - n_e\frac{\partial b}{\partial t}) - C'\,W}{n_e\, b} \tag{5.52}$$

The term $(S\frac{\partial \phi_f}{\partial t} + W - n_e\frac{\partial b}{\partial t})$ in equation 5.52 needs some explanation. This term was completely taken into account in the original MOC model for transient flow cases[7]. However, since December 4, 1980, this term was simplified, leaving only

---

[7]The original model of Konikow and Bredehoeft [1978] assumed that for $S < 0.005$, the aquifer would be confined and thus $\frac{\partial b}{\partial t} = 0$, while for $S \geq 0.005$ the model assumed $\frac{\partial b}{\partial t} = \frac{\partial \phi_f}{\partial t}$.

the sources and sinks term W by assuming $S\frac{\partial \phi_f}{\partial t} = n_e \frac{\partial b}{\partial t}$. This was realized in order to reduce numerical errors, as then errors in the groundwater flow equation could not propagate in the advection-dispersion equation. The modification led to a more simplified formulation of the advection-dispersion equation, the so-called flow-equation-removed equation [Goode, 1992]:

$$\frac{\partial C}{\partial t} = \frac{1}{b} \frac{\partial}{\partial x_i} \left(b \, D_{ij} \frac{\partial C}{\partial x_j} \right) - V_i \frac{\partial C}{\partial x_i} + \frac{W(C - C')}{n_e \, b} \tag{5.53}$$

Nevertheless, it was demonstrated that ignoring temporal changes in fluid-storage for transient flow ($S \neq 0$) could result in significant errors in solute travel time [e.g. Goode, 1992]. Subsequently, Goode and Konikow updated MOC once again in November, 1988 by accounting for the product $n_e b$ of porosity and aquifer thickness for temporal changes.

Note that the discussion mentioned above does not affect the adapted MOC model. As a matter of fact, in the adapted MOC model, the removal of the time derivative of the fluid-storage term from the advection-dispersion equation would not have consequences for two reasons: first, the simulated vertical profiles have a hypothetical *constant* thickness or width of *one foot* (unit of length), and second, the time scale of solute transport is so great that the transient component of the groundwater flow is of negligible importance.

Anyway, the rate of change of concentration $\frac{\partial C}{\partial t}$, as observed from a fixed point (e.g. the node or center of a grid cell), can be redefined by:

$$\frac{dC}{dt} = \frac{\partial C}{\partial t} + \frac{\partial C}{\partial x} \frac{dx}{dt} + \frac{\partial C}{\partial z} \frac{dz}{dt} \tag{5.54}$$

where

- $\frac{dC}{dt}$ = the so-called *material derivative* of concentration: the rate of change of concentration as observed when moving with the fluid particle,

- $\frac{\partial C}{\partial t}$ = rate of change of concentration as observed from a fixed point.

The material derivatives of position $\frac{dx}{dt}$ and $\frac{dz}{dt}$, which correspond with the movement of fluid particles through the flow field, in equation 5.54 are defined by the real velocity:

$$\frac{dx}{dt} = V_x \tag{5.55}$$

$$\frac{dz}{dt} = V_z \tag{5.56}$$

Thus, combination of the equations 5.53 to 5.56 yields:

$$\frac{dC}{dt} = \frac{1}{b} \frac{\partial}{\partial x_i} \left(b \, D_{ij} \frac{\partial C}{\partial x_j} \right) + \frac{W(C - C')}{n_e \, b} \tag{5.57}$$

The solutions of the system of equations 5.55, 5.56 and 5.57 are:

$$x = x(t); \; z = z(t); \; C = C(t) \tag{5.58}$$

which are called the *characteristic curves*. Garder, Peaceman and Pozzi [1964] were the first to introduce the so-called *method of characteristics* into the solution of multidimensional miscible displacement. They stated that:

> *"Each point corresponds to one characteristic curve, and the values of x,*
> *y and C are obtained as functions of t for each characteristic."*

The basic concept of the method of characteristics is to solve the components of the advection-dispersion equation separately [Konikow and Bredehoeft, 1978]:

a. the advection term (equations 5.55 and 5.56) through a so-called *particle tracking* procedure,

b. the dispersion term as well as the term for sources and sinks (equation 5.57) through finite-difference approximations, using a coordinate system at rest relative to the advective movement.

ad a. In fact, the method of characteristics is developed for solving the advective term. The solution of the equations 5.55 and 5.56 can be obtained by following the characteristic curves. This following of curves is numerically achieved by introducing moving points, namely particles that can be traced through the flow field within the stationary coordinates of the finite-difference grid. This process is called *particle tracking*.

The following procedure is performed in MOC. Each particle has a position and a concentration associated with it. The initial concentration assigned to each particle is the initial concentration associated with the node of the grid cell containing that particle. As a result, a number of particles are placed in each grid cell of the finite-difference grid to form a set of particles that is distributed in a geometrically uniform pattern. For each time level k, every particle is moved over a distance through the flow field in proportion to the length of the time step, the so-called *solute time step* Δt_s, and the flow velocity at the location of that particle:

$$
\begin{aligned}
x_p^k &= x_p^{k-1} + \delta x_p = x_p^{k-1} + \Delta t_s \, V_{x\,[x_p^k, z_p^k]} \\
z_p^k &= z_p^{k-1} + \delta z_p = z_p^{k-1} + \Delta t_s \, V_{z\,[x_p^k, z_p^k]}
\end{aligned}
\tag{5.59}
$$

where

- $p =$ index number for particle identification,
- $\delta x_p, \delta z_p =$ distances moved in the x and z-direction (L),
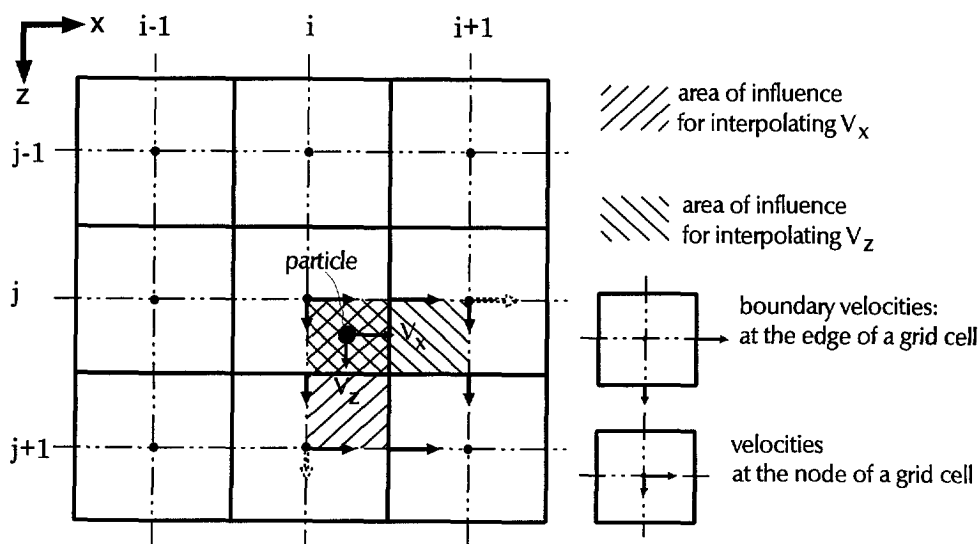- $\Delta t_s =$ solute time step at time level k (T),

Figure 5.2: Example of how to calculate the velocity of a particle by bilinear interpolation of the velocities (after Konikow and Bredehoeft, 1978).

- $V_{i\,[x_p^k,z_p^k]}$ = real velocity at the position of any particular particle p in the i-direction $(L\,T^{-1})$.

The velocity at the location of the particle is determined by *bilinear interpolation* of the velocities at adjacent nodes in combination with the so-called boundary velocities, which are situated at the edges of grid cells (see figure 5.2 and Konikow and Bredehoeft, 1978).

Obviously, particle path lines are sensitive to what technique is applied for spatial interpolation of the velocities within block-centered finite-difference schemes, especially for heterogeneous aquifers [Goode, 1990]. Goode evaluated three interpolation schemes: the linear, the bilinear and the so-called *grad scheme*, which applies bilinear interpolation of *head* gradients. It appears that the selection of the best interpolation scheme depends on how transmissivity changes: e.g. the grad scheme is the most accurate of the three in block-heterogeneous systems, that is if transmissivity changes abruptly. However, if transmissivity varies smoothly, the bilinear scheme appears to be more accurate than both the linear scheme and the grad scheme. As profiles in the Netherlands can be schematised by heterogeneous media, it might be worth to investigate the sensitivity of the solution for the applied spatial interpolation scheme used in the particle tracking procedure. Nevertheless, this investigation is beyond the scope of this thesis.

ad b. the changes in concentration caused by hydrodynamic dispersion, and fluid sources and sinks are solved by an explicit finite-difference approximation of equation 5.57:

$$\Delta C_{i,j}^k = \Delta t_s \left[\frac{1}{b} \frac{\partial}{\partial x_i} \left(b\, D_{ij} \frac{\partial C}{\partial x_j} \right) + \frac{W(C - C')}{n_e\, b} \right] \qquad (5.60)$$

or

$$\Delta C_{i,j}^k = (\Delta C_{i,j}^k)_I + (\Delta C_{i,j}^k)_{II} \qquad (5.61)$$

where

- $(\Delta C_{i,j}^k)_I$ = change in concentration by hydrodynamic dispersion,

- $(\Delta C_{i,j}^k)_{II}$ = change in concentration by sources and sinks.

As computation of the concentration gradient for a large number of particles appears to be laborious, equation 5.61 is solved in MOC at each node of the grid rather than directly at the location of each particle [Konikow and Bredehoeft, 1978]. The first right hand term in equation 5.61 can be rewritten as follows:

$$(\Delta C_{i,j}^k)_I = \frac{\Delta t_s}{b} \left[\frac{\partial}{\partial x}(b\, D_{xx} \frac{\partial C}{\partial x} + b\, D_{xz} \frac{\partial C}{\partial z}) + \frac{\partial}{\partial z}(b\, D_{zz} \frac{\partial C}{\partial z} + b\, D_{zx} \frac{\partial C}{\partial x}) \right]$$
$$(5.62)$$

Substitution of spatial derivatives of the concentration gives an explicit finite-difference approximation that is applied in Konikow and Bredehoeft [1978]. The second right hand term in equation 5.61 can also be rewritten by an explicit finite-difference approximation:

$$(\Delta C_{i,j}^k)_{II} = \frac{\Delta t_s}{n_e\, b_{i,j}^k} \left[W_{i,j}^k(C_{i,j}^{k-1} - C_{i,j}'^{\,k}) \right] \qquad (5.63)$$

The equations 5.55, 5.56 and 5.57 should be solved simultaneously. However, this is not achievable, since equations 5.55 and 5.56 are solved by particle movement on implicitly computed freshwater heads, while equation 5.57 (or rather equations 5.62 and 5.63) is solved explicitly with respect to concentrations. Obviously, the accuracy of estimating the concentration gradient affects the accuracy of the numerical results.

The change in concentration is the sum of the following terms:

$$C_{i,j}^k = C_{i,j}^{k^*} + \Delta C_{i,j}^k \qquad (5.64)$$

where

- $C_{i,j}^k$ = new nodal concentration at the end of time level k $(M\,L^{-3})$,

- $C_{i,j}^{k^*}$ = average of the concentration of all particles in cell $[i, j]$ for time level k after only advective transport $(M\,L^{-3})$,

- $\Delta C_{i,j}^k$ = change in concentration caused by hydrodynamic dispersion (dispersion term), sources and sinks ($M\,L^{-3}$).

The procedure is as follows:

1. first, the concentration gradients at the previous time level ($k-1$) are determined at each node,

2. second, based on equation 5.59, the particles are convected to new positions for time level k^*, which is a new time level k *prior* to the adjustments for concentration for dispersion and mixing (sources and sinks). The time index is distinguished with an asterisk $*$, because this temporarily assigned average concentration represents the new time level only with respect to advective transport [Konikow and Bredehoeft, 1978],

3. after all particles have been moved, the concentration at each node is *temporarily* assigned the average of the concentration $C_{i,j}^{k^*}$ of all particles which are at that moment located within the area of that specific grid cell,

4. at the new positions of the particles, the concentration gradients are computed again at each node from concentrations at the time level k^*,

5. finally, since the concentration gradients are continuously changing with time, e.g. from the $k-1$ to the k time level, a two-step explicit procedure is applied to adjust the concentration distribution at each node: thus first based on concentration gradients at $k-1$, and second based on concentration gradients at k^*. Thus, the change in concentration due to dispersion and sources and sinks is determined by:

$$\Delta C_{i,j}^k = \frac{0.5\,\Delta t_s}{b}\left[\frac{\partial}{\partial x_i}\left(b\,D_{ij}\frac{\partial C_{i,j}^{k-1}}{\partial x_j}\right) + \frac{W_{i,j}^{k-1}(C_{i,j}^{k-1}-C_{i,j}'^{k-1})}{n_e}\right]$$
$$+\frac{0.5\,\Delta t_s}{b}\left[\frac{\partial}{\partial x_i}\left(b\,D_{ij}\frac{\partial C_{i,j}^{k^*}}{\partial x_j}\right) + \frac{W_{i,j}^{k}(C_{i,j}^{k^*}-C_{i,j}'^{k})}{n_e}\right] \qquad (5.65)$$

5.3.3 Stability criteria

A number of stability criteria determine the explicit numerical solution of the advection-dispersion equation in Konikow and Bredehoeft [1978]. These criteria may require that the flow time step Δt, applied to solve the groundwater flow equation, must be subdivided into a number of smaller solute time steps Δt_s to accurately solve the advection-dispersion equation. During such a solute time step, particles are moved to new positions. The distance over which a particle is moved is proportional to the length of that solute time step and the velocity at the location of that particle (see equation 5.59).

Three stability criteria of the advection-dispersion equation, which must all three be satisfied in MOC, are discussed here:

1. The explicit solution of equation 5.62 is stable, according to Redell and Sunada [1970], if:

$$\frac{D_{xx}\Delta t_s}{(\Delta x)^2} + \frac{D_{zz}\Delta t_s}{(\Delta z)^2} \leq 0.5 \tag{5.66}$$

This expression is called the *Neumann-criterion*. Solving equation 5.66 for Δt_s yields:

$$\Delta t_s \leq \min{}_{\text{(over grid)}} \left[\frac{0.5}{\frac{D_{xx}}{(\Delta x)^2} + \frac{D_{zz}}{(\Delta z)^2}}\right] \tag{5.67}$$

From equation 5.67 can be deduced that the maximum permissible time step in the simulation is the smallest Δt_s computed for any individual node in the entire grid. Thus, the smallest permissible time step Δt_s for solving the advection-dispersion equation occurs in the node that has the greatest value of $\frac{D_{xx}}{(\Delta x)^2} + \frac{D_{zz}}{(\Delta z)^2}$.

2. Consider the mixing of groundwater of one concentration $C_{i,j}$ with injected or recharged (surface) water of a different concentration $C'_{i,j}$. The change in concentration in that specific source node is not allowed to exceed the difference between the concentration in the aquifer $C_{i,j}$ and the source concentration $C'_{i,j}$:

$$(\Delta C_{i,j}^k)_{II} \leq C_{i,j}^{k-1} - C_{i,j}'^k \tag{5.68}$$

In combination with equation 5.63, equation 5.68 produces:

$$\Delta t_s \leq \min{}_{\text{(over grid)}} \left[\frac{n_e\, b_{i,j}^k}{W_{i,j}^k}\right] \tag{5.69}$$

3. The last stability criterion for the maximum permissible time step Δt_s involves the particle movements to simulate advective transport. Equation 5.59 shows that the distance a particle moves is a linear spatial extrapolation from one time level to the next. However, as the streamlines are curvilinear, an error is introduced into the numerical solution. In order to suppress the deviation of the particles from the streamline, the solute time step should be such that no critical distance is exceeded:

$$\Delta t_s V_{x\,[x_p^k, z_p^k]} \leq \zeta \Delta x$$
$$\Delta t_s V_{z\,[x_p^k, z_p^k]} \leq \zeta \Delta z \tag{5.70}$$

where

- ζ = the maximum relative distance across a grid cell, in which a particle is allowed to move during one solute time step Δt_s. It is usually a fraction of the grid dimension $(0 < \zeta \leq 1)$ in order to ensure that the particle movements are controlled within one solute time step.

Obviously, this criterion is based on the Courant-number Co, see subsection 4.4.3.
Rewriting equation 5.70 gives:

$$\Delta t_s \leq \frac{\zeta \Delta x}{(V_x)_{max}}$$

$$\Delta t_s \leq \frac{\zeta \Delta z}{(V_z)_{max}} \tag{5.71}$$

where

- $(V_x)_{max}, (V_z)_{max}$ = the maximum real velocity at a node or boundary of
  a grid cell respectively in the x and z-direction.

Finally, the smallest solute time step Δt_s is applied which is determined by the
equations 5.67, 5.69 and 5.71. If the flow time step Δt is greater than the smallest
solute time step Δt_s, then the flow time step Δt is subdivided into the appropriate
number of smaller time steps Δt_s required to solve the advection-dispersion equation.
It may occur that the stability criteria are not so strict that the smallest required
solute time step Δt_s is greater than the flow time step Δt. Then, Δt_s must be equal
to Δt, as the flow time step is imposed in advance.

5.3.4 Numerical dispersion

Numerical dispersion is caused by the numerical calculation process. Although the
method of characteristics itself does not introduce numerical dispersion [Garder,
Peaceman and Pozzi, 1964], solving the advection-dispersion equation generates nu-
merical dispersion due to, among others, the movement and tracking of particles, the
conversion from particles to grid cells and finite-difference approximations. Examples
of how numerical dispersion occurs in MOC are:

- solving the concentration gradient by finite-difference approximations. For in-
  stance, the spatial derivatives of concentration in equation 5.62 are approxi-
  mated by the average (*weighted arithmetic mean*) of the concentration in adja-
  cent grid cells,

- averaging the concentration $C_{i,j}^{k^*}$ in a grid cell, based on all particles that are
  located within a grid cell at the time level k^*,

- assigning concentrations at nodes of sources and sinks to the entire area of
  the grid cell. Concentration variations within the area of the grid cell are
  eliminated,

- eliminating concentration variations within individual grid cells. This occurs
  when too many grid cells have become void of particles (e.g. two percents of all
  participating grid cells). Then, a procedure (called GENPT) is executed that
  initiates again a uniform distribution of tracer particles throughout the entire

grid. The procedure attempts to preserve an approximation of the previous concentration gradient within each grid cell,

- calculating zero change in concentration due to convective transport (equation 5.59) at nodes which became void due to divergent flow, though the nodal concentration is still adjusted due to hydrodynamic dispersion, fluid sources and sinks (equation 5.60).

Some special problems associated with MOC, in particular moving and tracking of particles in the particle tracking procedure, are pictured only briefly here. See for further information Konikow and Bredehoeft [1978]. Some special aspects are: ·

- in order to prevent that groundwater or solute cross a no-flow boundary, particles have to be relocated within the aquifer by reflection across the boundary, see figure 5.3,
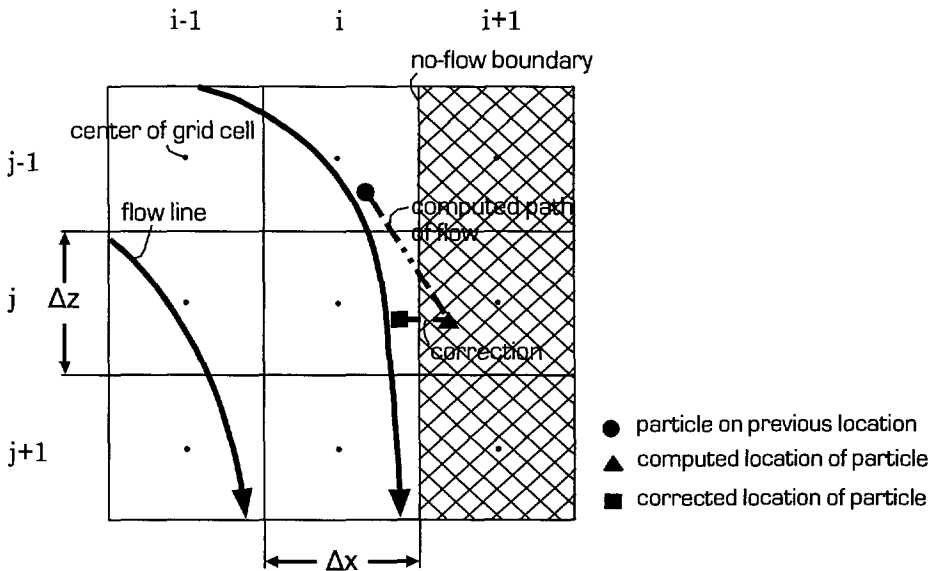
Figure 5.3: Possible movements of particles near an impermeable (no-flow) boundary [after Konikow and Bredehoeft, 1978].

- in areas with fluid sources or sinks in grid cells, a special procedure is required to maintain a reasonably uniform and continuous spacing of particles,

- in order to maintain the total number of particles in the entire flow field at a nearly constant value, new particles have to be created at sources and old particles have to be removed at sinks or discharge boundaries.

Changes in the solute concentration of particles due to chemical reactions or physical processes may also cause problems in the particle tracking procedure. However, as mentioned before, this is not considered in this thesis. Finally, numerical dispersion also occurs in combination with numerical instabilities in the (vertical) velocity field due to, among others, density differences. This phenomenon is discussed in subsection 5.5.1.

5.4   Parameters in MOC

In MOC, parameters are specified in the so-called *input data file* to properly compute the freshwater head distribution, the solute concentration distribution and both horizontal and vertical velocities as a function of specific moments in time. They are subdivided into:

- *model* parameters which determine the setup of the computation,

- *subsoil* parameters or *geohydrologic* parameters which determine the geometry and geohydrology of the schematised profile,

- initial and boundary conditions.

As MOC is adapted for density differences, two classes of parameters are distinguished: (1) those parameters that have the same meaning in the adapted as well as in the original MOC model: they are only discussed occasionally; and (2) those parameters that have a different physical meaning in the adapted MOC model or are additionally defined due to the density differences.

The sensitivity of the solution for both model and subsoil parameters is discussed in various case studies, e.g. sections 6.2, 6.3 and chapter 7.

5.4.1   Model parameters

As several parameters, such as the maximum permitted number of *iterations* for the groundwater flow equation and the printing output options, have the same meaning in both the original model and the adapted model, they are not discussed in this thesis. See for further information Konikow and Bredehoeft [1978].

1. Number of grid cells

MOC uses rectangular, block-centered grid cells, as the finite-difference method is applied to solve the groundwater flow equation and the advection-dispersion equation. Originally (1978), the maximum number of grid cells was 20 by 20 (with a maximum of 3200 particles). During the 1980's, the maximum number of grid cells was expanded to some 900 (e.g. $30 \cdot 30^8$ with 12,500 particles), if the program had

---

[8]MOC uses dummy grid cells around the finite-difference grid, thus in fact $32 \cdot 32$ grid cells were applied.

to be executed under *Conventional Memory* of 640 *Kb*. If more memory was available (the so-called *Extended Memory*), e.g. on the *Mainframe* or on *VAX*-computers, then more grid cells could be applied (e.g. 3600 or 60 · 60 grid cells with 20,000 particles). The adapted MOC model with larger numbers of grid cells was applied by: the Laboratory of Applied Geology and Hydrology of the State University of Ghent, Belgium (Lebbe); the National Institute of Public Health and Environmental Protection (RIVM, formerly RID) (van der Eem and Peters); the Testing and Research Institute of the Netherlands Waterworks (KIWA) [van der Eem, 1986]; and Gemeentewaterleidingen Amsterdam (Kooiman).

In the late 1980's, the boom in computer capacities had attained such proportions that even stand-alone Personal Computers with Extended Memory of several Mb RAM could accommodate a much larger number of grid cells than originally possible. For instance, during the first years of this study the author applied a 4 Mb RAM computer (Hewlett-Packard[9]) that could reproduce some 9000 (e.g. 250·36) grid cells with some 76,000 particles. The latest stand-alone PC the author applied, a 8 Mb RAM computer (Highscreen[10]), can reproduce some 20,000 (e.g. 500 · 40) grid cells with 180,000 particles. In order to address the Extended Memory RAM, a Lahey Fortran compiler[11] and a Lahey/Ergo Operating System[12] was utilized.

When vertical profiles are simulated, the number of grid cells in horizontal direction is usually greater than the number of grid cells in vertical direction. The shape of a grid cell can be rectangular. The ratio horizontal length Δx to vertical height Δz can range from 25 to 1 without numerical problems, as is demonstrated in the simulated case studies.

2. Number of particles

The following numbers of particles in a grid cell could be applied in the original MOC model of 1978: 4, 5 and 9 particles. Obviously, the solute transport is simulated more exact with more particles per grid cell. Since June 10, 1985, the computer code was adapted by Sanford in order to specify 16 particles per grid cell, as this could lead to an increase in numerical accuracy of the solution of the solute transport. Since August 12, 1985, it is allowed to specify 1 particle per grid cell in order to reduce the calculation time if input data files are only tested or if the interest is just focused on the groundwater flow equation. However, this leads to an increase in numerical inaccuracy of the solution of the solute transport.

---

[9]Some specifications: Hewlett-Packard Vectra RS/25C, 80386 micro processor, CPU with 4 Mb RAM, 25 MHz 80387 mathematical co-processor RS/25C. Price: about Dfl 21,000,-. Month of purchase: June 1990.

[10]Some specifications: Highscreen LE 1024, 80486 micro processor, CPU with 8 Mb RAM, 50 MHz 80487 mathematical co-processor. Price: about Dfl 6000,-. Month of purchase: August 1992. The calculation time is approximately 5 times faster than of the Hewlett-Packard of June 1990.

[11]Lahey Fortran compiler F77L-EM/32 (version 3.01). Price: about Dfl 2250,-. Month of purchase: June 1990.

[12]Lahey/Ergo Operating System (DOS Extender) OS/386 (version 2.1.04). Price: about Dfl 1000,-. Month of purchase: June 1990.
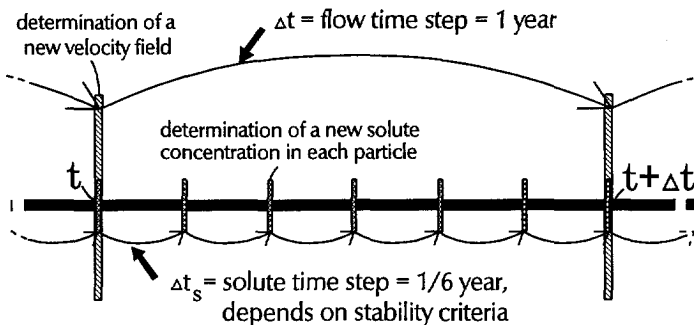
3. Solute time step Δt_s

The solute time step Δt_s is the time increment in which a particle is moved over a distance proportional to the length of that time increment and the velocity at the position of that particle. Several stability criteria determine the length of the solute time step (see subsection 5.3.3). Normally, several solute time steps are applied to simulate the solute transport during one flow time step of the groundwater flow equation.

4. Flow time step Δt

After each flow time step, the buoyancy is deduced from the computed solute concentration, and a new freshwater head distribution as well as a new velocity field is calculated.

   Note that the flow time step in the adapted MOC model should be chosen with care. The reason for this is that the groundwater flow equation depends on density differences, and thus the solute concentration also determines the solution. The salinity distribution changes after every solute time step, while the velocity field is kept constant during that flow time step (see figure 5.4). It may happen that the salinity distribution changes so rapid during one flow time step (there is a large number of solute time steps within one flow time step), that the velocity field does not closely match any more with the salinity distribution, and thus, with the current density. This could lead to numerical instabilities (see subsection 5.5.1). In order to remedy this problem, the length of the flow time step should be shortened. A flow time step of 1 *year* appears to be an appropriate value in a large number of case studies see, e.g., chapter 8.

determination of a new velocity field

Δt = flow time step = 1 year

determination of a new solute concentration in each particle

t

$t+\Delta t$

Δt_s = solute time step = 1/6 year, depends on stability criteria

* velocity field remains constant during 1 year
* solute concentration changes during each solute time step

Figure 5.4: Example of the relation between the flow time step and the solute time step.

5. Convergence criterion TOL

The convergence criterion TOL for the iterative calculation of the freshwater head in the groundwater flow equation is presented in ft, as MOC uses the Anglo-Saxon system of units. In the adapted MOC model, the criterion for the groundwater flow equation should range from about 10^{-4} to 10^{-6} ft. This criterion seems to be rather strict. Nonetheless, the freshwater head should be given precisely, especially at the constant piezometric level boundaries of vertical profiles where hydrostatic conditions ought to apply. At those boundaries, small deviations in the fixed freshwater head could lead to significant (erroneous) velocities in vertical direction. The accuracy of the solution of the groundwater flow equation can easily be enlarged by decreasing the value of the convergence criterion TOL.

6. Maximum relative distance ζ across one grid cell

The maximum relative distance ζ across one grid cell, in which a particle is allowed to move during one solute time step, is normally set to a fraction of a grid cell dimension. This is to ensure that particles do not move beyond several grid cells.

7. Observation points

Observation points can be designated in the nodes of grid cells. The model can follow changes in freshwater head and solute concentration as a function of time. In the adapted MOC model, a maximum of five observation points can be allocated, but this number can easily be expanded.

5.4.2 Subsoil parameters

The conversion from the original *horizontal* model to the adapted *vertical* model has its effects on several subsoil parameters. The following eight modifications in the adapted MOC model are implemented in comparison with the original model:

1. Anisotropic and heterogeneous media

The simulated geohydrologic profiles can be considered as anisotropic, since in each grid cell the hydraulic conductivity in horizontal direction can differ from the hydraulic conductivity in vertical direction through the so-called anisotropy factor: k_z/k_x. As each grid cell has a discrete hydraulic conductivity, the simulated groundwater systems can be considered as heterogeneous. In conclusion, MOC is suited for modelling anisotropic and heterogeneous geohydrologic systems.

2. Saturated thickness of the aquifer

As the adapted MOC model is applied, the saturated thickness b of the aquifer, that could vary spatially, represents the thickness of the aquifer *perpendicular* to the

vertical profile. This parameter is set to the unit length of *one foot*, the so-called *stretched foot*. As a consequence, the hydraulic conductivity k_i corresponds with the transmissivities T_{ii} through equation 5.72:

$$T_{ii} = b \cdot k_i \qquad (5.72)$$

3. Specific storativity S_s

MOC can simulate not only steady state, but also transient flow problems. The storage coefficient S which is applied in the original MOC model represents the specific storativity S_s in the adapted MOC model, as the saturated thickness b is equal to *one foot*: $S_s = S/1\ foot$.

The values of the storage coefficient S in the Netherlands, obtained from pumping tests, are in the range of 10^{-2} to 10^{-4} for (semi)-confined aquifers [Uffink, 1982]. Todd [1980] finds for most of the (semi)-confined aquifers values in the range of $0.5 \cdot 10^{-2}$ to $0.5 \cdot 10^{-4}$. In Maidment *et al.* [1993], some representative values of specific storativity S_s are given (see table 5.2). Todd [1980] gives the rule-of-thumb relationship $S_s = 3 \cdot 10^{-6} m^{-1}$. An empirically determined formula, developed by van der Gun [1979] who applied results of pumping tests of almost sixty cases in Dutch sandy aquifers, generates values of the specific storativity S_s of the geohydrologic system in the range of $0.5 \cdot 10^{-5} m^{-1}$ to $3 \cdot 10^{-5} m^{-1}$.

Table 5.2: Representative values of the specific storativity S_s [Maidment *et al.*, 1993].

Sediment type	Specific storativity S_s (m^{-1})
Unconsolidated clays	$10^{-2} - 10^{-4}$
Unconsolidated sands	$10^{-3} - 10^{-5}$
Unconsolidated gravels	$10^{-4} - 10^{-6}$
Compacted sediments	$10^{-5} - 10^{-7}$

The time lag of solute transport is so great in relation to the time lag of groundwater flow that the transient component of groundwater flow can be neglected, and thus, the specific storativity S_s can be taken equal to zero. A specific storativity S_s equal to zero significantly simplifies the calculations with the adapted MOC model. In section 6.2, the sensitivity for S_s is determined for a specific groundwater flow regime. Simulations in section 7.5 demonstrate that it is justified to set S_s equal to zero.

4. Hydraulic resistance

Aquitards, semi-pervious layers or resistance layers, such as a Holocene clayey layer, are normally characterized by the *hydraulic resistance c* in *days*. Aquitards, as they occur in geohydrologic systems, are represented in the hydraulic conductivity matrix

of the adapted MOC model after conversion with the following equation:

$$k_{(i,j)} = \frac{d}{c \cdot k_z/k_x} \cdot \tau_1, \quad \text{where} \quad \tau_1 = \frac{1}{86400} \tag{5.73}$$

where

- $k_{(i,j)}$ = data in the input data file of MOC which represents the (horizontal) hydraulic conductivity in grid cell $[i,j]$ (ft/s),

- d = thickness of the aquitard (ft). Note that, as rectangular grid cells of constant dimensions are applied in MOC, the thickness of the aquitard has to be schematised and subsequently to be inserted in the input data file as the height of the grid cell Δz or a multiple of Δz,

- c = hydraulic resistance of the aquitard $(days)$,

- k_z/k_x = anisotropy factor $(-)$,

- τ_1 = time conversion factor (1 day=86400 s) $(-)$.

In this thesis, the properties of aquitards (e.g. loam aquitards and clayey Holocene aquitards) remain constant. However, research has indicated that especially such aquitards may react chemically on changes of solutes in groundwater [Goldenberg et al., 1986; Mehnert and Jennings, 1985]. Irreversible changes in permeability may occur, especially due to the chloride-ion which flows through these layers. When saline groundwater is replaced by fresh groundwater, the hydraulic conductivity decreases with small fluctuations until a lower value of hydraulic conductivity is finally reached. This process takes place as a result of chemical processes, such as deflocculation of clay minerals. Thus, the hydraulic conductivity of such layers should be adapted in MOC for changes in solute content of passing groundwater. However, this adaptation is beyond the scope of this thesis.

5. Initial solute concentration

The initial distribution of solute concentration of the entire geohydrologic system must be known, as the density distribution is applied into the groundwater flow equation of the adapted MOC model. The conversion from chloride concentration to density is given in subsection 5.4.3.

6. Extraction and infiltration

MOC allows lines of extraction and injection wells in grid cells. The following conversion must be applied for the extraction of groundwater out of the medium or injection of surface water into the medium:

$$q_{(i,j)} = \frac{Q}{L_\perp} \cdot \tau_2, \quad \text{where} \quad \tau_2 = \frac{3.2808^2}{365.25 \cdot 86400} \tag{5.74}$$

where

- $q_{(i,j)}$ = data in the input data file of MOC that represents the rate of extraction or infiltration of water in grid cell $[i,j]$ $(ft^3/s/ft')$,

- Q = rate of extraction $(+)$ or infiltration $(-)$ (m^3/yr),

- τ_2 = time conversion factor $(1\ year \simeq 365.25\ days;\ 1\ m \simeq 3.2808\ ft)\ (-)$,

- $L_\perp$ = width over which water is extracted or infiltrated, *perpendicular* to the profile (m). Note that the applied data should be implemented in the input data file per unit length of *one foot*. As such, the three-dimensional situation must be schematised to a two-dimensional profile, which introduces a major problem. The width or the so-called *sphere of influence* $L_\perp$, over which injection and extraction wells perpendicular to the profile should be taken into account, is difficult to assess.

7. Recharge and discharge

Spatially varying (natural groundwater) recharge or discharge is simulated in the adapted MOC model as follows. The flux in or out of the geohydrologic system is computed by multiplying the recharge or discharge quantity (LT^{-1}) with the area of a grid cell $\Delta x \cdot \Delta z$, thus obtaining $L^3 T^{-1}$. In the adapted MOC model, however, a vertical profile is considered (see figure 5.5). Now, the area of the grid cell is $\Delta x \cdot 1$ *foot*. Nonetheless, as the adapted MOC model still uses the spatial area $\Delta x \cdot \Delta z$, the data has to be divided by the height of the grid cell Δz:

$$inf_{(i,j)} = \frac{f}{\Delta z} \cdot \tau_3, \quad \text{where} \quad \tau_3 = \frac{3.2808}{365.25 \cdot 86400} \tag{5.75}$$

where

- $inf_{(i,j)}$ = data in the input data file of MOC that represents the rate of recharge or discharge in grid cell $[i,j]$ $(ft/s/ft')$,

- f = rate of recharge $(-)$ or discharge $(+)$ (m/yr),

- Δz = height of the grid cell (ft),

- τ_3 = time conversion factor $(-)$.

The original groundwater recharge and discharge facilities can also be applied in the adapted MOC model. As vertical profiles are simulated, the supposition that groundwater flow perpendicular to the profile ought to be negligible, should be valid. It often happens, however, that cases with groundwater flow perpendicular to the profile occur, for instance when high rates of groundwater are extracted or when deep polder areas (several metres below $N.A.P.$) in the vicinity of the chosen profile

Original MOC model   Adapted MOC model
        Natural groundwater recharge f   Natural groundwater recharge f

Flux in original MOC model is f·Δx·Δz   Flux in adapted MOC model is f·Δx·1 foot
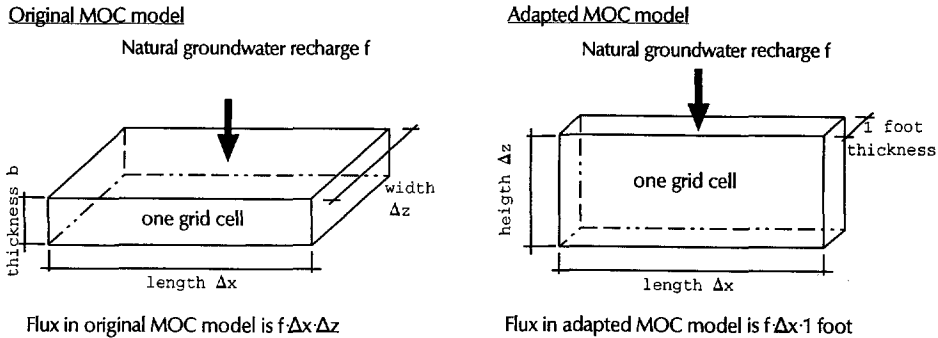
Figure 5.5: Determination of the natural groundwater recharge for both the original model and the adapted MOC model.

induce groundwater flow perpendicular to the profile. In those cases, a *groundwater discharge* out of the geohydrologic system can be introduced as a trick to counteract the effect in the third dimension. This facility is imposed in section 8.3, where groundwater is discharged in the central part of a profile in Noord-Holland.

8. Boundary conditions

Two[13] different types of boundary conditions for the groundwater flow can be imposed in MOC:

- a *constant flow* boundary, the so-called *Neumann problem*.
  This type of boundary can be implemented in the adapted MOC model by means of two tools: (1) 'Extraction and infiltration' (e.g. lines of extraction and injection wells), and (2) 'Recharge and discharge' (e.g. natural groundwater recharge into the geohydrologic system). A particular example of this constant flow boundary type is the *no-flow* boundary.

- a *constant piezometric level* boundary, the so-called *Dirichlet problem*.
  As MOC computes freshwater heads, the constant piezometric level boundary has to be converted into a freshwater head boundary in case density differs from fresh groundwater. This is further explained in subsection 5.4.4.

  In the adapted MOC model, a constant piezometric level boundary along specific segments of the model area is imposed by applying a parameter of the original MOC model: the so-called *leakage coefficient*[14]. If the leakage coeffi-

---

[13]The Cauchy or mixed boundary, which specifies a head-dependent flow, cannot be imposed in MOC.

[14]In the original MOC model, the piezometric level is separated from the phreatic groundwater level (e.g. a polder level) by an aquitard (e.g. the Holocene clayey aquitard). This leakage coefficient (T^{-1}) is the reciprocal value of the hydraulic resistance c (T). In the original MOC model, this leakage coefficient is called the *leakance coefficient*.

cient of the aquitards, which is in fact *imaginary* in the adapted MOC model, is set to a sufficient high value, e.g. 1 s^{-1}, the phreatic groundwater level nearly equates the (fictive) freshwater head. As such, a (nearly constant) boundary condition is imposed for the freshwater head. Konikow and Bredehoeft already indicated this application in 1978.

Fluxes of water and solute are still passing through the aquitard, though they should not be taken into account in the adapted MOC model. These fluxes make that the mass balances, applied in the original MOC model, cannot be employed any more for the adapted MOC model (see subsection 5.5.2).

Implementation of sea level rise
An additional procedure is implemented in the adapted MOC model by the author, using documentation of van der Eem. This procedure enables the user to change after each pumping period not only the rates of injection and extraction (this is standard in MOC), but also freshwater heads, solute concentrations and boundary conditions. Thus, sea level changes can be simulated in the adapted MOC model with this procedure by inserting in the input data file a number of pumping periods with different constant piezometric level boundaries.

Moreover, in order to simulate sea level rise in chapter 9 as accurate as possible, a brief procedure is implemented in the adapted MOC model to adjust the freshwater head in selected grid cells before every flow time step:

$$\phi_{f(i,j)}^{k+1} = \phi_{f(i,j)}^{k} + \Psi \cdot \Delta t \qquad (5.76)$$

where

- $\phi_{f(i,j)}^{k+1}, \phi_{f(i,j)}^{k}$ = freshwater heads respectively at the $(k+1)^{th}$ time level and the kth time level (L),

- Δt = flow time step (T),

- Ψ = rate of sea level rise $(L T^{-1})$.

5.4.3   Densities

As stated before, density should be considered to be a function of pressure, temperature of the fluid and concentration of dissolved solutes. However, the influence of pressure can be neglected under the given circumstances of the considered geohydrologic systems. Furthermore, the influence of temperature on the density is of minor importance with respect to the influence of dissolved solutes concentration within the range of the applied geohydrologic systems. Therefore, in this thesis, the density of groundwater is only related to the concentration of dissolved solutes in the groundwater, whereas the temperature is considered to be equal to 10 $^{\circ}C$. The concentration of dissolved solutes is subdivided into negative (anions, e.g. Cl^-, SO_4^{2-}, HCO_3^{2-}) and

positive ions (cations, e.g. Na^+, Mg^{2+}, K^+). Since in coastal groundwater chloride
(Cl^-) is the predominant negative ion, which is moreover investigated intensively,
the interest in this thesis is focused on the chloride distribution. When, in fact, only
changes in the chloride distribution are simulated with the adapted MOC model,
the distribution of all dissolved solutes is meant. In other words, the distribution of
chloride ions is considered to represent the distribution of all dissolved solutes. As
such, a proportional distribution of all dissolved solutes, which is present in ocean
water, is also assumed to be present in groundwater under consideration.

The applied classification of fresh, brackish and saline groundwater based on chlo-
ride concentrations according to Stuyfzand [1986b] is presented in table 5.3. Obvi-
ously, there are various other classification systems possible, e.g. because the def-
inition for fresh groundwater depends on the application of the groundwater. For
instance, the drinking water standard in the European Community equals 150 mg
Cl^-/l [Stuyfzand, 1986b], while according to the World Health Organization, a conve-
nient chloride concentration limit is 200 mg Cl^-/l [Custodio et al., 1987]. A chloride
concentration equal to 300 mg Cl^-/l indicates the taste limit of human beings ac-
cording to ICW [1976], while Todd [1980] gives 100 mg Cl^-/l as the limit when salt
can be tasted. The chloride concentration of sprinkler water for horticulture should
be less than 200 mg Cl^-/l, while livestock can endure higher concentrations: up
to 1500 mg Cl^-/l may be accepted, provided that the chloride concentration stays
constant.

Table **5.3**: Classification into six main types of fresh, brackish or saline groundwater de-
pending on the basis of chloride concentration, after Stuyfzand [1986b].

Main type of groundwater	Chloride concentration [mg Cl^-/l]
fresh	$Cl^- \leq 150$
fresh-brackish	$150 < Cl^- < 300$
brackish	$300 < Cl^- < 1000$
brackish-saline	$1000 < Cl^- < 10,000$
saline	$10,000 < Cl^- < 20,000$
hyperhaline or brine	$Cl^- \geq 20,000$

The conversion from chloride concentration to density, that is applied in the
adapted MOC model, is as follows:

$$\rho_{(i,j)} = \rho_f \cdot (1 + \frac{\rho_s - \rho_f}{\rho_f} \cdot \frac{C_{(i,j)}}{C_s}) \qquad (5.77)$$

where

- $\rho_{(i,j)}$ = density of groundwater in grid cell $[i, j]$ ($M\,L^{-3}$),

- ρ_f = reference density, usually the density of fresh groundwater (without dis-
  solved solids) at mean subsoil temperature ($M\,L^{-3}$),

- ρ_s = density of saline groundwater at mean subsoil temperature $(M\,L^{-3})$,

- $(\rho_s - \rho_f)/\rho_f$ = relative density difference $(-)$,

- $C_{(i,j)}$ = chloride concentration or the so-called *chlorinity* in grid cell $[i,j]$ $(mg\ Cl^-/l)$,

- C_s = reference chloride concentration $(mg\ Cl^-/l)$. In equation 5.77, a linear relation exists between ρ_s and C_s.

In this thesis, the following data are applied for the Dutch situation: $\rho_f = 1000$ kg/m^3; $\rho_s = 1025\ kg/m^3$; thus $(\rho_s - \rho_f)/\rho_f = 0.025$; and $C_s = 18{,}630^{15}\ mg\ Cl^-/l$.

In Dutch coastal aquifers, the chloride concentration of groundwater does normally not exceed 17,000 $mg\ Cl^-/l$, as sea water that intrudes the groundwater flow regime is mixed with water from mainly the river Rijn. The density of that saline groundwater ρ_s equals about 1022.8 kg/m^3.

Lebbe [1983], who also applied the adapted MOC model, used in equation 5.77 the salinity or the total dissolved solids (TDS) instead of the chlorinity for the conversion to groundwater density. Then, $C_{(i,j)}$ is the actual TDS in a grid cell $[i,j]$ and C_s is the reference TDS, e.g. the TDS of ocean water of 34,500 mg/l. The TDS of several oceans around the world is higher than 34,500 mg/l due to, among others, a high degree of evaporation and oceanic currents, and consequently, the density is higher than $\rho_s = 1025\ kg/m^3$. For instance, the chloride concentration in the Mediterranean Sea can be as high as 21,000 $mg\ Cl^-/l$, and the TDS of the Red Sea and some areas of the Mediterranean can reach some 45,000 mg/l.

5.4.4 Conversion to freshwater head

As a non-uniform density distribution in the groundwater flow regime is simulated with the adapted MOC model, the piezometric levels in fresh, brackish or saline groundwater must be converted into freshwater heads ϕ_f. The determination of the (fictive) freshwater head is as follows (see also figure 5.6):

$$\phi_f = (h - z_{obs}) \cdot \frac{\rho_{obs}}{\rho_f} + z_{obs} \tag{5.78}$$

where

- ϕ_f = freshwater head of the observation well with respect to the reference level (L),

- h = observed piezometric level relative to the reference level (L),

- z_{obs} = elevation of the point of observation relative to the reference level (L),

- ρ_{obs} = density of the water column in the observation well $(M\,L^{-3})$.
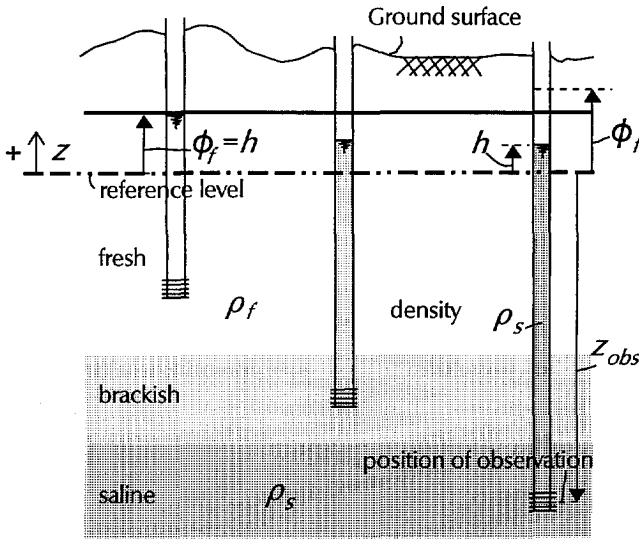
Figure 5.6: Conversion from observed piezometric level to freshwater head.

For example, at a vertical boundary with a constant piezometric level the freshwater head configuration can be assessed assuming that no vertical groundwater movements occur. This means the situation is supposed to be *hydrostatic*. If the piezometric level in the upper grid cell, $\phi_{f(i,2)}$[16], and the density distribution in vertical direction are known, the freshwater heads in all grid cells underneath the upper cell in the same column can be determined. For each grid cell at an increasing depth with respect to the reference level, e.g. *N.A.P.*, the freshwater head in the center of the grid cell $[i,j]$ is as follows:

$$\phi_{f(i,j)} = \phi_{f(i,j-1)} + \Upsilon_{(i,j)} \cdot \Delta z \tag{5.79}$$

where

- $\phi_{f(i,j)}, \phi_{f(i,j-1)}$ = freshwater heads respectively in the grid cells $[i,j]$ and $[i,j-1]$ (L),

- $\Upsilon_{(i,j)}$ = relative density difference, the buoyancy between the grid cells $[i,j]$ and $[i,j+1]$ $(-)$, see equation 5.19.

---

[15]According to Todd [1980], sea (ocean) water contains about $C_s = 19,300\ mg\ Cl^-/l$, while van Dam [1992a] proposes a chlorinity of $C_s = 19,000\ mg\ Cl^-/l$ for ocean water.

[16]MOC uses dummy grid cells around the finite-difference grid, thus the upper row which participates has the index $j = 2$.

5.4.5   Hydrodynamic dispersion

The mixing process of (hydrodynamic) dispersion not only depends on the velocity distribution, but also on the geometry of the geohydrologic systems with its good permeable aquifers and less permeable aquitards.

Mechanical (or convective) dispersion D_m

The determination of the longitudinal dispersivity α_L and the transversal dispersivity α_T is based on both laboratory and field experiments.

Laboratory experiments in homogeneous sand columns suggest that α_L is of the order of magnitude of the average sand grain [Bear and Verruijt, 1987]. According to literature studies, laboratory dispersion experiments report measurements of the longitudinal dispersivity α_L in the range of 10^{-4} to 10^{-2} m, thus the best estimates of laboratory experiments appear to be very small. Laboratory experiments [e.g. Bertsch, 1978] proved that dispersion is affected by molecular diffusion at groundwater flow velocities smaller than about $5 \cdot 10^{-6}$ m/s. For groundwater flow velocities greater than about $5 \cdot 10^{-6}$ m/s and smaller than about $1 \cdot 10^{-3}$ m/s, α_L equals 0.063 cm in a homogeneous, isotropic, sandy to gravelly porous medium.

By contrast, field experiments in heterogeneous sand and gravel aquifers (especially in the USA) are calibrated with much greater values of α_L, in the range of 1 to 100 m. Gelhar et al. [1992] reviewed 59 different field sites in order to classify the dispersivity data into three reliability classes. The representative scale of the cases ranges from 10^{-1} to 10^5 m. They found that for these cases, the longitudinal dispersivity ranges from 10^{-2} to 10^4 m. For instance, Bredehoeft and Pinder [1973] applied for the case study Brunswick, Georgia, USA, a longitudinal dispersivity of about 60 m as the best estimate in order to match the calculations with measurements. Also smaller values are found by trial and error, such as α_L=6.6 m for the Cutler area of the Biscayne aquifer near Miami, Florida [Segol and Pinder, 1976]. In conclusion, the variation in dispersivity reflects the influence of different degrees of aquifer heterogeneity at different field sites. The values determined appear to be *scale-dependent*. Gelhar et al. [1992] concluded that in general, longitudinal dispersivities in the lower part of the indicated range are more likely to be realistic for field applications. Furthermore, they indicated that there is a need for very large-scale, long-term experiments extending to several kilometres.

In contrast with the field sites in especially the U.S.A., the best estimates of the longitudinal dispersivities in Dutch (and Belgian) large scale groundwater flow regimes appear to yield rather small values. This observation is based on various case studies, such as Lebbe [1983], Lebbe and Pede [1986], Kooiman et al. [1986], van der Eem et al. [1989], Lebbe et al. [1990] and Walraevens et al. [1993]. According to Stuyfzand [1991], the order of magnitude of α_L for dune sand probably ranges from 0.04 to 0.1 m.

Much less information is available on transversal dispersion. Nonetheless, the ratio α_T/α_L is likely to range from 1:5 to 1:24 [Bear, 1979], though a ratio of 1:3 has

been widely applied in numerical simulations [Gelhar *et al.* 1992]. For the transversal dispersivity α_T, Stuyfzand and Stuurman [1985] determine for sand-dune areas the range 0.01-0.05 m.

In chapter 8, it is demonstrated that the calculated profiles best match field measurements when α_L is small (in the order of magnitude of cm to dm).

Molecular diffusion D_d

Molecular diffusion is defined as solute spreading in response to concentration gradients. The molecular diffusion D_d, which even occurs if groundwater does not flow, mainly depends on temperature. As mentioned before, the influence of diffusion on hydrodynamic dispersion becomes visible only at very small velocities of the groundwater (e.g. $< 1 \cdot 10^{-6}$ m/s, according to Bertsch [1978]). For a conservative solute as chloride, the molecular diffusion D_d for porous media is approximately 10^{-9} m^2/s at a temperature of 25 $^o C$.

5.5   Limitations of the adapted MOC model

5.5.1   Numerical instabilities

Numerical instabilities, which make the solution of the solute transport inaccurate, are caused by: (1) numerical approximations that already occur in the original MOC model; and (2) density flow that additionally arises in the adapted MOC model. The latter cause is discussed here.

Numerical instabilities in the (vertical) velocity field can occur when particles from a grid cell with a high solute concentration and thus a high density enter in a grid cell with a low solute concentration. At the end of every flow time step, new solute concentrations and thus new densities are determined for both the grid cells. This may lead to abrupt differences in density between the two adjacent grid cells. Subsequently, the groundwater flow equation is solved again at the beginning of a new flow time step, and thus a new velocity field is calculated. The new vertical velocity field could have changed significantly, as it depends on the changed density distribution. Occasionally, the direction of the vertical velocity may even alter in some grid cells, at least if the initial vertical velocity was small. During that subsequent flow time step, the new computed velocity field may move particles in the opposite direction. This may, once again, lead to new abrupt changes in density of some adjacent grid cells, etc., and the velocity fluctuations in vertical direction can cause numerical instabilities.

Figure 5.7 shows a schematisation of how numerical instabilities due to density flow occur. Several particles enter into other grid cells during the first flow time step (of 1 *year*). Subsequently, the solute concentration in each grid cell is determined by averaging over all available particles of the grid cell. When the groundwater flow
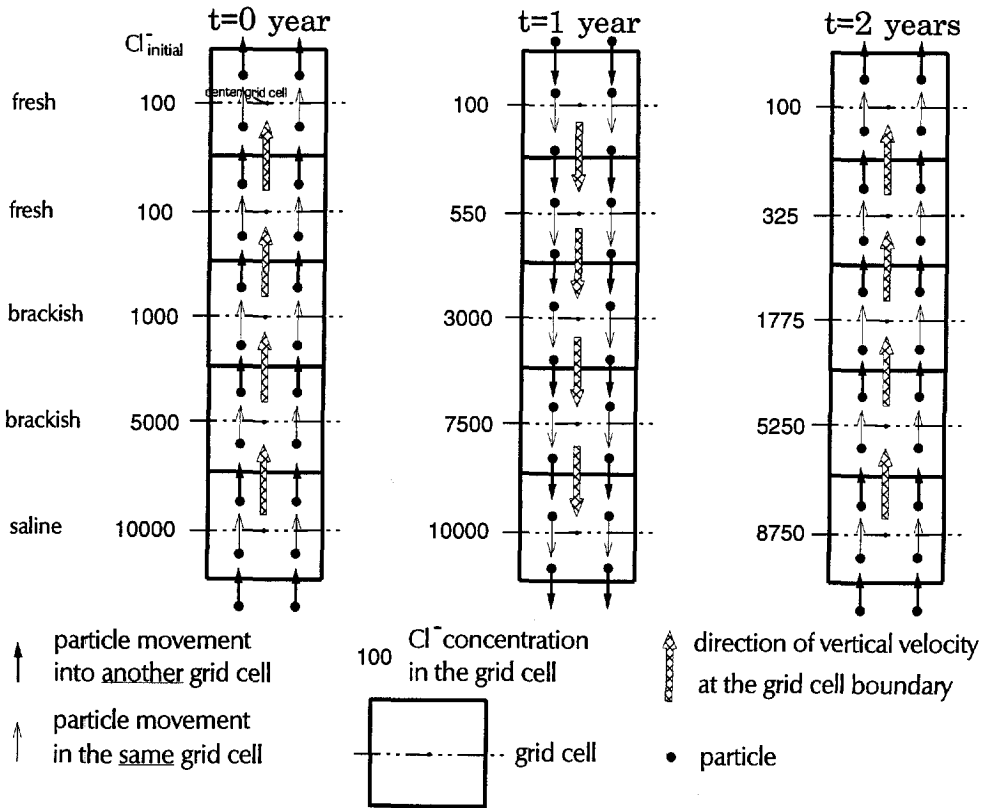
Figure 5.7: Schematisation showing how numerical instabilities due to density flow can occur. The solute and the flow time step have the same length of 1 *year*. Only the vertical groundwater flow is displayed. Because particles are moved to other grid cells, abrupt changes in solute concentration and thus in density in several grid cells can create fluctuations in vertical velocity.

equation is solved again at the beginning of the second flow time step, the vertical velocities at the boundaries of grid cells differ abruptly due to the differences in density, namely the vertical velocities have even changed in the opposite direction. During the second flow time step, particle movements cause lower solute concentrations. Once again, the solute concentrations of adjacent grid cells differ and the vertical velocities alter in the opposite direction. After solving the groundwater flow equation, vertical velocities may alter again, etc. This phenomenon of fluctuating vertical velocities due to density flow causes numerical instabilities. Under certain circumstances, these instabilities may get out of hand and could locally disturb the solute concentration to such an extent that the result of the simulation is not reliable anymore.

Numerical instabilities occur at those places where the densities in adjacent grid

cells differ rapidly, for example at places where the transition zone between fresh and saline groundwater is small or at places where surface water is injected with a density different from that of the original groundwater at that depth. It depends, among others, on the geometry of the geohydrologic system whether the vertical velocities in the grid cells fluctuate in direction with approximately equally small amplitudes, or diverge to (unacceptable) strong amplitudes. Anyhow, in the (adapted) MOC model, the particle tracking technique suppresses severe over and undershooting of respectively the maximum and minimum solute concentration.

In this subsection both model and subsoil parameters that can limit numerical instabilities in the velocity field due to density flow are briefly discussed:

1. **Number of particles in each grid cell**
   Changes in solute concentration and density are less abrupt if more particles per grid cell are present. Thus, more particles per grid cell counteract numerical instabilities and lead to a more exact simulation of the solute transport.

2. **The convergence criterion TOL**
   If the groundwater flow equation is solved more precisely (that is TOL is smaller), the velocity field and the particle movements are represented more accurately. As a result, numerical instabilities are counteracted, although this parameter has less influence on the exactness of the solute transport than the number of particles per grid cell.

3. **Size of the flow time step Δt**
   If too many solute time steps take place within one flow time step, the solution of the advection-dispersion equation may be changed too much to match the solution of the groundwater flow equation. As a result, numerical instabilities can occur. To limit them, the length of the flow time step should be shortened.

4. **Initial density distribution**
   The simulation of the geohydrologic system starts with an initial density distribution. If vertically adjacent grid cells have relatively great density differences in the initial situation, this may immediately create numerical instabilities in the vertical velocity field. In order to suppress this phenomenon, the initial solute (chloride) distribution must be as smooth as possible, though it must be in accordance with the measured distribution.

5. **Total number of grid cells**
   The groundwater flow equation is solved more accurately and the particles are moved more precisely, if the total number of grid cells increases. On the other hand, changing only the grid cells to smaller dimensions does not always counteract numerical instabilities. The explanation is as follows. If the grid cells are altered into smaller dimensions than originally and hydrodynamic dispersion is small, the brackish zone between fresh and saline groundwater can be also small. As the flow time step for recalculating the groundwater flow equation

remains the same, the new case with smaller grid cells applies more and smaller solute time steps due to the equations 5.67 and 5.71 than the original case. Thus, each particle is moved more often during one flow time step. As the velocity field remains the same during this flow time step, particles in a brackish (unstable) zone may pass adjacent grid cells with completely different density. The smaller the grid cells are, the more often particles enter adjacent grid cells with completely different densities. Consequently, abrupt changes in solute (chloride) concentration and in density may occur in several grid cells. The density of a grid cell in the brackish zone may fluctuate during the computations of the groundwater flow equation, and this may create or amplify numerical instabilities. An example of this phenomenon is given in section 6.3.

Fortunately, in general, the favourable characteristics of more and smaller grid cells dominate over the negative characteristics.

6. **Hydrodynamic dispersion**

When hydrodynamic dispersion is small, mixing of solute between adjacent grid cells is small too and a small transition zone may occur. Then, it is possible that a great difference in solute concentration and density can occur between adjacent grid cells, and subsequently, numerical instabilities in the vertical velocity field occur.

In conclusion, exercises with the parameters mentioned above have indicated that increasing the number of particles per grid cell seems to have the greatest influence on suppressing numerical instabilities, followed by shortening the length of the flow time step, and finally by lowering the value of the convergence criterion TOL. Furthermore, numerical instabilities can be counteracted if the initial density distribution is smoothed, especially in transition zones. Enlarging the total number of grid cells does not necessarily decrease numerical instabilities. However, reducing the dimension of the grid cells is effective in combination with shortening the length of the flow time step.

5.5.2   Accuracy of the solution

The accuracy of the numerical solution of the groundwater flow model MOC can be estimated by analysing the errors in both the groundwater volume and the solute mass balances. Unfortunately, the balances as derived in the original MOC model cannot be applied for the adapted MOC model. The reason is that the fluxes of both water and solute through the *imaginary* aquitard are also considered in the balance evaluation (see also subsection 5.4.2: item 8. Boundary conditions). Therefore, a new procedure is applied for the adapted MOC model to determine the errors in the balances. Obviously, it is still based on the principle of mass conservation for respectively groundwater and solute.

Accuracy of groundwater flow

The incoming and outgoing fluxes (groundwater volumes) over specific boundaries of the geohydrologic system are calculated by applying the velocities perpendicular to those boundaries and the total length of the boundaries. In addition, extractions, infiltrations, recharges and discharges are also considered. Figure 5.8 shows an example how the incoming and outgoing groundwater volumes in one grid cell are determined. For the determination of the error in the groundwater volume balance of an entire geohydrologic system, the following equation is applied:

Groundwater volume balance in a grid cell:

$$flow_{in} : q_{x\,(i-1/2,j)}{}^*\Delta z^*\Delta t_s + q_{z\,(i,j-1/2)}{}^*\Delta x^*\Delta t_s + source^*\Delta t_s$$

$$flow_{out} : q_{x\,(i+1/2,j)}{}^*\Delta z^*\Delta t_s + q_{z\,(i,j+1/2)}{}^*\Delta x^*\Delta t_s + well^*\Delta t_s$$

net volume flux = flow$_{in}$ - flow$_{out}$
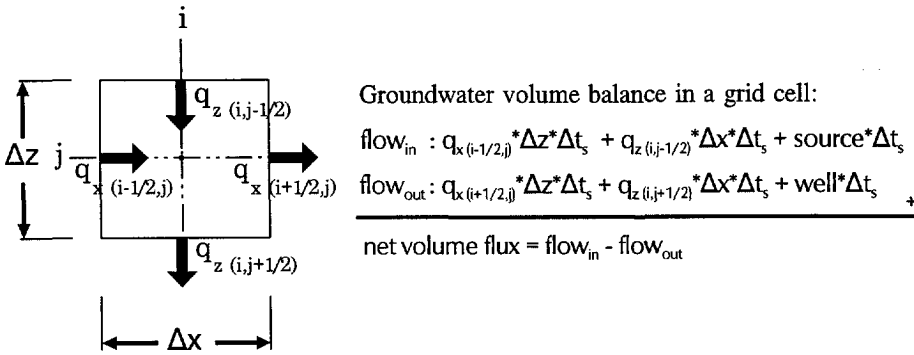
Figure 5.8: Example of the determination of incoming and outgoing groundwater volumes in one grid cell per stretched foot during one solute time step.

$$E_{water} = 100 \cdot \frac{flow_{in} - flow_{out}}{V_0} \quad (\%) \tag{5.80}$$

where

- E_{water} = error in the groundwater volume balance (%),

- V_0 = initial groundwater volume per stretched foot $(L^3\,L^{-1})$,

- flow$_{in}$, flow$_{out}$ = respectively the cumulative sums of incoming and outgoing groundwater volumes in the geohydrologic system per stretched foot $(L^3\,L^{-1})$.

The error in the groundwater volume balance appears to be insignificant for commonly used parameters (e.g. for TOL=10^{-5} ft): < order of magnitude 10^{-1}%. Even if initially a relatively great error in the groundwater volume balance would exist, it can easily be diminished by lowering the value of the convergence criterion TOL. For all cases with commonly applied parameters, the error in the groundwater volume balance is small compared to the error in the solute mass balance. An example of incoming and outgoing groundwater volumes is given in section 7.7: item **Water balances**.

Accuracy of solute transport

The accuracy of the solution of the solute transport equation is quantified by the error in the solute mass balance. In the original MOC model, three methods were defined to represent the error, while the MOC version 3.0 of 1989 computes even another error. The test problems, applied in the original MOC model, obtained errors in the solute mass balance of, mostly, in the range of -10 % to +10 %. Unfortunately, as stated before, all the methods given in the original MOC model cannot be applied due to the adaptation of the model for vertical profiles. Therefore, a new error in the solute mass balance is defined by applying: (1) the cumulative sums of the incoming and outgoing fluxes over the boundaries (*net mass flux M_f*) and (2) the change in mass stored in the system (*mass accumulation ΔM_s*). The error in the solute mass balance is expressed by:

$$E_{solute} = 100 \cdot \frac{R_m}{M_0} \qquad (\%) \qquad\qquad (5.81)$$

where R_m is the *mass residual* $(M\,L^{-1})$ (that is the difference between *net mass flux M_f* and *mass accumulation ΔM_s*) and M_0 is the *initial mass of solute* present in the entire geohydrologic system $(M\,L^{-1})$.

In general, the error in the solute transport is great in comparison with the error in the groundwater flow. The errors can be significant because changes in solute concentration are (mainly) caused by particle movements to *other* grid cells. These particles may cause relatively random changes in the solute concentrations of those grid cells. Abrupt changes in solute concentration directly affect the error in the solute mass balance. For instance, particles with high solute concentrations enter grid cells where the particles have low solute concentrations. After (arithmetic) averaging of solute concentrations over the currently available particles, the solute concentration in those grid cells may increase considerably. These described changes in solute concentration also occur at the boundaries of the system. At those places, the changes may induce a substantial change in mass stored in the system (*mass accumulation ΔM_s*), which directly affects the error in the solute mass balance.

Another significant cause of the error in the solute transport is the reposition of particles to a new uniform distribution throughout the entire grid, when too many grid cells become void due to particle movements (the procedure is called GENPT). The maximum number of grid cells that can be void of particles, NZCRIT, is initially set to 2 %. Though an approximation of the previous concentration gradient within each grid cell is preserved, relevant information, such as the exact position of particles, is eliminated whenever new particle distributions are generated. Consequently, as particle movements to *other* grid cells cause the main changes in concentration, discontinuities in the changes in concentration may occur, which lead to errors in the solute mass transport. If NZCRIT is too small, then a new particle distribution is generated too often which could amplify errors in solute mass transport.

The error in the solute transport E_{solute} is only slightly affected by the longitu-

dinal dispersivity and by model parameters such as the number of particles in each
grid cell, the convergence criterion TOL, and the dimensions of the grid cells.

5.6   Graphical presentation

In this section, a postprocessor is briefly described that provides the graphics ca-
pability for data output of the adapted MOC model. The package is based on the
graphical presentation of data output developed by Lebbe [personal communication,
1990]. The author adapted and added several (new) features[17] in the postprocessor[18]:

- Freshwater head and solute concentration
  The distributions of both freshwater head and solute concentration of the pro-
  files can be displayed for selected moments in the simulation time (at the end
  of the so-called pumping periods). The presentation can be twofold: (1) by
  contour lines (respectively the so-called freshwater head isohypses and lines of
  equal solute concentration) or (2) by a coloured block distribution (each grid
  cell is presented by a coloured rectangular block). The colour of the blocks cor-
  responds with a range in respectively freshwater head and solute concentration
  in a defined classification. Furthermore, the postprocessor is able to produce
  ASCII files of respectively the freshwater head and the solute concentration in
  each grid cell. These files can be applied in packages such as SURFER.

- Velocity field
  The real velocity in the center of a grid cell is deduced by linear interpolations
  between the velocities at the boundaries of the grid cell. The vector of the
  velocity in the center of a grid cell is determined by multiplying the velocity
  with a certain time step. The orientation and the length of the vector presents
  respectively the direction and the distance in the geohydrologic system that a
  groundwater particle in the center of that grid cell would displace during that
  time step, on condition that the velocity field is constant during that time step.

  The velocity vectors can be superimposed on the freshwater head contour lines
  and/or on the coloured block solute distribution in one single picture. That
  picture can be stored in an output data file as HPGL[19]-instructions. The
  output data file can be applied as a direct hardcopy print or can be retrieved
  in graphics packages such as WP Presentations for editing.

- Streamlines and travel times at one specific moment in time
  Two types of streamlines can be determined: (a) streamlines which indicate the

---

[17]Examples of the features are displayed in the following chapters.

[18]Unfortunately, the postprocessor, written in Pascal and available for the personal computer,
has not yet been made user-friendly due to lack of time. However, within a few man-weeks the
postprocessor can be made suitable for at least undergraduate students.

[19]HPGL stands for Hewlett-Packard's Graphics Language, which was originally developed to depict
pictures on plotters.

travel that particles would make if the velocity field is in a stationary situation, and (b) streamlines based on a non-stationary situation in the velocity field, which in fact occurs for the groundwater flow regimes with changing densities.

ad a. The streamlines based on a stationary velocity field can be computed in a straightforward way. The velocity field, taken at one specific moment in time, is not adjusted during the travel of the particles. Fluid particles at any location in the grid can be tracked, based on bilinear interpolation of the velocities at adjacent nodes and at boundaries (figure 5.2). The streamlines are constructed by continuous determination of the velocity at the position of the particles and moving the particles through the geohydrologic system during a certain time step. The travel time of a particle through the system is computed by adding up all time steps that particle needs to move through the system. Note that the condition of the boundaries of the entire geohydrologic system should be known in advance.

ad b. In a non-stationary situation, the *actual* streamlines, *path lines* or *flow paths* are assessed by tracking a number of particles through the geohydrologic system *during* the simulation. This is not difficult to accomplish as MOC already uses the particle tracking method. It generates a specific output data file in which information of the travel of certain particles through the grid is stored. The postprocessor constructs the path lines. Unfortunately, if a new uniform distribution of particles throughout the entire grid is generated (the procedure GENPT is applied), the coding of tracked particles may be assigned to other particles. If that happens, the positions of the assigned particles may be altered and as a result, the path lines are not functional anymore from that moment in time.

- Changes in volume distribution of groundwater
  At the end of each pumping period, the postprocessor counts the number of grid cells with fresh ($Cl^- \leq 300$ *mg* Cl^-/l), brackish ($300 < Cl^- < 10,000$) and saline ($Cl^- \geq 10,000$ *mg* Cl^-/l) groundwater. Subsequently, the change in salinity distribution in the geohydrologic system as a function of time can be quantified.

- Film option for changes in freshwater head and solute concentration
  The *film option* of the postprocessor can display changes in the distribution of freshwater head and solute concentration in the profile as a function of time. Note that in most of the cases a large number of pumping periods is required in order to visualize significant changes in the distribution as a function of time.

- Freshwater head and solute concentration in observation points
  The freshwater head and solute concentration at specific observations points can be displayed as a function of time. The postprocessor can generate ASCII files that can be applied in packages such as SigmaPlot for producing (sophisticated) diagrams or charts.

Chapter 6

Hypothetical cases with the adapted MOC model

6.1 Introduction

Model testing comprises, besides comparison with the results of other models and with reality, model verification of problems for which analytical solutions exist. Numerical models, that simulate not only groundwater flow but also solute transport, can be tested or *validated*[1] by various models with analytical solutions. Analytical solutions of solute transport can be complex, and therefore, mostly straightforward hypothetical cases are considered. For instance, analytical solutions are given for the one-dimensional form of the advection-dispersion equation by Ogata and Banks [1961], Shamir and Harleman [1966], Kinzelbach [1986, 1987a], Gelhar and Collins [1971], Freeze and Cherry [1979] and Uffink [1990]. Bear [1972, 1979] has summarized examples of analytical solutions of the hydrodynamic dispersion with specific boundary and initial value problems.

The original MOC model [Konikow and Bredehoeft, 1978] has already been tested intensively, e.g. by Huyakorn *et al.* [1984] and Beljin [1988]. The author has successfully tested his adapted MOC model, that, in addition, simulates density differences in vertical profiles, through comparing his results with results of others. For instance, the following cases have been reproduced: Lebbe [1983], Peters [1983] and Lebbe [1984] (movement of fresh water injected in a salaquifer), and van der Eem *et al.* [1989].

In this chapter, additional testing is done. The simulations with the adapted MOC model are compared with analytical solutions of the following three problems:

a. Case similar to Edelman's sudden change in boundary condition [1947], where unsteady one-dimensional flow is considered in a confined aquifer without recharge, density differences, solute transport and hydrodynamic dispersion.

---

[1] Often the testing of the computer codes for problems with known solutions is (erroneously) called *validation*. A mathematical model is said to be *validated*, if sufficient testing has been performed to show an acceptable degree of correlation [Huyakorn *et al.*, 1984]. However, as a matter of fact, the models can only be *invalidated*, since the testing is only a limited demonstration of the reliability of the model [Konikow and Bredehoeft, 1992].

b. Henry's problem [1964], where saline water intrudes in a hypothetical rectangular aquifer and merges by a constant dispersion coefficient,

c. Chan Hong's sharp interface [1989], where a sharp interface between fresh and saline groundwater is simulated.

It should be noted that several conclusions drawn in this chapter highly depend on the geometries and the (subsoil and model) parameters of these specific cases.

6.2   Case similar to Edelman's sudden change in boundary condition [1947]

A case is considered that is based on Edelman's type (a)[2] [1947]: sudden change in boundary condition, namely the open water level in a canal is changed which has its effects on the piezometric level in the adjacent aquifer (see figure 6.1). In this section, however, the aquifer is confined and a rise of the open water level at the boundary canal is implemented rather than a lowering of the open water level as occurs in Edelman's type (a). The rise in open water level can stand for a sudden sea level rise SLR. Then, the change in piezometric level in the confined aquifer is due to a sea level rise at the so-called seaside boundary. A fully penetrating ditch bounds the aquifer at the seaside boundary $x=0$. As MOC cannot simulate an infinite boundary, which occurs in the original types of Edelman, a no-flow boundary is supposed at the land side at $x=l$. The aquifer is situated above an impervious base or no-flow boundary. At the top, the confined aquifer is also bounded by an impervious layer, and thus, no natural groundwater recharge occurs. Before $t=0$, the open water level in the boundary canal equals that of the top of the aquifer. At $t=0$, the open water level has risen, e.g. due to a sudden sea level rise.

In subsection 6.2.1, the analytical solution of the case similar to Edelman's type (a) is given and the subsoil and model parameters used in the adapted MOC model are enumerated. In subsection 6.2.2 the results are discussed of the adapted MOC model which are compared with the analytical solution. The sensitivity of the aquifer for the specific storativity S_s is determined and the influence of the flow time step is analysed. Finally, in subsection 6.2.3, some conclusions are drawn.

---

[2]Edelman [1947] derived four types of solutions for unsteady one-dimensional flow in an unconfined aquifer of semi-infinite extend without recharge: (a) a sudden lowering of the water level in a boundary canal; (b) a suddenly occurring constant groundwater discharge into a canal; (c) a linearly increasing lowering of the water level in a boundary canal; and (d) a linearly increasing groundwater discharge into a canal. For the types (b) and (d), the water level in the canal is being lowered accordingly.
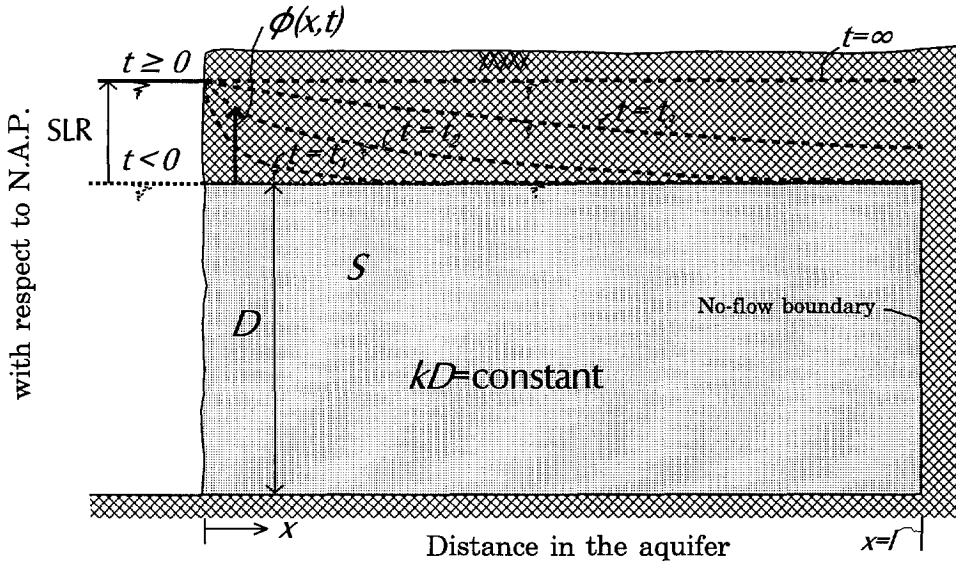
Figure 6.1: Schematic representation of the case similar to Edelman's type (a): a confined aquifer with a no-flow boundary at $x=l$.

6.2.1 Definition of the case similar to Edelman's case

Analytical solution

Equations 6.1 to 6.8 describe the flow problem, representing the unsteady one-dimensional flow in the aquifer [Carslaw and Jaeger, 1959; de Marsily, 1986]:

Darcy:
$$q = -kD\frac{\partial \phi}{\partial x} \tag{6.1}$$

continuity:
$$\frac{\partial q}{\partial x} = -S\frac{\partial \phi}{\partial t} \tag{6.2}$$

combined:
$$\frac{\partial^2 \phi}{\partial x^2} = \frac{S}{kD}\frac{\partial \phi}{\partial t}, \qquad \text{for } 0 \le x \le l, \quad t \ge 0 \tag{6.3}$$

initial condition:
$$\phi(x,0) = 0, \qquad \text{for } 0 < x \le l \tag{6.4}$$

at the first boundary:
$$\phi(0,t) = \text{SLR}, \qquad \text{for } t \ge 0 \tag{6.5}$$

at the second boundary:
$$\left(\frac{\partial \phi}{\partial x}\right)_{x=l} = 0, \qquad \text{for } t \ge 0 \tag{6.6}$$

$$\phi(x,t) = \text{SLR} \left(1 - \frac{4}{\pi} \sum_{n=0}^{\infty} \frac{(-1)^n}{(2n+1)} \exp \left[-\frac{(2n+1)^2 \pi^2 kDt}{4Sl^2} \right] \cos \frac{(2n+1)\pi(l-x)}{2l} \right)$$

(6.7)

or

$$\phi(x,t) = \text{SLR} \sum_{n=0}^{\infty} (-1)^n \left[\text{erfc} \frac{(2n+1)l - (l-x)}{2\sqrt{\frac{kDt}{S}}} + \text{erfc} \frac{(2n+1)l + (l-x)}{2\sqrt{\frac{kDt}{S}}} \right]$$

(6.8)

Complementary error function:

$$\text{erfc}(u) = 1 - \frac{2}{\sqrt{\pi}} \int_0^u e^{-u^2} du \quad \text{or} \quad \text{erfc}(u) = 1 - \frac{2}{\sqrt{\pi}} \sum_{n=0}^{\infty} \frac{(-1)^n u^{2n+1}}{n!(2n+1)}$$

(6.9)

where

- q = groundwater flow per unit width of the aquifer ($L^2 T^{-1}$),

- kD = transmissivity of the aquifer, considered as constant ($L^2 T^{-1}$),

- ϕ = piezometric level in the aquifer with respect to the reference level, that is the horizontal top of the aquifer (L),

- S = storage coefficient or specific yield of the aquifer ($-$),

- x = distance from the boundary canal (L),

- l = length of the aquifer up to the land side no-flow boundary (L),

- $\text{erfc}(u) = 1 - \text{erf}(u)$ = complementary error function ($-$). The solution of the $\text{erf}(u)$ is tabulated, among others, in Abramowitz and Stegun [1965] and Huisman [1972].

Density differences are not taken into account. Effects of tides, that make the problem unsteady, and recharge are neglected. Only changes in piezometric level are computed and analysed, as solute transport is not considered.

Carslaw and Jaeger [1959] also derived formulas for equivalent problems in the theory of conduction of heat in solids. Their analytical formulas are similar to those for groundwater flow in aquifers. For instance, for an aquifer with an initial piezometric level ϕ equal to 0 and for $t > 0$ ϕ=SLR at x=0 and ϕ=0 at x=1, the solution becomes:

$$\phi(x,t) = \text{SLR} \sum_{n=0}^{\infty} \left[\text{erfc} \frac{(2n+1)l - (l-x)}{2\sqrt{\frac{kDt}{S}}} - \text{erfc} \frac{(2n+1)l + (l-x)}{2\sqrt{\frac{kDt}{S}}} \right]$$

(6.10)

Subsoil and model parameters

The following reference case is defined for simulation with the adapted MOC model: an aquifer with a length of l=12,500 m and a height of D=100 m, containing fresh groundwater with a density equal to 1000 kg/m^3. Furthermore, the hydraulic conductivity equals k=20 m/d (the anisotropy factor k_z/k_x is set to 1 (−)) and the effective porosity is set to 0.35. As no solute transport is considered in this case, the dispersivities α_L and α_T are set to zero. In Dutch sandy aquifers, the specific storativity S_s ranges from 0.5·10⁻⁵ m^{-1} to 3·10⁻⁵ m^{-1} van der Gun [1979] (see also subsection 5.4.2: item 3. Specific storativity S_s). For the reference case, the specific storativity S_s is set to 1·10⁻⁵ m^{-1}. According to equation 5.13 ($S=S_s·b$), the storage coefficient S (−) is equal to the specific storativity S_s (L^{-1}) in the adapted MOC model, as the saturated thickness b of the aquifer perpendicular to the profile is set to the unit length.

The aquifer is schematised with 250·10=2500 grid cells, thus a grid cell has a length of 50 m and a height of 10 m. The convergence criterion TOL for the (iterative) calculation of the freshwater head in the groundwater flow equation is 10⁻⁵ ft. The initial flow time step is set to a small value of 1 day.

6.2.2 Discussion

The adapted MOC model compared with the analytical solution

Figure 6.2 shows that the computations of the adapted MOC model are in good agreement with the analytical solution of equation 6.7. As can be seen, the time lag, before a new state of dynamic equilibrium of the piezometric level distribution is reached, depends on the value of the specific storativity S_s, which ranges from S_s=3 · 10⁻⁶ m^{-1} to S_s=3 · 10⁻⁵ m^{-1}. The smaller the specific storativity S_s is, the faster the geohydrologic system reacts on sudden changes in open water level at the seaside boundary. For instance, for S_s=1 · 10⁻⁵ m^{-1}, 95 % of the ultimate elevation in piezometric level at x=7425 m is reached within some 100 $days$. Under normal conditions in sandy aquifers of the Netherlands, the time lag is for confined aquifers in the order of several hours (to at most several days at large distances from the changing boundary), whereas for unconfined aquifers the time lag is substantially greater, viz. in the order of weeks (to at most a few months at large distances from the changing boundary). It is evident that the time lag for both types of aquifers can be neglected compared to the time scale of sea level rise, which is in the order of decades or centuries, namely a sea level rise of approximately 60 cm takes place during one century. A relevant consequence of this observation is that it is justified to set the specific storativity S_s equal to zero when a sea level rise is simulated. The piezometric levels in the coastal groundwater flow regimes reach the new state of dynamic equilibrium almost immediately after a sudden sea level rise.

Obviously, the part of the aquifer that is situated near the seaside boundary reaches the new state of dynamic equilibrium earlier than the part of the aquifer near
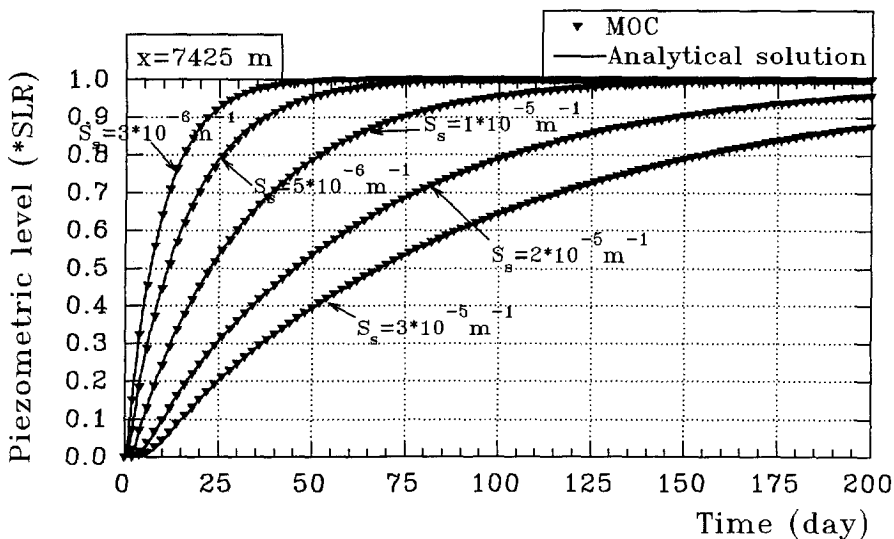
Figure 6.2: Influence of the specific storativity S_s on the change in piezometric level as a function of time in an observation point at $x=7475$ m from the seaside boundary, in case the open (sea) water level is changed suddenly. For MOC, the piezometric level at every second flow time step is displayed.

the land side boundary. This is demonstrated in figure 6.3, where the changes in piezometric level of four observation points are displayed. Here again, the computations of the adapted MOC model are in good agreement with the analytical solution of equation 6.7.

Figure 6.4 shows the changes in piezometric level due to the elevation at the seaside boundary as a function of the distance in the aquifer at several moments in time. After a number of days the piezometric level in the aquifer has already risen significantly due to the elevation at the seaside boundary. Within 100 *days* 95 % of the new state of dynamic equilibrium (ϕ=SLR) is reached.

The length of the flow time step

The length of the flow time step in the adapted MOC model is rather important, if the specific storativity S_s is not equal to zero. When the interest is focused on the development to a new state of dynamic equilibrium for the piezometric level, the length of the flow time step should not be too great, since the new state of dynamic equilibrium may be reached within some (tens of) days. Figure 6.5 shows the influence of the length of the flow time step on the development of the piezometric level to a new state of dynamic equilibrium. Simulations with great flow time steps generate inaccurate piezometric levels as a function of time, whereas simulations with small
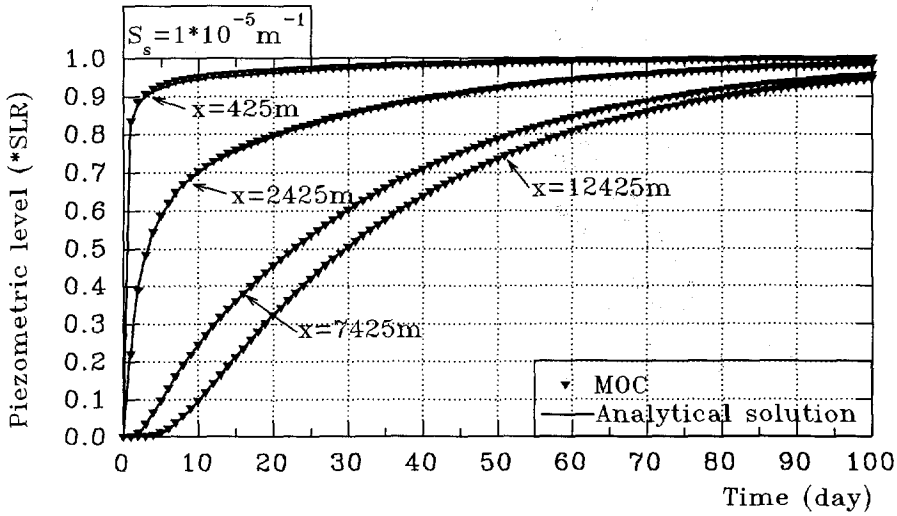
Figure 6.3: Changes in piezometric level for four observation points as a function of time. The specific storativity $S_s=1 \cdot 10^{-5}$ m^{-1}.
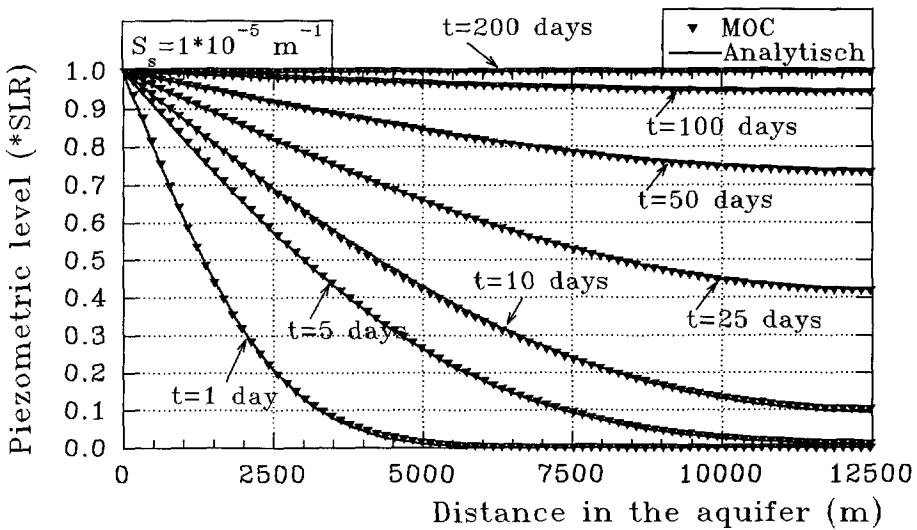
Figure 6.4: Change in piezometric level as a function of the distance in the aquifer at several moments in time. The specific storativity $S_s=1 \cdot 10^{-5}$ m^{-1}.
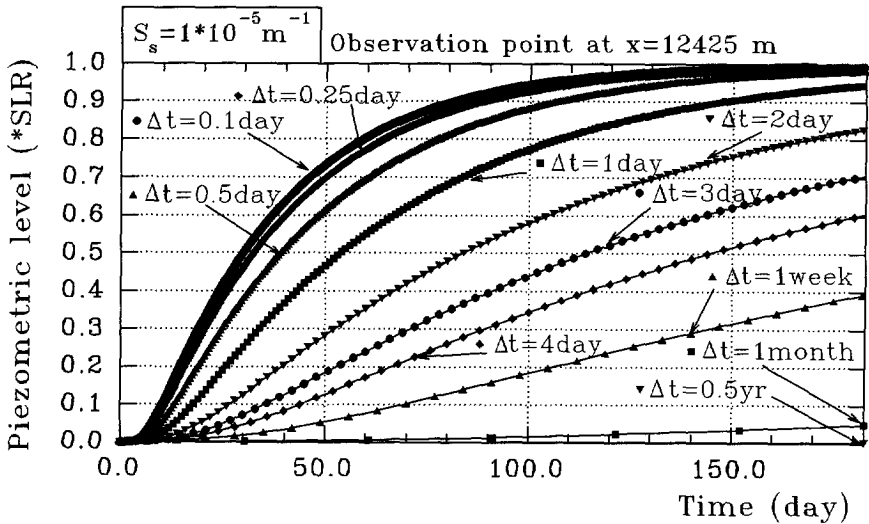
Figure 6.5: Influence of the length of the flow time step on the piezometric level as a function of time in an observation point at x=12425 m.

flow time steps, in the order of 0.1 day, appear to approach the exact development of the piezometric level sufficiently accurate.

6.2.3   Conclusions

In this hypothetical case which is inspired by Edelman's achievements, the piezometric levels in a finite confined aquifer are changing due to an instantaneous elevation in open water level in a canal boundary.

The simulations, computed with the adapted MOC model, are in good agreement with an analytical solution, borrowed from Carslaw and Jaeger [1959]. The specific storativity S_s highly determines the time lag before a new state of dynamic equilibrium of the piezometric level distribution is reached. In this specific hypothetical case, 95 % of the new state of dynamic equilibrium is reached at the land side no-flow boundary at x=12,500 m within *one year* for specific storativities S_s in the range of $0.5 \cdot 10^{-5}$ m^{-1} to $3 \cdot 10^{-5}$ m^{-1}. These values occur in the sandy aquifers of the Netherlands. This means that when long periods are simulated, such as when the impact of sea level rise on the groundwater flow regime is assessed, the specific storativity S_s can be set equal to zero.

For cases with a specific storativity S_s not equal to zero, the computations with the adapted MOC model should be performed with small flow time steps to suppress inaccurate solutions of the groundwater flow equation.

6.3   Henry's problem: sea water in coastal aquifers [1964]

In this section, some characteristics of the adapted MOC model are discussed through simulations of Henry's problem. In Henry's problem, saline water intrudes a coastal aquifer and merges by a constant dispersion coefficient. The results are compared with the solution of Henry himself and with various solutions of other techniques. It is common practice to apply Henry's problem [1964] as a benchmark for new two-dimensional groundwater flow models that can simulate solute transport and density flow [Segol, 1994]. Various researchers use Henry's problem to verify their own model. A few of these scientists, such as Lee and Cheng [1974], compared their numerical solutions with Henry's final steady state solution; other scientists, such as Pinder and Cooper [1970], Segol *et al.* [1975], Frind [1982], Voss [1984], Sanford and Konikow [1985] and Galeati *et al.* [1992], compared their solutions with the unsteady state solutions of Henry's problem. These unsteady state situations are stages in the evolution of the salt water intrusion. Originally, hydrodynamic dispersion could only be presented in MOC as a *velocity-dependent* hydrodynamic dispersion. As a *constant* dispersion coefficient has to be applied in Henry's problem, the author has also adapted the computer code to simulate a *constant* dispersion coefficient (see subsection 5.3.1).

In subsection 6.3.1, the geometry of Henry's problem is described and the applied subsoil and model parameters are summarized. In subsection 6.3.2, the solutions of the adapted MOC model and six other techniques are compared. Moreover, the results of computations with different numbers of grid cells, particles and values of dispersion coefficients are discussed, and an analysis of the simulation of a sharp interface and the development of the brackish zone is given. Finally, in subsection 6.3.3, some conclusions are drawn.

6.3.1   Definition of Henry's problem

Geometry

Henry formulated in 1964 the sea water intrusion in a homogeneous, isotropic, confined, rectangular aquifer including dispersion. The effect of dispersion on salt encroachment in coastal aquifers was investigated. He solved the equations with the Galerkin method by using Fourier series.

The boundary conditions of Henry's problem are shown in figure 6.6. The top and bottom boundaries are impermeable and thus no-flow boundaries. A constant fresh water flux Q enters the aquifer along the vertical at $x=0$. The seaside boundary at $x=l$ is a constant *saltwater head*. In the adapted MOC model, mass transport occurs over the seaside boundary. This is in contrast with the solution of Henry, where no mass transport over the seaside boundary occurs. Relevant dimensionless variables of this problem are defined as follows:

$$\xi = l/d, \qquad a = Q/k_1 d \quad \text{and} \quad b = D_h/Q \qquad (6.11)$$
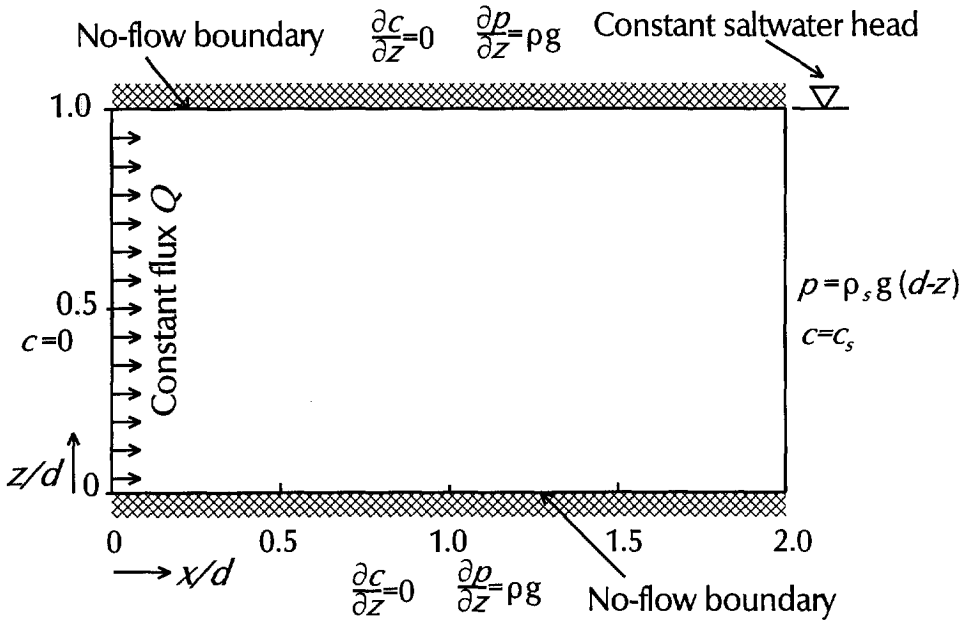
Figure 6.6: Schematic representation of Henry's problem.

where

- $\xi = l/d$ = aspect ratio $(-)$,

- l = length of the aquifer (L),

- d = height of the aquifer (L),

- D_h = coefficient of hydrodynamic dispersion $(L^2\,T^{-1})$,

- Q = net fresh water discharge per unit length of beach $(L^2\,T^{-1})$,

- $k_1 = k\frac{\rho_s-\rho_f}{\rho_f}$ = hydraulic conductivity k times the relative density difference $(L\,T^{-1})$,

- ρ_f, ρ_s = density of respectively fresh and saline water $(M\,L^{-3})$,

- $b = D_h/Q$ = inverse of the (seepage) Peclet-number Pe $(-)$.

The parameters in Henry's problem are set to $\xi=2$, $a=0.263$ and $b=0.1$. Effects of tides and recharge, that make the salt water intrusion problem unsteady, are averaged and all included in the value of the hydrodynamic dispersion coefficient D_h.

Subsoil and model parameters

In order to satisfy the parameters $\xi=2$, $a=0.263$ and $b=0.1$, the following character-
istics are applied in the reference case: a hypothetical aquifer of $d=1.0$ m by $l=2.0$
m; a hydraulic conductivity of $k=1$ cm/s; a fresh water discharge per unit length
of beach of $Q=6.6 \cdot 10^{-5}$ m^2/s, which is uniformly distributed over the number of
vertical grid cells; and an effective porosity of 0.35. No anisotropy occurs in Henry's
problem $(k_z/k_x=1.0)$ and the specific storativity S_s is set to zero.

The reference case has 800 grid cells: $40 \cdot 20$, thus the (square) grid cell has a length
Δx and a height Δz of 0.05 m. The convergence criterion TOL for the (iterative)
calculation of the freshwater head in the groundwater flow equation is 10^{-6} ft, and
the relative distance ζ in a grid cell, in which a particle is allowed to move during
one solute time step, is set to 1.0. Each grid cell has 9 particles. The flow time step
is set to 5 min.

The author has added a *constant* molecular diffusion coefficient D_d to the dis-
persion components in the computer code of the adapted MOC model (see subsec-
tion 5.3.1), as Henry's problem assumes that the hydrodynamic dispersion is repre-
sented by a *constant* dispersion coefficient rather than by a *velocity-dependent* dis-
persion coefficient. The *constant* molecular diffusion coefficient D_d is set to 0.066
cm^2/s.

In the initial condition of the reference case, the entire aquifer only contains
fresh groundwater, which has a density equal to 1000 kg/m^3. Saline groundwater
has a density equal to 1025 kg/m^3, thus the relative density difference $\frac{\rho_s - \rho_f}{\rho_f}$ is
0.025. During the evolution of the brackish zone, a brackish outflow at the seaside
appears in the upper part of the aquifer. It is assumed in this hypothetical case that
brackish groundwater, which flows out of the aquifer at the seaside, immediately
mixes with salt seawater outside the aquifer and is discharged immediately. Hence,
this boundary is kept constantly saline, and thus, a constant saltwater head rather
than a brackishwater head is simulated at the upper part of the seaside boundary.

Results of the reference case

Figure 6.7 shows the freshwater head distribution, several isolines of saltwater fraction
and the velocity field after a simulation time of 400 min. Near the seaside, a landward
flow of saline water occurs in the lower part of the aquifer and a seaward flow of fresh
water occurs in the upper part of the aquifer. Obviously, sea water mixes with
fresh water and circulates. Especially in the outgoing fresh water at the seaside the
velocities are great. Mixing, which is caused by hydrodynamic dispersion, restricts
the landward extent of salt water intrusion. This phenomenon was predicted by
Cooper [1964] and observed in the field by Kohout [1964].
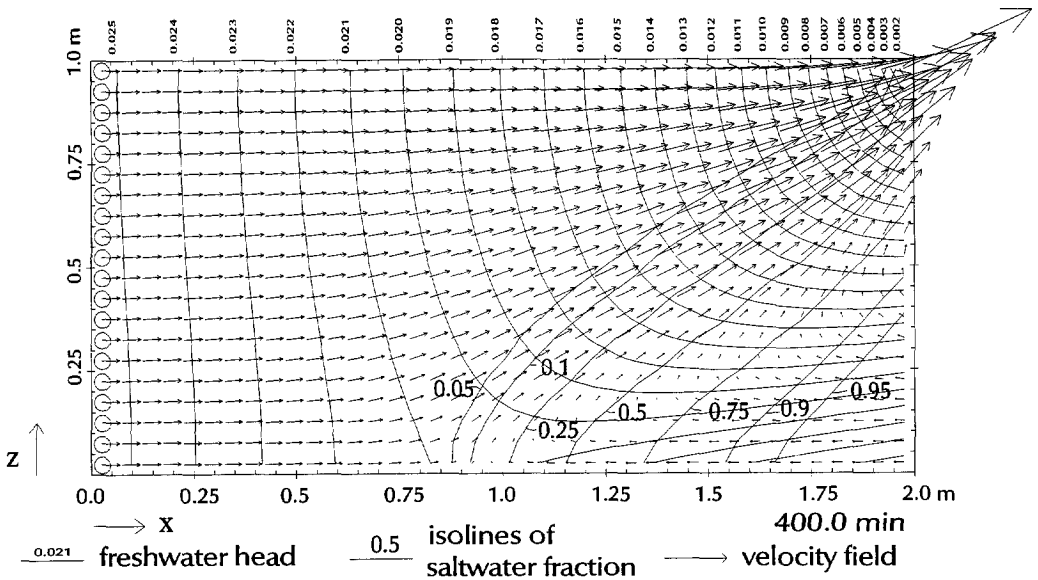
Figure 6.7: Freshwater head distribution (in m), several isolines of saltwater fraction and the velocity field of the reference case, computed by the adapted MOC model. The *constant* dispersion coefficient equals 0.066 cm^2/s. The simulation time is 400 min. The lengths of the arrows correspond with the displacement of groundwater during a time step of 4.0 min, beginning at the indicated moment in time.

6.3.2   Discussion

Solution of Henry's problem by the adapted MOC model compared with solutions by six other techniques

1. Pinder and Cooper [1970] were one of the first to use Henry's problem for testing their numerical model. In a way, their model is a precursor of MOC. They used the *method of characteristics* to solve the transport equation and the iterative *alternating-direction implicit* procedure (ADI) to solve the groundwater flow equation. They considered an unsteady flow development under conditions similar to Henry's problem, thus with the same seaside boundary. Pinder and Cooper assumed two initial conditions for the salinity distribution in the aquifer: (1) fresh groundwater, and (2) a steady state sharp interface between fresh and saline groundwater.

   Figure 6.8 shows the position of the isolines of 0.5 saltwater fraction, 30 and 100 min after the beginning of the salt water intrusion for the initially fresh condition. Although they deduced that their numerical solution approaches Henry's steady state solution after a long time, they only showed in their article the unsteady state solutions of the isolines of 0.5 saltwater fraction till 100 min
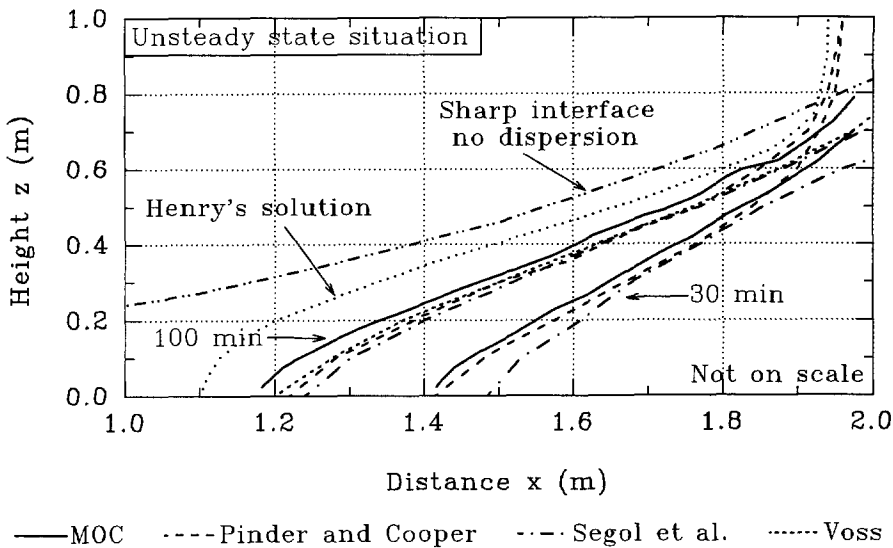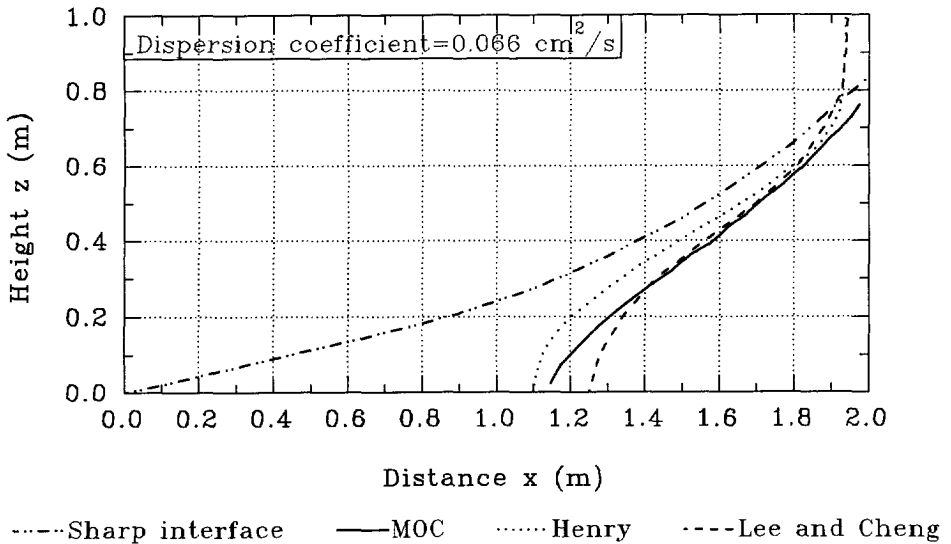
Figure 6.8: Unsteady state situation of the isoline of 0.5 saltwater fraction of Henry's problem, computed by the adapted MOC model (the reference case), Pinder and Cooper [1970], Segol et al. [1975] and SUTRA [Voss, 1984]. Also the solution of Henry [1964] and the steady state sharp interface with no dispersion are given.

for the initially fresh condition and till 70 *min* for the initially sharp interface condition. Their results for both conditions **cannot** clearly demonstrate that the computations are eventually in good agreement with Henry's steady state solution.

2. Segol *et al.* [1975] used a Galerkin Finite Element technique to solve the set of nonlinear partial differential equations. The positions of the isolines of 0.5 saltwater fraction after 30 and 100 *min* are shown in figure 6.8. Note that Segol *et al.* had to use another seaside boundary condition for the transport of solute than Henry because of the application of the finite-element method: the condition is modified to allow mass transport over the top portion of the seaward boundary. Therefore, the top parts of the isolines cannot be compared.

3. Frind [1982] applied the classical Galerkin Finite Element approach to simulate density-dependent transport problems, with emphasis on computing cost-saving measures. The positions of the isolines of 0.5 saltwater fraction of Frind appear to be in very good agreement with Segol *et al.*'s solutions that are shown in figure 6.8.

4. Galeati *et al.* [1992] compared computations of their technique (a 'modified' method of characteristics, implicit with backward tracking of particles) with

Frind's solution [1982]. They found that the comparison with Frind was good
except near the seaside boundary, which was treated in a different way.

5. Voss [1984] developed the finite-element simulation model SUTRA that employs
   a two-dimensional hybrid finite-element and integrated finite-difference method
   to approximate the governing equations (see also subsection 4.5.1). In figure 6.8,
   the position of the isoline of 0.5 saltwater fraction is given of the unsteady state
   situation after 100 min, which agrees with the results of the other solution
   techniques.

6. Lee and Cheng [1974] formulated and solved the coupled nonlinear conserva-
   tion equation of mass and salt in terms of stream functions by the finite-element
   method with the aid of iteration and underrelaxation. They used Henry's orig-
   inal seaside boundary condition. Nonetheless, figure 6.9 shows that the steady
   state position of the isoline of 0.5 saltwater fraction is **not** really in good agree-
   ment with the position of Henry's solution in the vicinity of the toe of the isoline.
   Note that this conclusion is in contrast with what Lee and Cheng deduced in
   1974.

Figure 6.9: Steady state situation of the isolines of 0.5 saltwater fraction of Henry's prob-
lem, computed by Henry [1964], the adapted MOC model (the reference case) and Lee and
Cheng [1974]. Also the solution of the steady state sharp interface is given (no dispersion).

In conclusion, the unsteady state solutions (namely 30 and 100 min after the be-
ginning of the salt water intrusion for the initially fresh condition) of the various
techniques are in good mutual agreement. By contrast, it appears that currently

no method has succeeded in duplicating Henry's steady state solution. Especially near the bottom of the aquifer, Henry's solution substantially differs from all numerical solution techniques. It appeared that the inaccuracies of Henry's results are a consequence of the limited computer facilities at the time [Segol, 1994].

Influence of number of grid cells

The sensitivity of the solution for the simulated number of grid cells is investigated. Four cases with different numbers of grid cells are compared, to observe differences in the position of the isoline of 0.5 saltwater fraction:

a. $20 \cdot 10 = 200$ grid cells: Δx and Δz is $0.1\ m$,

b. $40 \cdot 20 = 800$ grid cells: Δx and Δz is $0.05\ m$,

c. $80 \cdot 40 = 3200$ grid cells: Δx and Δz is $0.025\ m$,

d. $120 \cdot 60 = 7200$ grid cells: Δx and Δz is $0.0167\ m$.

The explicit numerical solution of the solute transport equation has several stability criteria (see equations 5.66 to 5.71). These criteria may require that the flow time step, used to solve the groundwater flow equation, is subdivided into a number of smaller solute time steps during which all particles are moved to new positions. For further information, see subsection 5.3.3.

Two stability criteria for the maximum permissible solute time step are affected by the number of grid cells:

- the stability criterion equation 5.67:

$$\Delta t_s \leq \min_{\text{(over grid)}} \left[\frac{0.5}{\frac{D_{xx}}{(\Delta x)^2} + \frac{D_{zz}}{(\Delta z)^2}} \right] \tag{6.12}$$

The smallest Δt_s occurs at the node having the greatest value of $\frac{D_{xx}}{(\Delta x)^2} + \frac{D_{zz}}{(\Delta z)^2}$. As the dimension of a grid cell $(\Delta x, \Delta z)$ decreases in case of an increasing number of grid cells, the value of $\frac{D_{xx}}{(\Delta x)^2} + \frac{D_{zz}}{(\Delta z)^2}$ in equation 5.67 increases. As a result, the maximum permissible solute time step decreases also.

- the stability criterion equation 5.71:

$$\Delta t_s \leq \frac{\zeta \Delta x}{(V_x)_{max}} \qquad \text{and} \qquad \Delta t_s \leq \frac{\zeta \Delta z}{(V_z)_{max}} \tag{6.13}$$

As the dimension of a grid cell $(\Delta x, \Delta z)$ decreases in case of an increasing number of grid cells, the maximum permissible solute time step also decreases if ζ remains the same. In this study, this stability criterion mostly dominates the simulation, and thus mostly determines the length of the solute time step for computing the solute transport equation.

In summary, if the number of grid cells increases, the number of calculations to move the particles during a flow time step of 5 *min* also increases. This observation is demonstrated in table 6.1. Initially, each grid cell has 9 particles during the computation of the reference case. The particles move from one grid cell to another. Some particles go out of the aquifer at the upper part of the seaside boundary and new particles enter into the aquifer at the land side and at the lower part of the seaside boundary (see figure 6.7). Therefore, more particle movements are counted than just the number that is determined by *the number of grid cells* times *the number of particles per grid cell* times *the number of solute time steps*.

Table 6.1: Some characteristics of the adapted MOC model for Henry's problem during the first 400 *min*: four cases with different numbers of grid cells; the total number of solute time steps; the mean number of solute time steps per flow time step of 5 *min*; the calculation time on the computer; and the total number of particle movements. The molecular diffusion is 0.066 cm^2/s and each grid cell initially has 9 particles.

Number of grid cells	Number of solute time steps	Mean number of solute time steps per flow time step	Calculation time† (*sec*)	Number of particle movements
200	322	4	70	625,969
800	666	9	420	5,219,227
3200	1624	21	3780	50,466,597
7200	2619	33	13,020	181,340,983

†: specifications of the computer applied: Highscreen LE 1024, 80486 micro processor, CPU with 8 Mb RAM, 50 MHz 80487 mathematical co-processor.

When more grid cells are used to simulate groundwater flow and solute transport in an aquifer, the solute transport equation should be solved more accurately. Figure 6.10 displays the isolines of 0.5 saltwater fraction of the four cases with different numbers of grid cells. The figure shows that the position of the isoline of 0.5 saltwater fraction of the case with 200 grid cells only deviates a little from the other three cases with more grid cells. The position of the isoline of 0.5 saltwater fraction of the case with 7200 grid cells is only a bit more smooth compared to the case with 800 grid cells. In conclusion, cases with 800 grid cells are accurate enough in comparison with the cases with 200 (less accurate), 3200 and 7200 grid cells. In addition, the calculation time of the computer is acceptable for the cases with 800 grid cells, namely 420 *sec* calculation time for a simulation of 400 *min*, see table 6.1.

Influence of the number of particles per grid cell

The influence of the number of particles in a grid cell on the accuracy of the solution appears to be small according to figure 6.11, unless only 1 particle in each grid cell is initially inserted. The difference between the cases with respectively 4, 5, 9 and
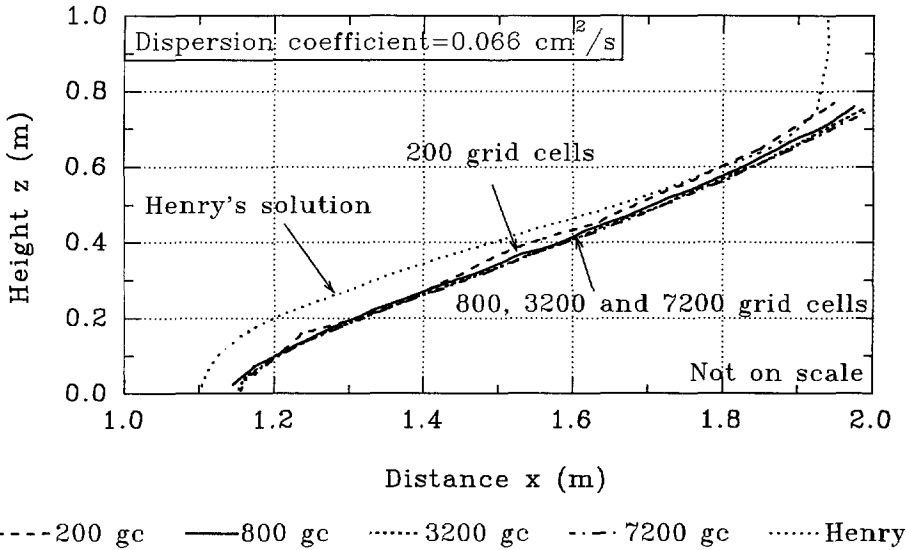
Figure 6.10: The isolines of 0.5 saltwater fraction of Henry's problem, computed by Henry himself and the adapted MOC model. Four cases with different numbers of grid cells are shown. The simulation time is 400 min.

16 particles in each grid cell can be neglected for the solution of Henry's problem, though these solutions deviate from the solution of Henry himself.

Several values of constant dispersion coefficients

Because the isoline of 0.5 saltwater fraction in the reference case with 800 grid cells lays near the isolines of 0.5 saltwater fraction of the cases with 3200 and 7200 grid cells (see figure 6.10), cases with 800 grid cells are chosen to assess the influence of several dispersion coefficients. Figure 6.12 shows four different coefficients of dispersion varying from 0 cm^2/s to 0.66 cm^2/s.

The greater the dispersion coefficient, the smoother the isolines of 0.5 saltwater fraction. If the dispersion increases, the isoline of 0.5 saltwater fraction moves towards the seaside and the brackish zone broadens. A greater dispersion coefficient implies a smaller maximum permissible solute time step Δt_s (see equation 5.67). Thus, the number of particle movements per flow time step increases with greater dispersion coefficients.

The smaller the dispersion coefficient, the larger the numerical instabilities for the solute transport may be (see figure 6.12). The reason is that in case the dispersion coefficient is small, mixing between adjacent grid cells is small too. Then it is possible that a great difference in density occurs between adjacent grid cells. When a particle in a grid cell with a high density (saline groundwater) moves to
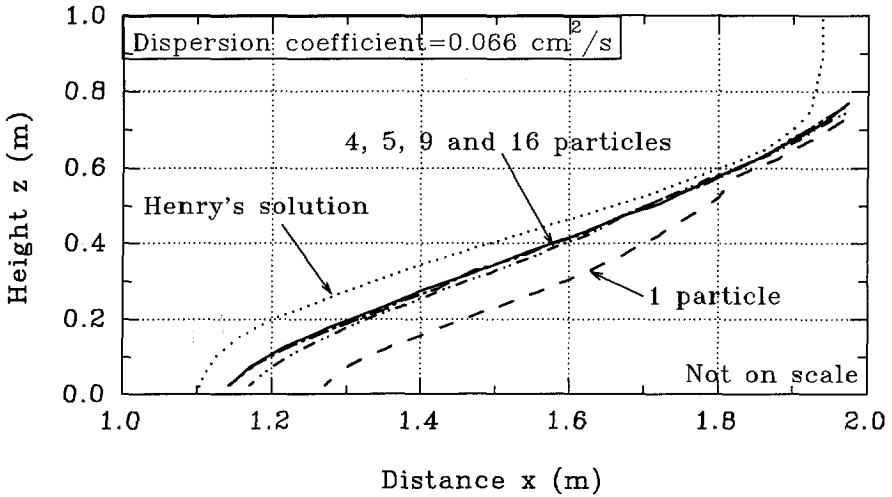
Figure 6.11: The isolines of 0.5 saltwater fraction of Henry's problem. The number of particles in a grid cell varies. All cases have 800 grid cells.
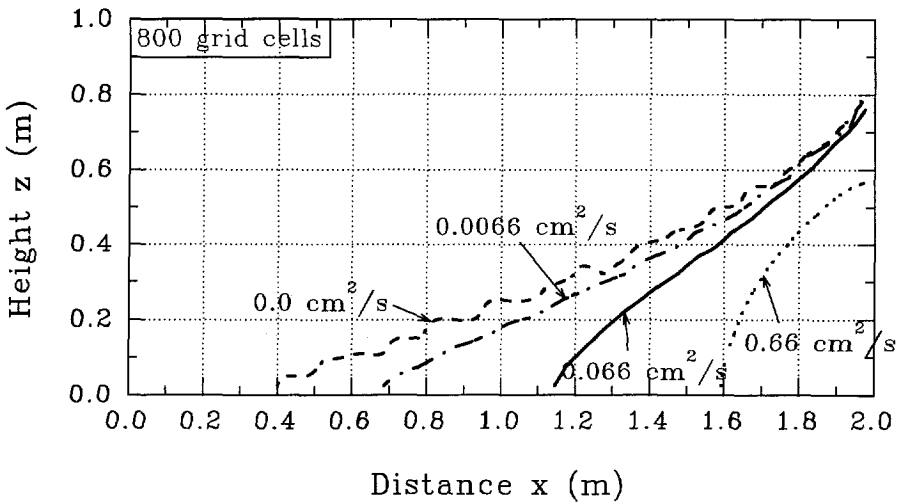
Figure 6.12: The isolines of 0.5 saltwater fraction of four cases with several *constant* dispersion coefficients.
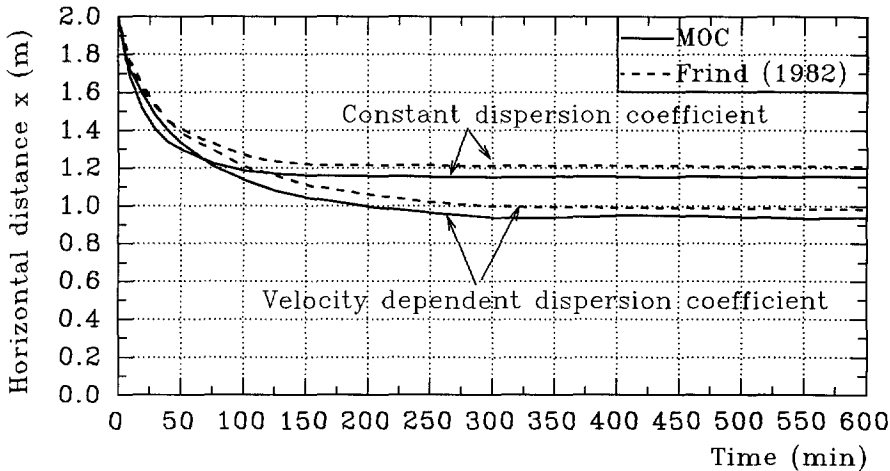
Figure 6.13: Advance of the position of the isoline of 0.5 saltwater fraction of Henry's problem at the bottom of the aquifer for both the *constant* dispersion coefficient and the *velocity-dependent* dispersion coefficient as a function of time, computed by the adapted MOC model and Frind [1982].

an adjacent grid cell that has a low density (fresh groundwater), the new density (e.g. brackish groundwater) may be completely different after averaging for the new flow time step. In this example, the density in such a grid cell is so much higher that the vertical velocity may subsequently alter in direction. In the next flow time step, the density of the grid cells in the evolved brackish zone may change once again due to particle movements in the other direction. At some grid cells, this process of alterations in vertical velocity due to changes in density could be repeated for the following flow time steps, and consequently, numerical instabilities are introduced. See subsection 5.5.1 for more information.

The constant versus the velocity-dependent dispersion coefficient

The *velocity-dependent* dispersion coefficient is represented by the dispersivities α_L and α_T (see the equations 5.46 and 5.47). In this case, both α_L and α_T are set to 0.035 m. Figure 6.13 shows the advance of the position of the isoline of 0.5 saltwater fraction at the bottom of the aquifer as a function of time for the *velocity-dependent* dispersion coefficient. The results of Frind [1982], who applies the classical Galerkin Finite Element approach, are compared with the computations with the adapted MOC model. As can be seen, both techniques are in reasonable agreement. The cases with the *constant* dispersion coefficient approach the steady state situation faster than the cases with the *velocity-dependent* dispersion coefficient.

Comparing figure 6.7 with figure 6.14 demonstrates that the displacement of the
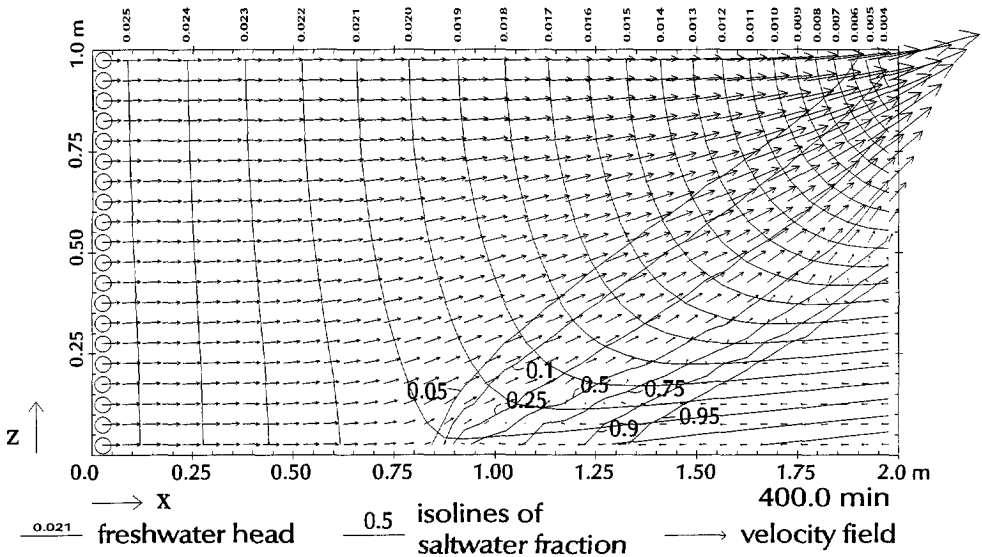
Figure 6.14: Freshwater head distribution (in m), several isolines of saltwater fraction and the velocity field of the case with the *velocity-dependent* dispersion coefficients α_L and α_T equal to 0.035 m. The simulation time is 400 min. The lengths of the arrows correspond with the displacement of groundwater during a time step of 4.0 min, beginning at the indicated moment in time.

isoline of 0.5 saltwater fraction in the aquifer is greater and the transition zone is smaller for the *velocity-dependent* dispersion coefficient than for the *constant* dispersion coefficient.

Simulation of a sharp interface

In figure 6.15, the isolines of 0.5 saltwater fraction are shown for four cases with different numbers of grid cells. As the dispersion coefficient is equal to 0.0 cm^2/s, these cases simulate a sharp interface. The results are in reasonable agreement with the solution for the sharp interface by Henry [1964], though the toe of the isoline of 0.5 saltwater fraction does not reach $x=0.0$ m as a result of numerical dispersion.

The figure shows that the cases with more grid cells, viz. 3200 and 7200, create more unstable isolines of 0.5 saltwater fraction. This is in contrast with the case where the *constant* dispersion coefficient is not equal to zero. For instance, when the dispersion coefficient is $D_h=0.066$ cm^2/s, the cases with 3200 and 7200 grid cells have more stable isolines of 0.5 saltwater fraction than the case with 800 grid cells (see figure 6.10). The explanation of this behaviour is as follows. Applying many grid cells for Henry's problem means small dimensions of the grid cells. The case with small grid cells must have small solute time steps in order to meet the stability
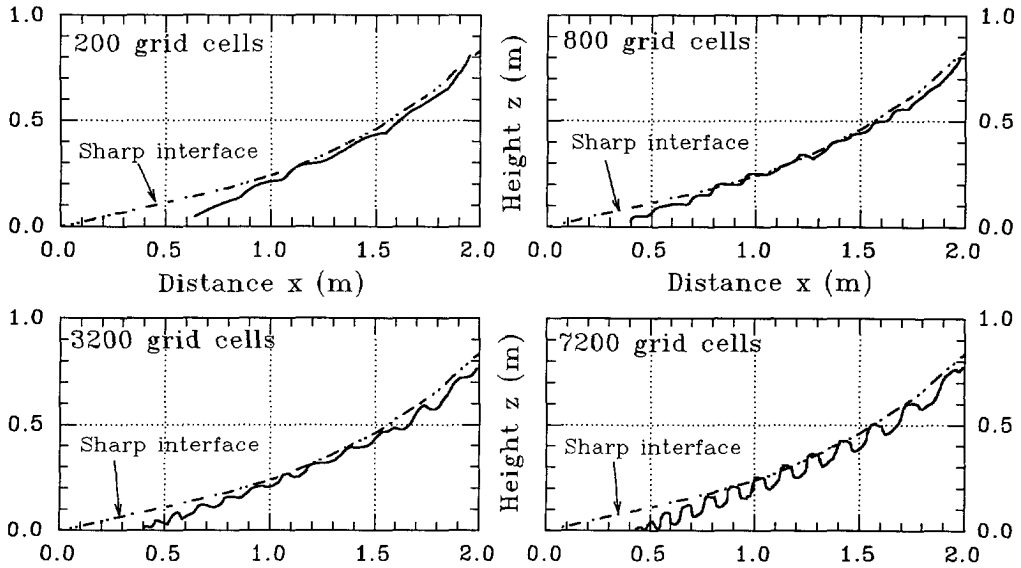
Figure 6.15: The isolines of 0.5 saltwater fraction of Henry's problem. The dispersion coefficient is 0.0 cm^2/s: a sharp interface is simulated. Four cases with different numbers of grid cells. The flow time step is 5 min. The simulation time is 600 min.

criteria (the equations 5.67 and 5.71). Consequently, when the flow time step remains 5 min, more solute time steps and thus more particle movements are necessary. As the velocity field is not adapted during the flow time step, particles in the brackish zone may pass several grid cells with a completely different density. In addition, if the dispersion coefficient equals zero, only a small brackish zone stretches over only a few grid cells due to numerical dispersion. Anyway, after the new density distribution is determined, abrupt changes in solute concentration and thus in density may occur in several grid cells. The densities of grid cells in the brackish zone may fluctuate during several flow time steps. This process could create unstable isolines (see figure 6.16). In conclusion, too many solute time steps within the same flow time step may induce numerical instabilities and numerical dispersion. Figure 6.17 shows that shortening the length of the flow time step creates more stable isolines.

Evolution of the brackish zone

In figure 6.18, the isolines of 0.5 saltwater fraction are shown during the development to the steady state situation. Calculations are made with two different initial conditions for the density distribution: (1) the aquifer is initially filled with saline groundwater and (2) the aquifer is initially filled with fresh groundwater. As can be seen, the salt water front is rapidly moving in the beginning of the simulation.
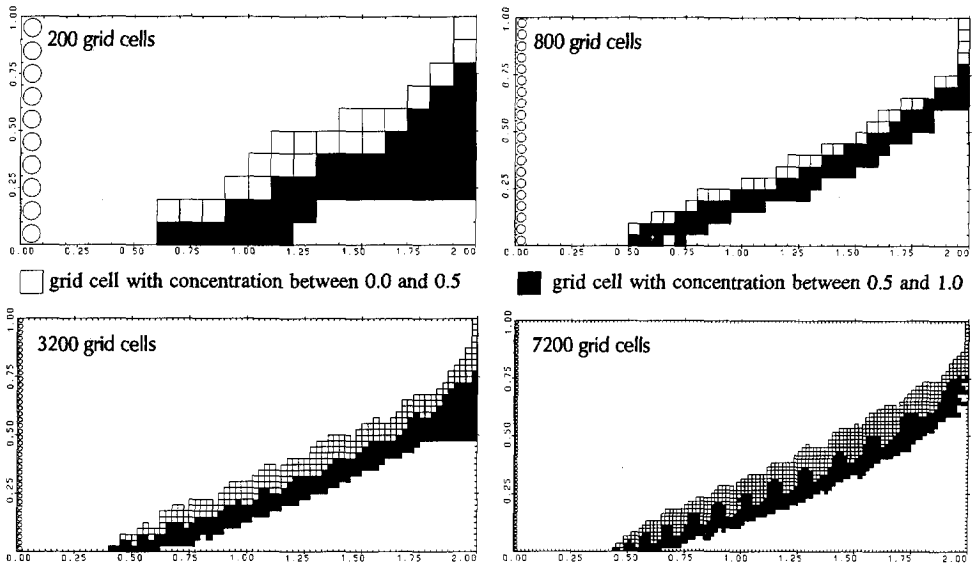
Figure 6.16: Grid cells with solute concentrations greater than 0.0 and smaller than 1.0. A sharp interface is simulated, thus D_h=0.0 cm^2/s. Four cases with different numbers of grid cells. The flow time step equals 5 min. The simulation time is 600 min.
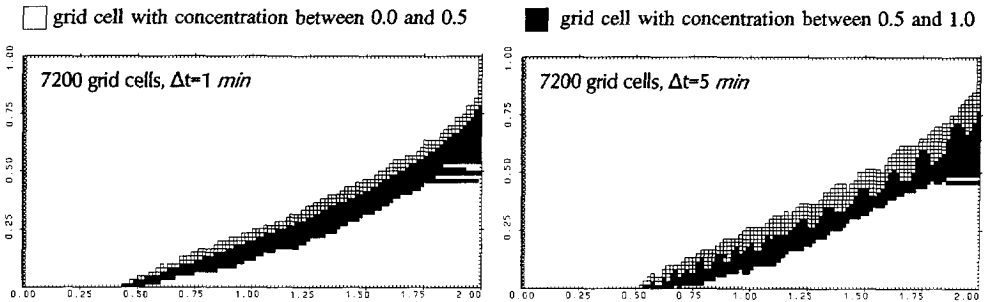
Figure 6.17: Grid cells with solute concentrations greater than 0.0 and smaller than 1.0. A sharp interface is simulated, thus D_h=0.0 cm^2/s. Both cases have 7200 grid cells. The flow time step is 1 and 5 min respectively. The simulation time is 200 min.

However, when the steady state situation is approached, the salt water front is moving slowly. These results are in good agreement with computations of Pinder and Cooper [1970] and Segol *et al.* [1975]. The final steady state situation of the whole simulation in Henry's aquifer is reached, when the toe of the isoline of 0.5 saltwater fraction near the bottom of the aquifer has approached about x=1.15 m.

Figure 6.19 shows the development of the solute concentration as a function of
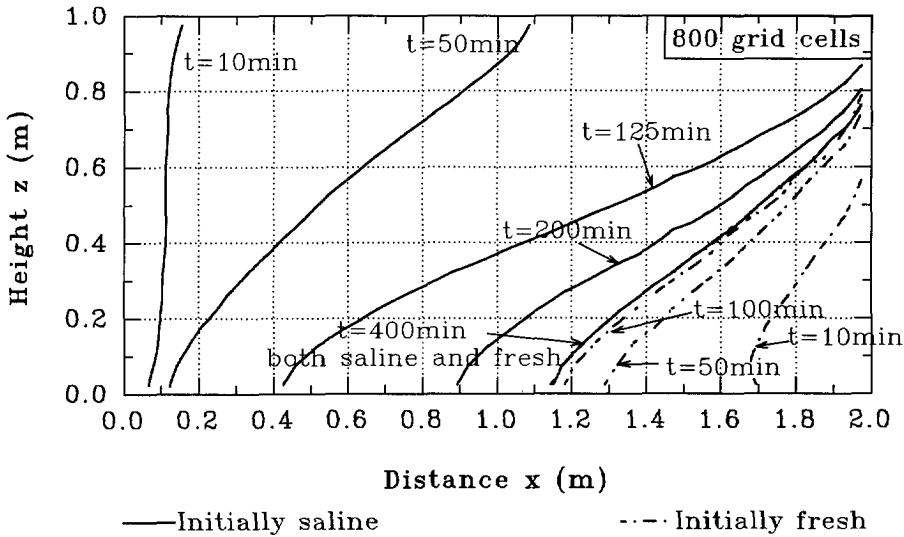
Figure 6.18: The isolines of 0.5 saltwater fraction of several unsteady situations. The cases have 800 grid cells and the dispersion coefficient is equal to 0.066 cm^2/s.

time for four observation points. From the observation point at $x=0.925$ m, $z=0.025$ m it can be deduced that a steady state situation in Henry's problem is reached after 190 min. Note that Voss and Souza [1987], who use the groundwater flow model SUTRA, suggested that the concentrations do not change appreciably after 100 min.

6.3.3   Conclusions

The adapted MOC model is used to simulate several unsteady state situations of Henry's problem. For steady state as well as unsteady state situations, the adapted MOC model is in good agreement with the six other solution techniques. Conversely, especially in the vicinity of the toe of the isoline of 0.5 saltwater fraction, the steady state solution of Henry himself does not match the adapted MOC model and the other solution techniques.

The results of computations with different numbers of grid cells show that the case with 800 grid cells is accurate enough. In general, the positions of the isolines of cases with more than 800 grid cells are smoother. However, if the dispersion coefficient is small (e.g. equal to zero, thus no dispersion occurs), the case with 7200 grid cells has unstable isolines due to numerical instabilities. A remedy to suppress the instability of isolines is to decrease the length of the flow time step. Solute transport in Henry's problem is about equally accurate for 4, 5, 9 and 16 particles per grid cell. Only if a
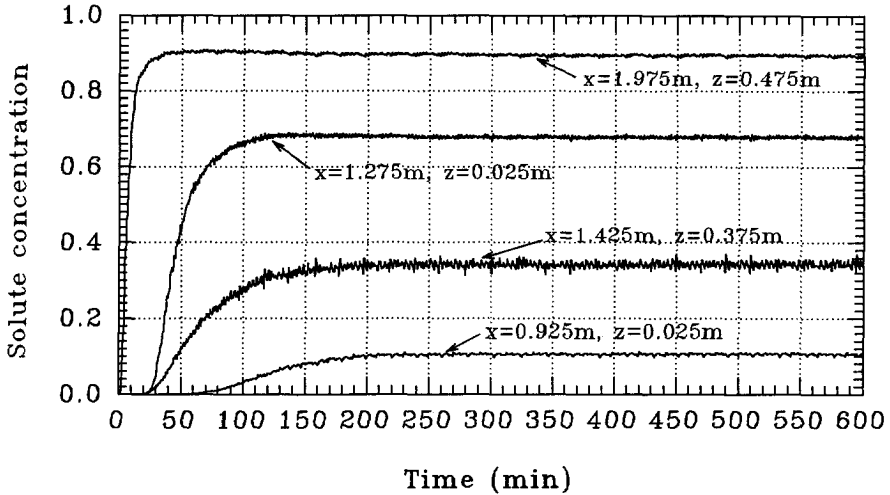
Figure 6.19: Solute concentration as a function of time for four observation points. The case has 800 grid cells and the dispersion coefficient is equal to 0.066 cm^2/s.

grid cell contains only 1 particle, the solution is unstable.

The salt water front approaches the steady state situation very slowly during the last phase of the unsteady state period. The final steady state simulation in Henry's problem is reached after 190 min.

6.4   Chan Hong et al.: sharp fresh-salt interface model [1989]

In this section, the adapted MOC model is compared with the numerical sharp fresh-salt interface model of Chan Hong et al. [1989]. Two-dimensional flow of fresh and saline groundwater in a homogeneous aquifer is simulated. It is assumed that no mechanical dispersion and no molecular diffusion occur, so the two fluids are supposed to be separated by a sharp fresh-salt interface. The density difference between fresh and saline groundwater induces a flow of the fluids. The exact displacement of the interface depends on the initial and the boundary conditions. Special attention is given to how the position of the salt-fresh interface evolves in time.

The ability of the adapted MOC model to simulate a sharp interface is tested and the influence of numerical dispersion is briefly evaluated. In subsection 6.4.1, the geometry of the simulated case and the numerical sharp interface model are described. In subsection 6.4.2, the results of the simulations are discussed. Finally, in subsection 6.4.3, some conclusions are drawn.

6.4.1 Definition of Chan Hong's case

Geometry

The problem consists of a homogeneous porous aquifer with fresh and saline ground-water, separated by a sharp fresh-salt interface. The flow is induced by density differences. All boundaries are impermeable: namely the two vertical boundaries and the two horizontal boundaries are no-flow boundaries. The sharp fresh-salt interface $u_{x,t}$ in Chan Hong's geometry initially obeys the following conditions (see figure 6.20):
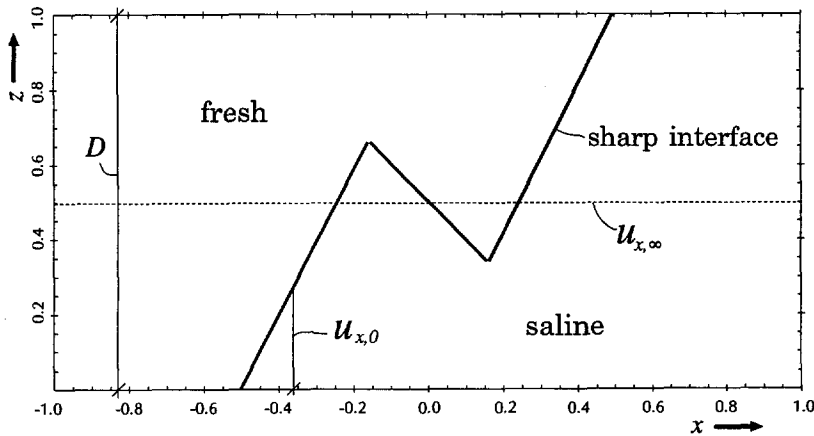
Figure 6.20: Homogeneous porous aquifer with fresh and saline groundwater, separated by a sharp fresh-salt interface $u_{x,t}$.

$$u_{x,0} = \begin{cases} 0, & -1 \leq x < -\frac{1}{2}, \\ 2x+1, & -\frac{1}{2} \leq x < -\frac{1}{6}, \\ -x+\frac{1}{2}, & -\frac{1}{6} \leq x < +\frac{1}{6}, \\ 2x, & +\frac{1}{6} \leq x < +\frac{1}{2}, \\ 1, & +\frac{1}{2} \leq x < +1. \end{cases} \qquad (6.14)$$

The results mentioned in Chan Hong *et al.* [1989] are rescaled to the following dimensionless variables:

$$x_r = x/D, \quad z_r = z/D, \quad u_r = u_{x,t}/D, \quad \Psi_r = \Psi/\Gamma D, \quad t_r = t\,\Gamma/D\,n_e, \qquad (6.15)$$

where

- r = an index that implies the rescaled parameter used in the numerical sharp fresh-salt interface model,

- x, z = respectively horizontal and vertical space coordinates (L),

- D = thickness of the homogeneous aquifer (L),

- $u_{x,t}$ = height of the fresh-salt interface at the horizontal space coordinate x as a function of time t (L),

- Ψ = stream function of the flow $(L^2\,T^{-1})$,

- $\Gamma = \frac{\kappa}{\mu}(\gamma_s - \gamma_f)\ (L\,T^{-1})$,

- κ = intrinsic permeability (L^2),

- μ = fluid viscosity $(M\,L^{-1}\,T^{-1})$,

- $\gamma_f, \gamma_s\,(= \rho_f g, \rho_s g)$ = respectively fresh and saline water specific weight $(M\,L^{-2}\,T^{-2})$,

- t = time (T),

- n_e = effective porosity $(-)$.

Background of the numerical sharp interface model

This brief theoretical description of the numerical sharp interface model is based on the article of Chan Hong *et al.* [1989]. The model is used by the Faculty of Technical Mathematics and Informatics, Delft University of Technology. It consists of a mathematical formulation which accurately determines the displacement of the sharp fresh-salt interface in a homogeneous aquifer.

The stream function is represented by a Poisson equation which is solved with the finite-element method. The moving fresh-salt interface is represented by a time evolution equation. A predictor-corrector method is used to follow the moving fresh-salt interface. The displacement of the fluid is based on the momentum balance equation (Darcy's law) and the continuity equation, assuming an incompressible fluid. The stream function Ψ is rewritten for the finite-element method, while the fresh-salt interface equation is described with a method called the $S^{\alpha,\beta}$ *second order explicit scheme*, introduced by Lerat and Peyret in 1973. The geometry is discretized with a mesh method that generates a triangular mesh. A fine mesh is generated near the interface and a coarse mesh further away. The triangular mesh is able to follow the displacement of the sharp fresh-salt interface. Consequently, only the values of the stream function Ψ at mesh points are required.

An interesting feature is the position of the x-coordinates, defined as $S_1(t)$ and $S_2(t)$, of the points where the interface reaches the bottom $z=0$ and the top $z=1$ of the aquifer respectively. Obviously, the location of the sharp fresh-salt interface is only computed between $S_1(t)$ and $S_2(t)$.

Subsoil and model parameters

For the reference case applied in the adapted MOC model, the following dimensions and parameter values are chosen:

- an aquifer with a length of 2 m and a height of 1 m,

- $n_e = 0.3$,

- $\kappa = 4.724 \cdot 10^{-11} \ m^2$ and $\mu = 10^{-3} \ kg/(ms)$,

- $\gamma_f = \rho_f \, g = 1000 \cdot 9.8 \ kg/(m^2 s^2)$ and $\gamma_s = \rho_s \, g = 1025 \cdot 9.8 \ kg/(m^2 s^2)$,

- $\Gamma = \frac{\kappa}{\mu}(\gamma_s - \gamma_f) = 1.157 \cdot 10^{-5} \ m/s = 1 \ m/d$,

- hydraulic conductivity: $k_x = \frac{\kappa \gamma_f}{\mu} = 4.630 \cdot 10^{-4} \ m/s = 40 \ m/d$,

- no anisotropy: $k_z/k_x = 1.0$,

- no hydrodynamic dispersion: α_L and $\alpha_T = 0.0 \ m$,

- dimension grid cell $\Delta x = \Delta z = 0.05 \ m$, so $40 \cdot 20 = 800$ grid cells,

- 16 particles per grid cell.

The most interesting parameter is the position of the fresh-salt interface at particular moments in time. The time parameter t_r used in the numerical sharp interface model is transformed to a value that is used in the adapted MOC model:

$$t = \frac{t_r \, D \, n_e}{\Gamma} = 0.3 \, t_r \quad (day). \tag{6.16}$$

The discretization of the sharp interface by the adapted MOC model differs from the discretization by the numerical sharp interface model. Since the adapted MOC model uses rectangular grid cells instead of triangular grid cells, the shape of the sharp interface can only be approximated roughly. In figure 6.21, the initial density distribution is given for both models. As the figure shows, the position of the fresh-salt interface for the adapted MOC model and the numerical model differs slightly one from another.

6.4.2   Discussion

In this subsection, the results of the computations with the adapted MOC model and the numerical sharp interface model are discussed on the basis of eight features.

During the simulation of the displacement of the fresh-salt interface, the adapted MOC model computes in several grid cells densities between fresh (1000 kg/m^3) and saline groundwater (1025 kg/m^3). These brackish grid cells are created due to numerical dispersion. From the moment these brackish grid cells originate, the exact
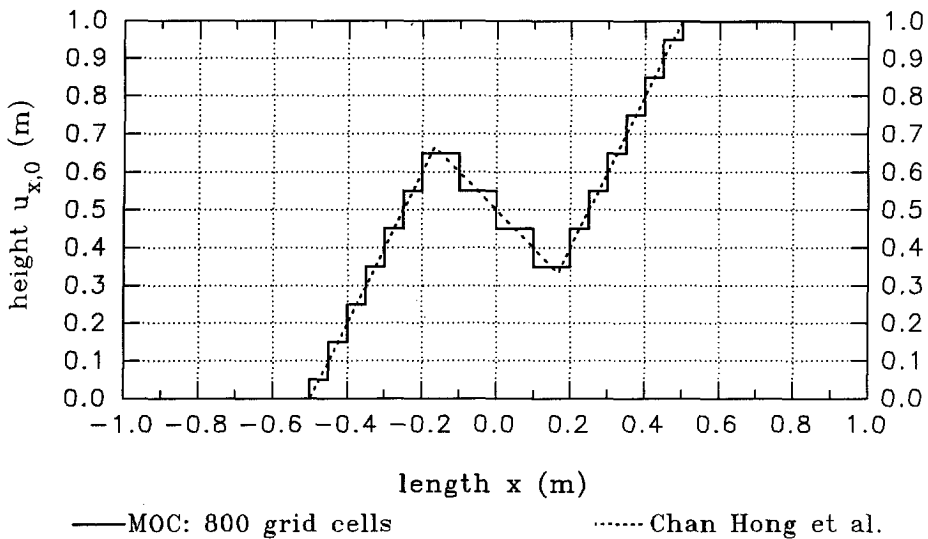
Figure 6.21: Position of the fresh-salt interface in the initial density distribution, used in the numerical sharp interface model as well as in the adapted MOC model.

position of the 'sharp' fresh-salt interface cannot be displayed any more. Subsequently, the position of the 'sharp' fresh-salt interface is estimated with an average density of 1012.5 kg/m^3 between that of fresh and saline groundwater. So, the position of the 'sharp' fresh-salt interface, shown in the figures of this subsection, equals in the adapted MOC model the 1012.5 kg/m^3-isoline for $t > 0$.

1. Number of grid cells

The displacement of the fresh-salt interface is also simulated with a fourfold increase of the number of grid cells: namely 3200 (80·40) instead of 800 (40·20) grid cells. The influence of the number of grid cells is limited, as the results in figure 6.22 show. The reference case with 800 grid cells computes about the same position of the fresh-salt interface as the more accurate case with 3200 grid cells.

2. Number of particles per grid cell

The number of particles per grid cell slightly affects the accuracy of the displacement of the fresh-salt interface. For instance, in figure 6.23 it is demonstrated that the difference between 5 or 16 particles per grid cell can be neglected.

By contrast, however, if only 1 particle per grid cell is used, then the accuracy of the simulation of the fresh-salt interface is much less accurate (figure 6.23). More numerical instabilities occur, and accordingly, the velocity distribution of the case

——MOC: 800 grid cells   ······ MOC: 3200 grid cells
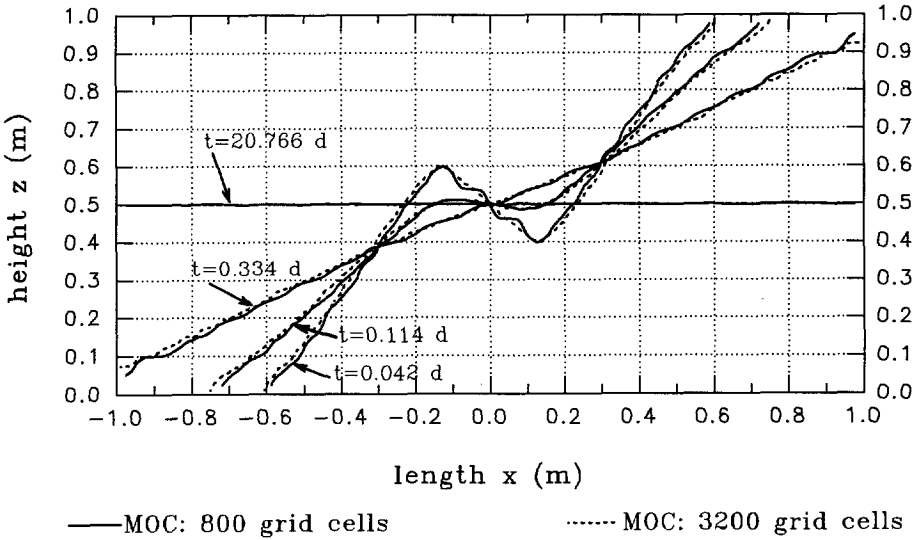
Figure 6.22: Influence of the number of grid cells in the adapted MOC model on the position of the fresh-salt interface at different moments in time. The moments in time $t=0.042$, $t=0.114$, $t=0.334$ and $t=20.766$ *days* are displayed.

——MOC, 16 particles   ----MOC, 5 particles   ········MOC, 1 particle
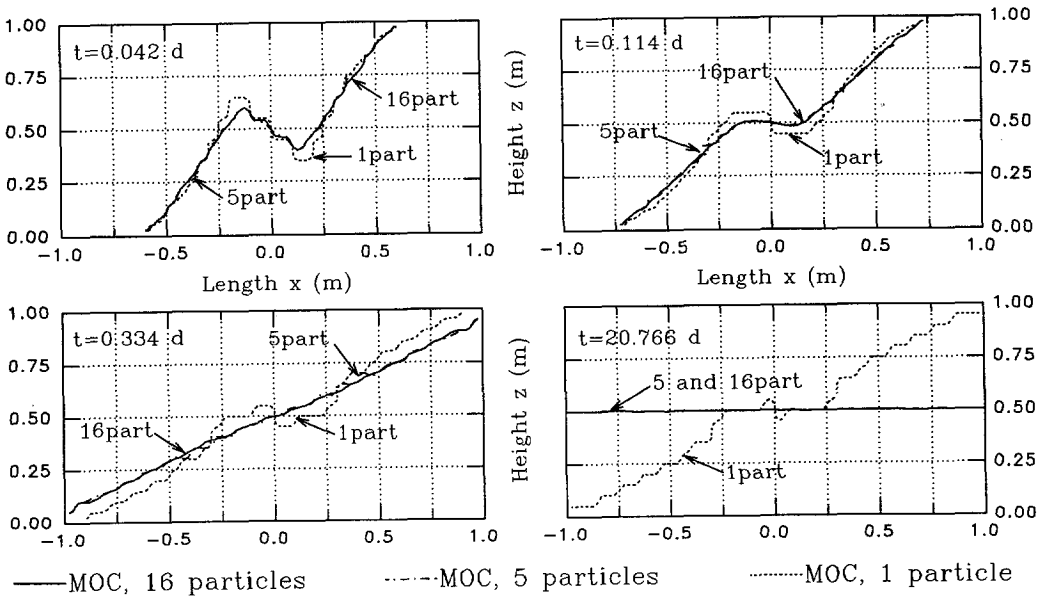
Figure 6.23: Influence of the number of particles in the adapted MOC model on the position of the fresh-salt interface. The moments in time $t=0.042$, $t=0.114$, $t=0.334$ and $t=20.766$ *days* are displayed. The cases with 16, 5 and 1 particles per grid cell are compared with each other.

with 1 particle per grid cell differs completely from the velocity field of the cases with 5 or 16 particles per grid cell as well as of the case with the numerical sharp interface model. Consequently, when the steady state situation is reached, the position of the fresh-salt interface is significantly different for the case with 1 particle per grid cell compared to the cases with 5 or 16 particles per grid cell.

3. Numerical dispersion

Since the dispersivities α_L, α_T are set to zero in the adapted MOC model, all grid cells should have densities equal to either fresh ($1000 \ kg/m^3$) or saline ($1025 \ kg/m^3$) water. Thus, numerical dispersion can be visualized when grid cells with densities between fresh ($1000 \ kg/m^3$) and saline ($1025 \ kg/m^3$) groundwater occur. In the figures 6.24 (800 grid cells) and 6.25 (3200 grid cells) can be seen that grid cells with a density between fresh and saline groundwater are created due to numerical dispersion. Note that the density of groundwater is nowhere smaller than $1000 \ kg/m^3$ or bigger than $1025 \ kg/m^3$, thus no over and undershooting occur. The figures show that the influence of numerical dispersion is limited to at maximum three grid cells in the vicinity of the supposed fresh-salt interface. Therefore, the case with 3200 grid cells has a smaller dispersion zone. Nonetheless, the position of the fresh-salt interface (the $1012.5 \ kg/m^3$-isoline) for both the cases is almost the same (see figure 6.22). Eventually, most of the brackish grid cells will disappear when the fresh-salt interface approaches the steady state situation.

4. Fresh-salt interface in the $2 \cdot 1 \ m^2$ aquifer

Figure 6.26 shows the development of the fresh-salt interface in the $2 \cdot 1 \ m^2$ aquifer. The fresh-salt interface rotates around the point $x=0 \ m$ and $z=0.5 \ m$. As can be seen, the fresh-salt interface rapidly smooths out between about $x=-0.3$ and $x=+0.3$ m. From roughly $t=0.334 \ day$ on, the shape of the fresh-salt interface is nearly a straight line. The difference with the numerical sharp interface model cannot be neglected during the first time steps, for instance at the situation $t=0.042 \ day$ and between $-0.15 \leq x \leq 0.15 \ m$. The main cause of this difference is likely to be the computation of the velocity field; for the adapted MOC model the velocities are computed *at the boundaries of the grid cells*, whereas for the numerical sharp interface model the velocities are computed *at exactly the fresh-salt interface*.

5. Fresh-salt interface in the $6 \cdot 1 \ m^2$ aquifer

The displacement of the fresh-salt interface is also simulated for an aquifer that is three times longer than the aquifer of the reference case, namely with a length of 6 m instead of 2 m (figure 6.27). Initially, the fresh-salt interface has the same shape as in the $2 \cdot 1 \ m^2$ aquifer. Obviously in this aquifer of $6 \cdot 1 \ m^2$, it takes more time until the state of dynamic equilibrium (steady state situation) is reached. Here again,
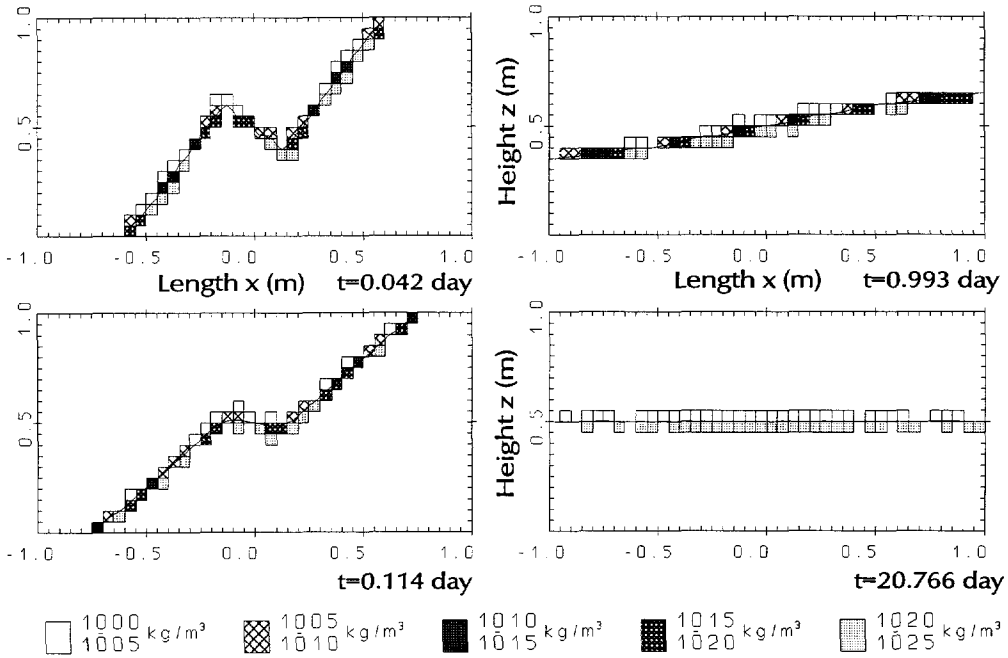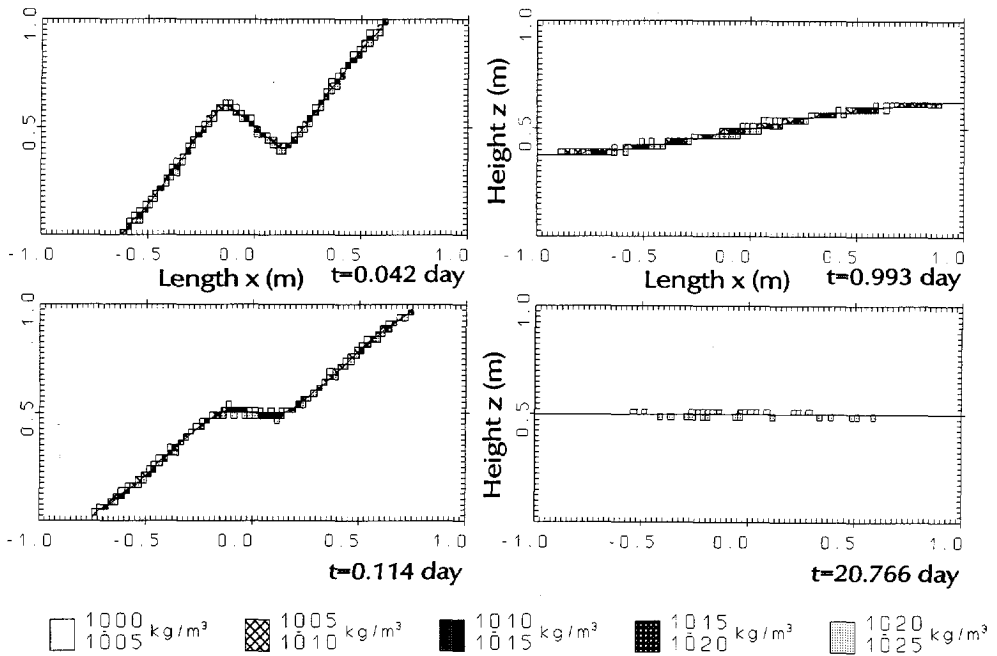
Figure 6.24: Visualization of numerical dispersion at some moments in time for the case with 800 grid cells. The grid cells with densities not equal to those of fresh or saline groundwater are displayed.

the results of the adapted MOC model and the numerical sharp fresh-salt interface model are in good mutual agreement.

6. Velocity distribution

Figure 6.28 shows the velocity distribution of the adapted MOC model in the $2 \cdot 1 \; m^2$ aquifer at the moment in time $t = 0.042 \; day$, $(t_r = 0.14)$. In figure 6.29, the velocity distribution of the numerical sharp interface model of Chan Hong *et al.* is shown. A comparison of these two figures is somewhat difficult, since the velocities are not given at precisely the same points. The adapted MOC model only computes velocities at the boundaries (and centers) of grid cells, whereas the numerical sharp interface model computes velocities at the exact position of the fresh-salt interface. This is an essential difference between the adapted MOC model and the numerical sharp interface model. The difference can be substantial in places where the fresh-salt interface is situated somewhere between the boundaries and the centers of grid cells. In that situation, the velocity *at* the fresh-salt interface is determined in the adapted MOC model by bilinear interpolation of the velocities at adjacent boundaries and centers of grid cells (see figure 5.2 in subsection 5.3.2). Thus, in the adapted MOC

Figure 6.25: Visualization of numerical dispersion at some moments in time for the case with 3200 grid cells. The grid cells with densities not equal to those of fresh or saline groundwater are displayed.

model the velocity at the interface is determined by an averaged value, whereas in the numerical sharp fresh-salt interface model the velocity is determined exactly.

Numerical dispersion generates grid cells with brackish densities, and consequently, the vertical velocity is affected. Therefore, the displacement of the fresh-salt interface in the adapted MOC model differs from the displacement of the fresh-salt interface in the numerical sharp interface model. This difference is significant in the beginning of the simulation, when the velocities are great and alter in direction over short distances (this means within a few grid cells), for instance near the interface between $-\frac{1}{6} \lesssim x \leq +\frac{1}{6}$ m. Nonetheless, the displacement of the fresh-salt interface in the adapted MOC model closely corresponds with the displacement in the numerical sharp interface model (see e.g. figure 6.26). This occurs in particular: (1) in the vicinity of the no-flow boundaries where the velocity does not alter in direction over short distances; and (2) when the fresh-salt interface has become smoother after several hours.

When the fresh-salt interface is moving towards its steady state situation, the velocities in the aquifer are decreasing. This can be seen in figure 6.30 which displays the evolution of the velocity field computed with the adapted MOC model. The
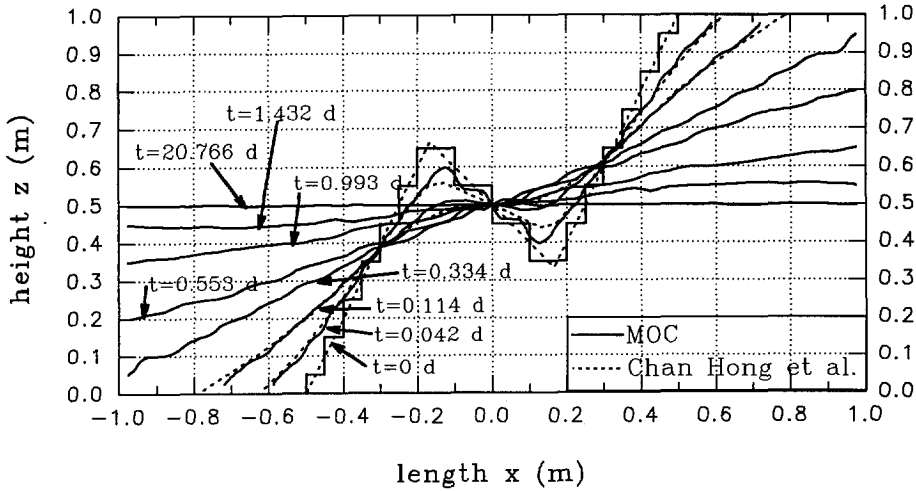
Figure 6.26: Development of the fresh-salt interface, computed with the adapted MOC model for the $2 \cdot 1 \ m^2$ aquifer. The interfaces are given for $t=0$, $t=0.042$, $t=0.114$, $t=0.334$, $t=0.553$, $t=0.993$, $t=1.432$ and $t=20.766$ *days*. Also the interfaces at three moments in time computed with the numerical sharp interface model are given [Chan Hong *et al.*, 1989].
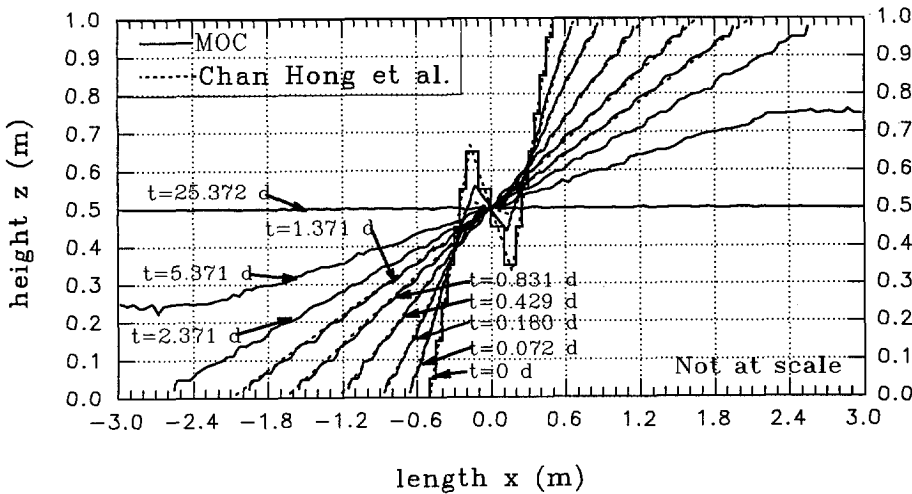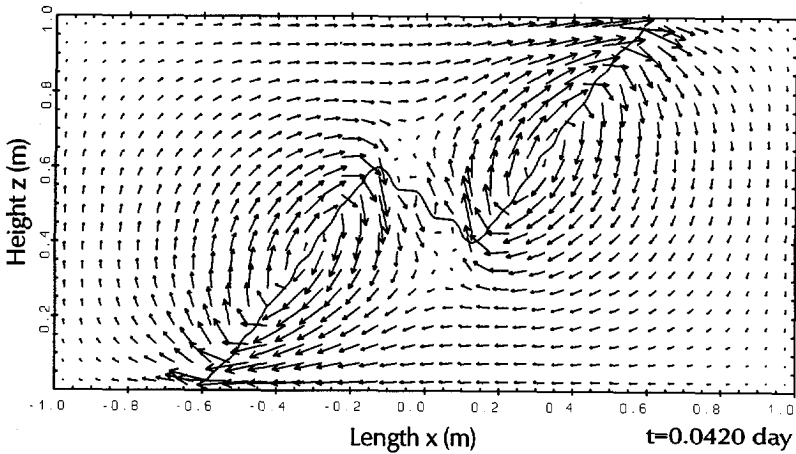

Figure 6.27: Development of the fresh-salt interface for the $6 \cdot 1 \ m^2$ aquifer computed with the adapted MOC model. The interfaces are given for $t=0$, $t=0.072$, $t=0.180$, $t=0.429$, $t=0.831$, $t=1.371$, $t=2.371$, $t=5.371$ and $t=25.372$ *days*. Also the interfaces at six moments in time computed with the numerical sharp interface model are given [Chan Hong *et al.*, 1989].

Figure 6.28: Velocity field computed with the adapted MOC model. This case has 800 grid cells. The moment in time is 0.042 *day*. The lengths of the arrows correspond with the displacement of groundwater during a time step of 1.5 *hour*, beginning at the indicated moment in time.
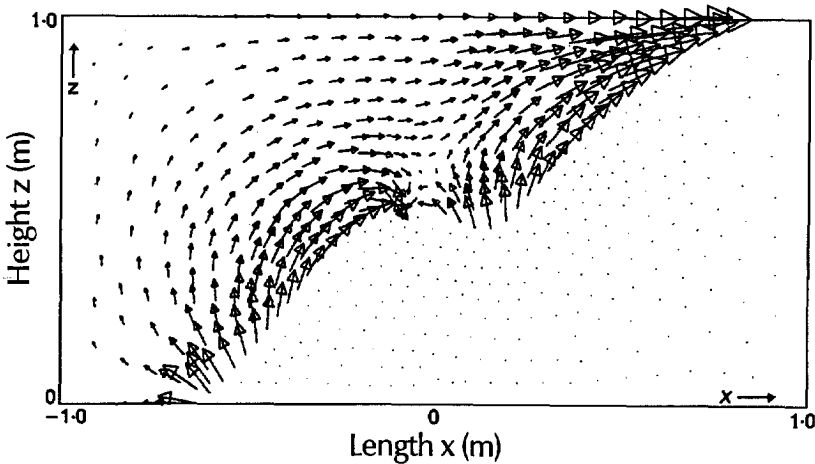
Figure 6.29: Velocity field computed with the numerical sharp interface model for the moment in time $t_r=0.14$, $t=0.042$ *day* [Chan Hong et al., 1989]. Source: *Chan Hong, J.R., Duijn, C.J., van, Hilhorst, D. & Kester, J., van. The interface between fresh and salt groundwater: a numerical study. IMA J. of Applied Mathem., 42: 209-240, p. 232.* Copyright ©1989 Oxford University Press, reprinted by permission of Oxford University Press.

velocities near the sharp interface are greatest at the beginning of the simulation, but they are decreasing during the evolution of the fresh-salt interface. The velocities are very small after a few days, which means that the state of dynamic equilibrium in density distribution is approached.
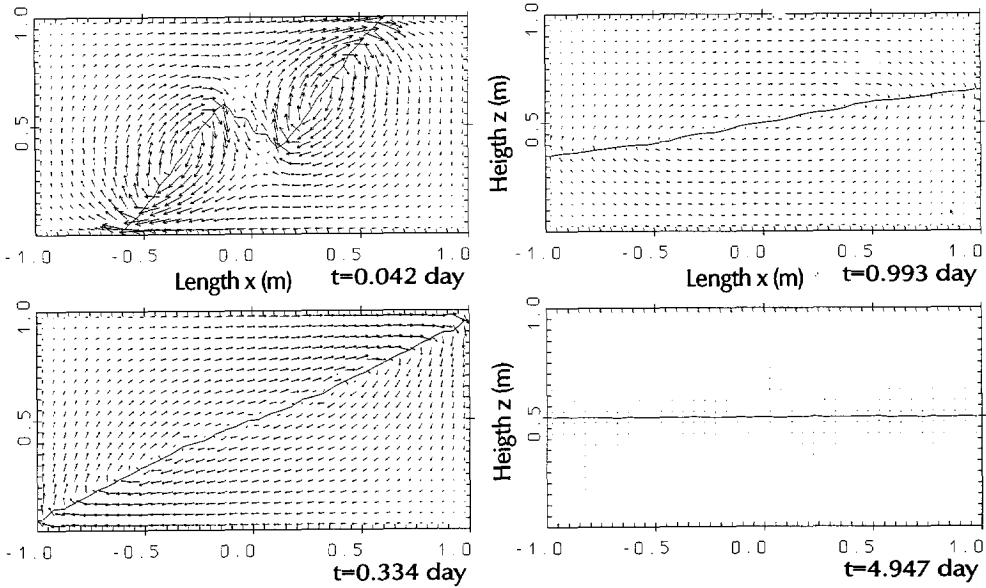
Figure 6.30: Evolution of the velocity field during the displacement of the fresh-salt interface. The moments in time are given for $t=0.042$, $t=0.334$, $t=0.993$ and $t=4.947$ *days*. The lengths of the arrows correspond with the displacement of groundwater during a time step of 1.5 *hour*, beginning at the indicated moment in time.

7. Approaching the state of dynamic equilibrium

Eventually, the state of dynamic equilibrium in density distribution will be approached. An *arbitrary* criterion is defined to follow the evolution of the fresh-salt interface to this state of dynamic equilibrium. The *equilibrium criterion* considers the average distance between the 1012.5 kg/m^3-isoline and the equilibrium position of the interface, with respect to the equilibrium position of the interface:

$$\text{equilibrium criterion } (t) = \frac{\sum_{i=1}^{n} |u_{x,t}^i - u_{x,\infty}|}{n \cdot u_{x,\infty}} \cdot 100 \ (\%) \tag{6.17}$$

where

- n = number of the horizontal grid cells (40 and 120 for respectively the $2 \cdot 1$ m^2 and $6 \cdot 1$ m^2 aquifers) $(-)$,

- $u_{x,t}^i$ = height of the 1012.5 kg/m^3-isoline at grid cell i (L),

- $u_{x,\infty}$ = equilibrium position of the interface: $u_{x,\infty}=0.5$ m for $x \in [-1,1\,m]$ $(2 \cdot 1\ m^2$ aquifer) and for $x \in [-3,3\,m]$ $(6 \cdot 1\ m^2$ aquifer).
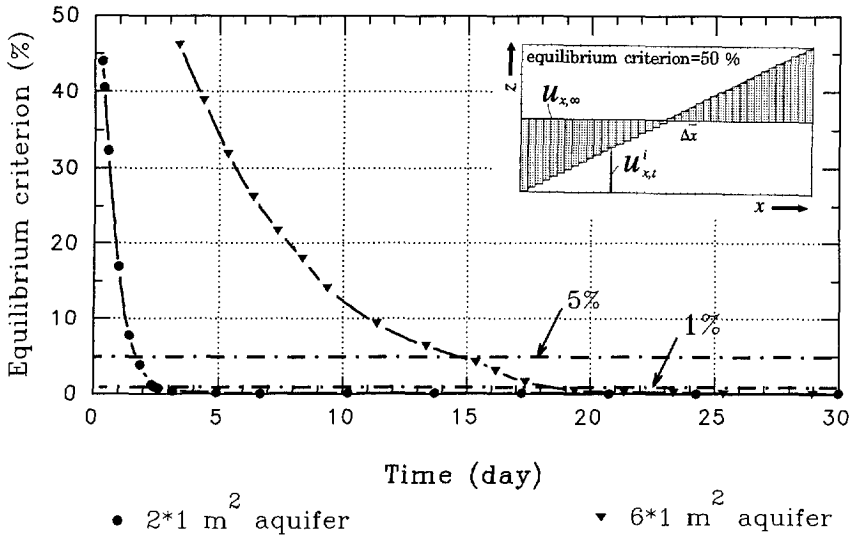
Figure 6.31: Equilibrium criterion which determines the time until the state of dynamic equilibrium is reached. Both aquifers are displayed: the $2 \cdot 1 \ m^2$ and the $6 \cdot 1 \ m^2$ aquifer. For example, the equilibrium criterion equals approximately 50 %, when the fresh-salt interface is located in the vicinity of the points $[-1, 0 \ m]$, $[0, 0.5 \ m]$ and $[1, 1 \ m]$ for the $2 \cdot 1 \ m^2$ aquifer.

The equilibrium criterion as a function of time is shown in figure 6.31. The equilibrium criterion is given from the moment the toe and top of the fresh-salt interface are situated in the vicinity of respectively the bottom left corner and the top right corner of the aquifer. The figure shows that the evolution of the fresh-salt interface to its equilibrium position is slower in the $6 \cdot 1 \ m^2$ aquifer than in the $2 \cdot 1 \ m^2$ aquifer. The time until the equilibrium criterion has a value equal to 5 % differs for both cases: after approximately 1.75 *days* and 14.90 *days* for the $2 \cdot 1 \ m^2$ and $6 \cdot 1 \ m^2$ aquifer respectively. Applying the equilibrium criterion equal to 1 %, the state of dynamic equilibrium in the density distribution of the $2 \cdot 1 \ m^2$ aquifer is reached after some 2.44 *days*, while in the $6 \cdot 1 \ m^2$ aquifer the fresh-salt interface takes some 18.45 *days* to reach the state of dynamic equilibrium.

8. Path lines with travel times

Some path lines with corresponding travel times are shown in figure 6.32 in the $2 \cdot 1$ m^2 aquifer (3200 grid cells). As it takes just a few days to reach the steady state situation, the path lines are simulated during only 3.5 *days*. In order to construct path lines, a number of groundwater particles are tracked during the simulation with the adapted MOC model (see section 5.6).

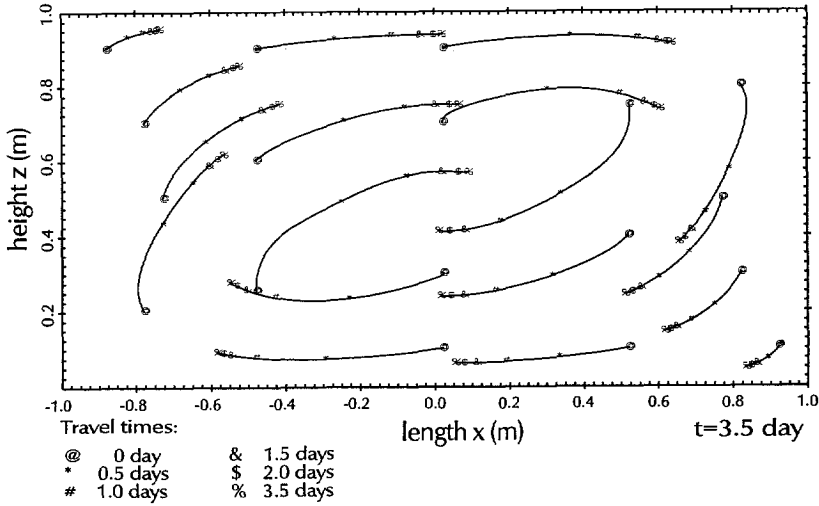Figure 6.33 shows several path lines in the $6 \cdot 1 \ m^2$ aquifer. At the beginning,

Figure 6.32: Some path lines with travel times through the $2 \cdot 1\ m^2$ aquifer (3200 grid cells) during the simulation of 3.5 *days*, computed with the adapted MOC model.
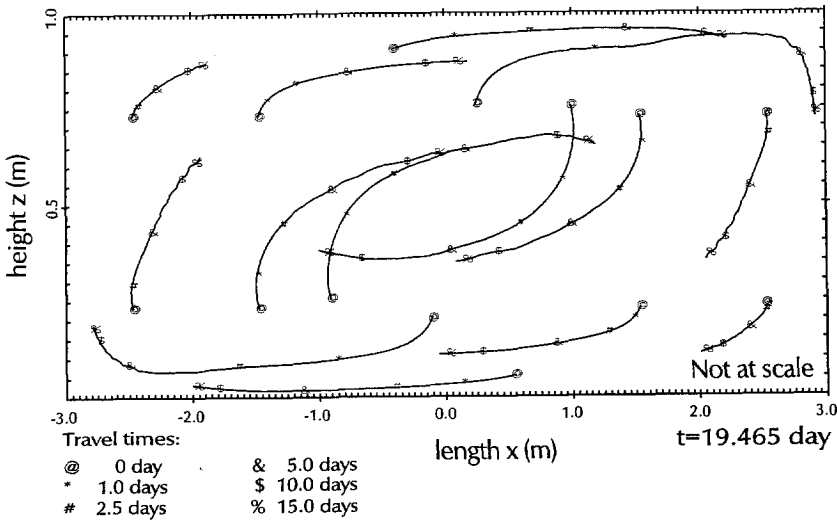

Figure 6.33: Some path lines with travel times through the $6 \cdot 1\ m^2$ aquifer during the simulation of 19.47 *days*, computed with the adapted MOC model. The vertical dimension is blown up with a factor three.

the displacement of groundwater is the greatest in the vicinity of the sharp fresh-salt interface. After some days, the fresh-salt interface approaches the boundaries, and subsequently, groundwater in the vicinity of the left and right no-flow boundaries will displace faster than at the beginning of the simulation.

6.4.3   Conclusions

The adapted MOC model is able to simulate a sharp fresh-salt interface of the geometry as chosen in this section. The results of the adapted MOC model are in good agreement with the results of the numerical sharp interface model of Chan Hong *et al.* [1989], except at places where the velocities alter in direction between adjacent grid cells.

Increasing the number of grid cells from 800 to 3200 grid cells does not significantly improve the accuracy of the displacement of the fresh-salt interface. The number of particles in a grid cell does not significantly affect the displacement of the fresh-salt interface, as long as the number of particles in a grid cell is more than 1. The adapted MOC model sometimes creates grid cells near the fresh-salt interface with densities between fresh (1000 kg/m^3) and saline (1025 kg/m^3) groundwater, which is the result of numerical dispersion. These brackish grid cells only occur in the close vicinity of the fresh-salt interface.

Chapter 7

Parameter analysis in a selected profile

7.1   Introduction

The main objective of this chapter is to analyse the influence of subsoil and model parameters applied in the adapted MOC model on the simulation of groundwater flow and solute transport in a profile in the southern part of Noord-Holland.

In section 7.2, the situation in the profile concerning phreatic groundwater levels and the deep groundwater extractions during the period 1853-1988 is described. In section 7.3, the schematised geohydrologic system is presented, and subsoil and model parameters applied in the simulation of the profile are given. In section 7.4, five approaches to calibrate the geohydrologic system are discussed. In section 7.5, the influence of several subsoil parameters is analysed, and in section 7.6, a model parameter analysis is executed. In section 7.7, the results of the simulated geohydrologic system (without sea level rise) are given. Finally, in section 7.8, some conclusions are drawn.

7.2   Present situation

The profile, simulated in this section, is located perpendicular to the Dutch coastline through the sand-dune area of Gemeentewaterleidingen Amsterdam, the Rijnland polders with its bulb fields up to halfway the Haarlemmermeer polder. The length of the profile equals 12,500 m perpendicular to the North Sea coastline. Figure 7.1 shows the map of the studied area. This area is selected because it has some representative characteristics of most of the groundwater flow regimes in the provinces of Noord and Zuid-Holland: namely a thick freshwater lens is present in the sand-dune area and a relatively strong seepage occurs in the low-lying polder area situated some kilometres inland.

The study of Kooiman [1989] is pursued in this research. His results constitute the basis for the present research. He simulated, among others, the development of the freshwater lens in the sand-dune area of Gemeentewaterleidingen Amsterdam from the end of 1853 till the end of 1987. Furthermore, he estimated effects of human interventions, such as the reclamation of the Haarlemmermeer, groundwater extractions for water supply, artificial recharge and deep-well infiltration.
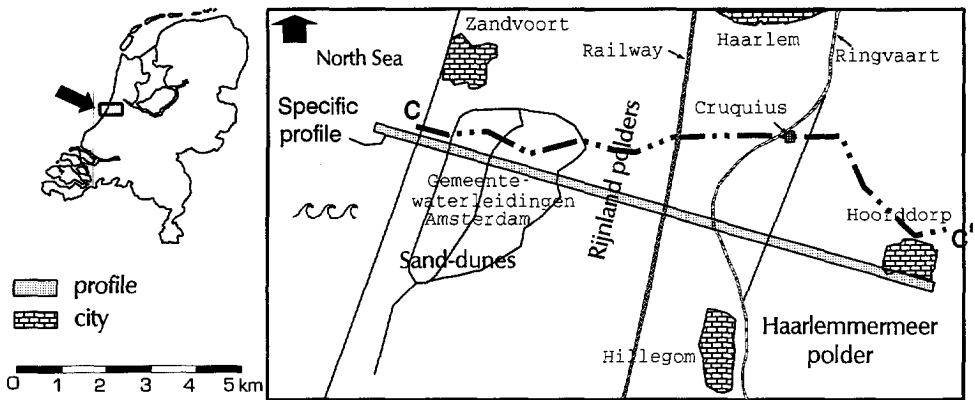
Figure 7.1: Map with the sand-dune area of Gemeentewaterleidingen Amsterdam, the Rijnland polders and the Haarlemmermeer polder. The profile $C - C'$ is from Stuyfzand [1988].

The sand-dune area of Gemeentewaterleidingen Amsterdam[1] has a surface of roughly $36 \cdot 10^6$ m^2: an average length of 9000 m parallel to the coastline and an average width of 4000 m perpendicular to the coastline. At present, the phreatic groundwater levels in the sand-dune area fluctuate around constant mean levels. The maximum differences in local phreatic groundwater levels due to seasonal effects and extraction rates appear to be small (in order of magnitude of decimetres), mainly because numerous infiltration gullies, drains and canals control the area. The Rijnland polders are situated more inland. The phreatic groundwater levels in this area, where horticulture (bulb cultivation) is practiced, are controlled at less than 1.0 m below $N.A.P.$ (-0.6 to -1.0 m $N.A.P.$[2]). More inland the low-lying Haarlemmermeer polder is situated. The lake Haarlemmermeer was reclaimed during the years 1840-1852 [Schultz, 1992]. The polder is separated from the Rijnland polders by the canal De Ringvaart. It has a controlled phreatic groundwater level that varies between -4.5 and -6.0 m $N.A.P.$

The evolution to the present situation in terms of the salinisation process is as follows. During many centuries, natural groundwater recharge has built up a freshwater lens in this geohydrologic system. Before the middle of the nineteenth century, the situation of the freshwater lens was supposed to be stationary [Venhuizen, 1971]. From the moment the lake Haarlemmermeer was reclaimed[3], a severe salt water in-

---

[1] Gemeentewaterleidingen Amsterdam is one of the greatest water supply company in the Netherlands.

[2] $N.A.P.$ stands for Normaal Amsterdams Peil and is the reference level in the Netherlands. $N.A.P.$ roughly equals Mean Sea Level.

[3] In this chapter, 1854 AD is taken as the moment the reclamation of the lake Haarlemmermeer was completed.
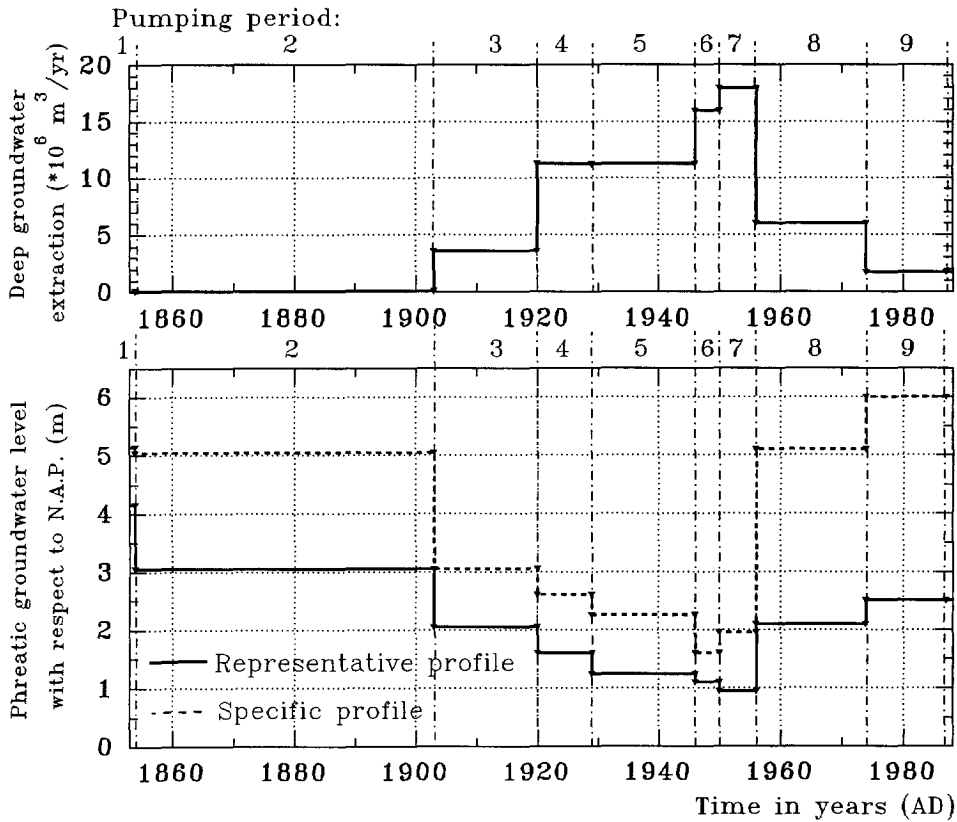
Figure 7.2: Deep groundwater extractions and phreatic groundwater levels in the sand-dune area of Gemeentewaterleidingen Amsterdam during the period 1854-1987. The whole period is subdivided in nine specific pumping periods. During each pumping period, the adapted MOC model simulates constant extraction rates and constant phreatic groundwater levels. The phreatic groundwater levels are given of the representative profile [after Kooiman, 1989] as well as of the specific profile (see section 7.3).

trusion has occurred from the sea. Meanwhile, Gemeentewaterleidingen Amsterdam had started the extraction of raw water from the sand-dune area [Schuurmans, 1983]. During the 49 years that followed (1854-1902), groundwater was withdrawn from the phreatic aquifer only. From 1903 on, shortage of drinking water made it necessary to extract also groundwater from the deeper semi-confined aquifer (figure 7.2). The extraction of groundwater by deep-wells increased from a few million m^3/yr to nearly 18 million m^3/yr during the period 1951-1956. The once 'sharp' salt-fresh interface in the sand-dune area moved upward and transformed into a brackish transition

zone. To counteract these negative consequences, Gemeentewaterleidingen Amsterdam started in 1957 with the injection of riverwater (Rijn water) at the surface, while the deep groundwater extractions were reduced to some 6 million m^3/yr. Until 1974, the situation of the freshwater lens did not change significantly. From 1974 on, the deep groundwater extraction was diminished to an average of some 1.75 million m^3/yr. During the past two decades, the effect of injection of fresh surface water in the aquifers (called *deep-well infiltration*) has been studied [e.g. Schuurmans and van den Akker, 1981; Kooiman *et al.*, 1984; Kooiman and Uffink, 1986]. Artificial recharge has increased the volume of the freshwater lens and has counteracted the salinisation process underneath the sand-dunes and towards the polders to some extent.

7.3 Schematisation

The reference case comprises the simulation of the profile from the reclamation of the lake Haarlemmermeer till the situation at the beginning of 1988. The sand-dune area of Gemeentewaterleidingen Amsterdam has been investigated intensively during at least the past century. These investigations have yielded sufficient data about the composition of the subsoil and the piezometric levels. Nevertheless, the values of some subsoil parameters are still inaccurate, such as the hydraulic conductivities of the aquifers, the hydraulic resistances and the exact position of the aquitards; the effective porosity; and the hydrodynamic dispersion. Since a two-dimensional profile is applied, the simulation always differs from the actual situation on-site. Therefore, two different profiles, namely *a representative profile* and *a specific profile* , are simulated in order to assess the effect of different values of the hydraulic resistances of the Holocene aquitard and the phreatic groundwater levels on the final solution.

   The data of the geohydrological schematisation of the area have been borrowed from the following sources:

- an article of Venhuizen [1971], presenting some data on groundwater flow masses through the studied area,

- the ICW report **Regionale Studies 9** [1976], displaying several important subsoil parameters of the central western part of the Netherlands,

- the **Grondwaterkaart van Nederland, Zandvoort en Amsterdam**, from the TNO Institute of Applied Geoscience [1979a], representing the position and composition of the geohydrologic system,

- an article of Schuurmans [1983], giving water balances of the sand-dune area of Gemeentewaterleidingen Amsterdam,

- a detailed report of Stuyfzand [1988], extensively describing the geohydrologic situation of the coastal area between Noordwijk aan Zee and Zandvoort,
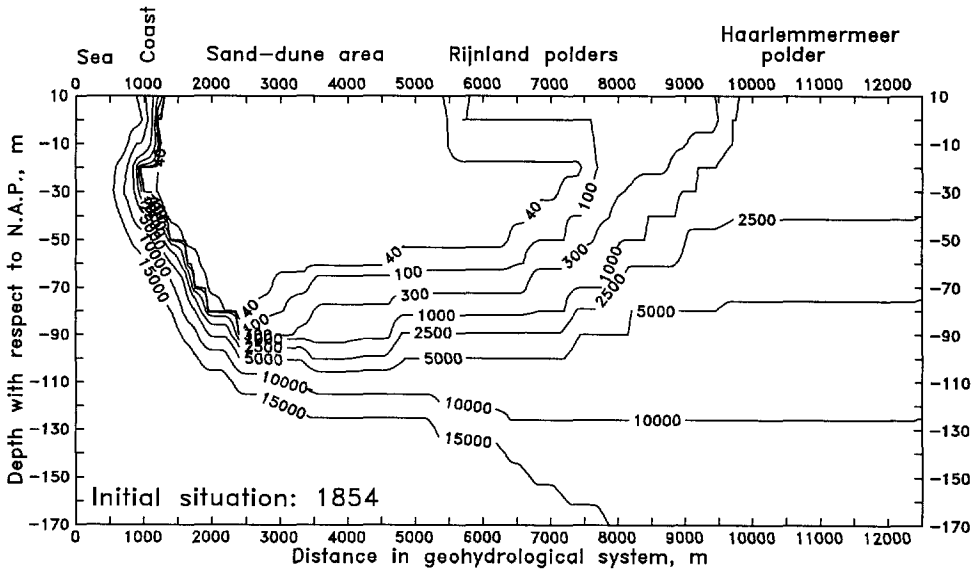
Figure 7.3: Initial chloride distribution (values in $mg\ Cl^-/l$) in 1854 [Kooiman, 1989].

- an article of Kooiman [1989], describing the representative profile applied in this case study.

In this section, relevant subsoil parameters of both the representative profile and the specific profile are given. The model parameters applied in the reference case are summarized below.

Subsoil parameters in the reference case

The anisotropy factor k_z/k_x (the ratio vertical and horizontal hydraulic conductivity) is 0.1 ($-$) and the effective porosity n_e is 0.35 ($-$). The longitudinal dispersivity α_L is equal to 0.02 m, see also Kooiman [1989], while the ratio transversal to longitudinal dispersivity α_T/α_L is 0.1 ($-$). The specific storativity S_s (L^{-1}) is set to zero. In figure 7.3, the initial chloride distribution is given at the beginning of 1854, as it is proposed by Kooiman [1989].

The geometries of the two profiles are discussed below:

a. Representative profile

Figure 7.4 shows the subsoil parameters of the representative profile that are applied by Kooiman [1989]. The subsoil parameters and the phreatic groundwater levels are averaged over an area of some 9000 m parallel to the coastline. The width of the sand-dune area is 4000 m (from 1500 to 5500 m).
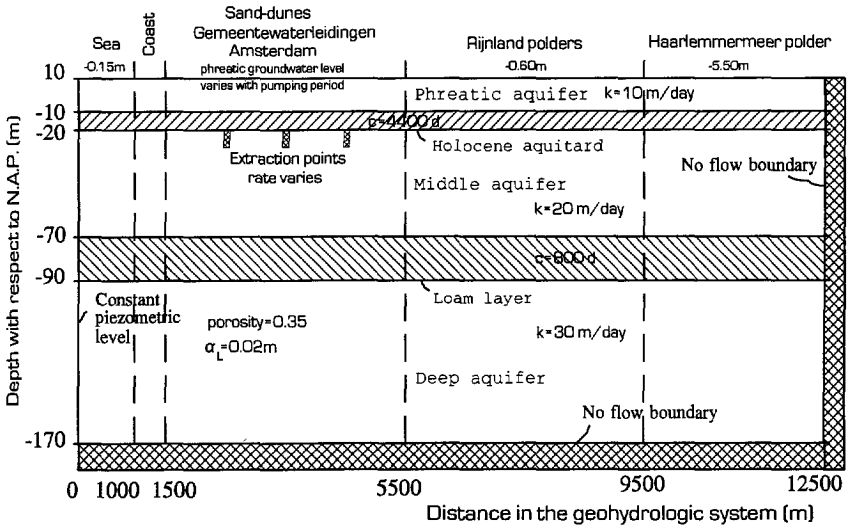
Figure 7.4: Subsoil parameters in the representative profile through the sand-dune area of Gemeentewaterleidingen Amsterdam and the polders lying inland.
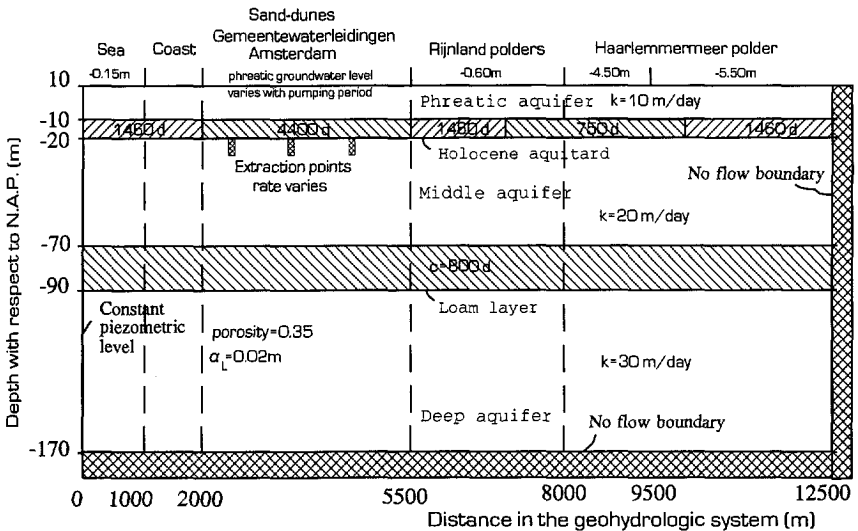

Figure 7.5: Subsoil parameters in the specific profile through the sand-dune area of Gemeentewaterleidingen Amsterdam and the polders lying inland.

b. Specific profile

Figure 7.5 shows the subsoil parameters of the specific profile. The (measured) subsoil parameters and phreatic groundwater levels best match a *particular*

profile perpendicular to the coastline, which exact position is given in figure 7.1. In this profile, local discontinuities in the Holocene aquitard are considered. The width of the sand-dune area is 3500 m (from 2000 to 5500 m).

As can be seen by comparing the figures 7.4 and 7.5, the value of the hydraulic resistance of the Holocene aquitard in both profiles differs. In reality, the hydraulic resistance in the Haarlemmermeer polder near the Cruquius pumping station is very low. As the hydraulic resistance in the representative profile is averaged over a length of 9000 m parallel to the coastline, a relatively high value of 4400 $days$[4] was found. This is in contrast with the hydraulic resistance of the Holocene aquitard in the specific profile, which equals a low value of only 750 $days$. The phreatic groundwater level at the upper boundary in the sand-dune area differs for both profiles during the nine pumping periods (see figure 7.2).

Model parameters in the reference case

The initial number of grid cells is 4500: 250 in horizontal direction and 18 in vertical direction. This means that a grid cell has a length Δx of 50 m and a height Δz of 10 m. Each grid cell has five particles. The flow time step is set to 1 $year$. The convergence criterion TOL, which represents the difference in freshwater head between two iterations, is set to 10^{-5} ft. The maximum relative distance ζ in a grid cell in which a particle is allowed to move during one solute time step is set to 0.5.

It appears that in the reference case with the given initial condition 42 solute time steps are required to simulate solute transport during a flow time step of 1 $year$. The main reason why so many solute time steps are necessary is that the velocity between some adjacent grid cells is relatively great due to a great difference in piezometric level. From equation 5.71 it can be deduced that in that case the solute time step should be small. Such a situation occurs at the boundary between the Rijnland polders and the Haarlemmermeer polder, where the piezometric level in the top row of grid cells changes very abruptly from -0.6 m to -5.5 m $N.A.P.$ respectively (see figure 7.4).

7.4   Calibration

The calibration of the groundwater flow model (or *history matching*) is executed in five approaches:

1. Chloride distribution of some years in the past

The calibration of the chloride distribution for this profile was done by Kooiman [1989]. He did this as follows:

---

[4]This value of the hydraulic resistance is derived from Schuurmans [1983], who calculated water balances for the phreatic aquifer and the deep aquifer in the sand-dune area of Gemeentewaterleidingen Amsterdam.

> *"The initial chloride distribution in 1854 was not known and had to be estimated. Starting with this estimated situation the chloride profiles of 1904 and 1974 are calculated and compared with existing profiles in a certain cross-section (...) of these years [Schuurmans, 1974]. By 'trial and error' the initial situation (...) was found, with the use of the calibration graphs (...). The differences, especially in 1974, are due to the fact that the real profiles are not completely 'representative': firstly because the supposed distribution to the three extraction points of the deep extraction differs from the real distribution, and secondly the map of 1974 does not exactly show the results of upconing."*

> [Kooiman, 1989]

2. Piezometric levels at two depths with respect to N.A.P.

The freshwater heads calculated with the adapted MOC model are compared with measured piezometric levels, given by Stuyfzand [1988], at: (a) -30 m ± 5 m N.A.P. and (b) -100 m ± 30 m N.A.P.

ad a. Figure 7.6 shows the piezometric levels, expressed in freshwater[5], at -30 m ± 5 m N.A.P. They are calculated with the adapted MOC model for both the representative and the specific profile[6] and measured by Stuyfzand [1988] for the specific profile. The reference level at -30 m ± 5 m N.A.P. is situated in the (middle) aquifer system underneath the Holocene aquitard. The measured piezometric levels have been converted to piezometric levels expressed in freshwater by correcting them in vertical direction for deviation of the groundwater density in an observation well from the standard density ρ_f=1000 kg/m^3.

In general, the calculated piezometric levels at -30 m ± 5 m N.A.P. of the specific profile under the Haarlemmermeer polder differ only some decimetres from the measured piezometric levels. By contrast, the calculated piezometric levels of the representative profile are higher, especially in the Rijnland polders and the Haarlemmermeer polder. The reason is that the subsoil parameters in the representative profile are averaged over the entire width of the area: 9000 m along the coast of the sand-dune area of Gemeentewaterleidingen Amsterdam.

ad b. Figure 7.7 shows the piezometric levels, expressed in *saltwater*[7], at -100 m ± 30 m N.A.P. They are calculated with the adapted MOC model for both profiles

---

[5] The adapted MOC model calculates freshwater heads which are in fact *fictive* piezometric levels. This means that in each grid cell the piezometric level is converted to a freshwater head with a standard reference density ρ_f of 1000 kg/m^3. This procedure is described in subsection 5.4.4.

[6] The exact position of the specific profile is displayed in figure 7.1.

[7] The freshwater heads, calculated with the adapted MOC model, are converted to piezometric levels expressed in saltwater in order to enable comparison of the calculated values with the measurements of Stuyfzand [1988]. The piezometric level expressed in saltwater has a reference chloride concentration of 16,500 mg Cl^-/l.
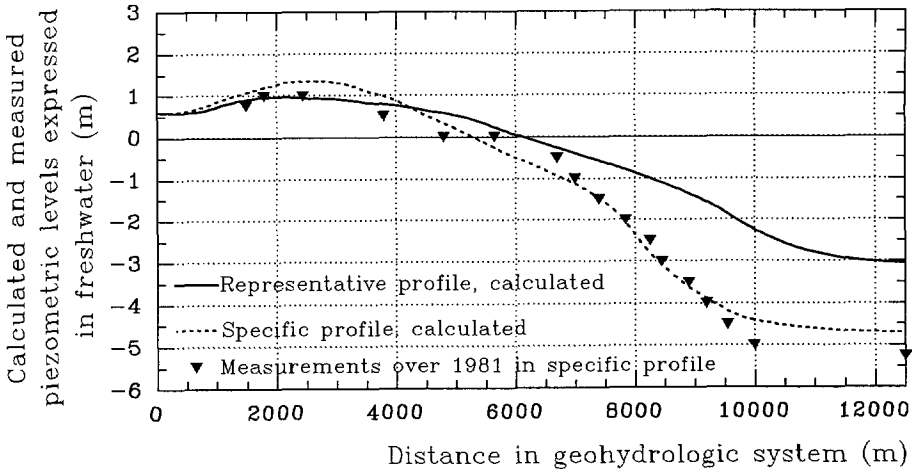
Figure 7.6: Piezometric levels, at -30 m ± 5 m N.A.P., expressed in freshwater. The levels, calculated with the adapted MOC model for both the representative profile and the specific profile, are compared with the levels, measured by Stuyfzand [1988] and averaged over 1981 for the specific profile.
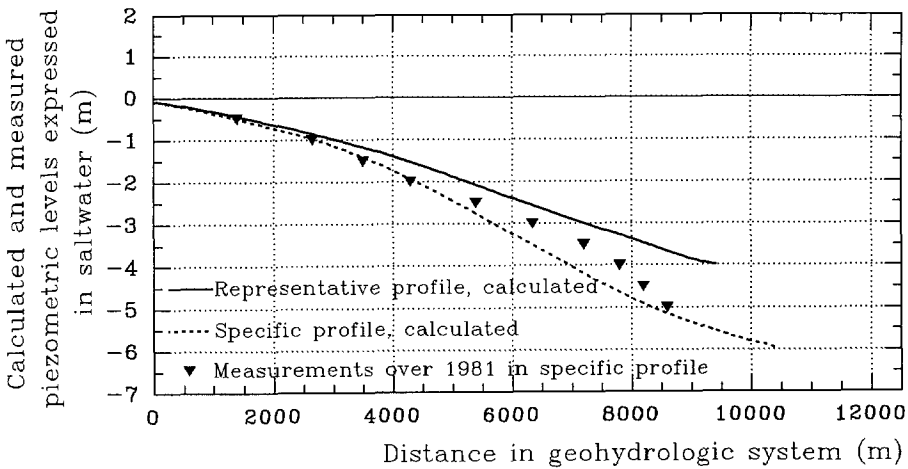

Figure 7.7: Piezometric levels, at -100 m ± 30 m N.A.P., expressed in saltwater. Only points with chloride concentrations higher than 15,000 mg Cl^-/l are shown. The levels, calculated with the adapted MOC model for both the representative profile and the specific profile, are compared with the levels, measured by Stuyfzand [1988] and averaged over 1981 for the specific profile.
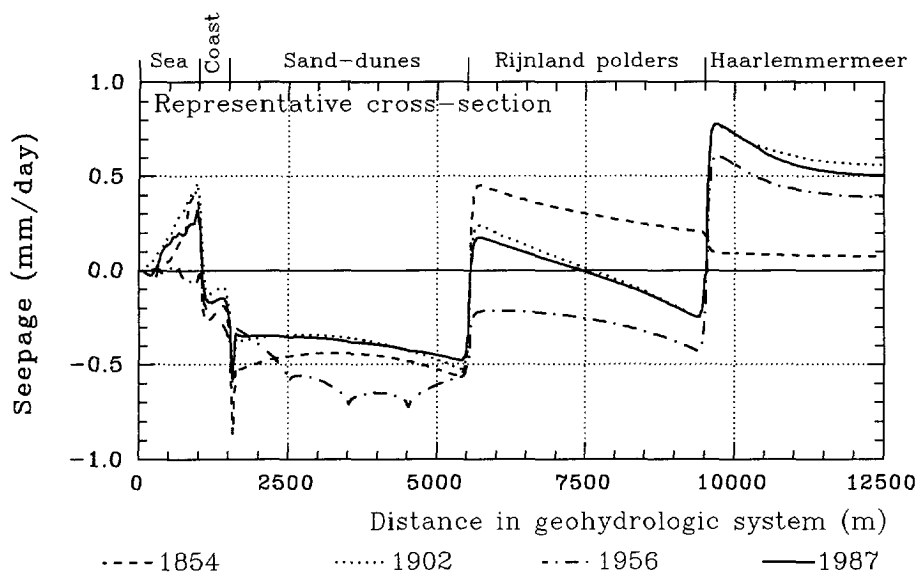
Figure 7.8: Calculated seepage and infiltration intensities through the Holocene aquitard at -20 m $N.A.P.$ of the representative profile at specific moments in time.

and measured by Stuyfzand [1988] for the specific profile. Stuyfzand only observed measurements at locations where the chloride concentrations are higher than 15,000 mg Cl^-/l. As no chloride concentrations higher than 15,000 mg Cl^-/l are calculated further inland than 9500 and 10,500 m for the representative and the specific profile respectively, the calculated piezometric levels in figure 7.7 are only given up to 9500 and 10,500 m inland respectively.

The measured piezometric levels correspond better with the calculated levels of the specific profile than with those of the representative profile, except at the location of the Rijnland polders.

3. Seepage through the Holocene aquitard in the Haarlemmermeer polder

Figure 7.8 shows the seepage and infiltration intensities through the Holocene aquitard at -20 m $N.A.P.$ of the representative profile, calculated with the adapted MOC model, at several moments in time. The figure shows that during periods with high extraction rates from the middle aquifer (e.g. 1951-1956), the infiltration through the Holocene aquitard is high in the vicinity of the lines of extraction wells. At the same moment, the seepage intensity in the Haarlemmermeer polder is lower than during periods with low extraction rates from the middle aquifer (e.g. 1975-1987), as a high extraction rate from the middle aquifer diminishes the seepage intensity in the Haarlemmermeer polder. It appears that the calculated seepage intensities in the
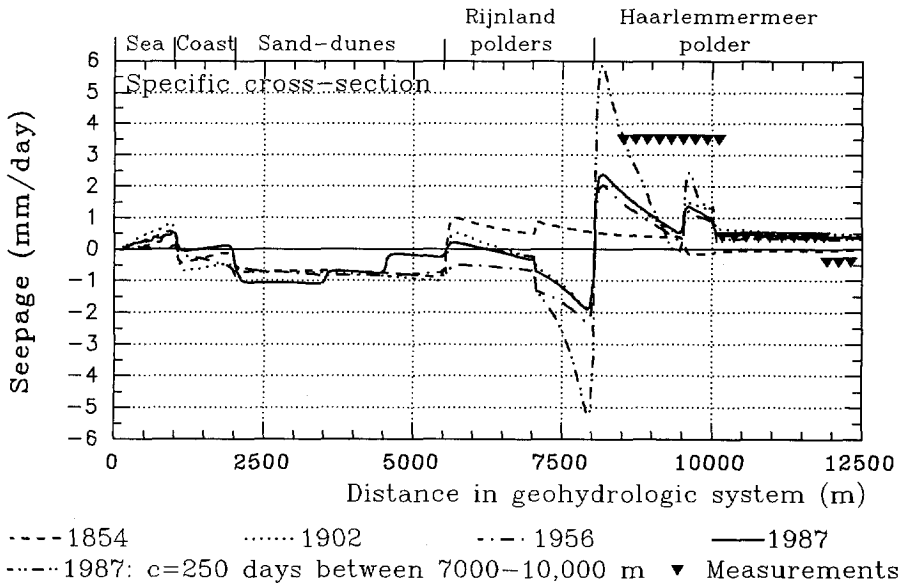
Figure 7.9: Calculated and measured seepage and infiltration intensities through the Holocene aquitard of the specific profile at several moments in time. The measurements in the Haarlemmermeer polder (1971) are averaged over specific subareas [Wit, 1974; ICW, 1976]. In addition, the intensities at the end of 1987 are given for a simulation with the hydraulic resistance in the reach 7000-10,000 m equal to 250 $days$ instead of 750 $days$.

Haarlemmermeer polder are substantially lower than the measurements in a small subarea situated next to the Rijnland polders [Wit, 1974]. The reason for this is that the representative profile does not include the local discontinuities in the Holocene aquitard near the Cruquius pumping station.

To overcome this discrepancy between reality and simulation, the specific profile has been simulated with a low hydraulic resistance of the Holocene aquitard of the subarea near the Rijnland polders and the Haarlemmermeer polder, namely the hydraulic resistance is 750 $days$ in the reach 7000-10,000 m (compare figure 7.4 with figure 7.5). Figure 7.9 shows the seepage and infiltration intensities of the specific profile, calculated with the adapted MOC model. Scarce comparative material is given by Wit [1974]. He calculated the magnitude of averaged seepage and infiltration intensities in the Haarlemmermeer polder by means of water balances for specific *subareas*. The calculations for the Haarlemmermeer polder correspond slightly better with the measurements of Wit.

It appears that the value of 750 $days$ for the hydraulic resistance of the Holocene aquitard in the specific profile is still too high. The hydraulic resistance of the Holocene aquitard in this area should lie in the reach 0-250 $days$ [Wit, 1974; ICW,

1976]. Hence, a simulation is made for the specific profile with a hydraulic resistance of 250 *days* in the reach 7000-10,000 *m*. The seepage and infiltration intensities in 1987 are given in figure 7.9. Though the calculated seepage intensity in the Haarlemmermeer polder (the reach 8000-10,000 *m*) is strong, the differences in seepage intensity between reality and simulation are still substantial. It is obvious that the value of the hydraulic resistance of the Holocene aquitard directly affects the seepage intensities in the Haarlemmermeer polder.

4. Deep groundwater percolation through the Holocene aquitard in the sand-dune area

In the sand-dune area, water from the surface[8] infiltrates in the phreatic aquifer as groundwater recharge. Part of the infiltrated water flows off through the upper aquifer and another part percolates through the Holocene aquitard, as the groundwater level in the phreatic aquifer is higher than the piezometric level in the middle aquifer. The latter part is called the *deep groundwater percolation*.

The deep groundwater percolation intensities in the sand-dune area of Gemeentewaterleidingen Amsterdam are determined by calculating the vertical flow through the Holocene aquitard with the adapted MOC model for all nine pumping periods (see table 7.1). The adapted MOC model simulates three different profiles: (1) the representative profile ('repre.'); (2) the specific profile ('spec.'); and (3) the so-called *percolation profile* ('perco.'). The profiles (1) and (2) have constant phreatic groundwater levels, whereas the percolation profile is defined as follows: it equals the representative profile but groundwater recharge into the phreatic aquifer of the sand-dune area is at a constant rate of 360 mm/yr[9]. This recharge into the phreatic aquifer includes three groundwater fluxes: the natural groundwater recharge, the artificial recharge of fresh surface water as well as the groundwater extraction from the phreatic aquifer.

The table shows that the deep groundwater percolation intensities through the Holocene aquitard of the representative profile correspond for several pumping periods with the values of Schuurmans. In the specific profile, the deep groundwater percolation intensity through the Holocene aquitard is the highest of the three simulated cases. The reason is that this profile is situated in the central part of the sand-dune area of Gemeentewaterleidingen Amsterdam where the phreatic groundwater level is the highest.

5. Inland boundary condition

The calculations of the reference case with a no-flow boundary (or a Neumann condition) at $x=12,500$ m from the seaside are compared with the actual situation in the geohydrologic system. Two maps of isohypses with piezometric levels at -25 and -80

---

[8]The sources of the surface water are natural (e.g. precipitation) as well as artificial (e.g. Rijn water by means of infiltration ponds).

[9]The groundwater recharge equals 12.96 million m^3/yr for the sand-dune area of Gemeentewaterleidingen Amsterdam of 9000 m by 4000 m.

Table 7.1: Deep groundwater percolation intensities through the Holocene aquitard in the sand-dune area in million m^3/yr for three cases, calculated with the adapted MOC model and compared with figures of water balances, estimated by Venhuizen [1971] and by Schuurmans [1983].

Period (years)	Duration (years)	Pumping period	adapted MOC model			Schuurmans [1983][2]	Venhuizen [1971][3]
			repre.	spec.[1]	perco.		
..-1853	–	1	6.3	8.5	5.7	6.4	7
1854-1902	49	2	5.2	9.9	6.0	5.9	8
1903-1920	18	3	4.5	7.0	6.3	4.9	7
1921-1929	9	4	6.2	8.7	7.6	4.9	7
1930-1946	17	5	5.7	8.1	7.5	5.4	7
1947-1950	4	6	7.1	8.5	8.3	6.0	7
1951-1956	6	7	7.5	9.5	8.7	6.0	7
1957-1974	18	8	5.8	11.5	7.0	6.8	8
1975-1987	13	9	5.2	8.0	6.3	7.1	–

[1]: a strip of 3500 m perpendicular to the coastline is considered: from x=2000 to 5500 m.
[2]: the geometry of Schuurmans' study equals the dimensions of the representative profile, namely 9000 m. The hydraulic resistance of the Holocene aquitard equals 4400 $days$.
[3]: the length of the sand-dune area of Gemeentewaterleidingen Amsterdam parallel to the coast is 8000 m instead of 9000 m.

m N.A.P. are considered. The observed values are corrected for density differences [ICW, 1976; Wit, 1974].

On the map at -25 m N.A.P. (figure 7.10), a waterdivide is situated in the center of the Haarlemmermeer polder near Hoofddorp. Surface water recharges into the geohydrologic system in the Westeinder plassen[10] and flows as groundwater into the direction of the waterdivide. Although on the map at -80 m N.A.P. (figure 7.11) a waterdivide is situated in the vicinity of the Groot-Mijdrecht polder (which is located some 30,000 m from the coast), the actual (flow) situation in the middle aquifer is best simulated with a no-flow boundary at x=12,500 m. Moreover, this boundary condition is also chosen for reasons of practicability, that is to limit the calculation time of the computer. Note that Kooiman [1989] also imposed a no-flow boundary at x=12,500 m.

However, when the impact of a substantial sea level rise on the geohydrologic system during the next centuries is assessed, the (fixed) inland boundary at x=12,500 m is located too close to the seaside. Then, the inland boundary should be located further inland. For instance, in section 8.2, the geohydrologic system is schematised with the inland boundary at x=39,000 m from the seaside.

---

[10]The Westeinder plassen have a relatively high open water level of about -0.6 m N.A.P.
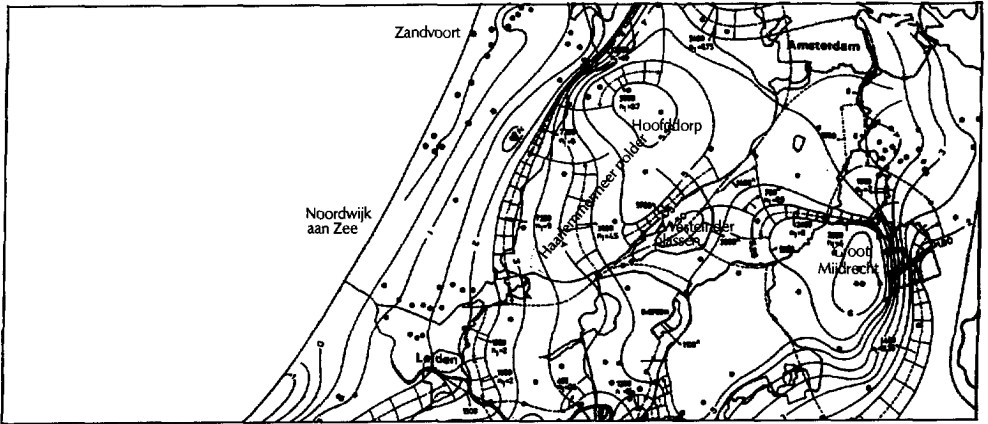
Figure 7.10: Map of isohypses at -25 m with respect to $N.A.P.$, averaged over 1971. Levels are with respect to $N.A.P.$ [after Wit, 1974]. By courtesy of Wit.
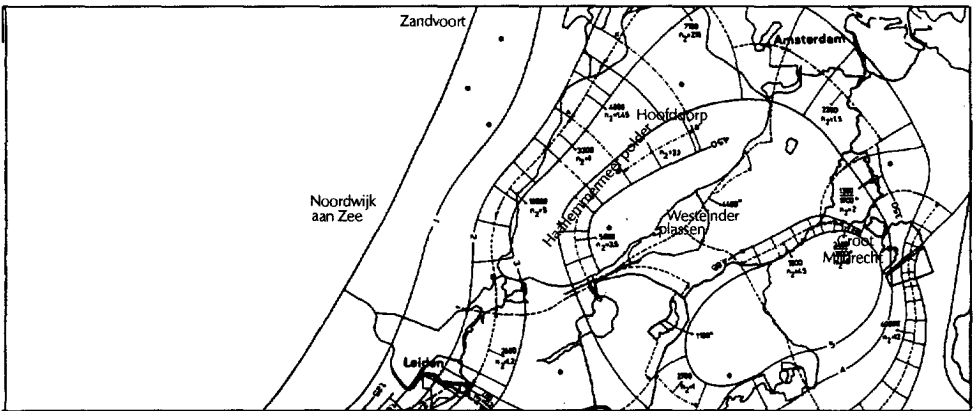

Figure 7.11: Map of isohypses at -80 m with respect to $N.A.P.$, averaged over 1971. Levels are with respect to $N.A.P.$ [after Wit, 1974]. By courtesy of Wit.

7.5   Influence of subsoil parameters

The influence of the following four subsoil parameters are analysed: (1) the specific storativity S_s; (2) the longitudinal dispersivity α_L; (3) the presence of the loam aquitard between -70 and -90 m $N.A.P.$; and (4) the groundwater recharge.

1. Specific storativity S_s

Figure 7.12 shows that the new state of dynamic equilibrium is reached within a time lag of several tens of days for all three realistic specific storativities S_s in the sand-

dune area of Gemeentewaterleidingen Amsterdam from $0.5 \cdot 10^{-5}$ to $3 \cdot 10^{-5} m^{-1}$ (derived by Uffink [1982] from pumping tests). In these simulations, the phreatic groundwater level in the Haarlemmermeer polder is changed instantaneously[11] from -0.6 m $N.A.P.$ (before 1854) to -5.5 m $N.A.P.$ (after the reclamation in 1854). The changes in freshwater head, calculated with the adapted MOC model, are recorded in a so-called observation point, positioned at x=7475 m and z=-105 m $N.A.P.$ As the interest is focused on the salinisation of the geohydrologic system, the new state of (dynamic) equilibrium of the piezometric level distribution is reached so fast that it is justified to take the specific storativity S_s equal to zero. This will simplify the calculations with the adapted MOC model significantly and not affect the results.
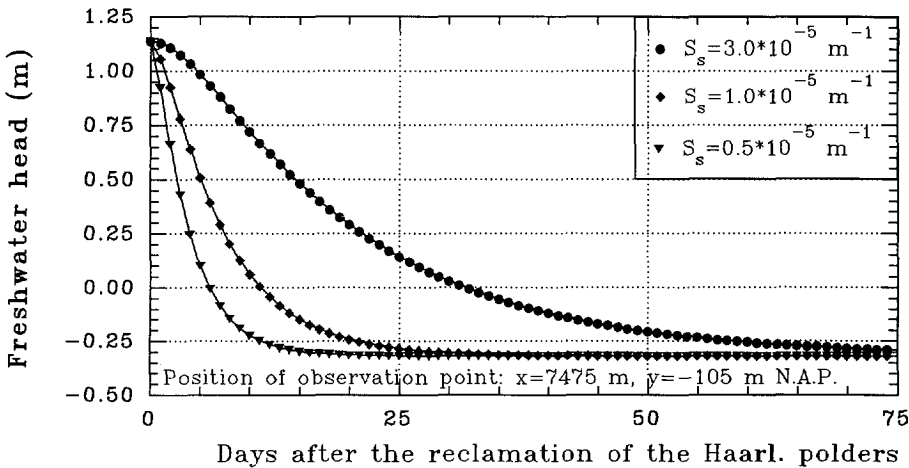
Figure 7.12: Influence of the specific storativity S_s on the calculated freshwater head as a function of time in an observation point with the position x=7475 m and z=-105 m $N.A.P.$, when the phreatic groundwater level in the Haarlemmermeer polder is lowered instantaneously in 1854. The flow time step is 1 day.

2. Hydrodynamic dispersion

The influence of the longitudinal dispersivity α_L is evaluated by comparing the results of simulations with five different values of longitudinal dispersivity α_L: 0 m, 0.02 m, 0.2 m, 2.0 m and 20.0 m. In figure 7.13, four chloride distributions of the profile are given after a simulation time of 134 years from the reclamation of the Haarlemmermeer polder (in 1854) till the end of 1987. The calculated chloride distribution matches the observed distribution best if small longitudinal dispersivities

---

[11]Note that, in reality, lowering the phreatic groundwater level in the Haarlemmermeer polder must have lasted about a year, so this is only a hypothetical case. Moreover, as a first approximation, the influence of phreatic storage is left out of consideration.
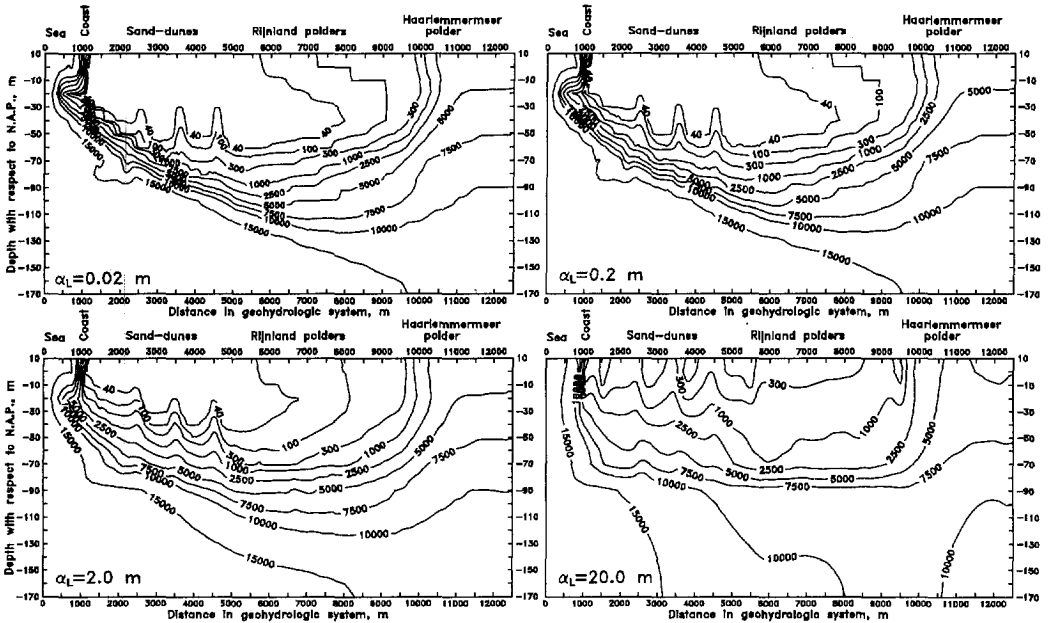
Figure 7.13: Chloride distributions (in $mg\ Cl^-/l$) at the end of 1987 for the reference case, calculated with four different longitudinal dispersivities: α_L=0.02 m, α_L=0.2 m, α_L=2.0 m and α_L=20.0 m.

are applied, namely α_L=0.02 m and α_L=0.2 m. By contrast, the case with α_L=2.0 m shows a freshwater lens that is too thin, whereas the case with α_L=20.0 m does not simulate a freshwater lens any more: the geohydrologic system only consists of a large zone with brackish groundwater. This situation does not occur in reality. It appears that for the case with α_L=0 m, the difference in chloride distribution with the cases with small longitudinal dispersivities is negligible.

Figure 7.14 shows the distribution of fresh ($Cl^-\leq 300\ mg\ Cl^-/l$), brackish ($300<Cl^-<10,000$) and saline ($Cl^-\geq 10,000\ mg\ Cl^-/l$) water in percentages of the total volume of water in the geohydrologic system during the past 134 years for five values of longitudinal dispersivities. The figure shows that especially the case with α_L=20.0 m differs from the case with α_L=0.02 m which is the best match. The fresh as well as the brackish volume fraction demonstrate that also the case with α_L = 2.0 m deviates from the cases with relatively small longitudinal dispersivities.

As a small longitudinal dispersivity is the best estimate, the influence of the transversal dispersivity α_T and the ratio α_T/α_L on the simulation of the chloride distribution is likely to be negligible.

The effective molecular diffusion D_d is of minor importance in the middle and deep aquifer. However, as the longitudinal dispersivity is small, the contribution of
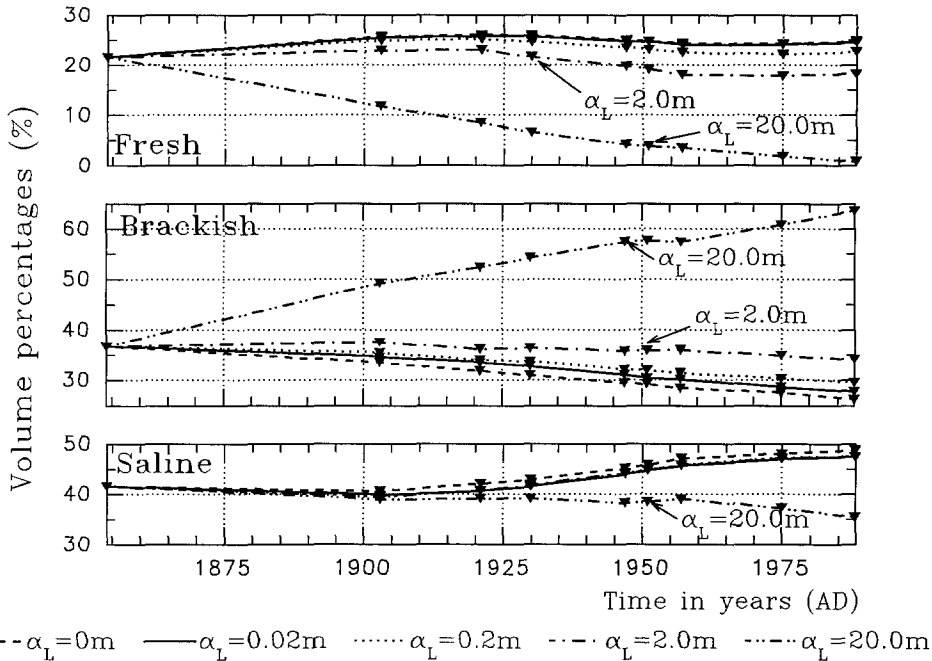
Figure 7.14: Volume percentages of fresh, brackish and saline groundwater in the geohydrologic system during the past 134 years after the reclamation of the lake Haarlemmermeer for five values of longitudinal dispersivity. The geohydrologic system is bounded in the horizontal direction by $x=0$ m and $x=12{,}500$ m, and in vertical direction by the levels $z=-10$ m and $z=-170$ m $N.A.P.$

the effective molecular diffusion D_d to the magnitude of the hydrodynamic dispersion is not insignificant in some places. For instance, in the center of the loam aquitard between -70 and -90 m $N.A.P.$ where only small (vertical) velocities occur, the ratio longitudinal dispersion coefficient to effective molecular diffusion D_L/D_d, where $D_L = \alpha_L |V|$ (see equation 5.46) and $D_d = 10^{-9}$ m^2/s, is smaller than 1.0. Thus, in the loam aquitard the effective molecular diffusion should not be neglected with respect to the longitudinal dispersion coefficient.

3. Loam aquitard

A case without the loam aquitard between -70 and -90 m $N.A.P.$ is simulated in order to assess the influence of the loam aquitard on the fresh, brackish and saline groundwater distribution. As groundwater flow is a slow process, the simulation time of 134 years appears to be not long enough to clearly detect the influence of the loam aquitard on the volume distribution of fresh, brackish and saline groundwater.
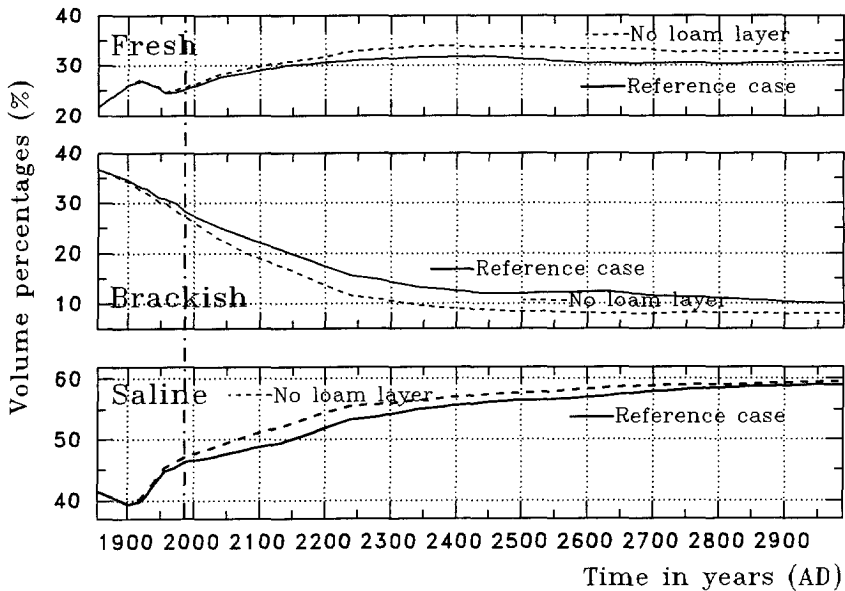
Figure 7.15: Volume percentages of fresh, brackish and saline groundwater in the geohydrologic system from 1854 till the end of the next millennium. Two cases with and without the loam aquitard are simulated in the representative profile. Groundwater recharge into the phreatic aquifer equals 360 mm/yr. The groundwater extraction rate during the next centuries equals the rate during the period 1975-1987.

Figure 7.15 shows that, during the past 134 years, the changes in volume of fresh and saline groundwater are caused, at first, by the reclamation of the Haarlemmermeer polder, and subsequently, by changes in groundwater extraction rates. During the past 134 years, the difference in volume percentage between the two cases with and without the loam aquitard is less than two percents. However, when the simulation time is one millennium[12], the differences increase. The groundwater extraction rate is low during the next centuries, so there is a surplus of fresh groundwater flowing into the geohydrologic system.

Based on results of the simulations not shown here[13], it is concluded that the loam aquitard only slightly affects the groundwater flow in the geohydrologic system. The loam layer decreases the seepage quantity and retards the oozing of mainly saline groundwater out of the deep aquifer into the middle aquifer. Accordingly, fresh groundwater, that infiltrates in the sand-dune area, intrudes in the middle aquifer and flows towards the Haarlemmermeer polder. What is more, the loam aquitard

---

[12]During this long simulation time, many processes that affect the geohydrologic system have not been considered, such as hydrological, morphological and man-induced processes.

[13]For instance, by means of the film-option (see section 5.6), changes in the solute distribution in the profile as a function of time can be compared for both cases with and without the loam aquitard.

appears to restrict the growth of the freshwater lens into the direction of the deep aquifer.

4. Groundwater recharge

The influence of a change in groundwater recharge into the phreatic aquifer of the sand-dune area of the representative profile is investigated by means of three ground-water recharge scenarios during the next millennium:

a. 216 mm/yr (-40 % compared with the reference case),

b. 360 mm/yr (during the past 134 years, this figure has been applied in the simu-
   lation of the reference case),

c. 432 mm/yr (+20 % compared with the reference case).

The groundwater recharge can alter due to a change in: (1) the natural component: e.g. change in precipitation due to climate change [IPCC, Houghton *et al.*, 1990], and (2) the anthropogenic component: e.g. change in artificial recharge or withdrawal of groundwater from the phreatic aquifer. Figure 7.16 shows the volume distributions of groundwater in the geohydrologic system during the next millennium for the three scenarios of groundwater recharge. Small changes in the volume percentages, espe-cially of brackish groundwater, are the result of the presence of the loam aquitard, which retards the inflow of saline groundwater in the middle aquifer. The volume of the freshwater lens changes considerably when the groundwater recharge in the phreatic aquifer of the sand-dune area is 216 mm/yr or 432 mm/yr. Even without a change in groundwater recharge, saline groundwater replaces brackish groundwater. The increase of the saline groundwater fraction due to a decrease in groundwater recharge (216 mm/yr) is already significant after several tens of years.

7.6   Influence of model parameters

The relation of model parameters to causes of numerical instabilities in the velocity field is investigated by means of comparing the reference case with a so-called ac-curate case. In this accurate case, three model parameters, which can increase the accuracy of the solution, are adapted: (1) the number of particles per grid cell; (2) the convergence criterion for the groundwater flow equation; and (3) the flow time step. The influence of these three model parameters on the solution is also analysed separately. Moreover, the influence of the dimension of the grid cells and the initial density distribution on the solution are also studied. Finally, the accuracy of the solute transport in the geohydrologic system is determined by assessing the error in the solute mass balance.
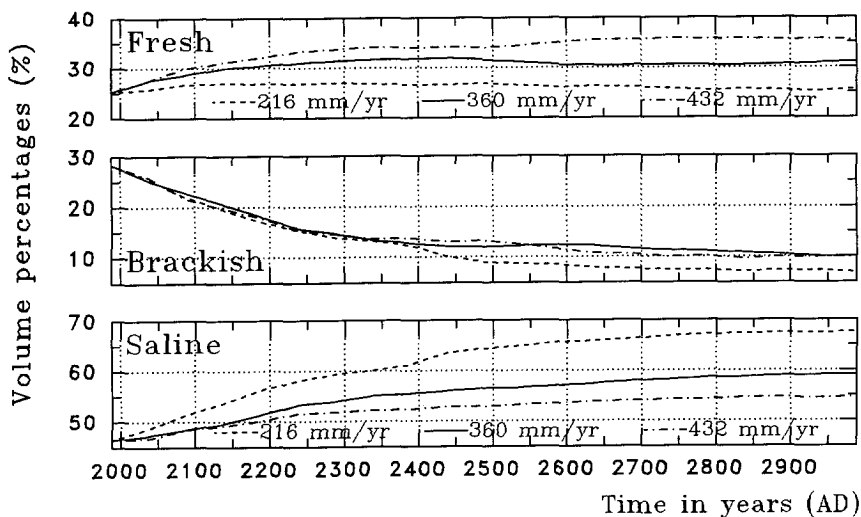
Figure 7.16: Volume percentages of fresh, brackish and saline groundwater in the geo-hydrologic system during the next millennium for three different scenarios of groundwater recharge: 216 mm/yr, 360 mm/yr, and 432 mm/yr.

Comparison of the reference case and the accurate case

Before model parameters are analysed separately, the combined influence of the following three model parameters are investigated by comparing the reference case versus the accurate case: (1) the number of particles per grid cell of 5 versus 16; (2) the convergence criterion TOL of 10^{-5} versus 10^{-10}; and (3) the flow time step of 1 *year* versus 1 *month*. The suppression of numerical instabilities in the velocity field by model parameters is clearly demonstrated by comparing figure 7.17 with figure 7.18. Nonetheless, numerical instabilities remain even for the accurate case.

Figure 7.19 shows the fluctuations of the chloride concentration as a function of time in a so-called observation point in the center of a grid cell for cases with different model parameters. Note that the observation point is situated in the transition zone between fresh and saline groundwater, thus the fluctuations in chloride concentration can be strong. After a simulation time of about 100 years, the observation point is located in saline groundwater and accordingly, (strong) fluctuations do not occur anymore. Fluctuations in the chloride concentration can be suppressed nearly completely when the accurate model parameters are applied.

Figure 7.20 shows the change in chloride concentration at the end of 1987 between the reference case and the accurate case. The differences in chloride concentration between the reference case and the accurate case are in most grid cells smaller than 250 mg Cl^-/l. However, in the surroundings of the transition zone under the sea,
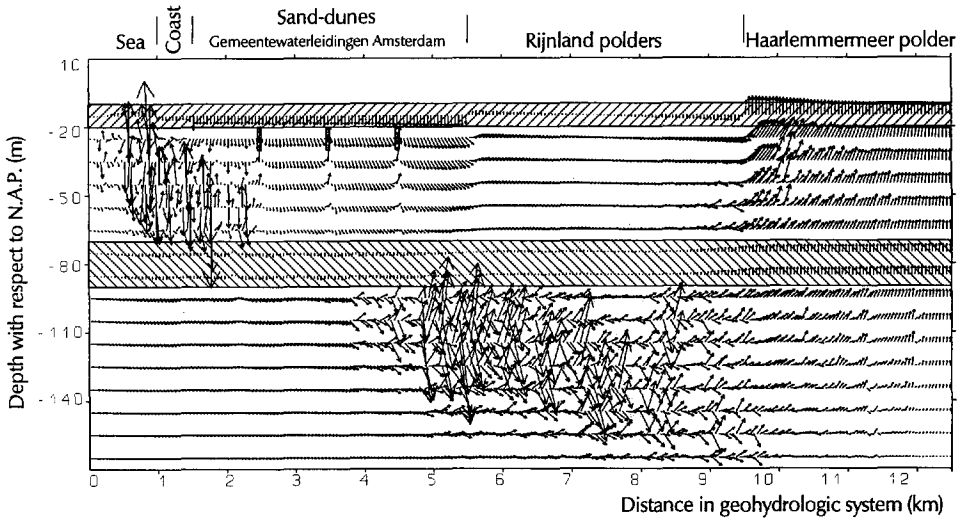
Figure 7.17: Velocity field in the geohydrologic system at the end of 1987. This is the reference case. The lengths of the arrows correspond with the displacement of groundwater during a time step of 10 years, beginning in 1987 and with a constant velocity field.
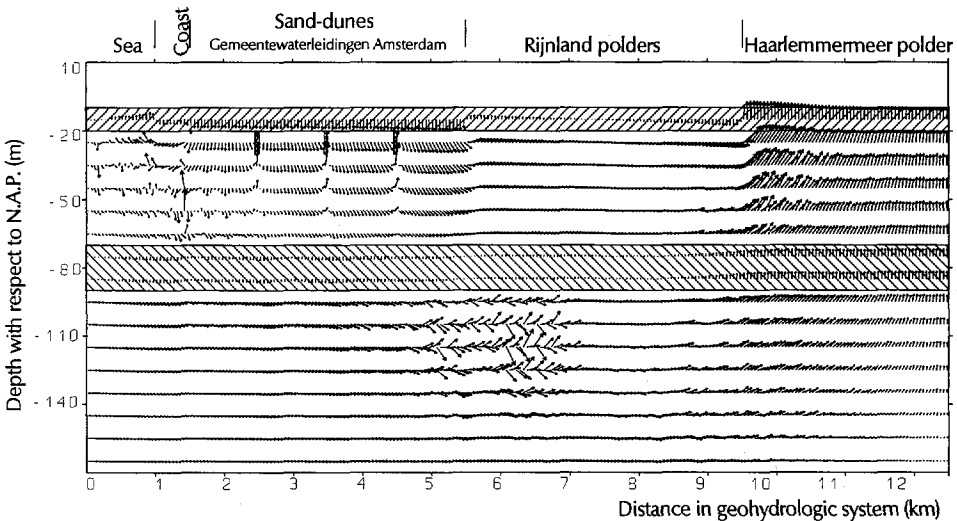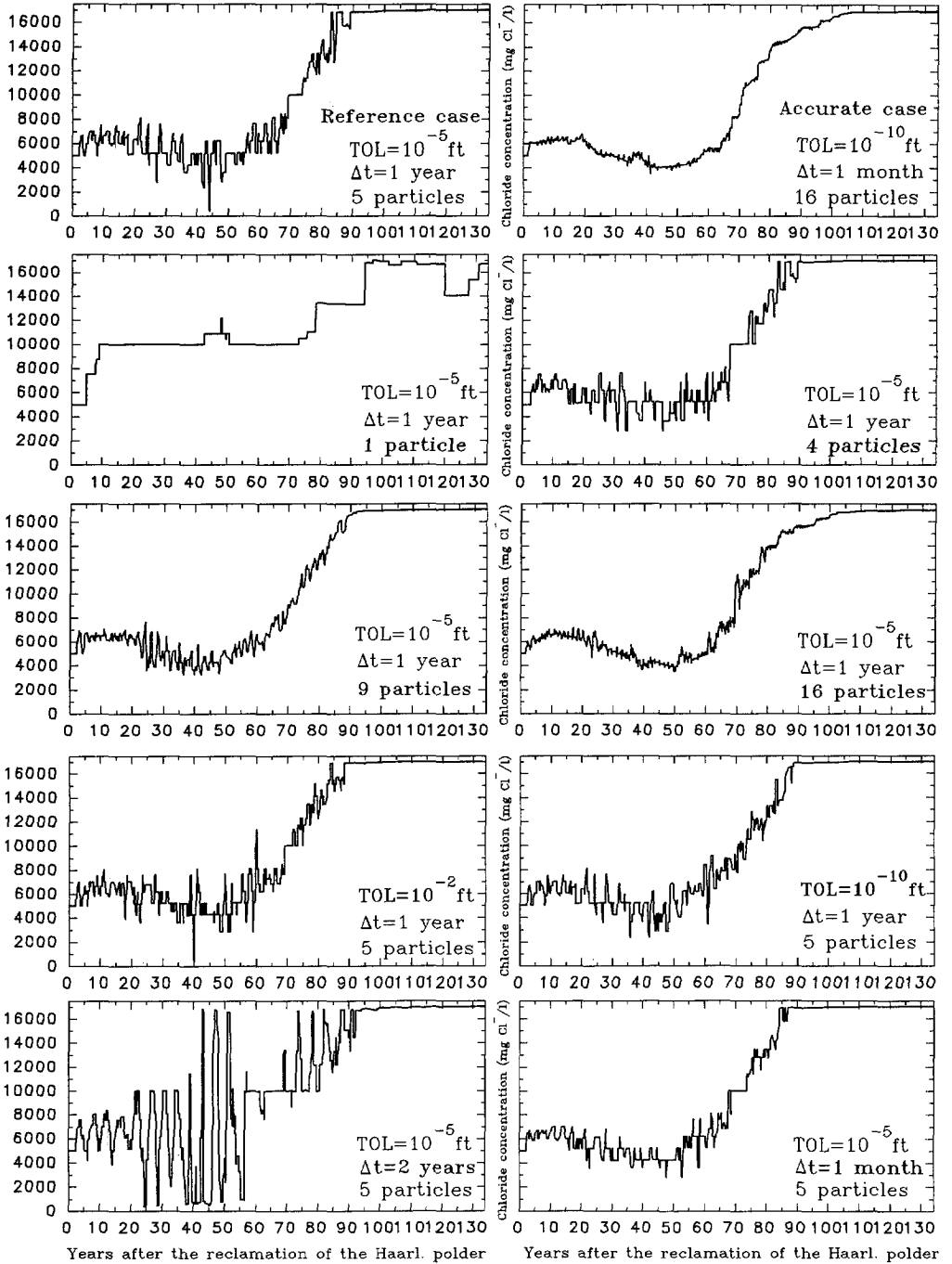

Figure 7.18: Velocity field in the geohydrologic system at the end of 1987. This is the accurate case. The lengths of the arrows correspond with the displacement of groundwater during a time step of 10 years, beginning in 1987 and with a constant velocity field.

Figure 7.19: Chloride concentration as a function of time in the observation point at $x=3475\ m$ and $z=-105\ m\ N.A.P.$ The influence of different model parameters is shown.
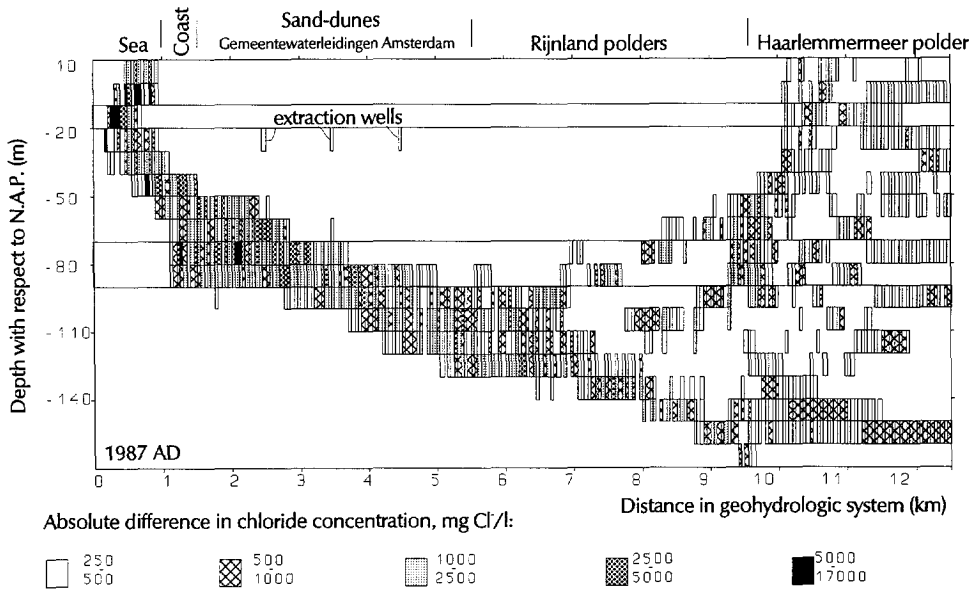
Figure 7.20: Absolute difference in chloride concentration in the geohydrologic system between the reference case and the accurate case after a simulation time of 134 years.

the coast and the sand-dunes, the difference in chloride concentration can go up to some thousands of $mg\ Cl^-/l$ in a few grid cells.

Numerical instabilities in the velocity field

Numerical instabilities in the velocity field due to density differences arise from the numerical approximation. They may occur at places where the transition zone between fresh and saline groundwater is small and where the vertical velocities are small. In subsection 5.5.1, the causes of numerical instabilities in relation with the model parameters have been discussed in detail.

For illustration, figure 7.21a shows the velocities through the geohydrologic system for the accurate case at the end of 1987, 134 years after the reclamation of the lake Haarlemmermeer in 1854. There are three lines of groundwater extraction wells in the sand-dune area. As can be seen, saline groundwater intrudes in the deep aquifer and vertical groundwater flow dominates in the aquitards. A downward groundwater flow occurs in the sand-dune area through the Holocene aquitard (that is deep groundwater percolation), while in the Haarlemmermeer polder groundwater flows in upward direction (that is seepage). Even for the accurate case, the velocities fluctuate in vertical direction in some places. This occurs especially in the middle aquifer in the coast segment in the vicinity of $x=1500\ m$, where a small transition zone between fresh and saline groundwater is present. The fluctuations seem to be strong
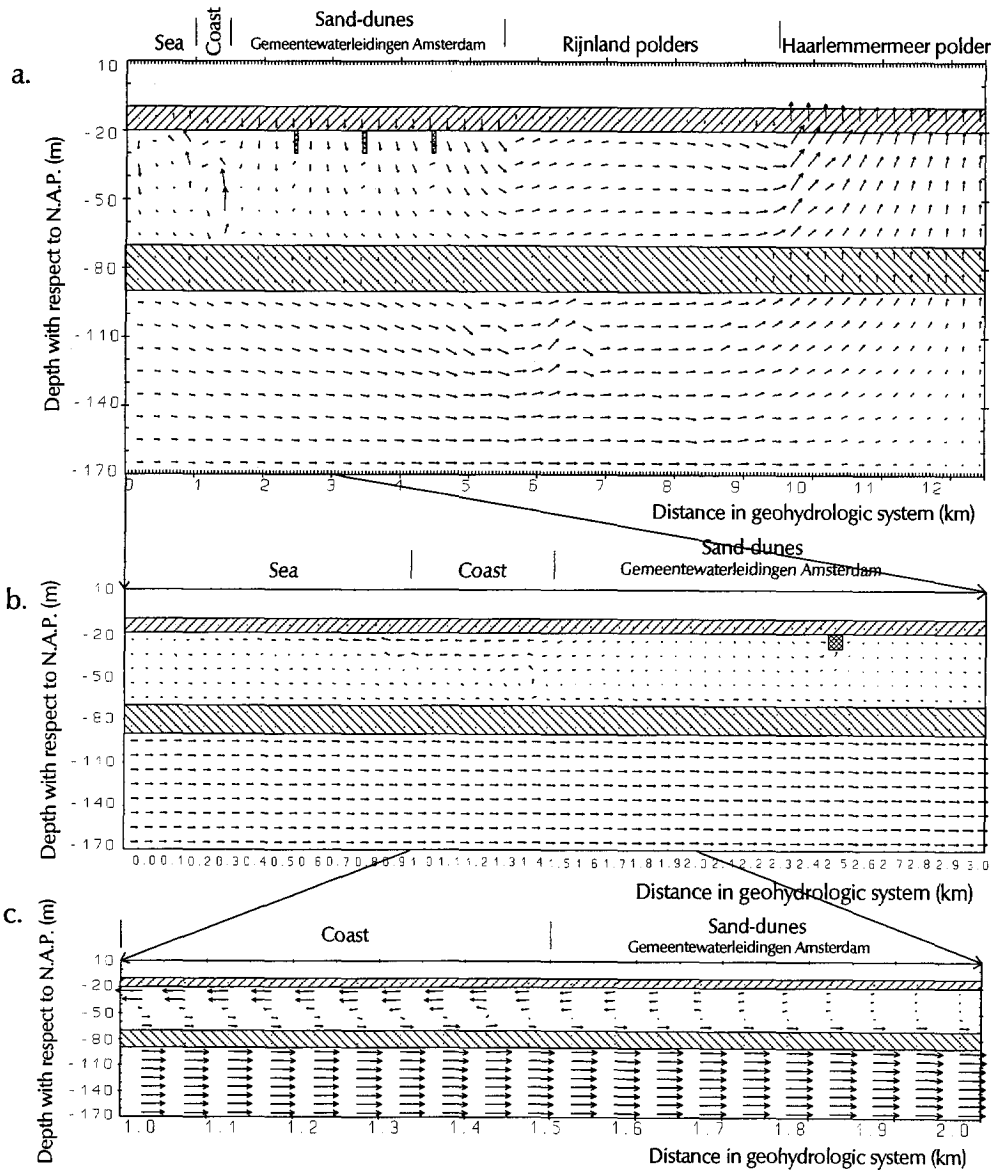
Figure 7.21: Velocity field in the geohydrologic system at the end of 1987 between a. $x=0$-12,500 m, b. $x=0$-3000 m, c. $x=1000$-2000 m. This is the accurate case. The distortion of the vertical direction with respect to the horizontal direction equals: a. a factor 35, b. a factor 5, c. no distortion. The lengths of the arrows correspond with the displacement of groundwater during a time step of a. 10 years, b. 3 years, c. 3 years. The velocity field is constant during that time. The velocity is displayed in the center of: a. every fifth grid cell, b. every grid cell, c. every grid cell.

because the vertical dimension is distorted with respect to the horizontal dimension with a factor 35. However, figure 7.21b and figure 7.21c show two segments of the geohydrologic system with smaller vertical distortions of the velocity field. In reality, the fluctuating vertical velocities appear to be small compared to the dominant horizontal velocities of groundwater in the geohydrologic system.

Number of particles per grid cell

When more particles per grid cell are present, the change in density at the end of a solute time step is less sudden after averaging the chloride concentration (and thus the density) over the available particles. As such, more particles per grid cell counteract numerical instabilities.

Figure 7.19 clearly shows that the chloride concentration as a function of time of the reference case (5 particles) has quite some fluctuations, while for the cases with 9 and 16 particles the chloride concentration is more smooth. The figure also shows that the simulation with only 1 particle per grid cell is completely inaccurate.

Convergence criterion TOL

When the convergence criterion TOL is smaller, the groundwater flow equation is solved more accurately, and thus, the velocities and particle movements are calculated more precisely. Figure 7.19 shows that this parameter has less influence on the accuracy of the solute transport than the number of particles per grid cell.

Length of the flow time step Δt

When too many solute time steps are simulated within one flow time step, the chloride distribution and thus the density distribution may be changed too much to match the solution of the groundwater flow equation. Figure 7.19 clearly shows that when this parameter Δt is too great (2 *year* instead of 1 *year*), the fluctuations are very strong and solute transport is simulated inaccurately.

Dimension of grid cells

More grid cells with smaller dimensions than used in the reference case does not always mean that the groundwater flow equation is also solved more accurately and that the particles are moved more precisely. Numerical instabilities may even be amplified, because particles in an unstable zone can enter more often adjacent grid cells with a completely different density. Note that this phenomenon applies on condition that the length of the flow time step is kept constant.

Cases with the following different numbers of grid cells are simulated: (1) the reference case: $250 \cdot 18 = 4500$ grid cells; (2) $50 \cdot 18 = 900$ grid cells; (3) $100 \cdot 36 = 3600$ grid cells; and (4) $250 \cdot 36 = 9000$ grid cells. In figure 7.22, the chloride concentrations for these four different numbers of grid cells are compared as a function of time in
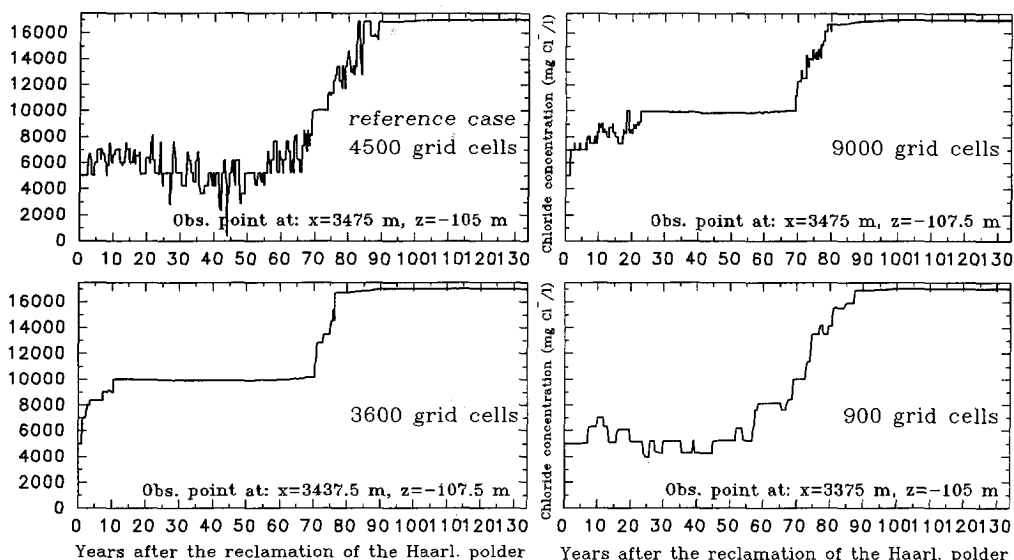
Figure 7.22: Chloride concentration as a function of time (in years after 1854). The influence of different numbers of grid cells is shown. As the observation points of the cases with 3600 and 9000 grid cells are located at -107.5 m N.A.P. instead of at -105 m N.A.P. (the cases with 900 and 4500 grid cells), see figure 7.23, the chloride concentrations as a function of time differ significantly.
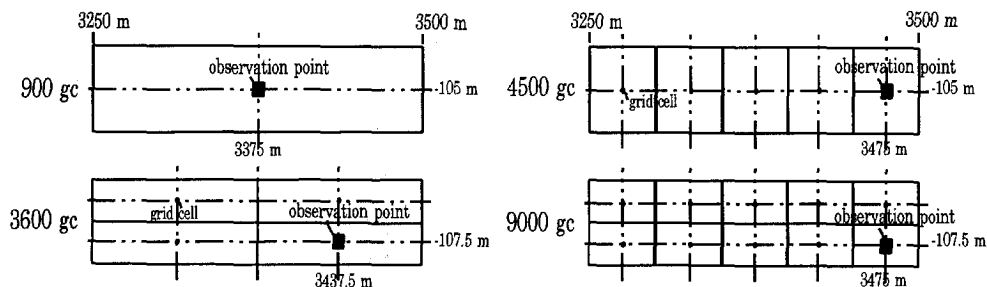

Figure 7.23: Position of the observation point in the four cases with different numbers of grid cells.

so-called observation points, which are located in a transition zone. The observation points of the three new cases have slightly different positions compared to the reference case, as an observation point must be situated in the center of a grid cell (see figure 7.23).

As can be seen in figure 7.22, the reference case has the strongest fluctuations in chloride concentration. So, in this particular situation, cases with less grid cells (900

and 3600 grid cells) do not necessarily lead to less accurate solutions. The length Δx of a grid cell is larger for the two cases with 900 and 3600 grid cells than for the reference case with 4500 grid cells, and thus, particles are displaced less frequently to adjacent grid cells. As a consequence, abrupt changes in chloride concentration occur less frequently. As the occurrence of numerical instabilities depends on the geometry of the geohydrologic system as well as on the location of transition zones, no general recommendation can be given for the most effective number of grid cells in horizontal direction.

More grid cells in vertical direction may reduce the fluctuations in chloride concentration as well. In this particular case, the favourable characteristics of smaller (and thus more) grid cells dominate and numerical instabilities are counteracted. This can be demonstrated by comparing the reference case (4500 grid cells) with the case with 9000 grid cells: the fluctuations are smaller for the case with more grid cells in vertical direction. In the transition zone, abrupt changes in density between adjacent grid cells are smaller, and numerical instabilities are counteracted. Note that the overall effect on the numerical instabilities also depends here on other (model) parameters, such as the length of the flow time step. Decreasing the length of the flow time step in combination with more grid cells will certainly suppress the numerical instabilities (see, for instance, figure 6.17).

Table 7.2 shows the influence of four cases with different grid cells on three geohydrologic features at the end of 1987: (1) the deep groundwater percolation through the Holocene aquitard, located in the sand-dune area in the reach 1500-5500 m; (2) the seepage quantity through the Holocene aquitard at -20 m $N.A.P.$, located in the Haarlemmermeer polder in the reach 9500-12,500 m; and (3) the volumes of fresh, brackish and saline groundwater, calculated for the geohydrologic system between $x=0$ and $x=12,500$ m, and between $z=-10$ and $z=-170$ m $N.A.P.$ Altogether, the results appear to be very similar. The greatest differences between the four cases are less than a few percents.

Table 7.2: Influence of different numbers of grid cells on some geohydrologic features at the end of 1987.

Number of grid cells	Percolation sand-dunes (m^2/yr)	Seepage Haarl. meer (m^2/yr)	Volumes in the geohydrologic system					
			fresh		brackish		saline	
			$(10^3 m^2)$	(%)	$(10^3 m^2)$	(%)	$(10^3 m^2)$	(%)
900	573.3	655.6	168.0	24.0	196.0	28.0	336.0	48.0
3600	560.0	653.3	165.1	23.6	198.4	28.3	336.5	48.1
4500	572.1	650.2	172.8	24.7	194.6	27.8	332.6	47.5
9000	562.2	650.0	165.8	23.7	199.1	28.4	335.1	47.9

Initial density distribution

The adapted MOC model requires an initial density distribution, and thus an initial chloride distribution, of the geohydrologic system. The initial density distribution

must be as smooth as possible in order to suppress numerical instabilities in the velocity field. Figure 7.24 shows that numerical instabilities in the velocity field occur already at the beginning of 1854, thus before the simulation has even started. The numerical instabilities especially occur in transition zones, where adjacent grid cells in vertical direction have relatively great differences in density. The chloride concentrations of adjacent grid cells in these vulnerable zones should be smoothed as much as possible, of course in accordance with the observed chloride distribution.
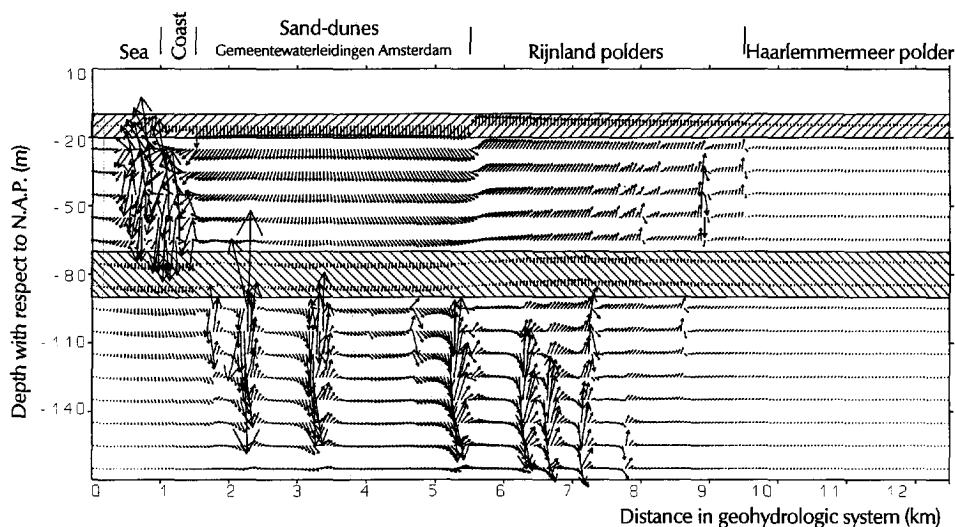

Figure 7.24: Velocity field in the geohydrologic system at the beginning of 1854. This is the reference case. The lengths of the arrows correspond with the displacement of groundwater during a time step of 10 years, beginning in 1854 and with a constant velocity field.

Error in solute mass balance

The accuracy of the solution of the solute transport equation is visualized by the error in the solute mass balance E_{solute}. This error is defined by equation 5.81 in subsection 5.5.2. The error E_{solute} is (mainly) caused by the particle tracking procedure: (a) particles are moved to other grid cells, which induce relatively random changes in the solute concentrations of those grid cells; and (b) particles are reposited to a new uniform distribution throughout the entire grid, when too many grid cells have become void due to particle movements.

Figure 7.25 shows the error E_{solute} during the simulation of the 134 years after the reclamation of the lake Haarlemmermeer. The effect of more accurate model parameters on E_{solute} is relatively small, because the initial mass of solute M_0 in the total geohydrologic system is some orders of magnitude greater than the solute
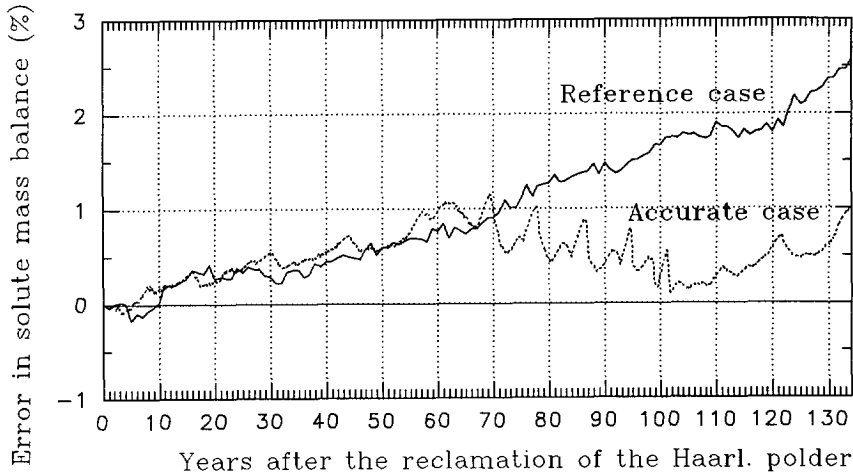
Figure 7.25: Error E_{solute} in the solute mass balance. The reference case is compared with the accurate case.

incoming and outgoing fluxes (net mass flux M_f).

7.7   Results of the simulated profile

In this section, the results of the simulated geohydrologic system are discussed, based on six features: (1) the chloride distribution at the end of 1987 and the change in chloride concentration between 1854 and 1987; (2) the freshwater head distribution (which are piezometric levels converted for the density of fresh water); (3) the velocities in the centers of the grid cells; (4) the change in volume distribution of fresh, brackish and saline groundwater; (5) the water balances during some specific years; and (6) streamlines from specific points in the geohydrologic system.

1. Chloride distribution

Figure 7.26a shows the chloride distribution for the representative profile at the end of 1987. The three lines of extraction wells create *upconing* of especially the isochlors[14] 40 and 100 $mg\ Cl^-/l$. Furthermore, the loam aquitard has retained brackish groundwater at some 1500 m from the seaside, while its surroundings has already become saline.

The change in chloride concentration between 1854 and 1987 is given in figure 7.26b. It shows that especially the geohydrologic system underneath the sanddune area and the Haarlemmermeer polder has become more saline.

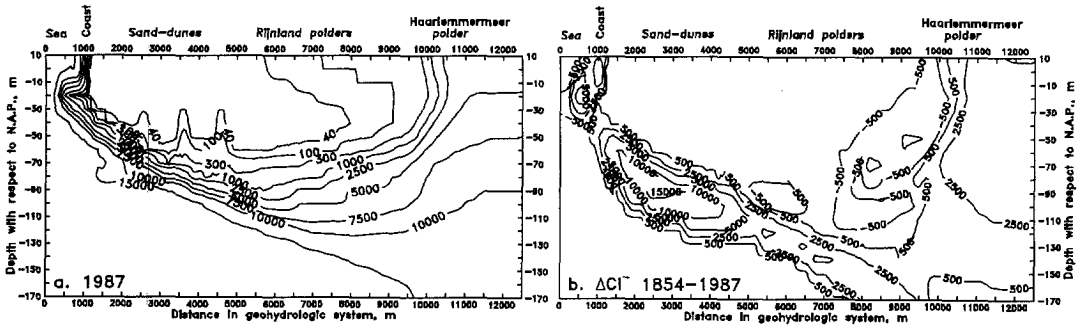[14] An isochlor is a line of equal Cl^--concentration.

Figure 7.26: a. The chloride distribution (values in $mg\ Cl^-/l$) at the end of 1987 calculated with the adapted MOC model for the reference case. b. The change in chloride concentration (values in $mg\ Cl^-/l$) between the years 1987 and 1854. Positive values mean that the area has become more saline, negative values mean that the area has become more fresh.

2. Freshwater head distribution

In figure 7.27a, the freshwater head is presented at the end of 1987 calculated with the adapted MOC model. At the seaside boundary, a hydrostatic situation occurs. The freshwater head is determined with equation 5.79. The freshwater head is high in the phreatic aquifer in the sand-dune area and groundwater recharge occurs through the Holocene aquitard. In the Haarlemmermeer polder, the freshwater head is low in the phreatic aquifer and groundwater oozes out of the middle aquifer through the Holocene aquitard.
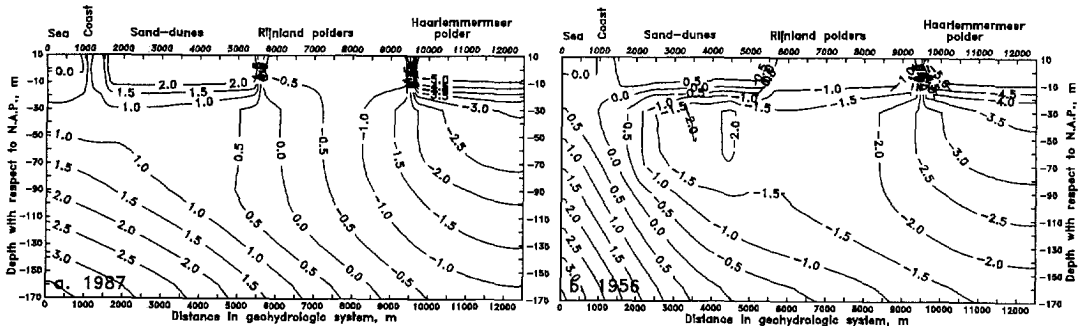

Figure 7.27: Freshwater head distribution (in m) of the geohydrologic system for the representative profile: a. at the end of 1987 and b. at the end of 1956.

The freshwater head in the middle aquifer in the sand-dune area changes throughout the pumping periods with different extraction rates and phreatic groundwater levels in the sand-dune area (see figure 7.2). For instance, figure 7.27b shows the freshwater head distribution at the end of 1956 calculated with the adapted MOC
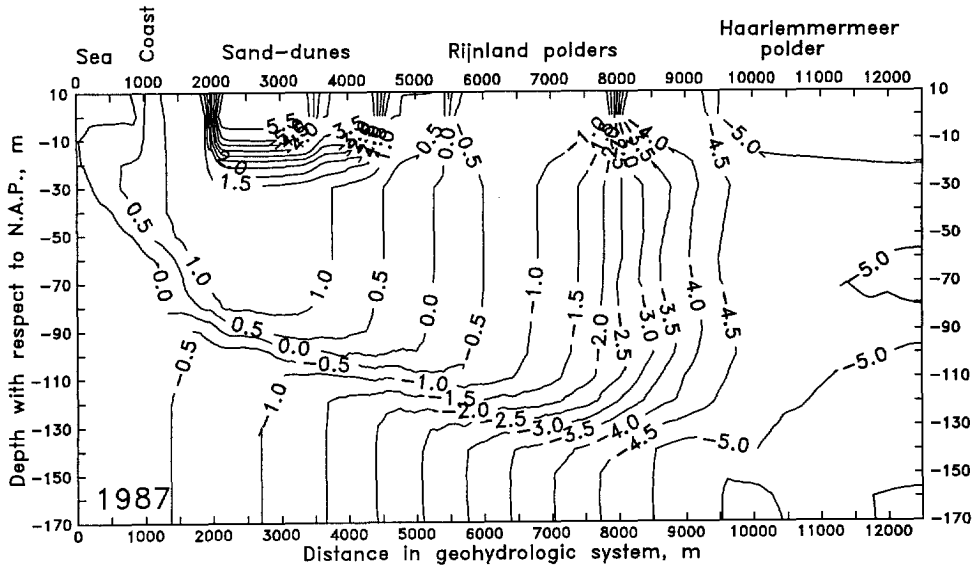
Figure 7.28: The *uncorrected* piezometric level distribution (in *m*) for the specific profile at the end of 1987.

model. As can be seen, a high groundwater extraction rate in the sand-dune area has its influence on the freshwater head distribution.

In figure 7.28, the *uncorrected* piezometric levels are presented for the specific profile at the end of 1987 (that is the end of the pumping period 1975-1987). To a certain extent, these levels correspond with the measured (uncorrected) piezometric levels, averaged over 1981, in profile **C** − **C′** of Stuyfzand [1988]. The position of the profile **C** − **C′** is indicated in figure 7.1.

3. Velocities

Figure 7.29 displays the velocities through the geohydrologic system at the end of 1956, when the extraction rates are the highest. Saline groundwater in the deep aquifer oozes through the loam aquitard into the direction of the lines of extraction wells. By comparing this figure with figure 7.18, it can be deduced that groundwater extractions seriously affect the grondwater flow in this geohydrologic system.

4. Volumes of fresh, brackish and saline groundwater

The change in chloride distribution is quantified by determining the total volumes of fresh, brackish and saline groundwater in the geohydrologic system. The tables 7.3 and 7.4 summarize the volume distributions in several years. Both tables show that, during the period 1854-1902, the volume of the freshwater lens has slightly increased;
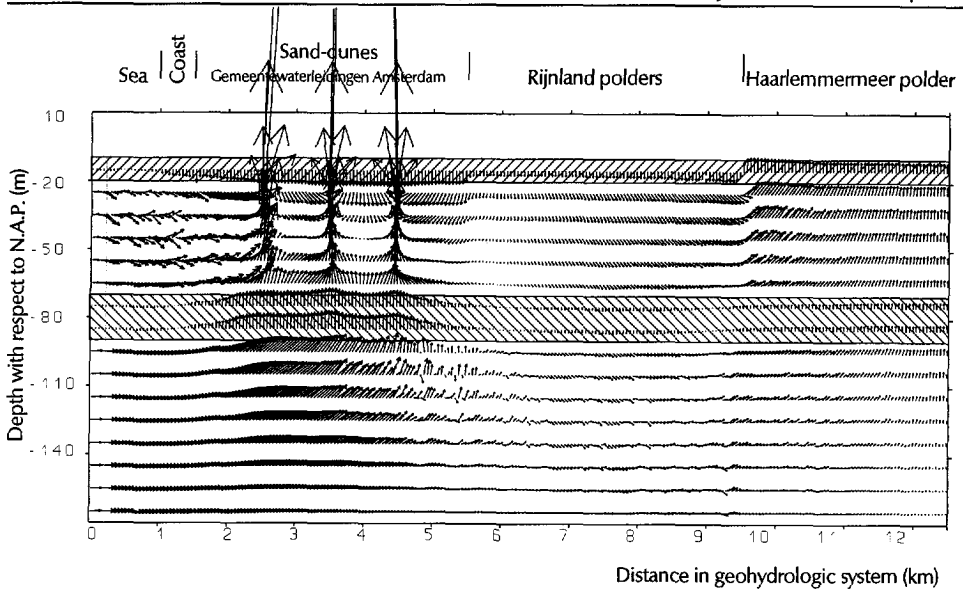
Figure 7.29: Velocity field in the geohydrologic system at the end of 1956. This is the accurate case. The lengths of the arrows correspond with the displacement of groundwater during a time step of 10 years, beginning in 1956 and with a constant velocity field.

Table 7.3: Percentages and volumes (in 10^3 m^3/m') of fresh, brackish and saline groundwater in the entire geohydrologic system in five striking years. This is the reference case. The porosity equals 0.35. The area is calculated between $x=0$ and $x=12,500$ m, and $z=-10$ and $z=-170$ m $N.A.P.$

The entire geohydrologic system						
Year	fresh		brackish		saline	
	(in 10^3m^2)	(%)	(in 10^3m^2)	(%)	(in 10^3m^2)	(%)
1854	151.6	21.7	257.2	36.7	291.2	41.6
1902	179.3	25.6	242.0	34.6	278.7	39.8
1956	168.3	24.0	211.2	30.2	320.5	45.8
1974	169.5	24.2	200.3	28.6	330.2	47.2
1987	172.8	24.7	194.5	27.8	332.7	47.5

this is due to natural groundwater recharge. Since the end of 1956, the distribution in fresh, brackish and saline groundwater is more or less stabilized. From then on, groundwater extraction for water supply from the deep aquifer was substantially reduced and artificial recharge of riverwater in the phreatic aquifer was started.

Table 7.4: Percentages and volumes (in 10^3 m^3/m') of fresh, brackish and saline ground-water in the sand-dune area in five striking years. This is the reference case. The porosity equals 0.35. The area is calculated between $x=1500$ and $x=5500$ m, and between $z=-10$ and $z=-170$ m $N.A.P.$

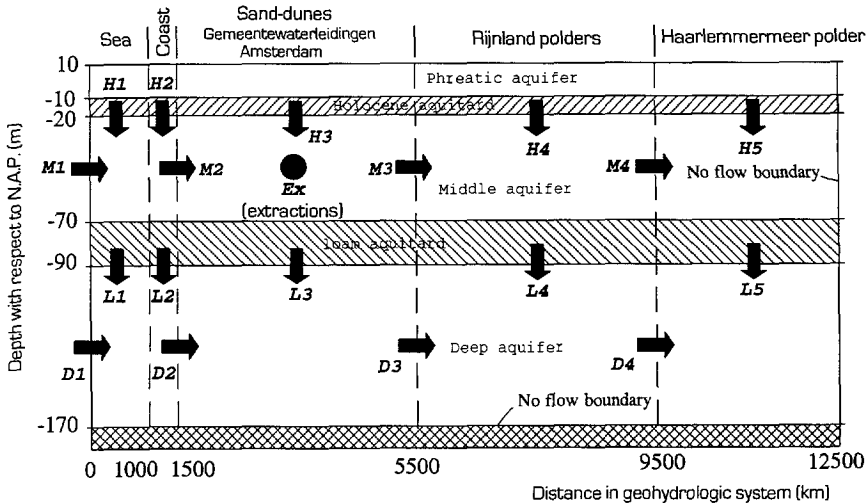| The sand-dune area						
Year	fresh		brackish		saline	
	(in $10^3 m^2$)	(%)	(in $10^3 m^2$)	(%)	(in $10^3 m^2$)	(%)
1854	95.7	42.7	33.8	15.1	94.5	42.2
1902	103.6	46.2	34.4	15.4	86.0	38.4
1956	80.0	35.7	27.3	12.2	116.7	52.1
1974	78.6	35.1	25.3	11.3	120.1	53.6
1987	80.6	35.9	25.2	11.3	118.2	52.8

Figure 7.30: Symbols of water masses in the geohydrologic system.

5. Water balances

The incoming and outgoing water masses over a boundary are determined from the velocities perpendicular to that boundary and the lengths of the boundary segments. In figure 7.30, the symbols and positive directions of the water masses are given flowing over specific boundary segments of the geohydrologic system. Table 7.5 shows the flow of water masses during specific years in million m^3/yr totalled over 9000 m parallel to the coastline. Some striking features of water masses over boundaries are:

- the salt water intrusion: **M1 and D1**
  The reclamation of the lake Haarlemmermeer in 1854 influences the salinisation

Table 7.5: Flow of water masses (in million m^3/yr) during some specific years. The water masses are totalled over 9000 m parallel to the coastline. See figure 7.30 for the meaning of the symbols.

Profile	repre.	repre.	repre.	spec.	repre.	repre.
year	1853	1956	1987	1987	1956	1987
Imposed condition in sand-dune area	phreatic groundwater level see figure 7.2				percolation 360 mm/yr	
Holocene aquitard						
H1	-0.4	0.1	-0.5	-0.9	0.0	-0.6
H2	0.4	0.4	0.3	0.0	0.3	0.1
H3	6.3	7.5	5.2	8.0	8.7	6.3
H4	-4.1	3.6	0.3	-2.5	3.4	0.1
H5	-0.8	-4.5	-5.9	-5.6	-4.6	-5.9
Middle aquifer						
M1	-1.2	2.8	0.3	0.4	2.5	0.0
M2	-2.2	3.1	-0.3	-1.0	2.6	-0.9
M3	2.2	-0.4	1.8	2.4	-0.2	1.8
M4	0.2	2.5	2.9	2.3	2.5	2.9
Loam aquitard						
L1	0.6	0.2	0.2	0.3	0.2	0.2
L2	0.4	0.0	0.2	0.2	0.0	0.2
L3	1.9	-6.9	1.4	2.9	-6.4	1.9
L4	-2.1	0.7	-0.8	-2.4	0.7	-1.0
L5	-0.6	-2.0	-3.0	-3.3	-2.1	-3.0
Deep aquifer						
D1	-0.2	8.0	2.0	2.3	7.6	1.7
D2	0.8	8.2	2.4	2.8	7.8	2.1
D3	2.7	1.3	3.8	5.7	1.4	4.0
D4	0.6	2.0	3.0	3.3	2.1	3.0
Extraction of groundwater						
Ex	0	17.9	1.7	1.7	17.9	1.7

in the geohydrologic system as follows: before 1854, groundwater has flown from the deep and middle aquifers towards the sea, while since 1854 salt water intrusion occurs. High groundwater extraction rates from the middle aquifer seriously affect the groundwater flow in the entire geohydrologic system. For instance, the salt water intrusion from the sea in both the deep aquifer and the middle aquifer is more severe during the period 1951-1956 than during the period 1975-1987, when the groundwater extraction rates from the middle aquifer are low.

- the seepage quantity in the Haarlemmermeer polder: **H5**
  The seepage quantity is much higher since 1854 than before the reclamation of the lake Haarlemmermeer. Furthermore, the seepage quantity in the Haarlemmermeer polder decreases when groundwater extraction rates during the period 1951-1956 are high.

- the flow through the loam aquitard in the sand-dune area: **L3**
  High groundwater extraction rates in the middle aquifer during the period 1951-1956 cause a great upward flow through the loam aquitard in the sand-dune area. This upward flow turns into a downward flow, when groundwater extraction rates in the middle aquifer are reduced during the period 1975-1987.

6. Streamlines

Two types of streamlines are determined (see also section 5.6): (a) streamlines which indicate the path that particles would make through the geohydrologic system when the velocity field is in a stationary situation, and (b) streamlines or path lines based on a non-stationary situation in the velocity field, which in fact occurs for geohydrologic systems with changing densities.

ad a. The velocity field, taken at one specific moment in time, is not adjusted during the travel of the particles. The travel time of a particle through the geohydrologic system is computed by adding up all time steps that particle needs to move through the system.

Figure 7.31 shows several streamlines and travel times through the geohydrologic system of the representative profile for the velocity field at the end of 1987. Saline groundwater particles, that intrude in the deep aquifer at the seaside boundary, have travel times of many centuries before the Holocene aquitard in the Haarlemmermeer polder is reached. In the long run, all groundwater particles in the deep aquifer will eventually reach the Haarlemmermeer polder on condition that the groundwater extraction rate from the middle aquifer is not too high. This situation occurred at the end of 1987.

By contrast, when the groundwater extraction rates from the middle aquifer are high (e.g. at the end of 1956, see figure 7.32), the situation is completely different. Then, great volumes of saline groundwater, that intrude in the deep aquifer at the seaside boundary, will ooze through the loam aquitard and will end in the lines of extraction wells. The travel times are shorter than when the groundwater extraction rates are low.

ad b. Path lines and travel times are determined by recording the movements of selected groundwater particles during the simulation with the adapted MOC model (see also section 5.6). This implies that the velocity distribution is constantly adapting, e.g. due to changes in phreatic groundwater levels, groundwater extraction rates or changes in density distribution. Since the particles can
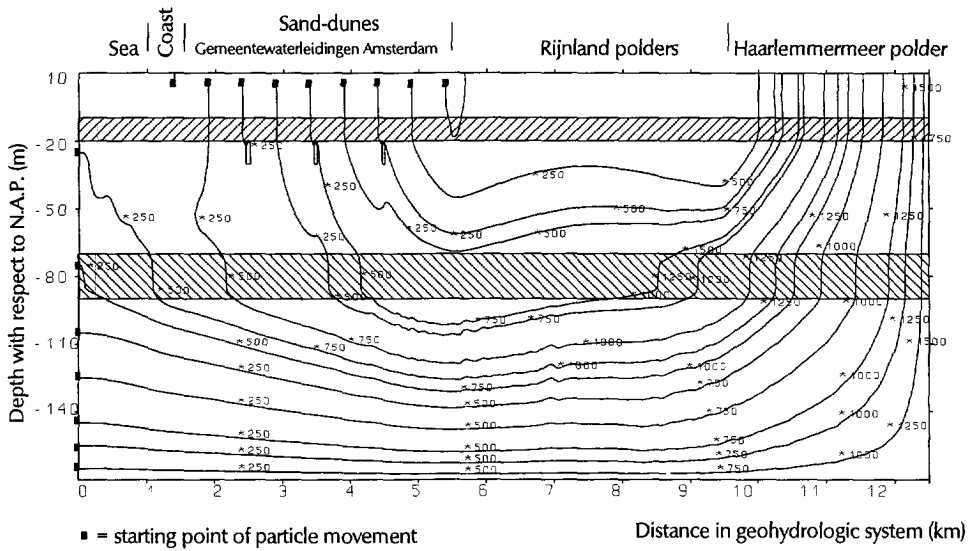
Figure 7.31: Some streamlines and travel times in years through the geohydrologic system, calculated with the velocity field that occurs at the end of 1987. This representative profile was simulated with model parameters of the accurate case.
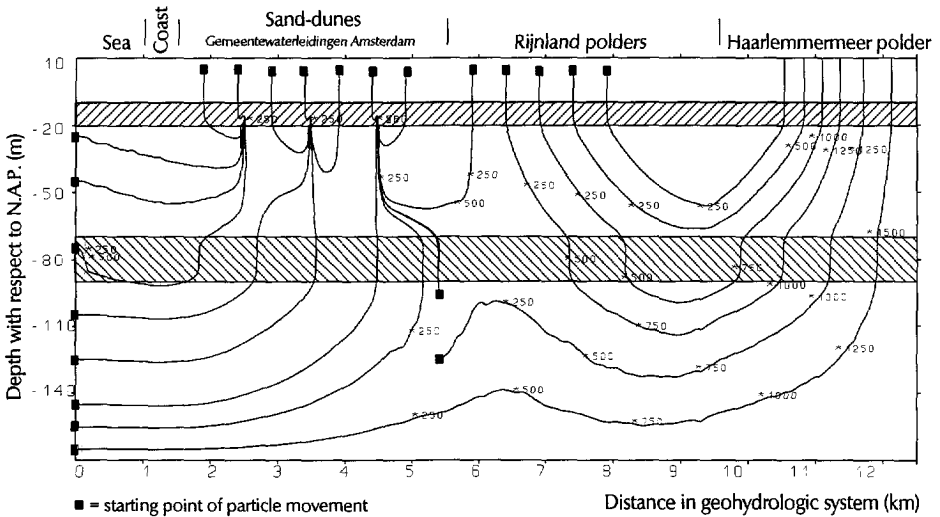

Figure 7.32: Some streamlines and travel times in years through the geohydrologic system, calculated with the velocity field that occurs at the end of 1956. This representative profile was simulated with model parameters of the accurate case.
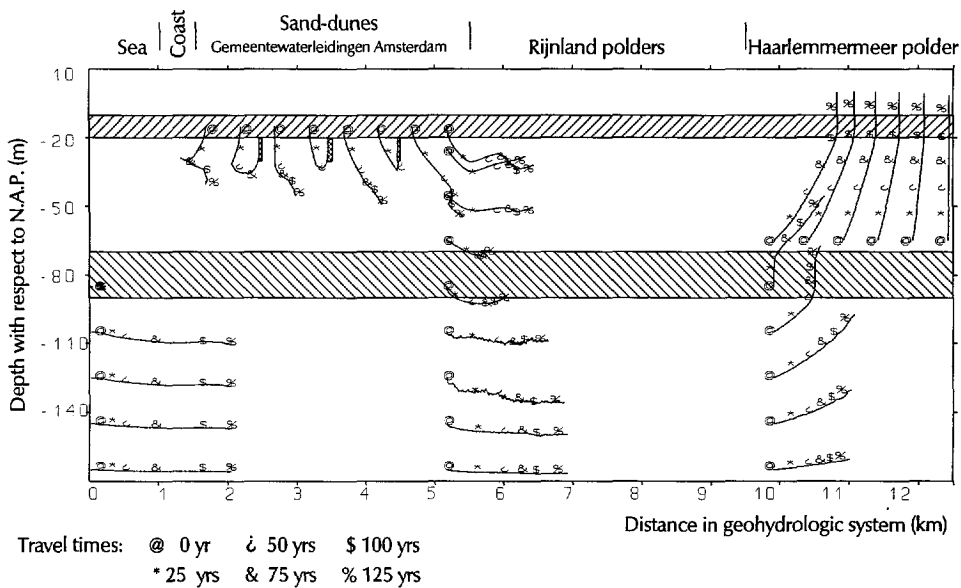
Figure 7.33: Some path lines with travel times in years through the geohydrologic system. This representative profile was simulated with model parameters of the reference case. Note that path lines may cross each other.

only be tracked during the simulation time, the selected groundwater particles are only followed during the 134 years after the reclamation of the lake Haar-lemmermeer (see figure 7.33). The figure shows that a groundwater particle, that started at $x=1625\ m$, $z=-15\ m$ N.A.P., was moving towards the seaside boundary during the first decades (that is exactly 67 years) after the recla-mation of the lake Haarlemmermeer. Subsequently, the flow direction of the groundwater particle altered towards the adjacent line of extraction wells, from the moment the groundwater extraction rate from the middle aquifer had been increased from some 3.6 million m^3/yr for the period 1903-1920 to some 11.2 million m^3/yr for the period 1921-1929 (see figure 7.2). From the beginning of 1975 on, the extraction from the middle aquifer has been reduced to such a low rate that the groundwater particle changes its flow direction towards the sea once again.

Concluding remarks on groundwater flow and solute transport in this profile

Based on the simulations with the adapted MOC model, the following conclusions can be drawn.

Since the 1850's, groundwater flow in this profile has been dominated by human activities. The lowering of the phreatic groundwater level in the Haarlemmermeer polder in 1854 has generated a strong saline groundwater flow from the sea through

the deep aquifer, inducing a severe salt water intrusion. During the first half of the 20th century, high groundwater extraction rates from the middle aquifer in the sand-dune area have decreased the volume of the freshwater lens and have increased the fraction of saline groundwater in the middle and deep aquifers. However, from 1957 on, the extraction of groundwater from the middle aquifer has been diminished and the freshwater lens has grown slightly. Moreover, artificial recharge in the phreatic aquifer since 1957 has accelerated the refreshening of the geohydrologic system.

In this section, human interventions have been simulated only tentatively to counteract the salinisation process of the geohydrologic system, to enlarge the freshwater lens and to diminish the seepage through the Holocene aquitard in the Haarlemmermeer polder. Some feasible countermeasures are probably: (1) extraction of saline groundwater from the deep or middle aquifer; (2) injection of fresh surface water into the aquifers (deep-well infiltration); and (3) raising the phreatic groundwater level in the polder area.

As the salinisation of the subsoil is a slow process, it takes many centuries before saline groundwater, that has intruded the geohydrologic system at the seaside boundary and that has flown through the deep aquifer, will ooze out of the geohydrologic system in the Haarlemmermeer polder as seepage. Hence, it takes many centuries before a state of dynamic equilibrium for the chloride distribution is reached.

7.8   Conclusions

The adapted MOC model is able to simulate the geohydrologic system of this profile perpendicular to the Dutch coastline where density flow cannot be neglected.

Subsoil parameters may seriously affect the groundwater flow and the solute transport in this profile. The loam aquitard between -70 and -90 m $N.A.P.$ retards the salinisation process in the geohydrologic system. The longitudinal dispersivity α_L, that represents the hydrodynamic dispersion in MOC, should be simulated with a small value (in the order of centimetres to decimetres), so that the calculated chloride distribution can match the observed chloride distribution.

Numerical instabilities in the velocity field occur due to a combination of both density flow and the numerical solution technique. The numerical instabilities due to density flow especially arise in those places where the transition zone between fresh and saline groundwater is small. The fluctuations in vertical velocities in those unstable zones can be counteracted by adapting several model parameters. Increasing the number of particles per grid cell is the most effective, followed by the length of the flow time step, and then by the convergence criterion TOL. Smoothing the initial density distribution also suppresses numerical instabilities in the velocity field. Reducing the dimension of the grid cells is usually only effective in combination with shortening the length of the flow time step.

Chapter 8

Simulation of two profiles perpendicular to the Dutch coastline

8.1 Introduction

The main objective of this chapter is to assess, by means of numerical modelling with the adapted MOC model, the impact of six scenarios of sea level rise on the following two vulnerable groundwater flow regimes perpendicular to the Dutch coastline during the next millennium:

1. a profile in the southern part of Noord-Holland from the coast through the intake area of Gemeentewaterleidingen Amsterdam, several polder areas behind the sand-dune area to the Vinkeveense plassen (a lake area) in the province of Utrecht. The length of the profile is 39,000 m.

   This profile resembles very much the profile in chapter 7. The reason[1] why the length of this profile is longer than that of the profile in chapter 7 is to assure that the inland boundary, which is situated far from the coast, does not affect the propagation of sea level rise in the geohydrologic system.

2. a profile in the northern part of Noord-Holland from a narrow sand-dune area near Petten to Enkhuizen at the IJsselmeer. The length of the profile equals 44,500 m.

In the sections 8.2 and 8.3, the impact of sea level rise on the two profiles is discussed. Moreover, an limited parameter analysis is carried out. The interest is focused on the following items:

---

[1] At the beginning of this study, the interest was focused only on the impact of sea level rise during just the next century. This implied that the sea level would rise only some decimetres. However, the first simulation results demonstrated that the changes in chloride distribution appeared to be insignificant during the next century. In order to observe substantial changes, the total simulation time was extended several centuries, which implied that the sea level would rise several metres. As a consequence, the inland boundary at x=12,500 m from the coast, as applied in the profile of chapter 7, could not be applicable any more. Therefore, the boundary was removed more inland, namely 39,000 m from the coast, where the conditions could be kept constant during the simulations. This is the profile in section 8.2.

233

a. propagation of sea level rise in the piezometric level distribution, thus the extent of the zone of influence of sea level rise is assessed.

b. changes in the chloride distribution, especially the salt water intrusion in the deep aquifers.

c. changes in the volumes of fresh, brackish and saline groundwater, that is the freshwater lens in the sand-dune area of Gemeentewaterleidingen Amsterdam (section 8.2).

d. changes in the seepage (both quantity and quality) in the low-lying polder areas, namely the Haarlemmermeer polder (section 8.2) and the polder area near Schagen (section 8.3).

e. effects of (hypothetical) countermeasures for the negative impact of sea level rise, such as extraction of saline groundwater, artificial recharge of fresh surface water (deep-well infiltration), raising the phreatic groundwater levels, and reclamation of land in front of the coast (only in section 8.2).

8.2   Profile to the Vinkeveense plassen

The selected groundwater flow regime is situated through the sand-dune area of Gemeentewaterleidingen Amsterdam with its thick freshwater lens, the Rijnland polders, the low-lying Haarlemmermeer polder to the polder and lake areas (the Groot-Mijdrecht polder and the Vinkeveense plassen) situated more inland (figure 8.1).
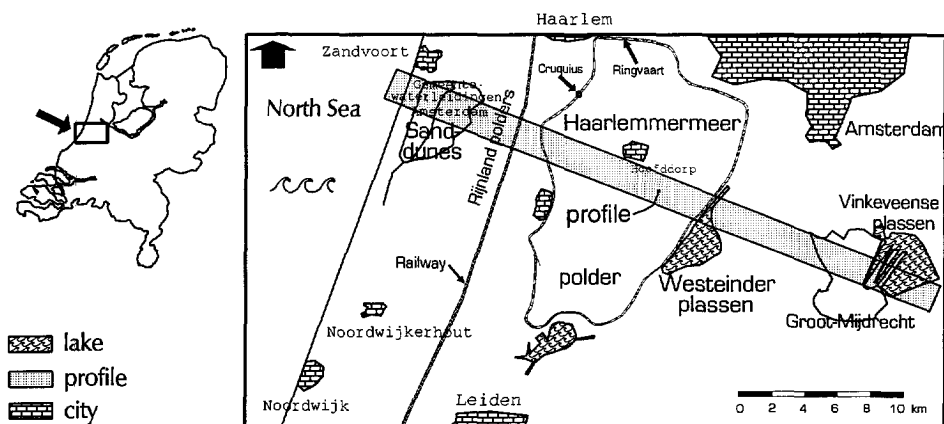

Figure 8.1: Map with the sand-dune area of Gemeentewaterleidingen Amsterdam, the Haarlemmermeer polder, and the polder and lake areas lying more inland.

This area is chosen because it contains some representative characteristics of groundwater flow regimes in Noord and Zuid-Holland (see figure 1.3): a freshwater

lens in the sand-dune area along the coast, and more inland relatively high seepage in the low-lying polder areas and surface water infiltration in relatively high-lying lakes. Moreover, the sand-dune area of Gemeentewaterleidingen Amsterdam has been investigated intensively, thus numerous subsoil parameters are known. The Groot-Mijdrecht polder, which is situated at some 30,000 m from the coastline, was reclaimed during the period 1872-1877. As it is a very low-lying polder (the controlled phreatic groundwater level varies between -5.60 and -6.25 m $N.A.P.$) and the hydraulic resistance of the Holocene aquitard is very low (order of magnitude: some tens to some hundreds of days), the seepage quantity is high, more than 5 mm/d.

The profile of this geohydrologic system is 39,000 m long, because the inland boundary must be located beyond the zone of influence of sea level rise. The supposition, that the groundwater flow perpendicular to the profile must be neglected, is not valid any more in all places of this entire geohydrologic system. Therefore, the interest in this study is mainly focused on the impact of sea level rise for about only the first tens of kilometres from the coast, where the supposition can still be justified.

In subsection 8.2.1, the geohydrologic system of the reference case is schematised, and relevant subsoil and model parameters are summarized. In subsection 8.2.2, the calibration of the geohydrologic system is discussed by means of two approaches: the piezometric levels and the groundwater flow through the Holocene aquitard. In subsection 8.2.3, a brief subsoil and model parameter analysis is executed. In subsection 8.2.4, the results follow of the simulated geohydrologic system for the year 1990, thus without sea level rise. In subsection 8.2.5, the impact of different sea level rise scenarios is quantified on the items of interest. In subsection 8.2.6, the effects of several (hypothetical) countermeasures are described. Finally, in subsection 8.2.7, some conclusions are drawn and a recommendation is given.

8.2.1   Schematisation

Subsoil parameters of the reference case

Figure 8.2 shows the geometry and subsoil parameters of the profile. The data of the geohydrological schematisation have been borrowed from the following sources: Kooiman [1989], Stuyfzand [1988], ICW [1976] and TNO Institute of Applied Geoscience [1979a]. For the first 12,500 m of the profile, the study of Kooiman [1989] is pursued (see also chapter 7). The longitudinal dispersivity α_L is set to a small value: 0.02 m [Kooiman, 1989]. The ratio transversal to longitudinal dispersivity α_T/α_L is set to 0.1 (−). The anisotropy factor k_z/k_x (the ratio vertical and horizontal hydraulic conductivity) is set to 0.1 (−). The effective porosity n_e equals 0.35 (−) and the specific storativity S_s is set to zero.

Figure 8.3 shows the chloride distribution of the profile in 1990, derived from ICW [1976], Stuyfzand [1988] and van Koppen [1985]. A freshwater lens occurs in the sand-dune area of Gemeentewaterleidingen Amsterdam. The inflow of saline groundwater from the sea in the geohydrologic system has increased due to the low
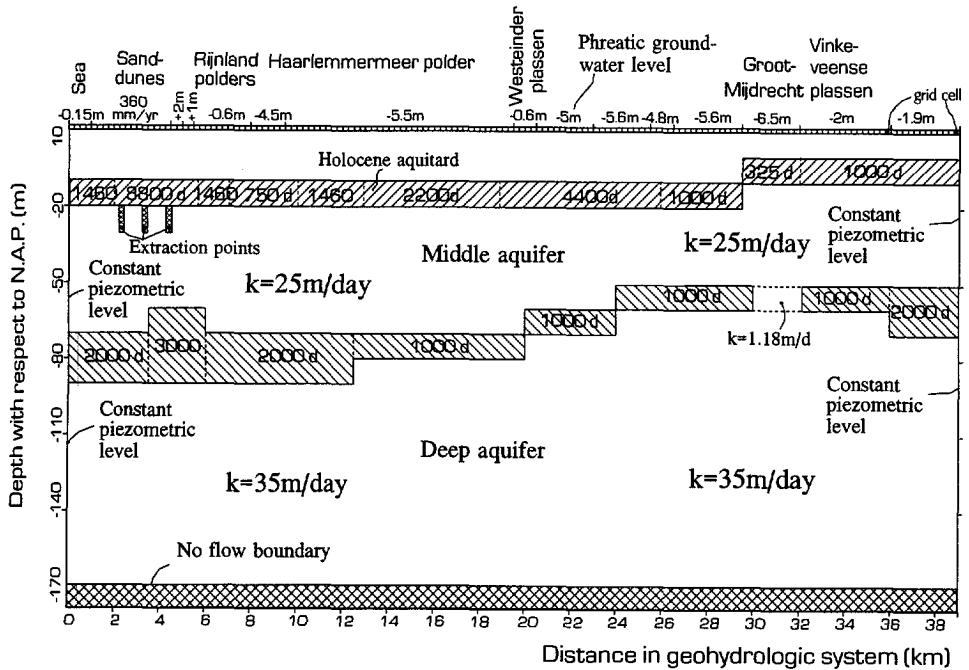
Figure 8.2: Subsoil parameters of the profile through the sand-dune area to the Vinkeveense plassen.

phreatic groundwater level in the Haarlemmermeer polder. Subsequently, a severe salt water intrusion occurs (see the 15,000 mg Cl^-/l-isochlor). Saline groundwater cones up in both the Haarlemmermeer polder and the Groot-Mijdrecht polder.

The phreatic groundwater levels in the polder and lake areas are derived from ICW [1976]. The levels at the upper boundary are kept constant during the simulation of the reference case. The groundwater recharge in the phreatic aquifer of the sand-dune area is 360 mm/yr. Three lines of extraction wells are placed in the middle aquifer of the sand-dune area, each line with a rate of about 64.1 $m^3/(m'yr)$. A constant piezometric level boundary is introduced for both the seaside boundary and the inland boundary. The situations are supposed to be hydrostatic. The piezometric level at the North Sea side is set to -0.15 m $N.A.P.$[2] and at the inland side to -1.90 m $N.A.P.$

Model parameters of the reference case

The applied number of rectangular grid cells is 2808: in horizontal direction 156 and in vertical direction 18 grid cells. Each grid cell has a length Δx of 250 m and a

---

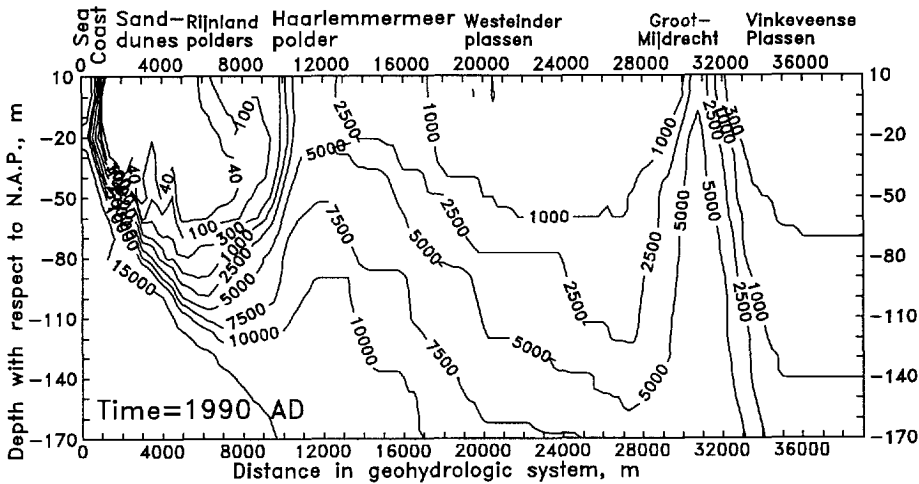[2]The average water level of the sea is not equal to $N.A.P.$ [Atlas van Nederland: Deel 15 Water, 1986].

Figure 8.3: Initial chloride distribution (values in $mg\ Cl^-/l$) in 1990.

height Δz of 10 m, thus the total geohydrologic system is 39,000 m long and 180 m high. Each grid cell contains five particles. The convergence criterion TOL is 10^{-5} ft. The flow time step Δt equals 1 $year$. The maximum relative distance in a grid cell ζ is set to 0.9. Under normal conditions, only two solute time steps are necessary to simulate solute transport during one flow time step.

8.2.2 Calibration

The calibration of this profile is carried out for piezometric levels at some depths relative to $N.A.P.$ and for seepage and infiltration intensities through the Holocene aquitard. The chloride distribution of the profile near the coastal zone was calibrated in the study of Kooiman [1989] at certain moments in time during the past (see section 7.4).

1. Piezometric levels at -25 m and -80 m with respect to N.A.P.

Figure 8.4 shows the piezometric levels, expressed in freshwater, at -25 m and -80 m $N.A.P.$. The levels, calculated with the adapted MOC model, are compared with measured piezometric levels [ICW, 1976 and Stuyfzand, 1988]. The measured piezometric levels are corrected for the density of groundwater in the observation well which differs from the standard reference density $\rho_f = 1000\ kg/m^3$. The (corrected) measured piezometric levels differ only some decimetres from the calculated piezometric levels. Only near and in the Groot-Mijdrecht polder and the Vinkeveense plassen the differences are greater than some decimetres, probably due to the following two reasons: (1) the simulated hydraulic resistance of the Holocene aquitard is too high, and (2)
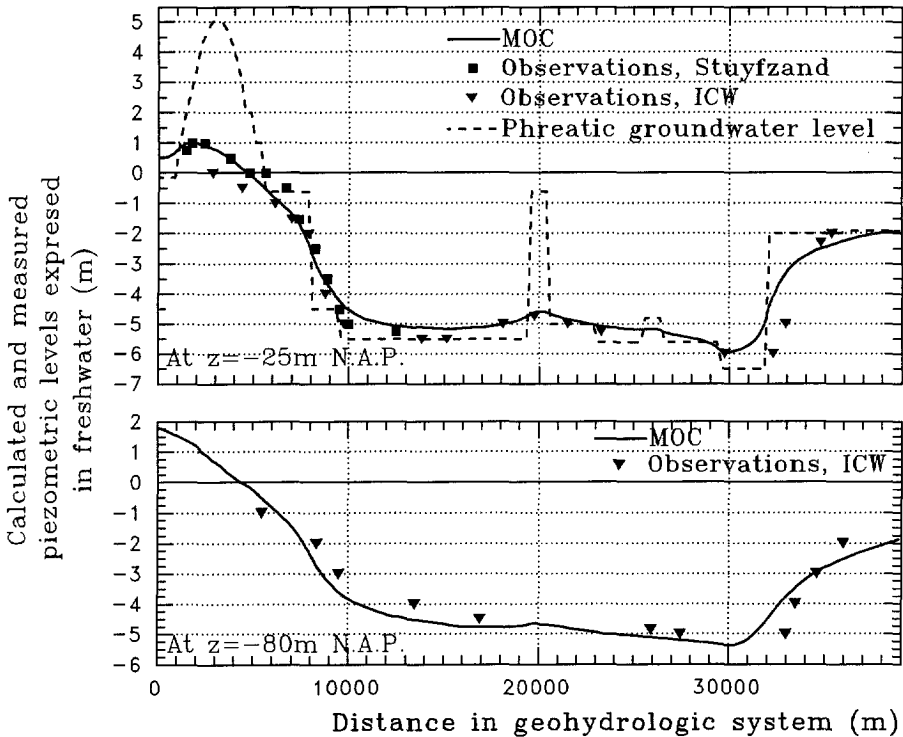
Figure 8.4: Calculated and measured piezometric levels, expressed in freshwater, at -25 and -80 m $N.A.P.$ The observations of Stuyfzand are only given in the first kilometres from the coast.

in the vicinity of the Groot-Mijdrecht polder groundwater flow perpendicular to the profile is not anymore of marginal importance.

2. Seepage and infiltration intensities through the Holocene aquitard

Figure 8.5 shows the (calculated) seepage and infiltration intensities at -15 m $N.A.P.$ The deep groundwater percolation through the Holocene aquitard in the sand-dune area of Gemeentewaterleidingen Amsterdam, calculated with the adapted MOC model, is about 700 $m^3/(m'yr)$ in 1990. Schuurmans [1983], who based his figure on water balances in the area, estimates about 785 $m^3/(m'yr)$ (see also table 7.1).

However, the hydraulic resistance of the Holocene aquitard in the profile varies significantly over short reaches. As a result, the calculated seepage intensities through the Holocene aquitard in the Haarlemmermeer polder cannot easily be matched with observed seepage intensities, which are determined by means of water balances of
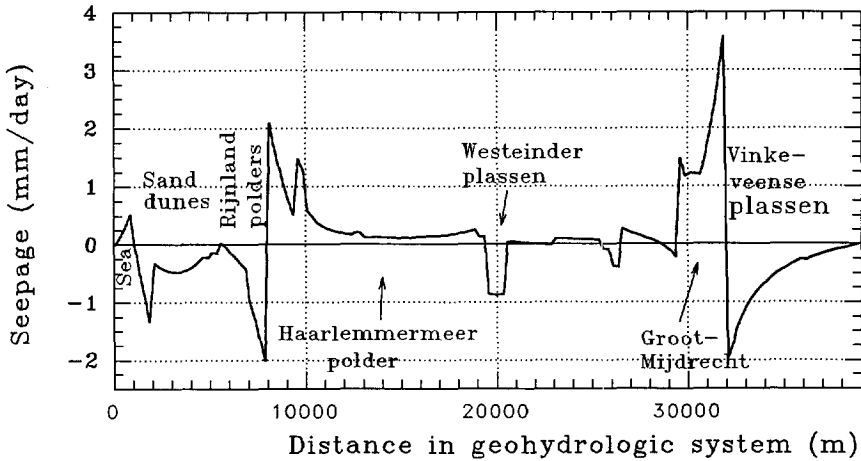
Figure 8.5: Calculated seepage and infiltration intensities at -15 m $N.A.P.$

specific subareas. In fact, the scale of the present schematisation of the geohydrologic system is too large (e.g. the length of a grid cell is 250 m) to describe local details. Nevertheless, the calculated seepage intensity in the Haarlemmermeer polder is in good agreement with the observed values. The overall influence of the local details in subsoil parameters on the deep groundwater flow appears to be of minor importance. Only in the Groot-Mijdrecht polder, the calculated seepage intensity appears to be too small, since the actual hydraulic resistance in situ seems to be (much) lower than the one applied in the model.

In figure 8.6, the differences are compared between the reference case and a case where the hydraulic resistances are lowered in specific segments of both the Haarlemmermeer polder and the Groot-Mijdrecht polder. In these specific segments of both polders, seepage and infiltration intensities are substantially higher in the case with lower hydraulic resistances than in the reference case. The average seepage intensity of the Groot-Mijdrecht polder is more in accordance with the observed seepage intensity in this case than in the reference case.

8.2.3 Parameter analysis

The influence of the following three parameters are briefly analysed: (1) hydrodynamic dispersion; (2) density differences; and (3) the error in the solute mass balance.

1. Hydrodynamic dispersion

The influence of the hydrodynamic dispersion on the salinisation of the geohydrologic system is assessed by simulating cases with different longitudinal dispersivities α_L. Figure 8.7 shows that the greater α_L, the greater the volume of brackish groundwater
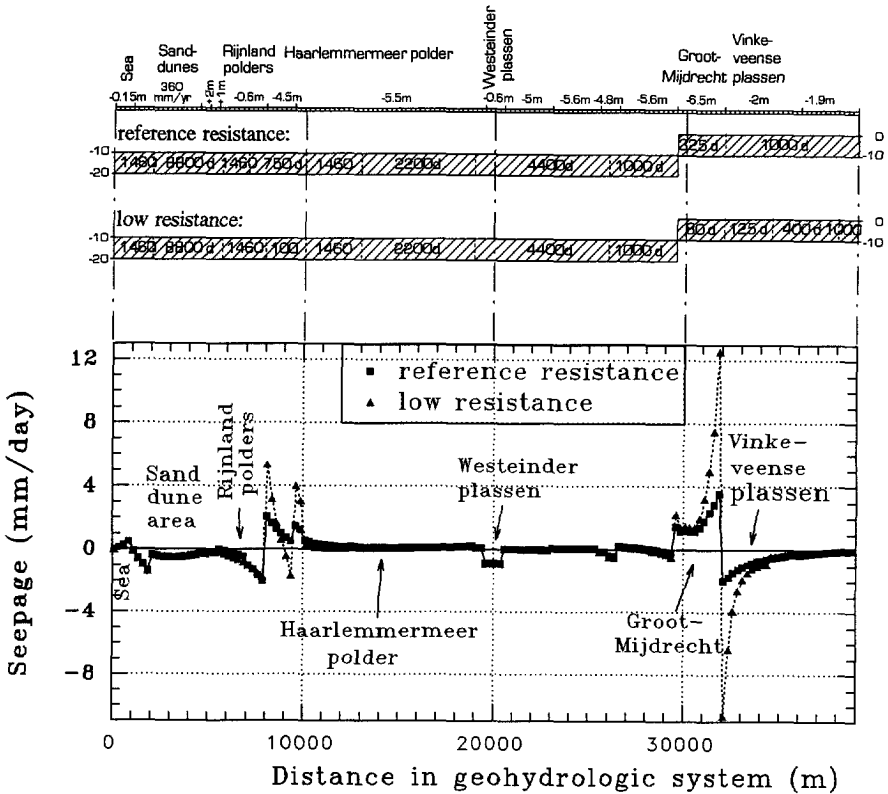
Figure 8.6: Calculated seepage and infiltration intensities at -15 m $N.A.P.$ for different hydraulic resistances of specific segments of the aquitard.

becomes in the geohydrologic system. For the two cases with great longitudinal dispersivities (α_L=2.0 m and α_L=20.0 m), the position of the *saline groundwater tongue* (the 15,000 mg Cl^-/l-isochlor) in the deep aquifer displaces in the direction of the seaside boundary during the next millennium. This phenomenon hardly seems to be realistic.

Obviously, the effect of molecular diffusion D_d on the salinisation process appears to be of minor importance. Figure 8.8 displays the difference in chloride distribution between the reference case with α_L=0.02 m and a case with only a molecular diffusion coefficient D_d equal to $1 \cdot 10^{-9}$ m^2/s.

2. Density differences

Figure 8.9 shows the influence of density differences on the geohydrologic system. This hypothetical case indicates the importance of taking into account density differences
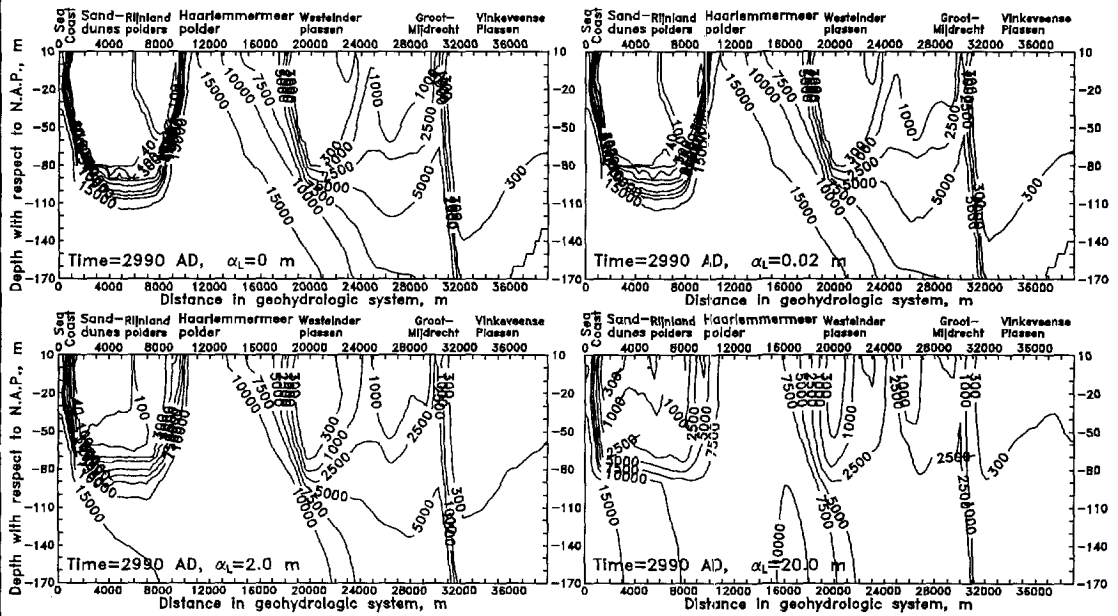
Figure 8.7: Chloride distributions (in $mg\ Cl^-/l$) in 2990, calculated with four different longitudinal dispersivities: α_L=0.0 m, α_L=0.02 m, α_L=2.0 m and α_L=20.0 m.

Figure 8.8: Influence of molecular diffusion D_d on the chloride distribution. The difference in chloride concentration (values in $mg\ Cl^-/l$) is given between the reference case with α_L=0.02 m and a case with α_L=0 m and D_d=1 · 10^{-9} m^2/s.

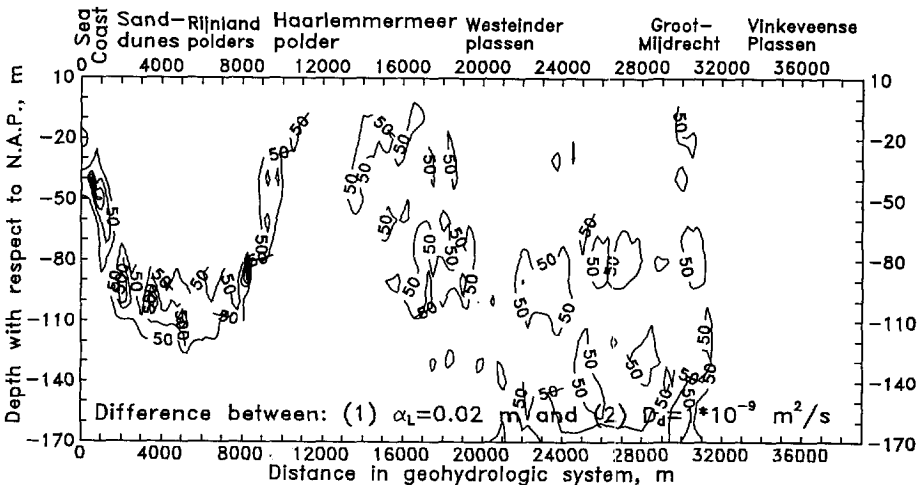in the coastal groundwater flow regimes in the Netherlands. If no density differences are taken into account $((\rho_s - \rho_f)/\rho_f = 0.0$ instead of 0.025), no salt water intrusion from the seaside boundary would occur, because natural groundwater recharge in the sand-dune area would dominate the entire flow regime in the vicinity of the coast. If the relative density difference is greater than in the reference case $((\rho_s - \rho_f)/\rho_f = 0.035$ instead of 0.025) a stronger inflow of saline groundwater occurs. As a consequence, the volume of the freshwater lens is substantially smaller and the seepage in the Haarlemmermeer polder consists of slightly more solutes.
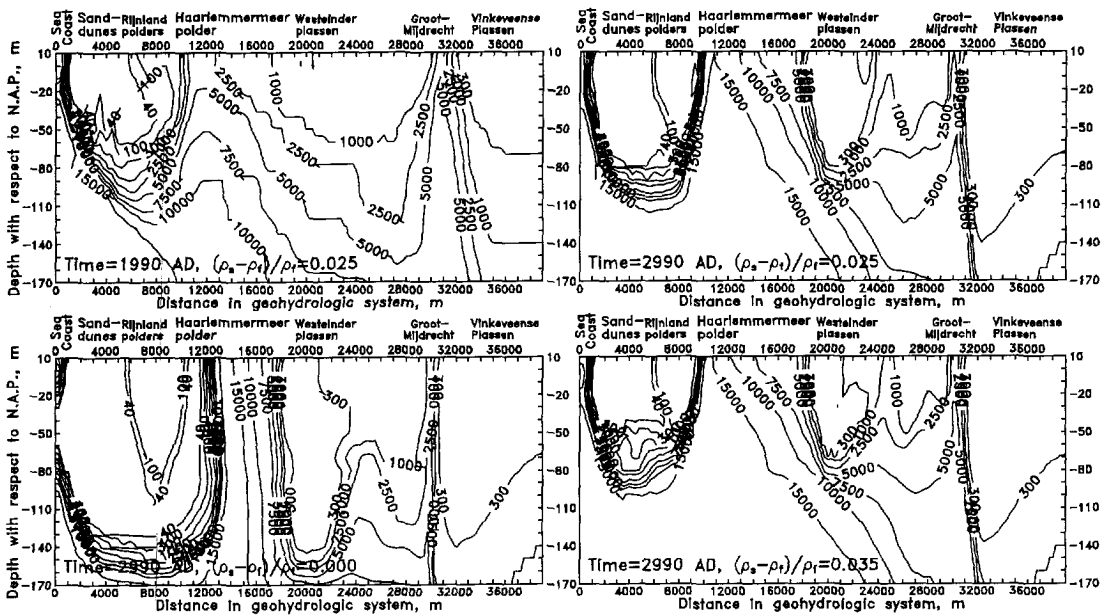

Figure 8.9: Influence of density flow on the chloride distribution (values in $mg\ Cl^-/l$) for cases with a relative density difference $(\rho_s - \rho_f)/\rho_f$ of 0.025 (the reference case: moments in time 1990 AD and 2990 AD); no density difference (2990 AD); and $(\rho_s - \rho_f)/\rho_f$ of 0.035 (2990 AD).

3. Error in the solute mass balance

The accuracy of the solution of the solute transport is assessed by comparing the reference case with a case with more accurate model parameters, namely 16 particles per grid cell instead of 5 and TOL is $10^{-10}\ ft$ instead of $10^{-5}\ ft$. Figure 8.10 shows that the error in the solute mass balance increases as a function of time for both cases: up to about 3 % in 2990. The difference in the error in solute mass balance between the reference case and the accurate case is insignificant.
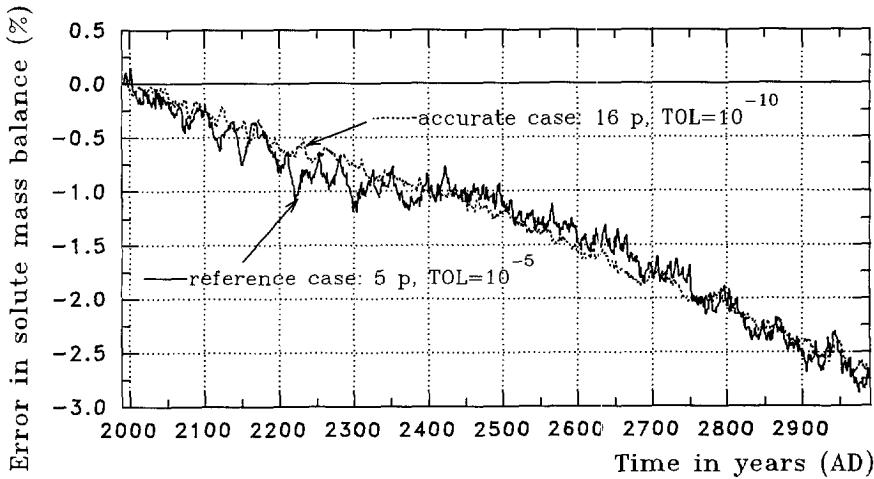
Figure 8.10: Error in the solute mass balance. The reference case is compared with the accurate case (16 instead of 5 particles per grid cell and $TOL=10^{-10}$ ft instead of 10^{-5} ft). One millennium is simulated.

8.2.4   Results of the simulated profile

Piezometric level distribution expressed in freshwater

Figure 8.11 shows the piezometric level distribution in 1990, expressed in freshwater (corrected for density differences), calculated with the adapted MOC model. A hydrostatic situation occurs at both the seaside and the inland boundary. Clearly, the low phreatic groundwater levels in both the Haarlemmermeer polder and the Groot-Mijdrecht polder induce low piezometric levels in the underlying aquifers.

Velocity field

Figure 8.12 shows the velocity field in the geohydrologic system in 1990. In the sand-dune area, a downward groundwater flow occurs through the Holocene aquitard. Saline groundwater intrudes in the deep aquifer at the seaside boundary. Ground-water flows upward as seepage in the Haarlemmermeer polder. Especially in the segment closest to the seaside, the seepage quantity is high due to the low hydraulic resistance of the Holocene aquitard. A very strong groundwater flow occurs in the Groot-Mijdrecht polder due to a combination of the low phreatic groundwater level, the low hydraulic resistance of the Holocene aquitard and an opening in the deep aquitard. Note that in some areas the velocities fluctuate in vertical direction, which is the result of numerical instabilities.
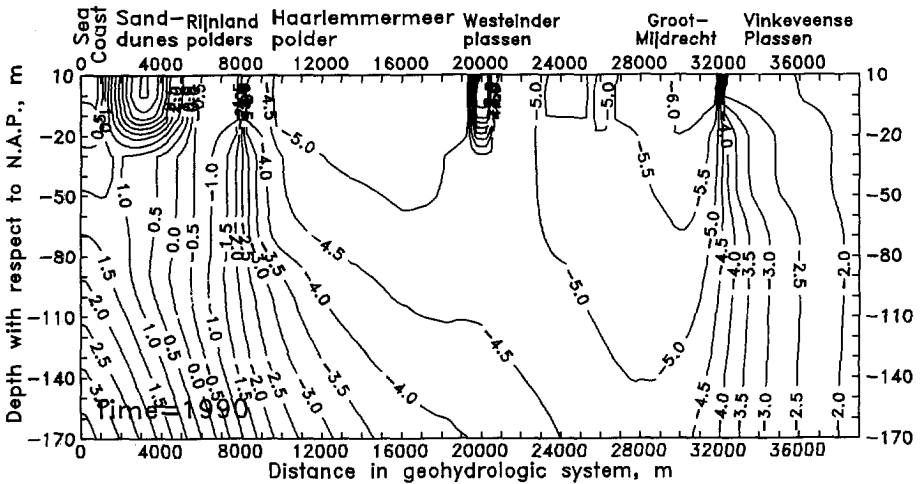
Figure 8.11: Calculated piezometric level distribution in 1990 (in m), expressed in fresh-water, of the geohydrologic system.

Groundwater fluxes

The groundwater fluxes over the following four segments of the geohydrologic system are analysed in table 8.1:

1. inflow of saline groundwater at the seaside boundary in the deep[3] aquifer between -90 and -170 m $N.A.P.$

2. deep groundwater percolation[4] in the sand-dune area through the Holocene aquitard in the reach 1000-4500 m.

3. seepage quantity through the Holocene aquitard in the Haarlemmermeer polder in the reach 8000-19,500 m.

4. seepage quantity through the Holocene aquitard in the Groot-Mijdrecht polder in the reach 29,500-32,000 m.

The groundwater fluxes in the geohydrologic system are analysed for (a) the reference case and for three (hypothetical) cases[5]: (b) no density flow; (c) inundation of the Haarlemmermeer polder (the phreatic groundwater level equals -0.6 m $N.A.P.$); and (d) inundation of the Groot-Mijdrecht polder (the phreatic groundwater level equals -0.6 m $N.A.P.$). The hypothetical case (b) indicates what happens if the effect of

---

[3] In the shallow aquifer between -20 and -70 m $N.A.P.$, the inflow of saline groundwater is limited due to the outflow of fresh groundwater from the sand-dune area, and hence, it is not considered.

[4] As defined in section 7.4 item 4., page 206.

[5] The hypothetical cases are simulated only to demonstrate the sensitivity of the groundwater flow regimes for changes in (boundary) conditions.
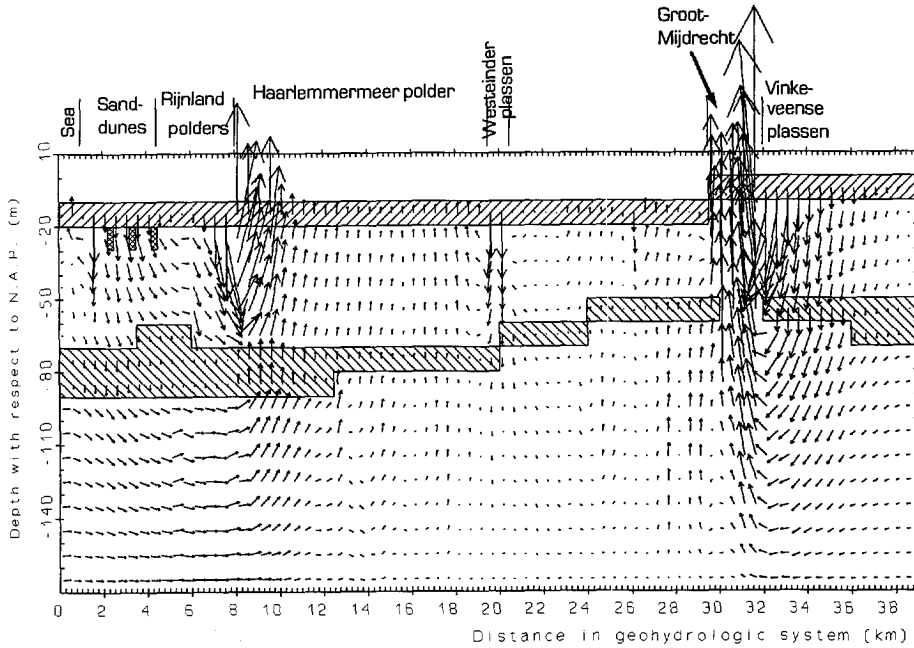
Figure 8.12: Velocity field in the entire geohydrologic system in 1990. The lengths of the arrows correspond with the displacement of groundwater during a time step of 20 years, beginning in 1990 and with a constant velocity field. The distortion of the vertical direction with respect to the horizontal direction equals a factor 110. The velocity is displayed in the center of every second horizontal grid cell.

density differences is not taken into account in this coastal groundwater flow regime, whereas the cases (c) and (d) demonstrate the substantial influence of the two low-lying polders on the groundwater flow in the geohydrologic system.

   Table 8.1 shows that, obviously, the differences in density cause a strong inflow of saline groundwater in the deep aquifer and reduce the deep groundwater percolation in the sand-dune area. Moreover, the present low phreatic groundwater levels in both the Haarlemmermeer polder and the Groot-Mijdrecht polder induce high seepage intensities. The low phreatic groundwater level in the Haarlemmermeer polder (with its western boundary situated at $x=8000\ m$) appears to cause a strong inflow of saline groundwater in the deep aquifer, namely the inflow of saline groundwater decreases from 417 to 222 $m^3/(m'yr)$ in case the phreatic groundwater level is raised from -5.5 (and -4.5 m) $N.A.P.$ to -0.6 $m\ N.A.P.$ Inundation of the low-lying polders (Haarlemmermeer as well as Groot-Mijdrecht) induces high infiltration rates of surface water, as can be seen by comparing the seepage quantities: from +1694 to -634 $m^3/(m'yr)$ for the Haarlemmermeer polder and from +1657 to -2601 $m^3/(m'yr)$ for the Groot-Mijdrecht polder.

Table 8.1: Groundwater fluxes in $m^3/(m'yr)$ in 1990 over four segments of the geohydro-logic system: the reference case and three other cases. Note that the error in the water balance between the incoming and outgoing groundwater volumes is insignificant.

Groundwater fluxes over segments:	(a) Reference case	(b) No density flow	(c) Inundation Haarl. meer -0.6 m	(d) Inundation Gr.-Mijdrecht -0.6 m
1. Inflow of saline groundwater	417	61	222	416
2. Percolation in sand-dune area	699	822	642	699
3. Seepage Haarlemmermeer	+1694	+1672	-634	+1806
4. Seepage Groot-Mijdrecht	+1657	+1980	+1751	-2601

8.2.5   Impact of sea level rise

In this subsection, the simulations of the geohydrologic system during the next millennium are discussed, though the interest is especially focused on the next century. As many prognoses of future sea level rise are conceivable (see section 3.6), six scenarios of sea level rise are imposed (see figure 8.13): -0.6 m/c; 0 m/c; 0.15 m/c; 0.6 m/c; 1.0 m/c; and 1.5 m/c. The simulations are initiated at the beginning of 1990. Sea level rises are imposed as step by step elevations of the piezometric level, expressed in freshwater head, at the seaside boundary for every 25 years. The first elevation takes place at the beginning of 2015, thus no sea level rise is imposed over the period 1990-2015[6].

Since a relatively long period is simulated, all processes that affect the geohydro-logic system should be considered. However, in the reference case, some processes are left out of consideration: for instance, hydrological processes (e.g. less precipitation, more evapotranspiration due to climate change), morphological processes (e.g. land-subsidence; shoreline retreat) and man-induced processes (e.g. reclamation of new land in front of the coast, sand-suppletion at the coast and creation of new sand-dune areas to counteract shoreline retreat).

Sea level rise induces a rise of the phreatic groundwater level in the sand-dune area. In reality, the rise of the phreatic groundwater level could be impeded due to a fixed land surface. In those places, sand-suppletion is supposed to nullify the possible impediment of the rise of the phreatic groundwater level.

Piezometric level expressed in freshwater and the zone of influence

Figure 8.14 shows the difference in piezometric level, expressed in freshwater, at -25 m $N.A.P.$ in 2090 for five scenarios of sea level rise with respect to the scenario with

---

[6]The sea level has risen some 0.1 m/c to 0.2 m/c over the past century (see section 3.5 item 3. The past few centuries, page 82). This fact is taken into account in the determination of the mean sea level at the beginning of the simulations in 1990.
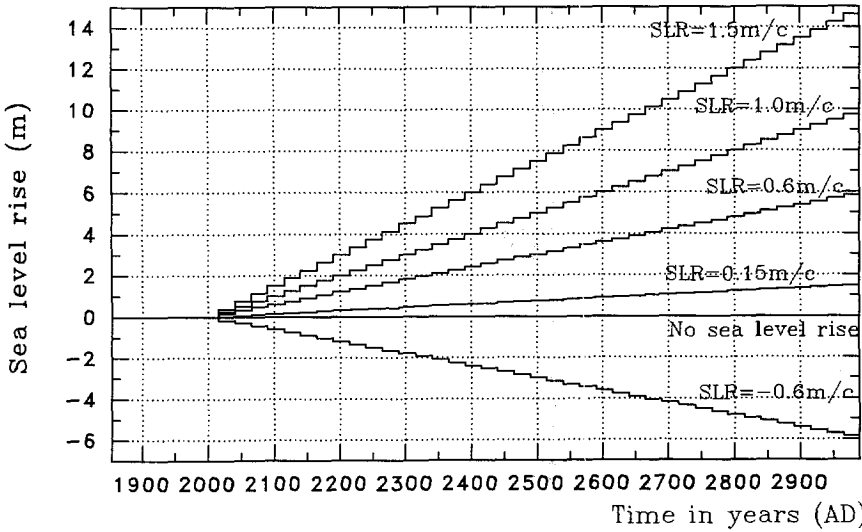
Figure 8.13: Scenarios of sea level rise, imposed at the seaside boundary during the next millennium.
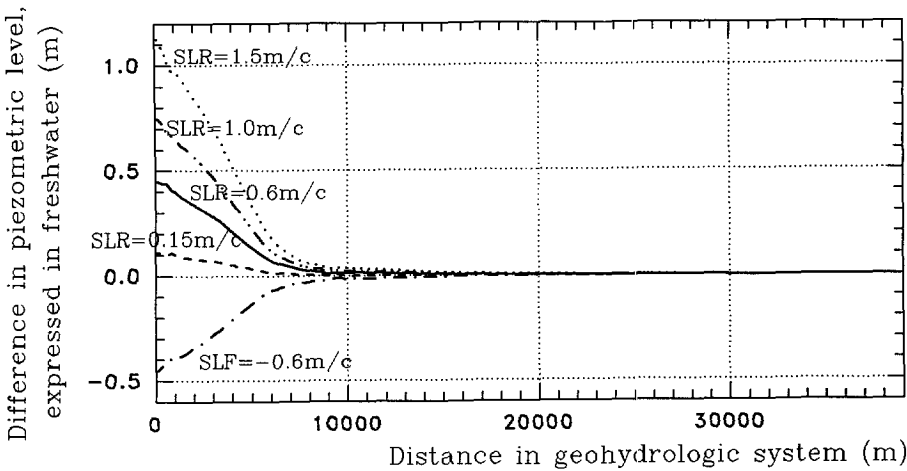
Figure 8.14: Differences in the piezometric level, expressed in freshwater, at -25 m $N.A.P.$ in 2090 for five scenarios of sea level rise with respect to the scenario with no sea level rise.

no sea level rise. Since the inland boundary is a constant piezometric level boundary for all scenarios, the rise in piezometric level at x=39,000 m from the seaside is equal to zero. The figure displays that the zone of influence of sea level rise in the geohydrologic system is some 8000 to 10,000 m. For instance, at 8500 m inland of

the seaside boundary, the rise in piezometric level is only about 5 % of the rise in sea level.

Path lines in the geohydrologic system

Figure 8.15 shows several path lines through the geohydrologic system during the next millennium for the reference case with no sea level rise. Saline groundwater particles enter the deep aquifer at the seaside boundary. The groundwater velocity is apparently small, e.g. a horizontal displacement of less than 20 *m per year* is rather common. A combination of three geohydrologic characteristics of the Groot-Mijdrecht polder causes a strong groundwater flow towards that polder: (1) the low phreatic groundwater level; (2) the low hydraulic resistance of the Holocene aquitard; and (3) an opening in the deep aquitard. Surface water infiltrates in the geohydrologic system in the Vinkeveense plassen and rapidly flows towards the Groot-Mijdrecht polder.
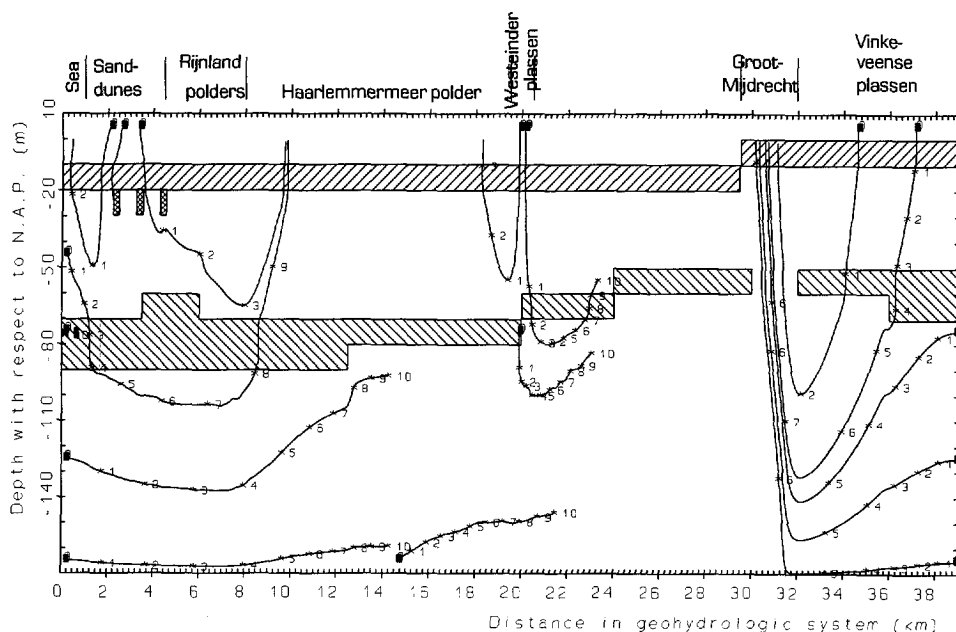
Figure 8.15: Some path lines and travel times in centuries through the geohydrologic system, calculated with a continuously adapted velocity distribution. The reference case with no sea level rise is simulated during the next millennium.

Figure 8.16: Chloride distribution (in $mg\ Cl^-/l$) in the geohydrologic system during the next millennium at different moments in time. The reference case with no sea level rise is simulated.

Chloride distribution

Figure 8.16 shows the chloride distribution during the next millennium for the reference case with no sea level rise. A severe salt water intrusion occurs in the geohydrologic system. Saline groundwater replaces brackish groundwater in the deep and middle aquifers behind the sand-dune area up to many kilometres inland. Nevertheless, the salinisation is a rather slow process. The freshwater lens not only remains during the next millennium but increases even slightly. This occurs as groundwater extraction rates during the past decades were higher than the rates that are applied in the reference case during the next millennium. Since the surface water level in the

Figure 8.17: Chloride distribution (in $mg\ Cl^-/l$) in the geohydrologic system during the next ten millennia at different moments in time. The reference case with no sea level rise is simulated.

Westeinder plassen (a lake area) and the Vinkeveense plassen is high with respect to their surroundings, fresh surface water infiltrates in the geohydrologic system. Subsequently, fresh groundwater bodies are formed under these lakes during the next millennium.

The chloride distribution is still changing after one millennium. This can be deduced from figure 8.17, where the change in chloride distribution is simulated during the next ten millennia for the reference case with no sea level rise. In the vicinity of the Groot-Mijdrecht polder, the state of dynamic equilibrium of the chloride distribution is reached after some seven to eight millennia. Saline groundwater is coning

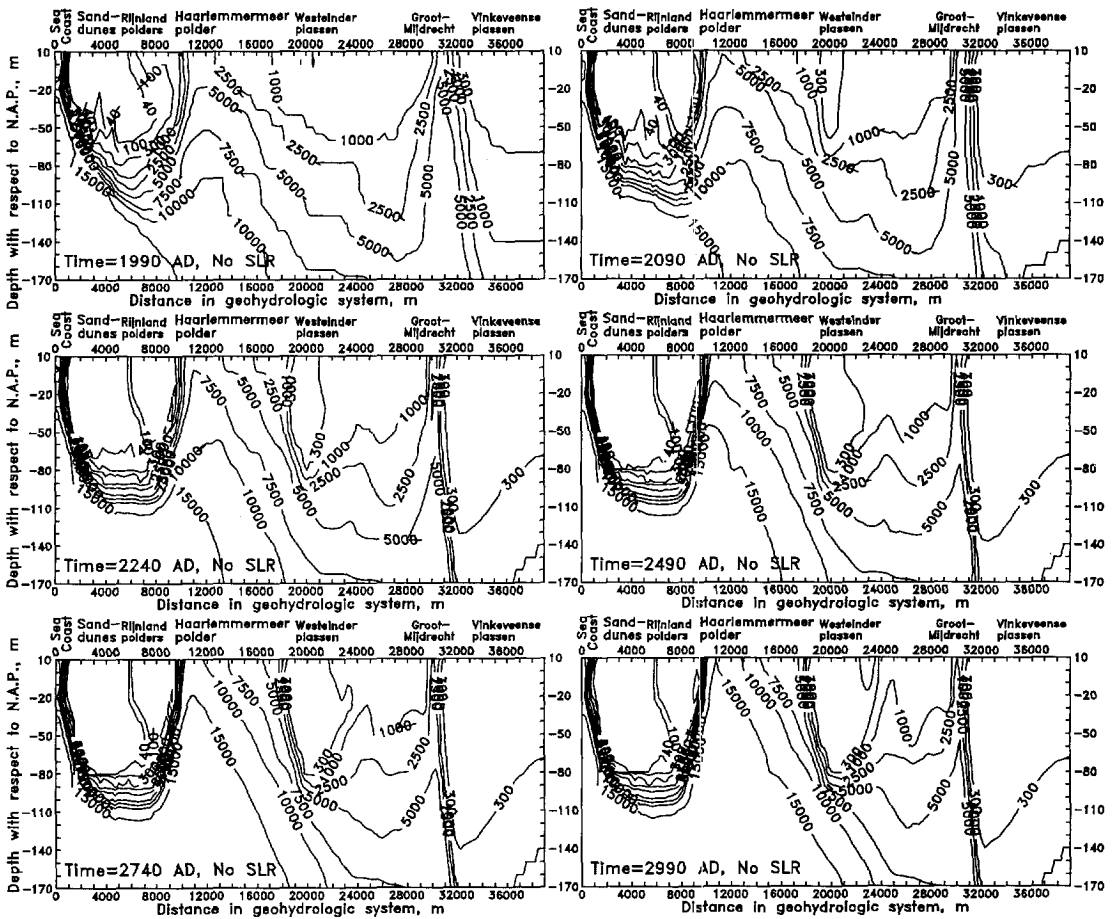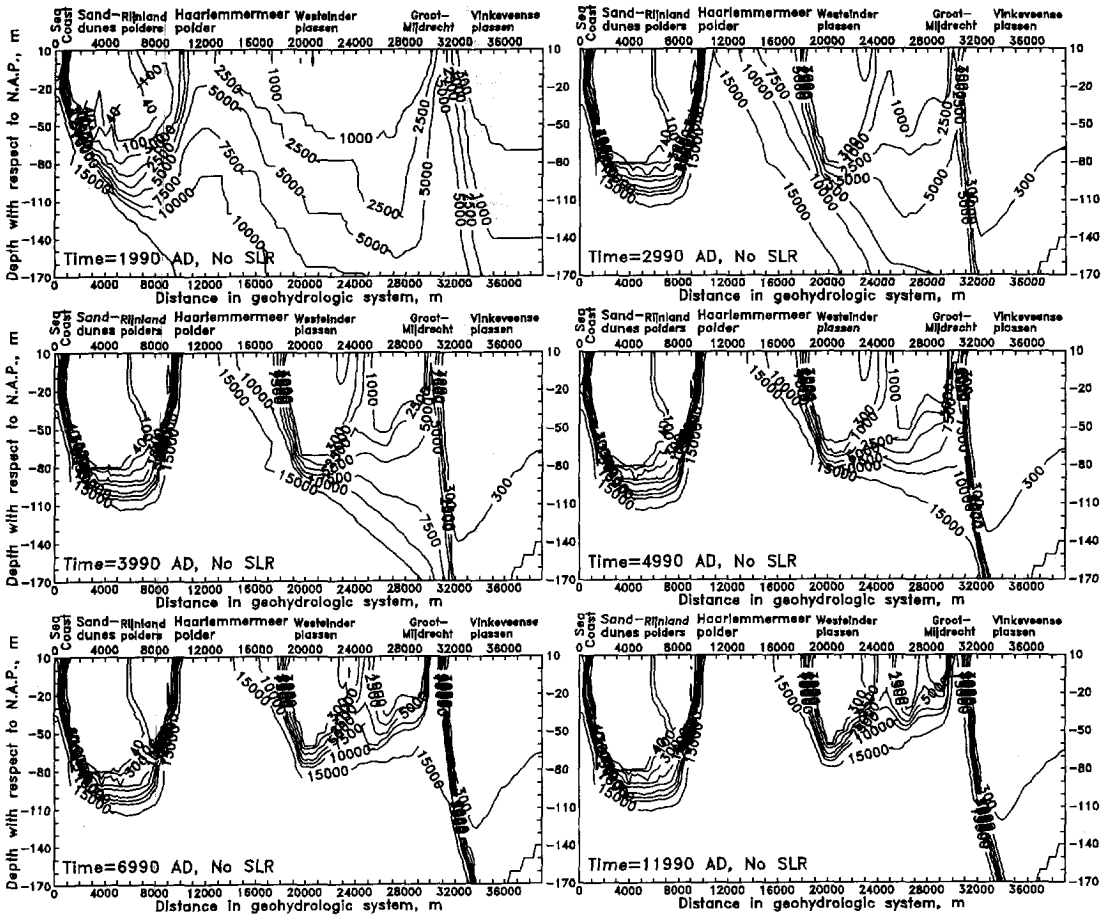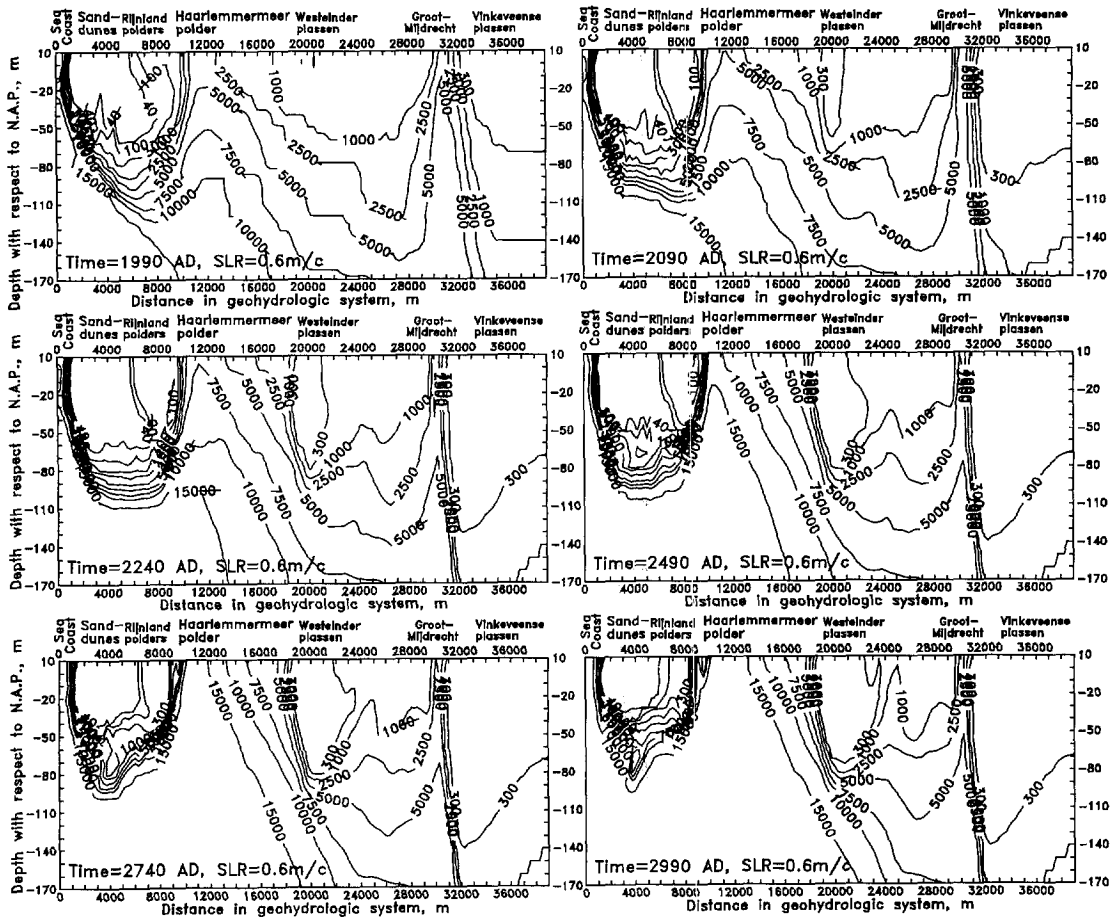**Figure 8.18**: Chloride distribution (in $mg\ Cl^-/l$) in the geohydrologic system during the next millennium at different moments in time. The constant rate of sea level rise is 0.6 m/c.

up in the Haarlemmermeer polder, because the polder water level is low and the hydraulic resistance of the Holocene aquitard is low. Saline groundwater, that originates from the sea, has reached the Haarlemmermeer polder after several centuries. As a result, seepage in this area consists of more chloride. Eventually, when the state of dynamic equilibrium is reached in this part of the geohydrologic system, the seepage in the central part of the Haarlemmermeer polder consists of saline groundwater (see figure 8.17).

Figure 8.18 shows the chloride distribution during the next millennium for the scenario with a sea level rise of 0.6 m/c. By comparing figure 8.18 with figure 8.16, it can be seen that the differences in chloride distribution between no sea level rise and

a sea level rise of 0.6 m/c appear to be small during the next centuries. However, after some more centuries, the freshwater lens diminishes and the seepage in the Haarlemmermeer polder consists of more saline groundwater due to sea level rise.

Figure 8.19 shows the chloride distribution in the geohydrologic system in 2990 for six scenarios of sea level rise. The influence of sea level rise can be neglected in the segment of the geohydrologic system that is situated more than about 20,000 m from the seaside boundary. However, it depends on the rate of sea level rise whether or not the freshwater lens in the sand-dune area remains during the next millennium. Furthermore, for all scenarios the seepage in the Haarlemmermeer polder consists of more brackish or saline groundwater than at present, though the quantity of seepage differs. The position of the saline groundwater tongue (15,000 mg Cl^-/l-isochlor) in the deep aquifer displaces from about 9500 m in 1990 (see figure 8.16) to about 19,500 m to 23,000 m in 2990 depending on the scenario of sea level rise: so with a rate of 1.0 km/c to 1.35 km/c for a sea level fall of -0.6 m/c and a sea level rise of 1.5 m/c respectively.

Volume distributions of fresh, brackish and saline groundwater

The change in chloride distribution due to sea level rise is quantified in figure 8.20 by calculating the distribution of fresh, brackish and saline water in percentages of the total volume of water in the geohydrologic system. In 2090, the differences in volume distribution between the six scenarios of sea level rise can still be neglected. Only after some more centuries, the differences in volumes become significant. The volume of brackish groundwater in the geohydrologic system decreases for all scenarios of sea level rise. Even when no sea level rise occurs, salinisation of the geohydrologic system clearly takes place during the next centuries compared to the situation in 1990. The reason for this is that the low-lying Haarlemmermeer polder has induced a strong inflow of saline groundwater from the seaside. Even when sea level falls, salinisation of the geohydrologic system is taking place during the next centuries. However, after some centuries (that is after 2540), less saline groundwater flows in the geohydrologic system from the sea than that saline and brackish groundwater flow out of the geohydrologic system through seepage. Consequently, the fraction of saline groundwater decreases. Note that no new state of dynamic equilibrium of the chloride distribution is reached during the next millennium (see figure 8.17).

Freshwater lens in the sand-dune area

Figure 8.21 shows the volume of the freshwater lens for six scenarios of sea level rise. Even when no sea level rise occurs, the volume of fresh groundwater slightly increases during the next centuries because lower groundwater extraction rates are simulated during the next millennium than during the period 1903-1973[7]. The change in volume

---

[7] The total extraction rate during the next millennium in the middle aquifer of the sand-dune area is about 192.3 $m^3/(m'yr)$ or about 1.73 million m^3/yr over 9000 m, see figure 7.2, page 197.
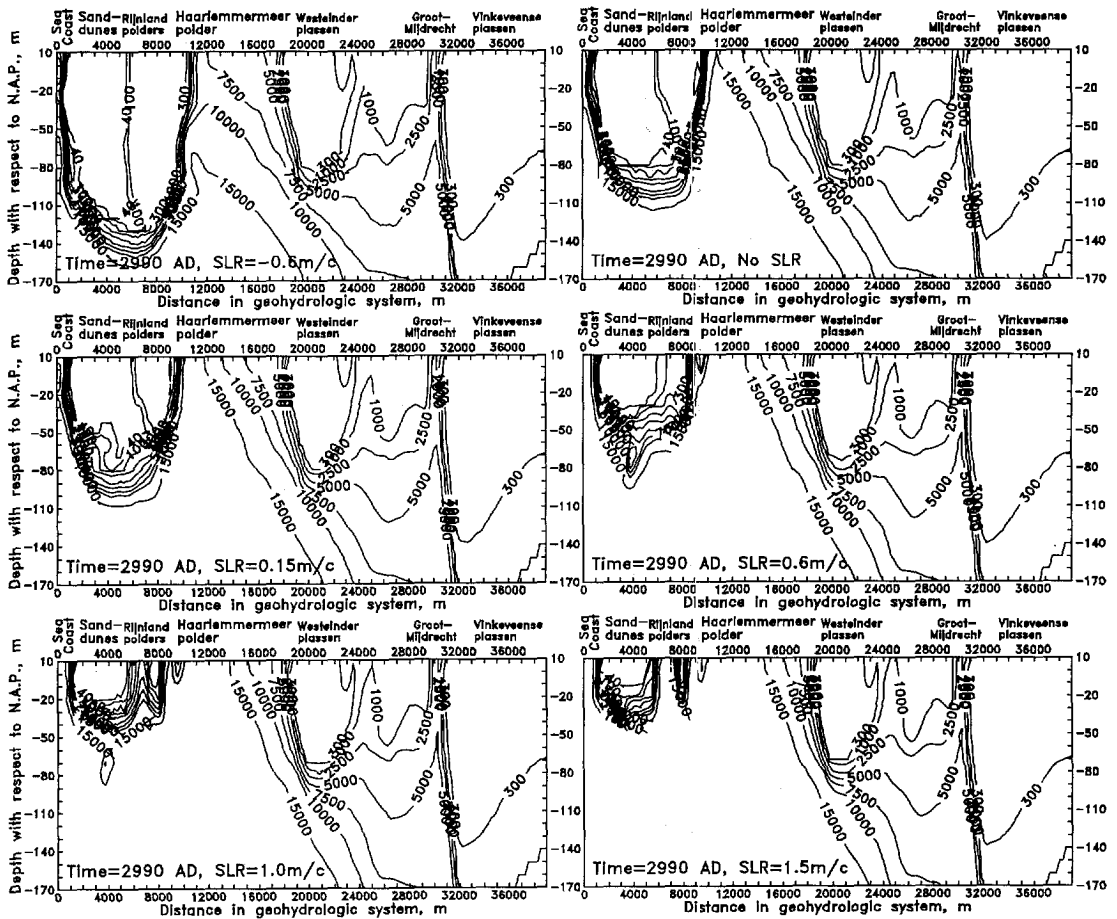
Figure 8.19: Chloride distribution (in $mg \ Cl^-/l$) in the geohydrologic system during the next millennium in 2990 for six scenarios of sea level rise.

of the freshwater lens due to sea level rise is of minor importance during the next two centuries. However, after a few centuries, the changes are considerable. For instance, when the sea level rises 0.6 m/c, the volumes of the freshwater lens in 2290 and 2990 decrease to about 87 % and 30 % respectively of the volumes of the freshwater lens when no sea level rise occurs.

Seepage quantity in the Haarlemmermeer polder

When no sea level rise occurs, the seepage quantity in the Haarlemmermeer polder decreases significantly during the next centuries (see figure 8.22). The reason for this
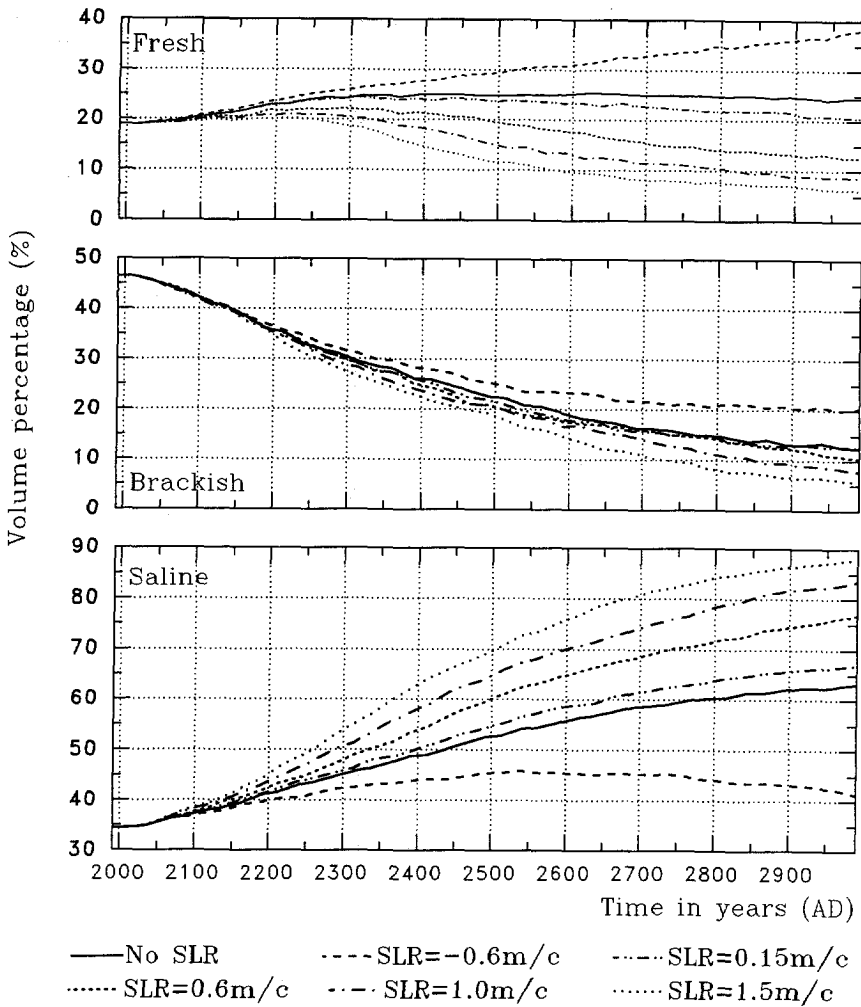
Figure 8.20: Volume percentages of fresh, brackish and saline groundwater during the next
millennium for six scenarios of sea level rise. The volume percentage is determined for the
segment of the geohydrologic system that is bounded in horizontal direction between $x=0$ m
and $x=19,500$ m (the inland side of the Haarlemmermeer polder) and in vertical direction
between $z=$-10 and $z=$-170 m $N.A.P.$

(unexpected) phenomenon is that salinisation of the geohydrologic system changes
the density distribution in especially the middle aquifer. As a result, groundwater
flow and seepage are influenced. When sea level rises, the seepage quantity in the
Haarlemmermeer polder increases substantially with respect to the reference case.
The increase in seepage quantity in the Groot-Mijdrecht polder due to sea level rise
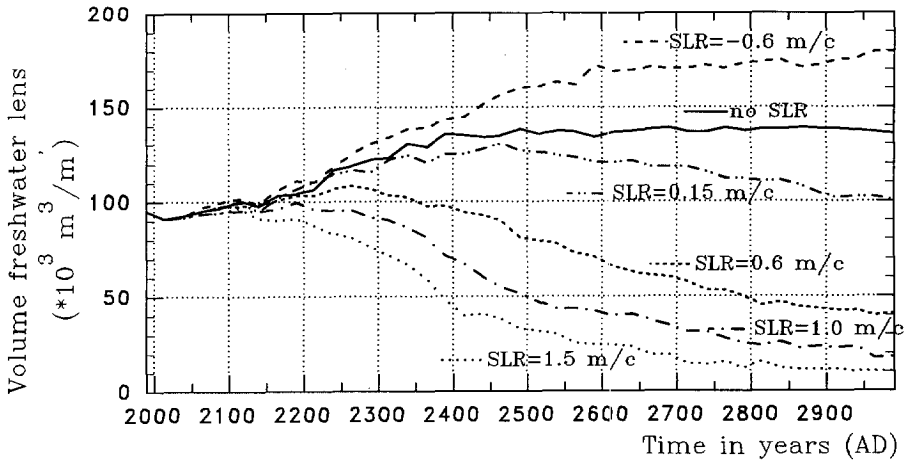
Figure 8.21: Change in the volume of the freshwater lens during the next millennium for six scenarios of sea level rise. For this special item, fresh groundwater is defined as ≤ 40 $mg\ Cl^-/l$. The considered segment is bounded in horizontal direction between $x=0\ m$ and $x=8000\ m$ (that is the western boundary of the Haarlemmermeer polder) and in vertical direction between $z=$-10 and $z=$-170 $m\ N.A.P.$

Figure 8.22: Seepage quantity through the Holocene aquitard of the Haarlemmermeer polder at -15 $m\ N.A.P.$ during the next millennium for six scenarios of sea level rise.

is insignificant, as the polder is situated beyond the zone of influence of sea level rise.

Figure 8.23 shows the development of the seepage quantity through the Holocene aquitard of both the Haarlemmermeer polder and the Groot-Mijdrecht polder during the ten millennia for the reference case with no sea level rise. As can be seen in figure 8.17, the state of dynamic equilibrium of the density distribution in the Haarlemmermeer polder is not yet completely reached after a few millennia, and subsequently, the seepage quantity stabilizes. The same phenomenon occurs in the Groot-Mijdrecht polder. During the next centuries, the chloride concentration in the geohydrologic system in the Groot-Mijdrecht polder is decreasing (see figure 8.25) and the seepage quantity is increasing. Till some two millennia from now, the chloride concentration and the seepage quantity stay constant. Subsequently, saline groundwater, that originates from the coastal aquifers, enters the aquifers in the area of the Groot-Mijdrecht polder, and thus, the seepage quantity decreases.

Figure 8.23: Seepage quantity through the Holocene aquitard of the Haarlemmermeer polder and the Groot-Mijdrecht polder during the next ten millennia.

Chloride concentration in the Haarlemmermeer polder

Figure 8.24 shows the mean chloride concentration[8] in the Holocene aquitard of the Haarlemmermeer polder at -15 m $N.A.P.$ as a function of time for six scenarios of sea level rise. For all scenarios, the mean chloride concentration in the Holocene

---

[8]The mean chloride concentration is determined by averaging the chloride concentrations in the Holocene aquitard over the total length of the Haarlemmermeer polder.
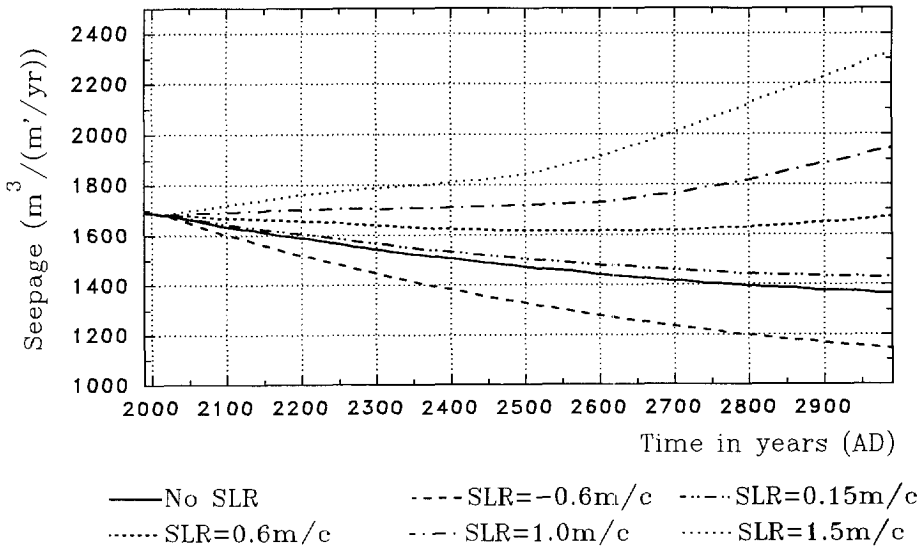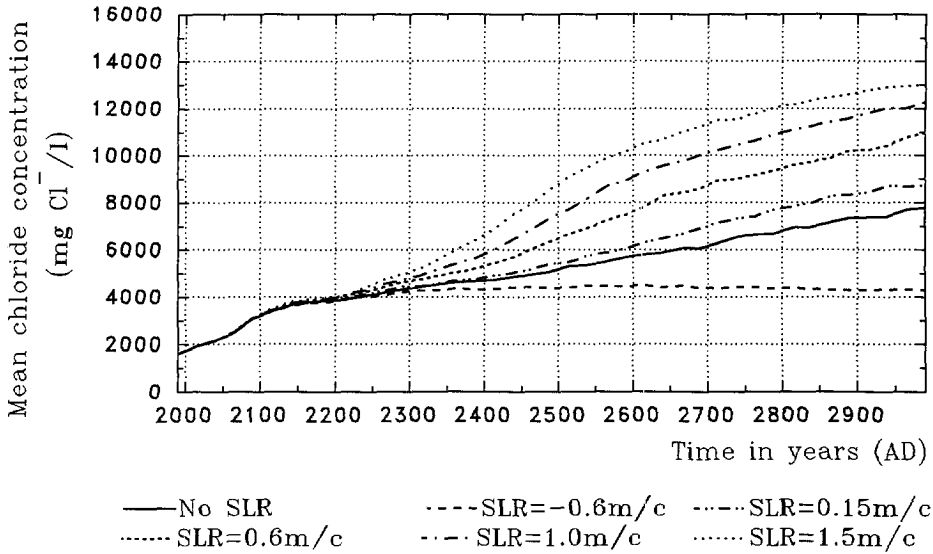
Figure 8.24: Mean chloride concentration in the Holocene aquitard of the Haarlemmermeer polder at -15 *m* *N.A.P.* during the next millennium for six scenarios of sea level rise.

aquitard increases significantly during the next two centuries, independent of the rate of sea level rise. From then on, the impact of different scenarios of sea level rise on the mean chloride concentration cannot be disregarded any more. The state of dynamic equilibrium is not yet reached after the next millennium, not even for the reference case with no sea level rise. Figure 8.25 shows that even during the next ten millennia, the mean chloride concentration is still increasing due to salinisation of the geohydrologic system.

Figure 8.26 shows the chloride distribution in the Holocene aquitard of the Haarlemmermeer polder for the reference case for several moments in time. The chloride concentration in the central part of the Haarlemmermeer polder increases significantly, even during the next century. The chloride concentration remains low at both sides of the polder, as fresh groundwater flows towards the polder from adjacent polder areas (western side) and lakes (eastern side).

Figure 8.27 shows the influence of sea level rise on the chloride distribution in 2990. Sea level rise increases the chloride concentration in nearly the entire Haarlemmermeer polder. Only near the inland boundary at 19,500 *m*, the chloride concentration remains low due to infiltration of fresh surface water. Even when the sea level falls -0.6 *m/c*, the overall chloride concentration in 2990 in the Holocene aquitard of the Haarlemmermeer polder is higher than the present concentration (compare with figure 8.26).
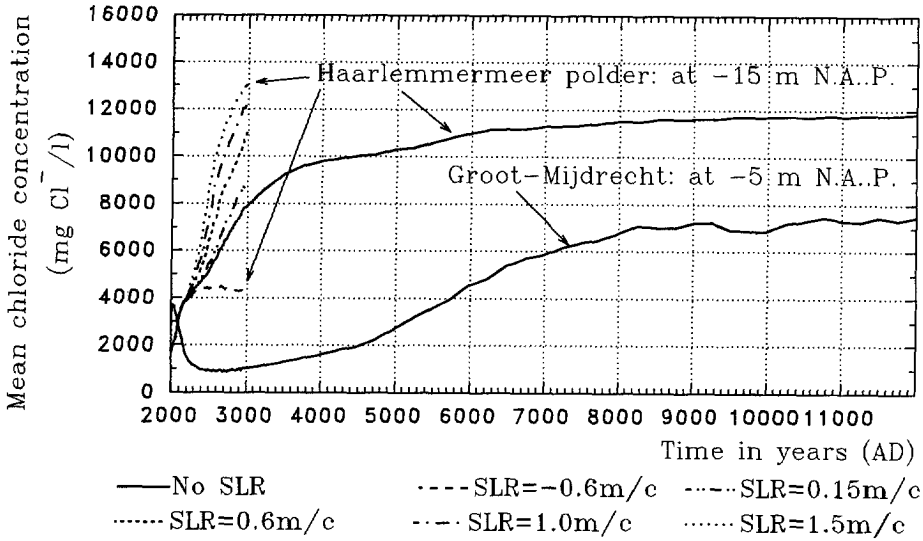
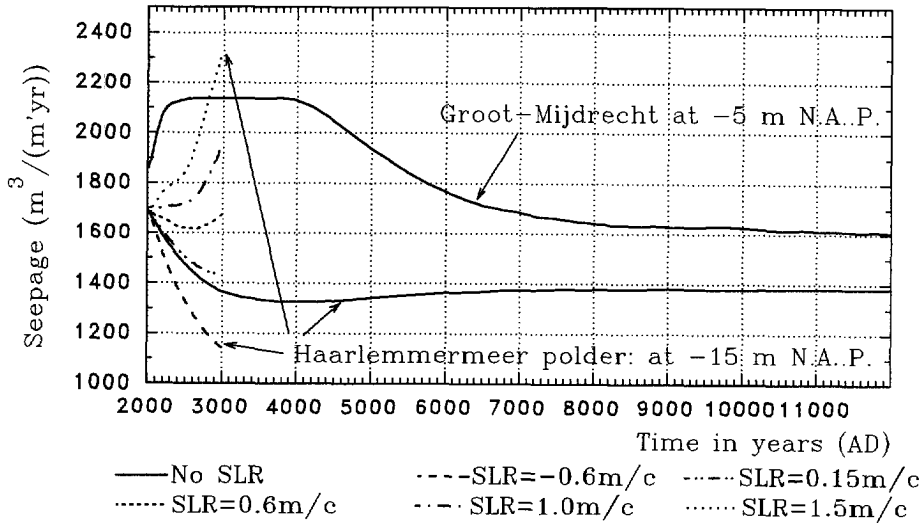**Figure 8.25**: Mean chloride concentration in the Holocene aquitard of the Haarlemmermeer polder and the Groot-Mijdrecht polder during the next ten millennia.
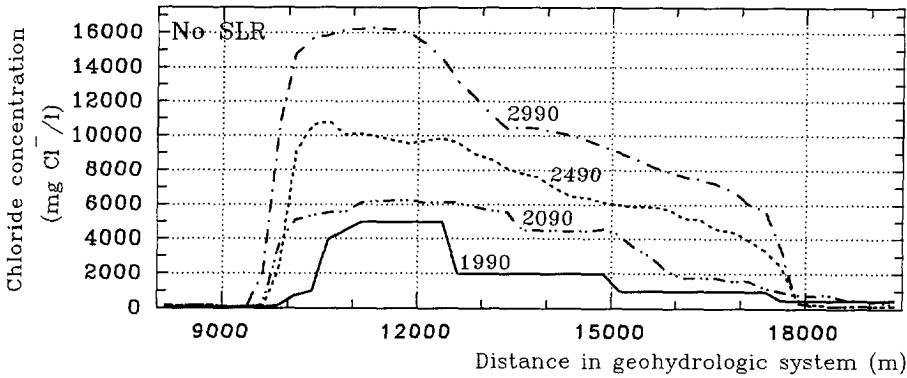
Figure 8.26: Chloride concentration in the Holocene aquitard of the Haarlemmermeer polder at -15 m N.A.P. for several moments in time for the reference case with no sea level rise.

Chloride load in the Haarlemmermeer polder

Figure 8.28 shows the chloride load[9] in $ton\ Cl^-/(m'yr)$ through the Holocene aquitard of the Haarlemmermeer polder at -15 m N.A.P. for six scenarios of sea level rise. High

---

[9] The chloride load through the Holocene aquitard has been calculated from calculated chloride concentrations and seepage quantities.
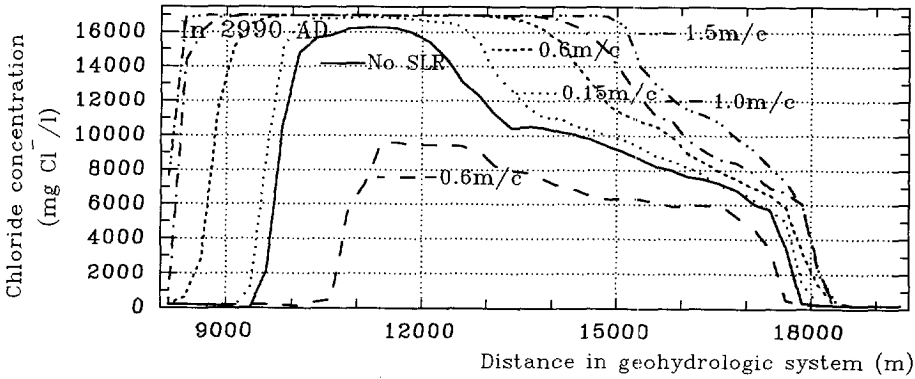
Figure 8.27: Chloride concentration in the Holocene aquitard of the Haarlemmermeer polder at -15 *m N.A.P.* in 2990 for six scenarios of sea level rise.
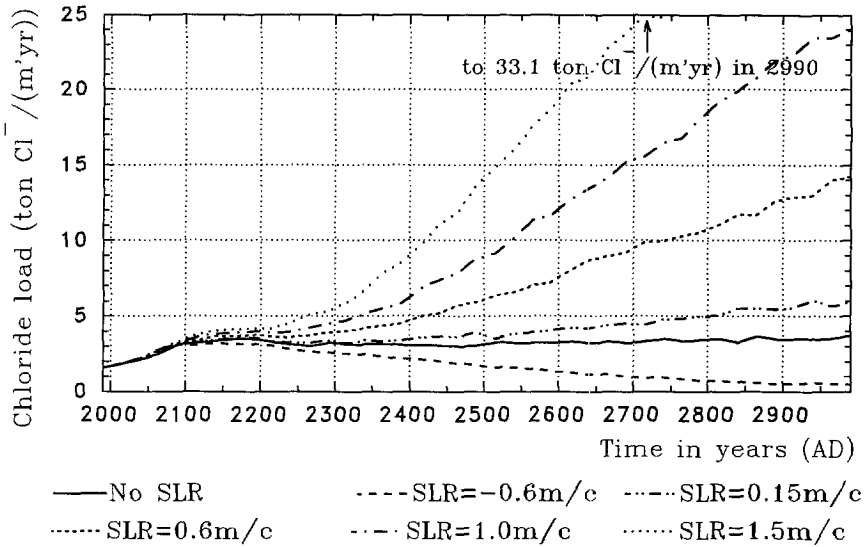
Figure 8.28: Chloride load in *ton* $Cl^-/(m'yr)$ through the Holocene aquitard of the Haarlemmermeer polder at -15 *m N.A.P.* for six scenarios of sea level rise.

rates of sea level rise generate high chloride loads in the Haarlemmermeer polder within a few centuries. Figure 8.29 shows that even after one millennium, the state of dynamic equilibrium for the chloride load is not yet completely reached for the reference case with no sea level rise. Note that this increase in chloride load is small compared with the increase in chloride load due to sea level rise.
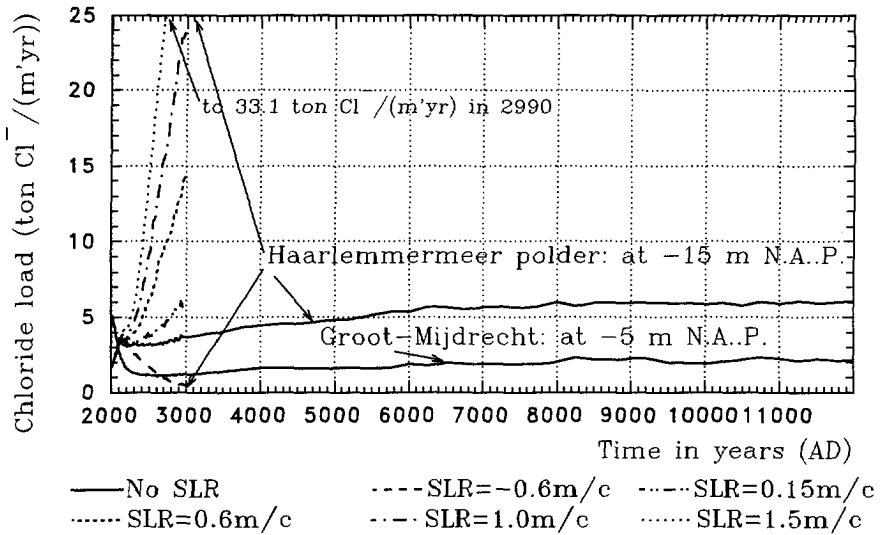
Figure 8.29: Chloride load in *ton $Cl^-/(m'yr)$* through the Holocene aquitard of the Haarlemmermeer polder and the Groot-Mijdrecht polder during the next ten millennia.

8.2.6   Effects of (counter)-measures

In this subsection, four measures (no. 1, 2, 3 and 5) to counteract the negative impact of sea level rise on the geohydrologic system and one measure (no. 4) to compensate for land-subsidence are evaluated. Whether or not some (counter)-measures are feasible from an economic, environmental or political point of view is not really the question here. These (counter)-measures should only be considered as interesting cases in order to gain a better insight into the range of conceivable human interventions. The following five (counter)-measures are evaluated:

1. **Extraction of saline groundwater**
   Six lines of extraction wells[10] are imposed in the sand-dune area, each with an extraction rate of about 128.2 $m^3/(m'yr)$[11]. The six well lines are positioned in horizontal direction at $x=4875$ m and in vertical direction at $z=-115$, $z=-$ 125, $z=-135$, $z=-145$, $z=-155$ and $z=-165$ m $N.A.P.$ The optimum position and extraction rate of the well lines should be derived at a later more decisive stage[12],

---

[10]As the six lines of extraction wells are positioned in vertical direction, they are in fact one line of extraction wells with filters on six different depths.

[11]The total extraction rate is four times as much as the total extraction rate of fresh groundwater from wells in the middle aquifer in the sand-dune area, simulated during the period 1974-1987.

[12]Note that several more cases with different positions and extraction rates of the well lines have been simulated. However, for the purpose of easy overview, only one case is presented.

2. **Deep-well infiltration of fresh surface water**

   Six lines of infiltration wells are imposed, each with an infiltration rate of about 128.2 $m^3/(m'yr)$. The six well lines are positioned in vertical direction at $z=$-115 m $N.A.P.$ and in horizontal direction at $x=3625$, $x=4125$, $x=4625$, $x=5125$, $x=5625$ and $x=6125$ m. The optimum position and infiltration rate of the well lines should be derived at a later more decisive stage,

3. **Raising the phreatic groundwater level in the Haarlemmermeer polder**

   It is obvious that this is a hypothetical countermeasure, as the polder accommodates Schiphol airport and has a high urbanisation rate. Nonetheless, this unfeasible countermeasure serves the purpose of illustrating what has unconsciously been provoked by reclaiming the lake Haarlemmermeer in the past century. The phreatic groundwater level is raised to -0.6 m $N.A.P.$,

4. **Lowering the phreatic groundwater levels in the polder areas due to land-subsidence**

   Land subsidence has been occurring because of compaction, shrinkage and oxidation of peat. In order to drain the polder areas efficiently, the phreatic groundwater level has to be lowered. Though this is not really a countermeasure in the strict sense that it counteracts the impact of sea level rise, this measure illustrates what has unconsciously been provoked by reclaiming land in the past centuries. The lowering of the polder levels equals 0.4 m during the next century and 0.15 m/c from then on,

5. **Land reclamation in front of the coast**

   Land reclamation in front of the coast can be utilized to alleviate socio-economic problems based on the shortage of space, e.g. the housing issue. A positive side effect of land reclamation in front of the coast is that it could counteract the impact of sea level rise on the salinisation of the geohydrologic system.

   During the beginning of the 1980's, the feasibility of a land reclamation project called Plan Waterman or Nieuw-Holland[13] was discussed at several decision levels. It comprises reclamation of land in front of the coast of the province of Zuid-Holland, between Scheveningen and Hoek van Holland [Overeem *et al.*, 1993; Stuurgroep Kustlocatie, 1995].

   Three scenarios of land reclamation in front of the coast in the sand-dune area of Gemeentewaterleidingen Amsterdam are simulated when no sea level rise occurs during the next millennium. Figure 8.30 displays for all three scenarios the schematisation and geometry of a model area with 10,000 m offshore.

Discussion

The analysis of the simulations comprises more results than is shown in the thesis. For instance, the chloride distributions of other moments in the simulation time, the

---

[13]The geometry of Nieuw Holland would be: a surface of 4000 ha, about 17,000 m long with an average width of 2500 m.
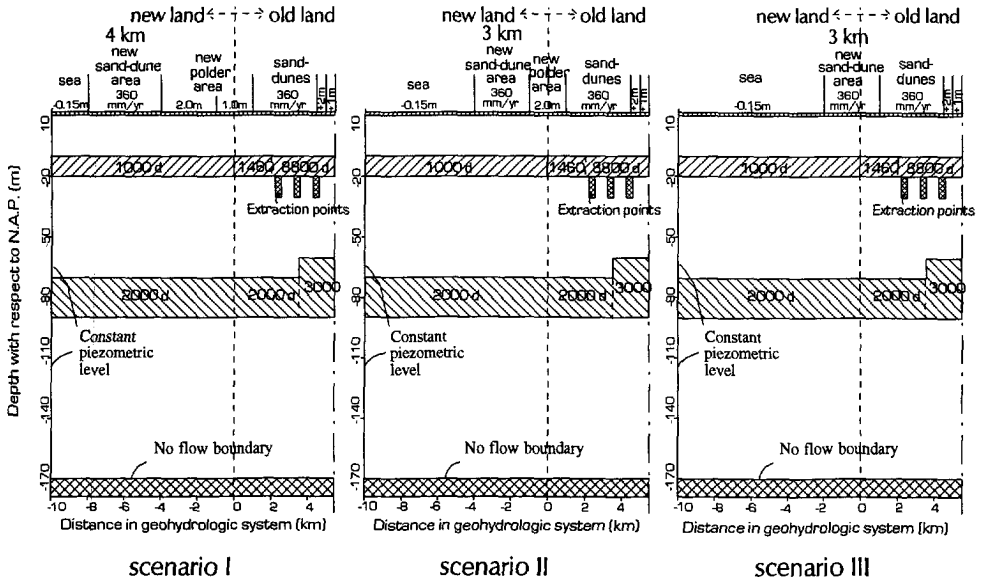
Figure 8.30: Schematisation of a part of the geohydrologic system for the three scenarios with land reclamation in front of the coast between $x=-10,000$ and $x=5000$ m. The seaside boundary at $x=0$ m of the reference case is moved to $x=-10,000$ m. The inland boundary at $x=39,000$ m remains the same. In all three scenarios, which are based on the geometry of the reference case, a new sand-dune area has been developed, whereas in the scenarios I and II, also a new polder area has been created.

changes in the volume distribution of fresh, brackish and saline groundwater and the seepage, the mean chloride concentration and the chloride load in the Haarlemmermeer polder are not shown here. In order to present the results as comprehensive as possible, only a selection of relevant results is displayed here.

The effects of the countermeasures 1 to 3 and the measure 4 are discussed by only showing the chloride distribution of the geohydrologic system in 2990 in figure 8.31. Two sea level rise scenarios are considered: no sea level rise and a sea level rise of 0.6 m/c. Some striking observations are:

- Salinisation of the geohydrologic system occurs for all (counter)-measures, which can be deduced when figure 8.31 is compared with figure 8.3 (the chloride concentration in 1990). The 15,000 mg Cl^-/l-isochlor is displaced significantly in the direction of the Groot-Mijdrecht polder, whether or not men intervenes with (counter)-measures, and whether or not the sea level rises. Moreover, the freshwater lens (chloride concentration ≤ 40 mg Cl^-/l) decreases with sea level rise, whether or not men intervenes with (counter)-measures. Less saline groundwater occurs in the middle aquifer in the Haarlemmermeer polder for the cases with the countermeasures 1 to 3 than for the reference case.
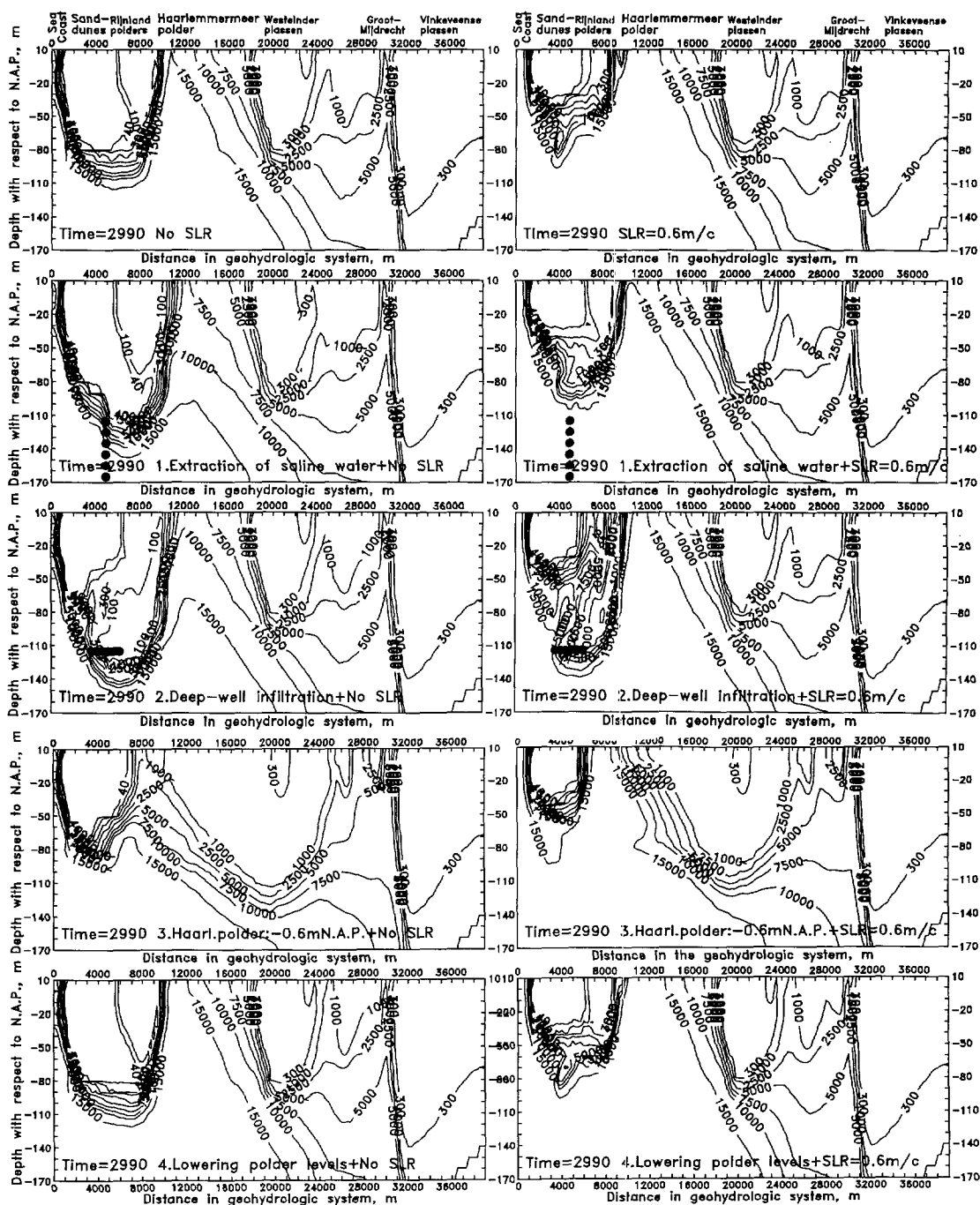
Figure 8.31: Chloride distribution (in $mg\ Cl^-/l$) in the geohydrologic system in 2990 for the reference case (for comparison), the three countermeasures 1 to 3 and the measure 4. Two sea level rise scenarios are considered: no sea level rise and a sea level rise of 0.6 m/c.

- Extraction of saline groundwater decreases the groundwater flow in the direction of the Haarlemmermeer polder. Moreover, this countermeasure decreases the seepage quantity in the Haarlemmermeer polder.

- Deep-well infiltration of fresh surface water slightly increases the volume of the freshwater lens in the Rijnland polders. Moreover, this countermeasure increases the seepage quantity in the Haarlemmermeer polder.

- Raising the phreatic groundwater level in the Haarlemmermeer polder to -0.6 m $N.A.P.$ (thus the polder would be inundated and becomes again Haarlemmermeer) reduces the groundwater flow in the geohydrologic system and the seepage quantity through the Holocene aquitard significantly. Although salt water intrusion in the deep aquifer is not stopped, the middle aquifer contains only (light) brackish groundwater when no sea level rise occurs. As a result, the chloride load in the Haarlemmermeer decreases significantly. However, when the sea level rises 0.6 m/c, saline seepage still occurs, though now in the Rijnland polders instead of in the Haarlemmermeer.

- The effect of lowering the phreatic groundwater levels in the polder areas due to land-subsidence appears to be minor, though this measure slightly amplifies the salinisation process. The main difference with the reference case is reflected by seepage with a somewhat higher chloride concentration in the Haarlemmermeer polder.

In figure 8.32, the effects of the countermeasure 5 is shown. As can be seen, a new freshwater lens has developed in the new sand-dune area in front of the coast. The seepage quantity in the Haarlemmermeer polder has increased significantly because the higher phreatic groundwater level in the (new) sand-dune area increases the deep groundwater percolation through the Holocene aquitard. For instance, compared with the reference case without sea level rise, the seepage quantity in the Haarlemmermeer polder increases about 5 % for scenario III immediately after creating the new sand-dune area and up to a maximum of about 14 % in 2990.

The salinisation of the upper part of the geohydrologic system is retarded due to land reclamation. This is demonstrated by comparing the positions of the 15,000 $mg\ Cl^-/l$-isochlor in 2990 for the reference case and the three scenarios. Figure 8.32 shows that, in case of no land reclamation, the 15,000 $mg\ Cl^-/l$-isochlor even passes through the Holocene aquitard, whereas for the scenarios with land reclamation, only the 10,000 $mg\ Cl^-/l$-isochlor passes through the Holocene aquitard. Hence, groundwater in the Haarlemmermeer polder is less saline. For instance, in 2990 the mean chloride concentration equals about 4800 $mg\ Cl^-/l$ for scenario III instead of 7800 $mg\ Cl^-/l$ for the reference case. As a consequence, the chloride load in the Haarlemmermeer polder is substantially smaller than in the reference case, e.g. in 2990 about 0.9 $ton\ Cl^-/(m'yr)$ for scenario III instead of 3.8 $ton\ Cl^-/(m'yr)$ for the reference case.
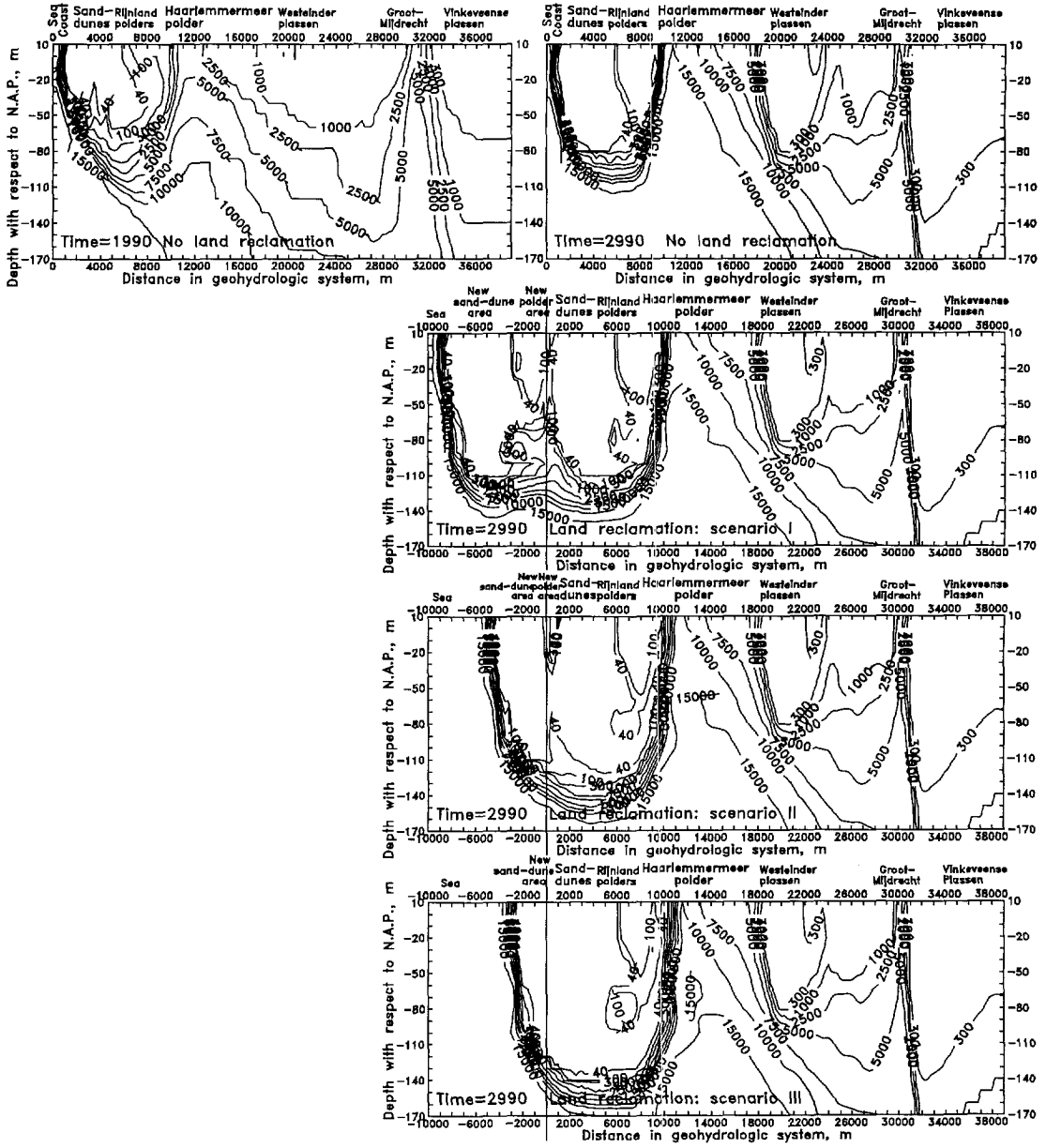
Figure 8.32: Chloride distribution (in $mg\ Cl^-/l$) in the geohydrologic system for three scenarios of land reclamation in front of the coast in 2990. No sea level rise is simulated.

8.2.7   Conclusions and a recommendation

Conclusions

The main conclusion is that during the next centuries not sea level rise but human interventions will dominate the salinisation of this geohydrologic system in the southern part of Noord-Holland. For instance, the reclamation of the low-lying Haarlemmermeer polder midway the 19th century has generated a substantial inflow of saline groundwater from the sea in the deep aquifer. Even when no sea level rise occurs, salinisation of the geohydrologic system becomes significant. The changes in quality of seepage in the Haarlemmermeer polder are substantial. In terms of salinisation, a time lag of some centuries occurs between the cause of changes and the ultimate effect. No state of dynamic equilibrium is reached at the inland side of the profile before several millennia have elapsed, as salinisation is proceeding slowly.

During the next century, the impact of sea level rise is mostly small. However, after several centuries, the sea has risen so much that the impact on the geohydrologic system is no longer of minor importance. Eventually, sea level changes considerably affect the distribution of fresh, brackish and saline groundwater in the geohydrologic system in this profile. Sea level rise accelerates the salinisation process significantly, though the zone of influence of sea level rise is only some 8000 to 10,000 m. The position of the saline groundwater tongue (the 15,000 mg Cl^-/l-isochlor) displaces in the deep aquifer with a velocity of 1.0 km/c to 1.35 km/c for a sea level fall of -0.6 m/c and a sea level rise of 1.5 m/c respectively. When the sea level rises 0.6 m/c (as generally accepted), the volume of the freshwater lens in the sand-dune area diminishes reasonably after at least some centuries (e.g. about -13 % after 300 years compared with no sea level rise). Moreover, when the sea level rises 0.6 m/c, the seepage in the low-lying Haarlemmermeer polder, increases both in quantity (e.g. about +22 % in 2990) and in quality (e.g. chloride load about +41 % in 2990).

Human interventions within the bounds of feasibility may slow down the salinisation of the geohydrologic system, but the salinisation process cannot easily be stopped completely. Countermeasures should be taken in time, since the time lag before changes in chloride distribution can be observed is considerable (several decades to centuries). Feasible rates of extraction of saline groundwater or deep-well infiltration of fresh surface water may at most reduce the impact of sea level rise. Note that the optimum position of the well lines should be derived at a later stage. Even more rigorous (hypothetical) countermeasures, such as raising the phreatic groundwater level in the Haarlemmermeer polder (not conceivable at all) or creating a sand-dune area in front of the coast by land reclamation, demonstrate once again that the salinisation process is difficult to restrain.

A recommendation

As a long period is simulated, the inland boundary of the schematisation has to be situated some tens of kilometres from the coast, at least beyond the zone of influence

of sea level rise. As only two-dimensional profiles are simulated, the geohydrologic situation in the vicinity of this profile is not considered. This could lead to a discrepancy between the simulated and the actual groundwater flow situation, e.g. at a few tens of kilometres from the coast. To overcome this discrepancy, three-dimensional modelling should be executed in order to account for groundwater flow perpendicular to the profile.

8.3 Profile to Enkhuizen at the IJsselmeer

In this section, the impact of six scenarios of sea level rise is simulated for the groundwater flow regime in a profile perpendicular to the Dutch coastline in the northern part of Noord-Holland (figure 8.33). This part of Noord-Holland, which is also called Westfriesland, is surrounded by the North Sea at the west side, and by the IJsselmeer at the east side. The IJsselmeer (former Zuiderzee) was brackish and in open connection with the North Sea till 1932. In 1932, the tidal inlet was closed by a dam (the so-called Afsluitdijk) and as a consequence, after some years, the former Zuiderzee became a freshwater lake, the IJsselmeer.
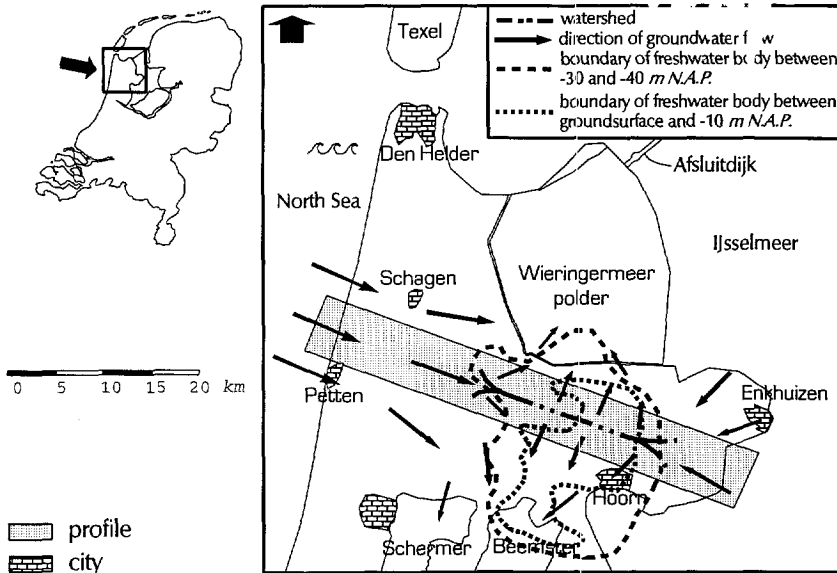
Figure 8.33: Map with the profile in the northern part of Noord-Holland.

In the central part of the profile the so-called freshwater body of Hoorn is situated (chloride concentration ≤ 200 mg/l). The freshwater body mainly occurs under the Eemian deposits and extends in some places to a depth of 90 m below mean sea level. The phreatic groundwater levels in the polders along the profile vary from about -0.5 m $N.A.P.$ near the coast to about -3.1 m $N.A.P.$ near the IJsselmeer. At

some kilometres in the direction perpendicular to the profile there are some large low-lying polder areas: at the north side the Wieringermeer polder, which was reclaimed in 1930, and at the south side the Beemster and the Schermer, reclaimed in 1612 and 1635 respectively [Schultz, 1992]. These reclaimed areas affect the groundwater flow, which can be deduced from piezometric levels at several depths below *N.A.P.* [ICW, 1982]. A minor freshwater lens occurs in the sand-dune area along the Dutch coastline, since the width of the sand-dunes through this profile is only about one kilometre.

In subsection 8.3.1, the geohydrologic system of the reference cases is schematised, and relevant subsoil and model parameters are summarized. In subsection 8.3.2, the calibration of the geohydrologic system is discussed. In subsection 8.3.3, the influence of some subsoil parameters on the solute transport in the geohydrologic system is analysed. In subsection 8.3.4, the simulations of the geohydrologic system are discussed and changes in groundwater flow and solute transport are quantified. In subsection 8.3.5, the impact of six scenarios of sea level rise is analysed. In subsection 8.3.6, the effects of three countermeasures are described. Finally, in subsection 8.3.7, some conclusions are drawn.

8.3.1   Schematisation

Subsoil parameters of the reference case

Figure 8.34 shows the geometry and subsoil parameters of the profile. The data of the geohydrological schematisation have been borrowed from the following sources:

- the M.Sc. thesis of Paap [1992] in which the geohydrologic situation is described,

- an article of de Wilde [1979] where the phreatic groundwater levels of the northern part of Noord-Holland are described,

- two articles of Pomper [1983a, 1983b] in which the geohydrologic situation of Noord-Holland is discussed,

- a report of Witt [1980] in which the chloride concentration of groundwater in a large part of the province of Noord-Holland is given,

- the ICW report **Regionale Studies 16** [1982] which shows several important subsoil parameters of the northern part of Noord-Holland,

- the **Grondwaterkaart van Nederland**, Alkmaar en Medemblik of the TNO Institute of Applied Geoscience [1979b] in which the composition of the geohydrologic system is presented.

The longitudinal dispersivity α_L is set to a small value: 0.021 m [e.g. like Kooiman, 1989]. A limited sensitivity analysis on this parameter is executed in subsection 8.3.3. The ratio transversal to longitudinal dispersivity α_T/α_L is set to 0.1 $(-)$, whereas
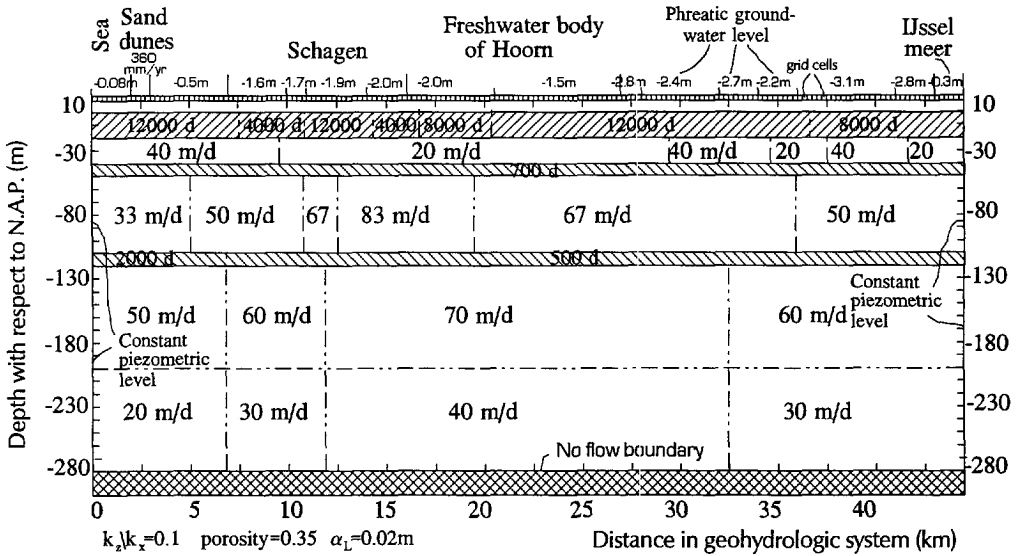
Figure 8.34: Subsoil parameters of the profile from the small sand-dune area near Petten to Enkhuizen at the IJsselmeer.

the anisotropy factor k_z/k_x (the ratio vertical and horizontal hydraulic conductivity) is also 0.1 (−). The effective porosity n_e is 0.35 (−) and the specific storativity S_s is set to zero.

Figure 8.35 shows the chloride distribution in the profile in 1988, derived from Witt [1980] and ICW [1982]. The chloride distribution is considered to represent the salinisation process. There are several hypotheses on the evolution to the present situation of the freshwater body of Hoorn.

According to de Vries [1981], the top of the Holocene sediments, which is slightly below the mean sea level at present, was formed about 3000 years ago. At that time, the elevation of this area has been about 1.5 m above mean sea level. In addition, the area was subsequently covered by a peat layer, though this layer has disappeared since. As such, the area has been elevated some metres above the mean sea level at those times for more than 1000 years. This high elevation, in combination with a relatively permeable soil, may have caused a deep infiltration of rainwater, and accordingly, the forming of the freshwater body of Hoorn. According to Beekman [1991], the refreshening of the freshwater body of Hoorn is induced by human activities since Medieval times in that particular geological situation. In the central part of the freshwater body, the age of groundwater appears to be younger than 250 years. Since Medieval times, peat areas, which occur throughout the area of the freshwater body, are subsiding due to land drainage. As a consequence, the tidal channels rose
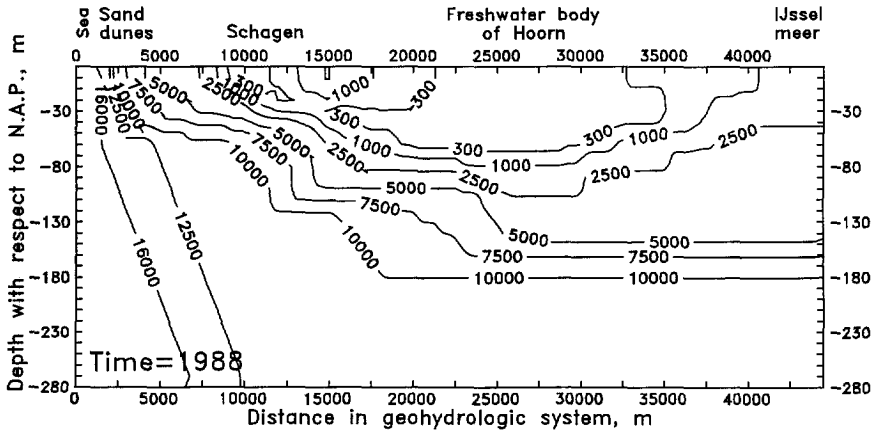
Figure 8.35: Initial chloride distribution (values in $mg\ Cl^-/l$) in 1988.

with respect to the peatland. Primarily, infiltration of fresh surface water took place within this complex system of tidal channels and peat areas. After the reclamation of lakes, especially since the 17th century, groundwater flow was induced both to the north and to the south. Salinisation of the aquifers in the west and refreshening of the freshwater body in the north are related to those changes in groundwater flow direction. According to ICW [1982] and Pomper [1983a], the lateral extend of the freshwater body is the result of a forced displacement of fresh groundwater by the (Eemian) seawater intrusion from the west and the presence of aquitards deposited simultaneously. These other hypotheses have in common that the formation of the freshwater body is dated to early Holocene or upper Pleistocene times, and that eventually the freshwater body will disappear.

The phreatic groundwater levels in the polders at the upper boundary, derived from de Wilde [1979], are kept constant. The groundwater recharge in the phreatic aquifer of the sand-dune area equals 360 mm/yr. A constant piezometric level boundary is introduced for both the seaside boundary and the lake side boundary, where the situation is supposed to be hydrostatic (see also subsection 5.4.4). At the seaside boundary, the chloride concentration of the incoming seawater is equal to 16,000 mg Cl^-/l. The piezometric level at the North Sea side is set to -0.08 m $N.A.P.$ (note that the average water level of the sea is not equal to $N.A.P.$ [Atlas van Nederland: Deel 15 Water, 1986]) and at the IJsselmeer side to -0.30 m $N.A.P.$

Model parameters of the reference case

The applied number of rectangular grid cells is 5162: in horizontal direction 178 and in vertical direction 29 grid cells. Each grid cell has a length Δx of 250 m and a height Δz of 10 m. The total profile is 44,500 m long and 290 m high. Each grid cell contains sixteen particles. The convergence criterion TOL is 10^{-5} ft. The flow time

step Δt equals 1 *year*. During this step, the velocity field remains constant. The maximum relative distance in a grid cell ζ is set to 0.5.

Groundwater flow perpendicular to the profile

As mentioned before, low-lying polder areas at the north (Wieringermeer polder) and at the south (Beemster and Schermer) induce groundwater flow perpendicular to the profile (figure 8.33). Thus, groundwater flow perpendicular to the profile should be introduced into the simulations. In order to simulate the effect of these low-lying polders, the reference case simulates a groundwater discharge out of the geohydrologic system in the central part of the profile.

8.3.2   Calibration

The calibration of this profile is carried out for piezometric levels at some depths relative to *N.A.P.* and for groundwater flow through the Holocene aquitard.

1. Piezometric levels relative to N.A.P.

Figure 8.36 shows the piezometric levels, expressed in freshwater, at -25, -65 and $-130\ m\ N.A.P.$ The levels, calculated with the adapted MOC model, are compared with measured piezometric levels [ICW, 1982]. These measured piezometric levels are corrected, as the density of the groundwater in an observation well deviates from the standard density $\rho_f = 1000\ kg/m^3$. The measured and corrected piezometric levels differ only some decimetres from the calculated piezometric levels, expressed in freshwater.

2. Groundwater flow through the Holocene aquitard

Figure 8.37 shows the difference between the phreatic groundwater level and the piezometric level at -25 $m\ N.A.P.$ [ICW, 1982]. Both the calculated and the observed values are displayed. Seepage and infiltration intensities can be deduced from these figures in combination with the hydraulic resistances. Observed seepage and infiltration intensities through the Holocene aquitard have been determined by means of water balances over specific subareas. Both the calculated and the observed intensities are almost everywhere smaller than 0.15 mm/d due to the high hydraulic resistance of the Holocene aquitard (see figure 8.34).

8.3.3   Parameter analysis

The influence of the following three parameters are briefly analysed: (1) the longitudinal dispersivity α_L; (2) the hydraulic conductivity k; and (3) the effective porosity n_e.
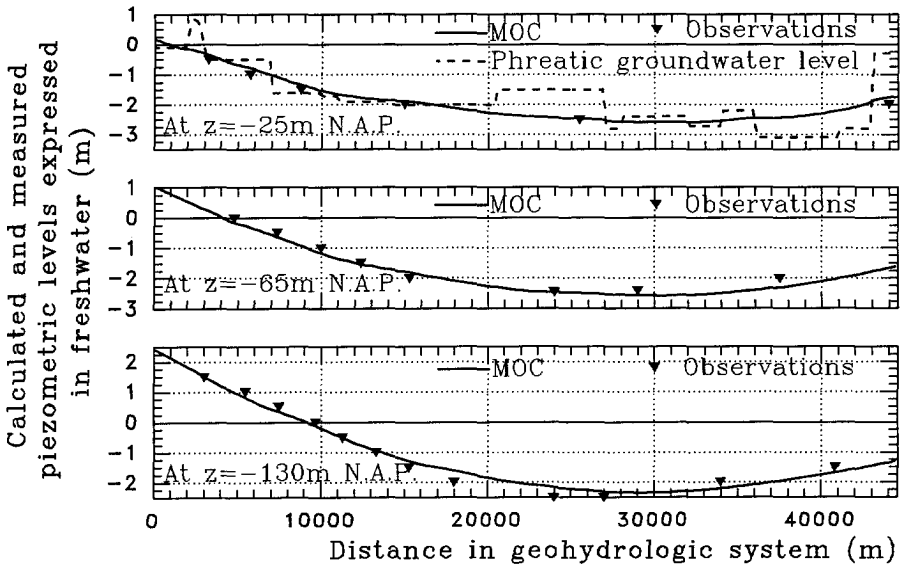
Figure 8.36: Calculated and measured piezometric levels, expressed in freshwater, at −25, -65 and -130 m $N.A.P.$ Some observations of (corrected) piezometric levels, borrowed from ICW [1982], are given for comparison.
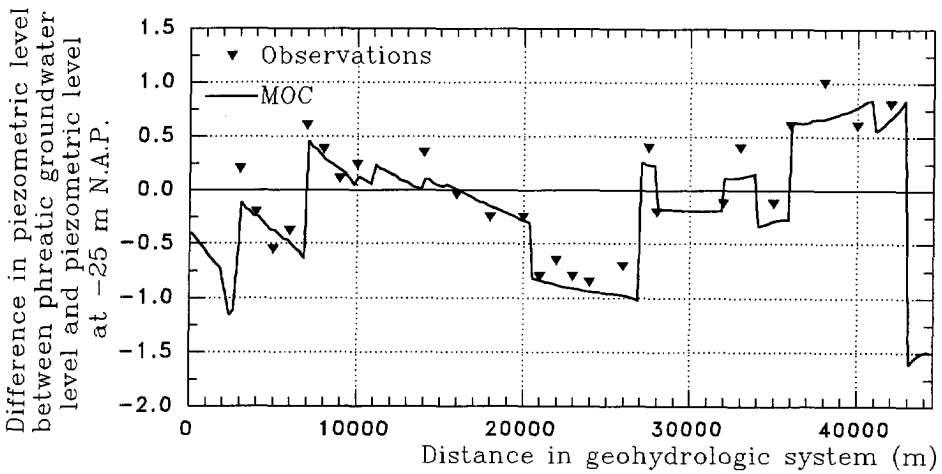
Figure 8.37: Difference in piezometric level between phreatic groundwater level and piezometric level at -25 m $N.A.P.$ for both calculations and observations.

1. Longitudinal dispersivity α_L

Figure 8.38 shows the chloride distributions in the geohydrologic system after a simulation time of 500 years, simulated with four different longitudinal dispersivities: $\alpha_L=0.021$ m (the reference case), $\alpha_L=0.21$ m, $\alpha_L=2.1$ m and $\alpha_L=21.0$ m. As can be seen, the two cases with small longitudinal dispersivities closely correspond with each other. Looking at the position of the 16,000 mg Cl^-/l-isochlor, the figure shows that no salt water intrusion occurs for the case with $\alpha_L=21.0$ m. The reason is that incoming saline groundwater mixes directly with fresh and brackish groundwater, and hence, the chloride concentration in the geohydrologic system is lower than 16,000 mg Cl^-/l. This is unlikely to believe, taking into account the significant inflow of groundwater at the seaside boundary. Furthermore, the case with $\alpha_L=21.0$ m shows that the freshwater body of Hoorn has disappeared and that the geohydrologic system eventually consists of only a large zone with brackish groundwater.

In conclusion, the longitudinal dispersivity α_L, as applied in the adapted MOC model, must be set to a small value (in the order of centimetres or decimetres), so that the calculated chloride distribution can match the observations.
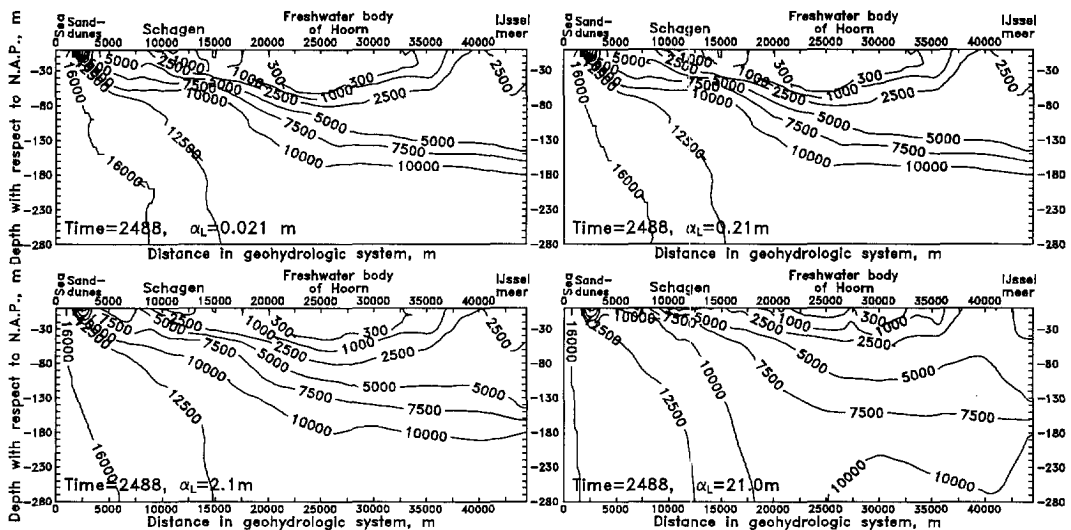
Figure 8.38: Chloride distributions (in mg Cl^-/l) in 2488, calculated with four different longitudinal dispersivities: $\alpha_L=0.021$ m (the reference case), $\alpha_L=0.21$ m, $\alpha_L=2.1$ m and $\alpha_L=21.0$ m.

2. Hydraulic conductivity

Obviously, the magnitude of the hydraulic conductivity in the geohydrologic system is quite important for the magnitude of the groundwater flow and thus for the solute transport. Figure 8.39 shows the distribution of fresh, brackish and saline water in percentages of the total volume of water in the geohydrologic system for several multiples of the hydraulic conductivity k. As can be seen the influence of the hydraulic conductivity is significant. This is especially due to the fact that, if transmissivities are high, salt water intrusion occurs rapidly. However, the influence of the anisotropy factor $(k_z/k_x$ up to 0.25, not shown here) on the volume distributions seems to be relatively small (differences of only a few percents in 2988).
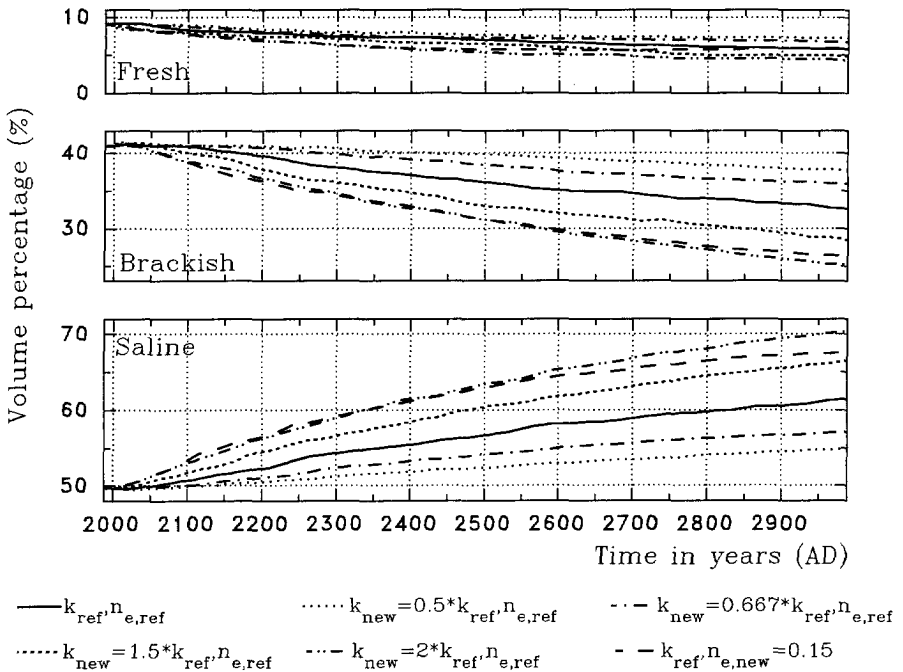
Figure 8.39: Volume percentages of fresh, brackish and saline groundwater during the next millennium for the reference case, four cases with different multiples of the hydraulic conductivity k and one case with $n_e=0.15$ instead of $n_e=0.35$.

3. Effective porosity

Effective porosities in the range 0.35-0.5 also seem to have relatively small effects on the volume distributions (not shown here). However, if the effective porosity is smaller than 0.35 (the reference case), then the volume distribution can differ significantly, as can be seen for $n_e=0.15$ in figure 8.39.

8.3.4 Results of the simulated profile

Chloride distribution

Figure 8.40 shows the chloride distribution at different moments in time during the next millennium. As can be seen, a strong inflow of saline groundwater occurs in the deep aquifers. The state of dynamic equilibrium is still not reached after one millennium. The freshwater body remains during the next centuries, yet the volume of fresh groundwater reduces a little. In the polder area, which is situated along the IJsselmeer, the low phreatic groundwater level causes the rise of brackish groundwater. As a result, the seepage consists of more chloride during the next centuries.
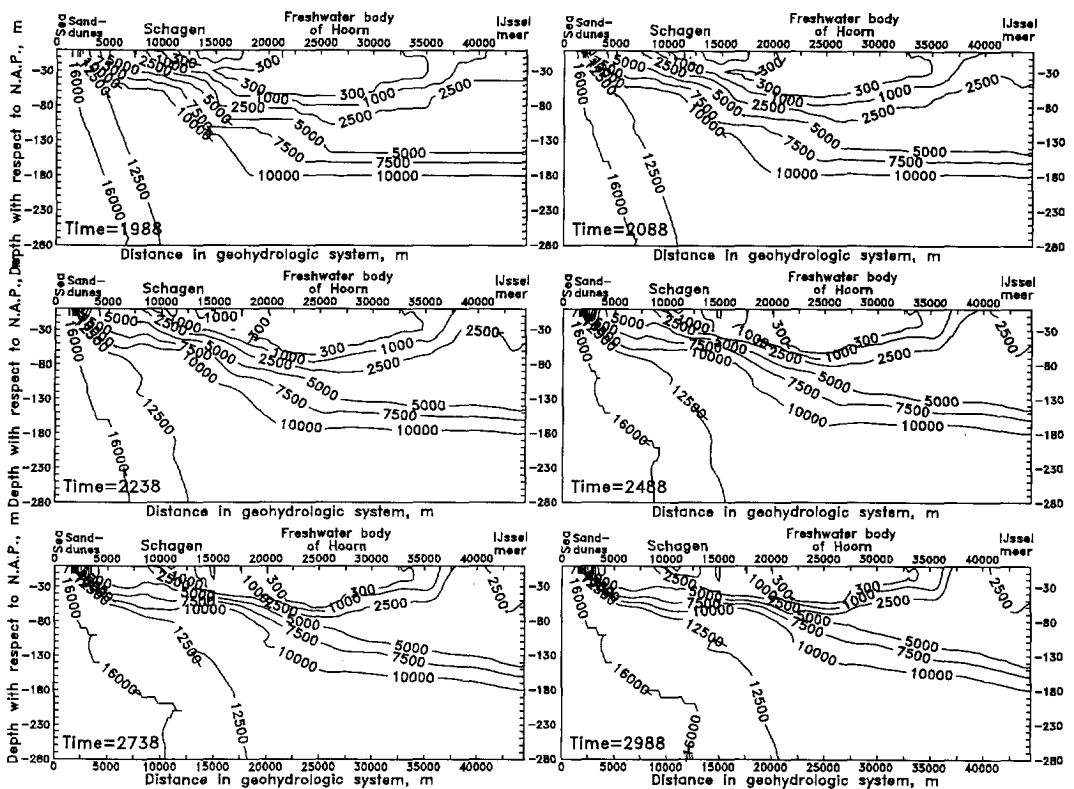
Figure 8.40: Chloride distribution (in $mg\ Cl^-/l$) in the geohydrologic system at different moments in time for the reference case: no sea level rise.

Piezometric level distribution expressed in freshwater

Figure 8.41 shows the calculated piezometric level distribution in 1988, expressed in freshwater (corrected for density differences). A hydrostatic situation occurs at both the seaside boundary and the lake side boundary. The piezometric level in the freshwater body of Hoorn is low compared to the phreatic groundwater level above the Holocene aquitard, that is situated between 0 and -20 m $N.A.P.$ Consequently, as the density in the freshwater body of Hoorn is (nearly) constant, it can be deduced that natural groundwater recharge occurs in this area.
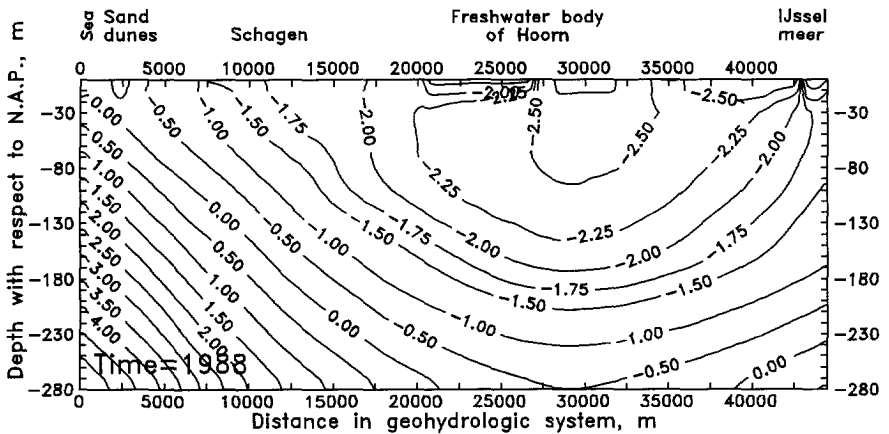
Figure 8.41: Calculated piezometric levels (in m), expressed in freshwater, in the geohydrologic system in 1988.

Velocity field

Figure 8.42 shows the velocity field in the geohydrologic system in 1988. As can be seen, a severe salt water intrusion is present in the deepest aquifer, in which the greatest intrusion occurs in the upper part of the aquifer where the hydraulic conductivity is the highest. Vertical velocity dominates in the aquitards. A downward groundwater flow through the Holocene aquitard occurs to the freshwater body of Hoorn, while groundwater flows upward in low-lying polders such as in the polder area near Schagen. The figure shows that in some places the velocities in the aquifers fluctuate in vertical direction, which is the result of numerical instabilities (see subsection 5.5.1).

Groundwater fluxes

The groundwater fluxes over the following five segments of the geohydrologic system are considered in table 8.2:
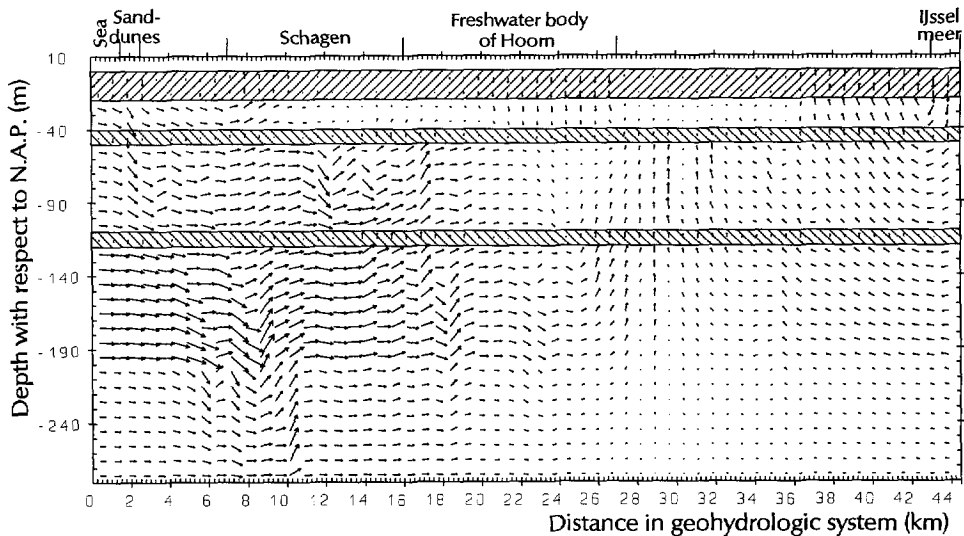
Figure 8.42: Velocity field in the entire geohydrologic system in 1988. The lengths of the arrows correspond with the displacement of groundwater during a time step of 50 years, beginning in 1988 and with a constant velocity field. The velocity is displayed in the center of every third horizontal grid cell. The distortion of the vertical direction with respect to the horizontal direction equals a factor 75.

1. inflow of saline groundwater at the seaside boundary in the aquifer between -20 and -40 m $N.A.P.$

2. inflow of saline groundwater at the seaside boundary in the aquifer between -50 and -110 m $N.A.P.$

3. inflow of saline groundwater at the seaside boundary in the aquifer between -120 and -280 m $N.A.P.$

4. seepage quantity through the Holocene aquitard in the polder area near Schagen in the reach 7000-16,000 m.

5. infiltration through the Holocene aquitard to the freshwater body of Hoorn in the reach 16,000-27,000 m.

The groundwater fluxes in the geohydrologic system are analysed for (a) the reference case and for four (hypothetical) cases: (b) no density flow; (c) no groundwater discharge out of the geohydrologic system in the central part of the profile, which implies that flow towards the low-lying polders north and south of the profile (viz. the Wieringermeer polder, the Beemster and the Schermer) is not taken into account; (d)

Table 8.2: Groundwater fluxes in $m^3/(m'yr)$ in 1988 over five segments of the geohydrologic system for the reference case and four other (hypothetical) cases. Depths of the three aquifers in m with respect to $N.A.P.$

Groundwater fluxes	(a) Reference case	(b) No density flow	(c) No low polders (Wieringermeer, Beemster & Schermer)	(d) Inundation polders in the profile	(e) No low polders & inundation polders in the profile
Inflow of saline groundwater at the seaside boundary					
1. -20 to -40 m	55.4	42.4	44.2	19.1	7.9
2. -50 to -110 m	176.4	112.1	146.9	82.4	53.0
3. -120 to -280 m	622.5	333.6	533.5	359.5	270.5
4. Seepage in the polder area near Schagen in the reach 7000-16,000 m					
(Seep. is positive: +)	+81.5	+10.1	+348.5	-211.1	+56.0
5. Infiltration to the freshwater body of Hoorn in the reach 16,000-27,000 m					
(Inf. is negative: -)	-215.2	-299.4	+178.8	-326.3	+67.6

inundation of all polders in the profile itself (the phreatic groundwater level equals $N.A.P.$); (e) no groundwater discharge out of the geohydrologic system and inundation of all polders in the profile itself, namely a combination of case (c) and (d). The hypothetical case (b) indicates what happens if the effect of density differences is not taken into account in this coastal groundwater flow regime, whereas the cases (c), (d) and (e) demonstrate the substantial influence of the polder areas on the groundwater flow in the geohydrologic system. Two striking features of the groundwater flow are:

- inflow of saline groundwater
  If no density differences are taken into account (see case (b), table 8.2), inflow of saline groundwater in the low-lying aquifer would be much smaller than for the reference case. The inflow of saline groundwater is more due to the present levels of the polders *in* the profile (case (d)) than due to the low-lying polders at several kilometres distance north and south the profile (case (c)). However, case (e) shows that if there were no polders in the profile itself as well as no low-lying polders north and south of the profile, the inflow of saline groundwater would be small but not insignificant due to density differences.

- groundwater flow through the Holocene aquitard
  If no low-lying polders north and south of the profile were present (case (c)), the freshwater body of Hoorn would diminish due to seepage quantities in the area of the freshwater body of Hoorn. If the polders in the profile were inundated to a polder level at $N.A.P.$ (case (d)), a very strong rate of infiltration would occur in the polder area near Schagen instead of a strong rate of seepage as in the reference case.

8.3.5 Impact of sea level rise

In this subsection, the simulations of the geohydrologic system during the next millennium are discussed. Six scenarios of sea level rise, which are defined in section 3.6, are imposed to estimate changes in groundwater flow and solute transport. The sea level rises are simulated as elevations of the piezometric level, expressed in freshwater, at the seaside boundary of the geohydrologic system every 25 years and from 2013 on. During the simulation of one millennium, the phreatic groundwater levels in the polder areas stay constant. Moreover, the groundwater recharge in the phreatic aquifer of the sand-dune area remains 360 mm/yr. Although a relatively long period is simulated, many hydrological, morphological and/or man-induced processes that could affect the geohydrologic system are not considered.

Piezometric level expressed in freshwater and the zone of influence

Figure 8.43 shows the difference in piezometric level, expressed in freshwater, at −25 m N.A.P. in 2088 for five scenarios of sea level rise with respect to the scenario of no sea level rise. Since the lake side boundary is a constant piezometric level boundary for all scenarios, the rise in piezometric level at 44,500 m from the seaside is equal to zero. The zone of influence of sea level rise is quite some kilometres which is mainly due to the high transmissivities of the aquifers. For instance, at 10,000 m inland of the seaside boundary, a rise in piezometric level of about 25 % of the rise in sea level is still present.
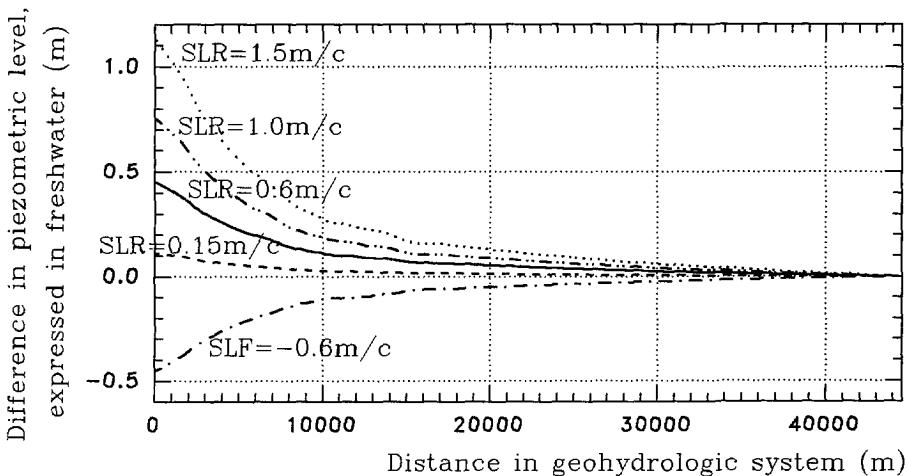
Figure 8.43: Differences in piezometric level, expressed in freshwater, at -25 m N.A.P. in 2088 for five scenarios of sea level rise with respect to the scenario of no sea level rise.

Groundwater flow through the Holocene aquitard

Figure 8.44 shows the upward flow (seepage is positive) and downward flow (infiltration) through the Holocene aquitard at -15 m $N.A.P.$ in 2088 for only four scenarios of sea level rise. It can be seen that infiltration in the polder area near the seaside (in the reach 3000-7000 m) changes into seepage if the rates of sea level rise are high. The seepage quantity in the polder area, that is situated near the IJsselmeer (in the reach 36,000-43,000 m), is already high due to the low phreatic groundwater level. There, the seepage quantity hardly changes due to sea level rise.
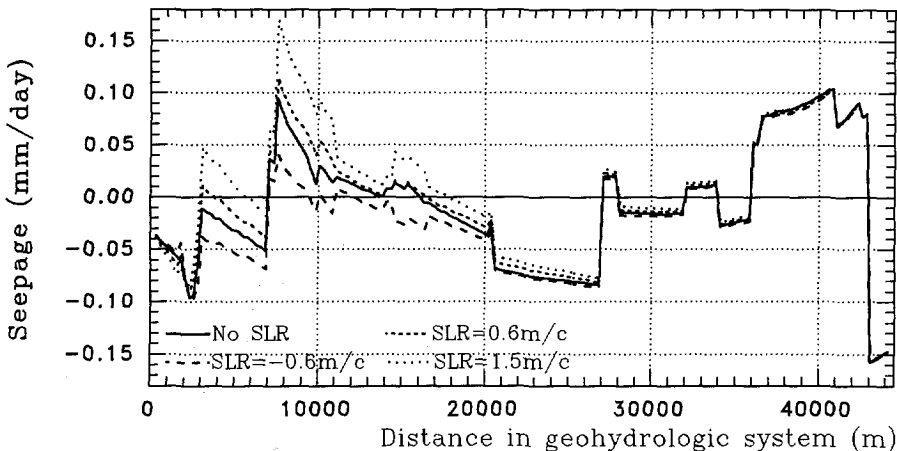
Figure 8.44: Calculated seepage and infiltration intensities through the Holocene aquitard at -15 m $N.A.P.$ in 2088 for four scenarios of sea level rise.

Chloride distribution

Figure 8.45 shows the chloride distribution during the next millennium for the scenario with a sea level rise of 0.6 m/c. As can be seen, the freshwater body of Hoorn slowly diminishes. Saline groundwater replaces brackish groundwater in the upper aquifers and aquitards in the first kilometres from the coast. Subsequently, the seepage through the Holocene aquitard in that area consists of more saline groundwater.

Figure 8.46 shows the chloride distribution in the geohydrologic system in 2488 for six scenarios of sea level rise. As can be seen, it depends on the rate of sea level rise whether or not the area between the sand-dunes and Schagen contains brackish or saline groundwater during the next 500 years. When sea level falls, even fresh groundwater occurs in the vicinity of Schagen.

Figure 8.47 shows the inflow of saline groundwater in $m^3/(m'yr)$ in the deep aquifer between -120 and -280 m $N.A.P.$ during the next millennium at the seaside boundary for seven scenarios of sea level rise. The figure shows that the increase in
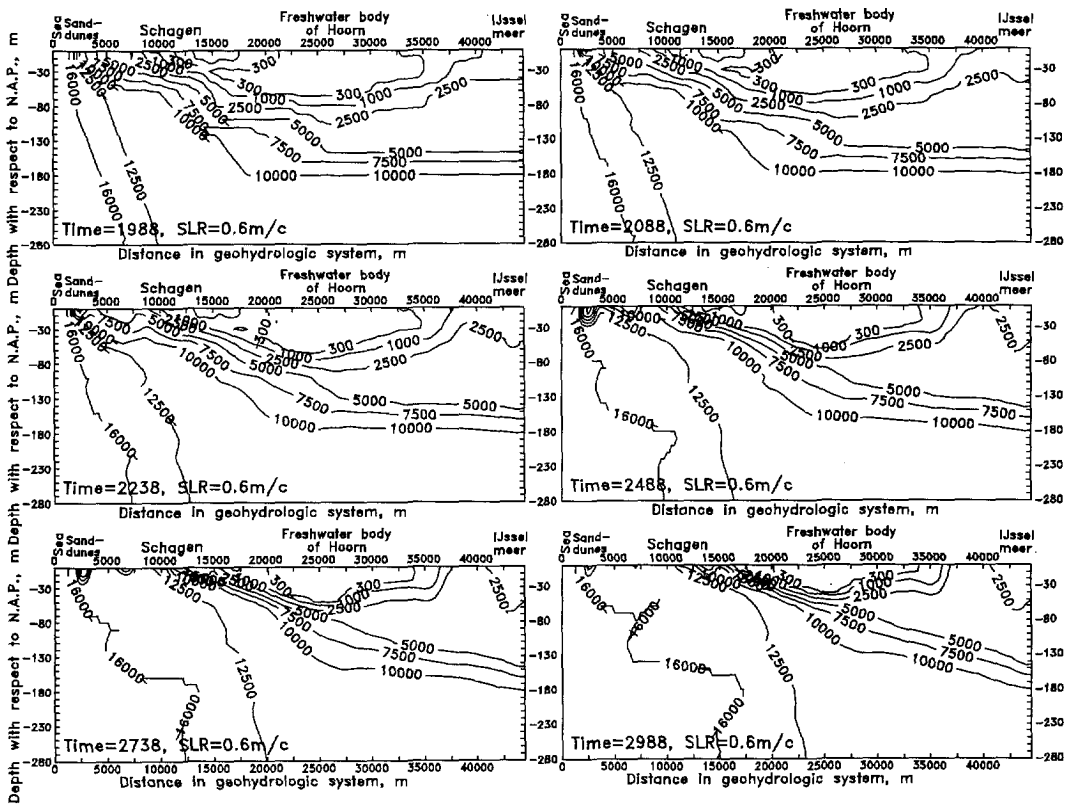
Figure 8.45: Chloride distribution (in $mg\ Cl^-/l$) in the geohydrologic system at different moments in time. A constant rate of sea level rise of 0.6 m/c is imposed.

inflow of saline groundwater at the boundary is nearly proportional to the rate of sea level rise. When no sea level rise occurs, the inflow of saline groundwater slightly decreases as a result of small changes in the density distribution. When the sea level falls -0.6 m/c, inflow of saline groundwater in the deep aquifer ends at the beginning of the 27th century and changes into outflow of groundwater from the geohydrologic system towards the sea. Furthermore, a case is simulated in which the water level in lake IJsselmeer rises at the same rate as the sea level rises (0.6 m/c). In this case, the inflow of saline groundwater at the seaside differs only marginal from that in the case with only a sea level rise of 0.6 m/c at the seaside boundary. The reason is that the gradient in piezometric level in the vicinity of the seaside boundary decreases only slightly.
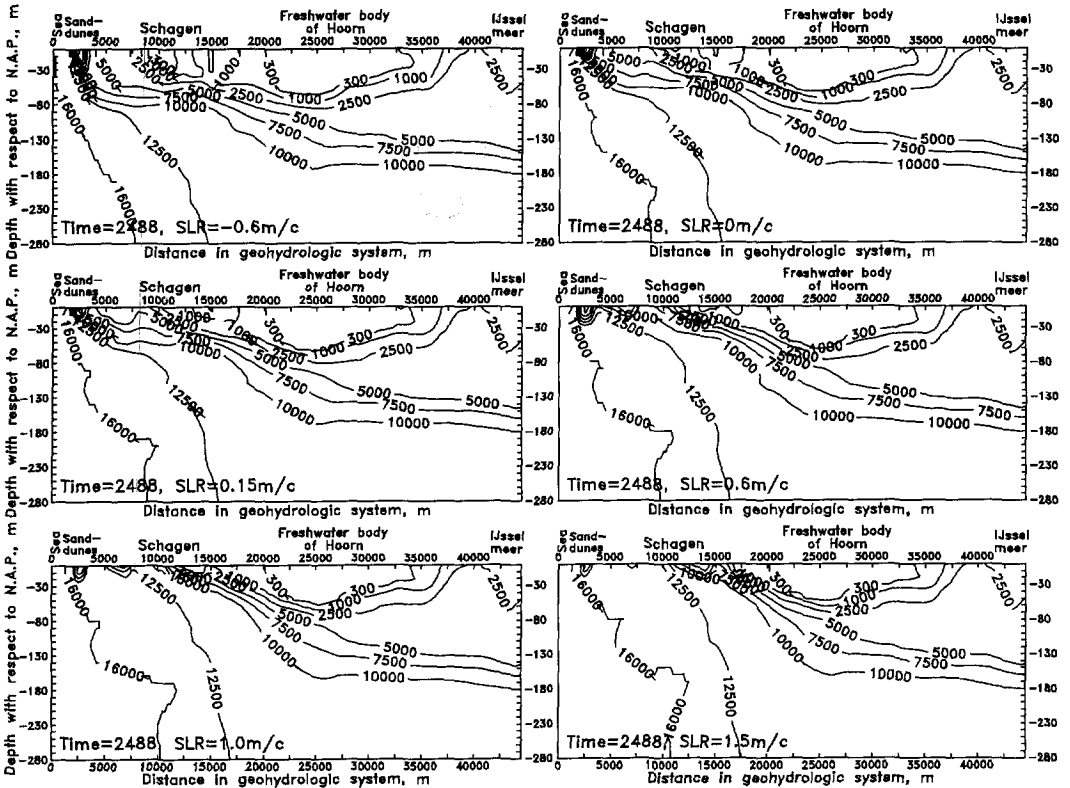
Figure 8.46: Chloride distribution (in $mg\ Cl^-/l$) in the geohydrologic system in 2488 for six scenarios of sea level rise.

Volume distribution of fresh, brackish and saline groundwater

The change in chloride distribution due to sea level rise is quantified in figure 8.48 by calculating the volume distributions of fresh, brackish and saline groundwater in percentages of the total volume of water in the geohydrologic system. Some striking observations are:

- when no sea level rise occurs, salinisation of the geohydrologic system clearly takes place during the next centuries, compared to the situation in 1988. Both the volumes of fresh and brackish groundwater in the geohydrologic system decrease several percents during the next centuries. On the other hand, the saline fraction increases, as saline groundwater is intruding from the sea in the direction of the low-lying polders,
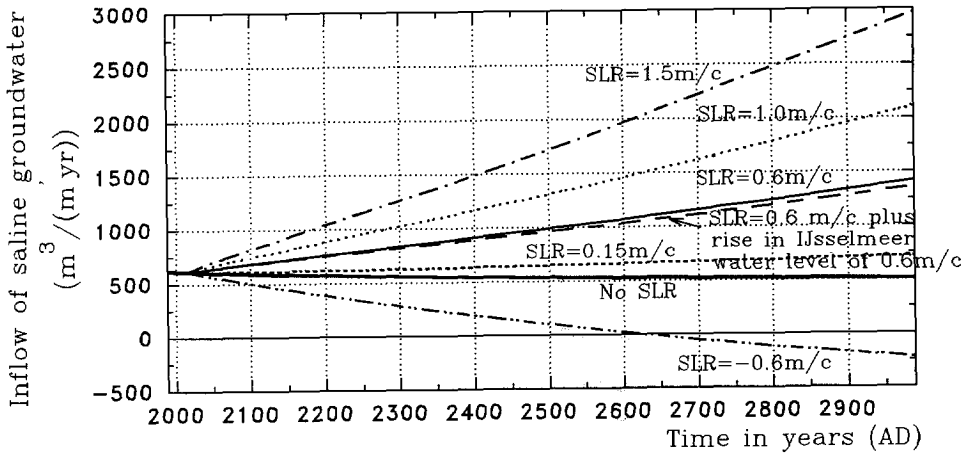
Figure 8.47: Inflow of saline groundwater in the geohydrologic system at the seaside in the deep aquifer between -120 and -280 m $N.A.P.$ for six scenarios of sea level rise plus a scenario with a water level rise at both sides of the geohydrologic system.

- even when sea level falls, salinisation of the geohydrologic system is occurring during the next centuries. Consequently, the volume of fresh groundwater is decreasing also. However, after some more centuries, the inflow of saline groundwater at the seaside boundary alters into a groundwater outflow, and subsequently, the volume of fresh and brackish groundwater in the geohydrologic system is increasing from that moment on,

- in 2088, the differences in volume distribution between the six scenarios of sea level rise can still be neglected. Only after some more centuries, the differences in volumes become significant,

- eventually, sea level rise considerably affects the distribution of fresh, brackish and saline groundwater in this geohydrologic system. Nonetheless, no (new) state of dynamic equilibrium in the volume distribution is reached during the next millennium.

Chloride concentration in the polder area near Schagen

Figure 8.49 shows the mean chloride concentration in the Holocene aquitard at -15 m $N.A.P.$ in the polder area near Schagen as a function of time for six scenarios of sea level rise. After about one century, the differences in chloride concentration between the scenarios of sea level rise become visible. For the scenarios with high rates of sea level rise, the mean chloride concentration in the Holocene aquitard increases rapidly to saline values.
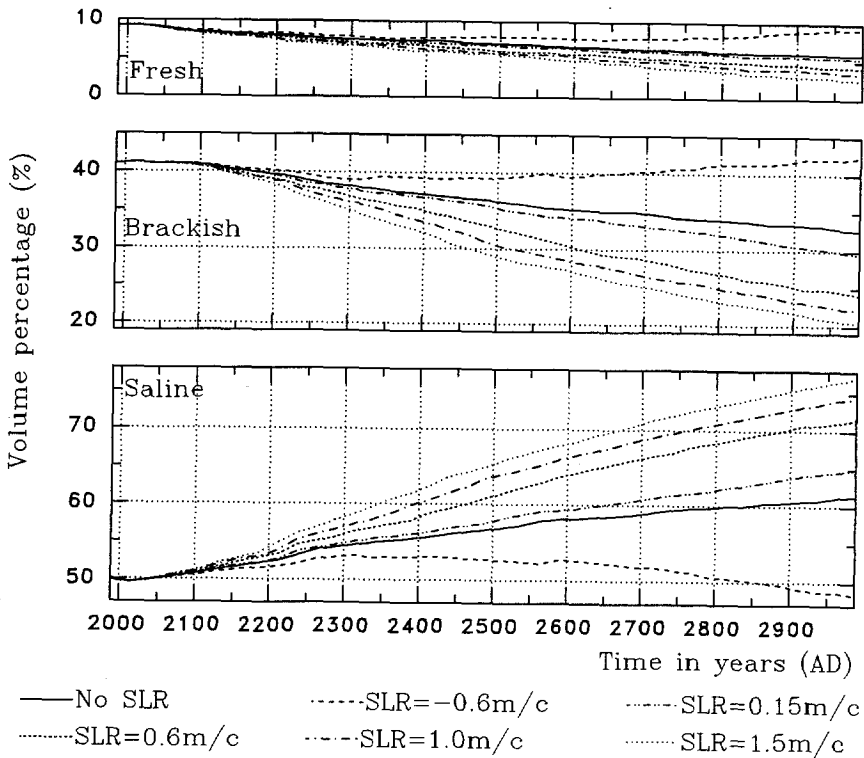
Figure 8.48: Volume percentages of fresh, brackish and saline groundwater during the next millennium for six scenarios of sea level rise. The volume percentage is determined for the entire geohydrologic system that is bounded in horizontal direction between $x=0$ and $x=44,500$ m and in vertical direction between $z=0$ and $z=-280$ m $N.A.P.$

Chloride load in the polder area near Schagen

Figure 8.50 shows the chloride load in $ton\ Cl^-/(m'yr)$ through the Holocene aquitard in the polder area near Schagen for six scenarios of sea level rise. It can be seen that high rates of sea level rise generate high chloride loads in the polder area within some centuries. Note that, at present, the chloride load in this polder area is small.

Changes in 2088 due to sea level rise: summary

In table 8.3, the changes due to sea level rise of some geohydrologic characteristics are summarized for the year 2088, as most interest is focused on changes during the next century. The decrease in inflow of saline groundwater with time (from 622.5 to 597.6 $m^3/(m'yr)$) for no sea level rise is the result of changes in density distribution through changes in chloride distribution. The increase in both seepage quantity and
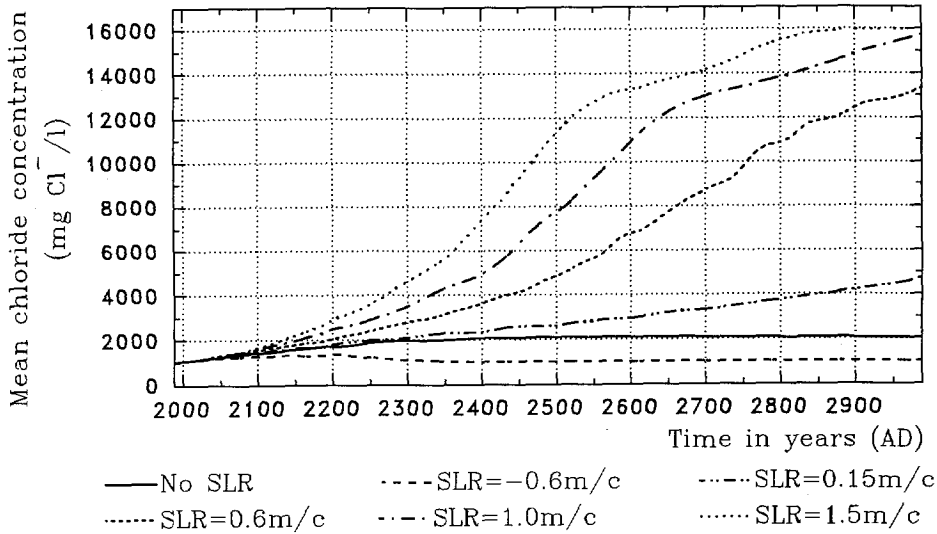
Figure 8.49: Mean chloride concentration in the Holocene aquitard of the polder area near Schagen in the reach 7000-16,000 m at -15 m $N.A.P.$ during the next millennium for six scenarios of sea level rise.
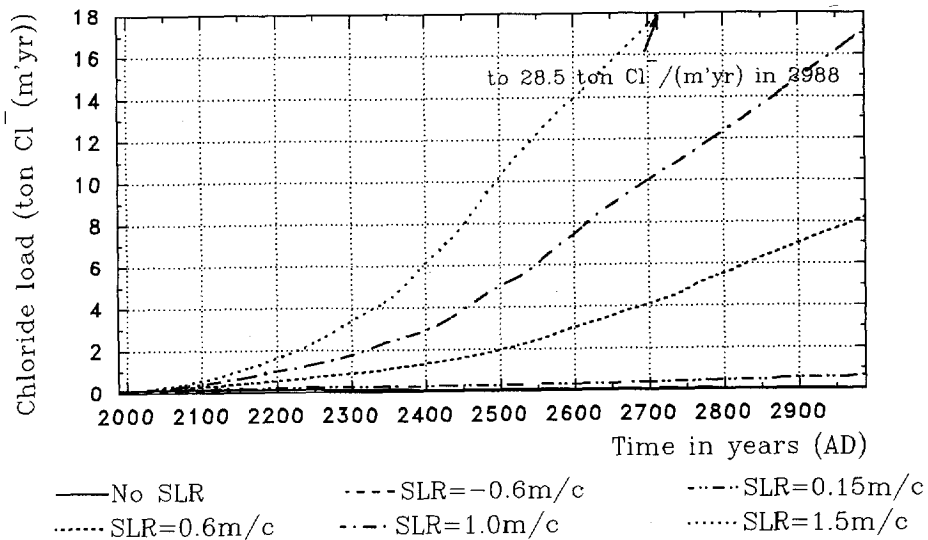
Figure 8.50: Chloride load in ton $Cl^-/(m'yr)$ through the Holocene aquitard of the polder area near Schagen in the reach 7000-16,000 m at -15 m $N.A.P.$ for six scenarios of sea level rise.

Table 8.3: Impact of six scenarios of sea level rise on some geohydrologic characteristics in 2088.

SLR	Time	Inflow of saline groundwater	Schagen polder area (7000-16,000 m)			Volumes in total system		
			Seepage	Mean Cl^-	Cl^- load	fresh	brackish	saline
m/c	AD	$m^3/(m'yr)$	$m^3/(m'yr)$	$mg\ Cl^-/l$	$ton\ Cl^-/(m'yr)$	%	%	%
0	1988	622.5	-81.5	1037	0.122	9.20	40.99	49.81
-0.6	2088	519.7	-19.7	1280	0.054	8.58	41.99	50.43
0	2088	597.6	-60.8	1406	0.153	8.41	40.97	50.62
0.15	2088	617.1	-72.9	1412	0.179	8.41	40.97	50.62
0.6	2088	675.2	-115.6	1468	0.277	8.35	40.88	50.77
1.0	2088	727.1	-155.0	1520	0.375	8.35	40.82	50.83
1.5	2088	792.9	-204.6	1563	0.497	8.39	40.78	50.93

chloride load as a function of sea level rise is significant for the scenarios with high rates of sea level rise. The changes in volume percentages of fresh, brackish and saline groundwater are insignificant during the next century.

8.3.6   Effects of countermeasures

The following three countermeasures for the negative impact of sea level rise on the geohydrologic system are investigated:

1. Extraction of saline groundwater

   Six lines of extraction wells are imposed, each with an extraction rate of about 73.3 $m^3/(m'yr)$[14]. Two scenarios with different positions of the six well lines are imposed[15]:

   Hor horizontal position: in horizontal direction at x=9875, x=11125, x=12375, x=13625, x=14875 and x=16125 m and in vertical direction at z=-95 m N.A.P.

   Ver vertical position; in vertical direction at z=-55, z=-65, z=-75, z=-85, z=-95 and z=-105 m N.A.P. and in horizontal direction at x=3625 m.

2. Deep-well infiltration of fresh surface water

   Six lines of infiltration wells are imposed, each with the same rate as in the countermeasure mentioned above in which saline groundwater is extracted: about 73.7 $m^3/(m'yr)$. The two scenarios with different positions of the six well lines are the same as in the countermeasure mentioned above[16].

---

[14]The rate of all six lines of extraction together is equal to the extraction from a canal with a rate of about 0.44 million m^3/yr over a length of one kilometre.

[15]Numerous schemes of position and extraction rate of the well lines have been simulated. One of the most effective, and yet realistic, schemes is the one applied here. Nonetheless, the optimum position and extraction rate of the well lines should be derived at a more decisive stage.

[16]As such, fresh surface water is infiltrated in a saline or brackish environment, which is not the most effective location of infiltration wells as mixing of saline and fresh groundwater would probably occur.

3. Raising the phreatic groundwater levels in some polder areas

Four scenarios are analysed: (a) inundation of all polders (the phreatic ground-water level equals $N.A.P.$); (b) raising the phreatic groundwater level to -0.5 m $N.A.P.$ for the polders in the reach 20,000-36,000 m; (c) raising the phreatic groundwater level to +1.0 m $N.A.P.$ for the polders in the reach 3000-7000 m; and (d) raising the phreatic groundwater level with 1 m for all polders.

It is obvious that these are hypothetical countermeasures, as the inundation would imply abandoning of valuable land. As such, these countermeasures should only be considered as interesting hypothetical cases in order to gain a better insight into the range of conceivable human interventions. Moreover, these unfeasible countermeasures serve the purpose of illustrating what has unconsciously been provoked during the past centuries by the creation of low-lying (polder) areas.

Discussion

The effects of these three countermeasures are discussed by comparing the counter-measures with the reference case. Some striking observations are:

• Comparison between extraction and infiltration

Figure 8.51 shows the chloride distribution in the geohydrologic system in 2988 in case of a sea level rise of 0.6 m/c for two countermeasures: extraction and infiltration. A severe salinisation of the deep parts of the geohydrologic system still takes place despite the extraction or infiltration activities to counteract the impact of sea level rise: that means the applied countermeasures appear to be insufficient[17]. However, for the year 2988, both extraction of saline groundwater and infiltration of surface water decrease the saline groundwater fraction com-pared to the reference case. Only in the upper part of the geohydrologic system at the inland side of the well lines, the salinisation is counteracted. Deep-well infiltration creates a larger brackish zone compared to both no countermeasure (the reference case) and extraction of saline groundwater. When sea level rises, the fresh groundwater fraction for all three scenarios (no countermeasure, ex-traction and infiltration) is smaller in 2988 than for the reference case in 1988 (figure 8.35).

ad 1. Extraction of saline groundwater

Figure 8.52 shows the influence of six extraction and infiltration well lines on the chloride load in the polder area near Schagen. When the sea level rises 0.6 m/c, the chloride load in the polder area near Schagen is less for the countermeasures with extraction of saline groundwater (see the two countermeasures with 'Ext' as well as 'SLR') than for the scenario with only a sea level rise of 0.6 m/c, because the applied extraction of saline groundwater lowers the seepage.

---

[17]Obviously, much higher rates of extraction and infiltration will counteract the impact of sea level rise more effectively, but these rates are probably unfeasible from an economic point of view.
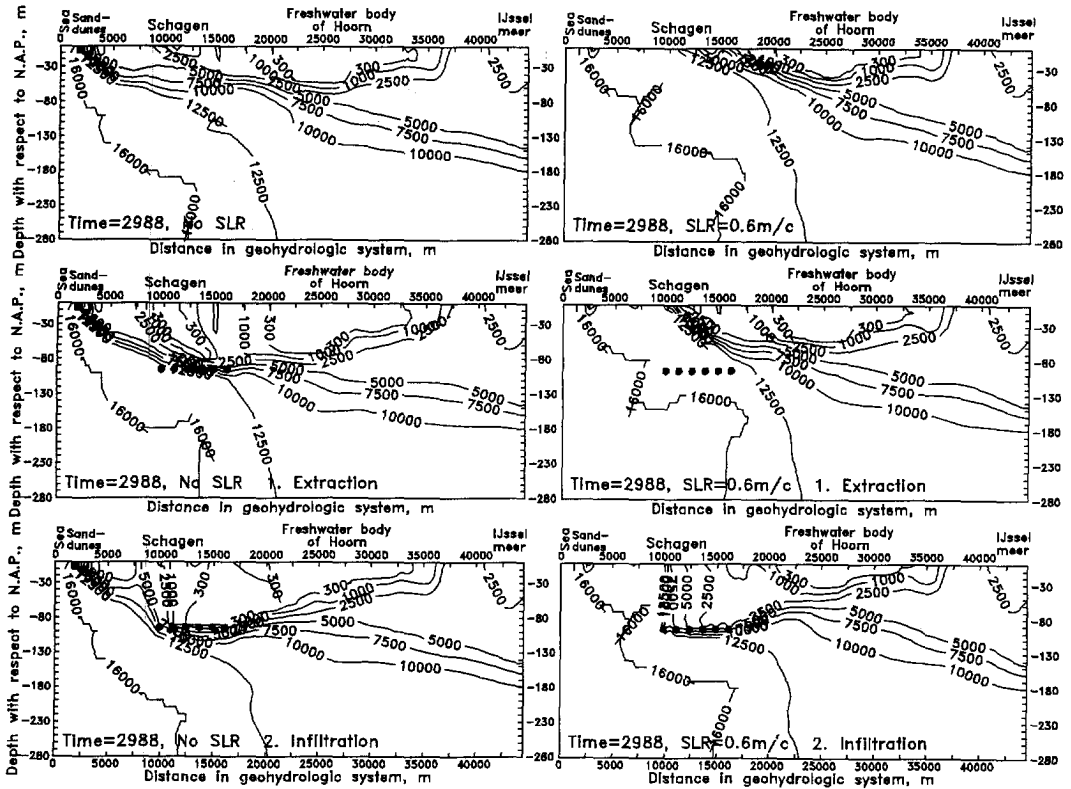
Figure 8.51: Chloride distribution (in $mg\ Cl^-/l$) in the geohydrologic system in 2988 in case of a sea level rise of 0.6 m/c for two countermeasures: extraction and infiltration. Only the scenario with the horizontal position of the six well lines (Hor) is shown. The symbol • represents the position of a well line.

Note that the position of the lines of extraction wells in the geohydrologic system is rather important. Obviously, the well lines must be situated near the seaside of the geohydrologic system, where the most serious impact of sea level rise is experienced. However, high extraction rates of saline groundwater near the coast also enlarge the inflow of saline groundwater from the sea. Therefore, the optimum position and capacity of the well lines should be derived at a more advanced stage.

ad 2. Deep-well infiltration of fresh surface water

The applied deep-well infiltration creates a strong groundwater flow in the geohydrologic system and raises the seepage quantity in the polder area near Schagen. The infiltrated fresh surface water is pushing brackish groundwater, which
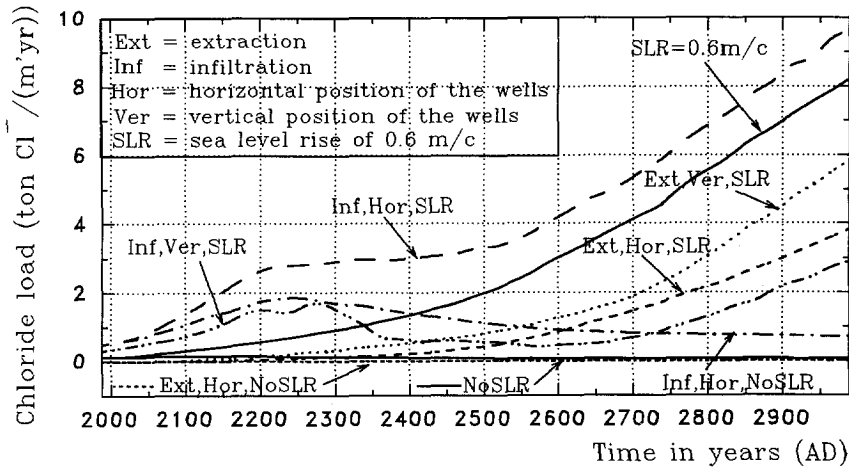
Figure 8.52: Chloride load in *ton $Cl^-/(m'yr)$* through the Holocene aquitard of the polder area near Schagen in the reach 7000-16,000 *m*. Two scenarios with different positions of the six well lines are imposed: in horizontal position Hor and in vertical position Ver. Both extraction of saline groundwater or infiltration of surface water are simulated in combination with a sea level rise of 0.6 *m/c*.

already occurs in the geohydrologic system, in the direction of the Holocene aquitard. Consequently, the seepage has a higher chloride concentration than in the reference case. This leads to a higher chloride load during the next centuries (figure 8.52: see the countermeasures with 'Inf'). When no sea level rise occurs, the applied deep-well infiltration creates a freshwater lens (see figure 8.51), and eventually, some fresh groundwater could be extracted from this lens above the filter depths of the infiltration well lines for domestic or industrial purposes. However, when the sea level rises 0.6 *m/c*, the chloride concentration in this (brackishwater) lens is too high to extract it for use.

Note that, here again, the position of lines of infiltration wells in the geohydrologic system is rather important (figure 8.52: compare 'Inf,Ver,SLR' with 'Inf,Hor,SLR'), and the optimum position and capacity of the well lines should be derived at a more advanced stage.

ad 3. Raising the phreatic groundwater levels in some polder areas.

Most of the changes in groundwater flow, seepage quantity and chloride load take place locally, in and nearby those polder areas where the phreatic groundwater levels have been raised.

Figure 8.53 shows changes in volume distribution of fresh, brackish and saline groundwater during the next millennium due to raising the phreatic ground-

——Reference case: no SLR   – – SLR=0.6m/c

······(a) Inundation all polder levels of N.A.P.

- - - -SLR=0.6m/c+(a) inundation all polder levels to N.A.P.

······(b) Raising polder levels in the reach 20,000–36,000 m to −0.5m N.A.P.

- · – (c) Raising polder levels in the reach 3000–7000 m to +1m N.A.P.

- · – (d) Raising all polder levels with 1 m
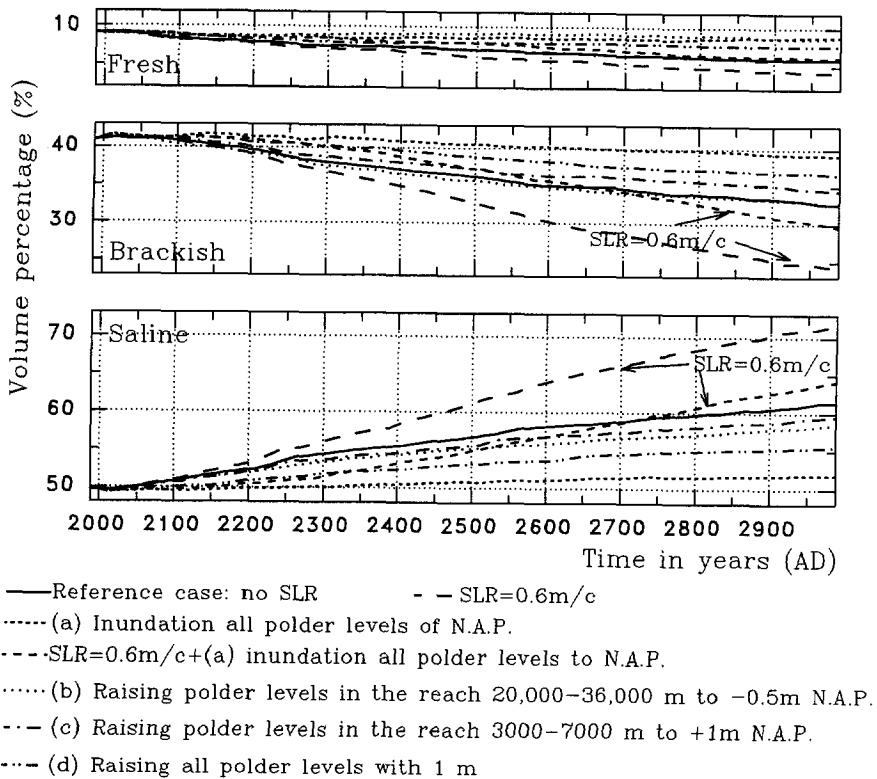
Figure 8.53: Volume percentages of fresh, brackish and saline groundwater in the geohydrologic system. The effects of five scenarios of raising the phreatic groundwater levels in some polder areas are given.

water level. As can be seen, the differences may be significant, which depends on the raising the phreatic groundwater level and on the area over which the raising occurs. For instance, for the scenario, in which the polder water levels for all polders are raised to *N.A.P.*, the changes in volume distribution are significant compared to the reference case. The reason is that such a raising the phreatic groundwater level reduces groundwater flow in the geohydrologic system extremely. Note, once again, that these last countermeasures are unfeasible.

8.3.7   Conclusions

A severe salinisation occurs already in this coastal geohydrologic system in the northern part of Noord-Holland, independent of sea level rise. The present salinisation process is dominated by human activities. The reclamation of the (low-lying) pold-

ers, which is already taking place during at least several centuries, has generated a strong inflow of saline groundwater from the sea in the deeper aquifers, though the salinisation of the geohydrologic system proceeds slowly. The freshwater body of Hoorn remains when the sea level does not rise. Note that a considerable time lag of some centuries occurs between the cause of changes (e.g. sea level rise or human interventions) and the ultimate effect on the salinisation process.

Sea level rise accelerates the salinisation process significantly. The zone of influence of sea level rise in the geohydrologic system is quite some kilometres, among others, due to high transmissivities in the deeper aquifer. As a consequence, the salt water intrusion extends several kilometres more inland in case of a sea level rise than in case of no sea level rise. In the low-lying polders near the coast, the seepage, both in terms of quantity and quality, increases significantly within some centuries in the low-lying polder areas in the first 15,000 m from the coast. Moreover, the upper part of the geohydrologic system in this area eventually contains only saline groundwater. The freshwater body of Hoorn disappears when the sea level rises 0.6 m/c.

Human interventions within the bounds of feasibility can counteract the impact of sea level rise on the geohydrologic system, but the salinisation process cannot easily be neutralized, and thus, it seems to be irreversible. Note that other schemes and rates of the extraction and infiltration well lines may lead to more positive effects, but these rates might be unfeasible from an economic point of view.

Chapter 9

Sensitivity analysis of Dutch groundwater flow regimes for sea level rise

9.1   Introduction

The sensitivity of the groundwater flow regime in the Netherlands for sea level rise is analysed[1] by simulating eight representative profiles perpendicular to the Dutch coastline. Each representative profile characterizes a specific coastal area[2] in the Netherlands. The influence of three main groups of cases are assessed through numerical modelling with the adapted MOC model: (I) scenarios with different rates of sea level rise; (II) (hypothetical) measures that counteract the negative impact of sea level rise; and (III) cases with different subsoil parameters. In this chapter, the objective is focused on the following impacts of sea level rise for each profile:

- the propagation of sea level rise in the piezometric level distribution

- the changes in salt water intrusion in the geohydrologic system

- the changes in the volumes of freshwater lenses in sand-dune areas

- the changes in seepage (both quantity and quality) in low-lying polders

In section 9.2, the eight representative profiles are chosen and described. In section 9.3, the three main groups of cases are selected. In section 9.4, the propagation of sea level rise in each geohydrologic system is considered. In section 9.5, the salt water intrusion in each geohydrologic system is described. In section 9.6, the evolution of the freshwater lens in four geohydrologic systems is evaluated. In section 9.7, the changes in seepage (both quantity and quality) in one selected polder of each profile are discussed. In section 9.8, the influence of several (hypothetical) countermeasures is described. In section 9.9, the influence of some important subsoil parameters is analysed. Finally, in section 9.10, some conclusions are drawn and recommendations are given.

---

[1]Note that the methodology followed in this chapter to investigate and to assess the impact of scenarios of sea level rise and human activities on Dutch coastal groundwater flow regimes could also be extended to similar vulnerable coastal groundwater flow regimes around the world.

[2]On this point, this chapter differs from chapter 8, where actual profiles have been considered.

9.2   Representative profiles along the Dutch coast

As the applied groundwater flow model is two-dimensional, profiles have been chosen perpendicular to the Dutch coastline. A general schematisation of the geohydrologic system perpendicular to the Dutch coastline is given in figure 9.1. Each profile represents a coastal zone with its own specific subsoil parameters which differ from the subsoil parameters of profiles in the vicinity. Strictly speaking, the number of conceivable profiles is infinite. For reasons of simplicity, however, the number of profiles has been limited to eight. Figure 9.2 shows the position of these eight so-called *representative profiles* perpendicular to the Dutch coastline. Note that the islands of the province of Zeeland are not modelled. This is argued later in this section. The names of the profiles are arbitrarily chosen: they refer to a city, region or province positioned in that profile. The subsoil parameters, which are representative for each dotted area, are reflected in each profile.
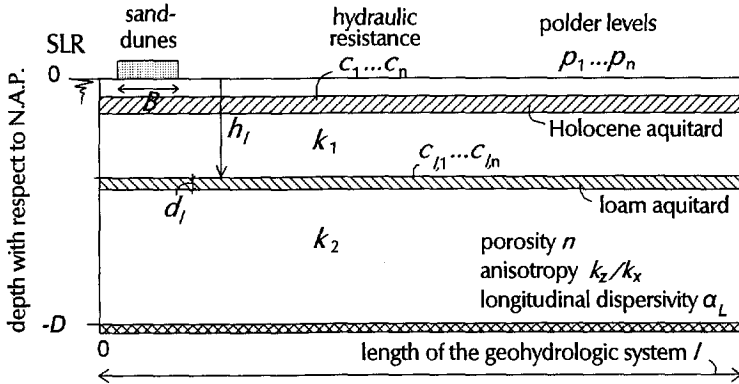
Figure 9.1: Schematised profile of the subsoil perpendicular to the Dutch coastline, the so-called Holland profile.

Apparently, three-dimensional effects, such as groundwater flow perpendicular to the profile due to groundwater extractions or low phreatic groundwater levels in polders, are left out of consideration. In fact, these effects may be very important for the interpretation of the results, but for the applied profiles, in which subsoil parameters are averaged over areas of several hundred square kilometres, the effects are probably of minor importance.

Subsoil parameters

The following subsoil parameters have been considered (see figure 9.1), accompanied by a conceivable range of the subsoil conditions along the Dutch coast:

- the thickness of the geohydrologic system D down to the geohydrologic base: it decreases from some 280 m (in the northern part of Noord-Holland) to some

profile	l km	$L_\perp$ km
1. Wie	30	25
2. Ber	30	30
3. Haa	40	25
4. Lei	40	15
5. Del	40	15
6. Vla	20	50
7. Grf	30	105
8. Wad	10	50

⟶ orientation of the profile

l = length of the geohydrologic system

$L_\perp$ = width perpendicular to the profile
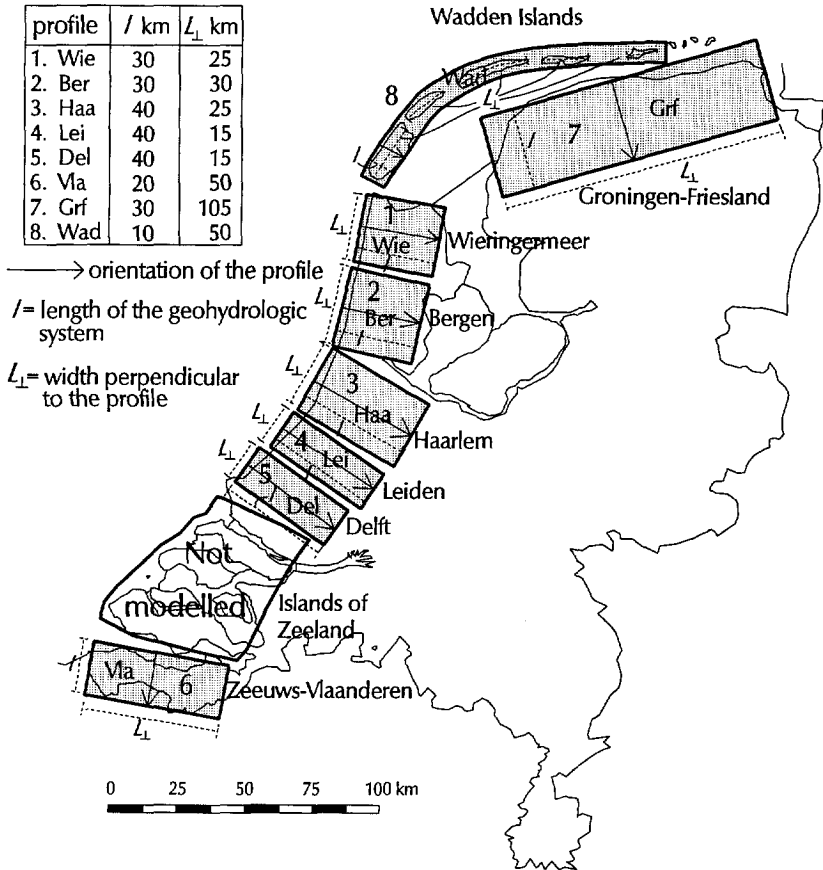
Figure 9.2: Location of the eight areas in which the eight representative profiles perpendicular to the Dutch coastline are defined. The islands of Zeeland are not modelled.

20 m (in Zeeuws-Vlaanderen).

- the hydraulic conductivity k: from 5 m/d to 70 m/d. The hydraulic conductivity of the aquifers can vary over short distances.

- the hydraulic resistance c of the Holocene aquitard: from 100 $days$[3] to 25,000 $days$. The hydraulic resistance of aquitards can vary considerably over short distances.

- the length of the geohydrologic system l: from 10,000 m to 40,000 m.

---

[3]In reality, even lower hydraulic resistances occur. As averaged values are applied in the profiles, a hydraulic resistance of 100 $days$ is taken as the lower limit.

- the depth h_l of the top of the loam aquitard with the hydraulic resistance c_l and the thickness d_l, where present: h_l from 30 m to 100 m, c_l from 500 $days$ to 2000 $days$ and d_l from 5 m to 20 m.

- the width of the sand-dune area B: from 0 m to 5000 m.

- the groundwater recharge f in the sand-dune area: the present average value of 360 mm/yr and 60 % and 120 % of it[4].

- the phreatic groundwater levels p in the polders: from +2.5 m to -6 m N.A.P.

The effective porosity n_e is set to 0.35; the longitudinal dispersivity α_L is set to 0.2 m; and the anisotropy factor k_z/k_x equals 0.1. The influence of these three subsoil parameters is analysed in subsection 9.9.

Based on the subsoil conditions mentioned above, eight profiles are formulated. Figure 9.3 shows the geometry, the values of the subsoil parameters and the phreatic groundwater levels in the polders of each profile. As can be seen, there is a great variety of subsoil conditions along the Dutch coast. The data of the geohydrological schematisation have mainly been borrowed from the following sources:

- the ICW reports Regionale Studies: no. 9 [1976] of the central western part of the Netherlands; no. 13 [1978] of the northern part of the Netherlands; and no. 16 [1982] of the northern part of the province of Noord-Holland.

- the RIVM report Landelijk Grondwatermodel; Conceptuele Modelbeschrijving [Pastoors, 1992],

- the reports of the geohydrologic situations of the coastal areas: between Noordwijk and Zandvoort aan Zee [Stuyfzand, 1988] and between Katwijk and Kijkduin [Stuyfzand et al., 1993].

- numerous Grondwaterkaarten van Nederland of the TNO Institute of Applied Geoscience, Delft: Zandvoort/Amsterdam [1979a], Alkmaar/Medemblik [1979b], 's Gravenhage/Utrecht [1980], Zeeuws-Vlaanderen [1982], Medemblik [1984a], Rotterdam [1984b], Goedereede, Zierikzee/Willemstad [1984c], Waddeneilanden [1987a], Leeuwarden/Groningen [1987b], Harlingen/Leeuwarden [1987c], and Middelburg/Bergen op Zoom [1985].

Figure 9.4 shows the phreatic groundwater levels in the polders as well as in the sand-dune areas. As can be seen, the phreatic groundwater levels in the polders are below N.A.P. in all profiles except in the profile VIa. Obviously, this situation reveals that a permanent salinisation process must be taking place in the direction of the (low-lying) polders.

---

[4]Changes in the groundwater recharge f could occur due to changes in natural groundwater recharge (e.g. due to climate change) and in artificial recharge of fresh surface water. In addition, changes in groundwater extraction rates from the phreatic aquifer may also affect the deep groundwater percolation through the Holocene aquitard.
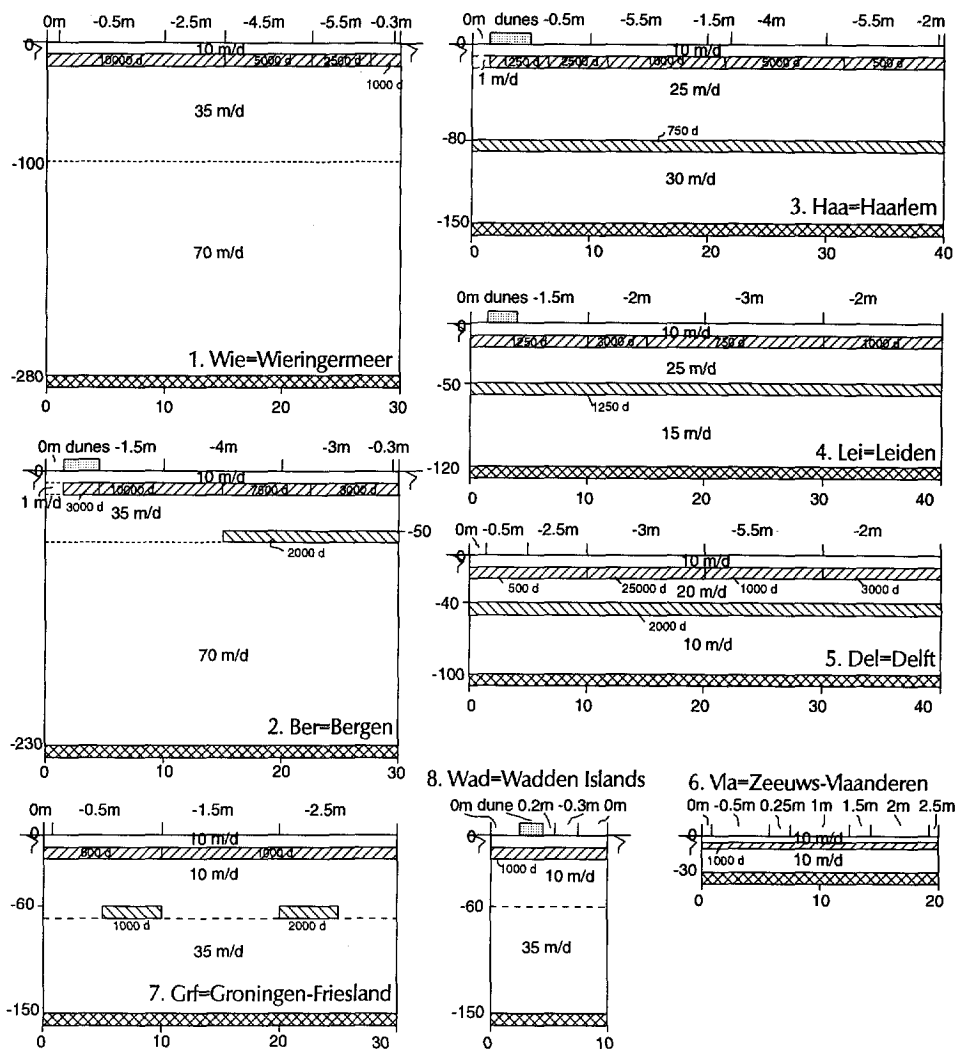
Figure 9.3: Geometry, subsoil parameters and phreatic groundwater levels with respect to *N.A.P.* (Normaal Amsterdams Peil) in the polders of the eight representative profiles.

Chloride distribution

Figure 9.5 shows the chloride distributions in 1990 in the eight profiles, derived from several different sources [e.g. ICW 1976, 1978, 1982; TNO-GG/RIZA, 1994a, 1994b]. Sand-dune areas with freshwater lenses occur in only four profiles: in Ber, Haa, Lei and Wad. As concentration measurements at great depths are generally rare, the chloride distribution in some places might be disputable.
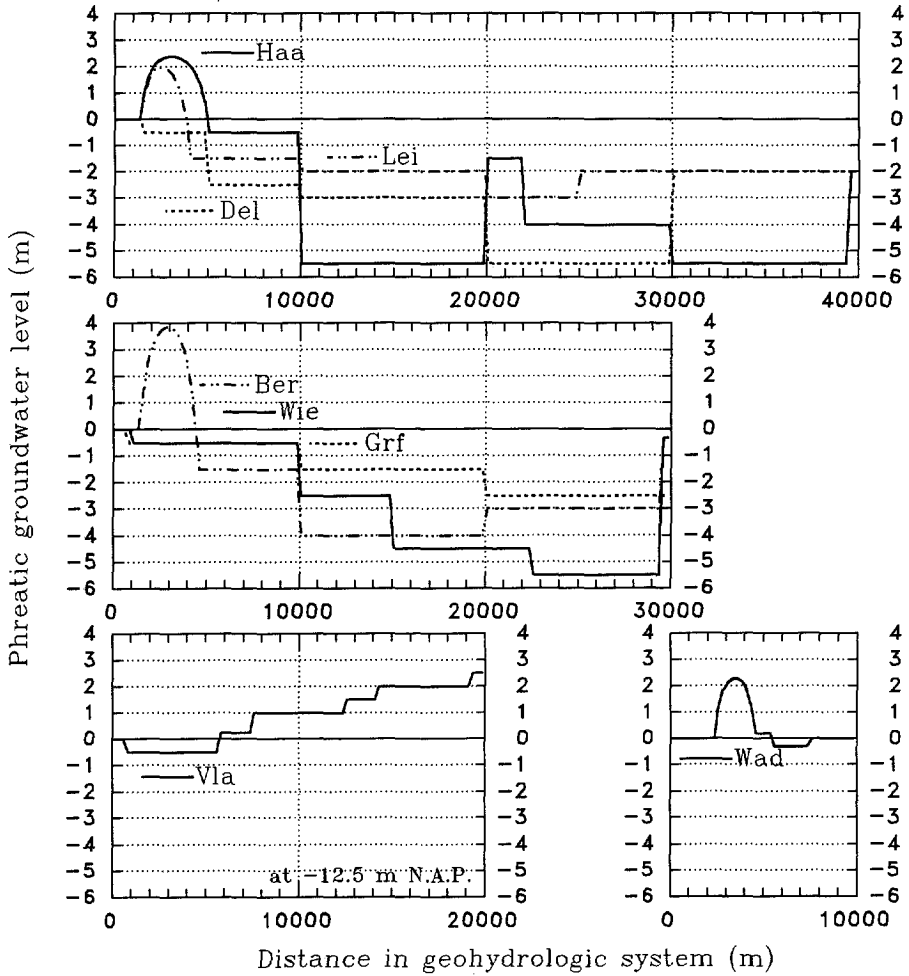
Figure 9.4: Phreatic groundwater levels with respect to *N.A.P.* in polders and in sand-dune areas, where present, of the eight profiles.

Characteristics of each profile

Specific characteristics of each profile are briefly discussed below:

1. *Wie=Wieringermeer*

   The transmissivity of this geohydrologic system is huge, as the thickness is enormous, some 260 m, and the hydraulic conductivity high. Moreover, the hydraulic resistance of the Holocene aquitard is high. The length of the system equals 30,000 m. No sand-dune area occurs. The polder (that is the Wieringermeer polder) in the reach 15,000-29,500 m has a very low phreatic groundwater
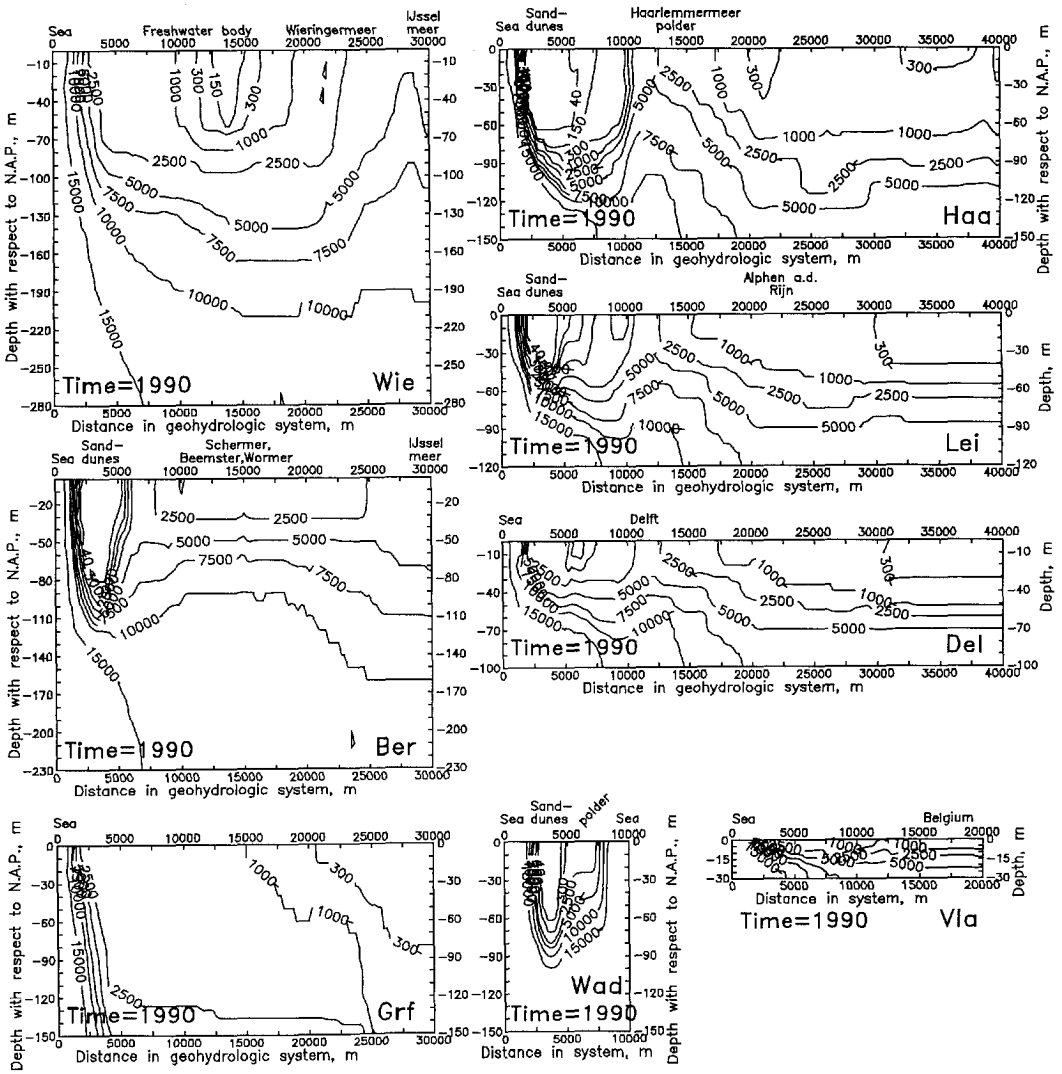
Figure 9.5: Chloride distributions (in $mg\ Cl^-/l$) in 1990 in the eight representative profiles.

level: between -4.5 and -5.5 m $N.A.P.$. At the inland boundary, the water level in the IJsselmeer is a constant piezometric level boundary. Fresh groundwater, which belongs to the freshwater body of Hoorn, is present in the central part of this profile.

2. **Ber=Bergen**
    The thickness of this geohydrologic system is some 230 m. In the central part of

this profile, a low-lying polder (-4 m $N.A.P.$) occurs, which represents the areas reclaimed in the seventeenth century: the Beemster (1608-1612), the Wormer (1625-1626), and the Schermer (1633-1635) [Schultz, 1992]. The main difference with the profile Wie in terms of chloride distribution is due to the presence of a simulated sand-dune area of 3000 m width under which a freshwater lens has evolved. The base of this lens can be found at a depth of at least 75 m below $N.A.P.$ Note that these figures are values which are averaged over a length $L_\perp$ of 30,000 m. In reality, however, in some places the width of the sand-dune area is greater (e.g. 5000 m) and the lens thicker (e.g. 130 m below $N.A.P.$) than simulated in this representative profile.

3. Haa=Haarlem

The length of this geohydrologic system equals 40,000 m. The thickness of the geohydrologic system is about 130 m, and the hydraulic conductivity is lower than in the two profiles mentioned above. Various low-lying polders are located at a considerable distance from the coast: e.g. the Haarlemmermeer polder in the reach 10,000-20,000 m. From the coastline, a broad sand-dune area extends to 3500 m inland. Gemeentewaterleidingen Amsterdam has pumped water from this area since the middle of the nineteenth century[5]. The freshwater lens reaches to a depth of at least 80 m below $N.A.P.$ Below this lens, saline groundwater flows in the direction of the low-lying Haarlemmermeer polder.

4. Lei=Leiden

This profile resembles the profile Haa to a certain extent. The main differences, however, are that (1) the thickness of the geohydrologic system is some 30 m less and (2) the phreatic groundwater levels of the polders is a few metres higher. The width of the sand-dune area is 2500 m, and hence, the thickness of the freshwater lens is somewhat smaller than in the profile Haa.

5. Del=Delft

Though, from a geohydrological point of view, this profile corresponds to a great extent with the profile Lei, a significant difference can be found in the hydraulic resistance of the Holocene aquitard in the reach 10,000-20,000 m: e.g. 25,000 $days$ in the profile Del instead of 3000 $days$ and 750 $days$ in the profile Lei. The sand-dune area, present in this profile, is too small to be simulated. Relatively low polders at some kilometres inland of the coast (-2.5 m $N.A.P.$ from x=5000 m) induce a flow of saline groundwater in the geohydrologic system. Close to the city of Delft, groundwater is extracted for industrial purposes. Two lines of extraction wells are simulated, located at x=13625 m, z=-25 m $N.A.P.$ and z=-35 m $N.A.P.$ The high extraction rate is equal to some 293 $m^3/(m'yr)$ per

---

[5]The total extraction rate in three lines of extraction wells in the middle aquifer of the sand-dune area is about 192.3 $m^3/(m'yr)$ for a simulation time of one millennium. This rate equals the rate in the period 1974-1987, see also figure 7.2 in section 7.2.

well line[6].

6. Vla=Zeeuws-Vlaanderen

   The Belgium hinterland is also considered in this profile. The length of the geohydrologic system equals 20,000 m. The phreatic groundwater levels in the polders at some kilometres inland of the coast are above $N.A.P.$ The thickness of the geohydrologic system is the smallest of all profiles, only some 20 m. In the past, a severe salinisation process has caused high chloride concentrations in this geohydrologic system.

7. Grf=Groningen-Friesland

   The length of the geohydrologic system equals 30,000 m. The phreatic groundwater levels are not very low in this profile. The hydraulic resistance of the Holocene aquitard is low, 500 and 1000 *days*. About halfway the system several small loam aquitards occur. The length of the saline groundwater tongue is limited to some kilometres. More inland of the tongue, brackish groundwater is present in the entire geohydrologic system.

8. Wad=Wadden Islands

   The Wadden Islands are schematised by this profile. At both boundaries, a sea level condition is present. A sand-dune area occurs at the North Sea side. At the Waddenzee side, polders are present with phreatic groundwater levels around $N.A.P.$ The thickness of the geohydrologic system[7] considered is set to some 130 m. The width of the sand-dune area is 2000 m, under which a freshwater lens has evolved with a thickness of about 80 m. Note that this profile closely corresponds with that of Texel.

The islands of Zeeland

   At first, the islands of Zeeland were modelled by means of a profile that corresponded with the geohydrologic system of Walcheren in northeast-southwest direction. However, it unfortunately appeared that it is not really possible to model the islands of Zeeland by means of a representative profile because the islands cannot be schematised in two dimensions[8]. Moreover, there are several reasons why the characteristics of these islands differ too much from each other to join them together in one representative profile. Firstly, the thickness of the geohydrologic system of these islands varies from about 100 m in the north to about 50 m in the south. Secondly, the phreatic groundwater levels of the polders vary from about $N.A.P.$ in Zuid-Beveland to about -3 m $N.A.P.$

---

[6]The rate of both well lines together is equal to the extraction from a drainpipe with a rate of about 0.59 million m^3/yr over a length of *one kilometre*.

[7]Just like in the profile Grf, the top of the third aquitard is taken as the geohydrologic base in the profile Wad [Pastoors, 1992].

[8]For instance, narrow sand-dune areas occur in the western seaside parts of the islands, which would complicate a proper selection of the orientation of the profile: in northeast-southwest direction or in northwest-southeast direction.

in Schouwen-Duiveland (the levels in this profile are relatively high compared with the levels in other profiles). Finally, the boundary conditions of the islands vary from a constant piezometric level boundary with fresh water (e.g. the northern side of Goeree-Overflakkee at the Haringvliet), a constant piezometric level boundary with saline water (e.g. the northern side of Schouwen-Duiveland at the Grevelingenmeer) to a piezometric level boundary that changes with sea level rise (namely Walcheren and the southern side of Zuid-Beveland).

As the impact of sea level rise could be significant in these coastal groundwater flow regimes, it is recommended to consider these islands through three-dimensional numerical modelling at a later stage.

9.3   Selection of cases

Obviously, innumerable cases regarding groundwater flow in coastal geohydrologic systems could be simulated for each profile. In this study, however, only some conceivable cases are chosen. They are subdivided into three main groups: (I) scenarios with different rates of sea level rise; (II) cases with (hypothetical) countermeasures; and (III) cases with different subsoil parameters for a sensitivity analysis. The cases of main group (II) are considered for two scenarios of sea level rise: one with no sea level rise and one with a sea level rise of 0.6 m/c. To arrive at a comprehensive view over the results of the simulations, a selection of relevant cases has been made. The selected cases are simulated with the adapted MOC model. Table 9.1 summarizes all relevant cases which are briefly described below:

a. Reference case: no sea level rise

This scenario with no sea level rise is applied as the so-called *reference case* for all cases. The present situation concerning boundary and initial conditions, phreatic groundwater levels in the polders and groundwater extraction rates is maintained during this scenario, which has a (long) simulation time of ten millennia. Accordingly, many processes[9] that may affect the geohydrologic system are left out of consideration. The results of this scenario may clarify the effect of (past) human activities, such as land reclamation which has created low-lying polder areas. Furthermore, the time lag has been determined before a state of dynamic equilibrium regarding the chloride distribution will be reached.

b.-f. Scenarios of sea level rise

In contrast with chapter 8, where all six scenarios of sea level rise were executed, here only three scenarios are considered for a simulation time of one millennium: (1) no sea level rise; (2) a sea level fall of -0.6 m/c; and (3) a sea level rise of 0.6 m/c. The change in sea level is added to the freshwater head in specific grid

---

[9]These processes are of a hydrological nature (e.g. less precipitation, more evapotranspiration due to climate change), a morphological nature (e.g. shoreline retreat) or a man-induced nature (e.g. sand-suppletion at the coastal zone to counteract shoreline retreat).

Table 9.1: Relevant cases regarding groundwater flow in coastal geohydrologic systems.

Cases		Representative profiles along the Dutch coast							
		1. Wie	2. Ber	3. Haa	4. Lei	5. Del	6. Vla	7. Grf	8. Wad
I. Scenarios of sea level rise									
a.	SLR=0 m/c: reference case	●	●	●	●	●	●	●	●
b.	SLR=-0.6 m/c	●	●	●	●	●	●	●	●
c.	SLR=0.15 m/c	−	−	−	−	−	−	−	−
d.	SLR=0.6 m/c	●	●	●	●	●	●	●	●
e.	SLR=1.0 m/c	−	−	−	−	−	−	−	−
f.	SLR=1.5 m/c	−	−	−	−	−	−	−	−
g.	Land-subsidence	−	−	−	−	−	−	−	−
h.	Groundwater recharge	n.a.	−	−	−	n.a.	n.a.	n.a.	−
II. Countermeasures									
i.	Constant level IJsselmeer	●	●	n.a.	n.a.	n.a.	n.a.	n.a.	n.a.
j.	Land reclamation	●	●	●	●	●	n.a.	●	●
k.	Extraction of groundwater	●	●	●	●	●	●	●	●
l.	Infiltration of surface water	●	●	●	●	●	●	●	●
m.	Inundation of polders	●	●	●	●	●	n.a.	●	●
n.	Widen the sand-dune area	●	●	●	●	●	●	●	●
o.	Physical barrier	●	●	●	●	●	●	●	●
III. Subsoil parameters									
p.	Hydraulic conductivity k	−	●	●	●	●	−	●	●
q.	Hydraulic resistance c	●	●	●	−	−	−	−	−
r.	Longitudinal dispersivity α_L	●	●	●	●	●	●	●	●
s.	Effective porosity n_e	●	●	●	−	−	−	●	−
t.	Anisotropy k_z/k_x	−	●	●	−	−	−	−	−
u.	Depth geohydrologic base D	●	●	●	●	●	−	●	●

● = case is executed; − = case is not executed; n.a. = not applicable

1. Wie=Wieringermeer	2. Ber=Bergen	3. Haa=Haarlem
4. Lei=Leiden	5. Del=Delft	6. Vla=Zeeuws-Vlaanderen
7. Grf=Groningen-Friesland	8. Wad=Wadden-Islands	

cells by means of equation 5.76 before every flow time step Δt. The time lag, in which the freshwater head in the geohydrologic system rises to a new state of dynamic equilibrium due to sea level rise, can be neglected with respect to the time lag in which the salinity distribution changes. Therefore, it is allowed to change the freshwater head in the geohydrologic system instantaneously by setting the specific storativity equal to zero. The range of sea level rise from -0.6 m/c to 0.6 m/c is such that a distinct view can be gained of the impact of sea level rise. Bear in mind that a sea level rise with a rate of e.g. 0.6 m/c means a sea level elevation of 6 m after a simulation time of one millennium.

The rise in sea level induces an elevation in phreatic groundwater level in the sand-dune area. In fact, the rise in phreatic groundwater level could be impeded if the position of the land surface is fixed. In order to assure that the phreatic groundwater level can rise freely, sand-suppletion is supposed to nullify the possible impediment.

g. Land-subsidence

Polder areas subside because of compaction, shrinkage and oxidation of peat as well as man-induced processes such as local mining activities (e.g. oil and gas) and groundwater recovery. Actually, land-subsidence is analogous to a relative sea level rise, on condition that the subsidence is the same everywhere. As the rate of land-subsidence is in the order of 0.15 m/c, this scenario is not considered separately.

h. Groundwater recharge

The groundwater recharge can alter due to a change in: (a) the natural component: e.g. change in the present precipitation pattern due to climate change [IPCC, Houghton et al., 1990], and (b) the anthropogenic component: e.g. change in artificial recharge or withdrawal of groundwater from the phreatic aquifer. Two scenarios are selected to assess the influence of a change in groundwater recharge on the salinity distribution in the profiles: (a) 216 mm/yr (60 % of the reference case) and (b) 432 mm/yr (120 % of the reference case). These scenarios are not executed in this chapter, as the effect of a change in groundwater recharge appears to be small (see section 7.5 item 4. Groundwater recharge).

i. Constant water level in the IJsselmeer when sea level rises

Unlike the scenarios with a sea level rise (b.-f.) where the water level in the IJsselmeer matches the sea level, in this case the water level in the IJsselmeer remains constant by means of pumping.

j. Land reclamation

Land reclamation off the coast can be applied to counteract the salinisation of the coastal geohydrologic system. Land reclamation may create a new groundwater flow situation in the geohydrologic system that might reduce the salinisation process. In subsection 8.2.6, land reclamation was briefly discussed in connection with the project Plan Waterman or Nieuw-Holland [Overeem et al., 1993; Stuurgroep Kustlocatie, 1995]. All profiles but one are executed with a certain strip of land, reclaimed on the seaside of the coastline. In the profile VIa, the presence of the Westerschelde estuary does not make this countermeasure realistic, and hence, it is not investigated.

k.-l. Extraction of saline groundwater and infiltration of surface water

Both extraction of saline groundwater and deep-well infiltration of surface water (chloride concentration is set to 500 $mg\ Cl^-/l$) may significantly affect the

salinisation process in each profile. The position of well lines and the exact rates of extraction or infiltration in the geohydrologic system is rather important (see table 9.2). The well lines should be situated in the vicinity of the seaside, where the greatest impact of sea level rise is to be expected. Only one well line scheme for each countermeasure is simulated, so the results are just indicative. Note that the positions and the rates of the well lines are not changed during the entire simulation, whereas, in reality, they will probably be adapted and optimized throughout the years based on changes in the salinisation of the subsoil.

Table **9.2**: Features of extractions of saline groundwater as well as deep-well infiltration of surface water in each profile: number of well lines and rates. The position of the well lines is shown in figure 9.26.

Wie	Ber	Haa	Lei	Del	Vla	Grf	Wad
Number of extraction and infiltration well lines							
10	10	8	13	8	8	10	6
Total rate for extraction and infiltration $(m^3/(m'yr))$							
1466	1466	704	381	352	118	528	498

m. **Inundation of polders**

Inundation of polders through raising the phreatic groundwater levels to $N.A.P.$ certainly influences both groundwater flow in the geohydrologic system and seepage quantity through the Holocene aquitard. Note that this countermeasure is only a hypothetical one, as it would imply abandoning of valuable land. In fact, this economically unfeasible countermeasure only serves the purpose of illustrating what has unconsciously been provoked during the last centuries by the creation of low-lying (polder) areas.

n. **Widen the sand-dune area**

The width of the existing sand-dunes B is increased with $1500\ m$ by converting polders to sand-dune areas through suppletion of sand. As a result, groundwater recharge occurs and a thicker freshwater lens evolves which is likely to retard the salinisation process. Whether or not this countermeasure is realistic depends on local circumstances. For instance, it is likely to believe that in the profile Haa, the polders inland of the sand-dune area will not be abandoned, as horticulture (bulb cultivation) is practiced there. In that case, this countermeasure is strictly hypothetical. In profiles where at present no sand-dunes occur, new sand-dunes were put in.

o. **Physical barrier**

Physical barriers are created in order to retard the salinisation process. Examples of physical barriers are sheet piles, clay trenches and injection of chemicals.

In this countermeasure, physical barriers are simulated through reducing the hydraulic conductivity in the reach 2500-2750 m (one grid cell) from the left seaside boundary. As such, the physical barriers are not completely impervious. In the three profiles (Wie, Ber and Wad) with a sea condition at the right boundary, a physical barrier is also implemented in the reach 2500-2750 m from the right boundary. The hydraulic conductivity k is reduced to 1 m/d in all profiles except in the profile Ber. In this profile, the hydraulic conductivity k is only reduced to 5 m/d, as it appeared that the groundwater flow equation did not converge to a solution for lower values of k.

p.-t. Subsoil parameters k, c, α_L, n_e and k_z/k_x

The exact values of these subsoil parameters are uncertain. As they may influence the simulation significantly, a limited parameter analysis is executed. Table 9.1 shows the profiles for which the analysis is executed. The following factors or values are considered (note that the values change one at a time whereas the other values equal the reference values), where the indices $_{ref}$ and $_{new}$ stand for the values applied in the reference case and the new case respectively:

p. Hydraulic conductivity: $k_{new} = k_{ref} \cdot 1.5$ and $k_{new} = k_{ref} \cdot 2/3$,

q. Hydraulic resistance: $c_{new} = c_{ref} \cdot 1.5$ and $c_{new} = c_{ref} \cdot 2/3$,

r. Longitudinal dispersivity: $\alpha_{L,new} = 0$ m and $\alpha_{L,new} = 2.0$ m,

s. Effective porosity: $n_{e,new} = 0.15$ and $n_{e,new} = 0.45$,

t. Anisotropy: $k_z/k_{x,new} = 0.05$ and $k_z/k_{x,new} = 0.25$.

u. Depth of the geohydrologic base D

The tops of the following formations of lower Pleistocene and Tertiary origin are preferred as the geohydrologic base in the reference case: in Noord and Zuid-Holland, the Maassluis Formation (fine grained marine sediments); in the northern part of the Netherlands, the Oosterhout Formation (marine clay of upper Pliocene and lower Pleistocene origin); and in the northeastern part of Groningen, the Breda Formation. These formations underlying the chosen base level in the reference case of all profiles are taken into account in this case, in order to assess their effect on the salinisation of the geohydrologic system. The thickness of these formations, which contain saline groundwater, is set to 50 m. The hydraulic conductivity k is set to 5 m/d. This value is probably too high, but it is taken as the upper limit to assess the maximum possible effect on the salinisation process.

9.4 Propagation of sea level rise

In straightforward terms, the so-called characteristic length λ of a formation indicates the zone over which a sea level rise at the seaside boundary influences the geohydrologic system: that is the *zone of influence*. In a simple geohydrological

schematisation, named the Holland profile, this characteristic length λ equals $\sqrt{kDc}$ (see equation 2.8). However, the profiles in this chapter are somewhat more complex and the propagation of a sea level rise is determined by calculating the difference in piezometric level, expressed in freshwater, in 2090 for the scenario SLR=0.6 m/c with respect to the scenario SLR=0 m/c. Figure 9.6 shows the zone of influence in the eight profiles. The following remarks can be made:

- in five profiles, the zone of influence of sea level rise in the geohydrologic system is only a few kilometres. Thus, the attenuation of sea level rise is great in these profiles. For instance, the distance in the geohydrologic system, over which a freshwater head elevation of 6 cm (10% of the sea level rise) can still be noticed, is as follows: in Haa 8000 m; in Lei 5300 m; in Del 2800 m; in Vla 1600 m; and in Grf 3000 m.

- conversely, in the two profiles Wie and Ber, the zone of influence of sea level rise is very long. Consequently, piezometric levels in the geohydrologic system elevate significantly due to sea level rise. The main cause for this substantial rise in piezometric level is that the transmissivities of the aquifers and the hydraulic resistance of the Holocene aquitard are very high.

  Moreover, another reason why the zone of influence of the profiles Wie and Ber is significant, is that the piezometric level at the IJsselmeer side boundary also rises[10] at the same rate as the sea level. Thus, the geohydrologic system is influenced at the seaside as well as at the IJsselmeer side, and consequently, the piezometric level in between rises due to both these rises.

- in the profile Wad, the zone of influence is significant, because the transmissivity is high and the geohydrologic system is short (the sand-dune area and the adjacent polder area together are 5000 m long). Moreover, the geohydrologic system of the profile Wad is also influenced by sea level rise at both boundaries.

9.5   Salt water intrusion in the geohydrologic system

In this section, the salt water intrusion in the geohydrologic system is displayed by three approaches: (a) by showing the chloride distribution in each profile for six situations; (b) by showing the change in volume distribution of fresh, brackish and saline groundwater as a function of time; and (c) by showing the change in chloride concentration in so-called observation points as a function of time. For approach (b), the time lag of each profile before a state of dynamic equilibrium in the salinisation process is reached is briefly discussed.

---

[10] In section 9.8, the effect of a constant piezometric level at the IJsselmeer side boundary on the zone of influence is discussed.
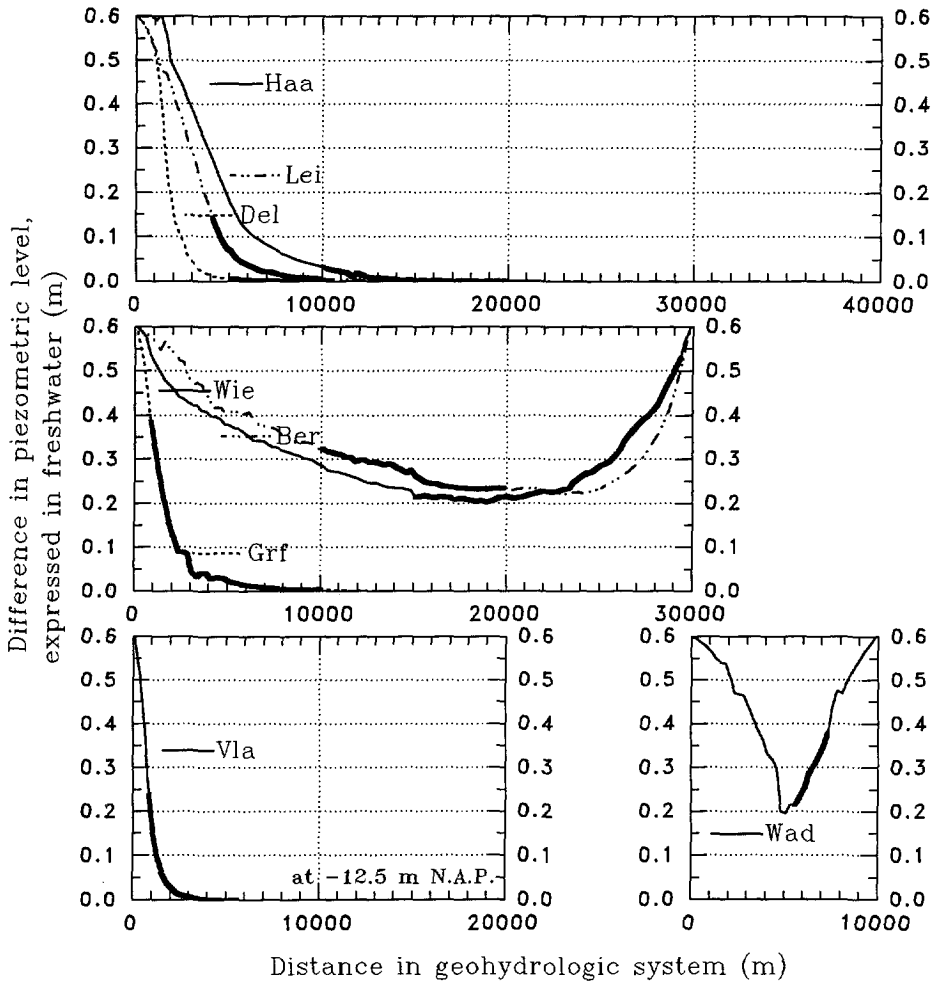
Figure 9.6: Differences in piezometric level, expressed in freshwater, at -25 m $N.A.P.$ (in the profile Vla at -12.5 m $N.A.P.$) in 2090 for the scenario SLR=0.6 m/c with respect to the scenario SLR=0 m/c in the eight profiles. The **bold** path points out the location of the selected polder of each profile (see also table 9.6).

9.5.1 Chloride distributions in each profile for six situations

The chloride distributions in each profile are shown for six situations: (1) no sea level rise in 1990, (2) in 2090, (3) in 2490 and (4) in 2990; (5) a sea level rise of 0.6 m/c in 2990; and (6) a sea level fall of -0.6 m/c in 2990. Some striking observations are:

1. Wie=Wieringermeer

   A severe salt water intrusion is caused in the geohydrologic system (see fig-
   ure 9.7), even without a sea level rise. Two main causes for the severe salini-
   sation are the high transmissivities and the low-lying Wieringermeer polder in
   the reach 15,000-29,500 m. When the sea level rises 0.6 m/c, the entire system
   will be saline in 2990.

2. Ber=Bergen

   In this profile, a severe salt water intrusion also occurs (see figure 9.8). The
   freshwater lens remains for each of the scenarios of sea level rise, though the
   volume obviously depends on the level of the sea. For each scenario, the aquifer,
   which underlies the low-lying polder in the central part of the profile, contains
   more saline groundwater in the future than in 1990.

3. Haa=Haarlem

   When no sea level rise occurs, the volume of the freshwater lens slightly increases
   (see figure 9.9) due to the fact that for the future lower groundwater extraction
   rates are planned than during the past decades. The freshwater lens narrows
   the height of the aquifer over which saline groundwater enters the hinterland.
   Consequently, salt water intrusion in the geohydrologic system, induced by the
   low-lying polder (e.g. the Haarlemmermeer polder), is rather limited. When
   the sea level falls -0.6 m/c, the freshwater lens (chloride concentration ≤ 300
   $mg\ Cl^-/l$) increases in such a way that salt water intrusion will eventually stop
   completely.

4. Lei=Leiden

   Salt water intrusion is rather limited for several reasons (see figure 9.10): (1) the
   freshwater lens is obstructing the inflow of saline groundwater to the hinterland;
   (2) the thickness of the geohydrologic system is 'only' 120 m; and (3) the
   phreatic groundwater levels of the polders are not as low as in the profile Haa.
   When the sea level rises 0.6 m/c, saline groundwater will eventually reach the
   polder which is located directly behind the decreasing freshwater lens.

5. Del=Delft

   The results correspond to some extent with those in the profile Lei. In the first
   kilometres inland of the coast, a severe salt water intrusion is taking place (see
   figure 9.11). Saline seepage occurs in the polder in the reach 5000-7500 m, be-
   cause there the phreatic groundwater level is relatively low (-2.5 $m\ N.A.P.$) and
   the hydraulic resistance is low (500 $days$). The industrial groundwater extrac-
   tions in the vicinity of Delft cause upconing of saline groundwater. Meanwhile,
   surface water infiltrates in the aquifer in the reach 8000-20,000 m, as the ex-
   tractions create a low piezometric level in the aquifer. From about 10,000 m
   inland of the coast, the impact of sea level rise is very limited due to the high
   hydraulic resistance of the Holocene aquitard. There is not much outflow by
   seepage and consequently not much inflow of saline groundwater.

Figure 9.7: Chloride distribution (in $mg\ Cl^-/l$) in the geohydrologic system of the profile Wie for six situations.

Figure 9.8: Chloride distribution (in $mg\ Cl^-/l$) in the geohydrologic system of the profile Ber for six situations.

6. Vla=Zeeuws-Vlaanderen

  The impact of sea level rise is limited to the first few kilometres from the coast (see figure 9.12), because the zone of influence is very short and the phreatic groundwater levels of the polders at some kilometres inland are situated above $N.A.P.$ As the thickness of this geohydrologic system is very small, groundwater
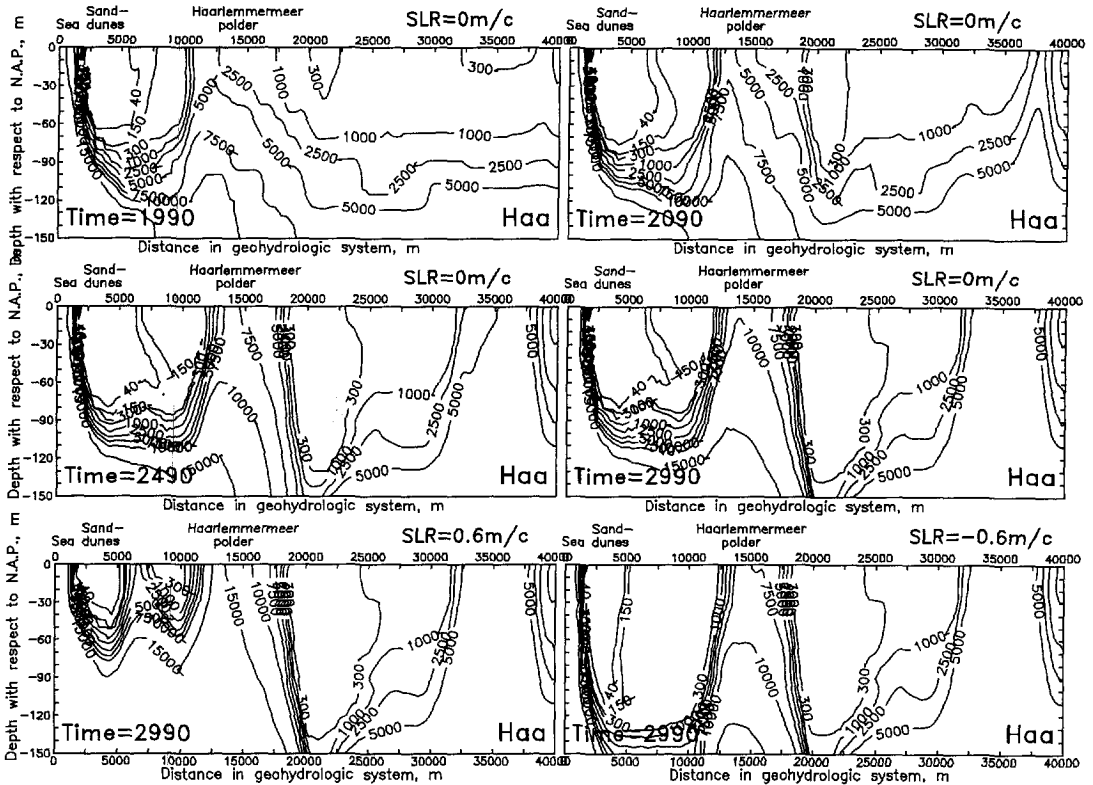
Figure 9.9: Chloride distribution (in $mg\ Cl^-/l$) in the geohydrologic system of the profile Haa for six situations.

flow is determined by local conditions. Consequently, salt water intrusion from the sea is restricted.

7. Grf=Groningen-Friesland

When no sea level rise occurs, saline groundwater only intrudes in the deeper parts of the geohydrologic system (see figure 9.13). When the sea level rises 0.6 m/c, the system will eventually be completely saline in the first kilometres inland of the coast. When the sea level falls -0.6 m/c, surface water infiltrates in the geohydrologic system after some centuries, and subsequently, brackish groundwater flows towards the sea.

8. Wad=Wadden Islands

The geohydrologic system underneath the polder becomes more saline at great pace for both the scenarios SLR=0 m/c and SLR=0.6 m/c (see figure 9.14). Even when the sea level rises 0.6 m/c, the freshwater lens remains, though the volume decreases. Note that the phreatic groundwater level in the sand-dune
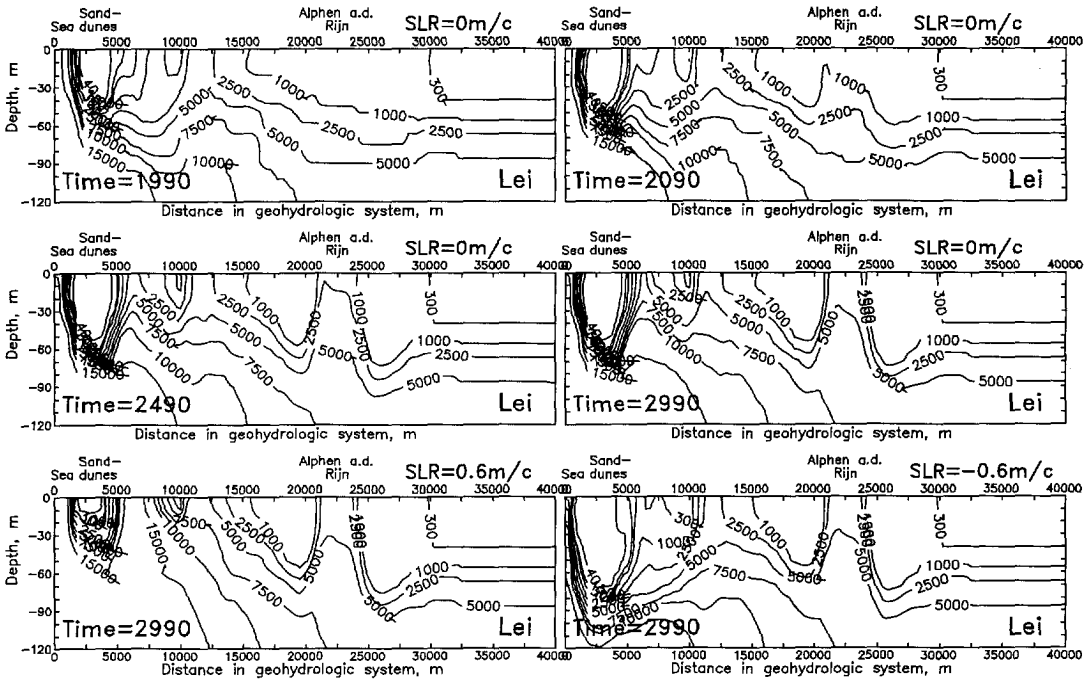
Figure 9.10: Chloride distribution (in $mg\ Cl^-/l$) in the geohydrologic system of the profile Lei for six situations.

area is supposed to rise with a sea level rise. Sand can be supplied where necessary in order to assure that the phreatic groundwater level can rise freely. When the sea level falls -0.6 m/c, the volume of the freshwater lens increases enormously. Nearly the entire system then contains fresh groundwater in 2990. It should be noted that in 2990 the controlled phreatic groundwater level of the polders in the reach 4500-7500 m is about 6 m higher than the level of the sea, and that, during the period 1990-2990, (fresh) surface water has infiltrated in the geohydrologic system.

9.5.2   Volume distribution of fresh, brackish and saline groundwater

In this subsection, the change in chloride distribution in the geohydrologic system due to sea level rise is quantified.

Salinisation of the geohydrologic systems

Figure 9.15 shows the distribution of fresh, brackish and saline water in percentages of the total volume of water in the geohydrologic system as a function of time in the
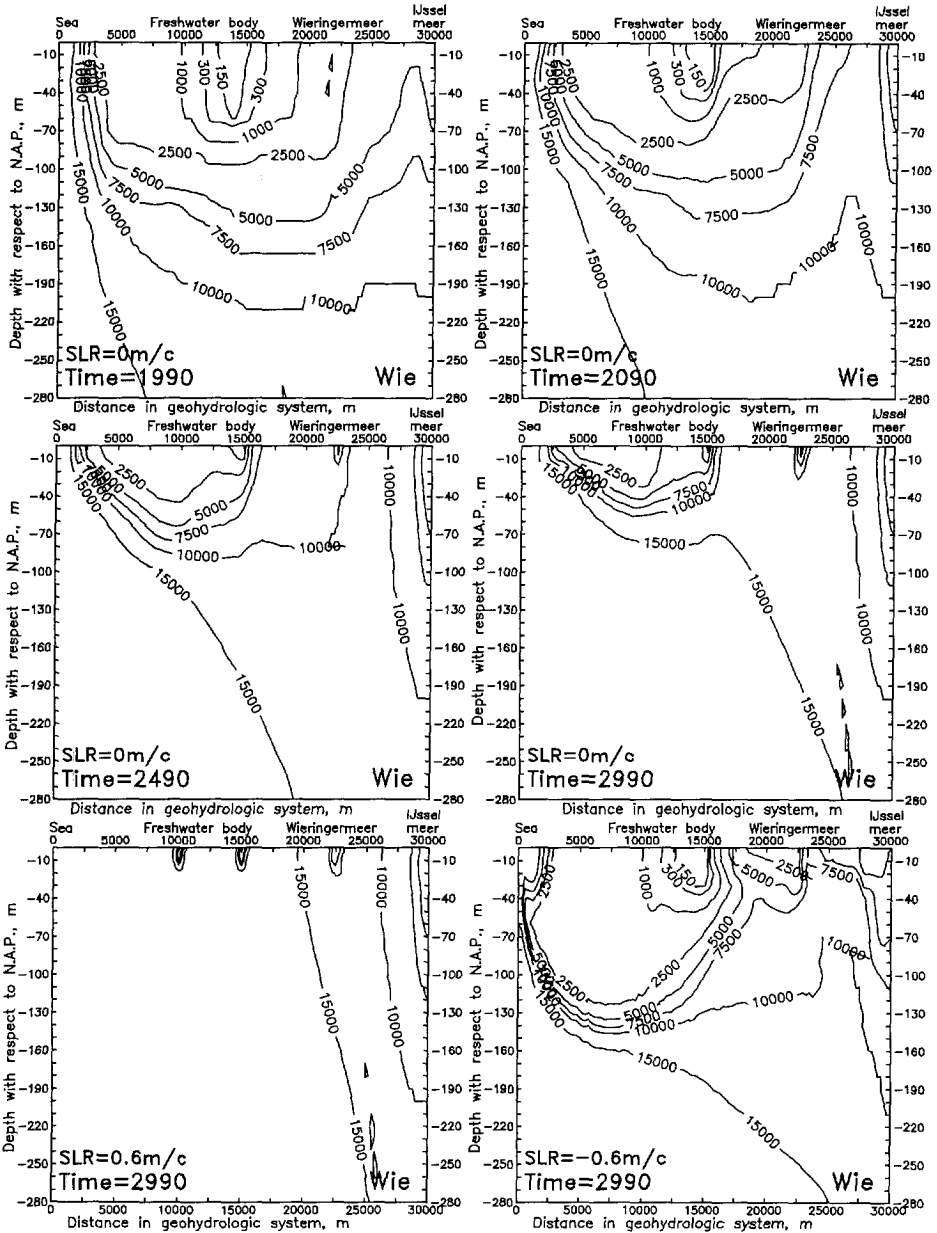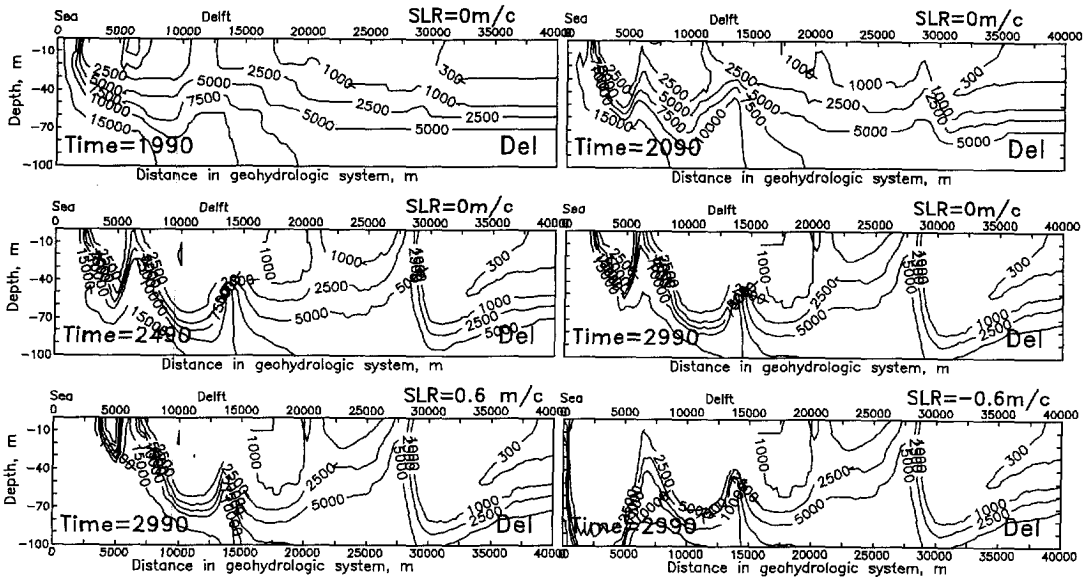
Figure 9.11: Chloride distribution (in $mg\ Cl^-/l$) in the geohydrologic system of the profile Del for six situations.
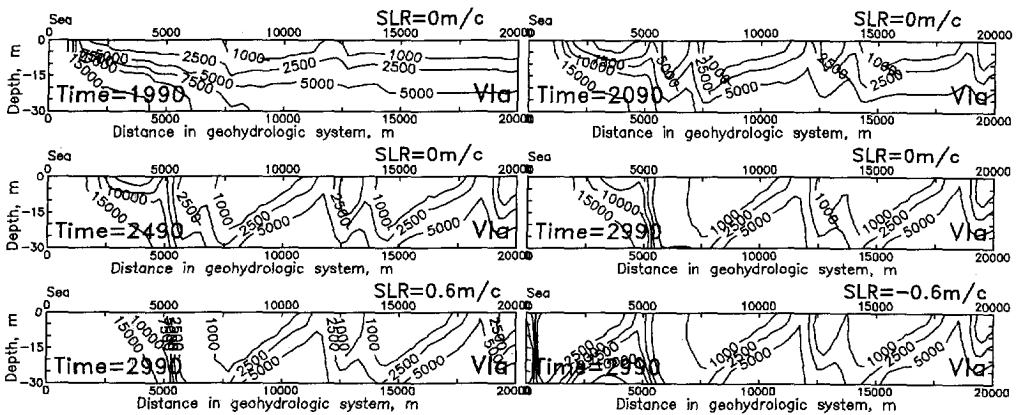
Figure 9.12: Chloride distribution (in $mg\ Cl^-/l$) in the geohydrologic system of the profile Vla for six situations.

eight profiles. The volume percentage of fresh groundwater is discussed separately in section 9.6.

Even when no sea level rise occurs, the salinisation process is severe during the next centuries in the northern part of the Netherlands in the profiles Wie, Ber and Grf. Conversely, no significant change in volume percentage occurs within the next
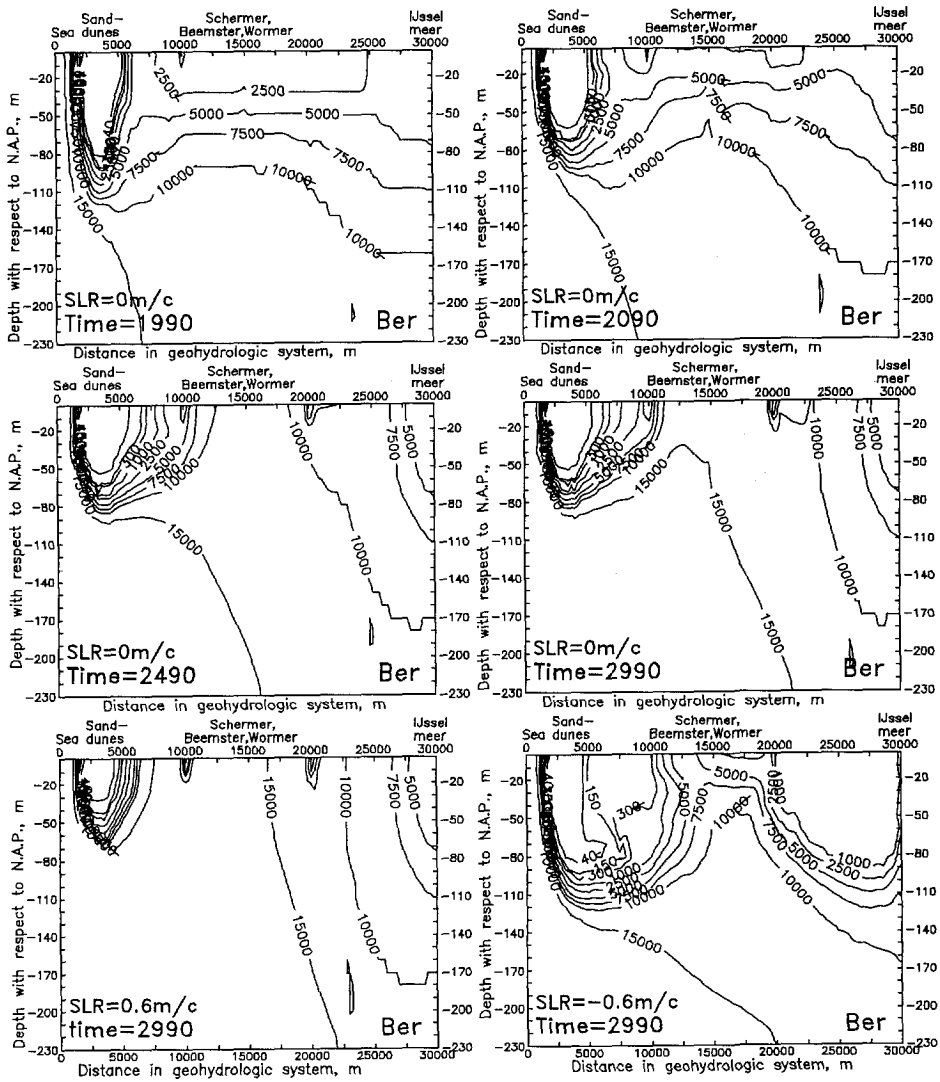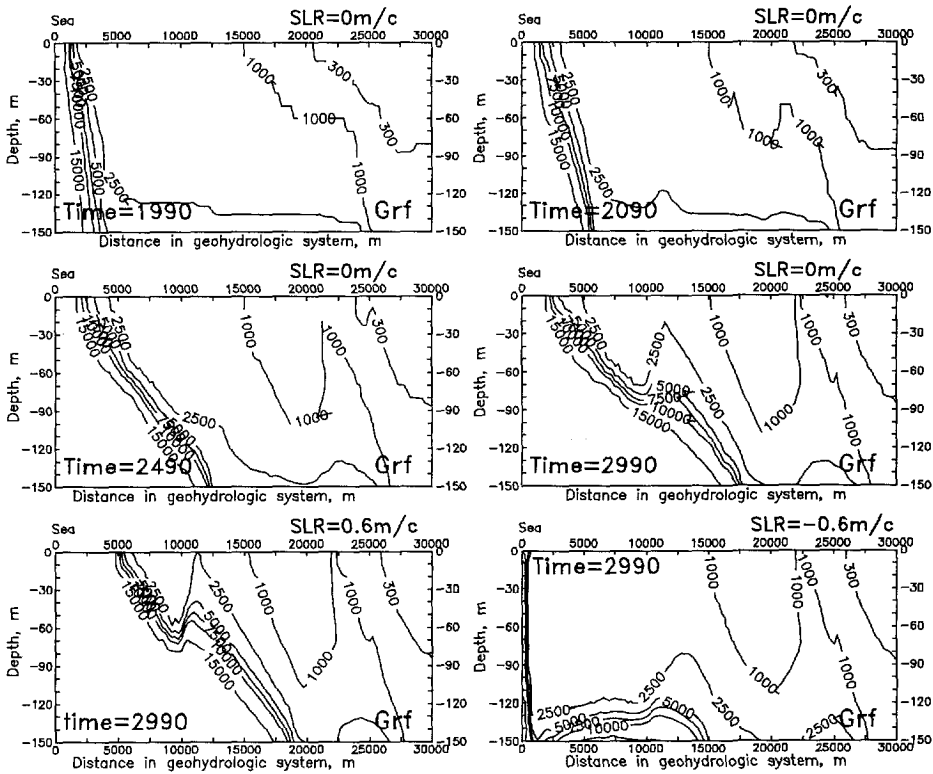
Figure 9.13: Chloride distribution (in $mg\ Cl^-/l$) in the geohydrologic system of the profile Grf for six situations.

centuries in the profiles Lei, Del and Vla.

Focusing on the next century, figure 9.15 shows that the impact of sea level rise appears to be of minor importance in the eight profiles, as the volume percentages of the three scenarios of sea level rise are in concordance with each other. This can also be observed in table 9.3, where the changes in volume percentage of saline groundwater in 2090 and 2990 are quantified for the three scenarios of sea level rise. For instance, table 9.3 shows that the change in volume percentage of saline groundwater in the profiles is less than 1.5 % in 2090 for the scenario SLR=0.6 m/c with respect to the scenario SLR=0 m/c.

Considering the absolute change in the volume of saline groundwater (see table 9.4), the salinisation appears to be greatest in the northern part of the Netherlands in the profiles Wie, Ber and Grf. Salt water intrusion is still substantial in the profiles of Zuid-Holland in the profiles Haa, Lei, Del. The salinisation is limited in the profiles Wad and especially Vla, which is obvious as the geohydrologic system of the profile Vla is small.
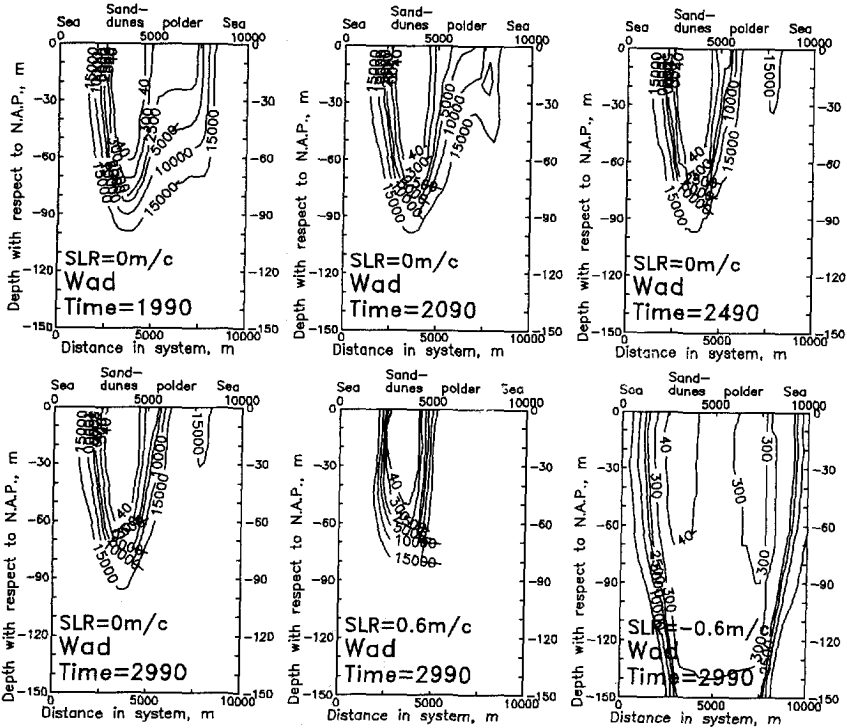
Figure 9.14: Chloride distribution (in $mg\ Cl^-/l$) in the geohydrologic system of the profile Wad for six situations.

Table 9.3: Change in volume percentage of saline groundwater due to the three scenarios of sea level rise in the eight profiles.

Change in saline	1.	2.	3.	4.	5.	6.	7.	8.
volume percentage	Wie	Ber	Haa	Lei	Del	Vla	Grf	Wad
in 2090 with respect to 1990								
SLR=0 m/c (%)	+8.6	+2.6	+1.0	0	+0.3	-0.6	+4.5	+5.5
SLR=0.6 m/c with respect to SLR=0 m/c								
in 2090 (%)	+0.8	+0.4	+0.1	+0.3	+0.3	+0.4	+0.7	+1.3
in 2990 (%)	+5.7	+2.7	+12.2	+8.8	+3.3	+0.8	+7.7	+5.3
SLR=-0.6 m/c with respect to SLR=0 m/c								
in 2090 (%)	-0.8	-0.3	-0.3	-0.4	-0.3	-0.4	-0.9	-2.5
in 2990 (%)	-30.2	-22.3	-9.2	-7.8	-13.3	-15.6	-27.1	-56.5
SLR=0.6 m/c with respect to SLR=-0.6 m/c								
in 2990 (%)	+35.9	+25.0	+21.4	+16.6	+16.6	+16.4	+34.8	+61.8
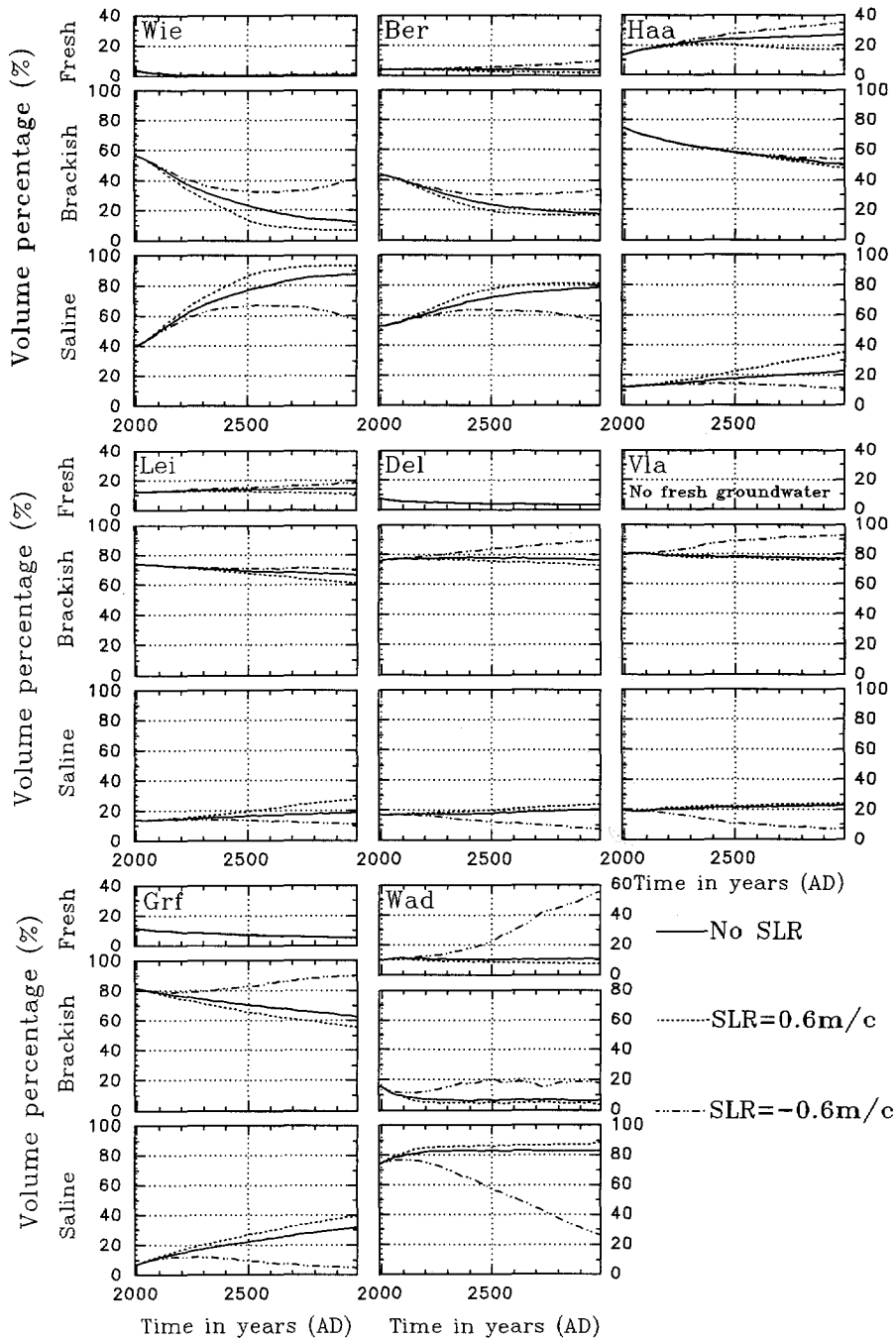
Figure 9.15: Volume percentages of fresh ($Cl^- \leq 300$ mg Cl^-/l), brackish ($300 < Cl^- < 10,000$) and saline ($Cl^- \geq 10,000$ mg Cl^-/l) groundwater during the next millennium (that is the period 1990-2990) in the eight profiles for the three scenarios of sea level rise.

Table 9.4: Absolute change in the volume of saline groundwater (in 10^3 m^3/m') in the eight profiles in 2990 with respect to 1990.

Absolute change in saline groundwater	1. Wie	2. Ber	3. Haa	4. Lei	5. Del	6. Vla	7. Grf	8. Wad
in 2990 with respect to 1990 (in 10^3 m^3/m')								
SLR=0 m/c	+1404	+614	+218	+81	+88	+7	+394	+50

Time lag before a state of dynamic equilibrium is reached

It clearly appears that most of the geohydrologic systems along the Dutch coast have at present not yet reached a state of dynamic equilibrium as far as the salinity distribution in the subsoil is concerned. The time lag of a geohydrologic system between the cause of changes and the ultimate effect on the salinisation process is mainly determined by three causes: (a) the driving force of the salinisation process, that is the phreatic groundwater levels in the polders and/or groundwater extractions; (b) the transmissivity and porosity of the geohydrologic system, that is the velocity with which groundwater can pass through the geohydrologic system; and (c) the geometry (size) of the geohydrologic system under consideration: for instance, a small geohydrologic system (e.g. 10,000 m) obviously reaches a state of dynamic equilibrium more rapidly than a large geohydrologic system (e.g. 40,000 m) under similar conditions. As the state of dynamic equilibrium will not be reached within one millennium, the simulation time has been extended to 10,000 years for the reference case of each profile. Based on the causes mentioned above, four durations of time lags can be classified:

I. A time lag of several centuries:
   geohydrologic systems with small geometries: the profiles Vla and Wad.

II. A time lag of a large number of centuries:
   geohydrologic systems with high transmissivities and low-lying polder areas: the profiles Wie and Ber. Both profiles become completely saline; only the freshwater lens in the profile Ber continues to exist.

III. A time lag of a few millennia:
   geohydrologic systems with moderate transmissivities and/or polder areas with high phreatic groundwater levels: the profiles Haa and Grf.

IV. A time lag of several millennia:
   geohydrologic systems with low transmissivities and/or polder areas with high phreatic groundwater levels: the profiles Lei and Del. Note that the high groundwater extraction rate in the Del profile causes only small changes in the volume distribution.

In conclusion, table 9.5 shows some geohydrologic characteristics of the groundwater flow regimes, on which the duration of the time lag is based.

Table 9.5: The duration of the time lag, before a state of dynamic equilibrium is reached, is based on geohydrologic characteristics of the groundwater flow regimes.

duration of time lag	(a) driving force		(b) subsoil parameters		(c) geometry
	polder level	extraction	transmissivity	porosity	
I. centuries	low	great	high	small	small
II. many centuries	|	|	|	|	|
III. millennia	↓	↓	↓	↓	↓
IV. many millennia	high	small	low	great	large

Sensitivity for sea level variation

In order to assess the sensitivity for sea level rise of each profile, the range in volume percentage of saline groundwater from a sea level rise of 0.6 m/c to a sea level fall of -0.6 m/c is determined for 2990 (see table 9.3). Three types of sensitivity can be perceived:

I. High sensitivity to sea level variation
    the profile Wad (+61.8 %), as (1) the level of the sea varies at both sides of the geohydrologic system and (2) the length of the geohydrologic system is small (namely 10,000 m).

II. Moderate sensitivity to sea level variation
    the profiles Wie, Ber and Grf (+35.9 %, +25.0 % and +34.8% respectively). In the profiles Wie and Ber, the level of the sea changes at both sides (see figure 9.6) and the transmissivities of the aquifers are high. In the profile Grf, the hydraulic resistance of the Holocene aquitard is low.

III. Low sensitivity to sea level variation
    the profiles Haa, Lei, Del and Vla (+21.4 %, +16.6 %, +16.6 % and +16.4 % respectively), as the zone of influence of sea level rise is limited (see figure 9.6).

9.5.3 Chloride concentration in observation points

Figure 9.16 shows the chloride concentration as a function of time in a specific observation point in each profile. As can be seen, the chloride concentration can change significantly due to sea level rise. It takes several decades before the changes in chloride concentration are noticeable, though the positions of the chosen observation points are located in areas where the impact of sea level rise is great.
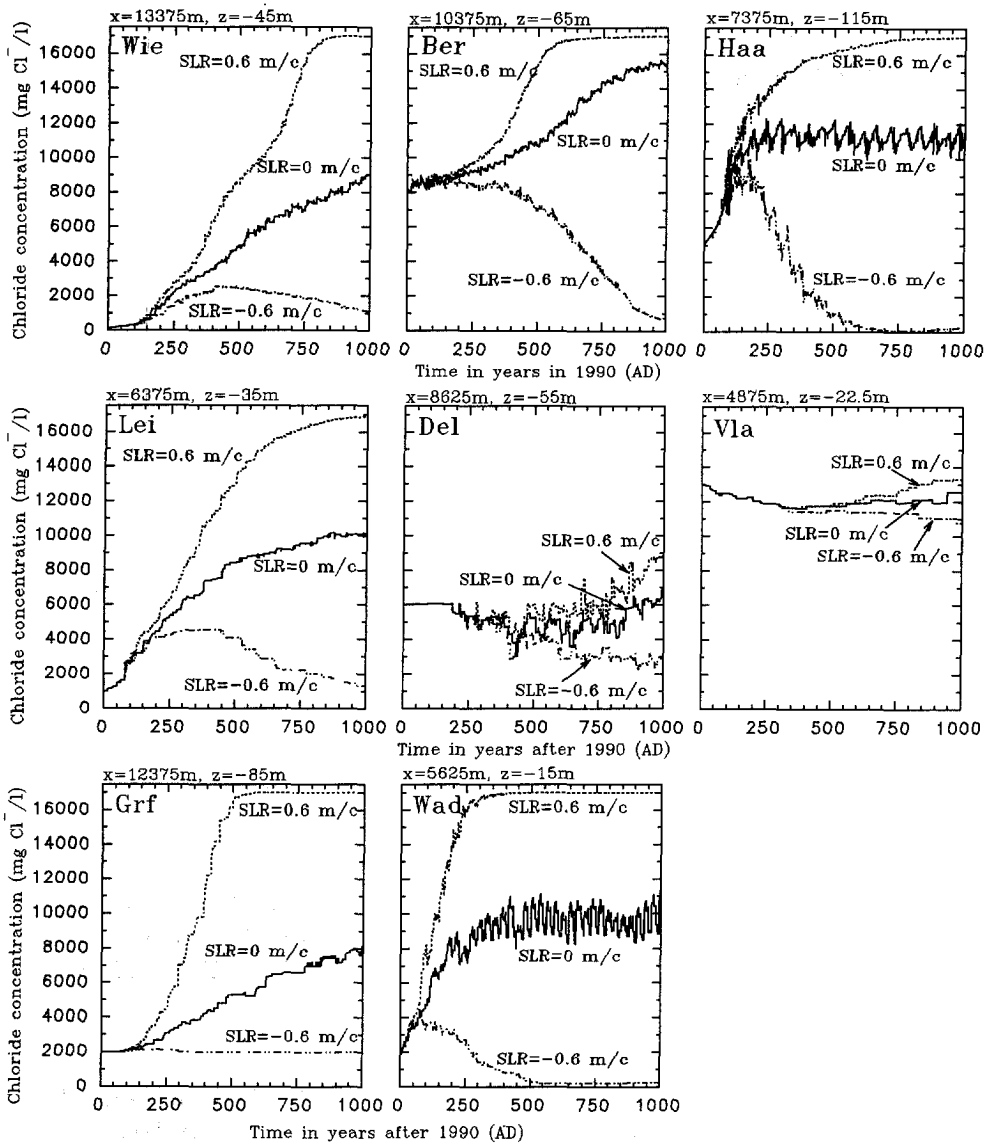
Figure 9.16: Chloride concentration as a function of time in each profile in a specific observation point for the three scenarios of sea level rise.

9.6 Freshwater lenses in sand-dune areas

Figure 9.17 shows the volume of fresh groundwater in the sand-dune areas as a function of time in the following four profiles: Ber, Haa, Lei and Wad. In this section,
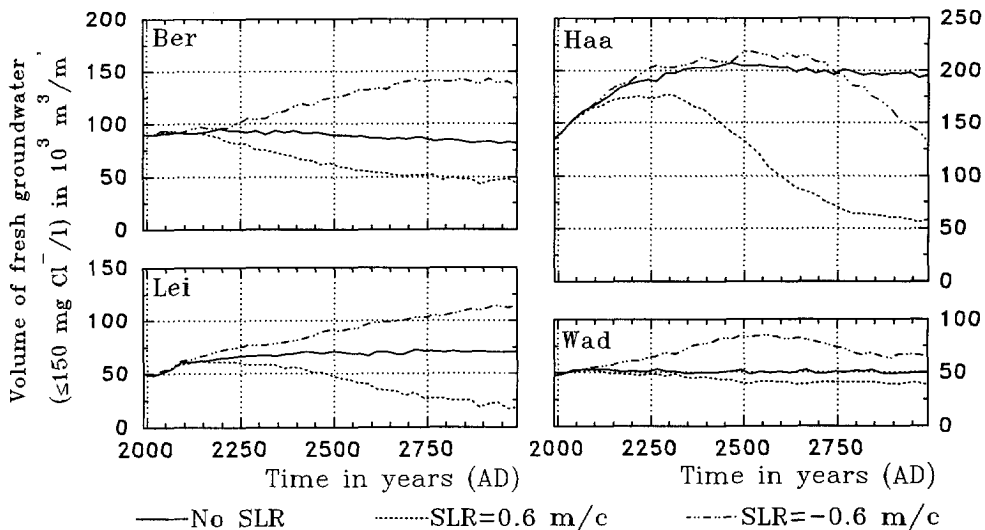
Figure 9.17: Volume of fresh groundwater ($\leq 150\ mg\ Cl^-/l$) in the sand-dune area in 10^3 m^3/m' as a function of time for the three scenarios of sea level rise.

groundwater with a chloride concentration $\leq 150\ mg\ Cl^-/l$ is defined as fresh groundwater. This is in contrast with the present definition of fresh groundwater (that is fresh groundwater is water with a chloride concentration $\leq 300\ mg\ Cl^-/l$, see, e.g., figure 9.15), in order to detect only groundwater that originates from the freshwater lens[11] in the sand-dune area.

Two phenomena occur in the profile **Haa** (see figure 9.17). Firstly, for the scenario SLR=0 m/c, the volume of fresh groundwater increases significantly, that is +23.4 % in 2090 with respect to 1990. The groundwater extraction rate has been decreased since 1956, which is one of the two reasons that the freshwater lens has been increasing ever since. The other reason is that the freshwater lens evolves towards the low-lying polder in the reach 10,000-20,000 m, and as a result, the volume increases. Secondly, the volume of the freshwater lens for the scenario SLR=-0.6 m/c drops below the volume for the scenario SLR=0 m/c after some seven centuries. The reason for this phenomenon is that, after some centuries, the groundwater flow in the sand-dune area alters in the direction of the sea, as the sea level is falling. The shape of the freshwater lens also changes, which results in a decreasing volume of fresh groundwater.

In the profile **Wad**, the volume of fresh groundwater decreases during the second half of the next millennium for the scenario SLR=-0.6 m/c. The reason is that, from

---

[11]The chloride concentration of water that recharges the sand-dune area as natural groundwater recharge is set to 30 $mg\ Cl^-/l$, whereas the chloride concentration of surface water that infiltrates through the Holocene aquitard in polders and lakes in these four profiles is set to at least 200 mg Cl^-/l.
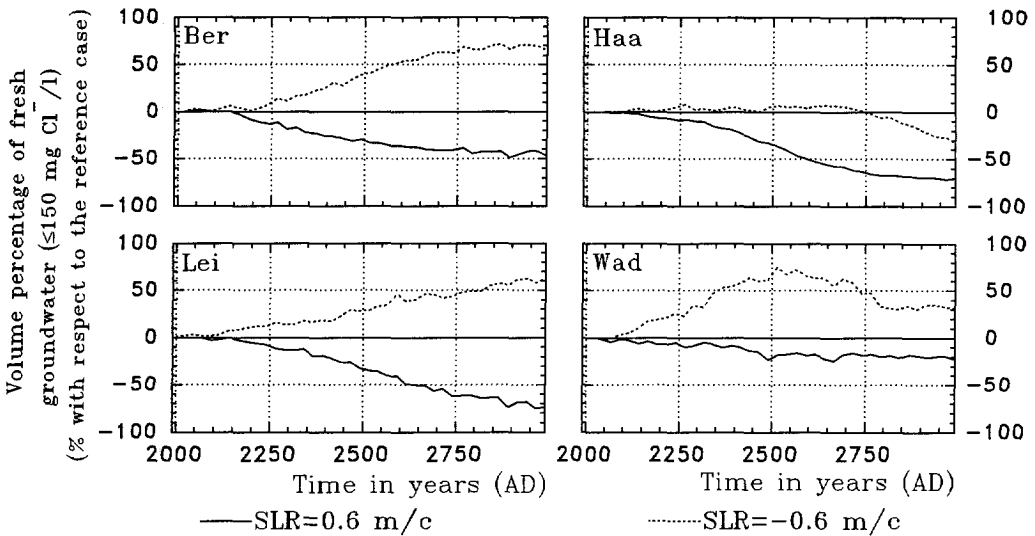
Figure 9.18: Change in volume percentage of fresh groundwater ($\leq$ 150 mg Cl^-/l) as a function of time for the scenarios SLR=0.6 m/c and SLR=-0.6 m/c with respect to the scenario SLR=0 m/c.

then on, sea level rise causes fresh surface water, which originates from the polder adjacent to the sand-dune area, to infiltrate in the geohydrologic system. This water, which contains a higher chloride concentration than 150 mg Cl^-/l, supersedes the fresh groundwater that recharges the sand-dune area.

Figure 9.18 shows the change in volume percentage with respect to the reference case with no sea level rise. During the next century, the impact of sea level rise on the fresh groundwater resources along the coast appears to be of minor importance, at most a few percents. After a millennium, however, the changes are (obviously) significant. The decreases in volume of fresh groundwater are in 2990: Ber -46.8 %; Haa -70.5 %; Lei -74.1 % and Wad -22.8 % for the scenario SLR=0.6 m/c with respect to the scenario SLR=0 m/c.

9.7 Seepage in selected polders

The impact of sea level rise on seepage is assessed for one selected polder of each profile. The characteristics of the selected polders are given in table 9.6. Most of the selected polders are located near the coast, in order to assure that those polders which are jeopardized most by sea level rise are considered.

The propagation of the sea level rise in the selected polder (see figure 9.6) already indicates the possible changes in seepage due to sea level rise. Obviously, if the sea

Table 9.6: Characteristics of the selected polders considered in the discussion on seepage and countermeasures.

Characteristics of selected polders	1. Wie	2. Ber	3. Haa	4. Lei	5. Del	6. Vla	7. Grf	8. Wad
Location of the selected polder, in km from the 'left' seaside boundary, see figure 9.3								
	15-29.5	10-20	10-20	4-10	5-10	0.75-5.75	0.75-10	5.5-7.5
Length of the selected polder, in km								
	14.5	10	10	6	5	5	9.25	2
Phreatic groundwater level in the selected polder, in m with respect to $N.A.P.$								
	-4.5/-5.5	-4.0	-5.5	-1.5	-2.5	-0.5	-0.5	-0.3
Propagation of sea level rise at the boundaries of the selected polder, in %, see figure 9.6								
at the seaside	91.8	53.9	5.3	26.4	1.0	53.8	72.3	68.6
at the land side	37.1	38.8	negl.	0.6	0.1	negl.	0.7	36.0
negl. = negligible								

level rise is attenuated considerably, the changes in seepage due to sea level rise are limited. This applies particularly for the selected polders of the profiles Haa and Del, as they are located at a considerable distance from the coast. Conversely, it can be deduced that the impact of sea level rise on seepage is great for the selected polders of the profiles Wie, Ber and Wad. In general, for Dutch polder areas at a great distance from the coast, the increase in seepage due to sea level rise appears to be of minor importance with respect to the already existing seepage quantities in those polder areas.

The changes in three seepage parameters for the selected polders of each profile are considered during the simulation time of one millennium: (1) seepage quantity; (2) mean chloride concentration; and (3) chloride load.

1. Seepage quantity

Apart from sea level rise, other processes also determine the seepage quantity as a function of time. Some of these processes are: (a) subsidence of the land surface due to compaction, shrinkage and oxidation of peat[12]; (b) decrease of the hydraulic resistance of aquitards due to oxidation of peat; and (c) excavations, dredging and perforations of aquitards, though the effects of these processes are limited by regulations of the water manager.

Figure 9.19 shows the seepage quantity through the Holocene aquitard during the next millennium in the selected polder of each profile. In the scenario SLR=0 m/c, the selected polders of the profiles show a decrease in seepage quantity due to the salinisation of the geohydrologic system. It appears that the impact of sea level rise during the next millennium is very serious for the selected polders of all profiles,

---

[12]Mankind shall be forced to lower the polder levels through drainage and pumping.
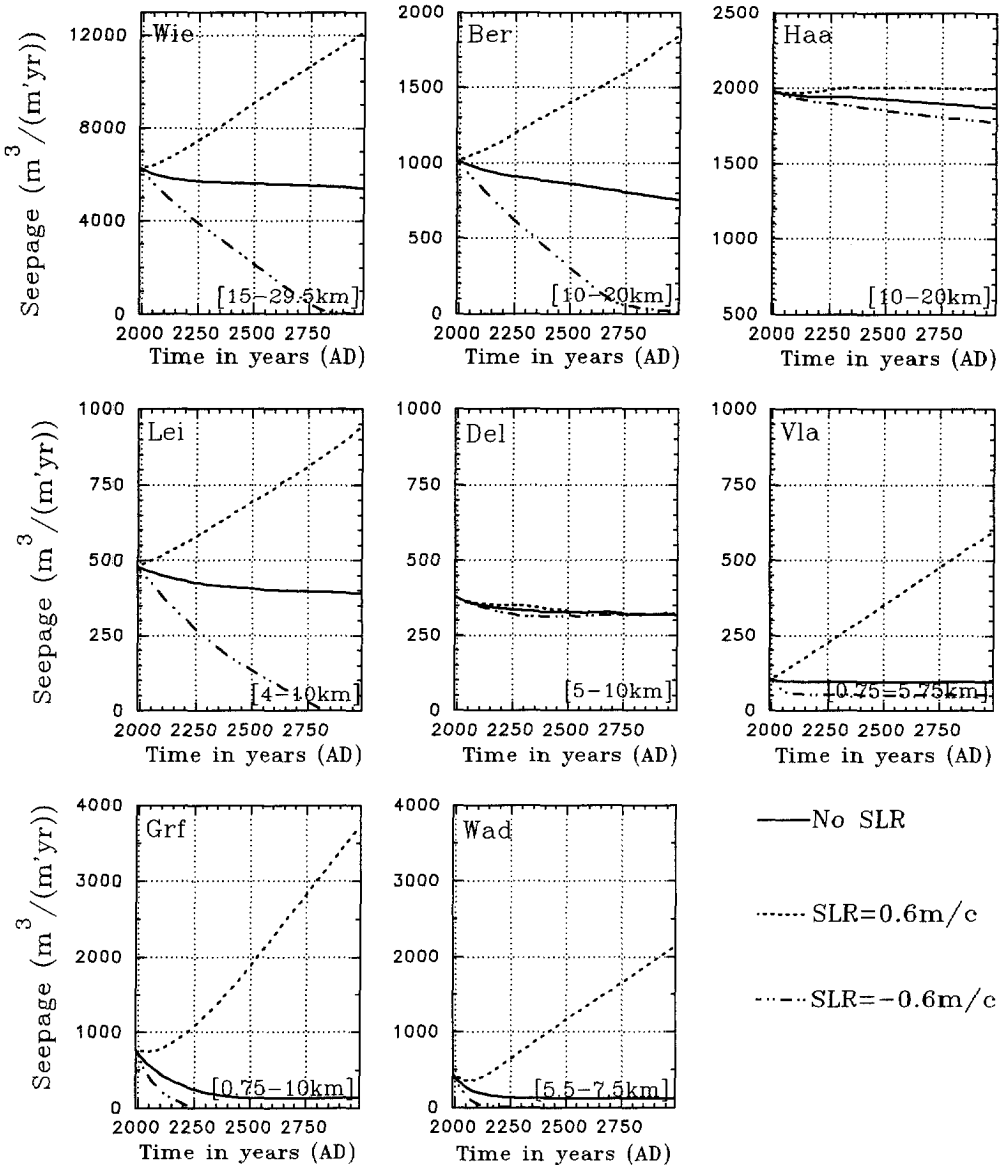
Figure 9.19: Seepage quantity $(m^3/(m'yr))$ through the Holocene aquitard at -15 m N.A.P. in the selected polder of each profile during the next millennium for the three scenarios of sea level rise. The reaches of the selected polders are indicated.

except for the selected polders of the profiles Haa and Del. As mentioned above, the main reason that the impact is relatively small in these two profiles is that the selected polders are situated at a distance beyond the zone of influence of sea level rise (see table 9.6).

Figure 9.20 shows the seepage quantity (in mm/d)[13] during the next century through the Holocene aquitard in the selected polder of each profile. As can be seen, the seepage quantity in 1990 in the selected polders of the profiles Wie, Haa and Wad is reasonable. Observing the scenario SLR=0 m/c (the reference case), the decrease in seepage quantity in the selected polders due to changes in density distribution is remarkable[14]. For instance, in the selected polder of the profiles Grf, the expected increase in seepage quantity due to sea level rise is nearly counterbalanced in 2090 with respect to 1990 due to changes in density distribution. By comparing the results in 2090 for the scenario SLR=0.6 m/c with the scenario SLR=0 m/c, the profiles are subdivided in the following three groups:

I. the profiles Haa and Del, where the selected polders experience a negligible increase in seepage quantity,

II. the profiles Wie, Ber and Lei, where the selected polders experience an increase in seepage quantity of about 10 %,

III. the profiles Vla, Grf and Wad, where the selected polders experience an increase in seepage quantity of at least 50%.

When comparing the seepage quantities in the selected polders due to SLR=0.6 m/c in 2090 with the seepage quantities in 1990, the following changes (in %) are calculated: Wie +3.9 %; Ber +6.3 %; Haa -0.6 %; Lei +6.3 %; Del -6.4 %; Vla +37.9 %; Grf +1.0 % and Wad -18.3 %. Even for the scenario SLR=0.6 m/c, the seepage quantity in 2090 is less than the seepage quantity in 1990 in the selected polders of the profiles Haa, Del and Wad.

2. Mean chloride concentration

Figure 9.21 shows the mean chloride concentration in the Holocene aquitard during the next millennium in the selected polder of each profile. When no sea level rise occurs, the mean chloride concentration in the Holocene aquitard increases very rapidly in the selected polders of the profiles Wie, Ber, Vla and Wad, even within one century. The subsoil of these selected polders becomes very saline during the next millennium. Conversely, the salinisation of the upper part of the geohydrologic system in the selected polders of the profiles Haa, Lei, Del and Grf is somewhat limited.

---

[13] The seepage quantity in $m^3/(m'yr)$, as presented in figure 9.19, is divided by the length of the selected polder in order to obtain, after conversion, the value in mm/d.

[14] Note that a very rapid change in density distribution might indicate that the initial chloride distribution could be incorrect.
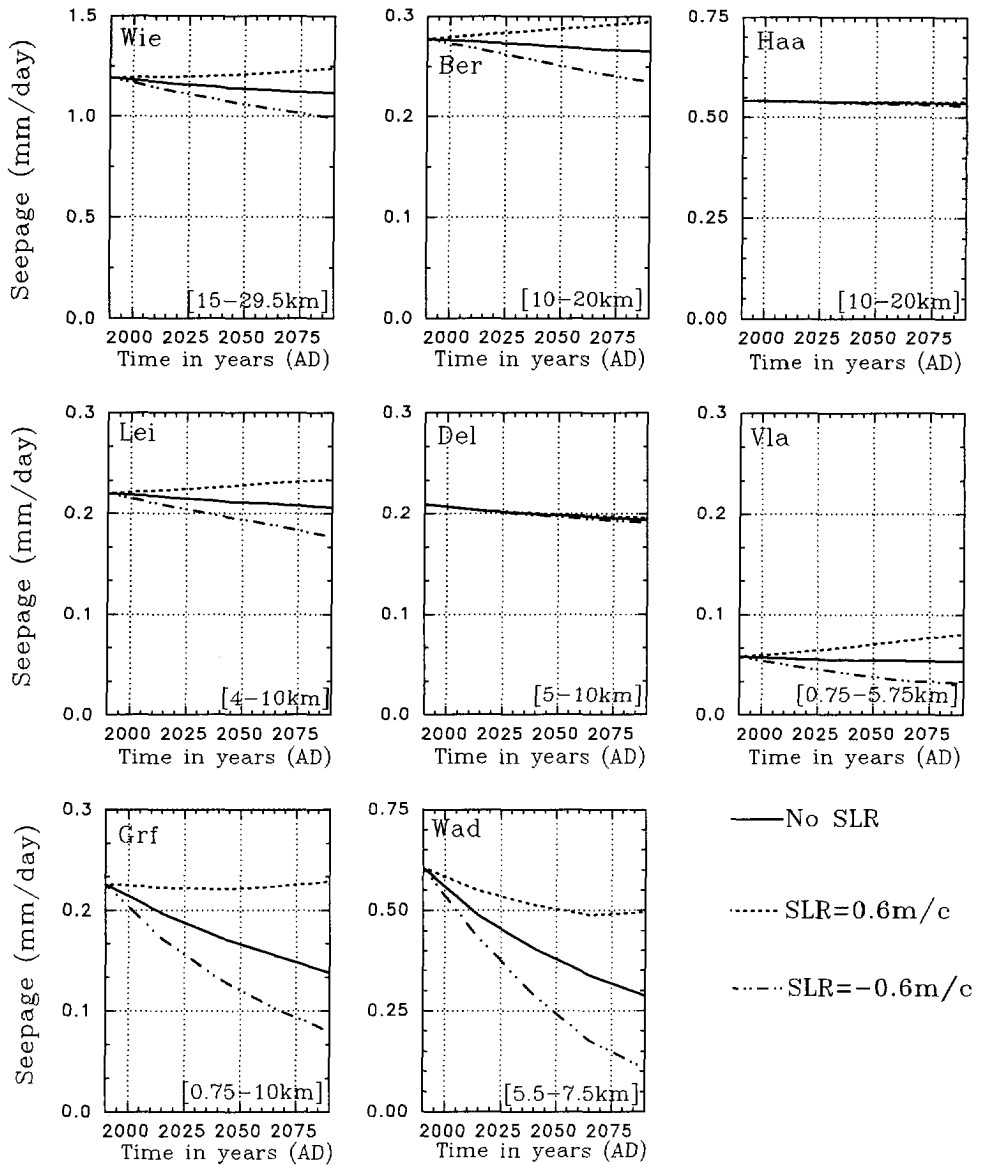
Figure 9.20: Seepage quantity (mm/d) through the Holocene aquitard at -15 m $N.A.P.$ in the selected polder of each profile during the next century for the three scenarios of sea level rise. The reaches of the selected polders are indicated.
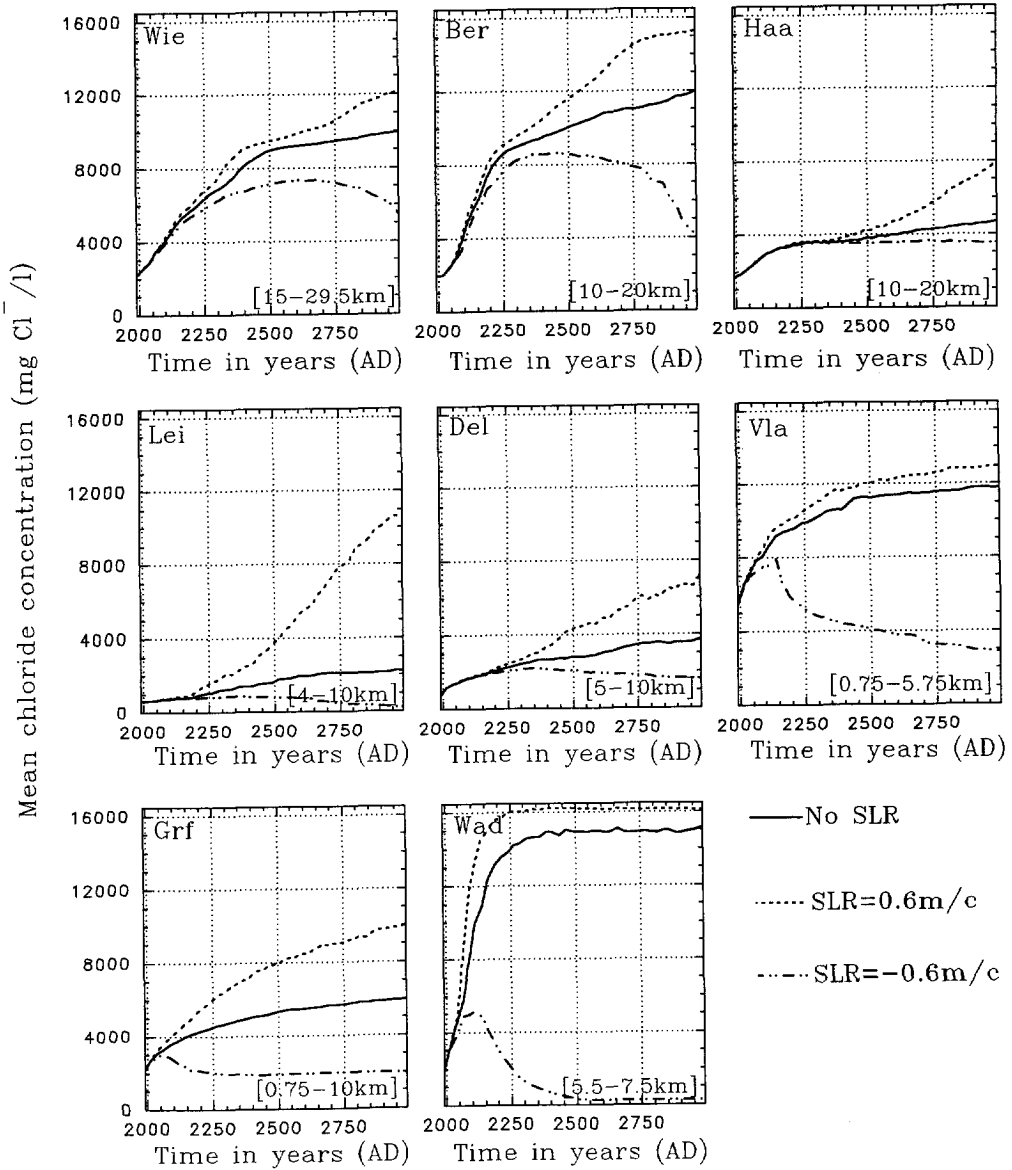
Figure 9.21: Mean chloride concentration in the Holocene aquitard at -15 m $N.A.P.$ during the next millennium for the three scenarios of sea level rise. The reaches of the selected polders are indicated.

During the next century, the influence of sea level rise on the change in mean chloride concentration is of minor importance in the selected polders of the four profiles Wie, Haa, Lei and Del. The selected polders of the profiles Ber, Vla, Grf show a slight change in mean chloride concentration between the three scenarios of sea level rise. The selected polder of the profile Wad, however, demonstrates a difference in mean chloride concentration of a few thousands of $mg\ Cl^-/l$ for the three scenarios of sea level rise.

Only after several centuries, the impact of sea level rise on the mean chloride concentration becomes substantial in all profiles, and as a consequence, considerable changes in the salinity of seepage occur in the distant future.

In general, it takes several decades or even centuries before brackish and saline groundwater reach the selected polders that are located several kilometres inland of the coast. It is clear that the nearer the polder is to the seaside boundary, the earlier the impact of sea level rise on the chloride distribution can be noticed. For instance, the change in mean chloride concentration due to sea level rise is retarded in the selected polder of the profile Haa with respect to the selected polder of the profile Grf, as the first-mentioned is located further inland.

3. Chloride load

Figure 9.22 shows the chloride load (in $ton\ Cl^-/(m'yr)$) during the next millennium in the selected polder of each profile. When the sea level falls -0.6 m/c, the chloride load is insignificant after one millennium in the selected polders of all profiles except in the selected polders of the profiles Haa and Del. In these two selected polders, seepage still occurs, even when the sea level has fallen 6 m in 2990 (see figure 9.19). A sea level rise of 0.6 m/c increases the chloride load enormously in all selected polders, especially when compared with the scenario SLR=0 m/c in the selected polders of the profiles Lei, Vla, Grf and Wad.

Figure 9.23 shows the impact of sea level rise on the chloride load in $kg\ Cl^-/(m^2yr)$[15] during a time span of one century. A sea level rise of 0.6 m/c influences the chloride load in the selected polders of all profiles considerably except in the selected polders of the profiles Haa, Lei and Del. The absolute increase in chloride load in 2090 for the scenario SLR=0.6 m/c with respect to the scenario SLR=0 m/c is great in the selected polders of the profiles Wie, Grf and Wad: +0.329, +0.392 and +1.294 kg $Cl^-/(m^2yr)$ respectively. Relative increases in chloride load in 2090 for the scenario SLR=0.6 m/c with respect to the scenario SLR=0 m/c are enormous in the selected polders of the profiles Vla, Grf and Wad, e.g. +92 %, +193 % and +167 % respectively. In addition, the relative increase in chloride load is also substantial in the selected polders of the profiles Wie, Ber and Lei, +14.4 %, +20.9 % and +18.8 % respectively. Note that the absolute chloride load in the selected polder of the profile Lei is still of minor importance.

---

[15]The chloride load in $ton\ Cl^-/(m'yr)$ is divided by the length of the selected polder in order to obtain, after conversion, the value in $kg\ Cl^-/(m^2yr)$.
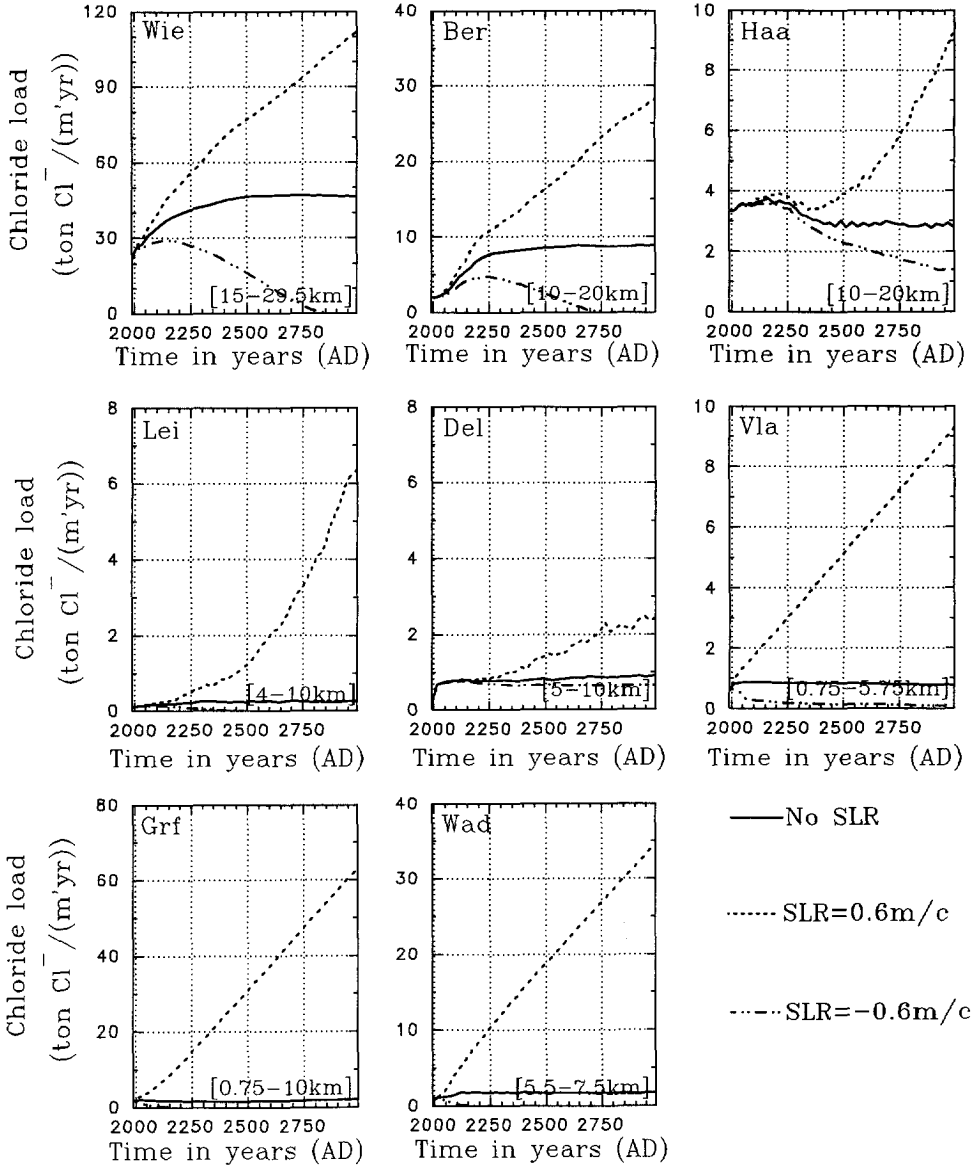
Figure 9.22: Chloride load $(ton\ Cl^-/(m'yr))$ through the Holocene aquitard at -15 m $N.A.P.$ in the selected polder of each profile during the next millennium for the three scenarios of sea level rise. The reaches of the selected polders are indicated.
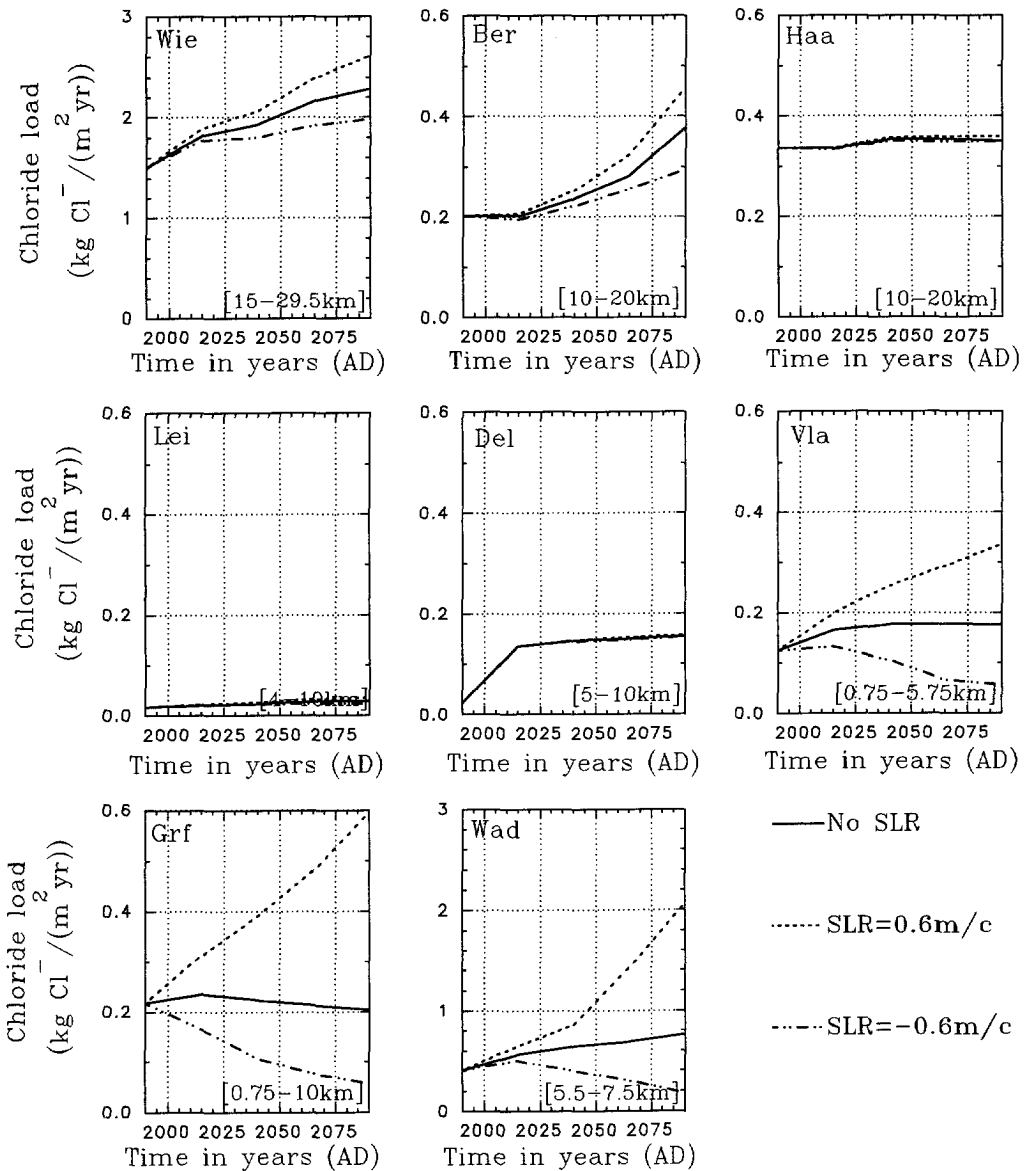
Figure 9.23: Chloride load $(kg\ Cl^-/(m^2yr))$ through the Holocene aquitard at -15 m $N.A.P.$ in the selected polder of each profile during the next century for the three scenarios of sea level rise. The reaches of the selected polders are indicated.

9.8   Effects of countermeasures

In this section, measures to counteract the negative impact of sea level rise are briefly discussed. Two scenarios of sea level rise are considered[16]: (1) SLR=0 m/c (the reference case) and (2) SLR=0.6 m/c. The discussion on the effects of the countermeasures mostly concerns the selected polders (see table 9.6). The countermeasures are defined in section 9.3.

i. Constant water level in the IJsselmeer when sea level rises

Whether the water level in the IJsselmeer matches the sea level or not makes no substantial difference on the chloride distribution in the profiles Wie and Ber. The constant water level in the IJsselmeer does not restrict the salinisation process of the geohydrologic system. No matter how, a severe salt water intrusion is still taking place in this scenario with a constant water level in the IJsselmeer. What is more, the constant water level in the IJsselmeer causes saline groundwater, which originates from the sea, to flow further towards the IJsselmeer boundary. Actually, the subsoil near the IJsselmeer boundary eventually becomes more saline than in the scenario with a water level rise at both boundaries.

However, the seepage quantity as well as the chloride load in the selected polders of both profiles do not increase as much in this scenario as they do in the scenario with a water level rise in the IJsselmeer. It can be deduced that, obviously, the propagation of sea level rise in the geohydrologic system is limited when the water level in the IJsselmeer is kept constant (see figure 9.24). With respect to the scenario with a water level rise at the IJsselmeer boundary, the seepage quantity in 2090 decreases in this case -9 % and -5 % and the chloride load decreases -12 % and -7 % for the selected polders of the profiles Wie and Ber respectively. The difference in seepage quantity is greater in the profile Wie than in the profile Ber, as the selected polder of the profile Wie is situated closer to the IJsselmeer boundary.

j. Land reclamation

This countermeasure comprises an additional strip of land of 5,000 m off the coast. Close to the old land, a new polder is reclaimed with a width of 2000 m and a phreatic groundwater level of +1.0 m $N.A.P.$ Adjacent to this polder, a new sand-dune area with a width of 3000 m is developed. A strip of sea of 5000 m is also simulated. The subsoil parameters in this strip of 10,000 m in total resemble the values of the old geohydrologic system; only the hydraulic resistance of the Holocene aquitard in all new sand-dune areas deviates from the old value: the new one equals 1000 $days$.

---

[16]To arrive at a comprehensive view over the results, only a selected number of the simulated cases is presented in figures in this section. Therefore, it may occur that conclusions drawn in the text are based on simulations not shown in figures in the thesis. Examples of such simulations are countermeasures in combination with the scenario SLR=0 m/c.
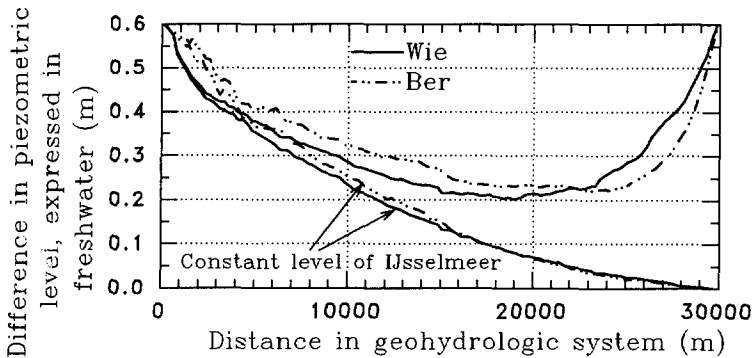
Figure 9.24: Differences in piezometric level, expressed in freshwater, at -25 m $N.A.P.$ in 2090 for the scenario SLR=0.6 m/c with respect to the scenario SLR=0 m/c in the profiles Wie and Ber. The influence of a constant water level at the IJsselmeer boundary is demonstrated.

Obviously, as a new sand-dune area is developed, a freshwater lens evolves in all profiles (figure 9.25). It takes a few decades to centuries before the new lenses are thick enough to withdraw groundwater from. Some remarks on the profiles follow here:

- Wie: when no sea level rise occurs, a very thick freshwater lens up to -85 m $N.A.P.$ evolves during the next centuries. The seepage quantity and chloride load in the selected polder in the reach 15,000-29,500 m do not differ from the reference case. In 2990, the volume of fresh groundwater (≤ 150 mg Cl^-/l) will be about $200 \cdot 10^3$ m^3/m', which is more than, for instance, the volume of fresh groundwater in the profile Haa in 1990 that equals about $135 \cdot 10^3$ m^3/m'.

  When the sea level rises 0.6 m/c, the lens only evolves to a volume of about $40 \cdot 10^3$ m^3/m' in 2990. Moreover, saline seepage ($> 15,000$ mg Cl^-/l) occurs around x=16,000 m (in the Wieringermeer polder).

- Ber: a twin freshwater lens is developed. When no sea level rise occurs, the total volume of fresh groundwater (≤ 150 mg Cl^-/l) is at least tripled till 2990 due to, among others, changes in the groundwater flow. Moreover, the chloride load in the selected polder in the reach 10,000-20,000 m decreases from some -6 % in 2090 to some -32 % in 2990.

  When the sea level rises 0.6 m/c, the total volume of both lenses only evolves to about 1.5 times the volume of the reference case in 2990. Moreover, saline seepage ($> 15,000$ mg Cl^-/l) occurs in the polders Schermer, Beemster and Wormer.
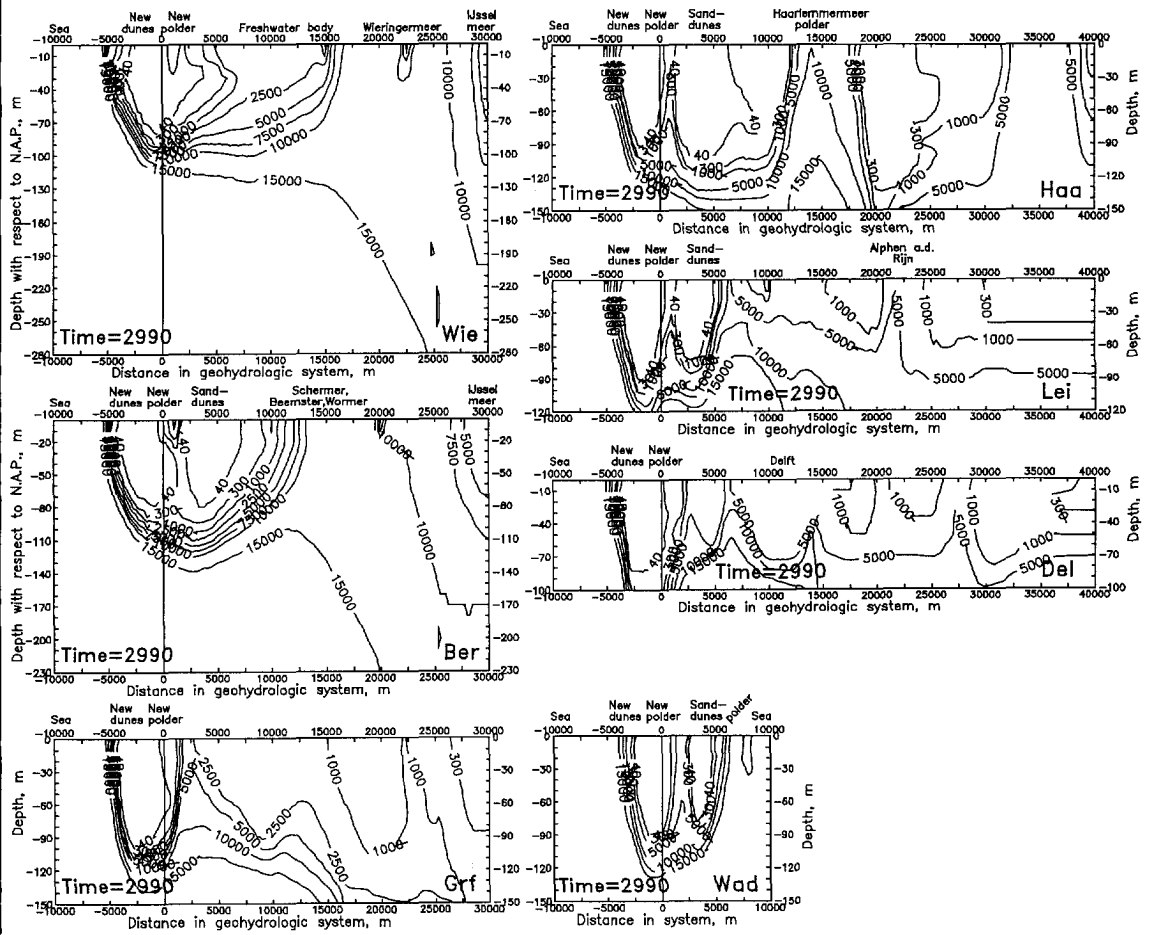
Figure 9.25: Effects of land reclamation on seven profiles in 2990. The level of the sea remains constant.

- Haa, Lei and Del: when no sea level rise occurs, the total volume of fresh groundwater in the profiles Haa and Lei increases significantly, since a twin lens evolves. In the profile Del, a completely new freshwater lens is developed. After some centuries, the (new) lens in these three profiles approaches the geohydrologic base. From then on, salt water intrusion in the geohydrologic system is (nearly) stopped and the surplus of saline groundwater inland of the blockade eventually leaves the geohydrologic system as saline or brackish seepage. During the next millennium, the changes in seepage quantity and chloride load with respect to the reference case are of minor importance for the low-lying polder areas.

When the sea level rises 0.6 m/c, the new freshwater lenses evolve, but they never reach the geohydrologic base. Thus, salt water intrusion in the geohydrologic system continues, though the lenses retard the salinisation.

- Grf: when no sea level rise occurs, a very thick freshwater lens evolves rapidly. The chloride load decreases substantially in the selected polder in the reach 750-10,000 m: in 2990 only to about 11 % of the value in the reference case.

  When the sea level rises 0.6 m/c, a somewhat smaller freshwater lens only retards the salt water intrusion. Meanwhile, the seepage in the reach 2500-3000 m contains more saline groundwater.

- Wad: when no sea level rise occurs, here again, a thick new freshwater lens is developed, though the chloride load in the selected polder in the reach 5500-7500 m does not change noticeably.

  When the sea level rises 0.6 m/c, both freshwater lenses are somewhat smaller, in 2990 nearly -40 % with respect to the scenario of SLR=0 m/c.

k. Extraction of saline[17] groundwater

Figure 9.26 shows the effects of this countermeasure on the chloride distributions in 2990 in the eight profiles. In general, the greater the geohydrologic system, the higher the extraction rates at more well lines must be before effects are significant. In all profiles, extraction of (saline) groundwater reduces the seepage quantity in polders in the vicinity. Obviously, the chloride load also decreases when the seepage quantity diminishes. On the other hand, groundwater extraction attracts saline groundwater from the sea, accelerating the salinisation process of the deeper regions of the geohydrologic system.

Table 9.7 summarizes the effects of extraction of (saline) groundwater on the three seepage parameters: (1) seepage quantity, (2) chloride load and (3) mean chloride concentration in the selected polders of the eight profiles. The table shows that the effects of groundwater extraction on the three seepage parameters can be very substantial for the selected polders of all profiles, except for the selected polder of the profile Wie. Although the extraction rate is high, the salinisation process cannot easily be stopped in the profile Wie with this extraction rate.

When the sea level rises 0.6 m/c, the salinisation process in most of the profiles cannot easily be stopped with extraction of (saline) groundwater at these moderate rates. The salinisation process (and thus the rise of groundwater with a higher chloride concentration) is only retarded to some extent. In the profile Vla, the size of the geohydrologic system and the extraction rates are such that salt water intrusion in the geohydrologic system is counteracted, even in case

---

[17]The changes in the salinity distribution of the subsoil may cause the well lines to extract brackish or even fresh groundwater on a certain moment.
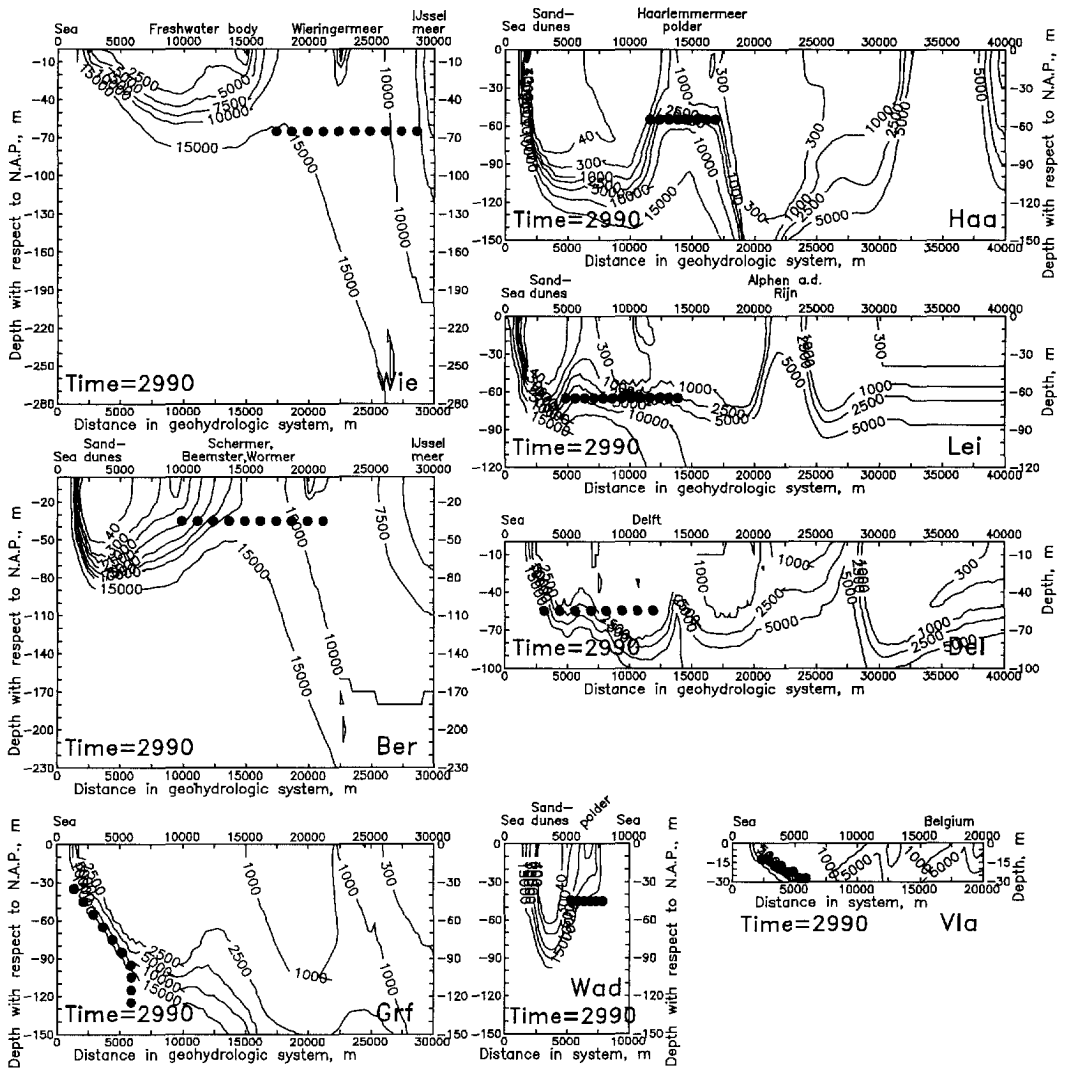
Figure 9.26: Chloride distribution (in $mg\ Cl^-/l$) in 2990 in the eight representative profiles in case saline groundwater is extracted. The level of the sea remains constant. A symbol • represents the position of a well line of extraction. In table 9.2, the number of well lines and the total rate of extraction are given for each profile.

of sea level rise. In most of the profiles, however, the effect on the salinisation process of this countermeasure appears to be of minor importance.

Table 9.7: Changes (in %) in 2990, with respect to the reference case, in the three seepage parameters in the selected polders of each profile due to two countermeasures: extraction of (saline) groundwater and infiltration of surface water. See table 9.2 for the number of well lines and the total rate of extraction. The level of the sea remains constant.

Wie	Ber	Haa	Lei	Del	Vla	Grf	Wad
Extraction of (saline) groundwater							
Change in seepage quantity in 2990 (%)							
-13	-45	-22	-15	-10	-43	-71	-38
Change in chloride load in 2990 (%)							
-18	-67	-88	-91	-37	-39	-76	-81
Change in mean chloride concentration in 2990 (%)							
-8	-32	-89	-92	-64	-59	-46	-60
Infiltration of surface water (500 $mg\ Cl^-/l$)							
Change in seepage quantity in 2990 (%)							
+16	+65	+43	+55	+76	+113	+450	+298
Change in chloride load in 2990 (%)							
-12	-46	+16	+307	+7	+4	+148	+26
Change in mean chloride concentration in 2990 (%)							
-40	-68	-67	+20	-51	-47	-13	-69

When the sea level rises 0.6 m/c and (saline) groundwater is extracted, the seepage quantity, chloride load and mean chloride concentration increase still considerably with respect to the scenario SLR=0 m/c (the reference case) in most of the selected polders of the profiles. For only the selected polders of the profiles **Haa** and **Del**, extraction of (saline) groundwater decreases these three seepage parameters, because these selected polders are located nearly beyond the zone of influence of sea level rise. As such, it can be expected that the rise in sea level affects only slightly the seepage parameters in these polders. When the sea level rises 0.6 m/c and (saline) groundwater is extracted, the seepage quantity, chloride load and mean chloride concentration decrease only slightly with respect to the scenario SLR=0.6 m/c and no (saline) groundwater is extracted.

I. **Deep-well infiltration of surface water**

Table 9.7 shows that, in general, the positive effects of this countermeasure are smaller than the effects of the countermeasure extraction of saline groundwater. Note that other schemes and rates of infiltration well lines could lead to more positive effects. In the near future, deep-well infiltration near the selected polders leads directly to a serious increase in seepage quantity. After some time, however, the mean chloride concentration in the Holocene aquitard decreases, as

the chloride concentration of the infiltrated surface water is low when compared with the original brackish groundwater. Only in the profile Lei, the infiltrated surface water pushes brackish groundwater towards the selected polder, causing an increase in mean chloride concentration, in 2990 with some +20 % of the value in the reference case (that is with no sea level rise and no countermeasure).

Based on the instantaneous increase in seepage quantity, the moment the deep-well infiltration begins, an increase in chloride load can be expected in most of the profiles for the next decades to even centuries. Especially in the profiles Haa, Lei, Grf and Wad, saline and brackish groundwater passes the infiltration well lines in the direction of low-lying polders, and the chloride load increases with respect to the reference case. In the profiles Wie and Ber, however, the chloride load eventually decreases as a result of the decrease in mean chloride concentration.

When the sea level rises 0.6 m/c, however, the same scheme and infiltration rate of the well lines, as considered above, does not really counteract the salinisation of the geohydrologic systems in all profiles, except in the profile Vla. In all profiles, the seepage quantity increases significantly. Only in the profiles Wie and Wad, the chloride load decreases after some centuries due to the deep-well infiltration of surface water.

m. Inundation of polders

Inundation of the selected polders mitigates the driving force of the salinisation process in the groundwater flow regime. The greater the difference between $N.A.P.$ and the original phreatic groundwater level, the more serious the effect of this countermeasure, as in the profiles Wie, Ber, Haa and Del (see figure 9.27). Obviously, the effects are significant near the selected polders themselves. As salinisation is still taking place, although at a lower rate, other (low-lying) polders with original phreatic groundwater levels now experience the rise of saline groundwater. This process is taking place in the profiles Wie (now in the reach 10,000-15,000 m) and Haa (now in the reach 7500-10,000 m in the Rijnland polders). In the profiles Grf and Wad, the differences in phreatic groundwater level due to inundation of the selected polders are too small to cause effects worth mentioning.

When the sea level rises 0.6 m/c, a severe salinisation process still occurs, even when the selected polders are inundated. Existing freshwater lenses decrease. After some centuries, both seepage quantity and chloride load significantly increase with respect to the reference case (that is no sea level rise) in those selected polders that are located within the zone of influence of sea level rise. However, seepage quantity and chloride load in the selected polders in question are lower in this case than in the case with only a sea level rise.

n. Widen the sand-dune area

The existing sand-dune area is widened with 1500 m. Note that this counter-
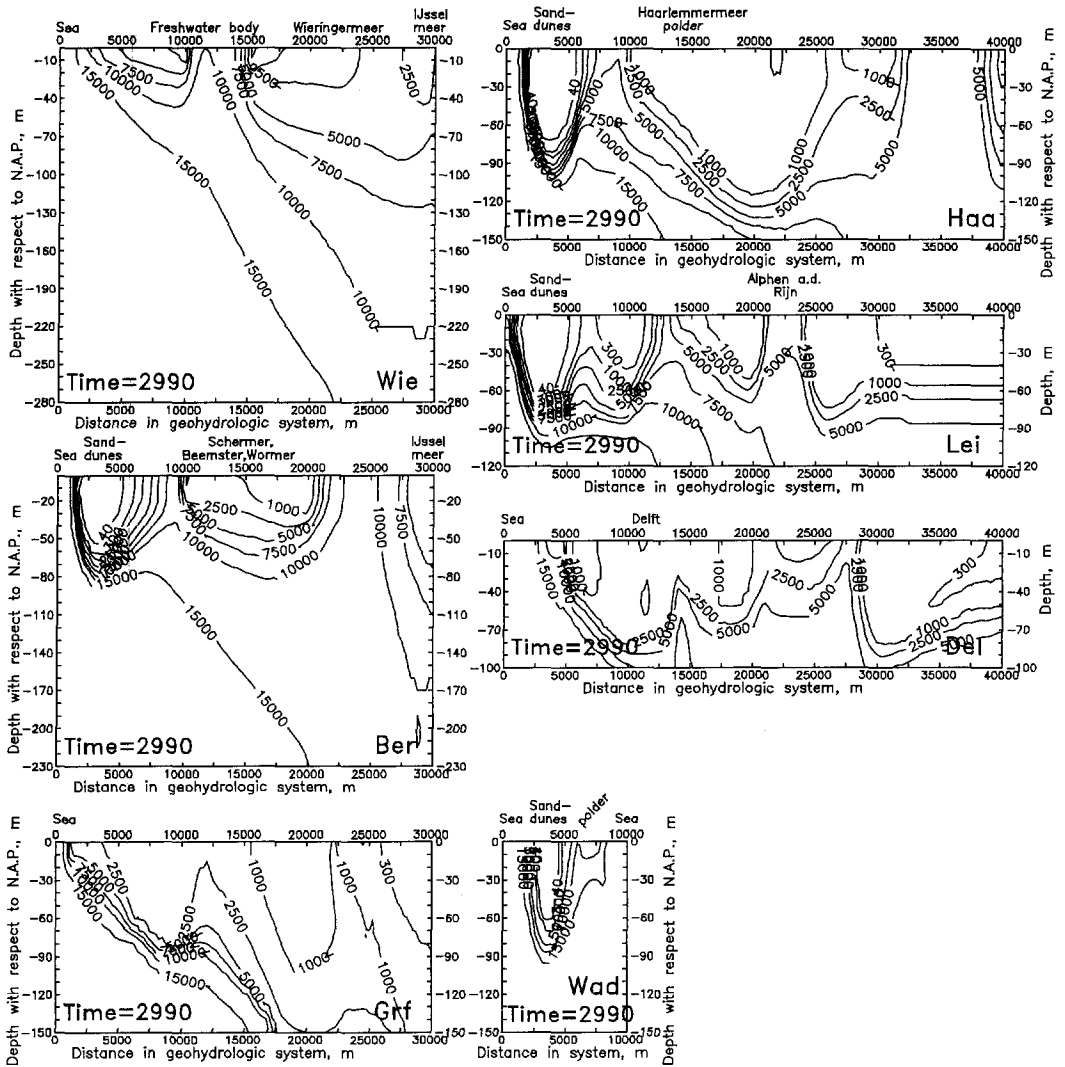
Figure 9.27: Chloride distribution (in $mg\ Cl^-/l$) in 2990 in the eight representative profiles in case the selected polders are inundated to $N.A.P.$ See table 9.6 for the position of the selected polder of each profile. The level of the sea remains constant.

measure resembles the countermeasure of land reclamation. When no sea level rise occurs, the phreatic groundwater level is heightened in the four profiles where already a sand-dune area occurs: about $+1.5\ m$ in the profiles **Ber** and **Lei**, and about $+0.7\ m$ in the profiles **Haa** and **Wad**. The volume of the freshwater lens increases significantly, e.g. after 100 year **Ber**=+48 %; **Haa**=+24 %;
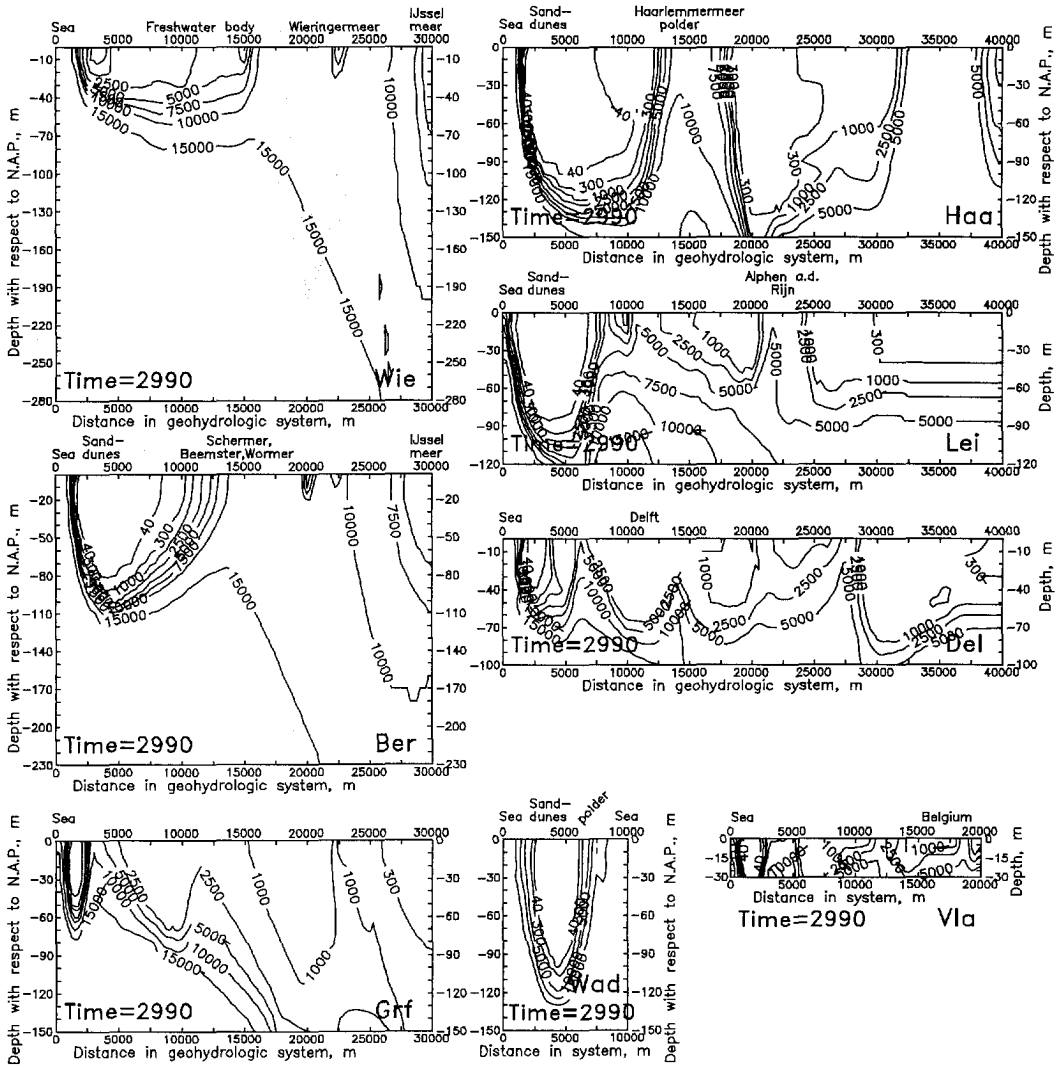
Figure 9.28: Chloride distribution (in $mg\ Cl^-/l$) in 2990 in the eight representative profiles in case the existing sand-dune area is widened with 1500 m. The level of the sea remains constant.

Lei$=+69$ %; and Wad$=+90$ % with respect to the reference case (no sea level rise) in 2090. In the profiles where no sand-dune area is present yet, a new fresh-water lens evolves (see figure 9.28). The time lag, when the lens has reached a new state of dynamic equilibrium, varies from profile to profile (e.g. several centuries in Wie to about 200 years in Grf). The volumes of the new freshwa-

ter lenses (≤ 150 mg Cl^-/l) become substantial (in 10^3 m^3/m')[18]: Wie=15, Del=34, Vla=20, and Grf=25. In the profiles Haa, Lei and Vla, the newly evolved freshwater lens obstructs saline groundwater to intrude towards the hinterland. Note that the inflow of saline groundwater is completely blocked in Vla.

The seepage quantity in the polder adjacent to the widened sand-dune area increases substantially. The reason is that the higher phreatic groundwater level in the sand-dune area increases the deep groundwater percolation through the Holocene aquitard, and as a result, (fresh) groundwater oozes out of the geohydrologic system in the adjacent polder. For instance, in the profiles Lei and Wad, the seepage quantity increases up to at least 25 % in the selected polders which are adjacent to the new (widened) sand-dune area. Subsequently, the chloride load in the adjacent polders increases temporarily due to the increase in seepage quantity. After some time, however, the mean chloride concentration decreases due to penetration of fresh (dune) groundwater. As a result, the chloride load in the adjacent polders diminishes, up to several tens of percents.

When the sea level rises 0.6 m/c, however, no freshwater lens can evolve in the profiles Wie, Del and Grf where no freshwater lens have existed before. The reason is that the rate of sea level rise is too high, so that the deep groundwater percolation through the Holocene aquitard is too small to build a freshwater lens. In the profiles Ber and Wad, the volume of the lens increases significantly with respect to the scenario with only a sea level rise. Meanwhile, however, salinisation of the subsoil in the vicinity of the low-lying polders is taking place. In the profiles Haa, Lei, but also in the profile Vla where the thickness is relatively small, new freshwater lenses are developed. These lenses block the salt water intrusion only temporarily. After some centuries, the lenses decrease due to sea level rise, and the salinisation process proceeds once again.

o. Physical barrier

Figure 9.29 shows the effects of this countermeasure on the chloride distributions in 2990 in the eight profiles. In general, physical barriers reduce the flow of groundwater in geohydrologic systems. In the chosen profiles, the seepage quantity in the polders in the vicinity of the physical barrier decreases. Moreover, the salinisation process is retarded, but not completely stopped. In the profiles Haa, Del and Lei, the rise of saline groundwater in low-lying polders is diminished. As a result, the chloride load can decrease substantially, especially in the polders in the vicinity of the physical barrier. The volume of the freshwater lens increases considerably in all four profiles with existing sand-dune areas, up to about: Ber=+11 %; Haa=+26 %, Lei=+9 % and Wad=+23 % with respect to the reference case in 2990. In the profile Haa, the thicker freshwater lens nearly blocks the salt water intrusion to the hinterland, causing a decrease

---

[18]The simulated volume of the freshwater lens in the profile Ber equals about 90 $\cdot 10^3$ m^3/m' in 1990.
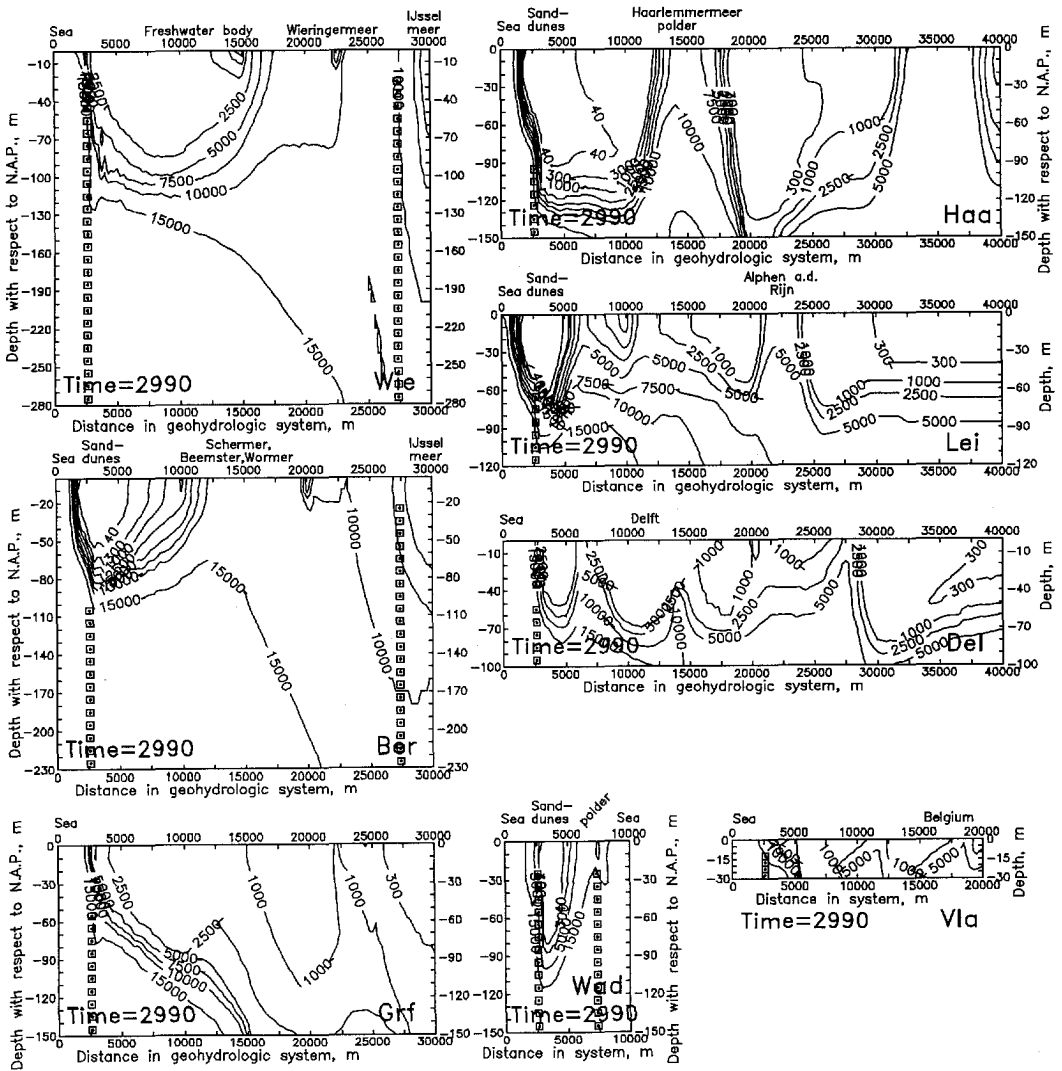
Figure 9.29: Chloride distribution (in $mg\ Cl^-/l$) in 2990 in the eight representative profiles in case a physical barrier is implemented. The level of the sea remains constant.

in chloride load. The effects of implementing a physical barrier are of minor importance in the profile Vla, mainly because the salt water intrusion is already limited. In two profiles in Noord-Holland, Wie and Ber, the salinisation process of the geohydrologic systems is retarded. Immediately after the construction of the physical barrier, both seepage quantity and chloride load in the selected polder of the profile Wie drop significantly, about -20 % and -13 % respectively

with respect to the reference case (no sea level rise). In the profile **Ber**, the barrier is more permeable (5 m/d instead of 1 m/d, see section 9.3 item o. **Physical barrier**, page 305), and consequently, the effects of this countermeasure are smaller than in the profile **Wie**. For instance, the moment the physical barrier has been installed, both seepage quantity and chloride load decrease about 6 % with respect to the reference case (no sea level rise).

When the sea level rises 0.6 m/c, the volumes of the freshwater lenses decrease. Inflow of saline groundwater still continues, though, due to the presence of the physical barrier, at a lower rate when compared with the scenario with only a sea level rise. In general, the physical barrier only retards the salinisation process, and thus, in the long run, most of the profiles eventually experience similar salinisation problems as in the scenario with only a sea level rise.

Conclusion

Human interventions cannot easily counteract the salinisation process in most of the Dutch coastal geohydrologic systems, though seepage quantity and chloride load in polder areas can be decreased substantially on a local scale. When sea level rises, the negative impact of sea level rise seems to be rather restricted for the next century and effective countermeasures might be feasible for the time being. However, within some centuries, saline groundwater replaces brackish groundwater, and polder areas in the zone of influence of sea level rise will experience brackish or saline seepage. Eventually, the salinisation process can only be retarded by countermeasures but not stopped, and only at the expense of great efforts.

9.9   Subsoil parameters

In this section, the effects of six subsoil parameters are briefly discussed:

p. **Hydraulic conductivity**[19]: $k_{new}=k_{ref} \cdot 1.5$ and $k_{new}=k_{ref} \cdot 2/3$
Obviously, the salinisation process significantly changes if the hydraulic conductivity is higher (multiplied with 1.5) or lower (multiplied with 2/3). The position of the saline groundwater tongue (that is the 15,000 $mg\ Cl^-/l$-isochlor) is largely affected by the hydraulic conductivity. For instance, in the profile **Grf**, the tongue would displace +3750 m ($k_{new}=k_{ref} \cdot 1.5$) and -3250 m ($k_{new}=k_{ref} \cdot 2/3$) with respect to the position of the tongue at $x=16,000\ m$ in 2990 in the reference case (no sea level rise). Upconing in the polders differs. Both seepage quantity and chloride load in the polders change very much: e.g. in the beginning of the simulations in 1990 in the selected polders of the profiles **Ber, Haa, Lei, Del, Grf** and **Wad** for $k_{new}=k_{ref} \cdot 1.5$ in the range from +25 % to +50 %, and for $k_{new}=k_{ref} \cdot 2/3$ in the range from -15 % to -33 %. The volume

---

[19] ref refers to the reference case, new refers to the case with the new subsoil parameter.

of the freshwater lens would increase significantly if the hydraulic conductivity $k_{new}=k_{ref}\cdot 2/3$: Ber=+19 %; Haa= only +2 %; Lei=+4 % and Wad=+15 % in 2090.

q. Hydraulic resistance: $c_{new}=c_{ref}\cdot 1.5$ and $c_{new}=c_{ref}\cdot 2/3$

In this case, the hydraulic resistance of the Holocene aquitard and the loam layer, where present, are adapted. Seepage through the Holocene aquitard is affected by another hydraulic resistance. Moreover, the chloride load in the low-lying polders changes. In the deep aquifers of the geohydrologic system, the changes in the chloride distribution due to different hydraulic resistances are insignificant. Furthermore, the volume of the freshwater lens does not alter substantially.

The vertical velocity through the aquitard increases, when the hydraulic resistance is multiplied with a factor 2/3. Subsequently, the seepage quantity in the polders also increases. For instance, in the profiles Wie, Ber and Haa, the seepage quantity would increase with +13 %, +27 % and +24 % respectively in 1990 with respect to the reference case. The chloride load increases simultaneously with the seepage quantity. Moreover, the saline groundwater replaces brackish and fresh groundwater more rapidly than in the reference case. Upconing in the polders goes faster, and thus, the chloride load is influenced once again. For instance, in the profiles Wie, Ber and Haa the chloride load would increase with +19 %, +27 % and +6 % respectively in 2990 with respect to the reference case.

r. Longitudinal dispersivity: $\alpha_{L,new}=0$ m and $\alpha_{L,new}=2.0$ m

The effect of different longitudinal dispersivities on the volume of the freshwater lens is significant in all four profiles with existing sand-dune areas Ber, Haa, Lei and Wad. For smaller α_L, the mixing of fresh, brackish and saline groundwater is smaller, and a greater freshwater lens is simulated. For greater α_L, the opposite phenomenon is accomplished. For instance, if $\alpha_L=0$ m respectively $\alpha_L=2.0$ m are applied instead of the reference value 0.2 m, the simulated volume of fresh groundwater (≤ 150 mg Cl^-/l) in 2090 would be much greater respectively smaller: Ber=+13 % respectively -36 %; Haa=+4 % respectively -29 %; Lei=+10 % respectively -41 % and Wad=+15 % respectively -28 %.

Moreover, for $\alpha_L=2.0$ m, the saline groundwater tongue (the 15,000 mg Cl^-/l-isochlor) retreats in the profiles Haa, Lei, Del and Vla. This retreat of the tongue does not occur if $\alpha_L=0.2$ m (or $\alpha_L=0$ m). On the contrary, for these two longitudinal dispersivities, saline groundwater intrudes further in the geohydrologic systems of these four profiles.

The changes in the volume percentages of fresh, brackish and saline groundwater due to different longitudinal dispersivities are significant in the three profiles Wie, Ber and Haa, up to some 20 % during the next millennium (see figure 9.30).
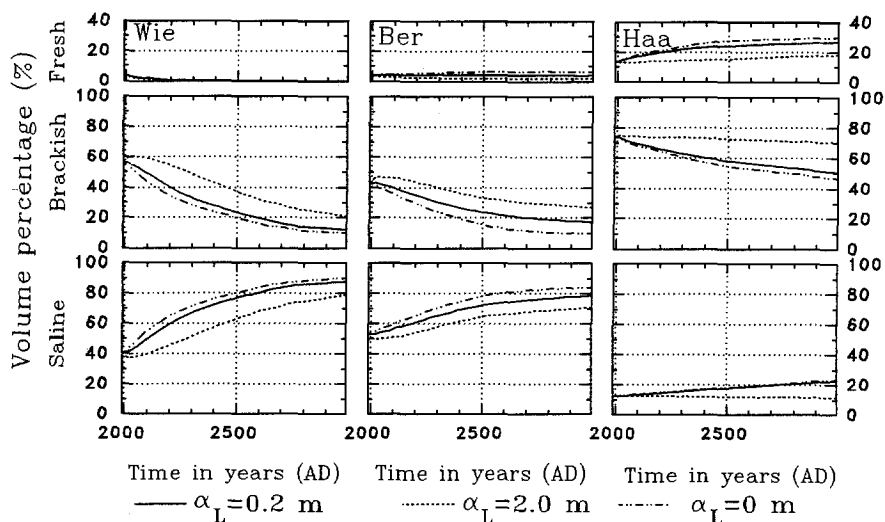
Figure 9.30: Volume percentages of fresh, brackish and saline groundwater during the next millennium in three profiles along the Dutch coast, calculated with three different values of longitudinal dispersivity: $\alpha_L=0.0$ m, $\alpha_L=0.2$ m and $\alpha_L=2.0$ m.

In the six other profiles, the difference within the next millennium between the reference case and the two cases are smaller than a few percents.

The (absolute) changes in chloride load are substantial for the selected polders of the profiles Ber, Haa, Lei and Del, as a change in chloride distribution has its influence on the chloride load in these polders. For instance, in 2990, the (absolute) difference between the case with $\alpha_L=2.0$ m and the reference case with $\alpha_L=0.2$ m would be (in ton $Cl^-/(m'yr)$): Ber=+0.345; Haa=+1.382; Lei=+0.399; and Del=+0.468. The changes in chloride load in the selected polders due to different longitudinal dispersivities are negligible in the other profiles.

s. **Effective porosity**: $n_{e,new}=0.15$ and $n_{e,new}=0.45$
   The real velocity in the geohydrologic system changes as follows: for $n_e=0.15$, $0.35/0.15=2.33$ times the reference velocity, and for $n_e=0.45$, $0.35/0.45=0.78$ times the reference velocity. The rate of the salinisation process of the geohydrologic system changes similar to the real velocity, and thus, the rate of the salinisation process is highly determined by the effective porosity. The smaller n_e, the greater the real velocity of the groundwater, and therefore, the higher the rate of salinisation of the geohydrologic system. Thus, the rise of saline groundwater is more severe. For instance, for the selected polders of the profiles Ber, Haa and Grf the chloride load would be greater in 2990 for $n_e=0.15$: +13%, +33 % and +23 % respectively with respect to the reference case. For

n_e=0.45, the change in chloride load in 2990 would only be a few percents with respect to the reference case. Moreover, for smaller n_e, the position of the saline groundwater tongue (the 15,000 $mg\ Cl^-/l$-isochlor) moves faster in the direction of low-lying polders. For instance, in the profile Grf the position of the saline tongue would be x=25,000 m and x=14,000 m in the geohydrologic system in 2990 for n_e=0.15 and n_e=0.45 respectively, whereas the position of the tongue in the reference case is x=16,000 m. Note that, eventually, the states of dynamic equilibrium of all three cases are equal to each other.

t. Anisotropy: $k_z/k_{x,new}$=0.05 and $k_z/k_{x,new}$=0.25

The value of the anisotropy factor affects, among others, the rise of brackish and saline groundwater in low-lying polders, and thus, seepage quantity and chloride load in these areas. In the case with k_z/k_x=0.25, the hydraulic conductivity in vertical direction k_z is greater than in the reference case with k_z/k_x=0.1. As a result, upconing in low-lying polders goes faster, and subsequently, seepage quantity and chloride load in these polders is considerably increased. With respect to the reference case, an increase of several tens of percents in both seepage quantity and chloride load has been calculated.

For instance, the following situation occurs in the profile Haa (see figure 9.31). As the vertical velocities are greater in the case with k_z/k_x=0.25 than in the reference case, fresh (surface) water infiltrates deeper in the groundwater flow regime. It appears that the salinisation process is to a certain extent blocked in the reach 9000-10,000 m and the inflow of saline groundwater is retarded. The chloride load in the selected polder (that is the Haarlemmermeer polder) decreases after some centuries, though the seepage quantity in this case remains much higher than in the two other cases k_z/k_x=0.05 and k_z/k_x=0.10. Figure 9.31 shows that the shape of the freshwater lens also differs for these two anisotropies. The more isotropic the medium (k_z/k_x=0.25), the smaller the width of the freshwater lens is.

u. Depth of the geohydrologic base D

Although the marine clayey sediments are not simulated in the reference cases of the eight profiles, saline (marine) groundwater in these sediments would probably participate in the salinisation process. Therefore, in this case, the geohydrologic base is lowered to simulate the effect of a lower geohydrologic base on the results. In geohydrologic systems with thick aquifers, e.g. in the profiles Wie and Ber, the effect on the results is small, because the distance between the base and the surface is great, and saline (marine) groundwater takes a very long time to reach the land surface. So, the seepage quantity and the chloride load are only slightly (one or two percents) greater.

Taking into account the marine clayey sediments in geohydrologic systems which are not so thick, e.g. $\leq$ 150 m, the effect of the marine clayey sediments on the salinisation process can be considerable. If the vertical velocities of groundwa-
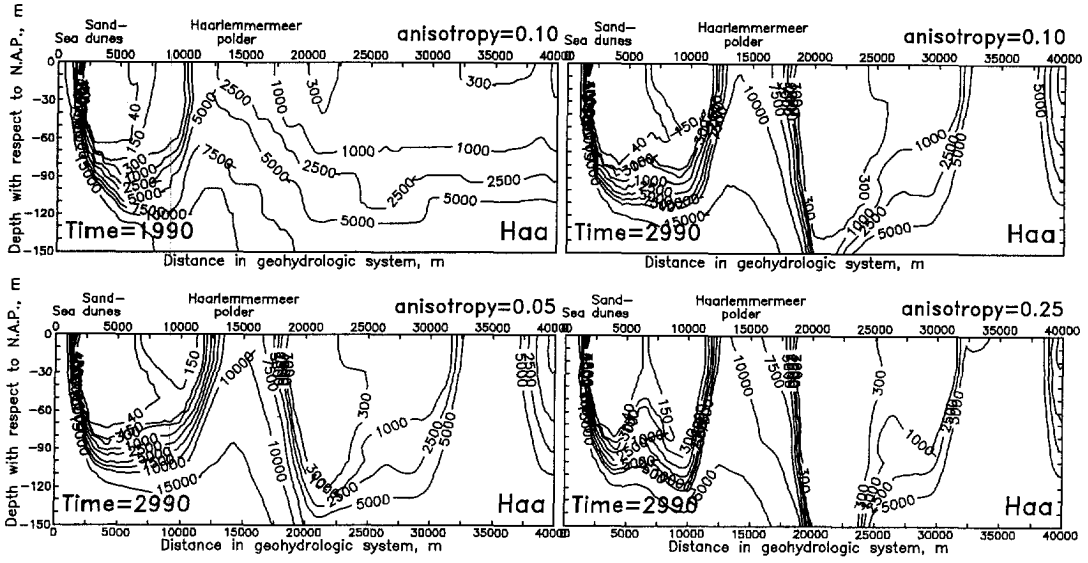
Figure 9.31: Chloride distribution (in $mg\ Cl^-/l$) in the geohydrologic system of the profile Haa, calculated with three different values of anisotropy: k_z/k_x=0.10 (in 1990 and 2990), k_z/k_x=0.05 (in 2990) and k_z/k_x=0.25 (in 2990).

ter in the marine clayey sediments are not too small, saline groundwater could be transported towards the upper part of the geohydrologic system. This process occurs in the profiles **Haa** and **Lei**, where the rise of brackish and saline groundwater in the direction of the low-lying polders is more severe than in the reference case. For instance, the chloride load in the selected polders of the profiles **Haa** and **Lei** would be greater in 2990, some +14 % and +19% respectively. In the profile **Del**, saline groundwater from the marine clayey sediments would be extracted by the well lines. In the profiles **Grf** and **Wad**, the marine clayey sediments do not affect the salinisation process of the geohydrologic systems.

In conclusion, it is recommendable to investigate whether or not the marine clayey sediments should be included in the schematisation of coastal geohydrologic systems over long simulation times of e.g. one millennium. Especially the geohydrologic systems in the provinces of Zuid-Holland and Zeeland might probably be sensitive to the choice of the position of the geohydrologic base. Note that the chosen hydraulic conductivity of the marine clayey sediments of 5 m/d is open for discussion.

9.10   Conclusions and recommendations

Conclusions

Even without a sea level rise, most of the eight profiles along the Dutch coast have not yet reached a state of dynamic equilibrium as far as the salinity distribution in the subsoil is concerned, because the current hydrological situation in the low-lying polders induces a severe salinisation process in the geohydrologic systems.

The shorter the distance of the propagation of sea level rise in the groundwater flow regime, the smaller the impact of sea level rise on the salinisation process. In the profiles Haa, Lei, Del, Grf and Vla, the so-called zone of influence of sea level rise is limited. In the profiles Wie, Ber and Wad, the zone of influence of sea level rise is extended, because, among others, the sea level rises at both sides.

When the sea level rises 0.6 m during the next century, the volume of the freshwater lenses in the four profiles with existing sand-dune areas decreases negligibly. However, after a few centuries, the decrease in volume may reach several tens of percents.

The impact of sea level rise in a polder can be significant in terms of seepage quantity, mean chloride concentration and chloride load in the following situations: the polder is situated directly inland of the coast; the phreatic groundwater level in the polder is low, namely several metres below $N.A.P.$; and/or the zone of influence of sea level rise in the geohydrologic system is long as a result of high transmissivities of aquifers.

When the sea level rises 0.6 m during the next century, both seepage quantity and chloride load change substantially in the selected polders of all profiles, except in the selected polders of the profiles Haa and Del, as these polders are located practically beyond the zone of influence of sea level rise. In the profiles with no sand-dune areas, the seepage quantity and chloride load increase seriously in those low-lying polder areas which are situated directly inland of the coast.

When no sea level rise occurs, effective human interventions may counteract the salinisation of the geohydrologic systems in all profiles, such as (a) reclaiming land off the coast, thus evolving new freshwater lenses; (b) extracting (saline) groundwater, thus decreasing the seepage quantity and chloride load in the polders; (c) inundating low-lying polders, thus removing the driving force of the salinisation process; (d) widening existing sand-dune areas, thus generating thicker freshwater lenses; and (e) creating physical barriers, thus blocking the free entrance of saline groundwater and retarding the salinisation process. Maintaining the water level of the IJsselmeer to reduce the salinisation process in the profiles Wie and Ber is not really an effective countermeasure. Moreover, the countermeasure deep-well infiltration of surface water increases the seepage quantity in polders, and thus, increases the chloride load, without really blocking the salinisation process towards the low-lying hinterland. Although the time lag before the countermeasures are effective is in the order of several decades to centuries, the measures may be technically feasible in the long-term. Note

that some of these countermeasures should only be considered as interesting hypothetical cases to gain a better insight into the range of conceivable human interventions.

When the sea level rises 0.6 m/c, however, even the effective countermeasures cannot easily stop the salinisation of the subsoil, though it can be retarded. Therefore, it is likely to believe that human interventions can only counteract the impact of sea level rise on the groundwater flow regimes in the long-term at the expense of major investments. Whether or not these investments are considered feasible depends on the prevailing economic, environmental and political circumstances at the moment when a (political) decision is taken.

The limited sensitivity analysis of the influence of subsoil parameters has demonstrated that some parameters affect the results of the salinisation process in the geohydrologic system to a large extent. In general, higher hydraulic conductivities, smaller porosities, lower hydraulic resistances and including marine clayey sediments accelerate the salinisation process.

Recommendations

In this chapter, the Dutch groundwater flow regimes have only been schematised and modelled in (two-dimensional) profiles. However, due to high groundwater extraction rates and due to the diversity and complexity of the Dutch polder landscape, groundwater flow is in fact three-dimensional, such as in the islands of the province of Zeeland. Therefore, three-dimensional modelling should be executed to cope with three-dimensional groundwater flow. Note that, for the time being, three-dimensional modelling is rather sophisticated, and that the enormous quantities of (reliable) groundwater data required in these models are not yet available.

It is recommended to derive, for a good decision, the optimum, and yet realistic, position of well lines and rates of extraction or infiltration. Note that it may even be necessary to adapt the positions and rates of extraction or infiltration of well lines in the course of the realisation of the countermeasure.

It is recommended to investigate whether or not the marine clayey sediments should be included in the schematisations of the coastal geohydrologic systems, because saline groundwater of these sediments might probably affect the salinisation of the upper part of the coastal geohydrologic systems of especially the provinces of Zuid-Holland and Zeeland during a long simulation times of, for instance, one millennium.

Chapter 10

Impact on three water management sectors

10.1 Introduction

As the ongoing sea level rise is expected to continue during the next century[1], it is relevant to know how water management sectors in the Netherlands will develop in the foreseeable future.

In this chapter, the direct perceptible impact of sea level rise is discussed on only three water management sectors[2]:

1. **domestic and industrial water supply from coastal sand-dune areas**
   The volumes of the freshwater lenses in the sand-dune areas are likely to decrease when sea level rises. Drinking water companies, which extract groundwater from these freshwater lenses for domestic and industrial purposes, should anticipate on possible changes in the storage of fresh groundwater in the (middle) long-term.

2. **flushing of water courses of low-lying areas**
   Sea level rise as well as previous human activities cause an increase in both seepage quantity and chloride load in the polders near the coast. The increased saline seepage in the polders is discharged by pumping the excess water into the surface water systems (boezems). In order to avoid deterioration of the

---

[1] The impact of sea level rise is discussed over a time span of one century because of three reasons: (1) over this time span, the impact of sea level rise, if any, can clearly be detected in all Dutch coastal groundwater flow regimes; (2) over this time span, other (complex) processes involved can be left out of consideration, though they may considerably affect the conditions of the groundwater flow regimes over a much longer time span; and (3) this time span corresponds with the life span of countermeasures to reduce the negative impact of sea level rise, comprising the following phases: initiative phase (exploration, planning, designing), development phase (realisation), operational phase and dismantling phase.

[2] The water management sectors are described in the PAWN-study [Pulles, 1985], which stands for Policy Analysis for the Watermanagement of the Netherlands. In this study, numerous models have been used to investigate intensively the following water management sectors in the Netherlands: agriculture, horticulture, domestic water supply, industry, power generation, navigation, recreation, environment, ecology and nature preservation.

surface water quality, the water courses have to be flushed more frequently and/or more intensively to diminish the solute concentrations of the polder areas and the surface water systems. When flushing is restricted, salt damage may increase.

3. agriculture in terms of salt damage

As the seepage in polders will contain more salt due to sea level rise and previous human activities, the salinity of the subsoil increases. When, subsequently, the salinity of the root zone also increases (depending on several conditions, such as the distances between drainage ditches and the thickness of the freshwater layer which builds up in the winter season), agriculture may suffer from salt damage, which could have economic implications.

In chapter 9, the impact of sea level rise has been assessed on sand-dune areas and on polders in (vertical) two-dimensional profiles only. In this chapter, however, the results of these simulations are interpreted spatially in order to assess the impact on entire regions along the Dutch coast[3]. This is accomplished by multiplying the results of chapter 9 with a width $L_\perp$, which is measured perpendicular to the considered profile. The geohydrologic conditions are supposed to be constant over the width $L_\perp$ (see figure 9.2 for the width $L_\perp$ of each profile). This implies that the seepage quantity and the chloride load in the (selected) polders, that have been given *per metre width* in chapter 9, are converted to m^3/yr and $kg\ Cl^-/yr$ respectively in this chapter.

The seepage quantities and chloride loads, mentioned in this chapter, should not be interpreted in terms of *absolute values*. The main reason for this is that the up-scaling from two-dimensional (vertical) figures to three-dimensional figures is rather elementary. This implies that many calculated figures cannot be matched with the observed figures. Nonetheless, the *changes* in seepage quantity and chloride load in the polders due to sea level rise and previous human activities can still give indicative estimates.

The results of the present study could be implemented as input data in various models, such as: (1) the models of the PAWN-study [Pulles, 1985]; (2) the integrated models ISOS [Peerbolte *et al.*, 1991], IMAGE and ESCAPE (see subsection 2.5.2); and (3) the model SWAP[4].

The impact of sea level rise on the three water management sectors is reviewed in the following sections. For each of these water management sectors, indicative conclusions are drawn.

---

[3]Note that the islands of the province of Zeeland are not modelled.

[4]Postma *et al.* [1994] assessed the impacts of sea level rise and climate change on crop production and water use in Voorne-Putten by means of the saturated/unsaturated groundwater flow and the crop growth model SWAP.

10.2   Domestic and industrial water supply from coastal sand-dune areas

Introduction

The total volume of water, delivered by the water supply companies, was about $1250 \cdot 10^6 \ m^3$ in 1993, about one third of which was extracted from surface water resources (including water from infiltration areas) and about two thirds from groundwater resources [Netherlands Central Bureau of Statistics, CBS]. The prognosis for 2020 is that the total annual volume of water, delivered by the water supply companies, will increase with some $+30$ to $+55$ % [Wieringa and Laan, 1989].

The contribution of groundwater, that originates from the deep parts of the freshwater lenses in the coastal sand-dune areas, to the national water supply is at present of minor importance. For instance, in 1989, the groundwater extractions for drinking water supply from the coastal sand-dune areas in the western part of the Netherlands amounted to some $206 \cdot 10^6 \ m^3$, of which the volume of artificial recharge was about $168 \cdot 10^6 \ m^3$ [Stuyfzand, 1993] and the volume of extracted groundwater, which originates from the deep parts of the freshwater lenses in the coastal sand-dune areas, was about $38 \cdot 10^6 \ m^3$ (compare 1976: $54 \cdot 10^6 \ m^3$ and 1993: $29 \cdot 10^6 \ m^3$) [CBS].

The objective of this section is to evaluate the future development of the fresh groundwater resources stored in the coastal sand-dune areas. For this purpose, only three profiles with sand-dune areas are considered: Ber, Haa and Lei. This selection implies that the fresh water resources in the Wadden Islands and in the islands of Zeeland are not considered in this evaluation. The main reason for not evaluating the profile Wad is that the results of the simulations in the vertical plane cannot simply be extended spatially by multiplying the results with a width $L_\perp$, as the geohydrologic conditions of the islands vary too much[5]. The main reason for not evaluating the freshwater lenses on the islands of Zeeland is that the islands cannot really be schematised in two dimensions (see section 9.2).

Impact of sea level rise

Figure 10.1 shows the change in volume of fresh groundwater (in $10^9 \ m^3$) due to sea level rise as a function of time. The calculated storage of fresh groundwater in 1990 for the three profiles is as follows: Ber=$2.7 \cdot 10^9 \ m^3$, Haa=$3.4 \cdot 10^9 \ m^3$ and Lei=$0.8 \cdot 10^9 \ m^3$. These appear to be conservative calculations. The reasons for the discrepancy between calculated and observed figures are numerous and diverse, though the main causes of discrepancy are the schematisation and modelling of the geohydrologic system in a (two-dimensional) profile. For instance, in some places,

---

[5]For instance, the width of the sand-dune areas of the islands under consideration (Texel, Vlieland, Terschelling, Ameland and Schiermonnikoog) differ significantly from each other. Vlieland has only a small polder named Kroon's polders at the tip of the island, whereas the profile Wad simulates a polder with a width of $3000 \ m$.
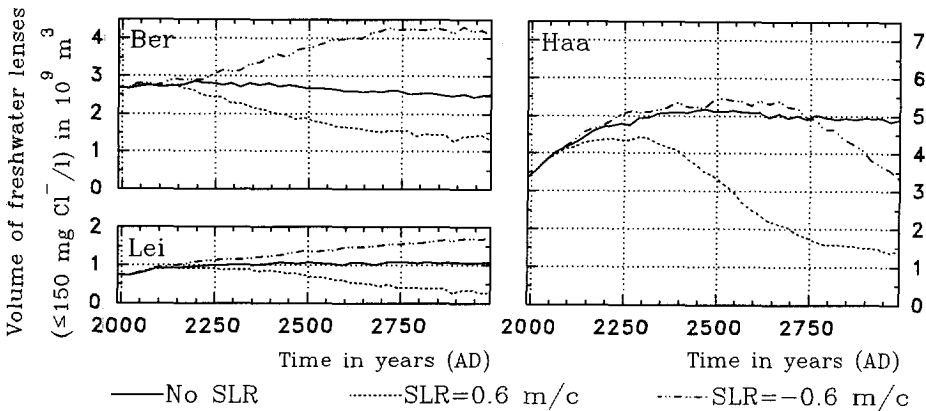
Figure 10.1: Volume of fresh groundwater ($\leq 150\ mg\ Cl^-/l$) in the profiles Ber, Haa and Lei in $10^9\ m^3$ as a function of time for the three scenarios of sea level rise. The volume in m^3/m' of figure 9.17 is multiplied with the width $L_\perp$ of each profile: for Ber $L_\perp=30\ km$, for Haa $L_\perp=25\ km$, and for Lei $L_\perp=15\ km$.

the width of the sand-dune area in the profile Ber is actually 5000 m instead of the simulated 3500 m. Therefore, a smaller volume of the freshwater body than observed in the profile Ber is calculated.

The figure shows that during the next century the impact of sea level rise on the fresh groundwater resources along the Dutch coast appears to be of minor importance. The volume of fresh groundwater will decrease only by a few percents at the utmost. In the profile Haa, the volume will even increase significantly with respect to the situation in 1990 till about the beginning of the 23th century, as extraction rates in the deep geohydrologic system have been reduced since the mid 1960's.

However, after a few centuries, the volumes of fresh groundwater will decrease substantially when the sea level rises 0.6 m/c. Severe upconing of saline groundwater is likely to occur at extraction points, even at low extraction rates. Obviously, the magnitude of the impact depends on local circumstances. For instance, in narrow sand-dune areas, where a severe shoreline retreat occurs due to sea level rise and where no sand-suppletion is applied, the volumes of the freshwater lenses could decrease rapidly. When, in addition, the phreatic groundwater level in the sand-dune area cannot adapt to sea level rise, groundwater extractions may eventually have to be stopped or at least to be diminished in order to prevent severe upconing of saline groundwater.

10.3   Flushing of water courses of low-lying areas

Introduction

Surface water systems, e.g. water courses in polders, boezems and lakes, have to be flushed in order to maintain an acceptable water quality. For instance, the volume of water, required for flushing to lower the salinity in the surface water systems and for water level control in the midwestern part of the Netherlands (between the open Rotterdam Seaway (Nieuwe Waterweg) and the navigation canal to Amsterdam (Noordzeekanaal): Rijnland, Delfland, Schieland and Amstelland) amounts to about $450 \cdot 10^6 \ m^3/yr$ under normal (average) conditions, whereas during (extremely) dry summers the total volume of water required in this part of the Netherlands is a multiple of this amount[6] [ICW, 1976; Wesseling, 1980; Abrahamse et al., 1982; Pulles, 1985].

The salinity in a surface water system originates from internal and external sources. Internal sources are seepage[7], precipitation and water discharged after domestic and industrial use. External sources are salt penetration by the lockage of ships to or from saline or brackish water and water intake from rivers and canals for water level control and for flushing.

In the future, the two main causes of the increases in seepage quantity and chloride load in the (low-lying) polders near the Dutch coast are the rise in sea level and the non-equilibrium state of the present salinisation process of the subsoil due to previous human activities (namely reclamation of lakes or parts of the sea). As a result of the salinisation of the subsoil, the salinity of the surface water systems increases, which has to be reduced through extra flushing[8].

Unfortunately, the exact estimates of the required (increases of) flushing quantities cannot be determined within the scope of this thesis, for several reasons. Firstly, seasonal effects of the incoming and outgoing surface water quantities make that a chloride concentration averaged over a year cannot be calculated. Secondly, the contribution of seepage and chloride load relative to other sources in the water and salt balance cannot easily be determined. Obviously, when the contribution of chloride load by seepage to the terms of the salt balance is of minor importance, an increase

---

[6] During the extremely dry summer of 1976 (a 2%-year), the water demand for flushing and for water level control exceeded the water supply. Especially in the waterboard of Delfland, the flushing discharges were too low. The total flushing demand of the boezems in the low-lying polders of the Netherlands was estimated at about $600 \cdot 10^6 \ m^3$ over the period April-August 1976, which equals some $45 \ m^3/s$ [van Boheemen and de Wilde, 1979]. For quantitative water management, e.g. for water level control, about twice the water demand for flushing was required in that area. In addition, a much greater volume of water was required to counteract salt water intrusion at outlets in the low-lying part of the Netherlands, namely some $715 \ m^3/s$.

[7] For instance, the chloride load of the seepage in the midwestern part of the Netherlands is estimated at some $180,000 \ ton \ Cl^-/yr$ [ICW, 1976; Wesseling, 1980].

[8] If the salt load of the Rijn decreases in the future due to agreements between the Rijn riparian states, this may probably reduce the volumes of water required for flushing the surface water systems in the low-lying parts of the Netherlands, as then, water which originates from the Rijn has a lower salinity.

of the chloride load by seepage due to sea level rise and (previous) human activities is generally also of minor importance.

Nonetheless, it is possible to assess flushing quantities with the tools applied in the PAWN-study. The 'old' exercises with the PAWN-models[9] can be executed once again, though now with a higher seepage quantity and a higher chloride load in the low-lying polders near the coast.

In this section, the data[10] on the increases in seepage quantity and chloride load are provided, as necessary in the PAWN-models. It is demonstrated that the increases in seepage quantity but above all the increases in chloride load can be substantial in numerous (low-lying) polders in the future.

In the reflections of this section, only the chloride ion is considered, which represents the solute concentration. Various other pollutants, such as phosphorus and nitrogen, influence the surface water quality as well. Within the scope of this thesis, these pollutants are not considered. Nonetheless, they can be very important for the overall water quality in surface water systems, which appears from the intensive investigations, now going on for preparation of the Fourth Policy Document for the Water Management of the Netherlands.

Impact of sea level rise on the seepage quantity in the polders near the Dutch coast

Figure 10.2 shows the seepage quantity at -15 m $N.A.P.$ in the polders of the eight profiles. The quantities in $m^3/(m'yr)$ of chapter 9 have been multiplied with the width $L_\perp$ perpendicular to the profile.

For reasons of completeness, the changes in both seepage quantity and chloride load are also calculated in the profile Wad. However, in the analysis of determining the required flushing quantities, display of the seepage quantity of the narrow polder in the profile Wad is disputable for two reasons. Firstly, in reality, flushing is not possible in the narrow polders of the Wadden Islands. Secondly, the simulated width of the polder in the profile Wad, which is equal to 3000 m, is not consistent with the widths of the Wadden Islands Vlieland, Terschelling, Ameland or Schiermonnikoog, and hence, it does not give a really representative picture of the actual situation.

The calculated seepage quantities may differ from the observed figures derived from e.g. water and salt balance studies. Nonetheless, based on the studies of the Institute for Land and Water Management Research (ICW) in Wageningen, the values are generally reasonable.

---

[9]The two relevant PAWN-models are: (1) the Water Distribution Model (DM) which describes the water management system of the Netherlands, and (2) the District Hydrologic and Agriculture Model (DISTAG) which calculates the flushing demand for each district. In case a water shortage occurs during dry summers, a minimum desired discharge is determined with the DISTAG model. When not enough surface water with sufficiently low salinity is available for flushing and for water level control, drought and salt damage may occur.

[10]The results of the simulations in chapter 9 are extrapolated spatially by multiplying them with a width $L_\perp$.
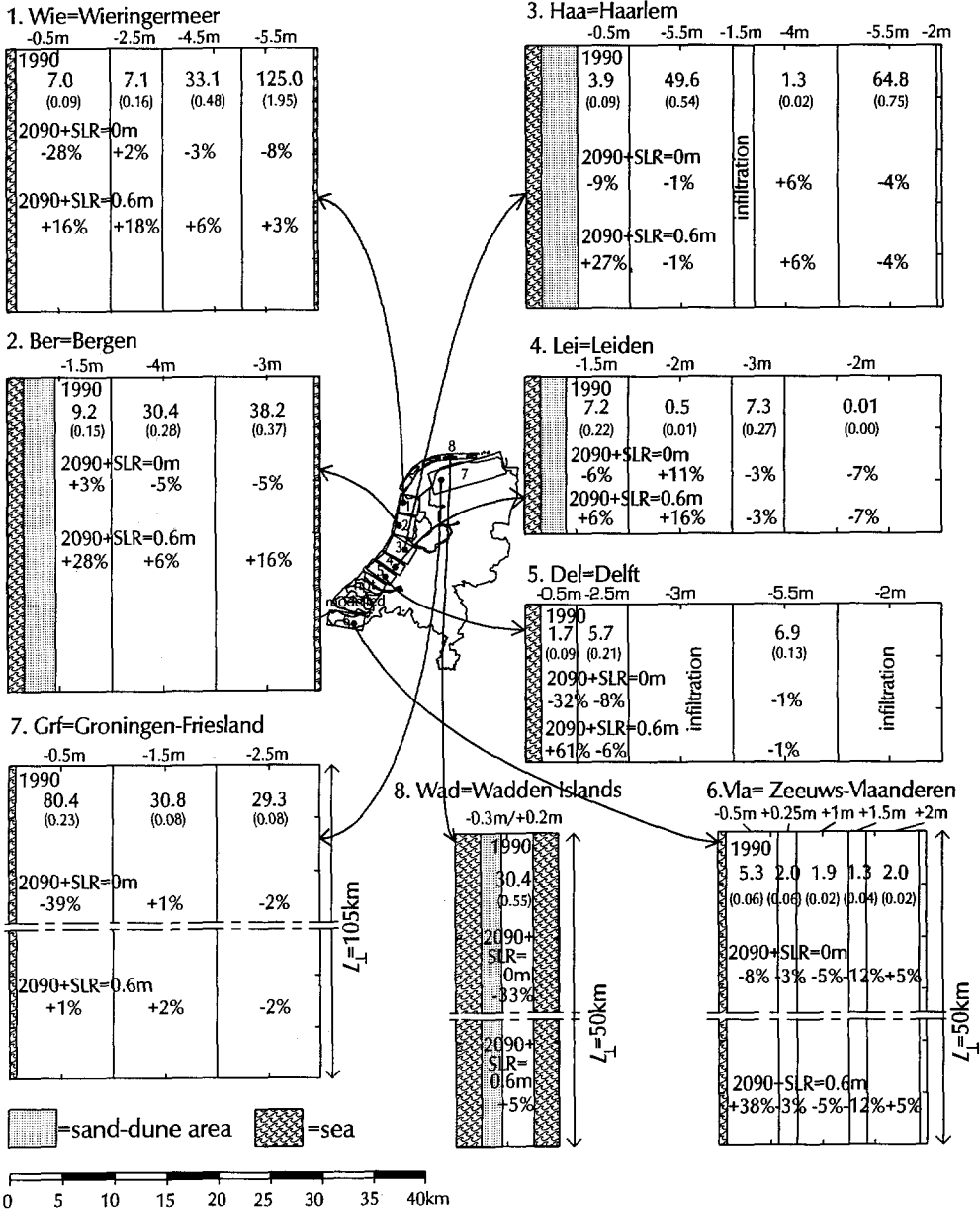
Figure 10.2: Seepage quantity in 10^6 m^3/yr (and in mm/d in brackets) at -15 m $N.A.P.$ (and at -7.5 m $N.A.P.$ in the profile VIa) in the polders of the eight profiles for three situations: (1) in 1990; (2) in 2090, relative to 1990 and without a sea level rise; and (3) in 2090, relative to 1990 and with a sea level rise of 0.6 m.

In the future, two processes occur simultaneously in the subsoil: (a) the non-equilibrium state of the present salinisation process of the subsoil due to previous human activities and (b) the rise in sea level:

ad a. Situation (2) of figure 10.2 shows that when no sea level rise occurs, the seepage quantity decreases some percents in nearly all polders in 2090 relative to 1990. This implies that the more saline the subsoil of the polders becomes due to the non-equilibrium state of the present salinisation process, the more the seepage quantity through the Holocene aquitard decreases.

ad b. Situation (3) of figure 10.2 shows that when the sea level rises 0.6 m during the next century, almost all polders near the coast can expect a great increase in seepage quantity in 2090 with respect to the present seepage quantity in 1990. For instance, polders near the sea are exceptionally vulnerable in the following provinces: Noord-Holland (Wie=+16%, Ber=+28%), Zuid-Holland (Haa=+27%, Del=+61%) and Zeeland (Vla=+38%). In the polders of the provinces of Groningen and Friesland, the increase in seepage quantity appears to be of minor importance. Note that some polders show a decrease in seepage quantity in 2090 with respect to the present seepage quantity in 1990 as a result of local geohydrologic circumstances.

Table 10.1 shows the total seepage quantity at -15 m $N.A.P.$ in all eight profiles. The salinisation in the subsoil causes a decrease in seepage quantity of some percents in most of the profiles and some tens of percents in the profiles Grf and Wad. When the sea level rises 0.6 m in 2090, the increase in seepage quantity in the coastal regions of the Netherlands is about +4 % with respect to the situation in 1990[11]. In absolute figures, the increase in seepage quantity is substantial in the profiles Wie (+8.6 · 10^6 m^3/yr) and Ber (+10.5 · 10^6 m^3/yr), whereas in relative figures, the increase in seepage quantity is significant for the profiles Ber (+14%) and Vla (+13%).

Impact of sea level rise on the chloride load in the polders near the Dutch coast

Figure 10.3 shows the chloride load in the polders of the eight profiles. The quantities in ton $Cl^-/(m'yr)$ of chapter 9 have been multiplied with the width $L_\perp$ perpendicular to the profile.

Local geohydrologic circumstances determine the actual chloride load in each polder. For instance, in the profile Haa, the relatively thick freshwater lens causes only fresh groundwater to ooze into the adjacent (lower lying) polder in the reach 5,000-10,000 m, and hence, the chloride load there in 1990 is low. When the sea level rises 0.6 m during the next century, the increase in chloride load will be very serious due to a combination of sea level rise and previous human activities. In some polders near the coast, the chloride load doubles, triples or even quadruples, whereas in other polders, the increase in chloride load will be limited. Though the chloride load in

---

[11]The increase in seepage quantity in percentage obviously depends on the area being considered.
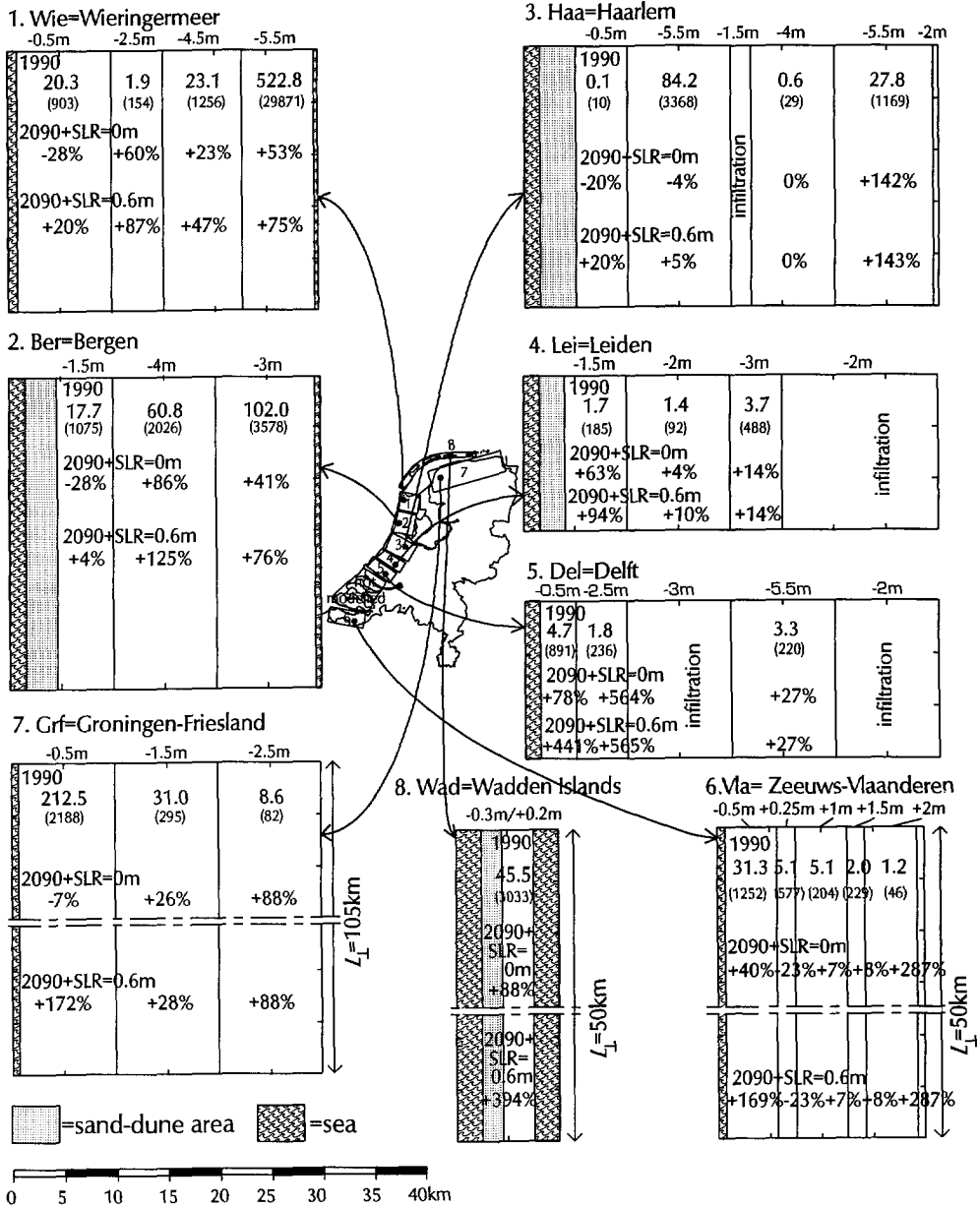
Figure 10.3: Chloride load in 10^3 *ton* Cl^-/yr (and in *kg* $Cl^-/ha/yr$ in brackets) at -15 *m N.A.P.* (and at -7.5 *m N.A.P.* in the profile VIa) in the polders of the eight profiles for three situations: (1) in 1990; (2) in 2090, relative to 1990 and without a sea level rise; and (3) in 2090, relative to 1990 and with a sea level rise of 0.6 *m*.

Table 10.1: Total seepage quantity in the eight profiles for three situations: (1) in 1990; (2) in 2090, relative to 1990 and without a sea level rise; and (3) in 2090, relative to 1990 and with a sea level rise of 0.6 m.

Total seepage quantity in the profiles at -15 m N.A.P.						
Profile	Width $L_\perp$	Seepage quantity in 1990	Increase of seepage quantity in 2090		Increase of seepage quantity in 2090	
Sea level rise			SLR=0 m		SLR=0.6 m	
	km	$10^6\ m^3/yr$	$10^6\ m^3/yr$	%	$10^6\ m^3/yr$	%
1. Wie	25	172.2	-12.0	-7	+8.6	+5
2. Ber	30	77.8	-3.1	-4	+10.5	+14
3. Haa	25	119.6	-3.8	-3	-1.9	-2
4. Lei	15	15.0	-0.6	-4	+0.3	+2
5. Del	15	14.3	-1.1	-7	+0.6	+4
6. Vla*	50	12.6	-0.9	-7	+1.6	+13
7. Grf	105	140.5	-31.6	-22	+1.0	+1
8. Wad	50	30.4	-10.1	-33	+1.5	+5
Total	315	582.4	-63.2	-11	+22.2	+4
* = seepage quantity at -7.5 m N.A.P.						

the Wieringermeer polder in the reach 15,000-29,500 m in the profile Wie increases several tens of percents, the absolute increase in $ton\ Cl^-/yr$ is enormous. Because of this prediction, it would be recommended in the future to discharge the seepage of this polder directly to the Waddenzee instead of to the IJsselmeer, to reduce the chloride load in this freshwater lake.

Table 10.2 shows the total chloride load at -15 m N.A.P. in all eight profiles. By comparing this table with table 10.1, it is clear that the changes in chloride load are much greater than the changes in seepage quantity. As an indicative estimate: the overall chloride load in 2090 in the low-lying coastal regions of the Netherlands increases +103 %, three fifths of which is caused by a sea level rise of 0.6 m and two fifths by the non-equilibrium state of the present salinisation process due to previous human activities. When no sea level rise occurs, the increase in chloride load is at least several tens of percents in 2090 with respect to 1990 (except in the profile Grf). This implies that, though the seepage quantity decreases, the subsoil becomes much more saline. When the sea level rises 0.6 m during the next century (as is generally accepted), the increase in chloride load is drastic in all profiles. In absolute figures, the increase of chloride load is very great in the northern part of the Netherlands in the profiles Wie, Grf and Wad. Note again that the estimate of the profile Wad is disputable. In relative figures, the chloride load increases the most in the profiles Del and Wad: with some +324 % and +395 % respectively in 2090 relative to 1990.

The figures mentioned above should clearly indicate that in polders where the seepage is the main contributor to chloride balances, the increase in this continuous

Table 10.2: Total chloride load in the eight profiles for three situations: (1) in 1990; (2) in 2090, relative to 1990 and without a sea level rise; and (3) in 2090, relative to 1990 and with a sea level rise of 0.6 m.

Total chloride load in the profiles at -15 m $N.A.P.$						
Profile	Width $L_\perp$	Chloride load in 1990	Increase of chloride load in 2090		Increase of chloride load in 2090	
Sea level rise			SLR=0 m		SLR=0.6 m	
	km	10^3 ton Cl^-/yr	10^3 ton Cl^-/yr	%	10^3 ton Cl^-/yr	%
1. Wie	25	568.6	+277.8	+49	+407.2	+72
2. Ber	30	180.5	+91.0	+50	+154.6	+86
3. Haa	25	112.7	+42.7	+38	+45.6	+40
4. Lei	15	6.7	+ 1.6	+24	+2.2	+33
5. Del	15	9.8	+14.5	+149	+31.5	+324
6. Vla*	50	44.6	+ 16.5	+37	+56.9	+127
7. Grf	105	252.1	-0.6	-0	+382.4	+152
8. Wad	50	45.5	+40.1	+88	+179.5	+395
Total	315	1220.5	+483.6	+40	+1259.9	+103
* = chloride load at -7.5 m $N.A.P.$						

source impels great adaptations in the present water distribution systems: that is the required flushing quantities should be increased substantially.

10.4   Agriculture in terms of salt damage

Introduction

Crop production depends, among others, on salinities in the (unsaturated) root zone[12]. When the salinity of the water in the root zone available to crops exceeds a certain critical value, the capacity of the plant to take up soil moisture decreases and the normal growth process is retarded. In addition, the resistance against frost diminishes. In conclusion, crop yields are reduced and the so-called salt damage occurs.

In general, salinisation of the (sub)soil and the root zone does not occur easily under the climatic conditions in the Netherlands[13]. Though salt accumulation is taking place in the soil in summer, the excess of precipitation in winter flushes the salt into the watercourses of the polder and subsequently into the boezems. However, in

---

[12] The root zone is defined as a relatively shallow top layer of soil (30 to 80 cm) depending on the type of the soil and the kind of vegetation.

[13] If any, salt damage to crops arises in the western (low-lying) parts of the Netherlands (Holland and Zeeland) and to a certain extent in the IJsselmeerpolders, as well as in the northern part of Groningen and Friesland.

those polders where seepage quantities and chloride loads are very high, the moisture in the root zone may contain high salinities in summer, which may cause salt damage to low salt-resistant crops.

The salinity in the root zone may originate from several sources. One important source is the salinity of surface water, which highly determines the salinity in the root zone via sprinkler irrigation[14]. Numerous sources contribute to the quality of surface water, such as gaswells, domestic and industrial waste water, fertilisers, de-icing chemicals on roads, pollution by recreation, seepage through dikes and precipitation (to a small amount). In addition, natural processes, such as accumulation of salt by evaporation, raise the salinity in the root zone even more. In regions near the coast, seepage with high salinities also contributes to higher salinities in the surface water as well as in the root zone (by means of capillary rise of groundwater from the saturated subsoil). Groundwater sprinkling in the low-lying regions of the Netherlands is limited by regulations, whereas surface water sprinkling during dry summers may be substantial in the low-lying polders. During dry summers, the water demand for flushing and for water level control exceed the water supply, which may cause salt damage. This occurred, for instance, during the extremely dry summer of 1976.

In the PAWN-study [Pulles, 1985], the salt damage was estimated at some 260 million *guilders* in an average year, whereas in an extremely dry year (a 2%-year) the salt damage would amount to some 530 million *guilders*. Nowadays, however, the figures are somewhat different: the PAWN-analysis underestimated the salt damage. For instance, the salt damage to agriculture in the year 1985 has been estimated later on nationally at some 586, 698, 716 and 949 million *guilders* for a 50%-average, a 10%-dry[15], a 5%-very dry and a 2%-extremely dry year respectively [Arnold, 1990]. The greater part of these calculations are based on the midwestern part of the Netherlands and Utrecht. Note that in these calculations the salt damage of crops under glass has been included, whereas in reality, alternatives for surface water sprinkling are applied when the chloride concentration exceeds 200 mg Cl^-/l.

Since in Dutch agriculture most salt damage is caused by chloride, only this specific ion is considered.

In this section, the method to assess salt damage, as applied in the PAWN-study, is discussed briefly first. The relation between the chloride concentration in the root zone, salt damage and crop values is explained. Secondly, the increase in chloride concentration in the Holocene aquitard of the coastal groundwater flow regions due to sea level rise and previous human activities is presented. As such, these results can be applied as boundary conditions in the PAWN-models.

---

[14]Note that sprinkling reduces the drought damage, whereas it may increase the salt damage.

[15]By comparison, the drought damage to agriculture in a 10%-dry year is estimated at some 1456 million *guilders* on a national level [Arnold, 1990].
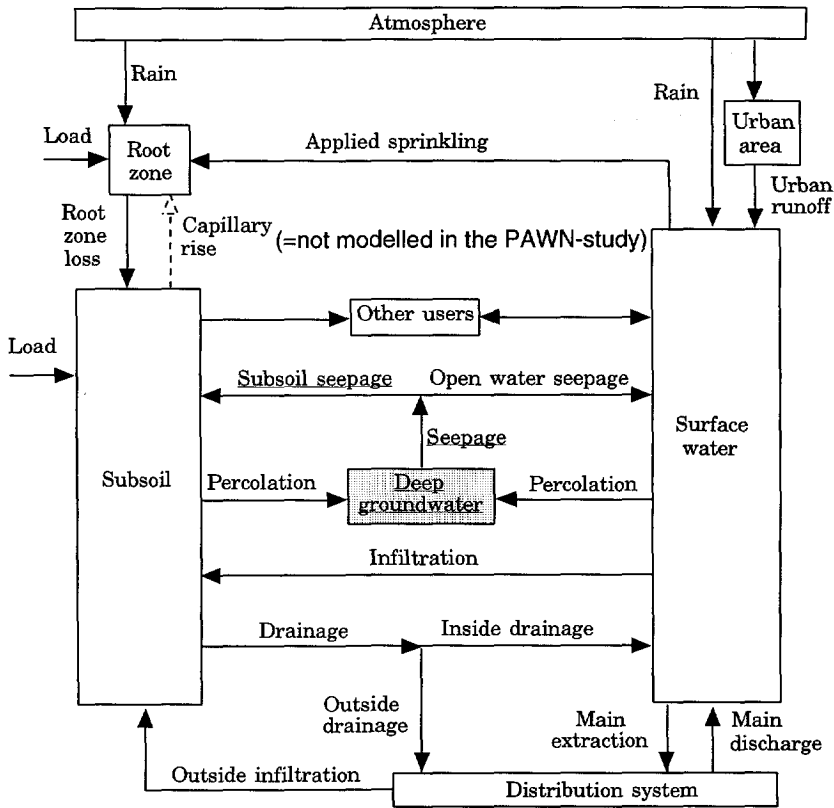
Figure 10.4: Schematisation of the salt flows in a district of the PAWN-study [modified from Abrahamse *et al.*, 1982]. In this thesis, the impacts of sea level rise and previous human activities are assessed for the deep groundwater and for the seepage to the subsoil. Note that the capillary rise from subsoil to root zone is not modelled in the Plot Salt Model.

Method applied in the PAWN-study

Three models are applied in the analysis of the PAWN-study to determine the salt damage [Abrahamse *et al.*, 1982]: (1) the so-called Plot Water Model, which simulates the water flows on plot level; (2) the Plot Salt Model, which calculates the salt flows on plot level [Baarse and van Beek, 1982]; and (3) the so-called Plot Damage/Cost Model, which calculates crop damages due to drought and/or excess chloride in the root zone.

It appears that the chloride concentration in the root zone depends highly on the chloride concentration of the surface water (boezem water) through surface water

sprinkling (see figure 10.4). Though, in theory, salt can flow from the subsoil to the root zone by capillary rise[16], this process is **not** modelled in the Plot Salt Model. The assumption is that a substantial freshwater layer is built up during the winter season, and that the salt in the subsoil hardly reaches the root zone.

As already mentioned, salt damage to crop occurs when the chloride concentration of the soil moisture in the root zone, C_{rt}, exceeds a certain value, C_{dam}. From that point onwards, a linear relationship can be assumed between the chloride concentration and the loss in crop yield. The following expression is defined:

$$L_{crop} = \begin{cases} 0 & \text{when} \quad C_{rt} < C_{dam} \\ \xi \cdot (C_{rt} - C_{dam}) & \text{when} \quad C_{dam} \le C_{rt} < C_{max} \\ 1 & \text{when} \quad C_{rt} \ge C_{max} \end{cases} \qquad (10.1)$$

where

- L_{crop} = fraction of loss in crop yield due to salt damage per decade (T^{-1}),

- C_{rt} = chloride concentration of the soil moisture in the root zone in $mg\ Cl^-/l$ $(M\ L^{-3})$,

- ξ = salt damage coefficient per $mg\ Cl^-/l$ per decade $(L^3\ M^{-1}\ T^{-1})$,

- $C_{max} = C_{dam} + 1/\xi$ in $mg\ Cl^-/l$ $(M\ L^{-3})$.

Salt damage to crop is determined over the entire productive period, because seepage is supposed to be almost constant during the season. For this purpose, the loss in crop yield Ψ in % is defined:

$$\Psi = L_{crop} \cdot T_{growth} \cdot 100\,\%, \text{ where } \quad L_{crop} = \xi \cdot 100\ mg\ Cl^-/l\ (T^{-1}) \qquad (10.2)$$

where

- Ψ = percentage of loss in crop yield during the entire productive period due to salt damage per 100 $mg\ Cl^-/l$ exceedance of the critical value C_{dam} $(-)$,

- T_{growth} = productive period of the crop in decades (T).

Table 10.3 shows the characteristics of some types of crops which have been applied in the PAWN-study. The salt damage for every crop on each plot is estimated by means of the loss in crop yield and the potential crop value[17]. The cumulative damage is carried out from one timestep of a decade to the next, taking into account that also drought damage may occur. A so-called survival fraction is defined, which is set to the fraction of the total crop that still survives at the end of each timestep.

---

[16]In the PAWN-study, the subsoil and the root zone are combined through a stationary relation between the soil moisture content in the bottom of the root zone, the capillary rise and the phreatic groundwater level.

[17]The potential crop value is the money value per hectare of crop, that is obtained from market observations of actual price data in the years 1975 and 1976 [Abrahamse *et al.*, 1982].

Table 10.3: Characteristics of some types of crops in relation with salt damage [after: Abrahamse *et al.*, 1982]. Most of the potential crop values depend on the drought in a given year.

Characteristics of some types of crops					
Crop type	Prod. period T_{growth} decade	Cl^--conc. root zone C_{dam} $mg\ Cl^-/l$	Salt damage coefficient ξ (per decade) $1/(mg\ Cl^-/l)$	Total loss crop yield Ψ %	Potential crop value [PAWN, 1985] $1000\ fl/ha$
1. Grass	18	1000	$12 \cdot 10^{-6}$	2.2	3-5
2. Consumption potatoes	13	700	$25 \cdot 10^{-6}$	3.3	10-16
3. Milling potatoes	13	700	$25 \cdot 10^{-6}$	3.3	3.8-5.8
4. Seed potatoes	10	700	$33 \cdot 10^{-6}$	3.3	13.5-20.3
5. Sugar beets	16	700	$24 \cdot 10^{-6}$	1.3	5.2*
6. Cereals (and others)	13	1000	$17 \cdot 10^{-6}$	2.2	3.1*
7. Cut corn	15	1000	$9 \cdot 10^{-6}$	1.4	3.6-6.0
8. Bulbs	14	200	$25 \cdot 10^{-6}$	3.5	27.4-30.1
9. Vegetables open air	21	500	$17 \cdot 10^{-6}$	3.6	15.6-20.3
10. Pit and stone fruits	18	500	$6 \cdot 10^{-6}$	1.1	10.4*
11. Ornamental trees	18	250	$17 \cdot 10^{-6}$	3.5	42.8*
12. Vegetables under glass	36	200	$17 \cdot 10^{-6}$	6.1	232.0-278.4
13. Flowers under glass	36	200	$17 \cdot 10^{-6}$	6.1	485.0-412.2
* = due to several reasons, the potential crop values of these crops were kept constant for each type of year [Abrahamse *et al.*, 1982].					

It should be noted that the PAWN method is not developed to accurately predict *absolute* agricultural damages. Instead, the instrument is developed to compare *relative* damages caused by *changes* in the quantity (drought damage) and/or quality (salt damage) of available water as a result of different initial situations [Abrahamse *et al.*, 1982].

The calculations of the PAWN-study have resulted in the following reflections: in general, open air crops do not suffer from salt damage because of two reasons: (1) most of the open air crops are not very sensitive to salt, and (2) salt brought into the root zone by sprinkling (which is the main source of salt[18]) is diluted and flushed out by rain. By contrast, glasshouse crops do suffer from salt damage[19] [Abrahamse *et al.*, 1982].

Impact of sea level rise

The simulations with the PAWN-models to estimate the values of salt damage are too time-consuming in the context of this study. Therefore, in this thesis, only the increase in mean chloride concentration of seepage through the Holocene aquitard

---

[18]Note again that salt from the seepage via the subsoil to the root zone by capillary rise was not modelled in the PAWN-study.

[19]The Plot Damage/Cost Model has predicted that in a extremely dry year (like 1976), about 15 % to 20 % of the greenhouse crops will be damaged by salt.

in the coastal groundwater flow regimes in the Netherlands are supplied. These indicative figures are based on the calculations of deep groundwater flow regimes in the eight profiles of chapter 9. The increase in mean chloride concentration of seepage is caused by sea level rise as well as by previous human activities. The present salinisation of the deep groundwater flow regime is not yet in a non-equilibrium state.

Figure 10.5 shows the mean chloride concentrations in the top layer of the polders of the eight profiles for three situations. As can be seen, several polders already contain brackish groundwater in the top layer. In the profiles Wie, Ber and Vla for instance, the polders contain mean chloride concentrations higher than 2000 mg Cl^-/l. The main feature of these polders is that they are located very near the coast (only in the profile Wie, the part of the polder in the reach 22,500-30,000 m is located near the IJsselmeer). In the profiles Haa and Lei, fresh groundwater originating from the sand-dune area reduces the salinity in the adjacent inland polders.

From the figures without a sea level rise in 2090 relative to 1990 (situation (2)), it can be deduced that the salinisation of the Dutch subsoil is still a dynamic process. Nonetheless, the increase in mean chloride concentration is limited in a number of polders. For example, the changes in mean chloride concentration are small for (see figure 10.5): three polders of Wie; two polders in Haa; the entire profile Lei; and the inland part of the profiles Del and Grf. In the profile Ber, the polder adjacent to the sand-dune area seems even to become more fresh due to seepage of fresh groundwater that originates from the sand-dune area.

When the sea level rises 0.6 m/c, the situation in terms of mean chloride concentration in the top layer will deteriorate in 2090 relative to 1990 in almost all polders which are located within the zone of influence of sea level rise (situation (3)). For instance, the mean chloride concentration in the top layer in coastal polders of the profiles Del, Vla, Grf and in the narrow polder in the profile Wad increases with several hundreds of mg Cl^-/l due to sea level rise.

As such, in the near future, extractions of fresh groundwater for sprinkling purposes in the low-lying parts of the Netherlands may have to cope with a serious salinisation of the subsoil. Subsequently, new locations for extraction of groundwater or the use of (fresh) surface water for sprinkling purposes should be considered.

Based on the figures mentioned above, it is recommended to change in the PAWN-model Plot Salt Model (see figure 10.4) the concept of **not** modelling the salt flow from the subsoil to the root zone by capillary rise. The reason is that the higher salinity level of the increased seepage quantity could affect the results, especially in the low-lying polders near the Dutch coast, where the seepage quantity is (already) strong (e.g. > 2 mm/d) and where the chloride concentration of the subsoil will probably increase significantly during the next century.

The loss in crop yield and thus the salt damage due to sea level rise and previous human activities can be assessed by applying the changes in seepage parameters (see the seepage quantity in figure 10.2, the chloride load in figure 10.3 and the mean chloride concentration in figure 10.5) as a function of time in the PAWN-models. Note that there are some restrictions on the applicability of this methodology, such
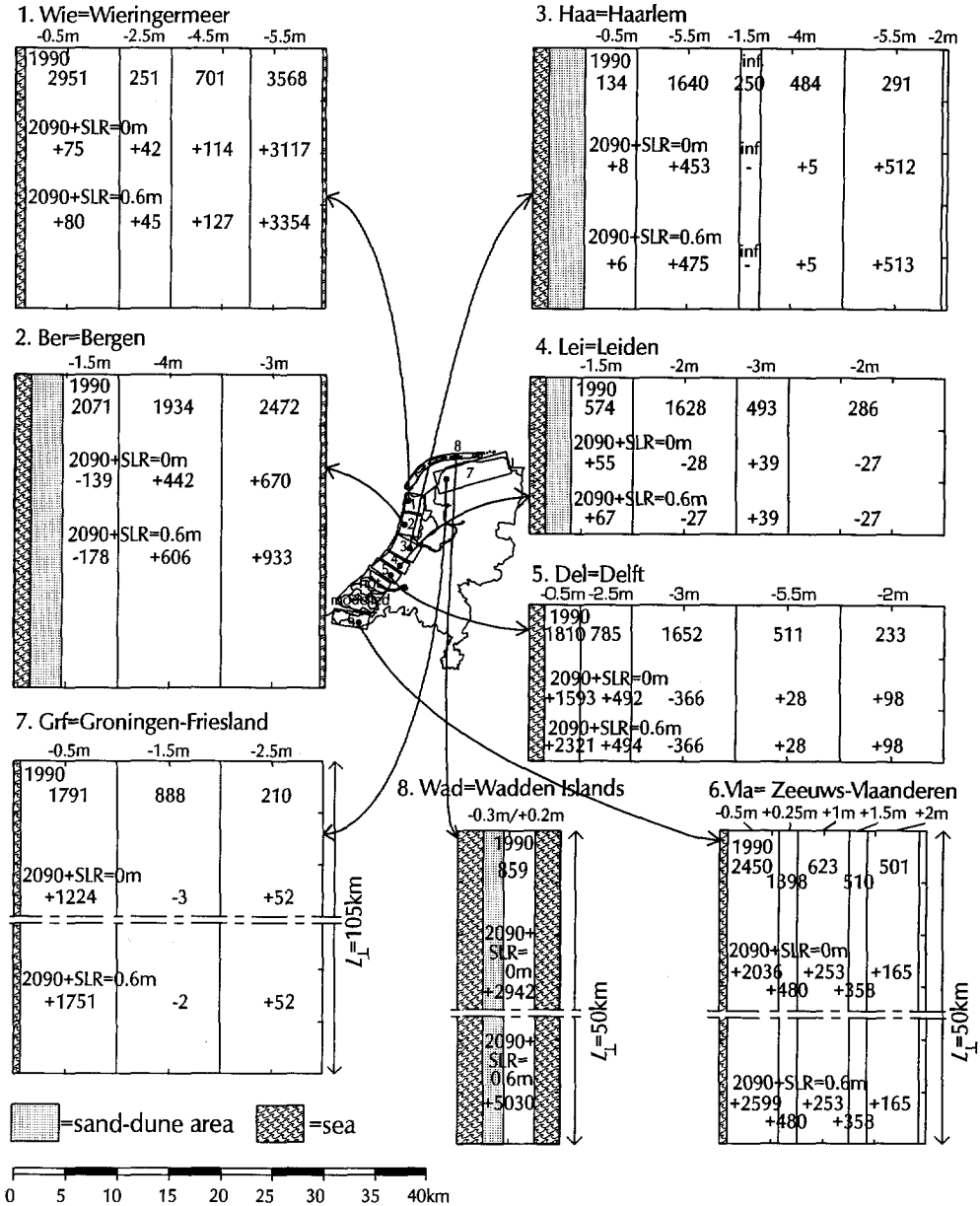
Figure 10.5: The (increase in) mean chloride concentrations (values in $mg\ Cl^-/l$) at -5 $m\ N.A.P.$ (and at -2.5 $m\ N.A.P.$ in the profile Vla) in the polders of the eight profiles for three situations: (1) in 1990; (2) in 2090, relative to 1990 and without a sea level rise; and (3) in 2090, relative to 1990 and with a sea level rise of 0.6 m.

as:

- the simulations of the eight profiles in chapter 9 are very rough, e.g. the top layer is represented by grid cells with a height of ten metre.

- the translation of the chloride concentration in the subsoil and in the surface water to the chloride concentration in the soil moisture of the root zone (via respectively capillary rise and sprinkler irrigation) is too elementary.

- several developments make that in the near future, the chloride concentration in the soil moisture of the root zone may not depend any more on the quality of (local) surface water. For instance, horticulture is already using groundwater, when available and not limited by regulations; rain water stored in reservoirs; and even water from the public water supply. Moreover, surface water with a good quality can also be supplied from external sources. For instance, the horticulture area Het Westland is supplied with surface water from the Brielse Meer.

- seasonal effects caused by changes in the chloride concentration of surface water are not considered in the analysis.

- the actual crop yield also depends on damages due to diseases, hail, frost, etc., and the income from the yields depends on developments on the market.

10.5   Conclusions

Absolute assessments of the impact of sea level rise on water management sectors such as domestic and industrial water supply, flushing and agriculture are beyond the context of this study. For instance, the extrapolation of results of the two-dimensional simulations of the profiles to descriptions in a three-dimensional plane should be handled with great caution. However, the results in this chapter can be implemented in integrated models such as the PAWN-models.

Despite the lack of absolute figures, some indicative trends can still be given for the next century:

1. **domestic and industrial water supply from coastal sand-dune areas**
   the impact of a sea level rise of 0.6 m on water supply from the freshwater lenses in coastal sand-dune areas is negligible.

2. **flushing of water courses of low-lying areas**
   the discharge system (pumping stations and water courses) in the polders near the coast only should probably be adapted and redesigned for greater capacity. The reason is that the impact of a sea level rise of 0.6 m on the change in seepage quantity is considerable (up to several tens of percents) in polders in

the first kilometres from the coast, whereas it is marginal (mostly up to only a few percents) in polders located further inland.

A substantial increase in volumes of water required for flushing could be required to counteract the deterioration of the water quality of the surface water systems in these low-lying regions. The reason is that the increase in chloride load due to the combination of a sea level rise of 0.6 m and the delayed effect of previous human activities (namely the reclamation of lakes or parts of the sea) on the future salinisation process is serious in nearly all polders in the low-lying regions of the Netherlands. Even those polders beyond the zone of influence of sea level rise are affected.

3. agriculture in terms of salt damage

the mean chloride concentration of the subsoil will probably increase with several hundreds of $mg\ Cl^-/l$ in many low-lying polders along the Dutch coast due to a sea level rise of 0.6 m as well as the state of dynamic equilibrium of the present salinisation process as a result of the delayed effect of previous human activities. Whether or not the loss in crop yield due to salt damage is substantial in these polders, depends on other conditions as well.

Chapter 11

Conclusions and recommendations

The conclusions drawn in this thesis serve to understand the mechanisms involving the possible impact of several scenarios of sea level rise and human activities on vulnerable coastal groundwater flow regimes in the Netherlands during the next millennium. The methodology followed to fulfil the main objective is universal, though it is focused on the geo(hydro)logic conditions in the Netherlands. The methodology can also be applied to vulnerable coastal groundwater flow regimes around the world with geo(hydro)logical conditions similar to those in the Netherlands. In the foregoing chapters, the following four phases of methodology have been analysed:

I. **Definition of the boundaries of the groundwater flow regime:**
   in chapter 2 (the physical condition of the coastal zone, the hinterland, the estuaries and the rivers due to sea level rise) and in chapter 3 (the future rate of sea level rise).

II. **Choice of the procedure of numerical modelling:**
   in chapter 4 (selection of a suitable computer code); in chapter 5 (description of the selected computer code); in chapter 6 (validation of the selected computer code); and in chapter 7 (sensitivity analysis of subsoil and model parameters).

III. **Simulation of the impact of sea level rise on groundwater flow regimes in the Netherlands:**
   in chapter 8 (simulation of two specific profiles) and in chapter 9 (simulation of eight representative profiles along the Dutch coast).

IV. **Assessment of the impact of sea level rise on three water management sectors:**
   in chapter 10 (domestic and industrial water supply, flushing and agriculture).

In section 11.1, conclusions are drawn for the phases of methodology I to IV mentioned above. In section 11.2, relevant recommendations are given for the following four target groups: (a.) for the climatic researcher; (b.) for the modeller; (c.) for the geo(hydro)logist; and (d.) for the water manager in practice.

11.1   Conclusions

I. Definition of the boundaries of the groundwater flow regime: chapter 2 and chapter 3

I.1   As virtually all literature on the impact of sea level rise discussed the coastal groundwater flow regimes only very superficially, this impact is until now the least known compared with the impact of sea level rise on the coastal zone, the hinterland, the estuaries and the rivers.

I.2   Since the beginning of the Industrial Revolution (about 1850 AD), the concentration of atmospheric greenhouse gases has rapidly increased as a result of intensive human activities such as burning of biomass and fossil fuels, deforestation and changes in land use. As a result of the increased concentration of greenhouse gases, the atmosphere is certain to warm up. This mechanism of global warming is called the *enhanced* greenhouse effect. Though several feedbacks, such as the effects of clouds and oceans, are not yet completely understood, and thus simulated inaccurately, the global mean temperature will probably rise approximately 3 $^{\circ}C$ with an uncertainty range of $\pm$ 1.5 $^{\circ}C$ until the end of the next century.

I.3   An important consequence of the rise in global mean temperature is the rise in sea level. The main contributors to sea level rise during the next century are thermal expansion of ocean water as well as melting of mountain glaciers and small icecaps, whereas accumulation on and ablation of polar ice sheets are supposed to be in balance. The majority of the predictions of the future sea level rise is in the range of 30 to 100 *cm* during the next century, with 60 *cm* as the best estimate (in 1996). This is significantly more than the sea level rise over the present century. For instance, the sea level has risen only about 10 to 20 *cm* in the period 1880-1980. Note that the expected rate of future sea level rise is in the same order of magnitude as the rate of sea level rise at the beginning of the Holocene, when the sea level has risen a few tens of metres within a geologically short period of some millennia.

II. Choice of the procedure of numerical modelling: chapter 4, chapter 5, chapter 6 and chapter 7

II.1   To suppress truncation and oscillation errors in the advection-dispersion equation, standard finite-difference and finite-element models should satisfy the condition that the spatial discretization (that is the dimension of a grid cell or grid block) should not be greater than a few times the magnitude of the (longitudinal) dispersivity that represents the hydrodynamic dispersion. When the dimension of the geohydrologic system in question is large, this strict condition of spatial discretization considerably restricts the practical application of three-dimensional codes with dispersive solute transport.

II.2 Whereas the finite-element models SUTRA and SWICHA cannot generate accurate solutions for the advection-dispersion equation in case of small longitudinal dispersivities, the adapted MOC model is very well capable of generating such solutions.

II.3 The method of characteristics of the original MOC model, which is applied to solve the advection-dispersion equation, does not cause numerical dispersion by itself. Nevertheless, numerical dispersion occurs in the MOC model as a result of the movement and the tracking of particles, the numerical (finite-difference) approximations and the conversion from particles to grid cells when solute concentrations are averaged.

II.4 Numerical instabilities in the vertical velocity field of the adapted MOC model do not only occur due to the numerical approximations that already occur in the original MOC model, but also due to numerical approximations in the density flow that additionally arise in the adapted MOC model. These numerical instabilities mainly arise in places where the transition zone between fresh and saline groundwater is small.

II.5 Currently, no method has been successful in duplicating the steady state solution of Henry. Especially near the bottom of the aquifer, Henry's solution differs substantially from those of other numerical solution techniques. This difference is probably a consequence of the limited computer facilities at the time of Henry calculations.

II.6 In the close vicinity of the fresh-salt interface of Chan Hong *et al.*, the adapted MOC model creates grid cells with brackish groundwater, which is the result of numerical dispersion.

II.7 Through adapting the vertical Darcian specific discharge in the groundwater flow equation by applying an additional term, the so-called *buoyancy* or *vertical density gradient velocity*, MOC is made suitable for simulating density dependent groundwater flow in the coastal geohydrologic systems where the density distribution is non-uniform.

III. Simulation of the impact of sea level rise on Dutch groundwater flow regimes: chapter 8 and chapter 9

III.1 The results from numerical modelling of the flow of groundwater and the movement of solutes in geohydrologic systems over time spans of several centuries should only be considered with a sound dose of reserve, as the extrapolation of the present processes to future situations is not really a careful procedure. Nonetheless, the conclusions drawn here on the predictions of the impact of sea level rise on groundwater flow regimes as well as on water management sectors

should be considered as (rough) indications of what might occur in the near future.

III.2 A single assessment of the impact of sea level rise for the Dutch groundwater flow regimes is unfeasible, since the exact impact of sea level rise is very site-specific and depends on features such as the geometry of the geohydrologic system, the subsoil parameters and human activities.

III.3 The present salinisation of the Dutch groundwater flow regimes is dominated by both past and present human activities. The most serious cause of salinisation is the lowering of phreatic groundwater levels as a result of the reclamation of lakes or parts of the sea in the past (from about 1200 AD up to present). These reclaimed areas have a delayed effect on the present and future salinisation process. Currently, extraction of fresh groundwater for water supply from the deep aquifers of the coastal sand-dunes causes upconing of brackish and saline groundwater, and contributes, as such, to the present salinisation of the subsoil. Sea level rise will intensify the salinisation process, above mentioned.

III.4 In the profile in the southern part of Noord-Holland (between the intake area of Gemeentewaterleidingen Amsterdam, several polder areas behind the sand-dune area and up to the Vinkeveense plassen), the reclamation of the low-lying Haarlemmermeer polder in the middle of the 19th century has generated a strong inflow of saline groundwater from the sea to the deep aquifers. Even when no sea level rise would occur, saline groundwater intrudes in the deep aquifers with a velocity of at least *one kilometre per century*. At the inland side at some tens of kilometres from the coast, a state of dynamic equilibrium in terms of the salinisation will only be reached after a few millennia.

Sea level rise accelerates the salinisation process in this geohydrologic system, though the zone of influence of sea level rise is only a few kilometres. During the next century, the impact of sea level rise on the distribution of fresh, brackish and saline groundwater in this geohydrologic system is still of minor importance. However, after several centuries, the sea has risen so much that the impact will be considerable. When the sea level rises 0.6 m/c, the volume of the freshwater lens in the sand-dune area will have diminished substantially after several centuries (e.g. about -13 % after 300 years compared with the scenario with no sea level rise). In addition, in the long-term, the seepage in the low-lying Haarlemmermeer polder increases both in quantity (e.g. about +6 % in 2290) and in quality (e.g. chloride load about +20 % in 2290).

Human interventions within the bounds of feasibility may slow down the salinisation of this geohydrologic system, but it is not easy to stop the process completely. Feasible rates of extraction of (saline) groundwater or (deep-well) infiltration of fresh surface water can, at best, reduce the impact of sea level rise. Even more rigorous, not really conceivable, (hypothetical) countermeasures, such as raising the phreatic groundwater level in the Haarlemmermeer

polder or creating a sand-dune area off the coast by land reclamation, also demonstrate that the salinisation process is difficult to restrain.

III.5 In the profile in the northern part of Noord-Holland (between a narrow sand-dune area near Petten to Enkhuizen at the IJsselmeer), a severe salinisation of the subsoil already occurs due to the reclamation of the (low-lying) polders in the vicinity. These polders have generated a strong inflow of saline groundwater from the sea to the deep aquifers. The freshwater body of Hoorn probably remains when no sea level rise occurs.

Sea level rise accelerates the salinisation process significantly, though the time lag between the cause of changes and the ultimate effect on the salinisation remains considerable, in the order of several to many centuries. The zone of influence of sea level rise in the geohydrologic system is quite some kilometres due to high transmissivities in the deep aquifers. Eventually, however, the upper part of the geohydrologic system contains only saline groundwater. Moreover, in the low-lying polders near the coast (e.g. the polder area near Schagen), the seepage (in terms of quantity and quality) will increase significantly within some centuries. The freshwater body of Hoorn probably disappears when the sea level rises 0.6 m/c.

Human interventions within the bounds of feasibility may slow down the salinisation process of this geohydrologic system in case of sea level rise, but it cannot easily be neutralized, and thus, the salinisation seems to be rather irreversible.

III.6 Most of the groundwater flow regimes of the eight studied profiles along the Dutch coast have not yet reached a state of dynamic equilibrium as far as the salinity distribution in the subsoil is concerned.

III.7 When no sea level rise occurs, the delayed effect of previous human activities (namely the creation of the low-lying polders) induces a severe salinisation process in most of the profiles. As a result, the subsoil in the polders becomes more saline in the future. Due to the changes in density distribution, the seepage quantity through the Holocene aquitard will decrease.

III.8 The shorter the length of the propagation of sea level rise in the geohydrologic system, the smaller the impact of sea level rise on the salinisation process. The zone of influence of sea level rise is limited in the profiles Haa, Lei, Del, Grf and Vla, whereas it is extensive in the profiles Wie, Ber and Wad, because, among others, the water level rises at both sides.

III.9 When the sea level rises 0.6 m during the next century, the volumes of the freshwater lenses in the four profiles with existing sand-dune areas hardly decrease. However, a few centuries later, the decrease in volume may reach several tens of percents.

III.10 The impact of sea level rise in a specific polder can be significant in terms of seepage quantity, mean chloride concentration and chloride load in the following situations: the polder is situated directly inland of the coast; the phreatic groundwater level in the polder is low, namely several metres below $N.A.P.$; and/or the zone of influence of sea level rise in the geohydrologic system is long as a result of high transmissivities of aquifers.

III.11 When the sea level rises 0.6 m during the next century, both seepage quantity and chloride load change substantially in the selected polders of most of the eight studied profiles. Exceptions are only the selected polders of two profiles Haa and Del in the province of Zuid-Holland, as these polders are located practically beyond the zone of influence of sea level rise.

III.12 When no sea level rise occurs, effective human interventions can probably counteract the long-term salinisation process in most of the profiles. Such interventions could be: (a) reclaiming land off the coast, thus evolving new freshwater lenses; (b) extracting (saline) groundwater, thus decreasing the seepage quantity and the chloride load in the polders; (c) inundating low-lying polders, thus removing the driving force of the salinisation process; (d) widening existing sand-dune areas, thus generating thicker freshwater lenses; and (e) creating physical barriers, thus blocking the free entrance of saline groundwater and halting the salinisation process. The countermeasure deep-well infiltration of surface water increases the seepage quantity in the polders, and thus, initially increases the chloride load as well. However, after some decades to centuries, the chloride load will drop substantially when the salinisation process towards the low-lying hinterland is blocked by the infiltrated surface water. Note that some of these countermeasures should only be considered as unfeasible but interesting hypothetical cases, in order to gain a better insight into the range of conceivable human interventions.

III.13 When the sea level rises 0.6 m/c, even the most effective countermeasures cannot stop the salinisation of the subsoil. Therefore, it is likely that human interventions can only retard the impact of sea level rise on the groundwater flow regimes in the long-term at the expense of major investments. Whether these investments are considered feasible or not depends on the prevailing economic, environmental and political circumstances at the moment when a (political) decision is taken.

IV. Assessment of the impact of sea level rise on three water management sectors: chapter 10

IV.1 The impact of a sea level rise of 0.6 m on safe extraction (for domestic and industrial water supply) from the freshwater lenses in coastal sand-dune areas is negligible during the next century.

IV.2 The impact of a sea level rise of 0.6 m during the next century on the change in seepage quantity is considerable (up to several tens of percents) in polders in the first kilometres from the coast, whereas it is marginal (mostly up to only a few percents) in polders located further inland.

IV.3 The increase in chloride load due to a combination of a sea level rise of 0.6 m during the next century and the delayed effect of previous human activities (namely the reclamation of lakes or parts of the sea) on the future salinisation is serious for nearly all polders in the low-lying coastal regions of the Netherlands, even for those polders beyond the zone of influence of sea level rise. As an indicative estimate: the chloride load through the Holocene aquitard in the low-lying coastal regions of the Netherlands will be doubled in 2090, three fifths of which is caused by a sea level rise of 0.6 m and two fifths by the delayed effect of previous human activities.

IV.4 The mean chloride concentration of the subsoil probably increases with several hundreds of $mg\ Cl^-/l$ in many low-lying polders along the Dutch coast due to the combined effect of a sea level rise of 0.6 m during the next century and previous human activities. Whether or not the loss in crop yield due to salt damage is substantial in these polders depends on other conditions as well.

11.2 Recommendations

a. For the climatic researcher

a.1 (from conclusion I.2):
The scientific community has to confirm statistically that human activities amplify the greenhouse effect on a different time scale than that of natural processes: within decades instead of millennia.

a.2 (from conclusion I.3):
In order to reliably predict a sea level rise during the next century, the scientific community has to investigate the mechanisms involved more intensively. Especially the influence of feedbacks such as oceans and clouds on the (enhanced) greenhouse effect has to be understood more distinctly.

b. For the modeller

b.1 (from conclusions II.1 and II.2):
To match calculated salinity distributions with observed ones along the Dutch coast, longitudinal dispersivities in the order of centimetres to decimetres should be applied to the simulations with the adapted MOC model for groundwater flow regimes with Holocene and Pleistocene deposits of marine and fluviatile origin.

b.2   (from conclusions II.3 and II.4):
       Numerical instabilities in the vertical velocity field of the adapted MOC model
       can be counteracted by the following measures, ranked in order of decreasing
       effectiveness: increasing the number of particles per grid cell; shortening the
       length of the flow time step, lowering the value of the convergence criterion
       TOL, and smoothing the initial density distribution, especially in transition
       zones. By contrast, only reducing the dimension of grid cells does not necessar-
       ily suppress numerical instabilities. However, this measure is rather effective in
       combination with shortening the length of the flow time step.

b.3   (from chapters 8 and 9):
       In this study, groundwater flow regimes have only been schematised and mod-
       elled in (two-dimensional) profiles. However, due to high groundwater extrac-
       tion rates and due to the diversity and complexity of the Dutch polder land-
       scape, groundwater flow is in fact three-dimensional in Dutch geohydrologic sys-
       tems, such as in the islands of the province of Zeeland and in the polder areas at
       several kilometres from the coast in the provinces of Noord and Zuid-Holland.
       Therefore, three-dimensional modelling should be executed as accurate as pos-
       sible to include this groundwater flow. A promising three-dimensional model
       could be an interconnected model of MODFLOW (made suitable for simulating
       density dependent groundwater flow) and the transport model MT3D.

b.4   (from conclusions IV.3 and IV.4):
       The salt source from the subsoil to the root zone by capillary rise should be
       modelled in the Plot Salt model of the PAWN-study for those low-lying polders
       along the Dutch coast, where seepage quantities are already high.

b.5   (from conclusions IV.1 to IV.4):
       In order to quantitatively describe the impact of sea level rise on water manage-
       ment (sectors), the results of the present study on changes in the subsoil due to
       sea level rise and previous human activities should be implemented in integrated
       models, such as applied in the PAWN-study, ISOS, IMAGE or the Fourth Policy
       Document for the Water Management of the Netherlands (in preparation).

c. For the geo(hydro)logist

c.1   (from conclusions III.4, III.5, III.12 and III.13):
       The optimum, and yet realistic, position and rate of well lines for extraction of
       (saline) groundwater or infiltration of surface water should still be determined
       when these countermeasures are considered at a more decisive stage.

c.2   (from subsection 5.4.2: item 4. Hydraulic resistance)
       The applied values for the hydraulic resistance of aquitards, such as loam
       aquitards and clayey Holocene aquitards, should depend on changes in the

solute content of passing groundwater [Goldenberg *et al.*, 1986; Mehnert and Jennings, 1985].

c.3   (from section 9.9: item u. Depth of the geohydrologic base D):
It is recommended to investigate whether or not the marine clayey sediments of lower Pleistocene and Tertiary origin should be included in the schematisations of the coastal geohydrologic systems, especially in the provinces of Zuid-Holland and Zeeland during a long simulation period of e.g. one millennium.

c.4   (from recommendation b.3):
The collection and the analysis of reliable groundwater data should be intensified, varying from subsoil parameters to records of solute concentrations and piezometric levels as functions of time and space. The present salinisation process, the seepage quantity and the chloride load should be monitored as functions of time to detect changes in the long-term. The geometry and geohydrologic parameters of the coastal groundwater flow regimes should be determined and described, particularly for those regimes which are possibly vulnerable to natural and man-induced processes.

d. For the water manager in practice

d.1   (from conclusion III.2):
A descriptive classification system should be developed to roughly assess the vulnerability of coastal groundwater flow regimes for sea level rise by determining the zone of influence of sea level rise; the time lag before the impact of sea level rise becomes noticeable; the occurrence of fresh water resources which can be affected; and the agricultural activities and the socio-economic consequences, now and in the future, for the areas where more saline seepage can be expected.

d.2   (from conclusions III.4, III.5, III.12 and III.13):
The economic feasibility of countermeasures should be investigated. Moreover, the countermeasures should be adapted and optimized throughout the years based on changes in the salinisation of the subsoil.

d.3   (from conclusions III.4, III.5, III.12 and III.13):
Countermeasures should be taken in time, since the time lag is considerable (several decades to centuries) before these measures result in effective changes in the salinity distribution of the subsoil.

d.4   (from conclusions IV.2 and IV.3):
When the sea level rises 0.6 m during the next century, the discharge system (pumping stations and water courses) in the polders near the coast only should probably be adapted and redesigned for greater capacity.

d.5 (from conclusion IV.3):
When the sea level rises 0.6 m during the next century, a substantial increase in volumes of water required for flushing could be necessary to counteract the deterioration of the water quality of surface water systems in the coastal regions of the Netherlands. Therefore, more detailed regional studies should be carried out.

d.6 (from conclusion IV.3):
The chloride load in the Wieringermeer polder (that is in the profile Wie in the reach 15,000-29,500 m) probably increases some tens of percents during the next century, even when no sea level rise occurs. Therefore, to reduce the chloride load in the IJsselmeer, the seepage of this polder should in the future be discharged to the Waddenzee instead of to the IJsselmeer.

List of symbols

Roman symbols			Dimension
A	$=$	cross-sectional area	L^2
A	$=$	height of the sea level with respect to the top of the aquifer, eq. 2.17	L
A_j	$=$	coefficient of the unknown piezometric level values in the alternating-direction implicit procedure, subsection 5.2.4	T^{-1}
B	$=$	width of sand-dunes without sea level rise	L
B_j	$=$	coefficient of the unknown piezometric level values in the alternating-direction implicit procedure, subsection 5.2.4	T^{-1}
B_{SLR}	$=$	width of sand-dunes after a sea level rise	L
b	$=$	thickness of the aquifer, chapter 5	L
b	$=$	inverse of the (seepage) Peclet-number Pe, section 6.3	$-$
C	$=$	content of the freshwater body, eq. 2.12	L^3
C_j	$=$	coefficient of the unknown piezometric level values in the alternating-direction implicit procedure, subsection 5.2.4	T^{-1}
C	$=$	concentration of dissolved solutes	$M\,L^{-3}$
C_{dam}	$=$	critical chloride concentration at the root zone above which salt damage to crop occurs, eq. 10.1	$M\,L^{-3}$
C_{rt}	$=$	chloride concentration of soil moisture in the root zone	$M\,L^{-3}$
C_{max}	$=$	$C_{dam} + 1/\xi$, eq. 10.1	$M\,L^{-3}$
$C_{(i,j)}$	$=$	chloride concentration or chlorinity in grid cell $[i,j]$	$M\,L^{-3}$
C_s	$=$	reference chloride concentration for which the density equals that of saline groundwater	$M\,L^{-3}$
C'	$=$	volume of fresh groundwater per unit coast length, eq. 2.10	L^2
C'	$=$	concentration of dissolved solutes in a source or sink	$M\,L^{-3}$
$C_{i,j}^k$	$=$	new nodal concentration at the end of time level k	$M\,L^{-3}$
$C_{i,j}^k$	$=$	average of the concentration of all particles in grid cell $[i,j]$ for time level k after only advective transport	$M\,L^{-3}$
Co	$=$	Courant-number	$-$
c	$=$	hydraulic resistance of the aquitard	T
c_{land}	$=$	hydraulic resistance of the aquitard at the inland side, eq. 2.16	T
c_{sea}	$=$	hydraulic resistance of the aquitard at the seaside, eq. 2.16	T
D	$=$	saturated thickness of the aquifer	L
D_j	$=$	the sum of all known parameters in the alternating-direction implicit procedure, subsection 5.2.4	$L\,T^{-1}$
D_d	$=$	molecular diffusion	$L^2\,T^{-1}$
D_h	$=$	hydrodynamic dispersion	$L^2\,T^{-1}$
D_m	$=$	mechanical (or convective) dispersion	$L^2\,T^{-1}$
D_{ij}	$=$	coefficient of hydrodynamic dispersion (a second-order tensor)	$L^2\,T^{-1}$
D_{num}	$=$	numerical dispersion	$L^2\,T^{-1}$
d	$=$	thickness of the semi-pervious layer	L
d	$=$	height of the aquifer, section 6.3	L
d	$=$	mean grain size or any other characteristic medium length (a measure of the pore spacing), eq. 5.44	L

Roman symbols			Dimension
E_{water}	=	error in the groundwater flow mass balance, eq. 5.80	–
Fr	=	Froude number, eq. 2.4	–
f	=	natural groundwater recharge. In eq. 5.75 recharge is $(-)$ and discharge is $(+)$	$L T^{-1}$
flow$_{in}$	=	cumulative sums of groundwater mass inflows in the geohydrologic system per stretched foot, eq. 5.80	$M L^{-1}$
flow$_{out}$	=	cumulative sums of groundwater mass outflows in the geohydrologic system per stretched foot, eq. 5.80	$M L^{-1}$
g	=	acceleration of gravity	$L T^{-2}$
G_a	=	overfill ratio, eq. 2.2	–
H	=	depth of the fresh-salt interface below mean sea level	L
H	=	height of profile taking part in the process of shoreline retreat, eq. 2.2	L
H_{max}	=	deepest position of the fresh-salt interface, eq. 2.10	L
h	=	water depth, chapter 2	L
h	=	phreatic groundwater level with respect to the reference level	L
I_b	=	bottom gradient of a river	–
I_t	=	slope of the topography	–
$in f_{(i,j)}$	=	rate of recharge $(-)$ or discharge $(+)$ in grid cell $[i,j]$ in the input data file of the adapted MOC model	T^{-1}
k	=	k^{th} time step	–
k	=	hydraulic conductivity of the aquifer	$L T^{-1}$
k_1	=	hydraulic conductivity k times the relative density difference, eq. 6.11	$L T^{-1}$
kD	=	transmissivity of the aquifer, considered as constant	$L^2 T^{-1}$
kD_s	=	average transmissivity of the aquifer, eq. 2.15 and eq. 2.16	$L^2 T^{-1}$
k_I	=	friction factor representing the stress along the interface, eq. 2.4	–
$k_{(i,j)}$	=	hydraulic conductivity in grid cell $[i,j]$	$L T^{-1}$
k_v	=	(vertical) hydraulic conductivity of the semi-pervious layer	$L T^{-1}$
$k_{x(i+1/2,j)}$	=	weighted harmonic mean of the hydraulic conductivity in the x-direction	$L T^{-1}$
$k_{z(i,j+1/2)}$	=	weighted harmonic mean of the hydraulic conductivity in the z-direction	$L T^{-1}$
L_{crop}	=	fraction of loss in crop yield due to salt damage per decade eq. 10.1	T^{-1}
L_w	=	length of the salt water wedge	L
$L_\perp$	=	width over which water is extracted or infiltrated perpendicular to the profile, eq. 5.74	L
$L_\perp$	=	width perpendicular to the profile in order to upscale the results of the simulations from a vertical plane to a horizonal plane, chapter 10	L
l	=	length of the geohydrologic system	L
l	=	length of the aquifer up to the land side no-flow boundary, eq. 6.8	L
M	=	Canter Cremers Number, eq. 2.3	–
M_0	=	initial solute mass per stretched foot, eq. 5.81	$M L^{-1}$
M_f	=	net mass flow per stretched foot, eq. 5.81	$M L^{-1}$
n_e	=	effective porosity of the medium	–
n	=	number of coefficients taken in the summation of eq. 6.7 to eq. 6.10	–
n	=	number of horizontal grid cells, eq. 6.17	–
P	=	volume of the tidal prism, eq. 2.3	L^3

Roman symbols			Dimension
Pe	$=$	Peclet-number	$-$
Pe_{grid}	$=$	grid-Peclet-number	$-$
$Pe_{grid,x}$	$=$	grid-Peclet-number in the x-direction	$-$
$Pe_{grid,z}$	$=$	grid-Peclet-number in the z-direction	$-$
p	$=$	pressure	$M\,L^{-1}\,T^{-2}$
p	$=$	subindex number for particle identification	$-$
Q	$=$	rate of extraction $(+)$ or infiltration $(-)$, eq. 5.74	$L^3\,T^{-1}$
Q	$=$	net freshwater discharge per unit length of beach, section 6.3	$L^2\,T^{-1}$
Q_r	$=$	fresh water river discharge	$L^3\,T^{-1}$
q	$=$	groundwater flow per unit width of the aquifer	$L^2\,T^{-1}$
q	$=$	filter velocity, subsection 2.4.1	$L\,T^{-1}$
$q_{x(i+1/2,j)}$	$=$	boundary velocity in the x-direction on the boundary between the nodes $[i,j]$ and $[i+1,j]$	$L\,T^{-1}$
$q_{z(i,j+1/2)}$	$=$	boundary velocity in the z-direction on the boundary between the nodes $[i,j]$ and $[i,j+1]$	$L\,T^{-1}$
q_0	$=$	natural groundwater outflow at the coastline x=0 , eq. 2.13	$L^2\,T^{-1}$
$q_{(i,j)}$	$=$	rate of extraction or infiltration of water in grid cell $[i,j]$ in the input data file of MOC, eq. 5.74	$L^2\,T^{-1}$
q_f	$=$	fresh groundwater flow from recharge in the uplands, eq. 2.17	$L^2\,T^{-1}$
q_s	$=$	saline groundwater flow underneath the freshwater lens	$L^2\,T^{-1}$
q_x	$=$	Darcian specific discharges in the x-direction	$L\,T^{-1}$
q_z	$=$	Darcian specific discharges in the z-direction	$L\,T^{-1}$
R	$=$	shoreline retreat or landward shift of the shoreline	L
R_c	$=$	radius of the sandy island without sea level rise, eq. 2.12	L
$R_{c,SLR}$	$=$	radius of the sandy island with sea level rise, eq. 2.12	L
R_m	$=$	solute mass residual per stretched foot, eq. 5.81	$M\,L^{-1}$
r	$=$	distance from the center of the circular island	L
r	$=$	subindex that implies the rescaled parameters used in the numerical sharp fresh-salt interface model, section 6.4	$-$
S	$=$	storage coefficient of the aquifer	$-$
S	$=$	salinity, subsection 5.4.3	$M\,L^{-3}$
SLR	$=$	sea level rise	L
S'	$=$	average rise in bottom level, eq. 2.2	L
S_s	$=$	specific storativity	L^{-1}
T	$=$	temperature	θ
t	$=$	time	T
t_r	$=$	rescaled time parameter, section 6.4	T
TOL	$=$	convergence criterion for the iterative calculation of the freshwater head in the groundwater flow equation in MOC	L
T_{xx}	$=$	horizontal transmissivity	$L^2\,T^{-1}$
T_{zz}	$=$	vertical transmissivity	$L^2\,T^{-1}$
T'	$=$	tidal period, eq. 2.3	T
$u_{x,t}$	$=$	height of the fresh-salt interface at the horizontal space coordinate x as a function of time t, section 6.4	L
$u_{x,\infty}$	$=$	equilibrium position of the height of the 1012.5 kg/m^3-isoline, section 6.4	L
$u_{x,t}^i$	$=$	height of the 1012.5 kg/m^3-isoline at grid cell i at time t, section 6.4	L
V_0	$=$	initial groundwater volume per stretched foot, eq. 5.80	L^2
V	$=$	eroded quantity of material, eq. 2.2	L^3
V	$=$	real velocity of groundwater	$L\,T^{-1}$
V'	$=$	deposited quantity of material, eq. 2.2	L^3

Roman symbols			Dimension
V_i	$=$	real velocity of groundwater in the i-direction	$L\,T^{-1}$
V_r	$=$	velocity in the river, upstream of the wedge, eq. 2.4	$L\,T^{-1}$
$(V_i)_{max}$	$=$	maximum real velocity at a grid cell in the i-direction, eq. 5.71	$L\,T^{-1}$
$|V|$	$=$	magnitude of the real velocity	$L\,T^{-1}$
W	$=$	width of profile taking part in the process of shoreline retreat, eq. 2.2	L
W	$=$	width of the coastal aquifer up to the water divide, eq. 2.14	L
$W(x,z,t)$	$=$	volume flux per unit area, chapter 5	$L\,T^{-1}$
$W'(x,z,t)$	$=$	source function, chapter 5	$M\,L^{-3}\,T^{-1}$
x	$=$	Cartesian coordinate	L
z	$=$	Cartesian coordinate	L
z_{obs}	$=$	elevation of the point of observation with respect to the reference level, eq. 5.78	L

Greek symbols			Dimension
α	$=$	relative density difference	$-$
α_{ijmn}	$=$	geometrical dispersivity tensor of the aquifer, eq. 5.45	L
α_L	$=$	longitudinal dispersivity of the aquifer	L
α_T	$=$	transversal dispersivity of the aquifer	L
β	$=$	angle of the bottom gradient of a river, eq. 2.5	$-$
Γ	$=$	a specific weight term, section 6.4	$L\,T^{-1}$
γ	$=$	specific weight	$M\,L^{-2}\,T^{-2}$
γ_f	$=$	specific weight of fresh water	$M\,L^{-2}\,T^{-2}$
γ_s	$=$	specific weight of saline water	$M\,L^{-2}\,T^{-2}$
$(\Delta C_{i,j}^k)_I$	$=$	change in concentration by hydrodynamic dispersion, chapter 5	$M\,L^{-3}$
$(\Delta C_{i,j}^k)_{II}$	$=$	change in concentration resulting from sources and sinks, chapter 5	$M\,L^{-3}$
$\Delta C_{i,j}^k$	$=$	change in concentration caused by hydrodynamic dispersion, sources and sinks, chapter 5	$M\,L^{-3}$
Δh	$=$	increase in water depth of the river because of climate change, eq. 2.7	L
ΔL_w	$=$	shift of the salt water wedge	L
ΔM_s	$=$	mass accumulation per stretched foot, eq. 5.81	$M\,L^{-1}$
Δp	$=$	difference between $M.S.L.$ and phreatic groundwater level	L
Δt	$=$	flow time step	T
Δt_s	$=$	solute time step	T
Δz	$=$	height of a grid cell	L
Δx	$=$	length of a grid cell	L
Δx_i	$=$	longest distance between sides of an element, eq. 4.17	L
δx_p	$=$	distance of a particle moved in the x-direction, eq. 5.59	L
δz_p	$=$	distance of a particle moved in the z-direction, eq. 5.59	L
∂	$=$	partial differential	$-$
ζ	$=$	factor of river bed elevation with respect to sea level rise, subsection 2.3.1	$-$
ζ	$=$	maximum relative distance across a grid cell, in which a particle is allowed to move during one solute time step Δt_s	$-$
η	$=$	length of the row or column under consideration in the alternating-direction implicit procedure, subsection 5.2.4	$-$
κ	$=$	intrinsic permeability	L^2
κ_x	$=$	intrinsic permeability in the x-direction	L^2
κ_z	$=$	intrinsic permeability in the z-direction	L^2

Greek symbols			Dimension
λ	$=$	characteristic length of the formation	L
λ_{land}	$=$	characteristic length at the inland side, eq. 2.16	L
λ_{sea}	$=$	characteristic length at the seaside, eq. 2.16	L
μ	$=$	dynamic viscosity of water	$M\,L^{-1}\,T^{-1}$
ξ	$=$	shape factor, eq. 2.1	$L^{1/3}$
ξ	$=$	aspect ratio, section 6.3	--
ξ	$=$	salt damage coefficient per $mg\ Cl^-/l$ per decade, eq. 10.1	$L^3\,M^{-1}\,T^{-1}$
ρ_f	$=$	density of fresh water	$M\,L^{-3}$
ρ_i	$=$	density of groundwater at point $[x,z]$	$M\,L^{-3}$
ρ_s	$=$	density of saline water	$M\,L^{-3}$
τ_1	$=$	time conversion factor in eq. 5.73	--
τ_2	$=$	time conversion factor in eq. 5.74	--
τ_3	$=$	time conversion factor in eq. 5.75	--
ϕ	$=$	piezometric level at the aquifer with respect to the reference level	L
ϕ_f	$=$	freshwater head	L
$\phi^k_{f(i,j)}$	$=$	freshwater head in grid cell $[i,j]$ at the kth time step	L
$\Upsilon_{(i,j)}$	$=$	relative density difference, buoyancy between the grid cells $[i,j]$ and $[i,j+1]$	--
Ψ	$=$	stream function of the flow, section 6.4	$L^2\,T^{-1}$
Ψ	$=$	rate of sea level rise, eq. 5.76	$L\,T^{-1}$
Ψ	$=$	percentage of loss in crop yield during the entire productive period due to salt damage per 100 $mg\ Cl^-/l$ exceedance of the critical value C_{dam}, eq. 10.2	--

Summary

The possible impact of several scenarios of sea level rise and human activities on vulnerable coastal groundwater flow regimes in the Netherlands for the next millennium is investigated in this thesis. The most important tool which led to this objective is numerical modelling. A two-dimensional groundwater flow model has been chosen which simulates density-dependent groundwater flow and solute transport in several specific groundwater flow regimes perpendicular to the Dutch coastline. Based on the achievements mentioned above, brief descriptions are given for the impact of sea level rise on three water management sectors: (1) domestic and industrial water supply from coastal sand-dune areas, (2) flushing of water courses of low-lying polder areas and (3) agriculture in terms of salt damage.

In chapter 1, the context of the thesis is discussed and four sub-objectives are formulated: (a) to assess the propagation of sea level rise in the piezometric level distribution of the coastal groundwater flow regimes; (b) to assess the changes in salinity of the coastal groundwater flow regimes; (c) to assess the changes in volumes of freshwater lenses in coastal sand-dune areas; and (d) to assess the changes in seepage (both quantity and quality) in low-lying polder areas. Moreover, the sub-objectives are related with the three water management sectors.

In chapter 2, an overview is given of the possible physical impacts of sea level rise on the coastal zone and the hinterland, the estuaries and the rivers, and the coastal aquifers. Moreover, the impact on two aspects of water management, seepage and discharge (of excess water), is described. Up to now, it appears that, in most of the descriptions, the impact of sea level rise on coastal aquifers is insufficiently dealt with, though it may be far-reaching.

In chapter 3, the causes of climate change, temperature rise and sea level rise are discussed. Moreover, the variations of the sea level in the past and the predictions of the sea level rise in the future are summarized. Though several mechanisms, such as the feedbacks of clouds and oceans, are not completely understood, the majority of the predictions of the future sea level rise is in the range of 30 to 100 cm during the next century, with 60 cm as the best estimate. The main contributors to this rise in sea level during the next century are the thermal expansion of ocean water as well as melting of mountain glaciers and small icecaps.

In chapter 4, a concise summary is given of groundwater flow models, suitable for this research. Three groundwater flow models are analysed: an adapted version of MOC [Konikow and Bredehoeft, 1978], SUTRA [Voss, 1984] and SWICHA [Lester, 1991]. A case study is defined to examine whether or not accurate solutions of the

chloride distributions can be generated in case the longitudinal dispersivity α_L is small (in the order of decimetres). It appears that SUTRA as well as SWICHA simulate inaccurate solutions due to oscillation errors (over and undershooting of maximum and minimum solute concentrations that are originally inserted in the applied model). In SWICHA, even artificial dispersion has to be added to the advection-dispersion equation matrix if α_L is small ($\leq$ decimetres), as otherwise, the solution does not converge. By contrast, the MOC model, adapted for density differences, is very well capable of generating accurate solutions with small longitudinal dispersivities due to the particle tracking technique. In this technique, particles are followed by means of the method of characteristics to simulate advective solute transport.

In chapter 5, the different theoretical aspects are described of the selected groundwater flow model MOC. To make the model suitable for simulating density dependent groundwater flow, the author has adapted the original MOC model (with the help of documentation of Lebbe and van der Eem) by applying an additional term to the vertical Darcian specific discharge in the groundwater flow equation, the so-called *buoyancy* or *vertical density gradient velocity*. Moreover, several subsoil parameters are modified to account for the conversion from the original *horizontal* MOC model to the adapted *vertical* MOC model.

In chapter 6, additional testing is done for the adapted MOC model for three hypothetical cases. In the first case, which is similar to the case of Edelman [1947], unsteady groundwater flow is simulated. In this case, the open water level at the seaside boundary is elevated suddenly. Computation results of the adapted MOC model correspond with analytical solutions. Small flow time steps should be applied to suppress inaccurate solutions of the groundwater flow equation. In the second case, the classical problem of Henry [1964] is considered. Two-dimensional groundwater flow in combination with solute transport and density flow is simulated for a confined aquifer. For steady state as well as for unsteady state situations, the results of the adapted MOC model are in good agreement with those of six other techniques that also solve this problem. Numerical instabilities in the vertical velocity field are caused due to a combination of both density flow and the numerical solution technique. These instabilities, which create unstable isolines, can, among others, be suppressed by reducing the dimension of the grid cells in combination with shortening the length of the flow time step. The solution of the advection-dispersion equation is unstable, if at the beginning of the simulation only 1 particle is placed in each grid cell. In the third case, a fresh-salt interface is simulated in a homogeneous aquifer with no hydrodynamic dispersion. The adapted MOC model is compared with the numerical sharp fresh-salt interface model of Chan Hong *et al.* [1989]. During the displacement of the fresh-salt interface, numerical dispersion is created by the adapted MOC model, though the numerical dispersion is limited to at maximum three grid cells in the vicinity of the supposed fresh-salt interface.

In chapter 7, a sensitivity analysis of both subsoil and model parameters is executed for a profile through a sand-dune area (Gemeentewaterleidingen Amsterdam) and a low-lying polder (the Haarlemmermeer polder). The value of the longitudinal

dispersivity α_L should be small (in the order of centimetres to decimetres), so that the calculated chloride distributions can match the observed ones. Moreover, the numerical instabilities in the vertical velocity field of the adapted MOC model are discussed extensively. They can be counteracted by (ranked in order of decreasing effectiveness): (a) increasing the number of particles per grid cell, (b) shortening the length of the flow time step, (c) lowering the value of the convergence criterion TOL, (d) and smoothing the initial density distribution, especially in transition zones. Reducing the dimension of grid cells is usually only effective in combination with shortening the length of the flow time step.

In chapter 8, the simulations of two specific profiles in Noord-Holland perpendicular to the Dutch coastline are discussed for six scenarios of sea level rise, varying from -0.6 m/c to +1.5 m/c. The profile in the southern part of Noord-Holland crosses the intake area of Gemeentewaterleidingen Amsterdam, the Haarlemmermeer polder and further east to the Vinkeveense plassen. The profile in the northern part of Noord-Holland crosses a narrow sand-dune area near Petten to Enkhuizen at the IJsselmeer. The simulations indicate that previous human activities are the main cause of the present salinisation in both profiles. The lowering of phreatic groundwater levels due to the reclamation of lakes or parts of the sea in the past (from about 1200 AD up to present) causes a permanent inflow of saline groundwater. As such, the so-called reclaimed lakes or polders have a delayed effect on the future salinity distribution. During the next century, the impact of sea level rise (0.6 m/c) on the (accelerated) salinisation process in the groundwater flow regimes of both profiles is mostly small. However, over a time span of a few centuries, the impact of sea level rise (0.6 m/c) is significant in the coastal parts of the groundwater flow regimes in both profiles, whereas the impact remains restricted at a distance of several kilometres from the coast. Moreover, the impact is greater in the northern profile than in the southern profile, as the zone of influence of sea level rise is longer in the northern profile. After many centuries, a sea level rise of 0.6 m/c causes the coastal parts of both groundwater flow regimes, that is the first 15,000 m to 20,000 m, to be completely saline. When the sea level rises 0.6 m/c, the seepage (in terms of quantity and quality) increases only slightly within some centuries in the low-lying Haarlemmermeer polder in the southern profile. On the other hand, the seepage increases significantly in the polder area near Schagen in the northern profile. When the sea level rises 0.6 m/c, the volume of fresh groundwater in the intake area of Gemeentewaterleidingen Amsterdam in the southern profile decreases substantially after at least some centuries. The freshwater body of Hoorn in the northern profile disappears eventually. In case of sea level rise, human interventions within the bounds of feasibility may slow down the salinisation process of these geohydrologic systems. However, the salinisation cannot be neutralized easily, and thus, the salinisation seems to be irreversible. Changes in the salinisation process due to countermeasures only become substantial after a lag of time of several decades to centuries.

In chapter 9, the sensitivity of the groundwater flow regime in the Netherlands for sea level rise is analysed, based on the simulations of eight profiles. Each profile

characterizes a specific coastal area in the Netherlands. Unfortunately, the groundwater flow regimes in the islands of the province of Zeeland cannot be modelled by (two-dimensional) profiles, and thus, this area in the low-lying regions of the Netherlands has not been considered in the simulations. The simulations are subdivided into three main groups of cases: (I) scenarios with three rates of sea level rise (-0.6 m/c, 0 m/c, and 0.6 m/c); (II) (hypothetical) countermeasures; and (III) cases with different subsoil parameters. Based on the simulations of the cases in main group (I), it appears that in most of the eight profiles the delayed effect of previous human activities have not yet reached a state of dynamic equilibrium as far as the salinity distribution in the subsoil is concerned. It is demonstrated that even without a sea level rise, the salinisation process is severe. Due to the fact that groundwater becomes more saline, the seepage quantity through the Holocene aquitard in the polders will slightly decrease. The impact of sea level rise in a polder can be significant in terms of seepage quantity, mean chloride concentration and chloride load in the following situations: the polder is situated near the coast; the phreatic groundwater level in the polder is low, that is several metres below $N.A.P.$; and the zone of influence of sea level rise in the geohydrologic system is long due to high transmissivities of aquifers. Effective countermeasures are: (a) reclaiming land in front of the coast, thus evolving new freshwater lenses; (b) extracting (saline) groundwater, thus decreasing the seepage quantity and chloride load in the polders; (c) inundating low-lying polders, thus removing the driving force of the salinisation process; (d) widening existing sand-dune areas, thus generating thicker freshwater lenses; and (e) creating physical barriers, thus blocking the free entrance of saline groundwater and halting the salinisation process. The countermeasure deep-well infiltration of surface water initially increases both seepage quantity and chloride load in the polders. However, after some decades or even centuries, the salinisation process towards the low-lying hinterland is blocked by the infiltrated surface water. When the sea level rises 0.6 m/c, it is likely that human intervention can only retard the salinisation of the groundwater flow regimes in the long-term at the expense of major investments. Whether or not these investments are considered feasible depends on the prevailing economic, environmental and political circumstances at the moment when a (political) decision is taken. However, it is clear that in the future, the Dutch have to cope with much more saline groundwater in their coastal groundwater flow regimes than at present.

In chapter 10, the results on the impact of sea level rise on the groundwater flow regime, described in the previous chapter, are interpreted for domestic and industrial water supply, flushing and agriculture. For that purpose, the results of the two-dimensional simulations of the profiles are extrapolated to descriptions in a three-dimensional plane by multiplying the two-dimensional results of chapter 9 with a width $L_\perp$, measured perpendicular to the considered profile. From simulations it is deduced that the impact of sea level rise on water supply from freshwater lenses in coastal sand-dune areas is probably negligible during the next century, as only a fraction of the total volume of extracted groundwater originates from the deep parts of the coastal freshwater lenses. The impact of a sea level rise of 0.6 m during the

next century on the change in seepage quantity is considerable (up to several tens of percents) in polders in the first kilometres from the coast, whereas they are marginal (mostly up to only a few percents) in polders located further inland. This implies that the discharge system (pumping stations and water courses) should probably be adapted and redesigned for greater capacities, only in the polders near the coast. The increase in chloride load due to the rise in sea level as well as due to the delayed effect of previous human activities is considerable for nearly all polders in the low-lying coastal regions of the Netherlands, even for those polders beyond the zone of influence of the sea on the distribution of the piezometric levels. Therefore, a substantial increase in flushing quantities could be required to counteract the deterioration of the water quality of surface water systems in the entire coastal region. Furthermore, the increase in (mean) chloride concentration of the subsoil will be substantial in many polders along the Dutch coast during the next century. This increase may cause an additional loss in crop yield due to salt damage, though this estimate depends on several other conditions as well, e.g. on how the increase in chloride concentration in the subsoil affects the chloride concentration in the root zone. The impacts mentioned above could be quantified by means of (numerical) techniques, like those applied in the PAWN-study. If the Plot Salt Model of the PAWN-study is applied, it is recommended to take into account the increased salt flux from the subsoil to the root zone in polders with already high seepage quantities.

In chapter 11, the main conclusions are drawn and some recommendations are given. The main conclusion is that a severe salinisation process, which is dominated by human activities, already occurs in the groundwater flow regimes along the Dutch coast, independent of sea level rise. The reclamation of the (low-lying) polders, which is already taking place during at least several centuries, has generated a strong inflow of saline groundwater from the sea to the deeper aquifers. The (irreversible) salinisation of the geohydrologic system proceeds slowly and will last for at least several centuries. It is to be expected that sea level rise intensifies this salinisation process. Feasible countermeasures may, to some extent, retard (but not stop) this process. Whether or not the impact of sea level rise for a specific polder is significant in terms of seepage quantity, mean chloride concentration and chloride load, depends on the following features: the distance to the coast, the phreatic groundwater level and the subsoil parameters. In the thesis, the impact of sea level rise on the three water management sectors is discussed only in indicative terms. The impact is probably significant in the coastal polder areas during the next century, both for flushing and for agriculture (salt damage) due to the increased salinity of the soil. The results mentioned above should be considered with a sound dose of reserve, as the modelling in two dimensions indicates that only (rough) schematisations of the reality are considered. In order to simulate the reality more accurately, three-dimensional modelling should be executed, among others, to account for groundwater flow perpendicular to the profile. Then, the islands of the province of Zeeland can also be considered.

Gualbert Oude Essink   Delft, may 1996.

Samenvatting

De mogelijke gevolgen van verschillende scenario's van zeespiegelstijging en van menselijke ingrepen op kwetsbare grondwaterstromingsregimes in het Nederlandse kustgebied voor het komende millennium zijn in dit proefschrift onderzocht. Het belangrijkste hulpmiddel om dit doel te bereiken is numeriek modelleren. Een tweedimensionaal grondwaterstromingsmodel is gekozen dat dichtheidsafhankelijke grondwaterstroming en stoftransport kan simuleren in verschillende grondwaterstromingsregimes loodrecht op de Nederlandse kustlijn. Gebaseerd op de bovengenoemde verrichtingen zijn bondige beschrijvingen gepresenteerd voor de effecten van een zeespiegelstijging op drie waterhuishoudkundige sectoren: (1) de drink- en industriewatervoorziening uit duingebieden in het kustgebied, (2) het doorspoelen van waterlopen in diepe poldergebieden en (3) de landbouw in diepe polders in termen van zoutschade.

In hoofdstuk 1 is de context van het proefschrift behandeld en zijn vier doelstellingen geformuleerd: (a) het inschatten van de voortplanting van een zeespiegelstijging in het stijghoogte-patroon van de grondwaterstromingsregimes in het kustgebied; (b) het inschatten van de veranderingen in de verdeling van zoet en zout water van de grondwaterstromingsregimes in het kustgebied; (c) het inschatten van de veranderingen in de volumes van de zoetwaterlenzen in de duingebieden in het kustgebied; en (d) het inschatten van de veranderingen in de kwel (zowel kwantitatief als kwalitatief) van diepe polders in de kuststreek. Voorts zijn de doelstellingen gerelateerd aan de drie waterhuishoudkundige sectoren.

In hoofdstuk 2 is een overzicht gegeven van de mogelijke fysische gevolgen van een zeespiegelstijging voor de kuststreek en het binnenland, de estuaria en de rivieren, en de watervoerende pakketten in het kustgebied. Tevens zijn de gevolgen van twee aspecten van de waterhuishouding, te weten kwel en afvoer van overtollig water, behandeld. Uit het overzicht komt naar voren dat de gevolgen van een zeespiegelstijging voor de watervoerende pakketten in het kustgebied tot dusver onvoldoende beschreven zijn, ofschoon deze gevolgen ingrijpend kunnen zijn.

In hoofdstuk 3 zijn de oorzaken van klimaatverandering, temperatuurstijging en zeespiegelstijging behandeld. Voorts zijn variaties in zeespiegelstijging in het verleden en voorspellingen van de zeespiegelstijging in de toekomst samengevat. Ofschoon verschillende mechanismen, zoals de terugkoppeling van wolken en oceanen, nog onvolledig begrepen zijn, is het gros van de voorspellingen van toekomstige zeespiegelstijgingen binnen het bereik van 30 cm tot 100 cm gedurende de komende eeuw, met 60 cm als de meest waarschijnlijke schatting. De voornaamste bijdragen tot deze stijging in zeespiegel gedurende de komende eeuw zijn de thermische uitzetting van

water in de oceanen en het afsmelten van gebergtegletsjers en kleine ijskappen.

In hoofdstuk 4 is een beknopte samenvatting gegeven van grondwaterstromings-modellen die geschikt kunnen zijn voor dit onderzoek. Drie grondwaterstromings-modellen zijn geanalyseerd: een aangepaste versie van MOC [Konikow en Brede-hoeft, 1978], SUTRA [Voss, 1984] en SWICHA [Lester, 1991]. Een case-studie is gedefinieerd om te onderzoeken of nauwkeurige oplossingen van de verdeling van het chloridegehalte verkregen kunnen worden als de longitudinale dispersiviteit α_L klein is (in de orde van grootte van decimeters). Er is aangetoond dat zowel SUTRA als SWICHA onnauwkeurige oplossingen simuleren door oscillatie fouten. Dit zijn instabiliteiten in de verdeling van het chloridegehalte, waarbij het model gehalten berekent hoger dan de hoogste en lager dan de laagste gehalten die oorspronkelijk zijn ingevoerd. In SWICHA moet zelfs kunstmatige dispersie toegevoegd worden aan de matrix van de advectie-dispersie vergelijking als α_L klein is ($\leq$ decimeters), omdat anders de oplossing niet convergeert. Daarentegen is het MOC model, dat is aangepast voor dichtheidsverschillen, uitstekend in staat om nauwkeurige oplossingen met kleine longitudinale dispersiviteiten te verkrijgen dankzij de zogenaamde deel-tjesverplaatsingstechniek. In deze techniek worden deeltjes gevolgd met behulp van de zogenaamde methode der karakteristieken om advectief stoftransport te simuleren.

In hoofdstuk 5 zijn de verschillende theoretische aspecten beschreven van het ge-selecteerde grondwaterstromingsmodel MOC. Om het model geschikt te maken voor het simuleren van dichtheidsafhankelijke grondwaterstroming, heeft de auteur het originele MOC model aangepast (met behulp van documentatie van Lebbe en van van der Eem) door een extra term toe te voegen aan de verticale specifieke Darcy-snelheid in de grondwaterstromingsvergelijking, het zogenaamde *drijfvermogen* of de *verticale dichtheidsgradiënt-snelheid*. Tevens zijn diverse geohydrologische parame-ters gemodificeerd als gevolg van de conversie van het originele *horizontale* MOC model naar het aangepaste *verticale* MOC model.

In hoofdstuk 6 is het aangepaste MOC model getest op drie hypothetische pro-blemen. In het eerste probleem, dat gelijksoortig is aan het probleem van Edelman [1947], is een niet-stationaire grondwaterstroming gesimuleerd. In dit geval is de open waterstand aan de randvoorwaarde van de zee plotseling verhoogd. Model-berekeningen met het aangepaste MOC model corresponderen met analytische op-lossingen. Kleine stromingstijdstappen moeten gebruikt worden om onnauwkeurige oplossingen van de grondwaterstromingsvergelijking te onderdrukken. In het tweede probleem is het klassieke probleem van Henry [1964] beschouwd. Twee-dimensionale dichtheidsafhankelijke grondwaterstroming in combinatie met stoftransport is gesi-muleerd voor een afgesloten watervoerend pakket. Voor stationaire alsmede niet-stationaire situaties zijn de resultaten van het aangepaste MOC model in overeen-stemming met die van zes andere technieken waarmee dit probleem ook is opgelost. Numerieke instabiliteiten in het verticale stroomsnelheidsveld worden veroorzaakt door een combinatie van dichtheidsstroming en de numerieke oplossingstechniek. Deze instabiliteiten, die onstabiele lijnen van gelijke chloridegehalte creëren, kun-nen onderdrukt worden door, onder andere, het verkleinen van de afmetingen van

de elementen in combinatie met het verkorten van de duur van de stromingstijdstap. De oplossing van de advectie-dispersie vergelijking is onstabiel als in het begin van de simulatie slechts 1 deeltje in elk element wordt geplaatst. In het derde probleem is een zoet-zout grensvlak gesimuleerd in een homogeen watervoerende pakket zonder hydrodynamische dispersie. Het aangepaste MOC model is vergeleken met het numerieke model voor een scherp zoet-zout grensvlak van Chan Hong *et al.* [1989]. Gedurende de verplaatsing van het zoet-zout grensvlak wordt numerieke dispersie gecreëerd door het aangepaste MOC model. Deze numerieke dispersie blijft beperkt tot een maximum van drie elementen nabij het veronderstelde zoet-zout grensvlak.

In hoofdstuk 7 is een gevoeligheidsanalyse uitgevoerd voor zowel geohydrologische als model parameters voor een profiel door een duingebied (namelijk het infiltratiegebied van Gemeentewaterleidingen Amsterdam) en een diepe polder (namelijk de Haarlemmermeerpolder). De waarde van de longitudinale dispersiviteit α_L moet klein zijn (in de orde van grootte van centimeters tot decimeters), opdat de berekende chloridegehalte-patronen corresponderen met de geobserveerde chloridegehalte-patronen. De numerieke instabiliteiten in het verticale stroomsnelheidsveld van het aangepaste MOC model zijn uitgebreid behandeld. In volgorde van afnemende effectiviteit kunnen zij geneutraliseerd worden door: (a) het vergroten van het aantal deeltjes per element, (b) het verkorten van de duur van de stromingstijdstap, (c) het verlagen van de waarde van het convergentie criterium TOL, (d) en het wegnemen van onregelmatigheden in het initiële dichtheidspatroon, voornamelijk in overgangszones tussen zoet en zout grondwater. Het verkleinen van de afmetingen van elementen is gewoonlijk alleen effectief in combinatie met het verkorten van de duur van de stromingstijdstap.

In hoofdstuk 8 zijn modelberekeningen van twee profielen in Noord-Holland loodrecht op de kustlijn behandeld voor zes scenario's van zeespiegelstijging, variërend van -0.6 *m/eeuw* tot +1.5 *m/eeuw*. Het profiel in het zuidelijke gedeelte van Noord-Holland doorkruist het infiltratiegebied van Gemeentewaterleidingen Amsterdam, de Haarlemmermeerpolder en verder oostwaarts tot de Vinkeveense plassen. Het profiel in het noordelijke gedeelte van Noord-Holland doorkruist een smal duingebied nabij Petten tot Enkhuizen aan het IJsselmeer. Modelberekeningen duiden aan dat menselijke ingrepen, die tot dusver hebben plaatsgevonden, de voornaamste oorzaak zijn van de huidige ondergrondse verzilting in beide profielen. Het verlagen van de freatische grondwaterstand ten gevolge van het droogleggen van meren en gedeelten van de zee in het verleden (van ongeveer 1200 AD tot heden) heeft een permanente toestroming van zout grondwater veroorzaakt. Als zodanig hebben de zogenaamde droogmakerijen ofwel polders nog steeds een vertragend effect op de toekomstige ondergrondse verzilting. De gevolgen van een zeespiegelstijging (0.6 *m/eeuw*) voor het (enigszins versnelde) verziltingsproces in de grondwaterstromingsregimes van beide profielen zullen gedurende de komende eeuw over het algemeen klein zijn. Over een tijdspanne van een paar eeuwen zijn de gevolgen van een zeespiegelstijging (0.6 *m/eeuw*) echter aanzienlijk in de gedeelten nabij de kust van beide grondwaterstromingsregimes, terwijl de gevolgen beperkt blijven op enige kilometers van de kust.

De gevolgen in het noordelijke profiel zijn groter dan in het zuidelijke profiel, omdat de invloedssfeer van een zeespiegelstijging groter is in het noordelijke profiel. Door een zeespiegelstijging van 0.6 $m/eeuw$ zal na vele eeuwen de ondergrond van beide grondwaterstromingsregimes volledig verzilten in de eerste 15.000 m tot 20.000 m van de kustlijn. De komende eeuwen zal bij een zeespiegelstijging van 0.6 $m/eeuw$ de kwel (in termen van kwantiteit en kwaliteit) slechts marginaal veranderen in de diepe Haarlemmermeerpolder in het zuidelijke profiel. Daarentegen zal de kwel aanzienlijk toenemen in het poldergebied bij Schagen in het noordelijke profiel. Pas na meerdere eeuwen zal bij een zeespiegelstijging van 0.6 $m/eeuw$ het volume van zoet grondwater in het infiltratiegebied van Gemeentewaterleidingen Amsterdam in het zuidelijke profiel substantieel afnemen. De zoetwaterbel van Hoorn in het noordelijke profiel zal uiteindelijk verdwijnen. Ingeval van een zeespiegelstijging kunnen menselijke ingrepen binnen de grenzen van uitvoerbaarheid het verziltingsproces in deze twee grondwaterstromingsregimes vertragen. Het verziltingsproces kan echter niet gemakkelijk tot stilstand gebracht worden. Het ziet er derhalve naar uit dat de ondergrondse verzilting vrijwel onomkeerbaar is. Veranderingen in het verziltingsproces ten gevolge van tegenmaatregelen zullen slechts substantieel worden na een tijdsbestek van vele decennia tot eeuwen.

In hoofdstuk 9 is de gevoeligheid van het grondwaterstromingsregime in Nederland voor een zeespiegelstijging geanalyseerd op basis van modelberekeningen in acht profielen. Elk profiel karakteriseert een specifiek kustgebied in Nederland. Helaas konden de grondwaterstromingsregimes op de eilanden van de provincie Zeeland niet geschematiseerd worden tot (twee-dimensionale) profielen. Derhalve is dit gebied in de laaggelegen contreien van Nederland niet beschouwd in de modelberekeningen. De modelberekeningen zijn opgedeeld in drie hoofdgroepen: (I) scenario's met drie verschillende zeespiegelstijgingen (-0.6 $m/eeuw$, 0 $m/eeuw$, and 0.6 $m/eeuw$); (II) (hypothetische) tegenmaatregelen; en (III) gevallen met verschillende geohydrologische parameters. Op basis van de modelberekeningen van de scenario's in hoofdgroep (I) is aangetoond dat in de meerderheid van de acht profielen nog geen dynamische evenwichtstoestand is bereikt voorzover het de verdeling van zoet en zout water in de ondergrond betreft. Dit wordt veroorzaakt door het vertraagde effect van de menselijke ingrepen die tot dusver hebben plaatsgevonden. Er is tevens aangetoond dat de ondergrondse verzilting zelfs zonder een zeespiegelstijging omvangrijk is. De hoeveelheid kwel door de Holocene slechtdoorlatende laag in de polders zal dan enigszins afnemen omdat het grondwater zouter wordt. De gevolgen van een zeespiegelstijging in een polder kunnen aanzienlijk zijn in termen van hoeveelheid kwel, gemiddeld zoutgehalte en zoutbelasting indien de volgende situaties zich voordoen: het poldergebied is gesitueerd nabij de kust; de freatische grondwaterstand is laag, te weten enkele meters onder $N.A.P.$; en de invloedssfeer van een zeespiegelstijging in het geohydrologisch systeem is groot als gevolg van met name een groot doorlaatvermogen van de watervoerende pakketten. Effectieve maatregelen ter compensatie van de ondergrondse verzilting zijn: (a) het aanwinnen van land voor de kust zodat nieuwe zoetwaterlenzen zich kunnen ontwikkelen; (b) het onttrekken van (zout) grondwater

zodat de hoeveelheid kwel en de zoutbelasting in de polders kunnen afnemen; (c) het inunderen van diepe polders zodat de drijvende kracht van het verziltingsproces wordt verwijderd; (d) het verbreden van bestaande duingebieden zodat zoetwaterlenzen zich kunnen verdiepen; en (e) het creëren van fysieke barrières zodat de vrije doorgang van zout grondwater wordt geblokkeerd en het verziltingsproces tot stilstand wordt gebracht. Kunstmatig infiltreren van (zoet) oppervlaktewater vergroot, als tegenmaatregel, aanvankelijk zowel de hoeveelheid kwel als de zoutbelasting in de polders. Pas na enkele decennia tot eeuwen zal het verziltingsproces naar het laaggelegen binnenland geblokkeerd zijn door het geïnfiltreerde oppervlaktewater. Wanneer de zeespiegel $0.6 \; m/eeuw$ stijgt, is het waarschijnlijk dat menselijke ingrepen de verzilting van de grondwaterstromingsregimes slechts op de lange termijn kunnen vertragen ten koste van grote investeringen. Of deze investeringen haalbaar zijn hangt af van de heersende economische, milieu en bestuurlijke omstandigheden op het moment wanneer een degelijke (politieke) beslissing genomen wordt. Het is echter duidelijk dat de Nederlanders in de toekomst het hoofd moeten bieden aan veel meer zout water in de grondwaterstromingsregimes in het kustgebied dan tegenwoordig het geval is.

In hoofdstuk 10 zijn de berekende gevolgen van een zeespiegelstijging op het grondwaterstromingsregime, die beschreven zijn in het voorafgaande hoofdstuk, vertaald naar drie waterhuishoudkundige sectoren: drink- en industriewatervoorziening, doorspoelen waterlopen en landbouw. Voor dit doel zijn de resultaten van de twee-dimensionale modelberekeningen geëxtrapoleerd naar beschrijvingen in een drie-dimensionaal vlak door de resultaten in hoofdstuk 9 te vermenigvuldigen met een breedte $L_\perp$, gemeten loodrecht op het beschouwde profiel. Uit de modelberekeningen kan worden opgemaakt dat de gevolgen van een zeespiegelstijging op de watervoorziening uit de zoetwaterlenzen in duingebieden in het kustgebied waarschijnlijk te verwaarlozen zijn gedurende de komende eeuw. Dit wordt mede veroorzaakt doordat slechts een fractie van het totale volume van onttrokken zoete grondwater afkomstig is uit de diepe gedeelten van de zoetwaterlenzen. De verandering in de hoeveelheid kwel door een zeespiegelstijging van $0.6 \; m$ gedurende de komende eeuw is groot (tot enige tientallen procenten) in polders die in de eerste kilometers van de kustlijn zijn gelegen, terwijl de verandering gering is (doorgaans tot slechts een paar procenten) in polders die meer landinwaarts zijn gelegen. Dit houdt in dat het afvoersysteem (te weten pompstations en waterlopen) moet worden aangepast en/of opnieuw ontworpen voor grotere capaciteiten in waarschijnlijk alleen de polders nabij de kust. De toename in zoutbelasting is aanzienlijk voor bijna alle polders in de laaggelegen regionen in het Nederlandse kustgebied. Deze toename is het gevolg van niet alleen de zeespiegelstijging maar ook van het vertraagde effect van menselijke ingrepen die tot dusver hebben plaatsgevonden. Zodoende geldt deze toename zelfs voor polders buiten de invloedssfeer van een zeespiegelstijging op het stijghoogte-patroon. Dientengevolge zal een substantiële toename van de doorspoeldebieten vereist zijn om de achteruitgang van de waterkwaliteit van de oppervlaktewatersystemen in het gehele kustgebied teniet te doen. Bovendien zal de toename in het (gemiddeld) zoutgehalte in de bodem groot zijn in de vele polders in het Nederlandse kustgebied

gedurende de komende eeuw. Deze toename zou een bijkomend verlies in gewas-opbrengst ten gevolge van zoutschade kunnen veroorzaken, alhoewel deze schatting eveneens afhangt van verschillende andere voorwaarden, zoals bijvoorbeeld inhoe-verre de toename in het zoutgehalte in de bodem het zoutgehalte in de wortelzone beïnvloedt. De bovengenoemde gevolgen kunnen gekwantificeerd worden door middel van (numerieke) technieken, zoals die gebruikt zijn in de PAWN-studie. Indien het zogenaamde Plotzoutmodel van de PAWN-studie wordt gebruikt is het aan te bevelen om de toegenomen zoutstroom van de bodem naar de wortelzone mee te nemen in die polders waar de hoeveelheid kwel reeds groot is.

In hoofdstuk 11 zijn de belangrijkste conclusies getrokken en worden enkele aan-bevelingen gedaan. De belangrijkste conclusie is dat de huidige verzilting van de grondwaterstromingsregimes in het Nederlandse kustgebied reeds omvangrijk is. Het verziltingsproces wordt beheerst door menselijke ingrepen en voltrekt zich onafhanke-lijk van een zeespiegelstijging. De aanleg van de laaggelegen droogmakerijen, die reeds gedurende enkele eeuwen plaats vindt, heeft een sterke toestroming van zout grond-water van de zee naar de diepe watervoerende pakketten veroorzaakt, ofschoon de onomkeerbare verzilting van het geohydrologisch systeem traag verloopt en nog ten-minste enige eeuwen zal duren. Het is te verwachten dat een zeespiegelstijging dit verziltingsproces versterkt. Uitvoerbare tegenmaatregelen zouden dit proces tot op zekere hoogte kunnen vertragen maar niet verhinderen. Of de gevolgen van een zee-spiegelstijging voor een specifieke polder aanzienlijk zijn in termen van hoeveelheid kwel, gemiddeld zoutgehalte en zoutbelasting hangt af van de volgende karakteris-tieken: de afstand tot de kust, de freatische grondwaterstand en de geohydrologische parameters. In het proefschrift zijn de gevolgen van een zeespiegelstijging voor drie waterhuishoudkundige sectoren slechts indicatief beschreven. De gevolgen voor de doorspoeling en voor de landbouw (zoutschade) in de polders in het kustgebied zijn waarschijnlijk groot gedurende de komende eeuw als gevolg van de toename van het zoutgehalte in de bodem. De bovengenoemde resultaten moeten beschouwd wor-den met een gezonde dosis terughoudendheid, omdat de modellering in twee dimen-sies aanduidt dat slechts (grove) schematisaties van de werkelijkheid in aanmerking genomen zijn. Om de werkelijkheid nauwkeuriger te simuleren moet het geohydrolo-gisch systeem in drie-dimensies gemodelleerd worden teneinde, onder andere, rekening te kunnen houden met grondwaterstroming loodrecht op het profiel. In dat geval kun-nen ook de eilanden van de provincie Zeeland in ogenschouw genomen worden.

Gualbert Oude Essink   Delft, mei 1996.

References

Abraham, G. 1976. Density currents due to differences in salinity. In: *Salt distribution in estuaries. Committee for Hydrological Research TNO. Proc. and Inform. No. 20. pp. 11-40.*

Abrahamse, A.H., Baarse, G. & Beek, E., van. 1982. Policy Analysis for the National Water Management in the Netherlands. Vol. **XII**. Model for regional hydrology, agricultural water demands and damages from drought and salinity. *The Rand Corporation & Delft Hydraulics.*

Abramowitz, M. & Stegun, I.A. 1965. Handbook of mathematical functions. *Dover.*

Anderson, M.P. & Woessner, W.W. 1992. Applied groundwater modeling. Simulation of flow and advective transport. *Academy Press, Inc., San Diego.*

Arnold, G.E. 1990. Beleidsanalyse landbouw. Eindverslag werkgroep landbouw t.b.v. derde Note Waterhuishouding). (in Dutch). *Ministerie van Verkeer en Waterstaat, Nota 90.007.*

Atlas van Nederland. 1986. Deel 15 Water. (in Dutch). Ven, G.P., van de *et al.* (eds). *Staatsuitgeverij, 's-Gravenhage.*

Baarse, G. & Beek, E., van. 1982. A methodology to determine consequences of variations in water management for agriculture. In: *Policy analysis for the national water management of the Netherlands. Committee for Hydrological Research TNO. Proc. and Inform. No. 29a. pp. 25-44.*

Bachmat, Y., Bredehoeft, J.D., Andrews, B., Holtz, D. & Sebastiaan, S. 1980. Groundwater Management: the use of numerical models. *American Geophysical Union. Water Resources Monograph Series 5.*

Barnett, T.P. 1983. Recent Changes in Sea Level and Their Possible Causes. *Clim. Change* **5**: *15-38.*

Barnola, J.M., Raynaud, D., Korotkevich, Y.S. & Lorius, C. 1992. Vostok ice core provides 160,000-year record of atmospheric CO_2. *Nature, 1 Oct.,* **329**: *408-411.*

Barth, M.C. & Titus, J.G. (eds). 1984. Greenhouse Effect and Sea Level Rise: A Challenge for This Generation. *Van Nostrand Reinhold Co. New York. 325 p.*

Bear, J. 1972. Dynamics of fluids in Porous Media. *American Elsevier Publishing Company, Inc., New York. 764 p.*

Bear, J. 1979. Hydraulics of Groundwater. *McGraw-Hill Book Company, New York.*

Bear, J. & Kapuler, I. 1981. A numerical solution for the movement of an interface in a layered coastal aquifer. *J. of Hydrol.,* **50**: *273-298.*

Bear, J. & Verruijt, A. 1987. Modeling Groundwater Flow and Pollution. *D. Reidel Publishing Company, Dordrecht, the Netherlands. 414 p.*

Beekman, H.E. 1991. Ion Chromatography of Fresh- and Seawater Intrusion. Multicomponent dispersive and diffusive transport in groundwater. *Ph.D. thesis. Free University of Amsterdam. ISBN 90-900 709-3. Drukkerij Fedo B.V. Enschede.*

Beljin, M.S. 1988. Testing and validation of models for simulating solute transport in ground-water. Code Intercomparison and Evaluation of Validation Methodology. *International Ground Water Modeling Center, GWMI 88-11.*

Berg, J. van den & Vries, M., de. (eds). 1979. Principles of River Engineering. The non-tidal alluvial river. *Pitman, London.*

Bertsch, W. 1978. Coefficients of Longitudinal and Transversal Hydrodynamic Dispersion, a Literature Review. (in German). *Sonderdruck aus Deutsche Gewässerkundliche Mitteilungen,* **22**, *H. 2, 37-46.*

Bijlsma, L., Vrees, L.P.M., de, Peerbolte, E.B., Vrijhof, H., Meyer, Th.J.G.P., Baarse, G. & Deursen, W.P.A., van. 1992. Analysis of vulnerability to the impacts of sea level rise. A case study for the Netherlands. *Rijkswaterstaat (Tidal Waters Division), Delft Hydraulics & Resource Analysis. DGW-93.034.*

Boheemen, P.J.M, van & Wilde, J.G.S., de. 1979. De watervoorziening van land- en tuinbouw in het droge jaar 1976. (in Dutch). *ICW, Institute for Land and Water Management Research. Wageningen. ICW Regionale Studies 15, 1979. 109 p.*

Bolin, B., Döös, B.R., Jäger, J. & Warrick, R.A. (eds). 1986. The Greenhouse Effect, Climate Change, and Ecosystems. *John Wiley & Sons.*

Bredehoeft, J.D. & Pinder, G.F. 1973. Mass Transport in flowing Groundwater. *Water Resour. Res., 9 (1): 194-210.*

Brouns, J.J.W.M. 1988. The impact of sea level rise on the Dutch coastal ecosystems. *Netherlands Institute for Sea Research. Research Institute for Nature Management. 102 p.*

Bruggeman, G.A. 1987. Increase in salt seepage along the Dutch coast with a sea level rise (global approach). (in Dutch). *National Institute of Public Health and Environmental Protection. Bilthoven, the Netherlands.*

Bruun, P. 1973. Port Engineering. *Gulf Publishing Company, Houston, Texas. 436 p.*

Calvache, M.L. & Pulido-Bosch, A. 1991. Saltwater intrusion into a small coastal aquifer (Rio Verde, Almuñecar, southern Spain). *J. of Hydrol., 129: 195-213.*

Carslaw, H.S. & Jaeger, J.C. 1959. Conduction of Heat in Solids. *Oxford University Press, London.*

Chan Hong, J.R., Duijn, C.J., van, Hilhorst, D. & Kester, J., van. 1989. The Interface Between Fresh and Salt Groundwater: A Numerical Study. *IMA J. of Applied Mathem., 42: 209-240.*

CHO-TNO: Committee for Hydrological Research. 1980. Research on possible changes in the distribution of saline seepage in the Netherlands. *Proc. and Inform. No. 26.*

CHO-TNO: Committee for Hydrological Research. 1986. Verklarende Hydrologische Woordenlijst. (in Dutch). *Rapporten en Nota's No. 16.*

Cooper, H.H., jr., Kohout, F.A., Henry, H.R. & Glover, R.E. 1964. Sea water in coastal aquifers. *U.S.G.S. Water Supply Paper 1613-C, 84 p.*

Cooper, H.H., jr. 1964. A hypothesis concerning the dynamic balance of fresh water and salt water in a coastal aquifer. In: *Sea water in coastal aquifers. Cooper, H.H., jr., Kohout, F.A., Henry, H.R. & Glover, R.E. 84 p. U.S.G.S. Water Supply Paper 1613-C, pp. C1-C11.*

CRC, Handbook of Chemistry and Physics. 1994. 75th Edition. Lide, D.R. (ed). *Chemical Rubber Company Press, Boca Raton, Florida.*

Custodio, E. & Bruggeman, G.A. (eds). 1987. Groundwater Problems in Coastal Areas. *Studies and Reports in Hydrology. UNESCO, International Hydrological Programme, Paris.*

Dam, J.C., van. 1976. Partial depletion of saline groundwater by seepage. *J. of Hydrol., 29: 315-339.*

Dam, J.C., van & Sikkema, P.C. 1982. Approximate solution of the problem of the shape of the interface in a semi-confined aquifer. *J. of Hydrol., 56: 221-237.*

Dam, J.C., van. 1992a. Geohydrology. Lecture notes. (in Dutch). *Delft University of Technology, Faculty of Civil Engineering, Section Hydrology, the Netherlands.*

Dam, J.C., van. 1992b. Problems associated with saltwater intrusion into coastal aquifers and some solutions. *Proc. ILT Seminar on Problems of Lowland Development, Saga, Japan, Nov. 1992. pp. 1-17.*

Dam, J.C., van. 1993. Impact of sea-level rise on salt water intrusion in estuaries and aquifers. *Keynote lecture Session III of the International Workshop SEACHANGE'93: Sea Level Changes and their Consequences for Hydrology and Water Management. Noordwijkerhout, the Netherlands. April, 1993. UNESCO, IHP-IV Project H-2-2. pp. 49-60.*

Das Gupta, A. & Loof, R. 1993. Effect of sea level rise on groundwater flow regime in coastal aquifer. In: *Sea Level Changes and their Consequences for Hydrology and Water Management. Noordwijkerhout, the Netherlands. April, 1993. UNESCO, IHP-IV Project H-2-2. pp. III 3-12.*

Day, J.W. Jr. 1987. Consequences of sea level rise : implications from the Mississippi Delta. In: *Impact of Sea level rise On Society. Report of a project-planning session, Delft, 27-29 Aug. 1986. Wind, H.G. (ed). A.A. Balkema, Rotterdam/Brookfield. pp. 83-84 and pp. 146-152.*

Day, J.W. Jr., Pont, D., Ibañez, C. & Hensel, Ph.F. 1993. Impacts of Sea Level Rise on Deltas in the Gulf of Mexico and the Mediterranean: Human Activities and Sustainable Management. In: *Sea Level Changes and their Consequences for Hydrology and Water Management. Noordwijkerhout, the Netherlands. April, 1993. UNESCO, IHP-IV Project H-2-2.*

Dean, R.G., Webster, W.C. *et al.* 1987. Responding to changes in sea level. Engineering implications. *National Research Council. National Academy Press, Washington, D.C.*

Delft Hydraulics. 1989. Stive, M.J.F. & Eysink, W.D. Prediction of the development shoreline 1990-2090, phase 3. (in Dutch). *Section report 3.1: Dynamic model of the Dutch coastal system.*

Delft Hydraulics & Rijkswaterstaat. 1988. Impact of Sea level rise On Society. A case study for the Netherlands. *United Nations Environment Programme. Government of the Netherlands. H 750-phase I. Delft Hydraulics & Rijkswaterstaat. Dec.*

Dickinson, R.E. 1986. How Will Climate Change? The Climate System and Modelling of Future Climate. In: *The Greenhouse Effect, Climate Change, and Ecosystems. Bolin, B., Döös, B.R., Jäger, J. & Warrick, R.A. (eds). John Wiley & Sons.*

Does, C., van der. 1990. The influence of sea level rise on the morphological evolutions of coastal lowlands: a literature survey. (in Dutch). *Institute of Geographical Research, Utrecht, the Netherlands. 50 p.*

Eem, J.P., van der. 1987. Adaption Konikow-Bredehoeft for Density Differences. (in Dutch). *Interne notitie KIWA. Aug. 1987.*

Eem, J.P., van der., Mulder, M.A.A. & Verlouw, J.G.W. 1989. Hydrological survey for deepwell-infiltration at the Leidsche Duinwater Maatschappij, Inc. (in Dutch). Hydrologisch onderzoek t.b.v. diepinfiltratie bij de N.V. Leidsche Duinwater Maatschappij. *KIWA SWE-88.017.*

El-Fishawi, N.M. 1989. Coastal erosion in relation to sea level changes, subsidence and river discharge, Nile Delta coast. *Acta Mineralogica-Petragraphica, Szeged, XXX, pp. 161-171.*

El-Fishawi, N.M. 1993. Recent sea level changes and their implications along the Nile Delta coast. In: *Sea Level Changes and their Consequences for Hydrology and Water Management. Noordwijkerhout, the Netherlands. April, 1993. UNESCO, IHP-IV Project H-2-2. pp. IV 3-11.*

El-Raey, M. 1990. Responses to the Impacts of Greenhouse-induced Sea Level Rise on Egypt. In: *Miami Conference on Adaptive Responses to Sea Level Rise and Other Impacts of Global Climate Change. Changing Climate and the Coast. Vol. 2. Report to Intergovernmental Panel on Climate Change (IPCC). UNEP, WMO. pp. 225-233.*

Elzen, M.G.J., den & Rotmans, J. 1988. Simulation model for a number of socio-economic impacts of the greenhouse effect for the Netherlands. (in Dutch). *Report number 758471008. National Institute of Public Health and Environmental Protection. Bilthoven, the Netherlands. 161 p.*

Elzen, M.G.J., den & Rotmans, J. 1992. The socio-economic impact of sea-level rise on the Netherlands: a study of possible scenarios. *Clim. Change 20: 169-195.*

Essaid, H.I. 1986. A comparison of the coupled fresh water-salt water flow and the Ghyben-Herzberg sharp interface approaches to modeling of transient behaviour in coastal aquifer systems. *J. of Hydrol., 86: 169-193.*

Farid, M.S. & Amer, A.M. 1986. An approach to handle sea water intrusion in Nile Delta aquifer. In: *Proc. 9th Salt Water Intrusion Meeting, Delft, the Netherlands, May 1986. pp. 329-341.*

Farid, M.S. 1989. A hydraulic management approach for salt-water intrusion using two-level pumping mechanism. In: *Proc. 10th Salt Water Intrusion Meeting, Ghent, Belgium, May 1988. pp. 238-244.*

Freeze, R.A. & Cherry, J.A. 1979. Groundwater. *Prentice-Hall, Inc. New Jersey.*

Frind, E.O. 1982. Simulation of long-term transient density-dependent transport in groundwater. *Adv. in Water Resour. 5: 73-88.*

Frind, E.O. & Pinder, G.F. 1983. The principle direction technique for solution of the advection-dispersion equation. *Proc. 10th IMACS World Congress on Systems Simulation and Scientific Computation, Concordia University, Montreal, Canada, Aug. 1982. pp. 305-313.*

Galeati, G., Gambolati, G. & Neuman, S.P. 1992. Coupled and Partially Coupled Eulerian-Lagrangian Model of Freshwater-Seawater Mixing. *Water Resour. Res., 28 (1): 149-165.*

Garder, A.O., Jr., Peaceman D.W. & Pozzi, A.L., Jr. 1964. Numerical calculation of multidimensional miscible displacement by the method of characteristics. *Soc. of Petroleum Eng. J., 4 (1): 26-36.*

Gelhar, L.W. & Collins, M.A. 1971. General analysis of longitudinal dispersion in nonuniform flow. *Water Resour. Res., 7 (6): 1511-1521.*

Gelhar, L.W., Welty, C. & Rehfeldt, K.R. 1992. A Critical Review of Data on Field-Scale Dispersion in Aquifers. *Water Resour. Res., 28 (7): 1955-1974.*

Ghassemi, F., Jakeman, A.J. & Jacobson, G. 1990. Mathematical modelling of sea water intrusion, Nauru Island. *Hydrological Processes*, 4: 269-281.

Gilbert, J.T.E., Vellinga, P., *et al.* 1990. Strategies for Adaptation to Sea Level Rise. *Intergovernmental Panel on Climate Change (IPCC), Response Strategies Working Group (III). Coastal Zone Management Subgroup (CZMS).*

Goldenberg, L.C., Mandel, S. & Magaritz, M. 1986. Fluctuating, non-homogeneous changes of hydraulic conductivity in porous media. *Quarterly J. of Eng. Geology, London*, 19: 183-190.

Goode, D.J. & Konikow, L.F. 1989. Modification of a method-of-characteristics solute-transport model to incorporate decay and equilibrium-controlled sorption or ion exchange. *U.S.G.S. Water-Resources Investigations Report 89-4030, Reston, Virginia.*

Goode, D.J. 1990. Particle velocity interpolation in block-centered finite difference groundwater flow models. *Water Resour. Res.*, 26 (5): 925-940.

Goode, D.J. 1992. Modeling transport in transient ground-water flow: an unacknowledged approximation. *Ground Water*, 30 (2): 257-261.

Gornitz, V., Lebedeff, S. & Hansen, J. 1982. Global Sea Level Trend in the Past Century. *Science*, 26 March, 215: 1611-1614.

Gun, J.A.M., van der. 1979. Estimate of the elastic storativity of sandy aquifers (in Dutch). Schatting van de elastische bergingscoefficient van zandige watervoerende pakketten. *Annual report. TNO Institute of Applied Geoscience: pp. 51-62.*

Haitjema, H.M. 1977. Numerical application of vortices to multiple fluid flow in porous media. *Delft Progress Report, Vol. 2: 237-248.*

Heide, P.K.M., van der & Boswinkel, J.A. 1982. The Fresh-saline Distribution of the Groundwater in the Netherlands. Part 2A. Theoretical Background. (in Dutch). *TNO Institute of Applied Geoscience.*

Henry, H.R. 1964. Effects of dispersion on salt encroachment in coastal aquifers. In: *Sea water in coastal aquifers. Cooper, H.H., jr., Kohout, F.A., Henry, H.R. & Glover, R.E. 84 p. U.S.G.S. Water Supply Paper 1613-C, pp. C70-C84.*

Hoffman, J.S. 1984. Estimates of Future Sea Level Rise. In: *Greenhouse effect and sea level rise: A challenge for this generation. Barth, M.C. & Titus, J.G. (eds). New York: Van Nostrand Reinhold.*

Hoog, B., de. 1988. The influence of climate change and sea level rise on water management in the Netherlands. *Report number 758471006. National Institute of Public Health and Environmental Protection. Bilthoven, the Netherlands. 40 p.*

Hosokawa, Y., Isobe, M. 1992. Vulnerability of coastal lowlands due to sea level rise –a review–. *Proc. ILT Seminar on Problems of Lowland Development, Saga, Japan, Nov. 1992. pp. 79-88.*

Houghton, J.T., Jenkins, G.J. & Ephraums, J.J. (eds). 1990. Climate Change. *The IPCC Scientific Assessment. Intergovernmental Panel on Climate Change (IPCC), Science Working Group (I). Cambridge University Press.*

Huisman, L. 1972. Groundwater Recovery. *MacMillan Press, London.*

Hull, C.H.J. & Titus, J.G. (eds). 1986. Greenhouse Effect, Sea Level Rise, and Salinity in the Delaware Estuary. *Washington DC: United States Environmental Protection Agency and Delaware River Basin Commission. 88 p.*

Huyakorn, P.S., Kretschek, A.G., Broome, R.W., Mercer, J.W. & Lester, B.H. 1984. Testing and validation of models for simulating solute transport in ground-water. Development, Evaluation, and Comparison of Benchmark Techniques. *International Ground Water Modeling Center, GWMI 84-13*

Huyakorn, P.S., Andersen, P.F., Mercer, J.W. & White, H.O., Jr. 1987. Saltwater Intrusion in Aquifers: Development and Testing of a Three-Dimensional Finite Element Model. *Water Resour. Res.*, 23 (2): 293-312.

ICW, Institute for Land and Water Management Research. 1976. Wageningen. Hydrologie en waterkwaliteit van Midden West-Nederland. (in Dutch). *Werkgroep Midden West-Nederland. ICW Regionale Studies 9. 101 p.*

ICW, Institute for Land and Water Management Research. 1978. Wageningen. Fysisch-chemische samenstelling van oppervlakte- en grondwater in het Noorden des lands. (in Dutch). *ICW Regionale Studies 13. 112 p.*

ICW, Institute for Land and Water Management Research. 1982. Wageningen. Kwantiteit en kwaliteit van grond- en oppervlaktewater in Noord-Holland benoorden het IJ. (in Dutch). *Werkgroep Noord-Holland. ICW Regionale Studies 16. 166 p.*

IGWMC. 1992. Software catalog. October. *International Ground Water Modeling Center. TNO Institute of Applied Geoscience, P.O. Box 6012, 2600 JA Delft, the Netherlands.*

INTERA. 1979. Revision of the documentation for a model for calculating effects of liquid waste disposal in deep saline aquifers. *Environmental Consultants, Inc. U.S.G.S. Water-Resources Investigations Report 79-96, 73 p.*

INTERCOMP. 1976. A model for calculating effects of liquid waste disposal in deep saline aquifers. *Resource Development and Engineering, Inc. U.S.G.S. Water-Resources Investigations Report 76-96, 263 p.*

Ippen, A.T. & Harleman, D.R.F. 1961. One dimensional analysis of salinity intrusion in estuaries. *U.S. Army Corps of Engineers, Waterways Experiment Station, Vicksburg, Mississippi Technical Bull., No. 5.*

Izrael, Yu.A., Hashimoto, M., Tegart, W.J.McG., *et al.* 1990. Potential impacts of climate change. *Intergovernmental Panel on Climate Change (IPCC), Impacts Working Group (II).*

Jeftic, L., Milliman, J.D. & Sestini, G. 1992. Climate change and the Mediterranean: Environmental and Social Impacts of Climate Change and Sea-level Rise in the Mediterranean Region. *Edward Arnold, London.*

Jelgersma, S., Zijp, M., van der & Brinkman, R. 1993. Sealevel Rise and the Coastal Lowlands in the Developing World. *J. of Coastal Res., 9 (3).*

Jensen, O.K. & Finlayson, B.A. 1978. Solution of the convection-diffusion equation using a moving coordinate system. *Second Int. Conf. on Finite Elements in Water Resour., Imperial College, London, July. pp. 4.21-4.32.*

Jong, C.H., de. 1986. The safety of the Netherlands in case of large sea-level rises (a preliminary study). (In Dutch). *Rijkswaterstaat, the Netherlands.*

Josselin de Jong, G., de. 1977. Review of vortex theory for multiple fluid flow. *Delft Progress Report, Vol. 2: 225-236.*

Kana, T.W., Michel, J., Hayes, M.O. & Jensen, J.R. 1984. The Physical Impact of Sea Level Rise in the Area of Charleston, South Carolina. In: *Greenhouse Effect and Sea Level Rise: A Challenge for this Generation. Barth, M.C. & Titus, J.G. (eds). New York: Van Nostrand Reinhold Co. pp. 105-150.*

Kaplin, P.A. 1990. Practical problems for coastal submergence in the light of secular trends. In: *Greenhouse Effect, Sea Level and Drought. Paepe, R., Fairbridge, R.W. & Jelgersma, S. (eds). Kluwer Academic Publishers, Dordrecht. pp. 385-393.*

Kashef, A.A.I. 1981. Technical and ecological impacts of the High Aswan Dam. *J. of Hydrol., 53: 73-84.*

Kashef, A.A.I. 1983a. Harmonizing Ghyben-Herzberg Interface with Rigorous Solutions. *Ground Water, 21 (2): 153-159.*

Kashef, A.A.I. 1983b. Salt-water Intrusion in the Nile Delta. *Ground Water, 21 (2): 160-167.*

Kinzelbach, W.K.H. 1986. Groundwater Modelling. An introduction with sample programs in BASIC. *Developments in Water Science, 25. Elsevier Science Publishers, Amsterdam.*

Kinzelbach, W.K.H. 1987a. Numerische Methoden zur Modellierung des Transport von Schadstoffen im Grundwasser. In German. *Schriftenreihe GWF Wasser-Abwasser. Band 21. R. Oldenbourg Verlag GmbH, Munchen.*

Kinzelbach, W.K.H. 1987b. Methods for the simulation of pollutant transport in ground water. A model comparison. In: *Proc. Solving Ground Water Problems With Models. Conference and Exposition. Vol. 1, Denver Colorado, U.S.A., Feb. 1987. pp. 656-675.*

Kipp, K.L. Jr. 1986. HST3D. A Computer Code for Simulation of Heat and Solute Transport in Three-dimensional Groundwater Flow Systems. *IGWMC, International Ground Water Modeling Center. U.S.G.S. Water-Resources Investigations Report 86-4095.*

Kohout, F.A. 1964. The flow of fresh water and salt water in the Biscayne aquifer of the Miami area, Florida. In: *Sea water in coastal aquifers. Cooper, H.H., jr., Kohout, F.A., Henry, H.R. & Glover, R.E. 84 p. U.S.G.S. Water Supply Paper 1613-C, pp. C12-C32.*

Konikow, L.F. & Bredehoeft, J.D. 1978. Computer model of two-dimensional solute transport and dispersion in ground water. *U.S.G.S. Techniques of Water-Resources Investigations, Book 7, Chapter C2, 90 p.*

Konikow, L.F. & Bredehoeft, J.D. 1992. Ground-water models cannot be validated. *Adv. in Water Resour.* **15**: 75-83.

Kooiman, J.W. 1989. Modelling the salt-water intrusion in the dune water-catchment area of the Amsterdam Waterworks. *Proc. 10th Salt Water Intrusion Meeting, Ghent, Belgium, May 1988. pp. 132-142.*

Kooiman, J.W., Schuurmans, R.A. & Steinmetz, J.J. 1984. Deep-well infiltration in the dune water-catchment area of the Amsterdam Waterworks. *Report of Amsterdam Waterworks.*

Kooiman, J.W., Peters, J.H. & Eem, J.P., van der. 1986. Upconing of brackish and salt water in the dune area of Amsterdam Waterworks and modelling with the Konikow-Bredehoeft program. *Proc. 9th Salt Water Intrusion Meeting, Delft, the Netherlands, May 1986. pp. 343-359.*

Kooiman, J.W. & Uffink, G.J.M. 1986. Deep-well infiltration in the dune area of Amsterdam Waterworks and modeling of the moving interface. *Proc. 9th Salt Water Intrusion Meeting, Delft, the Netherlands, May 1986. pp. 535-549.*

Koppen, P.C., van. 1985. Geohydrological survey of the polder Groot-Mijdrecht. (in Dutch). *M.Sc. thesis at the Delft University of Technology, the Netherlands. 94 p.*

Korevaar, R. 1989. EG loopt warm voor aanpak broeikaseffect. (in Dutch). *Toegepaste Wetenschap TNO. Feb., 47-51.*

Kranenburg, C. 1986. Density flow. (in Dutch). *Delft University of Technology, Faculty of Civil Engineering, the Netherlands. Lecture notes, 145 p.*

Lange, W., de. 1991. A groundwater model of the Netherlands. (Basisrapport derde Note Water-huishouding). (in Dutch). Ministerie van Verkeer en Waterstaat, Nota 90.066.

Langeweg, F. & Weerden, J.J., van. 1976. Empirical methods of forecasting movement of salt in estuaries. In: *Salt distribution in estuaries. Committee for Hydrological Research TNO. Proc. and Inform. No. 20. pp. 41-86.*

Lantz, R.B. 1971. Quantitative Evaluation of Numerical Diffusion (Truncation Error). *Transactions AIME, Soc. of Petroleum Eng. J.* **251**: 315-320.

Leatherman, S.P. 1984. Coastal Geomorphic Responses to Sea Level Rise: Galveston Bay, Texas. In: *Greenhouse Effect and Sea Level Rise: A Challenge for this Generation. Barth, M.C. & Titus, J.G. (eds). New York: Van Nostrand Reinhold Co. pp. 151-178.*

Lebbe, L.C. 1981. The subterranean flow of fresh and salt water underneath the western Belgian Beach. *Proc. 7th Salt Water Intrusion Meeting, Uppsala, Sweden, Sept. 1981. Sver. Geolog. Unders. Rap. Meddel.*, **27**, 193-219.

Lebbe, L.C. 1983. Mathematical model of the evolution of the fresh-water lens under the dunes and beach with semi-diurnal tides. *Proc. 8th Salt Water Intrusion Meeting, Bari, Italy. Geologia Applicata e Idrogeologia, Vol.* **XVIII**, *Parte* **II**: 211-226.

Lebbe, L.C. 1984. Numerische simulatie van grondwaterkwaliteitsproblemen als hulp bij het beheer van de watervoorraden in het Vlaamse kustgebied. (in Dutch). *Tijdschrift Becewa, Ghent, Belgium. Nr. 76.*

Lebbe, L.C. & Pede, K. 1986. Salt-fresh water flow underneath old dunes and low polders influenced by pumpage and drainage in the western Belgian Coastal Plain. *Proc. 9th Salt Water Intrusion Meeting, Delft, the Netherlands, May 1986. pp. 199-220.*

Lebbe, L.C., Walraevens, K. & Breuk, W., de. 1990. The evolution of the fresh and salt water flow and distribution in two cross-sections through the dune area of De Haan. *Proc. 11th Salt Water Intrusion Meeting, Gdańsk, Poland. pp. 72-97.*

Lee, C.H. & Cheng, R.T. 1974. On seawater encroachment in coastal aquifers. *Water Resour. Res., 10 (5): 1039-1043.*

Lennon, G.P., Wisniewski, G.M. & Yoshioka, G.A. 1986. Impact of increased river salinity on New Jersey aquifers. In: *Greenhouse Effect, Sea Level Rise, and Salinity in the Delaware Estuary. Hull, C.H.J. & Titus, J.G. (eds). Washington DC: United States Environmental Protection Agency and Delaware River Basin Commission. pp. 40-54.*

Lester, B. 1991. SWICHA. A Three-Dimensional Finite-Element Code for Analyzing Seawater Intrusion in Coastal Aquifers. *Version 5.05. GeoTrans, Inc., Sterling, Virginia, U.S.A. IGWMC, International Ground Water Modeling Center, Delft, the Netherlands. 178 p.*

Lisitzin, E. 1974. Sea-level Changes. *Elsevier Oceanography Series, Vol. 8.*

Maas, C. 1989. The origin of saline groundwater in the Netherlands. (in Dutch). Het vóórkomen van zout grondwater in Nederland. H_2O *(22), no. 7, 214-219.*

Maidment, D.R. (ed). 1993. Handbook of Hydrology. *McGraw-Hill, Inc.*

Manneh, A. 1993. Salinity Intrusion in the river Gambia. In: *Sea Level Changes and their Consequences for Hydrology and Water Management. Noordwijkerhout, the Netherlands. April, 1993. UNESCO, IHP-IV Project H-2-2. pp. III 13-22.*

Marsily, G., de. 1986. Quantitative Hydrogeology. Groundwater Hydrology for Engineers. *Academic Press, Inc., Orlando, Florida.*

Mazure, J.P. 1936. Geo-hydrologische gesteldheid van de Wieringermeer. *Rapporten en mededeelingen betreffende de Zuiderzeewerken No. 5. Algemeene landsdrukkerij, 's-Gravenhage 131 p.*

McDonald, M.G. & Harbaugh, A.W. 1984. A modular three-dimensional finite-difference groundwater flow model. *U.S.G.S. Open-File Report 83-875, 528 p.*

Mehnert E. & Jennings, A.A. 1985. The effect of salinity-dependent hydraulic conductivity on saltwater intrusion episodes. *J. of Hydrol.,* **80:** *283-298.*

Meinardi, C.R. 1973. The occurrence of brackish groundwater in the lower parts of the Netherlands. (in Dutch). Het zoutwatervoorkomen in de ondergrond van de lage gedeelten van Nederland. H_2O *(6), no. 18, 454-460.*

Meisler, H., Leahy, P.P. & Knobel, L.L. 1984. Effect of eustatic sea-level changes on saltwaterfreshwater in the northern Atlantic coastal plain. *U.S.G.S. Water-Supply Paper 2255.*

Miami Conference on Adaptive Responses to Sea Level Rise and Other impacts of Global Climate Change. 1990. *Changing Climate and the Coast. Report to Intergovernmental Panel on Climate Change (IPCC). UNEP, WMO.*

Miller, G.H. & De Vernal, A. 1992. Will Greenhouse warming lead to Northern Hemisphere icesheet growth ? *Nature, 16 Jan.,* **355:** *244-246.*

Mimura, N., Yasuhara, K., Isobe, M. & Hosokawa, Y. 1992. Vulnerability assessment to sea level rise –case studies of Japanese task team–. *Proc. ILT Seminar on Problems of Lowland Development, Saga, Japan, Nov. 1992. pp. 99-106.*

MOC: Computer Model of Two Dimensional Solute Transport and Dispersion in Ground Water. 1989. *International Ground Water Modeling Center, Delft, version 3.0, Nov.*

Naeem, A.S., Arshad, A. & Dilawer, A.R. 1993. The effects of sea level and manmade changes on the Indus River Estuary. In: *Sea Level Changes and their Consequences for Hydrology and Water Management. Noordwijkerhout, the Netherlands. April, 1993. UNESCO, IHP-IV Project H-2-2. pp. IV 35-44.*

Navoy, A.S. 1991. Aquifer-estuary interaction and vulnerability of groundwater supplies to sea level rise-driven saltwater intrusion. *Ph.D. thesis. Pennsylvania State University, U.S.A. 225 p.*

Noomen, P. 1989. Bodembeweging in Nederland. (in Dutch). In: *Zeespiegelrijzing en bodemdaling; welk scenario wordt werkelijkheid ? Symposium 12 april 1989, Delft University of Technology, Delft.*

Oerlemans, J. 1989. A projection of Future Sea Level. *Clim. Change,* **15:** *151-174.*

Oerlemans, J. 1993. Sea-level changes. In: *Hydrology and Water Management of Deltaic Areas. Volker, A., Boekelman, R.H., Koppen, P.C., van & Mulder, M.A.A. (eds). Centre for Civil Engineering Research and Codes (CUR), Report 93-5, Gouda, the Netherlands.*

Ogata, A. & Banks, R.B. 1961. A solution of the differential equation of longitudinal dispersion in porous media. *United States Geological Survey, Professional Paper No. 411-A.*

Olsthoorn, T.N. 1993. Modelling simultaneous flow of fresh and saline groundwater with a spreadsheet. *Proc. 12th Salt Water Intrusion Meeting, Barcelona, Spain, Nov. 1992. pp. 343-357.*

Ossenkoppele, H. 1993. Modellering van de verdeling en de beweging van zoet, brak en zout grondwater in het duingebied van Gemeentewaterleidingen Amsterdam. (in Dutch). *M.Sc. thesis at the Delft University of Technology, the Netherlands. 84 p.*

Oude Essink, G.H.P., Boekelman, R.H. & Bosters, M.C.J. 1993. Physical impacts of sea level change. *State of the Art Report UNESCO Workshop SEACHANGE'93: Sea Level Changes and their Consequences for Hydrology and Water Management. Noordwijkerhout, the Netherlands. April, 1993. UNESCO, IHP-IV Project H-2-2. pp. 81-137.*

Oueslati, A. 1990. Coastal Morphology and Sea Level Rise Consequences in Tunisia. In: *Miami Conference on Adaptive Responses to Sea Level Rise and Other Impacts of Global Climate Change. Changing Climate and the Coast. Vol.* **2.** *Report to Intergovernmental Panel on Climate Change (IPCC). UNEP, WMO. pp. 211-223.*

Overeem, M., van, *et al.* 1993. Nieuw-Holland. Kwaliteit in een nieuwe kustlokatie tussen Hoek van Holland en Scheveningen. *Stichting Maatschappij en Onderneming. Den Haag.*

Paap, H.A. 1992. De invloed van de stijging van de zeespiegel op het verziltingsproces. Het model Konikow-Bredehoeft toegepast op een doorsnede in Noord-Holland. (in Dutch). *M.Sc. thesis at the Delft University of Technology. 139 p.*

Pastoors, M.J.H. 1992. Landelijk Grondwatermodel; Conceptuele Modelbeschrijving. Onderzoek effecten grondwaterwinning. (in Dutch). *Report number 714305004. RIVM. National Institute of Public Health and Environmental Protection. Bilthoven, the Netherlands.*

Peaceman, D.W. 1977. Fundaments of numerical reservoir simulation. *Developments in Petroleum Science 6, Elsevier Scientific Publishing Company, Amsterdam.*

Peerbolte, E.B., Ronde, J.G., de, Vrees, L.P.M., de, Mann, M.A.M. & Baarse, G. 1991. Impact of Sea level rise On Society. A case study for the Netherlands. *Delft Hydraulics, Rijkswaterstaat & Resource Analysis. GWAO-90.016.*

Perdomo, M., Vellinga, P., *et al.* 1992. Global Climate Change and the Rising Challenge of the Sea. *Intergovernmental Panel on Climate Change (IPCC), Response Strategies Working Group (III). Coastal Zone Management Subgroup (CZMS).*

Peters, J.H. 1983. The movement of fresh water injected in salaquifers. *Proc. 8th Salt Water Intrusion Meeting, Bari, Italy. Geologia Applicata e Idrogeologia. Vol.* **XVIII**, *Parte* **II:** *145-155.*

Pinder, G.F. & Bredehoeft, J.D. 1968. Application of the Digital Computer for Aquifer Evaluation. *Water Resour. Res., 4 (5): 1069-1093.*

Pinder, G.F. & Cooper, H.H, Jr. 1970. A numerical technique for calculating the transient position of the saltwater front. *Water Resour. Res., 6 (3): 875-882.*

Pirazzoli, P.A. 1987. Sea-level changes in the Mediterranean. In: *Sea-level changes. Tooley, M.J. & Shennan, I. (eds). Oxford, Blackwell, UK. pp. 152-181.*

Pirazzoli, P.A. & Pluet, J. 1991. World Atlas of Holocene Sea-level Changes. *Elsevier Oceanography Series, Vol.* **58.**

Plassche, O., van de. 1982a. Zeespiegelbewegingen in Nederland gedurende de laatste 7000 jaar. (in Dutch). In: *Nederlandse organisatie voor zuiver-wetenschappelijk onderzoek, jaarboek 1982, bijlage.*

Plassche, O., van de. 1982b. Sea-level change and water-level movements in the Netherlands during the Holocene. *Mededelingen Rijks Geologische Dienst, Vol.* **36-1.**

Pomper, A.B. 1983a. Observations on the hydrochemical groundwater situation of the western Netherlands. *Geologie en Mijnbouw, 62, 585-592.*

Pomper, A.B. 1983b. Geohydrological situation of the western part of the Netherlands. *Geologie en Mijnbouw, 62, 3/4, 519-528.*

Postma, J., Stuyt, L.C.P.M. & Kabat, P. 1994. Effect of sea-level rise and climate change on groundwater salinity and agro-hydrology in a low coastal region of the Netherlands. Wageningen, DLO Winand Staring Center, Report 89.

Priem, H.N.A. 1989. De grootste milieu-catastrofe. (in Dutch). In: *N.R.C. Handelsblad, Wetenschap en Onderwijs. Feb. 28.*

Pulles, J.W. 1985. Policy Analysis for the Watermanagement in the Netherlands (PAWN). (in Dutch). Een beleidsanalyse van de waterhuishouding van Nederland. *Rijkswaterstaat, Hoofddirectie van de Waterstaat, Den Haag.*

Ramanathan, V. & W. Collins. 1991. Thermodynamic regulation of ocean warming by cirrus clouds deduced from observations of the 1987 El Niño. *Nature, 2 May,* **351:** *27-32.*

Rampino, M.R. & Sanders, J.E. 1980. Holocene transgression in south-central Long Island, New York. *J. of Sedimentary Petrology, Vol.* **50:** *1063-1080.*

Reilly, Th.E. & Goodman, A.S. 1985. Quantitative analysis of saltwater-freshwater relationships in groundwater systems – a historical perspective. *J. of Hydrol.,* **80:** *125-160.*

Reilly, Th.E. 1990. Simulation of dispersion in layered coastal aquifer systems. *J. of Hydrol.,* **114:** *211-228.*

Rijkswaterstaat. 1990. A new coastal defence policy for the Netherlands. *Ministry of Transport and Public Works, Den Haag.*

Rind, D. *et al.* 1991. Positive water vapour feedback in climate models confirmed by satellite data. *Nature, 7 Feb,* **349***: 500-503.*

Robin, G. deQ. 1986. Changing the Sea Level. Projecting the Rise in Sea Level Caused by Warming of the Atmosphere. In: *The Greenhouse Effect, Climate Change, and Ecosystems. Bolin, B., Döös, B.R., Jäger, J. & Warrick, R.A. (eds). John Wiley & Sons.*

Ronde, J.G., de & Ruijter, W.P.M. (eds). 1986. Zeespiegelstijging, worstelen met wassend water. (in Dutch). *GWAO-86.002, Rijkswaterstaat, Tidal Waters Division, Den Haag.*

Ronde, J.G., de. 1988. Past and future sea level rise in the Netherlands. In: *Workshop on Sea Level Rise and Coastal Processes. Palm Coast, Florida. 9-11 March, 1988. United States Department of Energy.*

Ronde, J.G., de. 1991. Rising waters. Impacts of the greenhouse effect for the Netherlands. *GWAO-90.026, Rijkswaterstaat, Tidal Waters Division, Den Haag.*

Rotmans, J. 1990. IMAGE: Integrated Model for the Assessment of the Greenhouse Effect. *Ph.D. thesis. Rijksuniversiteit Limburg, the Netherlands.*

Sahagian, D.L., Schwartz, F.W. & Jacobs, D.K. 1994. Direct anthropogenic contributions to sea level rise in the twentieth century. *Nature, Jan.,* **367***: 54-57.*

SALINA. 1987. Computer code for a sharp salt/fresh water interface in a non steady groundwater flow system, developed by Consultants for Water & Environment IWACO Ltd.

Samper, J. & García-Vera. 1993. A groundwater salinity model for the closed-basin area of Los Monegros, Spain. *Proc. 12th Salt Water Intrusion Meeting, Barcelona, Spain, Nov. 1992. pp. 99-117.*

Sanford, W.E. & Konikow, L.F. 1985. A two-constituent solute-transport model for ground water having variable density. *U.S.G.S. Water-Resources Investigations Report 85-4279.*

Santing, G. 1980. A problem with the flow of fresh and saline groundwater: the corrections on the hydraulic heads. (in Dutch). Een probleem bij de stroming van zoet en zout grondwater: de correcties op de stijghoogten. *H2O (13) 1980, no. 22.*

Sauter, F.J., Leijnse, A. & Beusen, A.H.W. 1993. METROPOL's User's Guide. *Report number 725205.003. National Institute of Public Health and Environmental Protection. Bilthoven, the Netherlands.*

Savenije, H.H.G. 1992. Rapid assessment technique for salt intrusion in alluvial estuaries. *Ph.D. thesis. Delft University of Technology. 186 p.*

Scheidegger, A.E. 1961. General theory of dispersion in porous media. *J. of Geophys. Res., 66 (10): 3273-3278.*

Schröder, P.C. (ed.). 1988. Sea-Level Rise, –A selective retrospection–. *Delft Hydraulics Emmeloord, the Netherlands. 100 p.*

Schultz, E. 1992. Water Management of the Drained Lakes in the Netherlands. (in Dutch). *Ph.D. thesis. Delft University of Technology. Rijkswaterstaat, Directie Flevoland, Lelystad. ISBN 90-369-1087-0. 507 p.*

Schuurmans, R.A. 1983. Restoring a briny catchment area. *Proc. 8th Salt Water Intrusion Meeting, Bari. Geologia Applicata e Idrogeologia. Vol.* **XVIII***, Parte II: 169-182.*

Schuurmans, R.A. & Akker, C., van den. 1981. Artificial removal of intruded saline water in a deep aquifer. *Proc. 7th Salt Water Intrusion Meeting, Uppsala, Sweden, Sept. 1981. Sver. Geolog. Unders. Rap. Meddel., 27, 239-246.*

Scientific Software Group. 1995. Catalog Environmental Software & Publications. 1995-1996. *P.O. Box 23041, Washington, D.C. 20026-3041, USA.*

Segol, G. 1994. Classic groundwater simulations. Proving and improving numerical models. *Prentice-Hall, Inc. New York. 531 p.*

Segol, G., Pinder, G.F. & Gray, W.G. 1975. A Galerkin finite-element technique for calculating the transient position of the saltwater front. *Water Resour. Res., 11* **(2)***: 343-347.*

Segol, G. & Pinder, G.F. 1976. Transient Simulation of Saltwater Intrusion in Southeastern Florida. *Water Resour. Res., 12 (1): 65-70.*

Selivanov, A.O. 1993. Modelling response of accumulative coasts to the possible future sea-level rise: general approach and examples from the former U.S.S.R. coasts. In: *Sea Level Changes and their Consequences for Hydrology and Water Management. Noordwijkerhout, the Netherlands. April, 1993. UNESCO, IHP-IV Project H-2-2. pp. IV 63-74.*

Sestini, G. 1990. Impacts of Global Climate Change in the Mediterranean Region: Responses and Policy Options. In: *Miami Conference on Adaptive Responses to Sea Level Rise and Other Impacts of Global Climate Change. Changing Climate and the Coast. Vol. 2. Report to Intergovernmental Panel on Climate Change (IPCC). UNEP, WMO. pp. 115-126.*

Sestini, G. 1992. The Impact of Climate Changes and Sea-level Rise on Two Deltaic Lowlands of the Eastern Mediterranean. In: *Impacts of Sea-level Rise on European Coastal Lowlands. Tooley, M.J. & Jelgersma, S. (eds). Blackwell Publishers, Oxford, UK. pp. 170-203.*

Shahin, M.M.A. 1991. Assessment of Groundwater Resources in Egypt. *IHE Report Series 23. International Institute for Hydraulic and Environmental Engineering, Delft, the Netherlands.*

Shamir, U. & Harleman, D.R.F. 1966. Numerical and analytical solutions of dispersion problems in homogeneous and layered aquifers. *M.I.T. Dept. Civil Eng., Hydrodynamics Lab. Rept. 89, May.*

Shearer, T.R. & Wonderen, J. van. 1993. Scavenger Wells -4- Simulation modelling. *Proc. 12th Salt Water Intrusion Meeting, Barcelona, Spain, Nov. 1992. pp. 583-598.*

Snead, R.E. 1972. Atlas of World Physical Features. *John Wiley & Sons, Toronto.*

Sorensen, R.M., Weisman, R.N. & Lennon, G.P. 1984. Control of erosion, inundation and salinity intrusion caused be sea level rise. In: *Greenhouse Effect and Sea Level Rise: A Challenge for this Generation. Barth, M.C. & Titus, J.G. (eds). New York: Van Nostrand Reinhold Co. pp. 179-214.*

Souza, W.R. & Voss, C.I. 1987. Analysis of an anisotropic coastal aquifer system using variable-density flow and solute transport simulation. *J. of Hydrol., 92: 17-41.*

Stanley, D.J. 1988. Subsidence in the Northeastern Nile Delta: Rapid Rates, Possible Causes, and Consequences. *Science, 22 April, 240: 497-500.*

Strack, O.D.L. 1989. Groundwater Mechanics. *Prentice Hall, New Jersey, U.S.A. 732 p.*

Stuurgroep Kustlocatie. 1995. Ruimte voor de kust. Eindrapport haalbaarheidsonderzoek kustlocatie Den Haag/Hoek van Holland. (in Dutch). *KuiperCompagnons, DHV, Coopers & Lybrand. 114 p.*

Stuyfzand, P.J. 1986a. Hydrochemistry and hydrology of dunes and adjacent polders between Zandvoort and Wijk aan Zee (map numbers 24F and 25A). (in Dutch). *KIWA SWE-86.016, 203 p.*

Stuyfzand, P.J. 1986b. A new hydrochemical classification of watertypes: principles and application to the coastal dunes aquifer system of the Netherlands. *Proc. 9th Salt Water Intrusion Meeting, Delft, the Netherlands. pp. 641-655.*

Stuyfzand, P.J. 1988. Hydrochemistry and hydrology of dunes and adjacent polders between Noordwijk and Zandvoort aan Zee (map no. 24H and 25C). (in Dutch). *KIWA SWE-87.007, 343 p.*

Stuyfzand, P.J. 1991. Composition, genesis and quality variations of shallow groundwater in coastal dunes. (in Dutch). Samenstelling, genese en kwaliteitsvariaties van ondiep grondwater in kustduinen. *KIWA SWE-91.008, 175 p.*

Stuyfzand, P.J. 1993. Hydrochemistry and hydrology of coastal dune area of the Western Netherlands. *Ph.D. thesis. Free University of Amsterdam. ISBN 90-74741-01-0. 366 p.*

Stuyfzand, P.J., Lüers, F. & Jonge, de, H.G. 1993. Hydrochemistry and hydrology of dunes and adjacent polders between Katwijk and Kijkduin. (in Dutch). *KIWA SWE-93.001, 165 p.*

Stuyfzand, P.J. & Stuurman, R.J. 1985. Experimental proof and modelling of a steady dune water lens on artificially recharged surface water. (in Dutch). *H2O (18), no. 19, pp. 408-415.*

Thatcher, M. & Harleman, D.R.F. 1972. A mathematical model for the prediction of unsteady salinity intrusion in estuaries. *R.M. Parsons Laboratory Rep. No. 144, MIT, Cambridge, Massachusetts.*

Thomas, R.H. 1986. Future Sea Level Rise and its early detection by satellite Remote Sensing. In: *Globaal overzicht van Nederlands onderzoek naar zeespiegelstijging. Delft Hydraulics.*

Thorborg, B.B.W. & Jousma, G. 1989. Development of a knowledge system for modelling fresh- and saline-groundwater flow. *Proc. 10th Salt Water Intrusion Meeting, Ghent, Belgium, May 1988, 200-209.*

Titus, J.G., Barth, M.C., et al. 1984. An Overview of the Causes and Effects of Sea Level Rise. In: *Greenhouse Effect and Sea Level Rise: A Challenge for this Generation. Barth, M.C. & Titus, J.G. (eds). New York: Van Nostrand Reinhold Co. pp. 1-56.*

Titus, J.G. 1987. The Causes and Effects of Sea Level Rise. In: *Impact of Sea level rise On Society. Report of a project-planning session, Delft, 27-29 Aug. 1986. Wind, H.G. (ed). A.A. Balkema, Rotterdam/Brookfield. pp. 104-125.*

TNO Institute of Applied Geoscience, Delft. 1979a. Grondwaterkaart van Nederland, Zandvoort (24) en Amsterdam (25 west, 25 oost). (in Dutch). Speelman, H. & Houtman, H. *Dec. 81 p.*

TNO Institute of Applied Geoscience, Delft. 1979b. Grondwaterkaart van Nederland, Alkmaar (19 west, 19 oost en 20A) en Medemblik (14 west, 14 oost). (in Dutch). Lageman, R. & Homan, M. *Dec. 70 p.*

TNO Institute of Applied Geoscience, Delft. 1980. Grondwaterkaart van Nederland, 's Gravenhage (30D, 30 oost) en Utrecht (31 west). (in Dutch). Boswinkel, J.A. & Cornelissen, C.M.L. *Jan. 39 p.*

TNO Institute of Applied Geoscience, Delft. 1982. Grondwaterkaart van Nederland, Zeeuwsch-Vlaanderen (47 oost, 48, 49 west; 53 oost, 54, 55 west). (in Dutch). Lekahena, E.G. *Nov. 43 p.*

TNO Institute of Applied Geoscience, Delft. 1984a. Grondwaterkaart van Nederland, Medemblik (14 west, 14 oost; 9D en 15C). (in Dutch). Lekahena, E.G. & Langbein, J.B.M. *May 45 p.*

TNO Institute of Applied Geoscience, Delft. 1984b. Grondwaterkaart van Nederland, Rotterdam (37 west, 37 oost). (in Dutch). Boswinkel, J.A. & Ritsema,.I.L. *Oct. 66 p.*

TNO Institute of Applied Geoscience, Delft. 1984c. Grondwaterkaart van Nederland, Goedereede, Zierikzee en Willemstad (36H, 42 west + oost, 43 west). (in Dutch). Cornelissen, C.M.L. *Oct. 76 p.*

TNO Institute of Applied Geoscience, Delft. 1985. Grondwaterkaart van Nederland, Middelburg/Bergen op Zoom (48, 49 west; 43C en D) (in Dutch). Hoogendoorn, J.H. *June 69 p.*

TNO Institute of Applied Geoscience, Delft. 1987a. Grondwaterkaart van Nederland, Waddeneilanden (in Dutch). de Wit, G.J. *May 107 p.*

TNO Institute of Applied Geoscience, Delft. 1987b. Grondwaterkaart van Nederland, Leeuwarden/Groningen (2G, H, 3C, D, 6 oost, 7 west). (in Dutch). de Heer, E. *June 49 p.*

TNO Institute of Applied Geoscience, Delft. 1987c. Grondwaterkaart van Nederland, Harlingen/Leeuwarden (2D, 5D, 5 oost, 6 west). (in Dutch). de Heer, E. & Hoogendoorn, J.H. *Nov. 65 p.*

TNO-GG/RIZA. 1994a. NAGROM: report 8: supra-regio Holland-Noord. *OS 94-44 TNO-GG and Rijkswaterstaat-RIZA.*

TNO-GG/RIZA. 1994b. NAGROM: report 9: supra-regio Holland-Zuid. *OS 94-45 TNO-GG and Rijkswaterstaat-RIZA.*

Todd, D.K. 1980. Groundwater Hydrology. *John Wiley & Sons, New York.*

Trescott, P.C., Pinder, G.F. & Larson, S.P. 1976. Finite-difference model for aquifer simulation in two dimensions with results of numerical experiments. *U.S.G.S. Techniques of Water-Resources Investigations, Book 7, Chapter C1, 116 p.*

Tsyban, A., Everett, J. & Titus, J. 1990. Chapter 6: World oceans and coastal zones. In: *Potential impacts of climate change. Intergovernmental Panel on Climate Change (IPCC), Impacts Working Group (II). Izrael, Yu. A., Hashimoto, M., Tegart, W.J.McG., et al. (eds).*

Tweede Kamer der Staten Generaal. 1989. Explanatory memory Wet op de waterkering. (in Dutch). *Vergaderjaar 1988-1989, 21 195, no. 1-2, Memorie van toelichting.*

Uffink, G.J.M. 1982. Determination of the elastic storativity from barometric efficiency. (in Dutch). De bepaling van de elastische bergingscoefficient aan de hand van de barometrische gevoeligheid. H_2O *(15), no. 19, pp. 530-533.*

Uffink, G.J.M. 1990. Analysis of dispersion by the random walk method. *Ph.D. thesis. Delft University of Technology. 150 p.*

United States Department of Energy. 1989. Workshop on Sea Level Rise and Coastal Processes. *9-11 March, 1988. Palm Coast, Florida.*

Venhuizen, K.D. 1971. Zoutwaterintrusies t.g.v. wateronttrekking langs de Nederlandse kust. (in Dutch). *Stichting Postakademische Vorming Gezondheidstechniek. Cursus Zout Grondwater in Nederland deel II. 1970-1971.*

Verruijt, A. 1970. Theory of Groundwater Flow. *Macmillan, London.*

Verruijt, A. 1980. The rotation of a Vertical Interface in a Porous Medium. *Water Resour. Res., 16 (1): 239-240.*

Vogel, P., Schelkes, K. & Giesel, W. 1993. Modeling of variable-density flow in an aquifer crossing a salt dome – first results. *Proc. 12th Salt Water Intrusion Meeting, Barcelona, Spain, Nov. 1992. pp. 359-369.*

Volker, A. 1970. Watercontrol and Reclamation of Deltaic and Coastal Areas. Hydrology, special subjects. *Delft University of Technology, Faculty of Civil Engineering, the Netherlands. Lecture Notes, 1969-1970.*

Volker, A. 1987. Impacts of a rapid rise of the sea level on flood protection and water management of low-lying coastal areas. In: *Impact of Sea level rise On Society. Report of a project-planning session, Delft, 27-29 Aug. 1986. Wind, H.G. (ed). A.A. Balkema, Rotterdam/Brookfield. pp. 167-176.*

Volker, A., Boekelman, R.H., Koppen, P.C., van & Mulder, M.A.A. (eds). 1993. Hydrology and Water Management of Deltaic Areas. *Centre for Civil Engineering Research and Codes (CUR). Report 93-5, Gouda, the Netherlands.*

Voss, C.I. 1984. SUTRA – A finite element simulation for saturated-unsaturated, fluid-density-dependent ground-water flow with energy transport or chemically reactive single-species solute transport. *U.S.G.S. Water-Resources Investigations Report 84-4369, 409 p.*

Voss, C.I. & Souza, W.R. 1987. Variable density flow and solute transport simulation of regional aquifers containing a narrow freshwater-saltwater transition zone. *Water Resour. Res., 23 (10): 1851-1866.*

Vries, J.J., de. 1981. Fresh and salt groundwater in the Dutch coastal area in relation to geomorphological evolution. *Geologie en Mijnbouw, 60, 363-368.*

Walraevens, K., Lebbe, L.C., et al. 1993. Salt/fresh-water flow and distribution in a cross-section at Oostduinkerke (Western Coastal Plain of Belgium). *Proc. 12th Salt Water Intrusion Meeting, Barcelona, Spain, Nov. 1992. pp. 407-420.*

Weiden, R.M., van der. 1988. Boundary integral equations for the computational modeling of three-dimensional steady groundwater flow problems. *Ph.D. thesis. Delft University of Technology. 253 p.*

Wieringa, K. & Laan, W.P.M. 1989. Toekomstige waterbehoefte in Nederland, trendscenario 1986-2020. (in Dutch). *Report number 738906001. RIVM. National Institute of Public Health and Environmental Protection. Bilthoven, the Netherlands.*

Wigley, T.M.L., Jones, P.D. & Kelly, P.M. 1986. Empirical Climate Studies. Warm World Scenarios and the Detection of Climate Change Induced by Radiatively Active Gases. In: *The Greenhouse Effect, Climate Change, and Ecosystems. Bolin, B., Döös, B.R., Jäger, J. & Warrick, R.A. (eds). John Wiley & Sons.*

Wilde, J.G.S., de. 1979. Begrenzing, oppervlakte, afvoer and peilen van de polders in Noord-Holland ten Noorden van het IJ en het Noordzeekanaal. (in Dutch). *Werkgroep Noord-Holland IX. Nota ICW 1160. Wageningen. 13 p.*

Wilson, J.L. & Sa da Costa, A. 1982. Finite element simulation of a saltwater/freshwater interface with indirect toe tracking. *Water Resour. Res., 18 (4): 1069-1080.*

Wind, H.G. (ed). 1987. Impact of Sea level rise On Society. Report of a project-planning session, Delft, 27-29 Aug. 1986. *A.A. Balkema, Rotterdam/Brookfield. 191 p.*

Wit, K.E. 1974. Hydrologisch Onderzoek in Midden-West-Nederland. (in Dutch). *Instituut voor Cultuurtechniek en Waterhuishouding (ICW). Nota 792^{II}.*

Witt, H. 1980. Het chloridegehalte van het grondwater in Noord-Holland benoorden het IJ en het Noordzeekanaal. (in Dutch). *Werkgroep Noord-Holland X. Nota ICW 1173, Wageningen. 25 p.*

Wolff, W.J., Dijkema, K.S. & Ens, B.J. 1993. Expected ecological effects of sea level rise. *State of the Art Report UNESCO Workshop SEACHANGE'93: Sea Level Changes and their Consequences for Hydrology and Water Management. Noordwijkerhout, the Netherlands. April, 1993. UNESCO, IHP-IV Project H-2-2. pp. 139-150.*

Zagwijn, W.H., Beets, D.J. & Berg, M., van den. 1985. Atlas van Nederland. Deel 13. Geologie. *Staatsuitgeverij, 's Gravenhage.*

Zijl, W. & Nawalany, M. 1993. Natural groundwater flow. *Lewis Publishers, Boca Raton, 321 p.*

Zwerver, S. 1989. Maatregelen tegen broeikaseffect hoeven niet veel te kosten. (in Dutch). Part of the report: 'Een paar graden meer ?'. In: *N.R.C. Handelsblad, Wetenschap en Onderwijs. March 31.*

Index

409

Curriculum Vitae

Gualbert Oude Essink was born in Rijswijk on the 22nd of December 1965. In June 1984, he obtained the Atheneum-B certificate at the secondary school Lodewijk Make-blijde College in Rijswijk.

In September 1984, he started to study Civil Engineering at the Delft University of Technology. After some two years, the specialization in hydrology and water management was chosen. His graduation work dealt with the effects of sea level rise on the behaviour of the interface between fresh and saline groundwater in a semi-confined aquifer along the Dutch coast. It was carried out under the guidance of Prof. dr ir J.C. van Dam. The ir degree in civil engineering (equivalent of M.Sc.) was obtained in October 1989. A supplementary examination in hydraulic engineering was also obtained.

In September 1989, the author was employed as an Assistent-In-Opleiding in the section Hydrology and Ecology of the Department of Water Management, Environmental and Sanitary Engineering of the Delft University of Technology. The research project comprises the possible impact of sea level rise on coastal groundwater flow regimes in the Netherlands, which led to the present Ph.D. thesis.

The author participated in the organizing committee of SEACHANGE'93, an international workshop of the UNESCO International Hydrological Programme IV on sea level changes and their consequences for hydrology and water management, which was held at Noordwijkerhout, the Netherlands, 19-23 April, 1993. He was asked by the FAO to participate in an expert consultation on sea water intrusion at Cairo, Egypt, 10-13 October, 1993 and to write a keynote on possible effects of a substantial rise in sea water level on the coastal aquifers. During his Ph.D. study, the author assisted undergraduate students and published about ten articles.

Since March 1995, the author worked freelance on the compilation of lecture notes of the subject Hydrological models.